

東北医科薬科大学 分子生体膜研究所年報 2018年度 研究成果報告書



2018 Annual Report of
Institute of Molecular Biomembrane and Glycobiology



ご挨拶

2018年度は、本学分子生体膜研究所が世話人を務め、第37回日本糖質学会年会を仙台国際センターで8月28-30日に開催いたしました。仙台での日本糖質学会年会は、昭和58年（第6回 松田和雄先生）、平成5年（第15回 鈴木茂生先生）、平成18年（第26回 宮城妙子先生）そして今年の第37回で4回目の開催となります。12年前の第26回では、宮城県立がんセンター、東北大学、弘前大学、東北薬科大学（現東北医科薬科大学）の糖質科学研究者が世話人となり、今回と同じ仙台国際センターで開催されました。この第26回年会が契機となり、東北糖鎖研究会が発足し、毎年一回の研究会を開催し活動しています（URL: <http://tohokut-tousa.strikingly.com/>）。現在、東北糖鎖研究会に参加している研究者の研究機関は、上記の4研究機関に加えて、北から鷹揚郷腎研究所、岩手医科大学、福島県立医科大学、新潟大学、新潟薬科大学、長岡技術科学大学、群馬大学の計11研究機関に発展し、第37回年会のプログラム委員、組織委員を担当していただきました。ここに厚く御礼申し上げます。

今回の年報では、各研究部門の研究活動報告に加えて、第37回日本糖質学会年会の内容報告、第2回箱守仙一郎賞の奨励賞および優秀論文賞のご紹介をいたします。

皆様からのなお一層のご指導、ご鞭撻のほど衷心よりお願い申し上げます。

平成31年3月

東北医科薬科大学分子生体膜研究所・所長

東北糖鎖研究会・会長

井ノ口 仁一

目次

- 所長挨拶・・・・・・・・・・・・・・・・・・・・・・・・・・・・・・・・ 1
分子生体膜研究所・所長 井ノ口 仁一

- 第37回日本糖質学会年会の開催報告・・・・・・・・・・・・・・・・ 4

- 山川民夫先生を偲んで・・・・・・・・・・・・・・・・・・・・・・・・ 7
東北医科薬科大学客員教授 鈴木明身

- 箱守仙一郎賞・・・・・・・・・・・・・・・・・・・・・・・・・・・・ 12
東北医科薬科大学分子生体膜研究所「箱守仙一郎賞」規約
平成30年度 箱守仙一郎賞
奨励賞 稲森 啓一郎（東北医科薬科大学分子生体膜研究所）
優秀論文賞 目黒 康洋（東北大学大学院農学研究科）
優秀論文賞 村上 友太（福島県立医科大学医学部）

- 研究報告・・・・・・・・・・・・・・・・・・・・・・・・・・・・ 21
機能病態分子部門
「GM3 ガングリオシドの生理的意義の解明に向けて」
井ノ口 仁一，稲森 啓一郎，永福 正和，狩野 裕考

生体膜情報部門
「生活習慣病に関連した G タンパク質共役受容体の機能と糖鎖および受容体相互作用による調節」
東 秀好，中川 哲人，黒田 喜幸

細胞制御部門
「糖鎖によるがん細胞の機能と中枢神経系における炎症反応の制御」
顧 建国，福田 友彦，伊左治 知弥

分子認識部門
「レクチンの抗腫瘍メカニズムの解明とがん薬物治療への応用」
細野 雅祐，菅原 栄紀，立田 岳生

- 学会発表記録・・・・・・・・・・・・・・・・・・・・・・・・・・・・ 37

- 学術論文・・・・・・・・・・・・・・・・・・・・・・・・・・・・ 42

第37回日本糖質学会年会の開催報告

井ノ口 仁一

平成30年8月28～30日に開催された今回の第37回年会では「次世代医療への糖鎖の貢献」をテーマに掲げ、糖鎖工学と糖鎖生物学における日本の強みを生かし、いかに次世代医療に向けた医療革命に貢献することができるのか。その現状と未来を様々な視点から展望する機会にしたいと思いました。参加者は、大変縁起の良い555名ぴったりで、一般からの参加者も2割を占め、盛会となりました。特別講演として2題、レジェンドレクチャー2題、シンポジウム1件、男女共同参画企画1題、奨励賞受賞講演1題、優秀講演賞第2次審査7題、一般演題77題、ポスター演題168題の発表が行われました。

1日目の朝は、一般演題と並行して、今回初めて企画された若手研究者を対象とした優秀講演賞候補者7名の講演がおこなわれました。いずれの発表内容もすばらしく、発表者の将来が楽しみです。その後の総会では、深瀬会長及び梶原副会長から、日本糖質学会の活動が報告されたあと、来年の名古屋大会の世話人代表の北島健先生から、記念すべき糖質学会40周年に当たる第38回年会を「不惑」というキーワードで行うとの抱負を述べられました。

続いて、第21回糖質学会奨励賞および第20回ポスター賞の授賞式が行われました。

平成30年度の受賞は、東北医科薬科大学 医学部の上村聡志博士（受賞タイトル：スフィンゴ糖脂質合成酵素の細胞内動態解析）です。上村博士は、今から20年前、私が北海道大学薬学部助教授時代の大学院生であり、この受賞を心より嬉しく思います。

男女共同参画企画では、東北大学の栗原和枝先生が「女性研究者活躍への期待と歩み」について講演されました。本企画は、群馬大学の松尾一郎先生がお世話され、栗原先生の女性研究者としての生き方を先生ご自身の体験と人生観をもとに率直にお話しされ大変好評でした。

特別講演では、東北大学 東北メディカル・メガバンク機構の機構長である山本雅之先生から、「東北メディカル・メガバンク計画の目標と進捗状況ー世界最先端のバイオバンクの構築を目指してー」と題して、圧巻のご講演をいただきました。7年前、東日本大震災からの医療復興を目指して開始された東北メディカル・メガバンク構想が、今や、世界をリードする遺伝子解析・ゲノム研究を組み合わせた「ゲノムコホート研究」に成長し、次世代の医療を牽引してく成果が続々と達成されおり、同じ仙台に住む一人として大変嬉しく思います。是非、糖鎖研

究をこの壮大なプロジェクト加えていただきたい、参加したいと思わず、フロアから発言させて頂きました。

次の特別講演は、遠藤玉夫先生です。「糖鎖生合成異常による先天性筋ジストロフィー」と題しての講演お願いし、学士院賞受賞に至った研究の経緯をじっくり1時間お話しいただいたのは、糖質学会では初めてで、先生の大学院生時代からの研究人生を楽しくそして興味深く拝聴できました。今後も、ますますのご活躍を願っています。

2日目の朝8時半からは、レジェンドレクチャーを鈴木邦彦先生にお願いし、「子供の遺伝性神経疾患：日本からの若い研究者と一緒に辿った路」としてご講演賜りました。先生は、「多くの小児の神経系の代謝疾患に関りましたが、散漫になるのを避けるために、このお話では、テーマを絞って、1970年以來、「核酸時代」も通して私の研究室の主なテーマの一つであった古典的な遺伝性脳白質変性症であるクラベ病 (globoid cell leukodystrophy, GLD) の病理機序の解明を追って来た道をお話してみたいと思います。」とされ、先生の米国での40年に渡る研究人生の一端をお話してくださいました。ご講演の中で、ミシガン大学の Norman Radin 教授との研究交流のお話がありました。それは、1970年代初頭のこと、「Radin 教授は、まだ未発表のガラクトシルセラミダーゼのアッセイ法を快く提供してくれたおかげで、クラベ病がガラクトシルセラミダーゼの欠損であることをいち早く証明することができた。彼の助けがなかったら、もっともっと時間がかかっていた。」と述べられました。私は Radin 研に 1985-87 年在籍し、グルコシルセラミド合成酵素阻害剤の開発研究がきっかけで糖鎖研究者としての道を歩み始めたことから、この逸話聞くことができ、嬉しく誇りに思いました。

2日目午前中の次のプログラムは、名古屋大の門松健治先生と岡崎研究機構の加藤晃一先生にオーガナイザーをお願いしてのパネルディスカッション形式のシンポジウム「糖鎖関連大型研究の現状と将来展望」です。「どうする！ニッポン・20年後の糖鎖科学を考える・シンポジウムで議論しよう！主役は学会参加者です。」と題した門松先生が作成されたパンフレットを学会初日から学会参加者全員に受付で配布し、5名のシンポジスト、3名の指定討論者とフロアとの様々な角度から活発な討論が予定調和は企図せずおこなわれました。議論を通して、糖鎖学界および各人の中に、おぼろげでも夢あるいは目指すべきものを描けていただけたなら、このシンポジウムの意義はあったと思います。

午後は、エクスカージョン (松島探訪、被災地訪問や宮城ニッカウイスキー工場見学、仙台新港と水族館など)、そして19時から懇親会が行われました。江陽グランドホテルで行われた懇親会では、世話人の私から、多数の参加者の皆様への感謝の意と山川民夫先生から「猛暑と足の具合がよろしくないなので、残念な

がら仙台には行かない。できれば、昨年執筆した東大医科研創立125周年・改組50周年記念誌への寄稿文—僕の青春時代-伝染病研究所の頃—を皆様にお配りしていただきたい。」と先週電話をいただいたことを報告いたしました。次に、レジェンドレクチャーをいただいた鈴木邦彦先生にお言葉をいただき、続いてカーンマイヤーアワードの受賞が決定された谷口直之先生のからお言葉をいただきました。乾杯のご発声は、名誉会員の長谷純宏先生にいただきました。宮城の地酒、牛タン、旬の魚介類などの郷土の味にご満足いただけただけでしょうか？この記事を書いているのは10月ですが、11月からの仙台は牡蠣のシーズンが始まります。また、「すずめ踊り」を-仙台すずめ踊り伊達の舞-さんのプロの指導もよろしく、皆様と楽しく一緒に踊ることができたのは大変良い思い出になりました。

3日目8時半からは、長谷純宏先生のレジェンドレクチャーは「還元末端糖残基の蛍光標識による解析」で、なぜ2-aminoptridine (PA) を蛍光剤として選ばれた経緯と発展の過程を、先生が影響を受けられた諸先輩の名言と共に語っていただきました。フロアからは、笠井献一先生が糖の標識試薬としてPAを選ばれなかったらフロンタルアフィニティークロマトグラフィーの成功はなかったと発言されました。

本年会は、多くの学会からの共催、協賛、後援をいただき、また、ご援助、展示、広告にてご支援いただきました財団、団体、企業に深く感謝申し上げます。また、ランチョンセミナーを共催いただきましたサーモフィッシャーサイエンティフィックと島津製作所に心からお礼申し上げます。そして、プログラム委員の先生方、アドスリー、JTB、東北医科薬科大分子生体膜研究所のスタッフ、学生アルバイトの皆さんのご協力にお礼申し上げます。

このレポートを執筆中に、山川民夫先生がご逝去されました。8月に糖質学会へのご出席のお願いで、山川先生とお電話でお話いたしましたこと昨日のように思い出しております。先生のお嬢様からは、「今となっては仙台に行けなかったことが残念でなりません。本人の決断ではありましたが、皆さまにお会いできていれば、良い思い出になったかと思います。」とのお言葉をいただきました。

ここに謹んで、ご冥福をお祈りいたします。

次項に山川先生の一歩弟子であられる本学客員教授の鈴木明身先生に「山川民夫先生を偲んで」を綴って頂きました。

山川民夫先生を偲んで

東北医科薬科大学客員教授 鈴木明身

先生は2018年10月7日、96歳で他界されました。直近まで、歩行が少し難しくなっていたことを除き、先生の特徴の一つであった度を越しての物事への好奇心も衰えず、すこぶるお元気でした。食欲も旺盛であったとお聞きしております。私がお見舞いした9月25日、10月5日は、意識がないとはいえ、寝姿は普段の先生のお姿に変わりはなく、まだまだ、大丈夫だと、思っていた矢先のことでした。先生の生涯の一時期を共有させていただいた者の素朴な感想として、先生の生涯はまれにみる極彩色にあふれたものであったことに疑いを持ちません。

先生は1921年10月19日（大正10年）、東北帝国大学医学部内科学山川章太郎教授の二男として、仙台市で生まれ、仙台第二中（現仙台第二高校）、旧制第二高等学校を卒業されるまで、仙台で過ごされました。仙台は先生の故郷でした。井ノ口仁一先生は世話人代表をされた第37回日本糖質学会年会（2018年8月28-30日）に山川先生を招待されました。先生は大変乗り気で、楽しみにされていましたが、猛暑と体調を懸念され、間際になって断念されました。大変心残りのご様子であったとお聞きしております。

先生は1944年9月（昭和19年）に東京帝国大学医学部を卒業されますが、学生の時から伝染病研究所（現医科学研究所）の有機化学の研究室で、化学合成の実験を体験します。伝染病研究所が選択されたのは、長兄の山川邦夫教授（東京帝国大学医学部卒業後、順天堂大学内科学教授）の後押しがあったとのこと。それとともに、有機化学を選択したのは、医学の研究を有機化学の知識を基礎として実践する決意があったと、聞いています。この実習中に、爆発の事故を起こします。トルエンをニトロ化し、生成したオルトとパラニトロトルエンを減圧蒸留で分離し、何度も繰り返して100gほどのパラニトロトルエンを貯めました。パラニトロトルエンのメチル基を酸化し、パラニトロ安息香酸にするために、100gほどの無水クロム酸を加えると、バーンと大爆発……。即入院され、その後、1週間ぐらいは意識がなく、ひどい痛みになやまされ、生死のはざまをさまよい、生還されます。私の学生時代は、学会で宿泊する旅館で、先生と一緒に風呂にはいる機会があったりしましたが、先生の胸部と腹部の半分はひどいケロイドでおおわれていました。この時、親身に心配された、薬科専門学校出身で実験助手をされていた女性がおられ、この方、恵津子夫人、と先生は生涯を共にされます。

この事故にもかかわらず、先生は卒業後に伝染病研究所の化学部に入られ、枝付き脂肪酸の合成、その実験動物体内での代謝の研究を行い、医学博士となられ

ます。伝染病研究所は北里柴三郎が私立伝染病研究所として創設し、その後内務省の国立伝染病研究所となり、紆余曲折を経て、東京帝国大学の所管となったことが知られています。伝染病研究所では、戦後まもなくまで、破傷風、ジフテリアなど感染症に対する抗血清が製造されていました。大量の血清を得るために、ウマに抗原を投与し、採血して得られた血液を凝固させ、固まった血球成分とフィブリンを除き、抗血清をえます。凝固物は、無用の長物として、捨て場に困っていたらうことが想像できます。先生はこの廃棄物に着目します。学生時代に化学の研究室に参加した経緯は上記のとおりですが、もう一つ気になっていた研究分野は川喜田愛郎教授のウイルス学だったようです。インフルエンザウイルスは赤血球を凝集することが知られています。さらに動物間で赤血球の免疫反応に種差があることも知られていました。伝染病研究所の先生の周辺では、感染症や免疫が関心事でした。上記の二つのことが先生の中で、融合したようです。培った脂肪酸の合成、分離、構造解析の手法を使って、困りもののウマの凝固塊からウマ赤血球に特異な物質を手に入れることは出来ないかと考えたようです。生理食塩水中で凝固塊を手でもみほぐし、遊離してきた赤血球を遠心して集め、そこへ、酢酸で酸性にした水を大量に加えて、低張処理します。加えた水の量が少ないと、放出されたヘモグロビンによる比重上昇のためか赤血球膜塊の沈殿が目視できません。大量の水であれば、目視で上清を取り除くことができます。沈殿を遠心し、沈査の stroma を集め、凍結乾燥します。この材料から有機溶媒で脂質を抽出して、アセトン不溶、エテール不溶、ピリジン可溶画分を集め、様々な分析に供しました。これらの実験結果から得られた糖脂質は hematoside と命名され、構造は sphingosine(d18:1)[-lignoceric acid (24:0)]-galactose-galactose-prehemataminic acid、prehemataminic acid は炭素 9 個の新しい糖であると J. Biochem. 38, 199-212, 1951 に報告されました。prehemataminic acid は当時構造が不明であった neuraminic acid あるいは sialic acid と同じ構造の単糖であることがその後明らかにされます。Sialic acid の正しい構造は 1955 年に Gottschalk によって炭素 9 個の単糖として報告されます。ウマ赤血球の hematoside の正しい構造は ceramide(d18:1-24:0)-glucose-galactose-(4-O-acetyl) N-glycolylneuraminic acid であることがその後報告されますが、様々な機器分析の手法が使えなかった時代に生体膜のモデルともなる赤血球膜の成分として糖脂質 hematoside が存在することを発見したことは、歴史に残る研究であることを示しています。

研究はヒト赤血球膜糖脂質の解析に展開され、globoside と命名された糖脂質が単離されます。Globoside の命名は先生によるものですが、ヒト赤血球の主要糖脂質の構造は Klenk による発表が先でありました。Globo-series の名前は

Gal α 1-4Gal β 1-4Glc β 1-Cer の骨格構造を持つ糖脂質に今でも使われています。日本生化学会大会でこれらの結果を発表した際に、東北大学医学部医化学教室正宗一教授が、globoside に ABO 式血液型の抗原活性はないのかと質問されたと、聞いています。正宗一先生は箱守仙一郎先生の恩師で、糖鎖生物学の先駆者のお一人です。この質問が契機になり、ヒト赤血球糖脂質の A 型、B 型抗原活性が調べられました。糖脂質は水溶液中で激しく攪拌することによりミセルを形成し、抗原糖脂質は multivalency を獲得して、抗体との反応性は飛躍的に上昇することが今では知られています。抗体と糖脂質水溶液を反応させ、その後に赤血球の懸濁液を加えて、赤血球凝集阻止活性を測定します。ヒト赤血球糖脂質画分は当時導入され始めたシリカゲルのカラムクロマトでクロロホルム-メタノール混液で分離溶出され、分画した画分で凝集阻止活性が調べられました。その結果、globoside (GalNAc β 1-3Gal α 1-4Gal β 1-4Glc β 1-Cer) よりも糖鎖の長い糖脂質の画分に阻止活性のあることが見出され、1953 年、1960 年に発表されます。その後、内貴、Marcus の研究で globoside は P 式血液型抗原であることが明らかにされます。さらにはがん関連抗原としての糖脂質の研究が箱守先生により精力的に行われ、多くの素晴らしい研究成果が発表されました。ABO 式血液型に関しては、分子生物学的な分子メカニズムが 1990 年に箱守仙一郎先生の研究で完成されます。

糖脂質の機能は多くの研究者によって研究されてきました。その中でも神経細胞の神経突起を増加させる、伸長させるという成果が注目されます。1980 年代には、イタリアの製薬企業が調製したウシ脳のガングリオシドを筋肉注射して、多発性硬化症、糖尿病などに効果があるという研究結果が発表されました。認知症の患者の脳室内にガングリオシドを注入し、効果があったという報告もなされました。しかし、筋肉注射による投与により、ウシ脳のガングリオシド製剤に含まれていた微量の N-glycolylneuraminic acid を含むガングリオシドが抗原となり、抗ガングリオシド抗体が産生され、それによるギランバレー症候群の発症が認められ、一連の研究は中止されました。井ノ口先生の研究室では山川先生が発見された hematoside (GM3, N-acetylneuraminic acid-Gal-GlcCer) の生理学、病理学的作用が研究されており、大変注目される成果が報告されてきています。ここ仙台的地で、hematoside の機能が明らかにされ、疾患の診断や治療に有効であることが示される日が来ることを願ってやみません。山川先生も見守ってくれていると信じます。

山川民夫先生 ご略歴

大正 10 年 10 月 19 日、仙台で生誕（西暦 1921 年）

昭和 19 年 東京帝国大学医学部医学科卒業

昭和 19 年 10 月 東京帝国大学伝染病研究所 入所

昭和 34 年 10 月 東京大学伝染病研究所化学研究部教授

昭和 41 年 4 月 東京大学医学部教授（生化学講座担当）

昭和 48 年 9 月 日本生化学会会長（～昭和 49 年 10 月）

昭和 57 年 4 月 財団法人 東京都臨床医学総合研究所所長（～平成 3 年 3 月）

昭和 62 年 12 月 日本学士院会員

平成 3 年 4 月 東京薬科大学学長（～平成 7 年 3 月）

平成 14 年 7 月 財団法人 微生物化学研究会会長（～平成 22 年 3 月）

昭和 30 年 10 月 日本生化学会奨励賞受賞

昭和 50 年 1 月 朝日賞受賞

昭和 57 年 4 月 日本学士院賞受賞

平成 3 年 1 月 東京都文化賞受賞

平成 3 年 11 月 勲二等瑞宝章受章

2014 年 11 月 文化功労者

参考文献

遠藤玉夫、石田秀治、北島 健 (2015) JSCR Newsletter 19-2, 8-12

山川民夫 (1981) 糖脂質物語 学術文庫 562 講談社

T. Yamakawa and S. Suzuki (1951) The chemistry of the lipids of posthemolytic residue or stroma of erythrocytes. I. Concerning the ether-insoluble lipids of lyophilized horse blood stroma. J. Biochem. 38, 199-212

A. Suzuki (2009) Tamio Yamakawa: Down of glycobiology. J. Biochem. 146, 149-156

写真

2015年8月2日 シアル酸研究会・JCGGによる文化功労者の顕彰をお祝いする会で談笑される先生。上野精養軒梅の間。鈴木邦彦先生撮影。



東北医科薬科大学分子生体膜研究所
「箱守仙一郎賞」(Sen-itiroh Hakomori Glycoscience Award) 規約

平成 30 年 9 月 22 日
東北医科薬科大学分子生体膜研究所
井ノ口 仁一

名称	箱守仙一郎賞
授与機関	東北医科薬科大学分子生体膜研究所
目的	生物系化学系を問わず広く糖鎖科学を専攻し、日夜努力を続けている東北エリアの研究者を顕彰することにより、日本の糖鎖科学研究の増進を図る。
賞の種別	奨励賞 1 名 顕彰楯および副賞 優秀論文賞 1~2 名 顕彰楯および副賞
対象	1) 奨励賞：東北エリア（新潟県および群馬県を含む）で研究に従事する応募時 45 歳までの研究者 2) 優秀論文賞：同地域で研究に従事し、申請時点で大学院生もしくは博士研究員である者 *いずれも指定された期間内に発表（accepted でも可）された学術論文に対して審査・授与する。
選考方法	自薦および他薦によるものとし、東北糖鎖研究会世話人が審査する。評価を点数化（次項参照）して決する。
授賞方法	東北糖鎖研究会開催時に授賞および受賞講演を行う。
運用方法	顕彰楯および副賞の購入費は、箱守賞基金を原資とし、分子生体膜研究所がこれを支弁する。
その他	事務局は分子生体膜研究所内に置く。

審査

(1) 応募資格および応募方法

東北6県、新潟県および群馬県（東北糖鎖研究会エリア）で研究を行っている45歳以下の糖鎖科学研究者（大学院生、博士研究員は自動的に優秀論文賞へのノミネートとなる）。対象論文は、その年度内（ただし応募締切以前）に **Impact factor** が付与されている英文学術雑誌（査読有）に出版、または掲載が決定されている原著論文（**accepted** でも可）とし、応募者が筆頭著者となっているものとする。要旨和訳と論文 **PDF** を添えて既定のエントリーフォームに記入してメールにて応募する。化学系・生物系は問わない。自薦および他薦どちらでも受け付ける。応募期間等についてはその都度決定し、周知する。

書類送付先：東北医科薬科大学 分子生体膜研究所 所長 井ノ口 仁一
メールアドレス：jin@tohoku-mpu.ac.jp

(2) エントリーフォーム（別添）

(3) 審査委員および審査方法

- 1) 分子生体膜研究所所長が審査員長を務める。
- 2) 東北糖鎖研究会世話人が審査員となる。ただし、世話人が推薦者または自薦者の所属責任者あるいは論文の共著者である場合は審査に参加しない。
- 3) 期限内に提出された論文について事務局が一次審査（下記基礎点による）を行い、奨励賞および優秀論文賞それぞれ上位3報を選定する。
- 4) 上位3報について審査員が下記評価項目を採点し、全員（その都度人数は異なる）の評価平均点+基礎点（100点満点、1点未満は四捨五入）から最上位者を受賞者として決定する。
- 5) 最高点が複数出た場合は審査員長の判断に委ねる。

基礎点	評価最高点
Impact factor 2.0 未満 10 点	独創性 10 点
4.0 未満 20 点	インパクト（重要性） 10 点
6.0 未満 30 点	論文構成 10 点
8.0 未満 40 点	将来性 10 点
10 未満 50 点	
10 以上 60 点	

平成30年度 箱守仙一郎賞
(Sen-itiroh Hakomori Glycoscience Award 2018)

東北糖鎖研究会 (<http://tohokut-tousa.strikingly.com>) の世話人による厳正な審査の結果、第二回箱守仙一郎賞の研究奨励賞および優秀論文賞の受賞者が決定し、弘前で行われた第12回東北糖鎖研究会で授賞式および奨励賞受賞講演が行われました。

奨励賞

稲森 啓一郎 東北医科薬科大学分子生体膜研究所 機能病態分子学 准教授
ガングリオシド生合成不全は肥満モデル KK^{Ay} マウスのレプチンおよびメラノコルチンシグナルを改善する
Deficient ganglioside synthesis restores responsiveness to leptin and melanocortin signaling in obese KK^{Ay} mice

優秀論文賞

目黒 康洋 東北大学大学院農学研究科 生物有機化学分野 博士後期課程二年
Glycosyl Bunte Salts: A Class of Intermediates for Sugar Chemistry
Organic Letters, 20, 76-79 (2018)

村上 友太 福島県立医科大学医学部脳神経外科学講座 博士研究員
Spontaneous intracranial hypotension is diagnosed by a combination of lipocalin-type prostaglandin D synthase and brain-type transferrin in cerebrospinal fluid
Biochim Biophys Acta Gen Subj, 1862, 1835-1842 (2018)



左より、井ノ口所長、村上友太博士、稲森啓一郎博士、目黒康洋さん(D2)

奨励賞

ガングリオシド生合成不全は肥満モデル KKAY マウスの レプチンおよびメラノコルチンシグナルを改善する

Deficient ganglioside synthesis restores responsiveness to leptin and melanocortin signaling in obese KKAY mice

稲森 啓一郎（東北医科薬科大学 分子生体膜研究所 機能病態分子学・准教授）

GM3 は a および b 系列ガングリオシドの前駆体で、肥満モデル動物の脂肪細胞や、2 型糖尿病または脂質異常症である肥満患者の血清中で増加がみられる。GM3 合成酵素(GM3S)をノックアウト(KO)した C57BL/6 マウスでは、インスリン感受性の亢進と、高脂肪食誘導性のインスリン抵抗性の発症が軽減される。しかし、摂食と代謝の中枢性制御における GM3 と関連ガングリオシドの病態生理的役割については不明である。我々は、黄色肥満マウス KKAY の GM3S 遺伝子を KO したモデルマウス(KKAY GM3S KO)において、肥満病態が著しく改善されることを見出した。KKAY マウスが過食で重度の肥満を発症するのに対し、KKAY GM3S KO マウスは著明な体重と摂餌量の減少、および、耐糖能とインスリン感受性の著しい改善を示した。KKAY マウスでは、レプチンの腹腔内投与に対する視床下部ニューロンの応答性が大幅に減弱していたが、KKAY GM3S KO マウスではレプチンに対する応答性が十分保たれていた。マウス視床下部由来神経細胞株を用いた実験では、GM3S 欠損細胞においてレプチン依存の ERK リン酸化が亢進していた。さらに、KKAY GM3S KO マウスは毛色の変化を呈しており、GM3S はメラノコルチンシグナルにも関与していることが示唆された。我々の発見により、GM3 関連ガングリオシドがレプチンおよびメラノコルチンシグナルにおいて重要な役割をもつことが示された(1)。

- (1) Inamori K, Ito H, Tamura Y, Nitta T, Yang X, Nihei W, Shishido F, Imazu S, Tsukita S, Yamada T, Katagiri H, Inokuchi J. Deficient ganglioside synthesis restores responsiveness to leptin and melanocortin signaling in obese KKAY mice. *J Lipid Res* 59, 1472-1481 (2018).

【経歴】

平成 7 年：九州大学理学部卒業，平成 9 年：九州大学大学院理学研究科修士課程修了，同年 日本学術振興会 特別研究員，平成 13 年：九州大学大学院医学系研究科博士課程修了(博士・理学)，同年 大阪大学大学院医学系研究科 博士研究員，平成 16 年：同 特任助手 (O・マンノース型糖鎖の生合成に関わる糖転移酵素の研究)，平成 18 年：米国アイオワ大学医学部・ハワードヒューズ医学研究所 Postdoctoral fellow，平成 24 年：同 Associate (ジストログリカンのラミニン結合性糖鎖の生合成に関する研究)，平成 25 年：東北薬科大学 分子生体膜研究所 機能病態分子学教室 准教授 (平成 28 年 大学名が東北医科薬科大学に改称)。現在、糖脂質ガングリオシドの生理機能に関する研究に従事。

【受賞の感想と抱負】

この度、平成30年度箱守仙一郎賞奨励賞を賜りましたこと、大変光栄に存じます。箱守先生はじめ東北糖鎖研究会の箱守賞審査委員の先生方に深く御礼申し上げます。糖鎖研究に携わって以来、箱守先生の偉大なるご業績と糖鎖生物学研究における多大なご功績を拝見しておりましたが、その箱守先生のお名前を冠した賞をいただきましたこと、深く感謝申し上げますとともに、大変身の引き締まる思いがいたします。

糖鎖研究に入っていくきっかけは、大学院時代に九州大学・岩永貞昭先生、川畑俊一郎先生のご指導のもと行ったカプトガニの生体防御レクチンの機能解析でした。その後、大阪大学・谷口直之先生のもとで糖転移酵素に関する研究に携わりました。そこで見つけた新規の酵素がO-マンノース型糖鎖の生合成に関与していたことから、当時、ジストログリカンの糖鎖異常と筋ジストロフィーの関係について研究を推し進めていたアイオワ大学・Prof. Kevin Campbellの研究室に飛び込みました。ここではジストログリカンのO-マンノース型糖鎖上に直接リガンド結合性多糖を付加する糖転移酵素の活性同定を行いました。現在は、東北医科薬科大学・井ノ口仁一教授のもと、糖脂質ガングリオシドの生理機能について、特にシアル酸転移酵素であるGM3合成酵素の欠損マウスを用いて肥満病態などの疾患における病態生理的役割の解明を目指しています。糖タンパク質糖鎖から糖脂質へと研究内容が大きくシフトし、四十を過ぎてからの新たな挑戦に未だに苦闘しておりますが、糖鎖の生理機能の解明を目指すといった点では一貫性をもって研究に取り組んでおります。今回の受賞対象となった論文からは、ガングリオシドの中枢性の摂食・代謝調節における役割とともに、予想外にも毛や皮膚の色素産生調節における関与が示唆されました。しかしながら、メカニズムの面では不明な部分が多くまだまだわからないことばかりで、今後ひとつひとつを明らかにしていきたいと考えております。

最後に、この研究を行うにあたり、井ノ口教授をはじめ、ご指導・ご協力いただきました共著者の先生方・大学院生、ご支援くださった研究室のメンバーに心より感謝申し上げます。今回の受賞を励みに、糖鎖科学のさらなる発展に少しでも貢献していけますよう引き続き精進して参りたい所存です。今後ともご指導ご鞭撻のほどよろしくお願い申し上げます。

稲森 啓一郎

優秀論文賞

Glycosyl Bunte Salts: A Class of Intermediates for Sugar Chemistry

Meguro Y, Noguchi M, Li G, Shoda SI

Organic Letters, 20, 76-79 (2018)

目黒 康洋（東北大学大学院農学研究科・博士後期課程二年）

我々は糖質合成における中間体として、これまでに前例の無いチオ硫酸糖を創製した。この新規糖誘導体であるチオ硫酸糖を、アルキルブンテ塩の発見者である19世紀のドイツ人化学者 Hans Bunte に因んでグリコシルブンテ塩と名付けた。すなわち、ホルムアミジン型脱水縮合剤を用いることにより、水溶液中にて無保護糖と安価なチオ硫酸ナトリウムから、一段階で新規糖化合物であるグリコシルブンテ塩の合成を達成した。本反応は水溶液中かつ0°Cの温和な条件下で進行し、水溶液中での反応であるため無保護オリゴ糖にも問題なく適用でき、信頼性の高い汎用的合成法である。さらに、グリコシルブンテ塩はこれまで未報告の化合物であることから、官能基変換による様々な有用糖質の合成中間体としての利用を試みた。本法は、従来法では多段階反応が必要であったグリコシルチオール、ジスルフィド糖、O-グリコシド、1,6-アンヒドロ糖など様々な糖質への変換が容易であることから、極めて利用価値の高い画期的な合成反応である。

【受賞の感想と抱負】

この度は、第二回箱守仙一郎賞・優秀論文賞を賜り一研究員として大変光栄に存じます。箱守先生はメチル化による多糖分析法の開発も有名ですが私の専門と関連する天然および生体関連糖鎖の探索・評価において素晴らしい研究成果を拝見しています。世界に先駆けて糖鎖化学の展開に多大なる功績を与えたことで名高い箱守先生の名前を冠した賞を頂くことは大変恐縮ではありますが、この賞を励みに私自身も糖鎖化学の発展に貢献できるよう努めていきたいと思っております。

私は正田晋一郎教授の下、1,2-アンヒドロ糖の形成を経由する新規グリコシル化反応の開発研究に従事していました。研究テーマを自ら設定し、実験、分析、そして論文執筆という一連の経験を経て、研究の奥深さを実感するとともに、研究成果を得ることがいかに困難かを痛感しています。しかしながら、困難に直面するたびに試薬を手にとって実験を繰り返し行ってきました。そのような研究生活の中で今回の受賞内容である有機/無機ハイブリッド構造を持つ新規糖誘導体グリコシルブンテ塩の発見に至りました。本反応は広範な無保護オリゴ糖にも問題なく適用でき、さらにグリコシルチオール、ジスルフィド糖、O-グリコシドなどへの変換も容易であることから利用価値の極めて大きな画期的反応であると考えています。この発見の感動は研究者として一生忘れられない財産になるでしょ

うがこのような経験ができたのもひとえに正田先生の自由な気風の下で研究を行えたおかげであると思っております。

修士課程時において、有機合成関連の学会にて特に天然物の全合成研究に関して拝聴する機会が多くありました。美しい!その当時、私には全合成の経験はありませんでしたが、さながら芸術的な絵画を見ているかのように直観的に美しいと感じました。もし、自分がこのような化学変換を自由自在に操ることができ、最終目的物を手にすることができるとしたら、これまでにない達成感を得られると確信しました。私はこのような経緯から有機合成ならびに全合成研究に魅了され、現在では桑原重文教授(東北大学農学)の下で糖含有天然物の全合成に従事しています。全合成に関連した医薬・農薬の開発は①天然物など、有用な生理作用を持つ薬剤の候補物質の探索・選抜②合成による構造最適化③臨床試験を経て行われることが多く、②を担う全合成研究者は中核的な存在です。そのため、全合成を志す私は様々な領域の研究者を結びつけるに足る広い知識と技量を蓄え、研究成果を社会に還元できるよう努めていきたいと考えております。合成化学者としての技量と知識に磨きをかけ、将来的には糖質合成の基礎研究から社会への還元までを包括する領域横断的な研究に従事したいと考えております。

最後に研究のご指導を頂いた正田晋一郎教授と研究室の皆様に深く感謝いたします。これまでの反応開発とは異なる発想や実験手法に満ちた新たな環境にて現在は生物活性天然物の全合成に挑戦しています。この新天地である東北大学農学研究科においても今回の受賞を励みに新たな研究成果を報告できるよう精一杯努力いたします。

目黒 康洋

優秀論文賞

Spontaneous intracranial hypotension is diagnosed by a combination of lipocalin-type prostaglandin D synthase and brain-type transferrin in cerebrospinal fluid

Murakami Y, Takahashi K, Hoshi K, Ito H, Kanno M, Saito K, Nollet K, Yamaguchi Y, Miyajima M, Arai H, Hashimoto Y, Mima T.

Biochim Biophys Acta Gen Subj, 1862:1835-1842 (2018).

村上 友太（福島県立医科大学医学部脳神経外科学講座・博士研究員）

【論文要旨】

特発性低髄液圧症候群（脳脊髄液漏出症）は脳脊髄液（髄液）漏出などにより起立性頭痛、めまい等の不定愁訴を示す疾患である。MRI、CTなどで診断されるが、画像上の変化が乏しい症例があり、この場合診断が極めて困難となる。本研究グループは髄液中のバイオマーカーを検索する研究を行った。本疾患の髄液タンパク質を系統的に調べて、脳型トランスフェリン及びリポカリン型プロスタグランジン D 合成酵素の増加を示し、両者を疾患マーカーとした場合に特発性低髄液圧症候群が感度 95%、特異度 73%で診断されることを示した。

この論文は特発性低髄液圧症候群におけるバイオマーカーの世界初の報告である。

付記：国立研究開発法人日本医療研究開発機構（AMED）のプレスリリース
(https://www.amed.go.jp/news/release_20180416.html)

【経歴】

平成 23 年 3 月 福島県立医科大学医学部 卒業

平成 25 年 4 月 福島県立医科大学医学部脳神経外科学講座 入局

平成 29 年 9 月 福島県立医科大学大学院医学研究科博士課程 修了

（同大学医学部生化学講座 橋本康弘教授のもと、脳脊髄液バイオマーカーの研究）

平成 31 年 1 月 福島県立医科大学医学部脳神経外科学講座 助教

【受賞の感想と抱負】

このたび、箱守仙一郎賞優秀論文賞を賜りまして大変光栄に存じます。箱守先生はじめ東北糖鎖研究会論文賞審査委員の先生方に御礼申し上げます。

受賞論文は、私が大学院研究で当講座（齋藤清教授）が同大学生化学講座（橋本康弘教授）と共同研究を行っている脳脊髄液（髄液）バイオマーカーについての研究内容の一部です。私が研究に関わらせていただく前段階で、髄液と血清との性状の違いとして、髄液中のトランスフェリン（Tf）というタンパク質には、血清型糖鎖をもつ血清型 Tf とは別に、髄液中に特有の脳型糖鎖をもつ脳型 Tf が存在する、ということが見いだされておりました。脳脊髄液の生理学としては、この数十年来教科書に記載されていた **bulk flow** 説（側脳室内の脈絡叢で髄液が産生されて、その後髄液はモンロー孔を経由し、第Ⅲ脳室、第Ⅳ脳室を通り、やがてくも膜下腔内に広がり、くも膜顆粒から吸収され上矢状静脈洞へ流れる、という髄液の産生や吸収に関する仮説）が近年疑問視され、新たな知見が増えてきた時期であったことから、髄液に興味を強く持ちました。

受賞論文内容は、特発性低髄液圧症候群の髄液診断は、ともに髄液特有の物質である、脳型 Tf、および、リポカリン型プロスタグランジン D 合成酵素の組み合わせによって高い診断精度で判断可能となることと、髄液生理学の考察です。特発性低髄液圧症候群は、診断困難な疾患であり有病率も高くありませんが、その診療を専門的に行っている山王病院の高橋浩一先生と美馬達夫先生との共同研究に関わる機会を、橋本教授のご高配により、幸運にもいただきました。本疾患に限らず、中枢神経系疾患の日常診療では、臨床症状が画像所見をはじめとした検査所見で説明できないという状況に遭遇することがあります。本研究が、髄液関連疾患の病態解明あるいは、臨床診断の一助になれば、これ以上の喜びはありません。

最後に、橋本教授、齋藤教授をはじめ、両講座の先生方にはこの場を借りまして深謝申し上げます。今後は、髄液、とくに糖鎖に着目した基礎研究は発展途上にある状態であるため、さらに同様の研究に関わっていきたいと考えております。今回の受賞を励みに研鑽を重ねていきたいと思っております。今後ともご指導ご鞭撻のほどよろしくお願いいたします。

村上友太

研究報告

GM3 ガングリオシドの生理的意義の解明に向けて
機能病態分子部門 井ノ口 仁一

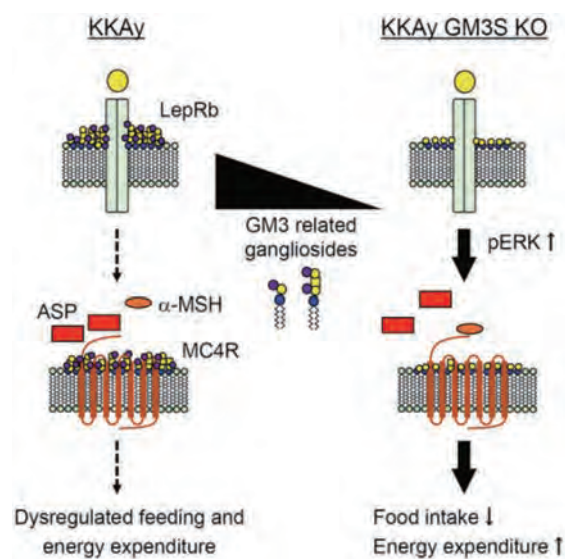
ガングリオシドファミリー生合成の最初の分子は、ラクトシルセラミドにシアル酸が転移して生成する GM3 ガングリオシドである。そもそも GM3 は、糖脂質研究の草分けである山川民夫博士がウマ赤血球からヘマトシドとして同定されたものである。我々にガングリオシド研究のきっかけを与えてくれたのは、1998 年に GM3 合成酵素 (GM3S, ST3GAL5) の遺伝子クローニングに参画したことである。2018 年度は、ジョンスホプキンス大の Ronald L. Schnaar 教授の依頼で GM3 ガングリオシドの生物学的意義についての筆者らの 20 年間の研究を “Biology of GM3 ganglioside” として以下のように集大成した総説を出版した(1)。

1. Molecular biology of GM3S/ST3GAL5
2. Insulin resistance in adipocytes and macrophages
3. Leptin signaling and resistance in hypothalamus
4. T-Cell immunity and immune disorders
5. GM3S deficiency and hearing loss

今年度の研究成果として、4つのトピックについて紹介する。

I. メラノコルチンシグナルにおけるガングリオシドの関与

黄色肥満マウス KKAy における GM3 合成酵素(GM3S)のノックアウト(GM3S KO)では、KKAy マウスの過食と肥満、耐糖能異常およびインスリン抵抗性の著明な改善がみられた。KKAy マウスではレプチン腹腔内投与に対する視床下部弓状核ニューロンの応答性が大幅に減弱していたが、KKAy GM3S KO マウスではレプチンに対する応答性が十分保たれていた。また、マウス視床下部由来神経細胞株における GM3S 欠損細胞では、レプチン依存の ERK リン酸化が亢進していた。さらに、KKAy/GM3S KO マウスは毛色の変化(黄色→灰色)を呈しており、GM3 関連ガングリオシドはレプチンとメラノコルチンシグナルにおいて重要な役割をもつことが示唆された(2)。



II. 腸管からのコレステロール吸収におけるガングリオシドの役割

今回我々は、GM3 合成酵素(GM3S)をノックアウト (KO) したガングリオシドが産生されない細胞(GM3S KO 細胞)を作成し、NPC1L1 を介したコレステロール吸収におけるガングリオシドの生理学的意義について解析した。外から与えたコレステロールは、細胞膜上にある NPC1L1 に結合すると、コレステロール依存的に NPC1L1・コレステロール複合体の細胞内移行(エンドサイトーシス)が起こり、体内にコレステロールが取り込まれる。ところが、GM3S KO 細胞ではコレステロール依存的な NPC1L1 のエンドサイトーシスが抑制され、細胞内コレステロール含量の増加も有為に抑制されていた。続いて、マウスにおいても、細胞レベルでの実験結果と一致するように、GM3S KO マウスはコレステロール負荷により引き起こされる血中のコレステロール値の上昇が著しく抑制されていた。さらに、高コレステロール血症モデルとして用いられる ApoE 変異マウスにおいて、ApoE 変異 GM3SKO マウスを作製したところ、ApoE 変異マウスが示す高コレステロール血症は ApoE 変異 GM3SKO マウスでは顕著に改善され、腸管からのコレステロール吸収率および小腸絨毛における NPC1L1 のエンドサイトーシスも抑制された。今回の研究から GM3 をはじめとするガングリオシドの発現を抑制することで、NPC1L1 の機能低下を引き起こし、高コレステロール血症の発症が抑制される可能性が見出された。ガングリオシドの発現制御が高コレステロール血症に対する新規治療標的として創薬につながることを期待される(3)。

III. T 細胞分化におけるスフィンゴミエリンの機能

T 細胞は細胞性免疫の中心的役割を担うリンパ球の一群であり、胸腺において多段階の生存増殖・分化を経て成熟し、末梢へ移出して免疫反応を担っている。本研究では、形質膜上でスフィンゴミエリン (SM) とコレステロールにより形成される微小領域 (脂質マイクロドメイン) の T 細胞の分化過程における生理的意義を解明を試みた。胸腺細胞の SM 発現量は一連の分化過程で大きく変動し、それはセラミドから SM を合成する酵素である SM 合成酵素 1 (SMS1) の発現レベルで厳密に制御されていることを見いだした。分化の初期段階から SM 発現は徐々に低下し、正負の選択の前後で SM 発現が再度大きく増加し、SM マイクロドメイン発現量は 10 倍以上増加し、正負の選択における SM マイクロドメインの関与が考えられた。*SMS1* 欠損マウス由来細胞では細胞死が亢進し、TCR 刺激後の TCR 近位のシグナル分子である ZAP-70 のリン酸化が亢進し、負の選択につながる ERK5 のリン酸化やアポトーシス促進分子である Bim, ERK5 の下流の伝達分子の Nur77 の発現も顕著に増加しており、*SMS1* 欠損胸腺細胞では TCR シグナル伝達が亢進することが判明した。*SMS1* 欠損胸腺細胞では TCR 刺激の閾値が下がり TCR シグナル強度が増強されて負の選択が亢進したと考えられる。このことは TCR シグナル強度の調節に SM に富んだ脂質マイクロドメインが寄

与することを示唆しており、胸腺細胞分化において SM 発現量の増減は厳密に制御され、正負の選択を決定する TCR 刺激の閾値を適正化しているものと考えられる。今後、自己免疫疾患患者の T 細胞における SM 発現の変化を解析することで、新たな診断や治療法の開発が期待される(4)。

IV. 糖尿病性腎症におけるスフィンゴ糖脂質の役割

本研究では、高脂肪食を KK マウスに 8 週間負荷し糖尿病性腎症モデルを作成した。この高脂肪食負荷 KK マウスの腎臓では、グロボ系糖脂質 Gb3 の発現が著しく増加していた。その分子種解析を、液体クロマトグラフ-タンデム質量分析計 (LC-MS/MS) を用いて行った結果、Gb3 のセラミド部分のアシル鎖に飽和の極長鎖 (C22, C23, C24) 有する分子種が特に増加していることを見出した。この結果より、グロボ系糖脂質の病態形成への関与が示唆されることから、糖尿病性腎症の病態形成に重要な炎症反応における、グロボ系糖脂質の炎症惹起活性の有無をヒト単球やマウス骨髄由来マクロファージを用いて評価した。その結果、極長鎖グロボ系糖脂質は、Toll-like receptor 4 (TLR4) リガンド (LPS, HMGB1) の存在下、TLR4 選択的なポジティブモジュレーターとして炎症促進活性を持つことが示唆された。また、彼はレプチン受容体に変異した *db/db* マウスでは Gb3 の発現が低く、レプチンの腹腔内投与で、Gb3 の発現が回復することを見いだしている。高脂肪食負荷により肥大した脂肪組織から分泌促進されたレプチンが、腎臓のグロボ系糖脂質の発現を増加させ、増加したグロボ系糖脂質が、TLR4 に作用することで炎症反応を促進し、糖尿病性腎症の病態形成に関与している可能性が本研究より示唆された。これらの研究成果は、糖尿病性腎症の新たな診断法や治療薬開発につながることを期待される。

2018 年度に発表した論文

1. Inokuchi J, Inamori K, Kabayama K, Nagafuku M, Uemura S, Go S, Suzuki A, Ohno I, Kanoh H, Shishido F. **Biology of GM3 ganglioside** (Book Chapter in Gangliosides in Health and Diseases). *Progress in Molecular Biology and Translational Science* (Schnaar RL., Lopez PHH., eds, Elsevier) page152-195 ISBN978-0-12-81234-6 (<https://doi.org/10.1016/bs.pmbts.2017.10.004>), 2018.
2. Inamori K, Ito H, Tamura Y, Nitta T, Yang X, Nihei W, Shishido F, Imazu S, Tsukita S, Yamada T, Katagiri H, Inokuchi J. (2018) Deficient ganglioside synthesis restores responsiveness to leptin and melanocortin signaling in obese KKAY mice. *J Lipid Res.* **59**, 1472-1481, 2018.
3. Nihei W, Nagafuku M, Hayamizu H, Odagiri Y, Tamura Y, Kikuchi Y, Veillon L, Kanoh H, Inamori K, Arai K, Kabayama K, Fukase K, Inokuchi J.

- NPC1L1-dependent intestinal cholesterol absorption requires ganglioside GM3 in membrane microdomains *J Lipid Res.* **59**, 2181-2187, 2018.
4. Toshima K, Nagafuku M, Okazaki T, Kobayashi T, Inokuchi J. Plasma membrane sphingomyelin modulates thymocyte development by inhibiting TCR-induced apoptosis. *International Immunology* doi:10.1093/intimm/dxy082, 2018.
 5. Nakayama H, Nagafuku M, Akemi Suzuki A, Iwabuchi K. and Inokuchi J. The regulatory roles of glycosphingolipid-enriched lipid rafts in immune systems. *FEBS letters* doi:10.1002/1873-3468.13275, 2018.
 6. 永福 正和, 豊島 かおる, 堀内 隼, 井ノ口 仁一. スフィンゴミエリンマイクロドメインは Jurkat 細胞の T 細胞抗原受容体依存性の活性化を負に制御する. *東北医科薬科大学研究誌* **65**, 29-42, 2018.
 7. Nitta T, Kanoh H, Inamori K, Suzuki A, Takahashi T, and Inokuchi J. Globo-series glycosphingolipids enhance lipopolysaccharide-induced inflammation and play a pathophysiological role in diabetic nephropathy *Glycobiology* **29**, 260-268, 2019.
 8. Hiraoka M, Ohkawa E, Abe A, Murata M, Go S, Inokuchi J, Ohguro H. Visual function in mice lacking GM3 synthase. *Curr Eye Res* <https://doi.org/10.1080/02713683.2019.1576206>, 2019.

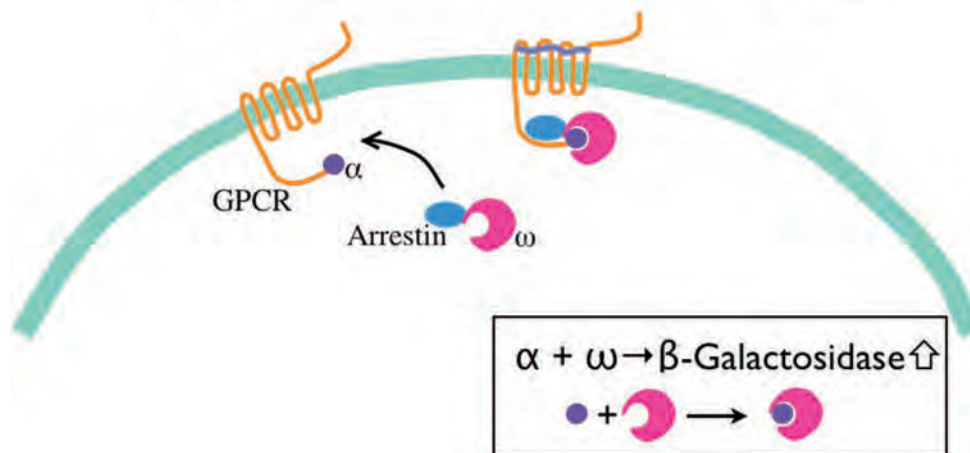
生活習慣病に関連した G タンパク質共役受容体の機能と糖鎖および受容体相互作用による調節

生体膜情報部門 東 秀好

1. GPCR α 相補アッセイの改良

近年、GPCR の活性測定法の 1 つとして α 補完が使われるようになってきた (1-3)。これは、大腸菌の β ガラクトシダーゼ (LacZ) をコードする lacZ の対立遺伝子の 1 つでアミノ末端付近の 11-41 アミノ酸配列を欠失し β ガラクトシダーゼ活性を持たない lacZ Δ M15 (ω フラグメントをコードしている) の産物と、それを相補して β ガラクトシダーゼ活性を復元させる LacZ タンパク質のアミノ末端 50 アミノ酸残基程度をコードする lacZ α の産物 (α フラグメント) の反応を利用した結合指標アッセイである。本来、大腸菌で利用されてきたものであるが、ホ乳類の細胞で利用できる。具体的には、測定対象の GPCR の C 末端に α フラグメントを、活性化により GPCR と結合するアレクチン等のタンパク質の C 末端に ω フラグメントをそれぞれ融合して培養細胞に発現させ、リガンド刺激により GPCR とアレクチンが結合するとそれらに融合した α フラグメントと ω フラグメントが結合して β ガラクトシダーゼ活性を表すので、これに測定可能な β ガラクトシダーゼの基質を導入すれば、結合が測定できる (下図)。

β -Galactosidase complementation assay



Arrestin 結合を指標とした GPCR 活性化の測定

従来法では G タンパク質の下流の反応を測るために特異性が緩かったが、本法では目的の GPCR に特定してシグナルをモニターできる利点がある。一部はアッセイキットとして市販されているが、目的遺伝子を発現させた培養細胞としてのみ入手可能である。従って、任意の GPCR とアレクチン等の組み合わせで研究するため、我々は、独自にプラスミドベクターを作製した。pAcGFP1-N1 (Clontech) の AcGFP1 を α フラグメント、または、 ω フラグメントに置換したベクターを用

いるという簡便なものである(4)。当初は、目的遺伝子発現細胞を 96 well plate に再播種後 1 時間でリガンド刺激するという方法をとったため、播種操作の物理的な刺激により細胞から相当量の ATP が分泌され、ATP をリガンドとする P2Y₂ 受容体等のアッセイには不便で工夫を要したが、トランスフェクションと同時に播種して 24 時間後にリガンド刺激する方法によりこの問題は改善された(5)。本法を用いて、P2Y₂R のホモダイマー形成におけるジスルフィド架橋の寄与を明らかにした(5)。

細胞内に発現された β ガラクトシダーゼを測定するためには、細胞膜を溶かして基質を加える必要がある。検出感度も必要なので Gal-Screen (Applied Biosystems) のような発光基質が必要であった。この基質は大変高価であることとともに、96 well plate との干渉があつて発光が不均一になるという問題があつた。96 well plate の不均一性は ELISA 等でも経験することで、現在の製造技術では完全には解決できないようだ。この問題を改善するため、発光基質に換えて蛍光基質である 4-methylumbelliferone (4MU) の使用を試みた。細胞膜を溶かすために SDS を添加した基質溶液とするだけで 4MU の分解が測定できた。GalScreen と遜色ない測定が可能であり、96 well plate との干渉も少なかった。こうして高価で不安定な基質を用いずともアッセイが可能となった。

2. GPCR 間親和性によるブラジキニン B₂ 受容体の脂質ラフトへのリクルート (6)

GPCR と脂質ラフトの関係はいくつか知られているが、ATP/UTP 受容体 P2Y₂ (P2Y₂R) はほぼすべてが脂質ラフトに局在する(7)。ブラジキニン B₂ 受容体(B₂R) は、脂質ラフトには 25-30%程度分画された。両者を共発現したところ、P2Y₂R の分布は不変であつたが、B₂R はより多くがラフト画分に移行した。このことは両受容体の相互作用が B₂R を脂質ラフトにリクルートしていることを示している。15 分間の UTP 刺激後、両者は細胞膜表面からほとんど消失し細胞内へ移行した。15 分間のブラジキニン刺激では両者の部分的なエンドサイトーシス像が共焦点蛍光顕微鏡で観察された。以前報告したように(8)、GT1b ガングリオシドとコンドロイチン硫酸 C で連続刺激すると B₂R は細胞膜表面から消失するとともに P2Y₂R も消失した。このように、P2Y₂R と B₂R 間にはシグナルクロストークが存在し、アレスチンのリクルート・エンドサイトーシスで挙動を共にするが、この両者の相互作用は脂質ラフト上で起こることが明らかになった。また、細胞表面へ移行できず多くは小胞体に留まる P2Y₂R の N 結合糖鎖欠損変異体もラフト画分に分画される(7)が、B₂R はこの変異体の共発現によってもラフト画分に集積し、多くは変異体と同様に小胞体に留まった。したがって、小胞体の脂質ラフトにおいて両者はすでに相互作用し、ラフトに親和性の高い P2Y₂R に牽引されることによって B₂R はラフトに移行することが明らかになった。

3. β_2 アドレナリン受容体 (β_2 AR) シグナルによるヒアルロン酸合成促進 (9, 10)

ヒアルロン酸 (HA) は、細胞外マトリックスの構成分子として、組織の弾性や物性維持に関わる他、創傷治癒や細胞増殖を制御する。 β 作動薬は、気管支の炎症反応をともなう気管支喘息の治療薬として使用されるが、長期連用は炎症反応の増悪やムチンの産生増加といった副作用も引き起こす。ヒアルロン酸はサイズ依存的に炎症反応の誘導や抑制に関与することから、 β_2 AR シグナルがヒアルロン酸の合成制御に関与する可能性を検討した。まず、 β_2 AR 発現細胞を β 作動薬で刺激すると、培養液中のヒアルロン酸量が上昇した。この分子機構を検討したところ、 β_2 AR は cAMP-PKA シグナルを介して STAT3 の転写活性を亢進させ、ヒアルロン酸合成酵素 2 (HAS2) の遺伝子発現を上昇させていることが分かった。

References

1. Wehrman, T.S., Casipit, C.L., Gewertz, N.M., and Blau, H.M. (2005) Enzymatic detection of protein translocation. *Nat. Methods*. **2**, 521-527
2. Hammer, M.M., Wehrman, T.S., and Blau, H.M. (2007) A novel enzyme complementation-based assay for monitoring G-protein-coupled receptor internalization. *FASEB J.* **21**, 3827-3834
3. von Degenfeld, G., Wehrman, T.S., Hammer, M.M., and Blau, H.M. (2007) A universal technology for monitoring G-protein-coupled receptor activation in vitro and noninvasively in live animals. *FASEB J.* **21**, 3819-3826
4. Yashima, S., Shimazaki, A., Mitoma, J., Nakagawa, T., Abe, M., Yamada, H., and Higashi, H. (2015) Close association of B2 bradykinin receptors with P2Y₂ ATP receptors. *J. Biochem., Tokyo*. **158**, 155-163
5. Abe, M., Watanabe, K., Kuroda, Y., Nakagawa, T., and Higashi, H. (2018) Homodimer formation by the ATP/UTP receptor P2Y₂ via disulfide bridges. *J. Biochem., Tokyo*. **163**, 475-480
6. Nakagawa, T., Takahashi, C., Matsuzaki, H., Kuroda, Y., and Higashi, H. (2018) Regulation of membrane raft recruitment of the bradykinin B2 receptor by close association with the ATP/UTP receptor P2Y₂. *Biochem. Biophys. Res. Commun.* **505**, 36-39
7. Nakagawa, T., Takahashi, C., Matsuzaki, H., Takeyama, S., Sato, S., Sato, A., Kuroda, Y., and Higashi, H. (2017) N-glycan-dependent cell-surface expression of the P2Y₂ receptor and N-glycan-independent distribution to lipid rafts. *Biochem. Biophys. Res. Commun.* **485**, 427-431
8. Shimazaki, A., Nakagawa, T., Mitoma, J., and Higashi, H. (2012)

Gangliosides and chondroitin sulfate desensitize and internalize B2 bradykinin receptors. *Biochem. Biophys. Res. Commun.* **420**, 193-198

9. 黒田喜幸, 中川哲人, 東 秀好, B2 アドレナリン受容体シグナルによるヒアルロン酸合成の上昇, 第 12 回東北糖鎖研究会, 弘前, 2018 年 9 月
10. 黒田喜幸, 中川哲人, 東 秀好, B 作動薬によるヒアルロン酸産生増加の分子機構, 第 57 回日本薬学会東北支部会, 仙台, 2018 年 10 月

糖鎖によるがん細胞の機能と中枢神経系における炎症反応の制御

細胞制御部門 顧 建国

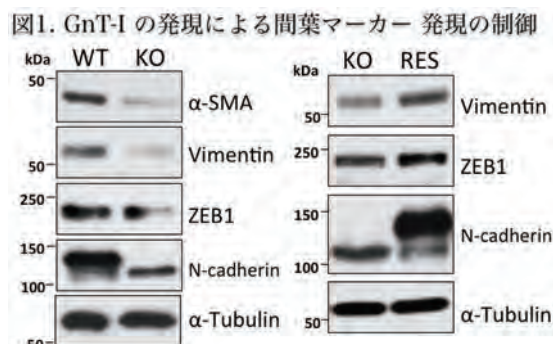
糖タンパク質は糖鎖と蛋白質が共有結合した生体分子である。蛋白質上の糖鎖の結合様式は一般的には N-型と O-型という 2 種類がある。糖鎖はタンパク質の物性に影響を与えると同時にタンパク質の機能、そして分子間の認識や細胞内シグナル伝達に大きな役割を持つ。細胞表面の糖鎖は、細胞増殖、細胞接着、移動および浸潤など多数の生物学的過程に関与することが知られている。インテグリンは α 鎖と β 鎖から成るヘテロ二量体で、細胞外マトリックス (ECM) への細胞の接着を媒介する主要な糖蛋白質で、細胞内蛋白質のチロシンリン酸化や低分子量 GTP 結合蛋白質の活性化を通じて細胞内骨格系の再編成や増殖・分化のシグナル伝達に関わる。また、インテグリンと細胞増殖因子受容体との相互作用は、細胞の増殖・移動・生存などの生理的な過程のみならず、がん細胞の増殖・転移・浸潤など病理的な過程にも重要な役割を担うと考えられている。これまで、我々は分岐型糖鎖の生合成に関わる N-アセチルグルコサミン転移酵素 III (GnT-III)、N-アセチルグルコサミン転移酵素 V (GnT-V)、 α 1,6 フコース(コアフコース)転移酵素 (Fut8) およびシアル酸転移酵素などの機能に注目し、細胞接着分子であるインテグリンがモデル分子として研究を行ってきた。その結果、糖鎖構造のみならず糖鎖付加サイトも分子の機能に重要であることを明らかにした。本年度は、我々は糖鎖生合成の新たな制御機構や糖鎖の機能に関して主に以下の 4 点について研究した。

I. インテグリン $\alpha 3 \beta 1$ と PI4 キナーゼ複合体によるシアル酸付加の制御

細胞膜タンパク質のシアル酸増加は、がん転移・浸潤に関連する現象とされ、細胞表面のシアル酸含量が転移能と相関するという報告も多くなされている。その多くは、シアル酸を付加するシアル酸転移酵素とシアル酸を除去するシアリダーゼの発現に焦点を当てて研究した結果である。Golgi phosphoprotein 3 (GOLPH3) は、多くの固形癌に高頻度で増幅され、がんの予後と負に相関する強力ながん遺伝子である。我々は、以前 GOLPH3 がシアル酸転移酵素の発現の調節ではなく、その転移酵素の働き効率を上昇させ、インテグリンへシアル酸修飾の増加、がん細胞の転移・浸潤に促進的に働くという全く新規な分子機構を見出している (Isaji, et al., JBC. 2014)。最近、さらに GOLPH3 の PH ドメインと結合する Phosphatidylinositol-4-phosphate (PI4P) に注目し、PI4 キナーゼがシアル酸修飾に必須であることを明らかにした。興味深いことに、その修飾にはインテグリン $\alpha 5 \beta 1$ ではなく、 $\alpha 3 \beta 1$ と PI4 キナーゼ間の相互作用が必要であることも明らかになった (1)。 $\alpha 3 \beta 1$ と PI4 キナーゼのどちらか欠失またはノックダウンさせるとシアル酸修飾が著しく低下した。今後、他の糖鎖構造の生合成への影響を含めた詳細な分子機序を解明して行く。

II. N-アセチルグルコサミン転移酵素-I (GnT-I) は上皮間葉転換(EMT)のスイッチとして働く

N-型糖鎖の構造の特徴から高マンノース型、混成型および複合型の3種の糖鎖に大別されている。これまで、複合型N-型糖鎖のインテグリン機能に関しては研究されてきたが、高マンノース型糖鎖しか持たないインテグリンの機能に関しては全く不明である。我々は高マンノース型と複合型およびハイブリッド型のN-型糖鎖の機能を明確に区別するために、高マンノース型の糖鎖しか作れないN-アセチルグルコサミン転移酵素-I (GnT-I) 欠失細胞 (KO) を樹立し、解析した(2)。その結果 GnT-I KO 細胞では、細胞凝集が誘導され、さらに細胞移動が著しく減少することが分かった。また興味深いことに、複合型糖鎖の喪失により間葉系細胞マーカーの低下および上皮系マーカーの増加が認められたことから、細胞に間葉上皮転換(MET)が生じていることが明らかになった。一方、KO 細胞に GnT-I を発現させた Rescue 細胞では、細胞凝集は抑制され、また MET とは逆の上皮間葉転換 (EMT) マーカーの発現およびがんの悪性化に関与する非受容体型チロシンキナーゼである FAK の活性が増強することを確認した(図1)。すなわち GnT-I は、がん細胞における形態、接着能および運動能をより悪性度の高い状態に維持することに貢献しており、これには細胞接着分子である $\beta 1$ インテグリンがもつ複合型N-型糖鎖が深く関与していることが示唆された。さらに GnT-I の発現が、細胞生存および抗がん剤に対する感受性に重要であることも分かった。本研究は、高マンノース型糖鎖が主に細胞間接着に寄与し、複合型糖鎖が ECM 接着や癌の悪性化や転移に重要な役割を果たす EMT に働くことを明らかにした。GnT-I が抗がん治療の新たな標的となる可能性を示したものと考えられる。

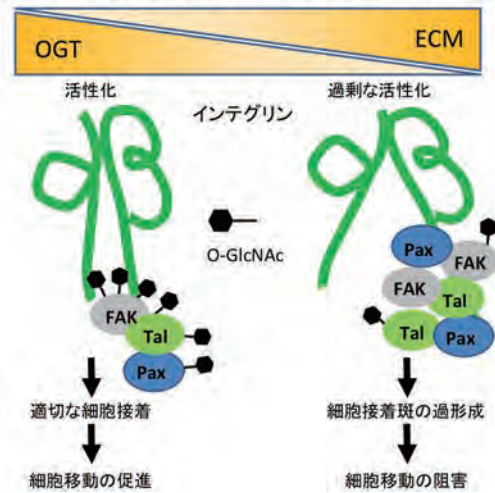


III. O-GlcNAc 付加によるインテグリンの inside-out シグナル制御

タンパク質の主要な糖鎖修飾は N-型と O-型糖鎖修飾だが、これらとは別に核や細胞質に存在するタンパク質に N-アセチルグルコサミン(GlcNAc)が 1 分子結合する O-GlcNAc 化がある。O-GlcNAc 化はタンパク質の修飾される部位がセリンまたはスレオニン残基の水酸基であることに加え、O-GlcNAc 転移酵素(OGT)により転移、O-GlcNAc 切断酵素 O-GlcNAcase(OGA)により加水分解されるため、リン酸化と同様にダイナミックに変化することが出来る。従って、O-GlcNAc 化は蛋白質の重要な機能制御機構の一つであると考えられている。実は、O-GlcNAc は、多数の癌組織において上昇し、細胞増殖・生存や転移に関わると考えられているが、どのように癌細胞の接着・浸潤を調節するのか不明点が多い。我々は、OGT ノックダウン細胞を樹立・解析し、O-GlcNAc が細胞接着、移動および接着斑 (FA) 複合体の重要な調節因子であることを明らかにした(3)。 OGT のノック

ダウン (KD) によって、フィブロネクチン上の細胞接着は有意に促進されたが、一方で、細胞移動は抑制される傾向を示した。対照細胞と比べて KD 細胞における細胞接着斑が有意に増加した。細胞接着斑には、インテグリン以外に Focal adhesion kinase (FAK)、パキシリン及びタリンなど分子が集積し複合体が形成される。KD 細胞にはそれらの複合体の過形成が観察された。即ち、接着斑の過剰な成熟化が KD 細胞で生じている可能性が示唆された。パキシリンやタリンへの O-GlcNAc 付加が確認された。さらに、これまでに報告がなかった FAK への O-GlcNAc 付加も初めて見出した。以上の結果から、O-GlcNAc 化は接着斑の複合体形成に重要であり、インテグリンを介した細胞接着・移動などの機能に新規な調節機構 (インテグリンの inside-out シグナル) である可能性が示唆される (図 2)。FAK にはリン酸化されるセリン、スレオニン残基が多数存在するので、O-GlcNAc がこれらと競合するかまたは特異的に修飾するか解析する必要がある。

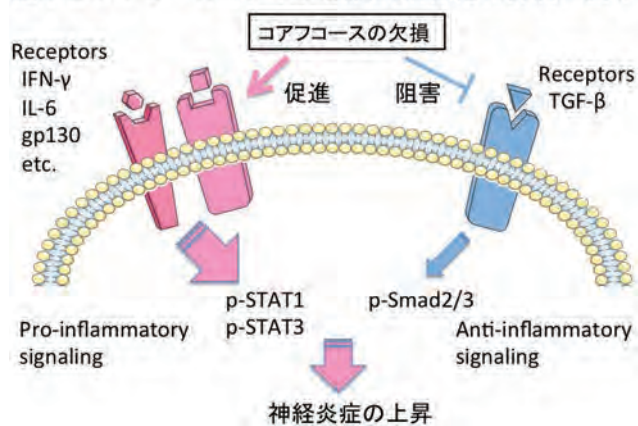
図2. O-GlcNAc化によるインテグリンと細胞移動の制御



IV. 神経炎症におけるコアフコースの機能

コアフコースは生体内で脳組織に最も高く発現している。コアフコース転移酵素(Fut8)を欠損させたマウスは、異常なホッピング、認知機能及び海馬ニューロンの長期増強(LTP)の減弱を含めた統合失調症様な症状を示す。最近、我々は、コアフコースと神経炎症反応の関連に注目して解析を行った(4)。Fut8 欠損マウスの脳組織をグリア細胞の一つで、中枢の免疫担当細胞として知られるミクログリアのマーカー抗 Iba1 抗体で染色したところ、野生型よりミクログリアのサイズ・数ともに有意に増加していた。これは、Fut8 欠損マウスのミクログリアは刺激を伴わない状況で活性化していることを示している。また、免疫担当細胞活性化作用をもつリポ多糖(LPS)を腹腔内に投与すると Fut8 欠損マウスは野生型マウスより感受性が高まっていた。ミクログリアの細胞株 BV2 細胞を炎症性サイトカイン IFN- γ で刺激するとコアフコースの発現が濃度依存的に増加した。さらに、コアフコースとミクログリア活性化の関連を明らかにするため、Fut8 欠損 BV2 細胞を作成し、IFN- γ による iNOS の発現誘導を検討したところ、野生型より Fut8 欠損 BV2 細胞のほう

図3. コアフコースはグリア細胞の活性化の抑制に働く



がより顕著であった。グリア細胞の一つであるアストロサイトもミクログリアとともに、炎症メディエーターや炎症促進性サイトカインを産生するので、C6 グリオブラストーマ細胞を用いて検討したところ、野生型より Fut8 欠損 C6 細胞のほうが IL-6/STAT3 シグナル伝達経路が活性化されることがわかった。野生型の初代培養アストロサイトに L-フコースのアナログである 2-fluorofucose (2FF) を添加することにより、フコシル化を抑制すると、C6 細胞と同様の結果が得られた。これらの結果は、コアフコシル化の欠損によりグリア細胞が容易に活性化状態になることすなわち、コアフコースはグリア細胞の活性化の抑制に働くことを示しており (図 3)、LTP の減弱など Fut8 欠損マウスの脳神経に見られる障害は、ニューロンだけではなくコアフコースが無くなることにより、グリア細胞の活性化の抑制が解除されたことに起因したものであることを強く示唆している。今後、Fut8 が基質とするタンパク質を介した炎症反応に関してより詳細な研究を行うことにより、統合失調症などの病態解析が大いに進展するであろう。

2018 年度に発表した論文

1. A complex between phosphatidylinositol 4 kinase II α and integrin α 3 β 1 is required for N-glycan sialylation in cancer cells. Isaji, T., Im, S., Kameyama, A., Wang, Y., Fukuda, T. and Gu, J. *J. Biol. Chem.* jbc.RA118.005208. doi: 10.1074/jbc.RA118.005208, 2019
2. N-Acetylglucosaminyltransferase I as a novel regulator of the epithelial-mesenchymal transition. Zhang, G., Isaji, T., Xu, Z., Lu, X., Fukuda, T. and Gu, J. *FASEB J.*, 33:2823-2835. doi: 10.1096/fj.201801478R, 2019
3. O-GlcNAcylation regulates integrin-mediated cell adhesion and migration via formation of focal adhesion complexes. Xu, Z., Isaji, T., Fukuda, T., Wang, Y. and Gu, J. *J. Biol. Chem.* jbc.RA118.005923. doi: 10.1074/jbc.RA118.005923, 2019
4. Deficiency of α 1,6-fucosyltransferase promotes neuroinflammation by increasing sensitivities of glial cells to inflammatory mediators. Lu, X., Zhang, D., Shoji, H., Duan, C., Zhang, G., Isaji, T., Wang, Y., Fukuda, T. and Gu, J. *Biochim. Biophys. Acta*, 1863:598-608, 2019
5. Core fucosylation of the T cell receptor is required for T cell activation. Liang, W., Mao, S., Sun, S., Li, M., Li, Z., Yu, Y., Ma, T., Gu, J., Zhang, J., Taniguchi, N. and Li, W. *Front. Immunol.* 9:78. doi: 10.3389/fimmu.2018.00078, 2018
6. β 4 integrin/PI3K Signaling Promotes Tumor Progression through Galectin-3-N-glycan Complex. Kariya, Y., Oyama, M., Hashimoto, Y., Gu, J. and Kariya, Y. *Mol. Cancer Res.*, 16:1024-1034. doi: 10.1158/1541-7786.MCR-17-0365, 2018
7. Core fucosylation of copper transporter 1 plays a crucial role in cisplatin resistance of epithelial ovarian cancer by regulating drug uptake. Lv, X., Song, T., Xue, K., Li, Z., Li, M., Cao, H., Wang, L., Song, W., Ma, T., Gu, J. and Li, W. *Mol. Carcinog.*, doi: 10.1002/mc.22971.

レクチンの抗腫瘍メカニズムの解明とがん薬物治療への応用

分子認識部門 細野 雅祐

(1) Raji 細胞におけるナマズ卵レクチン (SAL) 取り込み機構の解明

これまでに SAL は、浮遊系のヒトバーキットリンパ腫細胞株 Raji の細胞膜に高発現しているグロボトリアオシルセラミド (Gb3) の糖鎖に結合することにより、MEK-ERK 経路の活性化に起因する p21 の発現増加を介して細胞増殖抑制を引き起こすことを報告している。しかし、Gb3 に結合した SAL が細胞膜上に留まるのか、あるいは細胞内へ移行するかは明らかでなかった。本年度はこの点に着目し、HiLyte Fluor™ 555 Labeling kit を用いて蛍光標識 SAL (HL-SAL) を作製し、共焦点レーザー顕微鏡ならび次世代型フローサイトメーター ImageStream^X Mark II を用いて検討した。HL-SAL (50 µg/mL) で 24 時間処理した細胞を観察したところ、Raji の細胞膜および細胞内、特に核近傍に SAL が集積することが明らかとなった。細胞内の蛍光は、膜に結合した HL-SAL をハプテン糖により除去した後も残存していた。また HL-SAL は、処理 10 分後には細胞内に取り込まれることが示され、その後 24 時間まで時間依存的に細胞内の蛍光量が増加した。さらに、Gold Nanoparticle (20 nm) で金標識した SAL を用い、走査型電子顕微鏡で観察した結果から、SAL は細胞質内では液胞様の膜構造物の内部に取り込まれている可能性が示された。この結果から、SAL は Gb3 に結合した後エンドサイトーシスで取り込まれるのではないかと考え、クラスリン介在型エンドサイトーシス阻害剤 Pitstop2、脂質ラフト介在型エンドサイトーシス阻害剤であるメチル-β-シクロデキストリン (MβCD) およびエンドサイトーシス時に細胞膜から小胞体を分離する際に機能するダイナミンを阻害する Dynago-4a および Dynasore を用いて検討した。MβCD、Dynago-4a および Dynasore で前処理することにより HL-SAL の取り込みが阻害された一方、Pitstop2 前処理では阻害されなかった。これらの結果から、SAL は Raji 細胞膜に存在する Gb3 に結合し、脂質ラフトを介したエンドサイトーシスにより細胞内に取り込まれることが示唆された。

(2) Gb3 検出に利用する抗 Gb3 抗体 (1A4) の調製について

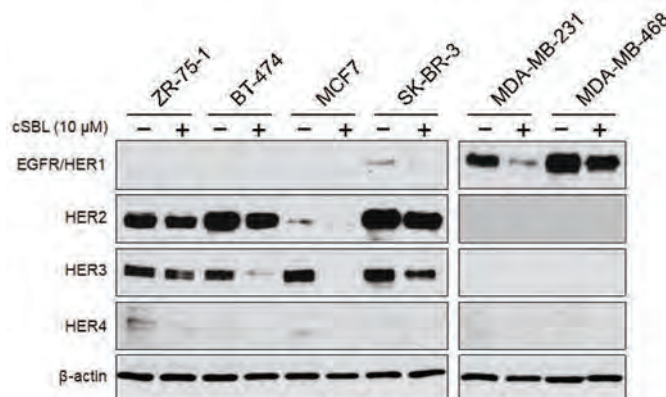
SAL の細胞膜レセプターである Gb3 の検出には、現在市販されているマウスモノクローナル抗体 BGR23 (IgG) およびラットモノクローナル抗体である 38-13 (IgM) が汎用されており、それぞれ Gb3 に対する反応性が異なる。一方で、箱守らにより樹立されたマウスモノクローナル抗体 1A4 (IgM) も一部の研究室で利用されている。今回、より反応性の高い抗 Gb3 抗体を効率よく取得するために 1A4 を産生するハイブリドーマを弘前大学医学部泌尿器科学講座から供与いただき、抗体の精製方法と貯法について検討しつつ Gb3 に対する反応性を

BGR23 と比較した。ハイブリドーマの培養上清を Protein L-Agarose カラムを通すことにより抗体を吸着させ、0.1M グリシン塩酸塩 (pH 2.5) により溶出させた。抗体の反応性は、Gb3 陽性細胞として Raji および腎がん細胞株 TOS1 を、同陰性細胞として慢性骨髄性白血病細胞株 K562 を用いてフローサイトメトリー法により検討した。はじめに K562 には反応を示さず、Raji に対して反応する 1A4 の濃度ならびに蛍光標識 2 次抗体の最適な条件を検討した。蛍光強度の分離の度合いから、1A4 の濃度を 0.6 $\mu\text{g}/\text{mL}$ とし、蛍光標識 2 次抗体を 500 倍希釈とすると、Gb3 を検出する際の感度として適切な条件であることが分かった。Raji に対し 1A4 0.6 $\mu\text{g}/\text{mL}$ で得られる蛍光強度は、BGR23 では 2.4 $\mu\text{g}/\text{mL}$ に相当し、重量比として 1A4 はおよそ 4 倍の反応性を示した。Gb3 の発現量が Raji より低い TOS1 に対しては、1A4 (0.6 $\mu\text{g}/\text{mL}$) と同程度の蛍光強度を得るのに BGR23 は 6.0 $\mu\text{g}/\text{mL}$ を要した。貯蔵方法に関しては、凍結保存しない場合、1 カ月程度であれば、スピニング後精製後中和処理を行い、そのまま (高塩濃度緩衝液中) 保存した方が、反応性が低下しないことが分かった。

(3) ウシガエル卵由来シアル酸結合性レクチン (cSBL) の乳がん細胞に対する抗腫瘍作用

cSBL は、レクチン活性およびリボヌクレアーゼ活性を有する多機能タンパク質であり、がん細胞に細胞死を誘導する。我々はこれまで、cSBL の悪性胸膜中皮腫 (MPM) に対する他剤との併用効果について明らかにしてきた。本年度は、種々の乳がん細胞に対する抗腫瘍効果と HER ファミリー分子の発現に及ぼす効果において得た新しい知見を論文発表した。

乳がんは、分子発現に多様性を示す疾患であり、主にエストロゲン受容体 (ER)、プロゲステロン受容体 (PgR)、ヒト上皮成長因子受容体 2 (HER2) の発現に基づいて分類されているが、これら受容体の過剰発現または遺伝子増幅の有無によって予後や選択治療が変わってくる。これまでに報告してきた ER や Bcl-2 および MAPK の発現・活性化に対する cSBL の効果に着目し、cSBL 処理乳がん細胞における鍵分子 (ER, PgR および HER ファミリー分子) や Bcl-2 ファミリー分子および MAPK の発現・活性化の調査を行った。その結果、p38 の活性化は、cSBL を処理した乳がん細胞で強く観察され、cSBL の抗腫瘍作用に深く関与していることが考えられた。Bcl-2 ファミリー分子に対する cSBL の影響は細胞の種類によって異なる可能性があ



ると考えられた。一方、乳がん関連分子（ER, PgR および HER2）の発現は、いずれも cSBL 処理により減少した。さらに、多数の細胞において、それぞれに発現する全ての HER ファミリー分子が減少し、cSBL は細胞種に関わらず HER ファミリー分子の発現を全般的に低下させる可能性が示唆された。HER ファミリーを標的とした分子標的薬では、EGFR の変異によって耐性を獲得したり、HER1 および HER3 を活性化したりすることが問題となっている。したがって、それらの薬剤と cSBL との併用は、乳がんの薬物治療における有効な選択肢になり得ると考えている。

2018 年に発表した論文

1. Sialic acid-binding lectin from bullfrog eggs inhibits human malignant mesothelioma cell growth in vitro and in vivo. Tatsuta T., Satoh T., Sugawara S., Hara A., Hosono M., *PLoS One*, **13**(1), e0190653 (2018).
2. Sialic Acid-Binding Lectin from Bullfrog Eggs Exhibits an Anti-Tumor Effect Against Breast Cancer Cells Including Triple-Negative Phenotype Cells. Tatsuta T., Sato T., Sato T., Sugawara S., Suzuki T., Hara A., Hosono M., *Molecules*, **23**(10), 2714 (2018).
3. ナマズ卵レクチンのがん治療への応用を目指した基礎研究, 菅原栄紀, 薬学雑誌, 138 (12), 1451-1459 (2018).
4. Gb3 検出に利用する抗 Gb3 抗体 (1A4) の有用性の検討. 菅原栄紀, 鷹觜祥子, 本田捷太, 立田岳生, 伊藤淳, 佐藤信, 大山力, 細野雅祐, *東北医科薬科大学研究誌*, **65**, 21-28 (2019).

■ 学会発表記録

<機能病態分子部門>

- New Paradigm for Chronic Inflammation Mediated by Ganglioside Molecular Species.
Jin-ichi Inokuchi, Hirotaka Kanoh
2018 Gordon Research Conference on “Glycolipid and Sphingolipid Biology”, Galveston, TX, USA
- ガングリオシド欠損による肥満モデルマウスの病態改善と受容体機能に与える影響
稲森 啓一郎, 伊藤 英樹, 田村 有美, 楊 燕華, 二瓶 渉, 宍戸 史, 突田 壮平, 山田 哲也,
片桐 秀樹, 井ノ口 仁一
日本生化学会東北支部 第 84 回例会, 岩手, 2018 年 5 月, 要旨集 p.35
- 肥満マウスにおける腎臓でのスフィンゴ糖脂質の発現変化
新田 昂大, 宮原 一樹, 狩野 裕考, 稲森 啓一郎, 廣瀬 卓男, 森 建文, 中村 保宏, 鈴木 明
身, 井ノ口 仁一
第 60 回日本脂質生化学会, 東京, 2018 年 5 月, 演題番号 2-28
- Ganglioside GM3 Molecular Species as Novel Endogenous Ligand for TLR4
Jin-ichi Inokuchi
24th IUBMB Congress & 15th FAOBMB Congress (IUBMB SEOUL 2018), IUBMB Eastern Asia Joint
Symposium on Glycoscience, June 2018.
- ガングリオシド欠損による肥満モデルマウスの病態改善および受容体機能に与える影響
稲森 啓一郎, 伊藤 英樹, 田村 有美, 新田 昂大, 楊 燕華, 二瓶 渉, 宍戸 史, 突田 壮平,
山田 哲也, 片桐 秀樹, 井ノ口 仁一
第 37 回日本糖質学会年会, 仙台, 2018 年 8 月, 要旨集 p.91
- マウス GM3 合成酵素における新規肝臓特異的 mRNA バリエーションの同定
宍戸 史, 上村 聡志, 新田 昂大, 井ノ口 仁一
第 37 回日本糖質学会年会, 仙台, 2018 年 8 月, 要旨集 p.096
- 糖尿病性腎症におけるグロボ系糖脂質の機能的役割
新田 昂大, 宮原 一樹, 狩野 裕考, 稲森 啓一郎, 森 建文, 廣瀬 卓男, 中村 保宏, 鈴木 明
身, 井ノ口 仁一
第 37 回日本糖質学会年会, 仙台, 2018 年 8 月, 演題番号 3A-18
- ガングリオシド欠損による肥満モデルマウスの病態改善と受容体シグナルへの影響
稲森 啓一郎, 伊藤 英樹, 田村 有美, 新田 昂大, 楊 燕華, 二瓶 渉, 宍戸 史, 突田 壮平,
山田 哲也, 片桐 秀樹, 井ノ口 仁一
第 91 回日本生化学会大会, 京都, 2018 年 9 月, ポスター番号 1P-364
- Ganglioside GM3 Molecular Species as Novel Endogenous Ligand for TLR4
Jin-ichi Inokuchi, Hirotaka Kanoh
2nd Japan-Korea Lipid Joint Symposium, Hokkaido University, Sapporo, Japan, September 2018
- ガングリオシド生合成不全は肥満モデル KKAY マウスのレプチンおよびメラノコルチンシグナルを改善する

- 稲森 啓一郎, 伊藤 英樹, 田村 有美, 新田 昂大, 楊 燕華, 二瓶 渉, 宍戸 史, 今津 進, 突田 壯平, 山田 哲也, 片桐 秀樹, 井ノ口 仁一
第 12 回東北糖鎖研究会, 弘前, 2018 年 9 月, 要旨集 p.17
- ガングリオシド生合成不全による KKAy マウスの肥満病態改善と受容体機能への影響
稲森 啓一郎, 伊藤 英樹, 田村 有美, 新田 昂大, 楊 燕華, 二瓶 渉, 宍戸 史, 今津 進, 突田 壯平, 山田 哲也, 片桐 秀樹, 井ノ口 仁一
第 11 回セラミド研究会 学術集会, 東京, 2018 年 10 月, 要旨集 p.21
 - 糖尿病性腎症におけるグロボ系糖脂質の機能的役割
新田 昂大, 狩野 裕考, 稲森 啓一郎, 鈴木 明身, 井ノ口 仁一
第 11 回セラミド研究会学術集会, 東京, 2018 年 10 月, 演題番号 O-1
 - ガングリオシド欠損による KKAy マウスの肥満病態の改善
稲森 啓一郎, 伊藤 英樹, 田村 有美, 新田 昂大, 楊 燕華, 二瓶 渉, 宍戸 史, 突田 壯平, 山田 哲也, 片桐 秀樹, 井ノ口 仁一
第 57 回日本薬学会東北支部大会, 仙台, 2018 年 10 月, ポスター番号 PB-26
 - B4GalNAcT1 新規アイソフォームの同定と arginine-based motif による細胞内輸送機構の解析
宍戸 史, 上村 聡志, 檜村 まどか, 井ノ口 仁一
第 57 回日本薬学会東北支部大会, 仙台, 2018 年 10 月, 要旨集 p.101
 - 細胞膜スフィンゴミエリンが TCR シグナルの調節を介した自己反応性 T 細胞の産生に関わる
豊島 かおる, 永福 正和, 岡崎 俊郎, 小林 俊秀, 井ノ口 仁一
第 57 回日本薬学会東北支部大会, 仙台, 2018 年 10 月, 要旨集 p.101
 - New Paradigm for Chronic Inflammation Mediated by Glycosphingolipid
Jin-ichi Inokuchi
MicrobiotaMi2018, University of Milano-Bicocca, Aula Martini, November 2018
 - NPC1L1-dependent intestinal cholesterol absorption requires ganglioside GM3 in membrane microdomains
Wataru Nihei, Masakazu Nagafuku, Hirotaka Hayamizu, Yuta Odagiri, Yumi Tamura, Yui Kikuchi, Lucas Veillon, Hirotaka Kanoh, Kei-ichiro Inamori, Kenta Arai, Kazuya Kabayama, Koichi Fukase, Jin-ichi Inokuchi
10th 2018 Asian Community of Glycoscience and Glycotechnology Conference, Taiwan, November 2018, Abstract OR37
 - Sphingomyelin microdomain modulates TCR signal intensity during thymocyte development
豊島 かおる, 永福 正和, 岡崎 俊郎, 井ノ口 仁一
第 47 回日本免疫学会学術集会, 福岡, 2018 年 12 月, 3-A-WS22-10-P
 - Membrane lipid microdomain enriched in sphingomyelin modulates T cell receptor-mediated activation
Masakazu Nagafuku, Kaoru Toshima, Jun Horiuchi, Jin-ichi Inokuchi
日本免疫学会第 47 回年会, 福岡, 2019 年 12 月, 演題番号 3-A-WS23-5-P
 - 糖脂質ガングリオシドの欠損による肥満モデルマウスの病態改善および受容体シグナルへの影響
稲森 啓一郎

第 7 回 AAA (Academy of Aging and Cardiovascular-Diabetes Research), 東京, 2019 年 1 月

- Homeostatic and pathogenic roles of GM3 ganglioside molecular species in TLR4 signaling in obesity.
Hirotaka Kanoh, Takahiro Nitta, Jin-ichi Inokuchi
KeyStone Symposium (Innate Immune Receptors: Roles in Immunology and Beyond). Taipei, Taiwan, March 2019, P# 2009
- Globo-series glycosphingolipids enhance Toll-like receptor 4-mediated inflammation and play a pathophysiological role in diabetic nephropathy.
Takahiro Nitta, Hirotaka Kanoh, Kei-ichiro Inamori, Akemi Suzuki, Jin-ichi Inokuchi
KeyStone Symposium (Innate Immune Receptors: Roles in Immunology and Beyond). Taipei, Taiwan, March 2019, P# 2053

<生体膜情報部門>

- $\beta 2$ アドレナリン受容体シグナルによるヒアルロン酸合成の上昇
黒田喜幸, 中川哲人, 東 秀好
第 12 回東北糖鎖研究会, 弘前, 2018 年 9 月, 演題番号 O-1
- ブラジキニン B2 受容体は ATP/UTP 受容体 P2Y2 との高い親和性によって脂質ラフトにリクルートされる
中川哲人, 高橋千央, 松崎仁美, 黒田喜幸, 東 秀好
第 91 回日本生化学会大会, 京都, 2018 年 9 月, 演題番号 2T11m-04 (2P-049)
- β 作動薬によるヒアルロン酸産生増加の分子機構
黒田喜幸, 中川哲人, 東 秀好
第 57 回日本薬学会東北支部会, 仙台, 2018 年 10 月, 演題番号 OB-15

<細胞制御部門>

- Functional expression of N-glycans in cell adhesion and EMT
顧建国
The 11th International Symposium on Glycosyltransferases, 青島, 2018 年 6 月, 要旨集 p22
- GlcNAc 化が細胞接着・移動における接着斑複合体におよぼす影響
徐志偉, 張国偉, 陸需, 伊左治知弥, 福田友彦, 顧建国
第 37 回日本糖質学会年会, 仙台, 2018 年 8 月, 演題番号 3A-11
- GnT-I は上皮間葉転換と間葉上皮転換を制御する
張 国偉, 伊左治知弥, 陸需, 徐志偉, 福田友彦, 顧建国
第 37 回日本糖質学会年会, 仙台, 2018 年 8 月, 演題番号 P-016
- $\alpha 1,6$ -フコース転移酵素欠損によるグリア細胞の活性化
陸需, 福田友彦, 庄子隼人, 段程偉, 張冬梅, 徐志偉, 張国偉, 伊左治知弥, 顧建国
第 37 回日本糖質学会年会, 仙台, 2018 年 8 月, 演題番号 P-120
- GlcNAc 修飾による細胞接着斑と細胞移動の制御に関する研究
伊左治知弥, 徐志偉, 福田友彦, 顧建国
第 12 回東北糖鎖研究会, 弘前, 2018 年 9 月, 演題番号 O-3
- グリア細胞におけるコアフコースの役割に関する研究

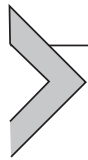
- 福田友彦, 陸需, 庄子隼人, 張冬梅, 伊左治知弥, 顧建国
第 12 回東北糖鎖研究会, 弘前, 2018 年 9 月, 演題番号 O-6
- Fut8 欠損によるグリア細胞の活性化とその機序に関する研究
庄子隼人, 福田友彦, 陸需, 張冬梅, 伊左治知弥, 顧建国
第 12 回東北糖鎖研究会, 弘前, 2018 年 9 月, 演題番号 P-6
 - GlcNac 修飾による細胞接着と細胞移動の制御
伊左治知弥, 徐志偉, 福田友彦, 顧建国
第 91 回日本生化学会大会, 京都, 2018 年 9 月, 演題番号 3P-050
 - グリア細胞における $\alpha 1,6$ フコースの役割に関する研究
福田友彦, 陸需, 庄子隼人, 張冬梅, 伊左治知弥, 顧建国
第 91 回日本生化学会大会, 京都, 2018 年 9 月, 演題番号 1P-036
 - GlcNac 修飾による細胞接着斑と細胞移動の制御
伊左治知弥, 徐志偉, 福田友彦, 顧建国
第 57 回日本薬学会東北支部会, 仙台, 2018 年 10 月, 演題番号 OB-01
 - 糖転移酵素 GnT-I は上皮間葉転換と間葉上皮転換を制御する
張国偉, 伊左治知弥, 福田友彦, 顧建国
第 57 回日本薬学会東北支部会, 仙台, 2018 年 10 月, 演題番号 PB-23
 - グリア細胞の活性化に及ぼすコアフコースの機能
庄子隼人, 福田友彦, 陸需, 張冬梅, 伊左治知弥, 顧建国
第 57 回日本薬学会東北支部会, 仙台, 2018 年 10 月, 演題番号 PB-24
 - Importance of glycosylation and its relationships with diseases
顧建国
大連理工大学学術講座 (学生教育セミナー), 遼寧省盤錦市, 2018 年 11 月
 - Glycosylation in cancer cells and towards clinical application
顧建国
大連医科大学学術セミナー, 大連市, 2018 年 11 月
 - Functions of N-glycan in EMT and cancer cells: switching of EMT by N-acetylglucosaminyltransferase I (GnT-I)
顧建国
第 10 回南京腫瘍診断治療国際会議, 南京市, 2018 年 11 月, 要旨集 p18.
 - Functions of glycosylation in cell adhesion and EMT of cancer cells
顧建国
中国科学院過程工程研究所・生化工程国家重点実験拠点研究セミナー, 北京市, 2019 年 3 月
 - PTM of glycosylation in cell adhesion and EMT of cancer cells and diseases
顧建国
北京大学・生命科学学院学術セミナー, 北京市, 2019 年 3 月
 - Glycosylation in cancer cells and diseases

顧建国

天津医科大学・基礎医学院学術セミナー, 天津市, 2019年3月

<分子認識部門>

- ナマズ卵レクチンは腎癌細胞において Sunitinib の効果を増強する
伊藤淳, 菅原栄紀, 岩村大径, 阿南剛, 海法康裕, 立田岳生, 細野雅祐, 佐藤信,
第106回日本泌尿器科学会総会, 京都, 2018年4月, 演題番号 PP2-013
- 新規悪性中皮腫治療薬の開発を目指したウシガエル卵由来シアル酸結合性レクチン (cSBL)
の応用研究
立田岳生, 佐藤 稔之, 菅原 栄紀, 細野 雅祐
日本生化学会東北支部第84回例会, 矢巾, 2018年5月, 演題番号 O-13
- がん細胞によって異なるナマズ卵レクチンの効果の比較
菅原栄紀, 石川幼尋, 本田捷太, 立田岳生, 伊藤淳, 佐藤信, 細野雅祐
第37回日本糖質学会年会, 仙台, 2018年8月, 要旨集 p.170
- ナマズ卵レクチンのヒトセミノーマ細胞株 JKT-1 に対する作用
菅原栄紀, 石川幼尋, 本田捷太, 立田岳生, 伊藤淳, 佐藤信, 大山力, 細野雅祐
第12回東北糖鎖研究会, 弘前, 2018年9月, 要旨集 p.22-24
- Sialic Acid-Binding Lectin from Bullfrog Eggs Exhibits an Anti-Tumor Effect Against Breast Cancer
Cells
Tatsuta T., Sato S., Sato T., Sugawara S., Suzuki T., Hosono M.
第91回日本生化学会大会, 京都, 2018年9月, 演題番号 1P-013
- ナマズ卵レクチンの細胞内輸送機構の解明
本田捷太, 菅原栄紀, 石川幼尋, 立田岳生, 細野 雅祐
第91回日本生化学会大会, 京都, 2018年9月, 演題番号 3P-194
- ナマズ卵レクチンは腎癌細胞において Sunitinib の効果を増強する
伊藤淳, 菅原栄紀, 立田岳生, 細野雅祐, 佐藤信
第77回日本癌学会学術総会, 大阪, 2018年9月, 演題番号 P-2330
- HeLa 細胞における SAL 取り込み機構の解明
星ひかり, 菅原栄紀, 石川幼尋, 本田捷太, 立田岳生, 細野雅祐
第57回日本薬学会東北支部大会, 仙台, 2018年10月, 要旨集 p.92
- 抗 Gb3 抗体である BGR23 および 1A4 の Gb3 に対する反応性の比較
鷹觜祥子, 菅原栄紀, 石川幼尋, 本田捷太, 立田岳生, 細野雅祐
第57回日本薬学会東北支部大会, 仙台, 2018年10月, 要旨集 p.93
- バーキットリンパ腫細胞株 Raji におけるナマズ卵レクチンの取り込み機構の解明
菅原栄紀, 石川幼尋, 本田捷太, 立田岳生, 細野雅祐
第41回日本分子生物学会年会, 横浜, 2018年11月, 演題番号 2P-0383



Biology of GM3 Ganglioside

Jin-ichi Inokuchi^{*,1}, Kei-ichiro Inamori^{*}, Kazuya Kabayama[†],
Masakazu Nagafuku^{*}, Satoshi Uemura[‡], Shinji Go^{*}, Akemi Suzuki^{*},
Isao Ohno[§], Hirotaka Kanoh^{*}, Fumi Shishido^{*}

^{*} Institute of Molecular Biomembrane and Glycobiology, Tohoku Medical and Pharmaceutical University, Sendai, Miyagi, Japan

[†] Osaka University, Toyonaka, Osaka, Japan

[‡] Tohoku Medical and Pharmaceutical University, Sendai, Miyagi, Japan

[§] Center for Medical Education, Tohoku Medical and Pharmaceutical University, Sendai, Miyagi, Japan

¹ Corresponding author. E-mail address: jin@tohoku-mpu.ac.jp

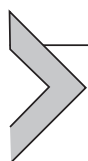
Contents

1. Introduction	152
2. Molecular Biology of GM3S/ST3GAL5	153
2.1 Tissue Distribution of GM3S mRNA Transcriptional Variants	155
2.2 Translation of GM3S Isoforms by Leaky Scanning System	155
2.3 Regulation of ER Export of GM3S by R/K-Based Motif	155
2.4 Regulation of Retrograde Transport of M1-GM3S Isoform by R-Based Motif	156
2.5 Golgi Retention and Maturation of <i>N</i> -Glycans in GM3S	157
2.6 Perspectives	158
3. Insulin Resistance in Adipocytes and Macrophages	159
3.1 GM3 is an Inducer of Insulin Resistance	159
3.2 Insulin Resistance as a Membrane Microdomain Disorder	161
3.3 GM3 Functions as a Physiological Regulator for Insulin Signaling and Adipogenesis	162
3.4 Serum GM3 as a New Biomarker of Metabolic Syndrome	163
3.5 Pathogenic Control of Adipocytes by Increased Expression of GM3	165
3.6 Perspectives	165
4. Leptin Signaling and Resistance in Hypothalamus	168
4.1 Leptin Receptor Signaling	169
4.2 Leptin Resistance	170
4.3 Leptin Signaling in Ganglioside-Deficient Mice	172
4.4 Perspectives	173
5. T-Cell Immunity and Immune Disorders	174
5.1 Ganglioside Expression in CD4 ⁺ and CD8 ⁺ T-Cell Subsets	174
5.2 Ganglioside Expression in TCR-Mediated T Cell Activation	176
5.3 T Cell Gangliosides in Autoimmune and Allergic Diseases	178
5.4 Perspectives	180

6. GM3S Deficiency and Hearing Loss	180
6.1 GM3S Deficiency in Humans	180
6.2 Significant Increase of GSLs During Postnatal Maturation of Murine Cochlea	182
6.3 Glycocalyx Integrity and Membrane Cycling in GM3S-Deficient Mice	182
6.4 GM3-Enriched Membrane Organization, PTPRQ-Myosin VI Complex Localization and Hair Cell Morphology	183
6.5 Perspectives	185
7. Conclusions and Future Directions	185
Acknowledgments	186
References	187

Abstract

Since the successful molecular cloning in 1998 of GM3 synthase (GM3S, ST3GAL5), the enzyme responsible for initiating biosynthesis of all complex gangliosides, the efforts of our research group have been focused on clarifying the physiological and pathological implications of gangliosides, particularly GM3. We have identified isoforms of GM3S proteins having distinctive lengths of N-terminal cytoplasmic tails, and found that these cytoplasmic tails define subcellular localization, stability, and in vivo activity of GM3S isoforms. Our studies of the molecular pathogenesis of type 2 diabetes, focused on interaction between insulin receptor and GM3 in membrane microdomains, led to a novel concept: type 2 diabetes and certain other lifestyle-related diseases are membrane microdomain disorders resulting from aberrant expression of gangliosides. This concept has enhanced our understanding of the pathophysiological roles of GM3 and related gangliosides in various diseases involving chronic inflammation, such as insulin resistance, leptin resistance, and T-cell function and immune disorders (e.g., allergic asthma). We also demonstrated an essential role of GM3 in murine and human auditory systems; a common pathological feature of GM3S deficiency is deafness. This is the first direct link reported between gangliosides and auditory functions.



1. INTRODUCTION

The presence of sialic acid at the surface of animal cell membranes was first demonstrated in 1951 by Tamio Yamakawa.¹ He isolated a sialic acid-containing glycolipid, which he called “hematoside,” from 100 g of dried ghosts obtained from 10 L of packed horse erythrocytes.^{1,2} Hematoside (now termed “GM3 ganglioside”) is the first product in the biosynthetic pathway of ganglio-series gangliosides, and the common precursor of complex gangliosides, such as a- and b-series gangliosides (Fig. 1). Gangliosides are expressed in a cell type-specific manner on the outer leaflet of cell membranes, and interact with various molecules on plasma membranes and certain intracellular membranes based on potentials of noncovalent bondings, for example,

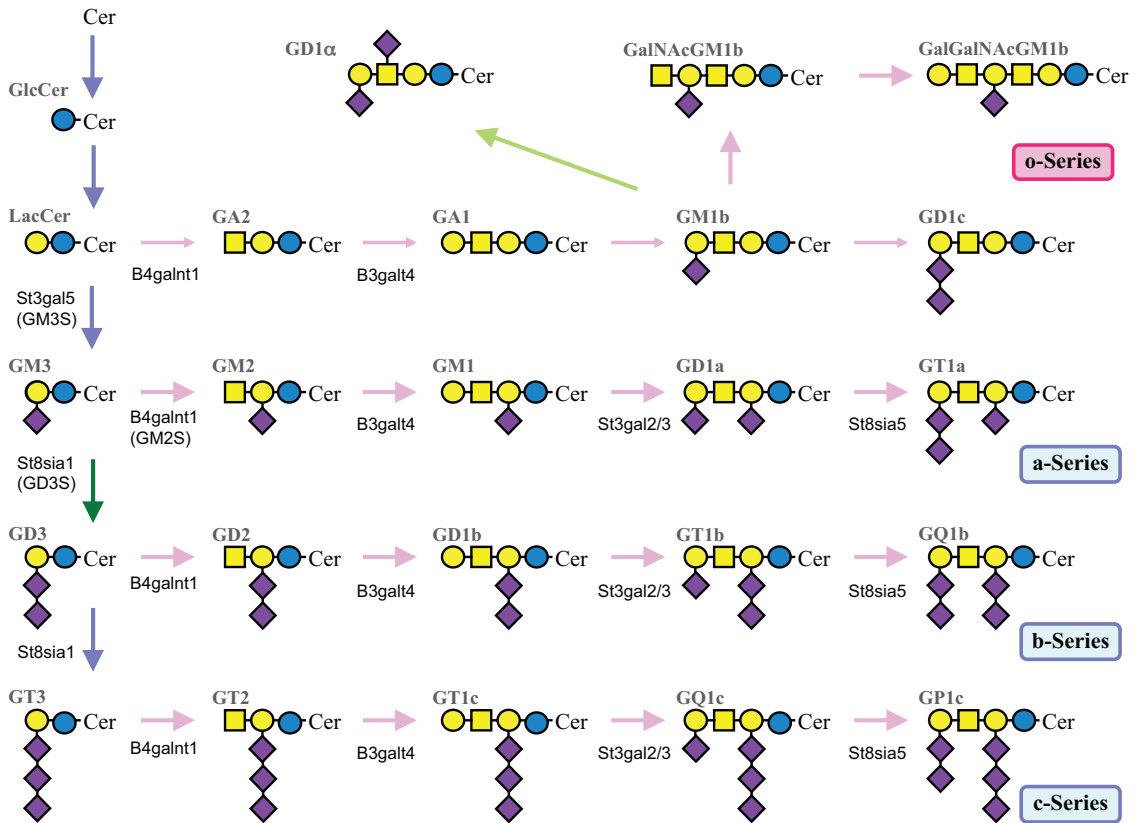
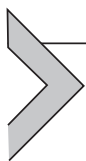


Fig. 1 Biosynthetic pathway of gangliosides.

hydrogen bonding and electrostatic and hydrophobic interactions. Members of the various ganglioside families participate in numerous cellular activities by forming dynamic functional complexes termed “membrane microdomains” or “lipid rafts.”^{3,4} Expression levels of cellular gangliosides are affected by various extracellular stimuli, including inflammatory cytokines. The presence of gangliosides in membrane microdomains thus reflects characteristics of individual cells under various physiological and pathological environments. Since molecular cloning of GM3S was achieved in 1988,⁵ the activity of our research group has been focused on elucidating the biological functions of GM3 and related gangliosides. Here, we review our recent discoveries and advances regarding the molecular biology of GM3S, and the pathophysiological significance of GM3 and related gangliosides.^{6–8}



2. MOLECULAR BIOLOGY OF GM3S/ST3GAL5

GM3S is a type II membrane protein having a catalytic domain in the luminal side (Fig. 2). Human and mouse GM3Ss initially undergo modification with two or three *N*-glycans, respectively, in the endoplasmic

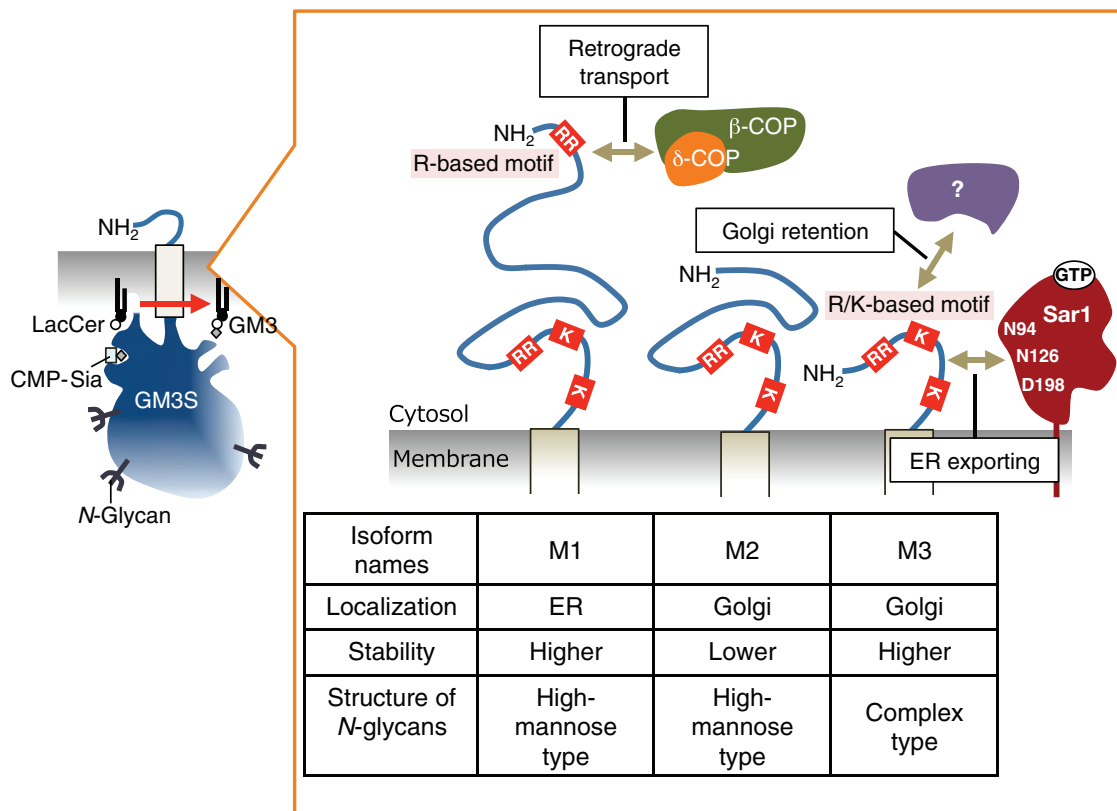


Fig. 2 Regulation of intracellular dynamics of GM3S isoforms by R-based and R/K-based motifs located within cytoplasmic tails. All isoforms have an R/K-based motif, which functions as an endoplasmic reticulum (ER) export signal by interacting with Sar1 protein. The R/K-based motif also functions as a Golgi retention signal in M3 isoform only, leading to stabilization of this isoform in Golgi. R/K-based motifs of M1 and M2 isoforms are presumably unable to function as Golgi retention signals because of their long cytoplasmic tails. Only M3 carries highly matured N-glycans. M1, which has R-based motif in its cytoplasmic tail, is targeted for ER by interaction with β -COP- δ -COP complex. The significance of ER targeting of M1 is unclear.

reticulum (ER).⁹ N-glycans are further modified in the Golgi apparatus, and glycan structures are converted from high-mannose type (immature form) to complex type (mature form). The presence of high-mannose type sugar chains is essential for enzyme activity.⁹ Lactosylceramide (LacCer), the acceptor substrate for GM3S, is synthesized in the luminal side of Golgi.¹⁰ CMP-sialic acid, a donor substrate for GM3 synthesis, is synthesized in cytosol and transported to the luminal side by CMP-sialic acid transporter localized in Golgi.¹¹ GM3 synthesis occurs subsequently in the luminal side of *trans*-Golgi.¹² This section describes regulation of intracellular dynamics of three GM3S isoforms (M1, M2, and M3) we discovered.

2.1 Tissue Distribution of GM3S mRNA Transcriptional Variants

Human GM3S has five mRNA variants,^{5,13–15} which are categorized into a-, b-, and c-type based on differences in transcription start sites (TSSs).¹⁶ a-Type and b-type are further subdivided into a1- (type 1), a2- (type 2), b1- (type 3), and b2-type (type 4) based on differences in splicing. a2-Type is expressed in a variety of tissues.¹⁶ c-Type (type 5) is expressed specifically and exclusively in pancreas.¹⁵

Mouse GM3S has two transcriptional variants: a- and b-type.^{13,17} The TSSs of these variants are very close, and their transcriptional regulation is therefore considered to be similar. Tissue distribution of the two variants is nearly identical.¹⁶ We recently discovered a liver-specific transcriptional variant, c-type.¹⁸ The c-type TSS is located downstream and far away from the TSSs of a- and b-type. We are currently investigating the liver-specific expression mechanism of c-type.

2.2 Translation of GM3S Isoforms by Leaky Scanning System

In general, the first AUG codon is recognized by ribosomes as an initiation codon (first-AUG rule).¹⁹ In mammals, the optimal context for recognition of the AUG start codon is GCCRCCAUGG (underline: initiation codon; R: A or G). When the first AUG residue is presented in a weak context, in particular, lacking both R in position -3 and G in position +4, the first AUG codon is sometimes skipped and a downstream AUG is recognized as an initiation codon. This process is termed a leaky scanning system.¹⁹ By using this system, GM3S isoforms (M1, M2, M2', and M3 in human; M1, M2, and M3 in mice), each having a distinctive length of N-terminal cytoplasmic tail, are translated from each mRNA variant. The lengths of isoforms M1, M2, M2', and M3 are respectively 69, 42, 47, and 14 aa.

Three isoforms (M1, M2, M3) or two isoforms (M2, M3) were detected, respectively, in cells expressing mouse a- or b-type variant. In contrast, one isoform (M3) or two isoforms (M1 and M3) were detected respectively in cells expressing human a1- or a2-type variant.¹⁶ M2' and M3 isoforms were detected in cells expressing human c-type variant.²⁰ Thus, the leaky scanning system seems to elicit coexistence of various GM3S isoforms in cells.

2.3 Regulation of ER Export of GM3S by R/K-Based Motif

Transport of GM3S from ER to Golgi is the first regulatory step for GM3 synthesis. Glycosyltransferases are loaded efficiently into COPII vesicles through interaction between [R/K](X)[R/K] motifs in the cytoplasmic tail

and small GTPase Sar1, a COPII coated-protein.^{21,22} All GM3S isoforms carry RR sequence just above the transmembrane domain. However, two lysine residues located downstream of the RR sequence are also involved in ER export signal [$^2R^3R(X)_5^9K(X)_3^{13}K$] in M3-GM3S.²³ We therefore propose this “R/K-based motif” as a new ER export signal (Fig. 2).

Formation of COPII-coated vesicles begins with conversion from Sar1-GDP to Sar1-GTP by the guanine nucleotide exchange factor, Sec12.²⁴ Sar1-GTP is anchored to ER membrane and recruits Sec23–Sec24 complex by interacting with Sec23.²⁵ The Sar1–Sec23–Sec24 complex recruits many cargo proteins containing ER export signals (DXE and FF sequences) through interaction with Sec23 or Sec24 to generate a prebudding complex.^{26–30} Sec23 also exhibits GTPase-activating protein activity for Sar1-GTP. Once Sar1 forms a prebudding complex, Sar1-GTP is hydrolyzed by Sec23 and is dissociated from prebudding complex.³¹ Prebudding complex without Sar1 is unstable, but Sar1 is immediately reactivated by Sec12 and incorporated into the complex. When prebudding complex without Sar1 contains unfolded proteins, it breaks before reassembly of Sar1-GTP because of weak interaction between the proteins and Sec23/Sec24. The GTP/GDP cycle of Sar1 thus functions as a selective sorting system for cargo proteins.³¹ If R/K-based motif interacts only with Sar1, the cargo proteins dissociate from prebudding complex when Sar1-GTP is converted to Sar1-GDP. The interaction by itself is therefore insufficient for glycosyltransferases to be efficiently concentrated in COPII-coated vesicles. Our current hypothesis is that R/K-based motif functions as a guide to prebudding complex through interaction with Sar1.²³ Glycosyltransferases carrying R/K-based motif may be transferred to other cargo proteins (receptors) in prebudding complex.

2.4 Regulation of Retrograde Transport of M1-GM3S Isoform by R-Based Motif

Among three isoforms, only M1-GM3S has a retrograde transport signal (R-based motif) in its N-terminal cytoplasmic tail (Fig. 2).¹⁶ Accordingly, most M1-GM3S is transported from Golgi to ER by R-based motif, and localized in ER. As R-based motifs interact with an acidic pocket of β -COP- δ -COP complex in COPI subunits, proteins carrying R-based motif are efficiently concentrated in COPI-coated vesicles involved in retrograde transport.³² R-based motifs must be positioned at a certain distance from the lipid bilayer to function,³³ indicating that R/K-based motif (ER export signal) just above transmembrane domain cannot function as a retrograde transport signal. In

vivo enzymatic activity of M1-GM3S is lower than those of M2-GM3S and M3-GM3S. However, GM3 synthesis is not completely eliminated when GM3S-KO cells express only M1-GM3S, suggesting that some M1-GM3S is sorted to *trans*-Golgi by escaping retrograde transport.

What is the biological significance of ER targeting of M1-GM3S? One possibility is that M1-GM3S has functions other than GM3 synthesis in ER. For instance, protein O-fucosyltransferase (OFUT1) is known as a glycosyltransferase localized in ER, similar to M1-GM3S.³⁴ OFUT1 has an ER targeting signal (KDEL-like motif) in its C-terminus and is localized in ER. OFUT1 glycosylates the epidermal growth factor (EGF)-like domain of Notch in Golgi, but displays Notch chaperone activity in ER.³⁴ Glycosylation activity of OFUT1 is not necessary for chaperone activity. The strong protein-protein interaction between OFUT1 and EGF-like domain of Notch presumably allows the unusual function. In contrast, GM3S recognizes the glycosphingolipids (GSLs), LacCer and galactosylceramide (GalCer) as substrates. GM3S does not display sialylation activity toward lactose and *N*-glycans of glycoproteins,¹⁷ so the active site of GM3S presumably recognizes both carbohydrate (hydrophilic) and ceramide (hydrophobic) portions. The partial hydrophobic pocket may interact with unfolded proteins, but the folding site is limited within the lipid bilayer. It therefore seems unlikely that M1-GM3S is involved in protein folding, in contrast to OFUT1.

Another possibility is that M1-GM3S regulates expression levels of M2-GM3S and M3-GM3S in Golgi. As indicated by expression patterns of mRNA variants in tissues, three GM3S isoforms usually coexist within a single cell. All GM3S isoforms are capable of interacting with each other (unpublished data); therefore, M2-GM3S and M3-GM3S may partially localize in ER by coexpression with M1-GM3S. Total amounts of GM3S isoforms in Golgi are consequently maintained at low level. We were able to establish stable clones expressing M2-GM3S or M3-GM3S only at low level, but easily established stable clones expressing M1-GM3S at high level. These findings suggest that excessive amounts of GM3S in Golgi are cytotoxic. M1-GM3S may promote cell survival by suppressing accumulation of M2-GM3S and M3-GM3S in Golgi.

2.5 Golgi Retention and Maturation of *N*-Glycans in GM3S

Golgi cisternae (*cis*, *medial*, and *trans*) are characterized by Golgi-resident enzymes. In the cisternal maturation model, the Golgi apparatus is regarded as a dynamic structure.^{35,36} According to this model, a new *cis* cisterna is continually formed by vesicles supplied from ER, and progressively matures

to a *medial* cisterna and then a *trans* cisterna. Retrograde transport of Golgi-resident enzymes by COPI-coated vesicles explains their distinctive distribution and Golgi retention. The (F/L)(L/I)XX(R/K) motif of Kre6, which is involved synthesis of β 1-6 glycans synthesis, functions as a Golgi retention signal in *Saccharomyces cerevisiae*.³⁷ This motif interacts with Vps74 in COPI-coated protein complex. Golph3 and Golph3L, the mammalian homologs of Vps47, cannot function complementarily in *vps47* Δ strain and (F/L)(L/I)XX(R/K) motif is not conserved in mammalian glycosyltransferases. Golgi retention of enzymes in mammals therefore presumably occurs by other mechanisms.

The half-life of M3-GM3S is longer than that of M2-GM3S, although both are localized in Golgi.¹⁶ We recently found that partial mutations of R/K-based motif (R2A, R3A, R2A/R3A, K9A/K13A) in M3-GM3S lead to altered localization from Golgi to endosomes and to rapid degradation,²³ suggesting that R/K-based motif also functions as a Golgi retention signal (Fig. 2). The motif is presumably involved in retrograde transport from Golgi. Masking of R/K-based motif by the long cytoplasmic tail of M2-GM3S may contribute to its low stability.

The differences of *N*-glycan structures among GM3S isoforms are noteworthy. The *N*-glycan structure of M1-GM3S is high-mannose type (immature form), as evidenced by the immediate relocation of M1-GM3S from Golgi to ER by R-based motif. The *N*-glycan structure of M2-GM3S localized in Golgi is also high-mannose type, whereas that of M3-GM3S is complex type (mature form).¹⁶ The proportion of mature *N*-glycans in M3-GM3S is reduced by mutations (R2A, R3A, R2A/R3A, K9A/K13A) of Golgi retention signal (R/K-based motif).²³ Our findings, taken together, suggest that Golgi-retention time of glycoprotein determines maturation level of *N*-glycans. For full maturation of *N*-glycans, glycoproteins must undergo modification by several glycosyltransferases in dynamic Golgi cisternae. A single passage through Golgi is not sufficient to convert all glycosyltransferases to mature forms.

2.6 Perspectives

Our studies of GM3S isoforms help clarify the regulatory mechanism of ganglioside synthesis in dynamic Golgi cisternae. Issues to be addressed in the future studies include:

1. Determination of three-dimensional structure of GM3S by X-ray crystallography.
2. Identification of molecules involved in ER export and Golgi retention of GM3S.

3. Examination of the heterooligomer formation by GM3S isoforms, and cytotoxic effects of GM3S by the accumulation in Golgi.
4. Elucidation of *N*-glycan maturation mechanism through analysis of *N*-glycan structures of GM3S isoforms and their mutants, which cannot be tethered to Golgi.

Elucidation of the posttranslational regulation of GM3S will contribute to more effective therapeutic strategies for pathological conditions resulting from abnormal GM3 synthesis.



3. INSULIN RESISTANCE IN ADIPOCYTES AND MACROPHAGES

Visceral adipose tissues are comprised of not only adipocytes; but also immune cells, including resident macrophages, T lymphocytes, and other types of cells.^{38–41} It remains unclear how interactions between adipocytes and resident macrophages are affected by expression of specific GSLs. We have shown that expression of GSLs and their corresponding synthase genes in adipocytes is maintained by soluble factors secreted from resident macrophages under not only inflammatory states, but also steady-state physiological conditions. Obese *GM3S*-deficient mice fed a high-fat diet were resistant to development of proinflammatory states in adipose tissues. This section focuses on association of GM3 with metabolic syndrome, and the physiological and pathological implications of GM3 present in adipose tissues.

3.1 GM3 is an Inducer of Insulin Resistance

Insulin elicits a wide variety of biological activities, which can be categorized into metabolic and mitogenic actions. Binding of insulin to insulin receptor (IR) activates IR internal-tyrosine (Tyr) kinase activity. Tyr-phosphorylated and activated IR is able to recruit and phosphorylate adaptor proteins, such as IR substrate (IRS). Phosphorylated IRS activates PI3-kinase (PI3K). Activated PI3K is translocated to lipid rafts and converts PIP₂ to PIP₃, and PIP₃ then recruits PDK1 to phosphorylate Akt. Full activation of Akt may be required for signaling by phosphorylation of the other site by mTORC2 (mTOR complex 2).⁴² This IR-IRS-PI3K-Akt signaling cascade is a representative metabolic pathway triggered by insulin, and results in translocation of glucose transporter 4 (GLUT-4) to plasma membrane to facilitate glucose uptake.

When mouse adipocytes were cultured in low concentrations of TNF α that did not cause generalized suppression of expression of adipocyte genes (e.g., IRS-1, GLUT-4), TNF α interfered with insulin action.⁴³ Prolonged treatment (≥ 72 h) was required for this effect, in contrast to many acute effects of this cytokine. The slowness of the effect suggests that insulin resistance in adipocytes treated with 0.1 nM TNF α was associated with progressive increases in cellular GM3 content, GM3S activity, and GM3S mRNA content, and that such treatment upregulates GM3 synthesis at the transcriptional level in cultured adipocytes.^{44,45} In contrast, ceramide levels under TNF α treatment increased transiently up to 6 h, and returned to normal by 24 h. These observations reflect the distinct and independent roles of GM3 and ceramides in development of insulin resistance in adipocytes.^{44,45} To determine whether elevated GM3 in 3T3-L1 adipocytes treated with TNF α is involved in insulin resistance, we used D-threo-1-phenyl-2-decanoylamino-3-morpholino-1propanol (D-PDMP), an inhibitor of glucosylceramide synthase,⁴⁶ to deplete cellular GSLs derived from GlcCer. D-PDMP treatment counteracted TNF α -induced increase of GM3 content in adipocytes, and reverted to normal the TNF α -induced defect in Tyr phosphorylation of IRS-1 in response to insulin stimulation.⁷ These findings are consistent with the observation that insulin signaling was enhanced in GM3S-knockout mice.⁴⁷ It has been reported that TNF α treatment of adipocytes induces an increase in serine phosphorylation of IRS-1.⁴⁸ Such phosphorylation is important because immunoprecipitated IRS-1 that has been serine phosphorylated in response to TNF α is a direct inhibitor of IR Tyr kinase activity. We found that TNF α -induced serine phosphorylation of IRS-1 in adipocytes was completely suppressed by D-PDMP inhibition of GM3 biosynthesis, suggesting that TNF α -induced increase of GM3 synthesis causes upregulation of serine phosphorylation of IRS-1.⁴⁵ An improved PDMP analog and a different type of GlcCer synthase inhibitor,^{49,50} had therapeutic value when orally administered in diabetic rodent models.

TNF α levels were fairly high in two obese diabetic rodent models (Zucker *fa/fa* rats and *ob/ob* mice),⁴⁸ but much lower in adipose tissues from lean control animals. We, therefore, examined GM3S mRNA expression in epididymal fat of the diabetic models. Northern blot analysis showed that GM3S mRNA content in adipose tissues of the two models was significantly higher than in lean controls.⁴⁵ TLC comparison of GM3 band mobility revealed the appearance of GM3 species with lower mobility (i.e., more hydrophilic) in the models.

We also examined GM3 expression in diet-induced obese (DIO) mice.⁵¹ Following 10 weeks of feeding, mean body weight of standard diet (SD) and high-fat diet (HFD) groups were 31.0 ± 0.6 g and 46.0 ± 0.8 g and fasted blood glucose levels were 137 and 203 mg/dL, respectively.⁵¹ GM3 level in epididymal fat was threefold higher in HFD than in SD group. mRNA level of *GM3S* gene was also threefold higher in HFD group.⁵¹

These findings strongly indicate that increased expression of GM3 in abdominal adipose tissues tends to induce malfunctions of adipose tissue, for example, chronic low-grade inflammatory states in obesity. In recent studies of omental adipose tissues in obese and insulin-resistant women, adipocyte hypertrophy, and macrophage infiltration were associated with increases of GM3 content and *GM3S* gene expression.⁵² Therefore, drugs that target GM3 biosynthesis may be useful for treating insulin resistance in obesity.

3.2 Insulin Resistance as a Membrane Microdomain Disorder

In studies of TNF α -induced insulin resistance in adipocytes, we showed that transformation to a resistant state might result from increased GM3 biosynthesis following upregulation of *GM3S* gene expression. Increased GM3 level during chronic exposure to TNF α may therefore suppress insulin signaling.⁴⁵ GSLs, including GM3, are important components of lipid rafts. We considered the possibility that increased GM3 levels in lipid rafts confer insulin resistance in TNF α -treated adipocytes. We examined GM3-protein interactions within plasma membranes of living cells by performing cross-linking assay with a photoactivatable, radioactive GM3 derivative. Adipocytes were preincubated with [³H]GM3(N3) and then irradiated to induce crosslinking of GM3. Target proteins were separated by SDS-PAGE and visualized by autoradiography. A specific radioactive band corresponding to the 90-kDa IR β -subunit was immunoprecipitated with anti-IR β antibodies, indicating direct association of GM3 with IR. We concluded that IR forms complexes with caveolin-1 and GM3 independently in 3T3-L1 adipocytes.⁵³

Lipids are asymmetrically distributed in the outer and inner leaflets of plasma membranes. In typical mammalian cells, most acidic phospholipids are located in the inner leaflet, and acidic GSLs, such as sulfatides and gangliosides are in the outer leaflet. Binding of proteins to lipid membranes is often mediated by electrostatic interactions between protein basic domains and acidic lipids. Gangliosides, which bear sialic acid residues, are ubiquitously present in the outer leaflet of vertebrate plasma membranes. GM3 is the most abundant ganglioside, and the primary ganglioside found in adipocytes.⁵⁴ Glycan chains of GSLs, including gangliosides are oriented

at a defined angle to the axis of ceramide.⁵⁵ GM3s spontaneously form clusters via hydrophobic interaction between their own saturated acyl chains, regardless of any repulsion between negatively charged sialic acids in the glycan chains.⁵⁶ GM3 clusters, together with other cell surface gangliosides, thus form GSL-enriched microdomains (GEM) and produce a negatively charged environment just above the plasma membrane. On the other hand, IR has a sequence in its transmembrane domain, that is, homologous (conserved) in mammals and presents the basic amino acid lysine (IR944) just above the transmembrane domain. During lateral diffusion, electrostatic interaction may occur between the lysine residue at IR944 and the negative charge of GM3 cluster, because of their close topological proximity on the plasma membrane. In a study using FRAP technique in living cells, we found that the mechanism for dissociation of IR-caveolin-1 complex is based on interaction of a lysine residue localized just above the transmembrane domain of IR β -subunit with GM3 clusters at the cell surface.⁵³ Based on these observations, we proposed a mechanism that determines insulin resistance state through localization shift of IR from caveolae to GEM in adipocytes.

Insulin signaling in skeletal muscle was shown to be higher in *GM3S* knockout (*GM3S*-null) mice than in wild-type (WT) C57BL/6 mice.⁴⁷ On the other hand, inhibition of insulin signaling by exogenous addition of saturated fatty acids into C2C12 myotubes was not eliminated by treatment with a GlcCer synthase inhibitor (D-PDMP analog).⁵⁷ The involvement of GM3 in pathophysiology of insulin resistance in mammalian skeletal muscle requires further study.

We explored the role of acyl chain length of ceramides in insulin signaling using ceramide synthase 2 (CerS2)-null mice that lack the ability to synthesize very long acyl chain (C22-C24) ceramides.⁵⁸ These mice did not display IR or Akt phosphorylation in liver in response to insulin. The absence of IR phosphorylation was correlated with its inability to translocate into detergent-resistant membranes (DRMs). The properties of DRMs in the CerS2-null mice differed significantly from those in WT mice, indicating that altered sphingolipid acyl chain length directly affects IR translocation to lipid rafts and subsequent signaling.

3.3 GM3 Functions as a Physiological Regulator for Insulin Signaling and Adipogenesis

Visceral adipose tissues, particularly mesenteric adipose tissue, play key roles in the pathogenesis of metabolic syndrome.^{38-40,59-63} To investigate the fundamental characteristics of mesenteric adipocytes, we established a

physiologically relevant differentiation system in which rat mesenteric-stromal vascular cells (mSVC) were induced to differentiate into mesenteric-visceral adipocytes (mVAC).^{64,65} We optimized the concentrations of insulin and insulin-like growth factor (IGF-1) at levels comparable to those in vivo: 0.85 and 200 ng/mL. IGF-1 and insulin were shown to function synergistically; IGF-1 by itself enhanced CCAAT/enhancer binding protein alpha (C/EBP α) and adipocyte lipid binding protein (aP2) mRNA expression, but in the absence of insulin at physiological concentration IGF-1 did not induce lipid droplet accumulation associated with adipocyte maturation.

We used the same differentiation system to elucidate the role of resident macrophages in mesenteric adipose tissue in physiological adipogenesis. Adipogenesis of mSVCs in the system was increased by removal of resident macrophages, along with enhanced insulin signaling and concomitant decrease of GSLs, including GlcCer, LacCer, and GM3. Phosphorylation levels of IR and IRS-1 after insulin stimulation were enhanced by depletion of macrophages, and protein level of IR per se was increased in mSVCs.⁵¹

Levels of GSLs (particularly GM3) in preadipocytes and mature adipocytes are thus precisely maintained by soluble factors secreted from resident macrophages to control physiological adipogenesis (Fig. 3). Adipogenesis of MEFs prepared from GM3S-null mice was accelerated, in combination with enhanced insulin signaling.⁵¹ GM3 is directly involved in insulin signaling and adipogenesis.

3.4 Serum GM3 as a New Biomarker of Metabolic Syndrome

GM3 is the major ganglioside in serum and is associated with serum lipoproteins.⁶⁶ We examined the relationships of serum GM3 levels with: (i) adiposity indices, and (ii) metabolic risk variables.⁶⁶ Serum GM3 levels were significantly elevated in type 2 diabetes patients with severe obesity (visceral fat area > 200 cm², BMI > 30). GM3 level was positively correlated with LDL-c (0.403, P = 0.012) in type 2 diabetes mellitus, but not related to blood pressure. High levels of small dense LDL (>10 mg/dL) were associated with increased GM3. Serum GM3 levels were affected by abnormalities of glucose and lipid metabolism, and by visceral obesity. Small dense LDL levels are associated with atherosclerosis development,^{67,68} and GM3 has been detected in atherosclerotic lesions.^{67,68} Thus, GM3 is a potentially useful marker for management of metabolic syndrome, including insulin resistance, and for early diagnosis of atherosclerosis.

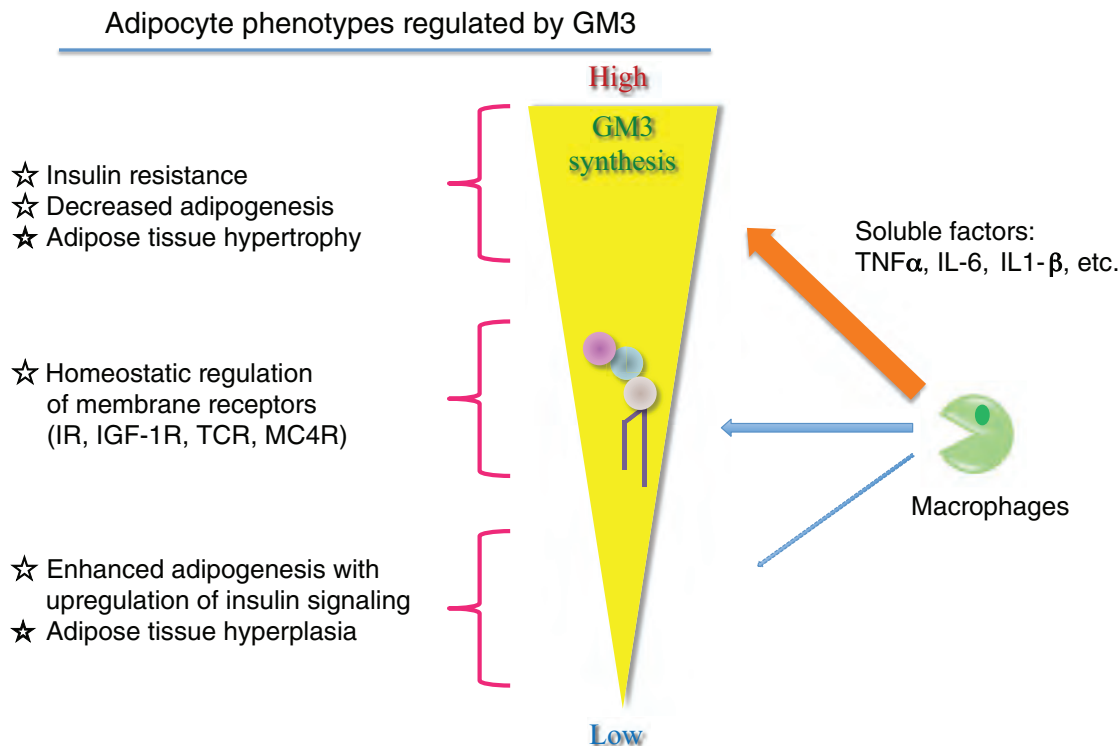


Fig. 3 GM3 as homeostatic and pathogenic mediator in adipogenesis and insulin signaling. Interactions between macrophages and adipose progenitor cells may influence the number of preadipocytes and/or their differentiation capacity, and induce adipose tissue dysfunction by inhibiting overall adipogenic capacity. Control of GM3 levels is a potential therapeutic intervention strategy for restoring healthy adipose tissue function in obese individuals, distinct from weight-reduction strategies.

The structural diversity of ceramide species arises from several types of modification in *N*-acyl chains [chain length (C16–24); α hydroxylation; desaturation] and in sphingoid bases (d18:1, d18:0; hydroxylation at C4), resulting in a large number of possible molecular species. We performed LC–MS/MS analysis to identify serum GM3 molecular species in 125 Japanese residents.⁶⁹ Individuals were categorized based on presence versus absence of metabolic disease risk factors, including visceral fat accumulation, hyperglycemia, and dyslipidemia. A total of 23 GM3 molecular species were identified, of which 8 were significantly elevated in individuals with visceral fat accumulation and metabolic disease (defined as the presence of hyperglycemia and dyslipidemia). All of the GM3 molecular species were composed of sphingenine [d18:1(Δ 4)], and six of the eight elevated species contained α -hydroxylated acyl chains. Hydroxylated GM3 species were, in order of decreasing abundance, d18:1-h24:0 = d18:1-h24:1 > d18:1-h22:0 >> d18:1-h20:0 > d18:1-h21:0 > d18:1-h18:1. We conducted univariate and multiple linear regression

analyses using numerous clinical health variables associated with obesity, type 2 diabetes, metabolic disease, atherosclerosis, and hypertension. GM3 (d18:1-h24:1) was selected as the best candidate for metabolic screening. This molecular species showed significant correlation with intima media thickness (a criterion for diagnosis of atherosclerotic disease in humans) and other metabolic disease risk factors, including autotaxin, LDL-c, and homeostatic model assessment insulin resistance (HOMA-IR).⁶⁹

3.5 Pathogenic Control of Adipocytes by Increased Expression of GM3

Adipose tissue macrophages are classified into two major subtypes: M1 and M2. A concept of M1/M2 polarization has been developed based on expression patterns of cytokines, surface markers, and metabolic enzymes.⁷⁰ M1 macrophages are potent effector cells that produce inflammatory cytokines, such as TNF- α , IL1- β , and IL-6. M2 macrophages are present as resident cells in nearly all organs under physiological conditions, and help maintain tissue homeostasis.^{71,72} They exert antiinflammatory effects by producing IL-10 and arginase I enzyme (Arg1). IL-10 potentiates insulin signaling in adipocytes,^{72,73} and Arg1 reduces nitric oxide synthesis and inflammation by metabolizing arginine to ornithine.⁷¹ Consumption of HFD shifts cytokine expression of murine adipose tissue macrophages from M2- to M1-like patterns by decreasing expression of IL-10 and Arg1 and increasing expression of TNF α and iNOS.⁷³

We analyzed gene expression profiles in epididymal adipose tissue of *GM3S*-null mice fed with HFD, but not with SD.⁵¹ In comparison with expression levels in *GM3S*^{+/-} mice, proinflammatory cytokine TNF α was significantly decreased, whereas antiinflammatory cytokine IL-10 was increased. Levels of adiponectin were increased, while those of atherogenic genes, such as *PAI-1* and *iNOS* were reduced. M2 signature genes, such as *MGL1* and *Arg1* showed increased expression in the *GM3S*-null mice. Glucose tolerance test (GTT) and insulin tolerance test (ITT) both revealed significant improvement of insulin resistance under HFD condition. Thus, GM3 plays key roles in development of obesity-induced chronic low-grade inflammatory states and of insulin resistance (Fig. 4).⁵¹

3.6 Perspectives

Adipocytes are more than inert energy depots; adipose tissue is a biologically active organ responsible for important physiological processes, including energy homeostasis and whole-body insulin sensitivity. Dynamic remodeling

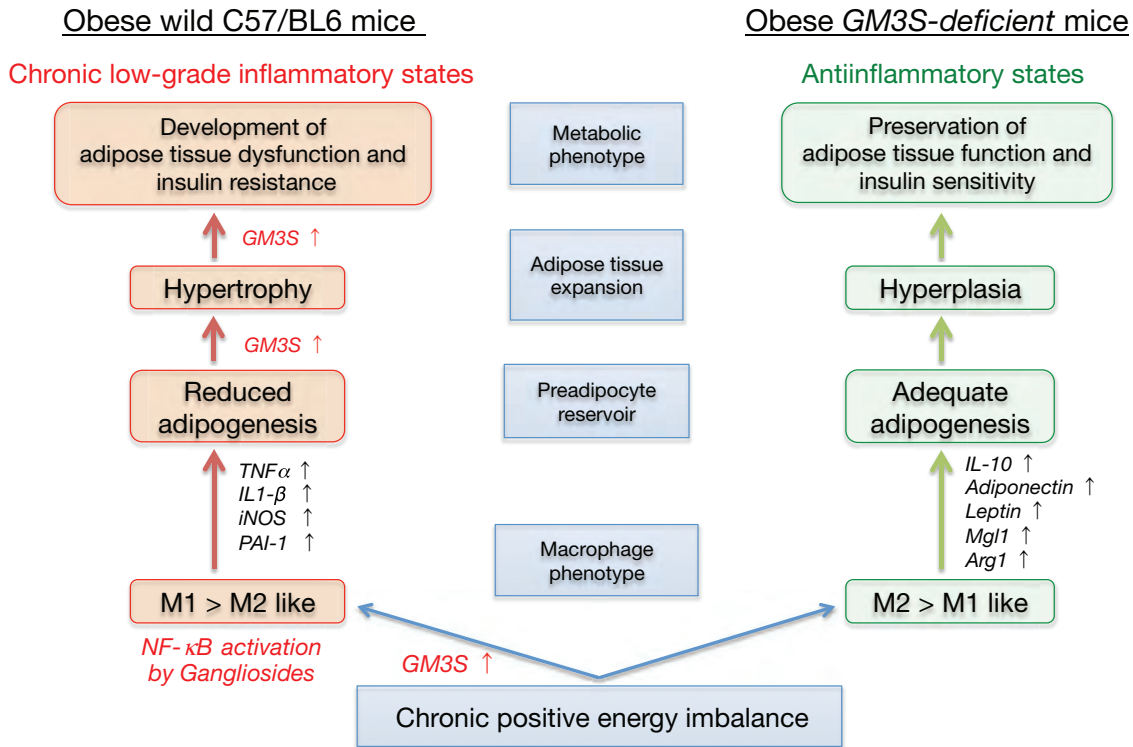


Fig. 4 Regulation of adipose tissue remodeling by GM3 during chronic positive energy imbalance. Chronic positive energy imbalance [high fat diet (HFD)] leads to obesity. Macrophage phenotype may affect the mechanism whereby adipose tissue expands. In the obese state, an adipose tissue mass increase through hyperplasia and hypertrophy, and the latter is associated with activation of stress signaling. When proinflammatory M1 macrophages are predominant, the preadipocyte reservoir may be inadequate because of reduced preadipocyte survival, proliferation, and/or adipogenic capacity. Energy storage occurs via exaggerated adipose hypertrophy, resulting in dysfunctional adipose tissue and contributing to an inflamed insulin-resistant state. Chronic increase of GM3 through upregulation of *St3gal5* gene by proinflammatory cytokines, such as *TNFα* and *IL-β* may promote development of insulin resistance.^{45,53} In obese *St3gal5*-deficient mice, insulin action was enhanced without any significant impact on diet-induced obesity.⁵¹ These mice showed anti-inflammatory M2-like phenotypes in visceral adipose tissue (epididymal fat),⁵¹ and significant increases of adiponectin and interleukin-10 (IL-10) in comparison with obese WT mice. IL-10 and adiponectin play essential roles in maintaining insulin sensitivity of adipocytes.^{72,73}

of adipose tissue architecture occurs during its expansion. Under positive caloric balance, development of metabolic disease is more closely related to how fat is stored (through adipocyte hypertrophy vs. hyperplasia) than simply to the amount of stored fat. Inhibitors of adipogenesis were frequently proposed in the past as potential antiobesity drugs. However, results from a variety of recent mouse and human experiments indicate that adipogenesis inhibitors are poor candidates for amelioration of metabolic disease states, because limitation of fat cell expansion is associated with insulin resistance. It

was proposed over a decade ago that type 2 diabetes might result from failure of adipocyte differentiation.⁷⁴ This hypothesis is now generally accepted, and has been supported by several independent lines of investigation in adipocyte biology.

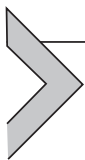
Interactions between macrophages and adipose progenitor cells must be considered, because macrophages affect numbers of preadipocytes and/or their differentiation capacity, and induce adipose tissue dysfunction by inhibiting overall adipogenic capacity. The existence of resident and infiltrating macrophages is well documented, and studies during the past decade suggest that such macrophages are modulated in obesity and type 2 diabetes. Proinflammatory TNF α ⁷⁵ and IL1- β ⁷⁶ are potent inhibitors of adipocyte differentiation, and both of these cytokines induce insulin resistance in adipocytes.^{77,78} TNF α expression is induced in adipose tissue of obese diabetic rodents⁴⁸ and humans.⁷⁹ TNF α detected in adipose tissue has been shown to be secreted from macrophages.⁸⁰ These studies, taken together, indicate that macrophages in adipose tissue produce TNF α and IL1- β , which can inhibit differentiation of preadipocytes and induce insulin resistance in mature adipocytes. Less attention has been paid to the ability of these cytokines to induce insulin resistance by inhibiting adipogenesis. Recent studies using new model systems demonstrate that limitation of adipose tissue expansion is associated with insulin resistance. Mice that are very obese but have unlimited adipose tissue expansion are metabolically healthy and insulin-sensitive.⁸¹ Overall, these studies support the concept that adequate numbers of differentiation-competent preadipocytes allow for hyperplastic growth by preserving metabolic function in obesity.

As described earlier, our studies using *GM3S* gene and *GM3S*-knockout mice have shown that GM3 is crucially involved in both homeostatic adipogenesis (by controlling insulin signaling) and development of obesity-induced chronic low-grade inflammatory states and insulin resistance in adipose tissue. GM3 expression in adipocytes is controlled by soluble factors secreted from resident macrophages, to execute physiological adipogenesis. GM3 expression in adipose tissue is further increased under obesity-induced proinflammatory conditions, and *GM3S*-deficient mice fed a high-fat diet are less likely to develop insulin resistance or chronic low-grade inflammatory states (Fig. 4).⁵¹ GM3 thus functions as a novel homeostatic and pathogenic mediator in adipose tissue (Fig. 3).

Our findings provide a rationale for design of novel therapies against metabolic syndrome (including type 2 diabetes) through inhibition of GM3 biosynthesis to maintain homeostatic insulin signaling. Extensive reduction

of all complex gangliosides by inhibition of GM3 biosynthesis produces widespread physical and chemical modifications of all cellular plasma membranes, particularly of lipid microdomains, and is therefore drastic and of little therapeutic value. Such extensive ganglioside depletion is not necessary for treatment of metabolic disorders. We have demonstrated the effectiveness of D-PDMP on impaired insulin signaling in TNF α -treated 3T3-L1 adipocytes, and that normalization of elevated GM3 levels was sufficient to ameliorate the state of insulin resistance.⁴⁵

In humans, GM3 is expressed predominantly in insulin-responsive organs (skeletal muscle, liver, adipose tissue) and lymphocytes. The presence of GM3-enriched membrane microdomains (lipid rafts) reflects the characteristics of individual cells. For accumulation of gangliosides in lipid rafts, critical roles are played by hydrogen donors and acceptors; and the abundance of (relative to phospholipids) long, saturated acyl chains in the ceramide backbone of gangliosides. Structural diversity of sphingoid bases and *N*-acyl chains in the ceramide moiety is essential in determining the behavior of gangliosides in cell membranes, and the localization of lipid rafts. A “sphingolipidomics” approach must be used to precisely characterize the ceramide structures actually present in cell membranes.



4. LEPTIN SIGNALING AND RESISTANCE IN HYPOTHALAMUS

Leptin is a 16-kDa protein required for maintenance of energy homeostasis and body weight.⁸² White adipose tissue produces and secretes leptin into the bloodstream, and circulating levels are correlated with body fat content.⁸³ Leptin signals adiposity status to the brain, particularly to the mediobasal hypothalamus (MBH), which plays a key role in control of feeding, body weight, and energy expenditure. Within the MBH, the arcuate nucleus (ARC) is an important site of leptin action. The ARC contains two interconnected groups of neurons. One group is orexigenic and releases agouti-related peptide (AgRP) and neuropeptide Y (NPY). The other group is anorexigenic and releases α -melanocyte-stimulating hormone (α -MSH), generated from proopiomelanocortin (POMC) precursors, which binds to melanocortin receptor 4 (MC4R) in the paraventricular nucleus (PVH) and other hypothalamic regions, and exerts anorectic effects. NPY binds to its cognate receptor, thereby stimulating feeding and reducing basal energy expenditure. AgRP acts as an inverse agonist of MC4R and inhibits

α -MSH activity.⁸⁴ AgRP/NPY neurons and POMC neurons thereby regulate melanocortin signaling in a coordinated manner to maintain energy balance.

Elevated levels of leptin reduce food intake and body weight through the long form of the leptin receptor, LepRb,⁸⁵ which is highly expressed in certain hypothalamic nuclei, including the ARC and ventromedial hypothalamus (VMH). LepRb is expressed in both AgRP/NPY neurons and POMC neurons. Leptin regulates energy balance by inhibiting neuronal activity and expression of NPY and AgRP in AgRP/NPY neurons, and promoting synthesis of α -MSH in POMC neurons.⁸⁶ Leptin increase can generate a strong, beneficial signal to prevent or reduce obesity. However, leptin activity may be disrupted by development of leptin resistance, a phenomenon defined by reduced ability to suppress food intake and body weight gain.⁸⁷

Gangliosides play important roles in neural development and functions.^{88,89} Recent studies using ganglioside-deficient mouse models have helped elucidate the functions of specific gangliosides in hypothalamic leptin signaling.

4.1 Leptin Receptor Signaling

Leptin action is transmitted by long form receptor LepRb, which is highly expressed in brain regions involved in control of feeding and energy expenditure.⁹⁰ LepRb is a transmembrane receptor and a member of the class I cytokine receptor family.⁸⁵ Six LepR isoforms (LepRa, b, c, d, e, f) have been identified in mice; they arise from the single *Lepr* gene by alternative mRNA splicing,^{91,92} and have been categorized into three classes: secreted (LepRe), short (LepRa, LepRc, LepRd, LepRf), and long (LepRb) forms. The six isoforms share an N-terminal extracellular domain with the ability to bind leptin, but differ in their C-terminal cytoplasmic domains. Only long-form LepRb is capable of mediating leptin signaling. LepRb-deficient *db/db* mice have an obese phenotype similar to that of leptin-deficient *ob/ob* mice.⁹³ LepRb has no inherent enzymatic activity, but produces a signal through binding to a cytoplasmic Tyr kinase, Janus kinase 2 (JAK2).⁹⁴ Leptin binding to the extracellular domain of LepRb results in conformational change of the receptor and JAK2 activation, and JAK2 subsequently phosphorylates other Tyr residues within LepRb and JAK2 itself.⁹⁵ Three tyrosine residues in LepRb (Tyr⁹⁸⁵, Tyr¹⁰⁷⁷, Tyr¹¹³⁸) undergo phosphorylation, and recruit Src homology 2 (SH2) domain-containing proteins to the LepRb-JAK2 complex, thereby enabling JAK2 to phosphorylate these signaling proteins.⁹⁶

In addition to JAK2, certain members of the Src Tyr kinase family are involved in control of leptin signaling. Phospho-Tyr¹¹³⁸ binds to the SH2 domain of signal transducer and activator of transcription 3 (STAT3). STAT3 is subsequently phosphorylated by JAK2, resulting in nuclear translocation and transcriptional initiation of target genes including POMC and suppressor of cytokine signaling 3 (SOCS3), a negative-feedback regulator of leptin signaling.⁹⁷ Numerous studies have demonstrated the essential role of the JAK2/STAT3 pathway in antiobesity action of leptin in the brain. STAT5 is similarly recruited to phospho-Tyr¹⁰⁷⁷ in response to leptin, and phosphorylated and activated by JAK2. Phospho-Tyr⁹⁸⁵ serves as a binding site for the SH2 domain of protein Tyr phosphatase 2 (SHP2), which mediates leptin-dependent activation of the extracellular signal-regulated kinase (ERK) pathway. The SHP2/ERK pathway is also involved in the antiobesity effect of leptin.^{98,99}

4.2 Leptin Resistance

Leptin resistance is a key risk factor for obesity. Diet-induced obese (DIO) mice and obese human patients typically show high circulating leptin levels and reduced responsiveness to leptin's antiobesity effects.⁸⁷ Even after exogenous leptin administration, obese subjects do not show reductions of food intake or body weight.¹⁰⁰ Various molecular mechanisms have been proposed to explain leptin resistance; these include impairment of leptin transport across the blood-brain barrier (BBB), suppressed leptin signaling, and impaired leptin-targeted neural circuits.^{96,101}

4.2.1 The BBB and Leptin Resistance

Circulating leptin, as an energy regulator, must cross the BBB to reach the neurons responsible for suppressing food intake and increasing energy expenditure. Impaired leptin transport across the BBB has been observed in obese mice,^{102,103} suggesting a possible cause of leptin resistance in obese humans and rodents.¹⁰⁴ The median eminence (ME), located on the floor of the third ventricle, forms a BBB structure that regulates passage of metabolic hormones and nutrients from blood to cerebrospinal fluid and energy-sensing MBH neurons.¹⁰⁵ Tanycytes, which are specialized radial glial cells that line the walls of the third ventricle, have been identified as gatekeepers controlling entry of leptin into the hypothalamus.¹⁰⁶ Tanycytes express all six LepR isoforms, activate STAT3 and ERK in response to leptin, and thereby take up leptin through clathrin-coated vesicles. Internalized leptin is then released into the MBH under the control of LepRb-ERK signaling. This pathway is disrupted in DIO mice.

4.2.2 Suppression of LepRb Signaling

In obese rodents and humans, chronically elevated levels of circulating leptin activate an inhibitory negative feedback mechanism, resulting in impairment of LepRb signaling. SOCS3 is a member of a large family of cytokine-inducible inhibitors of signaling. Its gene expression is induced by leptin, and also by cytokines, such as interleukin-6.^{97,107} SOCS3 binds to JAK2 and inhibits its kinase activity,¹⁰⁸ and also inhibits LepRb signaling through binding to phospho-Tyr⁹⁸⁵ of LepRb.¹⁰⁹ Peripheral leptin administration rapidly induces SOCS3 mRNA in the hypothalamus of leptin-deficient *ob/ob* mice, but not of LepRb-deficient *db/db* mice.¹¹⁰ In leptin-resistant obese mouse model *Ay/a*, SOCS3 expression in the ARC and dorsomedial hypothalamic nuclei is elevated, suggesting that SOCS3 is a mediator of leptin resistance in obesity. Mice with heterozygous *Socs3* deficiency or neuron-specific *Socs3* knockout showed increased leptin sensitivity and resistance to DIO,^{111,112} supporting the concept that SOCS3 is a physiological negative regulator of LepRb signaling.

LepRb signaling is also suppressed by many other molecules, including protein Tyr phosphatases (PTPs). PTP1B, a nonreceptor Tyr phosphatase known to inhibit insulin signaling, suppresses LepRb signaling in vivo by dephosphorylating and thereby inhibiting JAK2.¹¹³ PTP1B-null mice are hypersensitive to leptin and resistant to DIO.^{113,114} Mice with neuronal deletion or POMC-neuron-specific deletion of PTP1B show increased leptin sensitivity and energy expenditure, and are less susceptible to DIO.^{115,116} These findings suggest that increased PTP1B expression mediates leptin resistance in obesity.

4.2.3 Impairment of Downstream Signaling of LepRb

Melanocortin receptor 4 (MC4R) plays a central role as a leptin-targeted neural circuit in energy homeostasis. MC4R gene mutations with associated loss of function are the most common monogenic form of obesity in humans.¹¹⁷ *Mc4r*-deficient mice develop obesity associated with hyperphagia,¹¹⁸ and do not respond to the anorectic action of MTII, a synthetic analogue of α -MSH.¹¹⁹ In *Ay/a* mice, melanocortin signaling is systemically disrupted by ectopic expression of agouti signaling protein (ASP), a homologue of AgRP.¹²⁰ Constitutive expression of ASP in the *Ay/a* hypothalamus blocks the effect of α -MSH and inhibits activation of MC4R, resulting in disruption of hypothalamic control of feeding and energy expenditure, and in development of leptin resistance.¹⁰⁰ Downstream of MC4R, expression of brain-derived neurotrophic factor (BDNF) in the VMH is regulated by the

leptin-MC4R axis, and inhibition of the BDNF/TrkB pathway results in leptin resistance.^{121,122}

4.3 Leptin Signaling in Ganglioside-Deficient Mice

Adult mammalian brain gangliosides consist mainly of a- and b-series gangliosides, such as GM1, GD1a, GD1b, and GT1b (Fig. 1).⁸⁹ GM3S-deficient mice that lack these ganglioside species have enhanced insulin signaling and are less susceptible to DIO.^{47,51} On the other hand, GD1a has an enhancing effect on EGFR activation.¹²³ In a 2013 study of mice with deletion of inducible neuron-specific *Ugcg* (the gene encoding GlcCer synthase), Nordstrom *et al.* reported possible functions of neuronal ganglioside species in LepR.¹²⁴ These mice lacked gangliosides, as well as GlcCer and LacCer in distinct populations of forebrain neurons following administration of tamoxifen. Loss of GlcCer synthase in hypothalamic neurons inhibited LepR signaling, and the mice developed progressive obesity. The authors demonstrated that GM1 and GD1a in hypothalamic neuronal cell line N-41 interact closely with LepR, suggesting that these a-series gangliosides enhance the action of leptin in hypothalamic neurons. Ji *et al.*, in 2015 and 2016 studies, showed that GD3 synthase (GD3S)-null mice, which lack all b-series gangliosides, show reduced leptin secretion from adipocytes and increased leptin sensitivity.^{125,126} Serum leptin levels in the *GD3S*-null mice were strongly reduced and leptin was accumulated in adipose tissues, indicating impaired leptin secretion. Addition of exogenous b-series gangliosides into medium of primary adipocyte culture restored leptin secretion.¹²⁵ These findings suggest that b-series gangliosides are involved in leptin secretion from adipocytes, although the mechanism is unknown. *GD3S*-null mice did not develop obesity, even though levels of circulating leptin were greatly reduced. Leptin signaling was altered in the hypothalamus of these mice. LepRb signaling in the hypothalamus, as measured by phosphorylated STAT3 levels, was enhanced in the mice, and *GD3S* overexpression in N-41 cells reduced responsiveness to leptin.¹²⁶ Increased levels of a-series gangliosides in *GD3S*-null mice enhance leptin sensitivity, which may explain the apparently normal energy expenditure observed.

An obese mouse model, KK-Ay, was established by introducing *Ay* mutation into KK mice, resulting in more severe and earlier onset of obesity and diabetic pathology.¹²⁷ Based on our finding that *GM3S*-null mutation in C57BL/6 mice resulted in no overt difference in obesity phenotype relative to WT,^{47,51} we introduced *GM3S*-null mutation in KK-Ay mice to evaluate the pathophysiological roles of GM3 and related gangliosides in obesity.

Whereas KK–Ay mice were hyperphagic and developed morbid obesity, the KK–Ay/*GM3S*-null mice had much lower body weight and food intake, comparable to values in control KK mice (unpublished data). The KK–Ay/*GM3S*-null mice were less susceptible to central leptin resistance, suggesting that GM3 and/or related ganglioside species negatively regulate hypothalamic leptin signaling.

4.4 Perspectives

Numerous recent studies indicate that GM3 and related gangliosides play essential roles in hypothalamic control of energy homeostasis. GM1 and GD1a have been implicated as positive regulators of leptin signaling. KK–Ay/*GM3S*-null mice, which do not express a- or b-series gangliosides, are less susceptible to leptin resistance. We observed enhancement of leptin-dependent ERK phosphorylation in *GM3S*-deficient hypothalamic neuronal cells (unpublished data), suggesting differential roles of specific gangliosides in LepR signaling (Fig. 5). Altered expression of gangliosides may also affect other signaling pathways (e.g., insulin signaling) involved in hypothalamic control of feeding and energy balance.

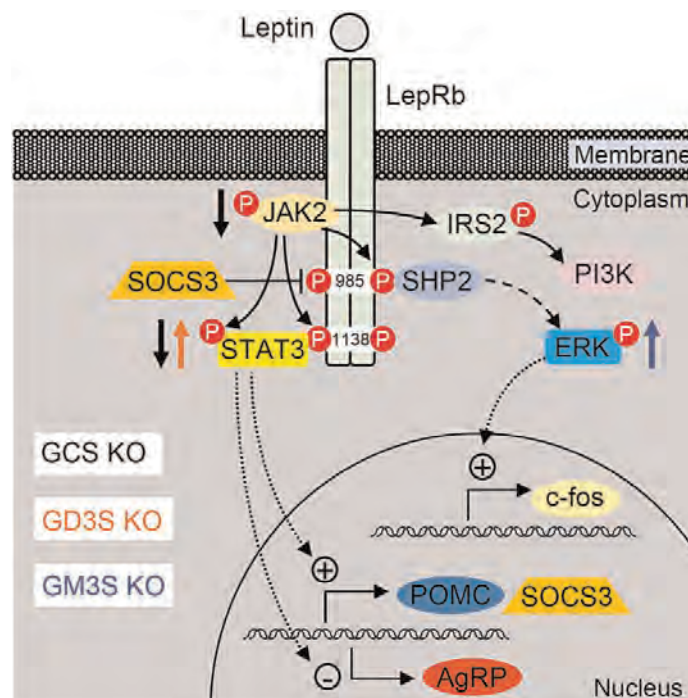


Fig. 5 Leptin receptor-signaling pathway, and alterations in signals observed in ganglioside-deficient models. Increased or decreased activation of each pathway component is indicated by an arrow with respective color.

There is increasing evidence for association of hypothalamic inflammation with development of leptin resistance and obesity.¹²⁸ Activation of inflammatory pathways in the hypothalamus is increased by DIO, even without overt weight gain. GM3 levels are elevated in visceral fat of obese model animals and in sera of obese patients.^{45,64,69} It is therefore conceivable that inflammation resulting from DIO alters ganglioside expression in the hypothalamus. Such alteration could affect interactions between neurons and nonneuronal cell populations and play a pathophysiological role in regulation of energy homeostasis.



5. T-CELL IMMUNITY AND IMMUNE DISORDERS

T cells are lymphocytes that have differentiated under the influence of the thymus and are responsible for cell-mediated immunity. T-cell activation, mediated by T cell antigen receptors (TCRs) in combination with costimulatory receptors, requires recruitment of both extracellular and intracellular molecules into specific cell membrane regions termed “lipid rafts.”¹²⁹ T cells are functionally subdivided into T helper (Th) cells and T cytotoxic (Tc) cells, which typically express specific cell surface molecules CD4 and CD8, respectively. CD4⁺ Th cells and CD8⁺ Tc cells have distinctive immunological functions, but are similar in terms of mechanisms of TCR-mediated signaling. Th and Tc cells have differing ganglioside levels and ganglioside species composition, providing distinctive intracellular signaling events for their respective immune functions.¹³⁰ This section summarizes ganglioside species-specific functions in activation of the two T cell subsets, and roles of gangliosides in immune diseases.

5.1 Ganglioside Expression in CD4⁺ and CD8⁺ T-Cell Subsets

Gangliosides are classified into several series based on the absence (o-series) or presence of one (a-series) or two (b-series) sialic acid residues linked to the galactose residue in the second position from ceramide backbone (Fig. 1).^{131,132} GM3, the simplest member of the a-series, is synthesized by GM3S. GM3 can be altered by GM2/GD2 synthase (GM2/GD2S, also termed B4galnt1) to form GM2 (a downstream a-series ganglioside), or by GD3S to form GD3 (the simplest b-series ganglioside). GM2/GD2S also elongates LacCer to form GA2, the simplest precursor of the o-series gangliosides. At each branching point in the various ganglioside biosynthetic

pathways, competition among responsible enzymes determines the relative expression levels of o-, a-, and b-series gangliosides.

T cells interact with and help activate antigen-presenting cells (APCs) through a unique immunological synapse, and lipid rafts are involved in this interaction.^{133–137} GM1 (a downstream a-series ganglioside) accumulates at the site of contact between TCRs and beads coated with TCR-stimulating antibodies in CD4⁺ T cells, but not in CD8⁺ T cytotoxic cells.¹³⁸ GM1 and GM3 define different types of raft membrane domains that segregate respectively to the leading pole or the trailing uropod of polarized human T cells.¹³⁹ Expression of GM1 varies depending on cell type and developmental stage, and staining with cholera toxin B subunit (CTx-B) is commonly used for visualization of rafts. CTx-B also reacts with an o-series ganglioside termed extended-GM1b (Fig. 1). Elucidating the ganglioside compositions of CD4⁺ and CD8⁺ T cells is essential for understanding the role of rafts in differentiation, maturation, and activation processes of these two T-cell subsets. Differences have been reported in ganglioside composition of primary T-cell subsets freshly isolated from lymphoid organs versus cultured T cells, including cloned cell lines and blasted cells stimulated by concanavalin A.

Biochemical analyses (TLC, HPLC) of whole T cell populations have traditionally been used to evaluate ganglioside expression patterns in primary T cells. However, whole T cell populations (i.e., all cells that express TCRs) are highly mixed populations, and such results are therefore of limited value for studies of specific T cell subsets. Flow cytometric techniques allow multiparameter analysis of target cells at the single-cell level, and therefore provide a valuable tool for determining levels of specific gangliosides in each T cell subset. Flow cytometric analyses using mAbs specific for various gangliosides revealed differential ganglioside expression by mature CD4⁺ and CD8⁺ T cells.^{140,141} We used LC-MS/MS for structural analysis of gangliosides in immature thymocytes, and in CD4⁺ and CD8⁺ T cells isolated from mouse lymphoid organs.¹³⁰ The two T cell subsets both express six ganglioside species (GM1a, GM1b, GD1b, GD1c, GalNAcGM1b, extended-GM1b), but differ markedly in their expression levels of these six species. Expression of o-series gangliosides (GalNAcGM1b, extended-GM1b) increases greatly following differentiation of thymocytes to CD4⁺ and CD8⁺ T cells. Most of the gangliosides expressed in CD8⁺ T cells are o-series. GM1b is expressed strongly in both subsets, whereas GM1a is expressed strongly in thymocytes and CD4⁺ T cells; but at only trace levels in CD8⁺ T cells.

GM2/GD2S gene expression is markedly higher in $CD4^+$ and $CD8^+$ T cells than in thymocytes. *GM3S* gene expression is higher in $CD4^+$ T cells and lower in $CD8^+$ T cells relative to thymocytes.¹³⁰ These gene expression patterns account in part for the differential ganglioside expression profiles during the differentiation processes from immature thymocytes to mature $CD4^+$ and $CD8^+$ T cells. In regard to GD1c, $CD4^+$ T cells can be separated into GD1c-positive IL-2-producing Th1-like cells and GD1c-negative IL-4-producing Th2-like cells.¹⁴¹ Thus, it is possible to classify T cell subsets into distinctive functional subpopulations based on differences in ganglioside expression profiles.

5.2 Ganglioside Expression in TCR-Mediated T Cell Activation

T cell activation is initiated and maintained by engagement of TCRs with major histocompatibility complex (MHC)-peptide complex on APCs, and by engagement of costimulatory molecules. CD4 and CD8 are coreceptors that bind to nonpolymorphic regions of MHC and facilitate signaling by TCRs during T cell activation. T cell activation requires recruitment of both extracellular and intracellular molecules into specific cell membrane regions (lipid rafts).

Cholesterol, a major raft lipid component, plays a key role in maintaining raft structure. It fills the space between hydrocarbon chains of sphingolipids, and functions as a “glue” holding the raft assembly together. Treatment with drugs (e.g., methyl- β -cyclodextrin) that deplete cholesterol from cell membranes typically results in disruption of raft-mediated cellular functions.¹⁴² In spite of some concerns regarding side effects of the drug on signaling events,¹⁴³ experimental approaches involving methyl- β -cyclodextrin have been widely used to document the important functions of cholesterol in rafts. Many studies have been based on manipulation of cholesterol level in lipid rafts, but a much smaller number have addressed the role of gangliosides in raft functions.

We highlighted one important aspect of ganglioside expression in T cells in our 2012 study of two strains of mice with distinctive genetic characteristics.¹³⁰ One strain, carrying a defective *GM3S* enzyme, expressed o-series, but not a- or b-series gangliosides. The other strain had an altered form of *GM2/GD2S* enzyme, and expressed GM3 and GD3; but no other gangliosides (Fig. 1). In WT mice, expression of a-series GM1a is higher in $CD4^+$ than in $CD8^+$ T cells. In *GM3S*-null mice, $CD4^+$ T cells show severe impairment of TCR-mediated proliferation and cytokine production. These defects are reversed by preincubation of cells with a-series

(GM3, GM1a), but not with b-series gangliosides. Most gangliosides expressed in WT CD8⁺ T cells are o-series (GA1, GM1b, GalNAcGM1b, extended-GM1b). T cells from *GM2/GD2S*-null mice also show severe impairment of TCR-mediated proliferation and cytokine production. These defects are reversed by preincubation of cells with o-series GA1 and GM1b, but not with a- or b-series gangliosides. These findings indicate that the two T cell subsets have specific raft microenvironments involving different gangliosides, and that these raft microenvironments are the basis of distinctive functions following TCR stimulation (Fig. 6). The two T cell subsets, although they have common mechanisms of TCR-mediated signaling, have differing cellular and molecular modifications. CD4 and CD8 are

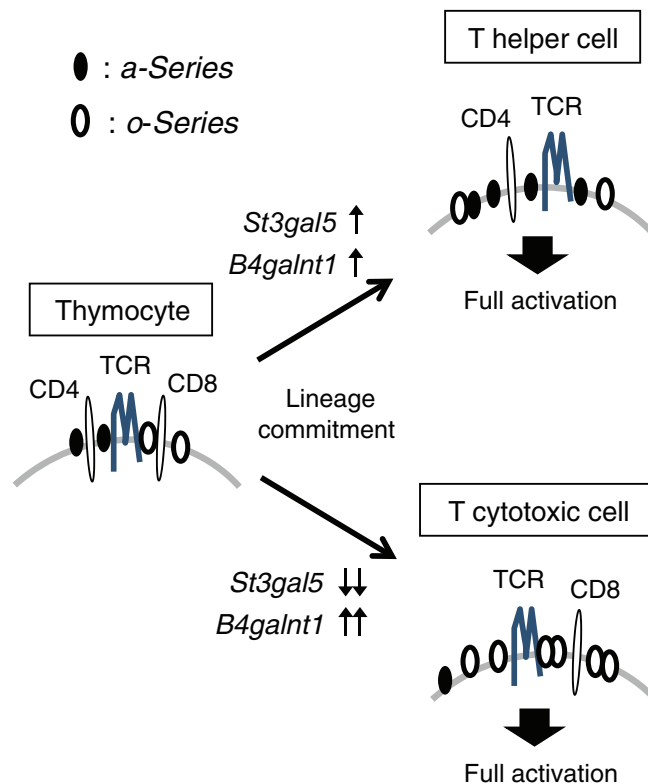


Fig. 6 Distinct expression signatures of ganglioside species during T-cell development. Lineage commitment from thymocytes (CD4/CD8 double positive) to mature single positive T cell subsets is accompanied by selective ganglioside expression. CD4⁺ T helper (Th) cells express predominantly a-series gangliosides because of upregulation of *St3gal5* gene, while CD8⁺ T cytotoxic (Tc) cells carry o-series gangliosides because of downregulation of *St3gal5* and upregulation of *B4galnt1* genes. Evidently, each T cell subset has unique lipid rafts composed of differing ganglioside species, and these rafts are the basis for distinctive functions in intracellular events following TCR-mediated stimulation. The ganglioside selection process is thus essential for formation of distinct, functional lipid rafts in mature T cells.

localized to lipid rafts by palmitoylation (a process whereby lipids are attached to other molecules), but raft localization is not determined solely by this process.^{144,145} To ensure movement of CD4 and CD8 to specific, correct locations on the membrane, it may be essential that these molecules interact with rafts carrying specific ganglioside species. Specific roles of the various gangliosides in regulation of membrane microenvironments remain to be elucidated.

5.3 T Cell Gangliosides in Autoimmune and Allergic Diseases

Almost all T cells that recognize self or harmless antigens are killed or inactivated in normal individuals. Failure of normal self-tolerance mechanisms leads to development of autoimmune and allergic diseases. The four T helper cell subpopulations (Th1, Th2, Th17, Treg) produce different cytokines and have distinctive effector functions, presumably based on differing organization of TCR signaling complexes in lipid rafts.¹⁴⁶ Lipid composition of lipid rafts and TCR signaling ability differ in Th1 versus Th2 cells.^{147–150} Studies of clinical cases and mouse models indicate that some of these disease processes are related to ganglioside composition of T cells; we will review three of these diseases in this section.

Allergic asthma, a type 1 hypersensitivity reaction, is a manifestation of immediate and late-phase reactions in the lung. Innate immune cells, such as mast cells, basophils, and eosinophils are the effector cells of airway inflammation.^{151,152} Adaptive immunity contributes to initiation of allergic reactions. CD4⁺ T cells play a crucial role in production of Th2 cytokine (IL-4 and IL-13), which then help B cells produce IgE antibodies specific for the “harmless” antigens.^{153,154} We examined mechanisms of allergic airway inflammation and airway hyperresponsiveness triggered by inhalation of ovalbumin (OVA) antigen in OVA-sensitized mice. GM3S-null mice showed striking reduction of allergic airway responses normally induced by OVA inhalation, that is, extensive mucus hypersecretion (characteristic of asthma), airway infiltration of inflammatory cells, OVA-specific IgE production, and increased Th2 cytokine levels in serum.¹³⁰ CD4⁺ T cells from these mutant mice lack GM1a, and self-reactive CD4⁺ T cells display enhanced GM1a expression resulting in persistence of abnormal cell activation.^{155,156} Karman *et al.* demonstrated suppression of airway inflammation by administration of antisense oligonucleotides against GM3S gene.¹⁵⁷ These findings indicate that a-series ganglioside GM1a is essential for T helper cell function. The novel CD4⁺ T cell subsets Th17 and Treg were described recently. In allergic airway inflammation, the balance between

effector Th2 cells and suppressive Treg cells is skewed toward Th2 predominance.¹⁵⁸ It has been suggested that Th17 cells contribute to neutrophilic, steroid-resistant severe asthma and enhance Th2-mediated airway inflammation, although the precise role of Th17 cells in asthma remains unclear.¹⁵⁹ *GM3S*-null mice displayed a reduction of Th17 cell number induced by in vitro culture.¹⁶⁰

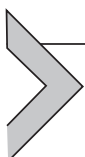
Systemic lupus erythematosus (SLE), one of the most common autoimmune diseases, presents with multisystem clinical manifestations, including rashes, arthritis, glomerulonephritis, hemolytic anemia, thrombocytopenia, and central nervous system involvement.^{161,162} A variety of autoantibodies are typically found in sera of SLE patients, and autoreactive T and B cells are involved in pathogenesis of this disease. T cells from SLE patients have intrinsic alterations of lipid components of lipid rafts.^{155,163,164} GM1a expression levels in CD4⁺ T cells (but not CD8⁺ T cells) from SLE patients, in comparison with healthy controls, are significantly higher. LacCer, GA2, Gb3, GM1a, and GD1a are also upregulated in SLE CD4⁺ T cells.¹⁶⁵ Increased GM1a expression is more marked in CD45RO-positive CD4⁺ T cells (memory T cells) from active SLE patients than from inactive SLE patients.¹⁵⁵ Activated human T cells show upregulation of GM1a levels.^{155,164,166,167} GM1a expression is also enhanced in self-reactive CD4⁺ T cells, resulting in persistence of abnormal cell activation.^{155,156} These findings, taken together, clearly indicate that gangliosides are key factors in SLE pathogenesis and pathology. In a 2014 study by McDonald *et al.*, SLE CD4⁺ T cells were stimulated for 72 h with a combination of anti-CD3 mAb, anti-CD28 mAb, and GlcCer synthase inhibitor NB-DNJ. In the treated cells, expression levels of GM1a and LacCer were similar to those observed in healthy controls, and defects in TCR signaling were partially reversed.¹⁶⁵ Expression levels of cellular GSLs are determined by the coordinated effects of de novo synthesis, turnover, and recycling.¹⁶⁸ The increased GSL expression in SLE CD4⁺ T cells was associated with accelerated internalization of GSLs from plasma membrane into intracellular compartments and rapid recycling of GSLs back to plasma membrane, resulting in a net increase in plasma membrane expression. SLE T cells display both increased GSL biosynthesis and accelerated trafficking to and from plasma membrane, which presumably lead to aberrant accumulation of gangliosides in lipid rafts.¹⁶⁹

Rheumatoid arthritis (RA), another common autoimmune disease, is characterized by synovial inflammation associated with destruction of joint cartilage and bone.¹⁷⁰ Both cell-mediated and humoral immune responses evidently contribute to RA development. Fluid around inflamed synovia and joints contains numerous types of inflammatory cells (Th1 cells, Th17

cells, activated B cells, macrophages) and cytokines (IL-1, IL-8, TNF α , IL-6, IL-17, IFN γ).^{171,172} GM3 and GM3S gene expression levels were higher in synovia of RA patients than in those of patients with osteoarthritis, which is not an autoimmune disease.¹⁷³ Progression of collagen-induced inflammatory arthritis, a mouse model of RA, was accelerated in GM3S-null mice, and induction of IL-17-producing cells in regional lymph nodes was enhanced by collagen immunization.¹⁷³ In another report, on the other hand, GM3S-null mice exhibit a decreased number of Th17 cells induced by in vitro culture.¹⁶⁰ Future studies will clarify whether a-series gangliosides expressed in Th17 cells are involved in RA development. CD4⁺ T cells can be separated into GD1c-positive IL-2 producing Th1-like cells and GD1c-negative IL-4 producing Th2-like cells.¹⁴¹ It appears likely that each subpopulation of CD4⁺ T cells has a unique, characteristic ganglioside expression pattern in its lipid rafts, and these patterns are responsible for specific functions of Th effector cells.

5.4 Perspectives

Results of numerous recent studies indicate that pathogenesis of allergic and autoimmune diseases are controlled in part by a variety of lipid rafts with differing ganglioside profiles in individual CD4⁺ T cell subsets. Differentiation events of T cells in thymus are associated with differential ganglioside expression patterns in individual T cell subsets. The various subpopulations of effector CD4⁺ T cells in peripheral lymphoid organs appear to have unique ganglioside expression patterns in their rafts, which are responsible for specific Th functions. Thus, the ganglioside selection process is essential for formation of distinct, functional lipid rafts in mature T cells. Although allergic reactions share certain common features, they differ greatly in the types of antigens involved. Reduction of a-series gangliosides by GM3S inhibition, and consequent modulation of ganglioside expression in lipid rafts, is potentially a powerful technique for therapy of immune system disorders.



6. GM3S DEFICIENCY AND HEARING LOSS

6.1 GM3S Deficiency in Humans

GM3S deficiency is a rare neurological disorder in which mutations of this enzyme result in a complete lack of GM3 and its downstream biosynthetic derivatives. The clinical manifestations of GM3S

deficiency include infantile-onset epilepsy, severe intellectual disability, irritability, failure to thrive, blindness, choreoathetosis, and cutaneous dyspigmentation. The disorder was first reported in Old Order Amish^{174,175} and more recently in French and Korean families or individuals.^{176,177}

Infants with GM3S deficiency display feeding difficulties and vomiting within the first few weeks after birth, which prevent normal growth and weight gain. Seizures begin to occur within the first year and worsen over time. Multiple types of seizures have been reported, and include symptoms, such as muscle rigidity, convulsions, and loss of consciousness. Affected children typically have severe intellectual disability and do not develop skills, such as speaking, unsupported sitting, walking, and reaching for objects. Vision and hearing abilities decline over time, although they are present at birth.^{174–182} In some cases, there are alterations of skin coloring on the arms, legs, and face (e.g., dark freckle-like spots or light patches),¹⁷⁸ or respiratory chain dysfunction.

Two homozygous mutations have been reported: c.862C>T (p.Arg288*) and c.994G>A (p.Glu332Lys). The nonsense mutation c.862C>T in Old Order Amish patients results in protein truncation between sialyl motif L and S. The c.994G>A mutation in an African-American family, within sialyl motif S, results in disruption of sialyl motif S function (interaction with LacCer acceptor and a sugar donor). The reported Korean patients had compound heterozygous and missense mutations in sialyl motif L (c.584G>C/p.Cys195Ser, and c.601G>A/p.Gly201Arg). These patients displayed various Rett-like phenotypes, but not epilepsy or blindness. These differences in symptoms may reflect differences in the mutation region of *ST3GAL5*. Humans who lack all a- and b-series gangliosides because of *ST3GAL5* c.694C>T mutations display major disruptions of auditory function, neonatal-onset hearing impairment, weak or absent middle ear muscle reflexes (MEMRs) and distortion product otoacoustic emissions (DPOAEs), abnormal auditory brainstem response (ABR) morphology and thresholds, absent cochlear microphonics (CMs), and delayed cortical auditory evoked potentials (CAEPs). Absent DPOAEs and CMs indicate severe outer hair cell (OHC) impairment. The presence of ABRs in seven of eight patients in our 2015 study suggested at least partial inner hair cell (IHC) function. However, numerous abnormalities revealed by MEMR and ABR testing indicated significant dysfunction of IHCs and/or central auditory pathways.¹⁸¹

6.2 Significant Increase of GSLs During Postnatal Maturation of Murine Cochlea

We investigated GSL expression in WT murine cochlea during the postnatal period of auditory system maturation. Mice began to recognize sound by postnatal day 12 (P12), designated the “onset of hearing.” On P1, GM3 was the dominant cochlear GSL. After P3, there were marked increases of cochlear GM3 GlcCer, complex gangliosides (GM1, GD1a, GD3, GD1b, GT1b), and sulfatides (SM3, SM4). In contrast, cerebral gangliosides achieved stable, mature expression as early as P3.¹⁸¹

Significant alterations of ganglioside expression in murine cochlea after P3 reflect their essential role in hearing onset.¹⁸¹ Following auditory maturation, GM3 and GM1 are distributed discretely among IHCs, OHCs, Deiters cells, and pillar cells of the organ of Corti (Table 1). Both IHCs and OHCs express GM3, which is localized on the apical surface, cuticular plate, and stereocilia. GM1 is the primary IHC ganglioside. It is also the predominant ganglioside on the apical surface of supporting cells, but is largely absent from OHCs.¹⁸¹

6.3 Glycocalyx Integrity and Membrane Cycling in GM3S-Deficient Mice

Apical membranes of stereocilia are covered with a glycocalyx composed of sialic acid-containing glycoproteins and glycolipids (including gangliosides),¹⁸³ creating a dense negative charge field that normally prevents fusion of adjacent stereocilia. In animal models, aminoglycoside administration reduced expression of sialoglycoconjugates in the OHC glycocalyx and enhanced fusion of stereocilia.^{184,185}

To elucidate the roles of various ganglioside species in hearing, we compared auditory function in *GM3S*-null versus *GM2/GD2S*-null mice, which have distinctive GSL expression patterns within the organ of Corti. *GM2/GD2S*-null cochlea had high GM3 content and was associated with

Table 1 Comparison of GM3 and GM1 Expression of Specific Regions in the Organ of Corti at P14.

	OHC			IHC			DC	PC
	Stereocilia	Cuticular Plate	Cell Body	Stereocilia	Cuticular Plate	Cell Body	Cell Surface	Cell Body
GM3	++	+	—	++	+	—	—	+
GM1	—	—	—	++	+	+	++	+

DC, Deiters cell; IHC, inner hair cell; OHC, outer hair cell; PC, pillar cell.

intact hair bundles and normal auditory function; whereas *GM3S*-null cochlea had no GM3 and was associated with deafness. Confocal laser microscopy with phalloidin staining revealed normal IHC and OHC morphology in 4-week-old *GM2/GD2S*-null mice. In contrast, OHCs in *GM3S*-null mice had blebs and intracellular vesicles composed of membranous structures, indicative of lack of balance between endocytosis and exocytosis.¹⁸¹ GM3 is expressed in IHCs and OHCs of WT mice, whereas only IHCs express GM1. This may account for the observation that OHCs in *GM3S*-null mice degenerate prior to IHCs.

6.4 GM3-Enriched Membrane Organization, PTPRQ-Myosin VI Complex Localization and Hair Cell Morphology

Cochlear hair cells are specialized for auditory and vestibular transduction. Projecting from their apical surface are filopodial processes (stereocilia) that contain hundreds of cross-linked actin filaments. Proteins, such as unconventional myosins, Usher proteins, and deafness-related gene products [protein Tyr phosphatase receptor Q (PTPRQ), cadherin23, protocadherin15, usherin, VLGR1] are expressed predominantly or exclusively in stereocilia, forming a structured interactive network for mechanoelectrical transduction.¹⁸⁶

In the normal organ of Corti, functional PTPRQ-myosin VI complexes are essential to maintain integrity of this network.¹⁸⁷ PTPRQ, a shaft connector at the tapered base of stereocilia, consists of an extracellular domain with 18 fibronectin III (FNIII) repeats, a membrane spanning domain, and a cytoplasmic domain having phosphatidylinositol and Tyr phosphatase activities.^{187,188} Myosin VI is an actin-based motor protein whose complex with PTPRQ mediates interactions between plasma membrane and cytoskeleton.¹⁸⁹ PTPRQ-deficient mice are deaf and have fused stereocilia that do not taper at the base.¹⁹⁰ Myosin VI-deficient mice are also deaf and have comparable structural changes of hair cells, accompanied by maldistribution of PTPRQ along the stereocilia.^{190–192}

In bullfrogs (*Rana catesbeiana*), PTPRQ is colocalized with ganglioside-rich membrane domains in basal stereocilia.¹⁹³ We examined the relationship between gangliosides and basal PTPRQ-myosin VI complex by immunostaining (Fig. 7). PTPRQ is localized exclusively in bases of stereocilia in WT murine IHCs. In contrast, in *GM3S*-null mice PTPRQ is maldistributed along shafts of fused stereocilia (Fig. 7B), and myosin VI is present from base to midshaft but absent from distal regions (Fig. 7A). These structural disruptions presumably result in loss of normal ciliary motor action. In

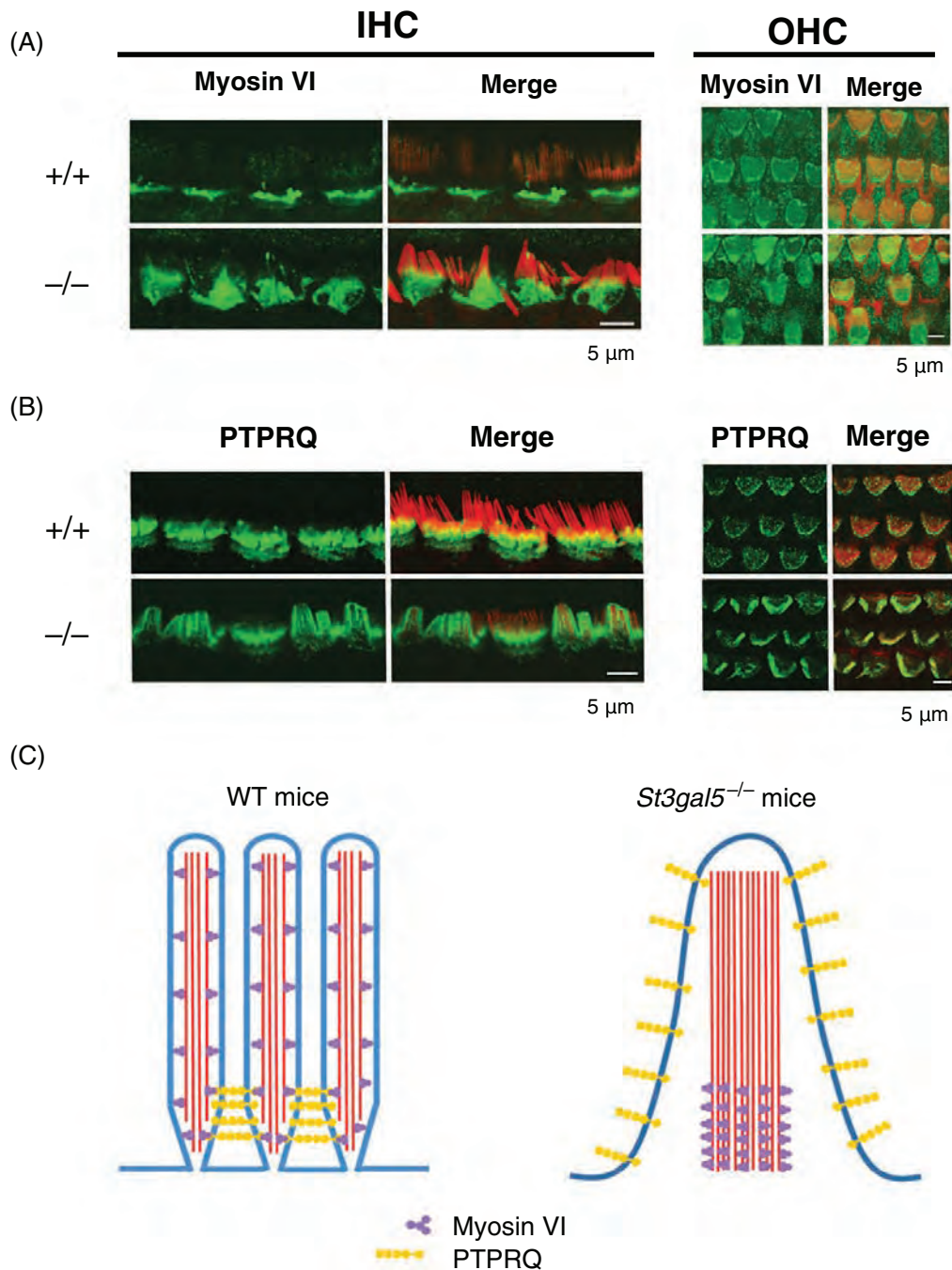


Fig. 7 Maldistribution of protein Tyr phosphatase receptor Q (PTPRQ) and myosin VI in stereocilia of *GM3S*-null mice. (A) Confocal images show stereocilia of inner hair cells (IHCs) and outer hair cells (OHCs) from WT and *GM3S*-null mice stained for myosin VI, (B) PTPRQ (green), and F-actin (phalloidin; magenta). (C) Schematic depiction of maldistributed PTPRQ and myosin VI in *GM3S*-null IHC stereocilia.¹⁸¹

OHCs of *GM3S*-null mice, myosin VI is expressed mostly at the cuticular plate surface, close to vestigial kinocilia.

These findings, taken together, indicate that GM3-enriched membrane microdomains are essential for formation and proper localization of

PTPRQ-myosin VI complexes in hair cells. Aberrant expression of PTPRQ-myosin VI complexes resulting from absence of GM3 alters the structure of stereocilia and impairs their ability to transduce auditory signals (Fig. 7C).

6.5 Perspectives

GM3 plays a specific and essential role in development, function, and viability of cochlear hair cells. In humans with GM3S deficiency, hearing is already impaired at birth. However, studies of auditory phenotype in GM3S-null mice suggest that ganglioside addition may partially restore auditory function during a critical postnatal “window.” These findings are relevant to our understanding of hearing loss in humans with GM3S deficiency, but do not explain the broader neurological phenotype associated with this condition. Further studies are needed to more precisely characterize the role of lipid rafts generally, and GM3 specifically, in development and function of the central nervous system.

New concepts and techniques are giving rise to novel strategies to reverse hearing impairment. Oshima *et al.* generated functional hair cell-like cells from embryonic and induced pluripotent stem cells.¹⁹⁴ Such strategies will help promote research on the auditory functions of GSL-enriched microdomains, and lead to new, more effective therapies to overcome hearing loss in humans.



7. CONCLUSIONS AND FUTURE DIRECTIONS

Functional roles of GM3 have been investigated indirectly based on addition of exogenous GM3 to culture medium, or on depletion of precursor GSLs by GlcCer synthase inhibitors.¹⁹⁵ Results of these studies suggested that GM3 is involved in transmembrane signaling through regulation of growth factor receptor activities, and in cell adhesion and motility through interaction with integrins and/or integrin-related molecule(s). However, it was not possible to definitively conclude that the effects of exogenously added or pharmacologically depleted gangliosides reflected the physiological functions of endogenous GM3.

Our studies during the past decade using GM3S-null mice have helped demonstrate the crucial roles of GM3 in diabetes, insulin resistance, leptin resistance, helper T cell function, and hearing function. Our findings provide a foundation for novel therapies against metabolic

syndrome, type 2 diabetes, and immunological disorders (e.g., allergies), based on inhibition of GM3 biosynthesis. Extensive depletion of all gangliosides by GM3 biosynthesis inhibition results in excessive physical and chemical modifications of all plasma membranes, and particularly of lipid microdomains in membranes. However, effective treatment of metabolic disorders will not require such extensive ganglioside depletion. In our study of D-PDMP effect on impaired insulin signaling in TNF α -treated 3T3-L1 adipocytes, normalization of elevated GM3 levels was sufficient to restore proper insulin resistance status.¹³⁰ We expect that comprehensive studies of functional suprabiomolecular complexes consisting of gangliosides and functional proteins in microdomains will lead to a novel concept and strategy of “membrane microdomain orthosignaling therapy.”

Our studies have shown that GM3 functions as a physiological regulatory factor to maintain homeostasis in adipocytes by modulating insulin signaling,^{45,51,53,130} and that serum GM3 concentration is elevated in patients with metabolic syndrome.⁶⁹ Further analysis of these sera by LC-MS/MS revealed increased levels of GM3 containing very long acyl chains with or without α -hydroxy modification (C24:0, α OH-C24:0), and reduced levels of GM3 carrying long acyl chains (C16:0, C18:0).⁶⁹ Inflammatory cytokines, hypoxic conditions, and ER stress increase the biosynthesis of GM3 in the adipocytes, and inflammatory reactions in GM3S null mice are suppressed when these mice are fed with high fat diets.⁵¹ Our ongoing studies are focused on the molecular mechanisms underlying these responses. We have observed that C24:0-GM3 and α OH-C24:0-GM3 induce secretion of inflammatory cytokines when monocytes or macrophages are stimulated by TLR4 ligand, LPS, or HMGB1; whereas C16:0-GM3, 18:0-GM3, and 24:1-GM3 suppress secretion of inflammatory cytokines. The effects are triggered by induction of TLR4/MD2 supramolecular complex formation and upregulation of signal transduction. Based on these findings, we propose a novel inflammation loop triggered by specific GM3 molecular species (MS submitted).

ACKNOWLEDGMENTS

The authors' studies described in this review were supported by the Core Research for Evolutional Science and Technology division of the Japan Science and Technology Agency (to J.I.), a Grant-in-Aid for Scientific Research (B) from MEXT (J.I.) (16H04767), Mizutani Foundation for Glycoscience (J.I.), Naito Foundation (J.I.), ONO Medical Research Foundation (J.I.), Uehara Memorial Foundation (J.I.), Yamada Science Foundation (J.I.), and the MEXT-Supported Program for the Strategic Research Foundation at Private Universities (S1201031). The authors are grateful to Dr. S. Anderson for English editing of the manuscript.

REFERENCES

1. Yamakawa T, Suzuki S. The chemistry of the lipids of posthemolytic residue or stroma of erythrocytes. Concerning the ether-insoluble lipids of lyophilized horse blood stroma. *J Biochem.* 1951;38:199–212.
2. Yamakawa T. Studies on erythrocyte glycolipids. *ProcJap Acad SerB.* 2005;81:52–63.
3. Todeschini AR, Hakomori S. Functional role of glycosphingolipids and gangliosides in control of cell adhesion, motility, and growth, through glycosynaptic microdomains. *BiochimBiophys Acta.* 2008;1780:421–433.
4. Sabourdy F, et al. Functions of sphingolipid metabolism in mammals—lessons from genetic defects. *BiochimBiophys Acta.* 2008;1781:145–183.
5. Ishii A, et al. Expression cloning and functional characterization of human cDNA for ganglioside GM3 synthase. *J Biol Chem.* 1998;273:31652–31655.
6. Inokuchi J. Membrane microdomains and insulin resistance. *FEBS Lett.* 2010;584:1864–1871.
7. Inokuchi J. Physiopathological function of hematoside (GM3 ganglioside). *ProcJpn Acad SerB.* 2011;87:179–198.
8. Inokuchi J. GM3 and diabetes. *GlycoconjJ.* 2014;31:193–197.
9. Uemura S, et al. Substitution of the N-glycan function in glycosyltransferases by specific amino acids: ST3Gal-V as a model enzyme. *Glycobiology.* 2006;16:258–270.
10. Burger KN, van der Bijl P, van Meer G. Topology of sphingolipid galactosyltransferases in ER and Golgi: transbilayer movement of monohexosyl sphingolipids is required for higher glycosphingolipid biosynthesis. *J Cell Biol.* 1996;133:15–28.
11. Eckhardt M, Muhlenhoff M, Bethe A, Gerardy-Schahn R. Expression cloning of the Golgi CMP-sialic acid transporter. *Proc Natl Acad Sci USA.* 1996;93:7572–7576.
12. Stern CA, Braverman TR, Tiemeyer M. Molecular identification, tissue distribution and subcellular localization of mST3GalV/GM3 synthase. *Glycobiology.* 2000;10:365–374.
13. Kapitonov D, Bieberich E, Yu RK. Combinatorial PCR approach to homology-based cloning: cloning and expression of mouse and human GM3-synthase. *GlycoconjJ.* 1999;16:337–350.
14. Kim KW, Kim SW, Min KS, Kim CH, Lee YC. Genomic structure of human GM3 synthase gene (hST3 Gal V) and identification of mRNA isoforms in the 5′-untranslated region. *Gene.* 2001;273:163–171.
15. Berselli P, et al. Human GM3 synthase: a new mRNA variant encodes an NH₂-terminal extended form of the protein. *BiochimBiophys Acta.* 2006;1759:348–358.
16. Uemura S, Yoshida S, Shishido F, Inokuchi J. The cytoplasmic tail of GM3 synthase defines its subcellular localization, stability, and in vivo activity. *Mol Biol Cell.* 2009;20:3088–3100.
17. Kono M, et al. Molecular cloning and functional expression of a fifth-type alpha 2,3-sialyltransferase (mST3 Gal V: GM3 synthase). *Biochem Biophys Res Commun.* 1998;253:170–175.
18. Shishido F, Uemura S, Nitta T, Inokuchi J. Identification of a new liver-specific c-type mRNA transcriptional variant for mouse ST3GAL5 (GM3/GM4 synthase). *GlycoconjJ.* 2017;34(5):651–659.
19. Kozak M. Pushing the limits of the scanning mechanism for initiation of translation. *Gene.* 2002;299:1–34.
20. Zava S, Milani S, Sottocornola E, Berra B, Colombo I. Two active and differently N-glycosylated isoforms of human ST3Gal-V are produced from the placental mRNA variant by a leaky scanning mechanism. *FEBS Lett.* 2010;584:1476–1480.
21. Giraud CG, Maccioni HJ. Endoplasmic reticulum export of glycosyltransferases depends on interaction of a cytoplasmic dibasic motif with Sar1. *Mol Biol Cell.* 2003;14:3753–3766.

22. Quintero CA, Giraudo CG, Villarreal M, Montich G, Maccioni HJ. Identification of a site in Sar1 involved in the interaction with the cytoplasmic tail of glycolipid glycosyltransferases. *J Biol Chem*. 2010;285:30340–30346.
23. Uemura S, Shishido F, Kashimura M, Inokuchi J. The regulation of ER export and Golgi retention of ST3Gal5 (GM3/GM4 synthase) and B4GalNAcT1 (GM2/GD2/GA2 synthase) by arginine/lysine-based motif adjacent to the transmembrane domain. *Glycobiology*. 2015;25:1410–1422.
24. Barlowe C, Schekman R. SEC12 encodes a guanine-nucleotide-exchange factor essential for transport vesicle budding from the ER. *Nature*. 1993;365:347–349.
25. Yoshihisa T, Barlowe C, Schekman R. Requirement for a GTPase-activating protein in vesicle budding from the endoplasmic reticulum. *Science*. 1993;259:1466–1468.
26. Aridor M, Weissman J, Bannykh S, Nuoffer C, Balch WE. Cargo selection by the COPII budding machinery during export from the ER. *J Cell Biol*. 1998;141:61–70.
27. Kuehn MJ, Herrmann JM, Schekman R. COPII-cargo interactions direct protein sorting into ER-derived transport vesicles. *Nature*. 1998;391:187–190.
28. Peng R, Grabowski R, De Antoni A, Gallwitz D. Specific interaction of the yeast cis-Golgi syntaxin Sed5p and the coat protein complex II component Sec24p of endoplasmic reticulum-derived transport vesicles. *Proc Natl Acad Sci USA*. 1999;96:3751–3756.
29. Springer S, Schekman R. Nucleation of COPII vesicular coat complex by endoplasmic reticulum to Golgi vesicle SNAREs. *Science*. 1998;281:698–700.
30. Votsmeier C, Gallwitz D. An acidic sequence of a putative yeast Golgi membrane protein binds COPII and facilitates ER export. *EMBOJ*. 2001;20:6742–6750.
31. Sato K, Nakano A. Dissection of COPII subunit-cargo assembly and disassembly kinetics during Sar1p-GTP hydrolysis. *Nat Struct Mol Biol*. 2005;12:167–174.
32. Michelsen K, et al. Novel cargo-binding site in the beta and delta subunits of coatomer. *J Cell Biol*. 2007;179:209–217.
33. Shikano S, Li M. Membrane receptor trafficking: evidence of proximal and distal zones conferred by two independent endoplasmic reticulum localization signals. *Proc Natl Acad Sci USA*. 2003;100:5783–5788.
34. Okajima T, Xu A, Lei L, Irvine KD. Chaperone activity of protein O-fucosyltransferase 1 promotes notch receptor folding. *Science*. 2005;307:1599–1603.
35. Losev E, et al. Golgi maturation visualized in living yeast. *Nature*. 2006;441:1002–1006.
36. Matsuura-Tokita K, Takeuchi M, Ichihara A, Mikuriya K, Nakano A. Live imaging of yeast Golgi cisternal maturation. *Nature*. 2006;441:1007–1010.
37. Tu L, Tai WC, Chen L, Banfield DK. Signal-mediated dynamic retention of glycosyltransferases in the Golgi. *Science*. 2008;321:404–407.
38. Chawla A, Nguyen KD, Goh YP. Macrophage-mediated inflammation in metabolic disease. *Nat Rev Immunol*. 2011;11:738–749.
39. Samaan MC. The macrophage at the intersection of immunity and metabolism in obesity. *Diabetol Metab Syndr*. 2011;3:29.
40. Suganami T, Ogawa Y. Adipose tissue macrophages: their role in adipose tissue remodeling. *J Leukoc Biol*. 2010;88:33–39.
41. Sun S, Ji Y, Kersten S, Qi L. Mechanisms of inflammatory responses in obese adipose tissue. *Annu Rev Nutr*. 2012;32:261–286.
42. Zoncu R, Efeyan A, Sabatini DM. mTOR: from growth signal integration to cancer, diabetes and ageing. *Nat Rev Mol Cell Biol*. 2011;12:21–35.
43. Guo D, Donner DB. Tumor necrosis factor promotes phosphorylation and binding of insulin receptor substrate 1 to phosphatidylinositol 3-kinase in 3T3-L1 adipocytes. *J Biol Chem*. 1996;271:615–618.
44. Kabayama K, et al. TNFalpha-induced insulin resistance in adipocytes as a membrane microdomain disorder: involvement of ganglioside GM3. *Glycobiology*. 2005;15:21–29.

45. Tagami S, et al. Ganglioside GM3 participates in the pathological conditions of insulin resistance. *J Biol Chem*. 2002;277:3085–3092.
46. Inokuchi J, Radin NS. Preparation of the active isomer of 1-phenyl-2-decanoylamino-3-morpholino-1-propanol, inhibitor of murine glucocerebrosidase. *J Lipid Res*. 1987;28:565–571.
47. Yamashita T, et al. Enhanced insulin sensitivity in mice lacking ganglioside GM3. *Proc Natl Acad Sci USA*. 2003;100:3445–3449.
48. Hotamisligil GS, Shargill NS, Spiegelman BM. Adipose expression of tumor necrosis factor- α : direct role in obesity-linked insulin resistance. *Science*. 1993;259:87–91.
49. Aerts JM, et al. Pharmacological inhibition of glucosylceramide synthase enhances insulin sensitivity. *Diabetes*. 2007;56:1341–1349.
50. Zhao H, et al. Inhibiting glycosphingolipid synthesis improves glycemic control and insulin sensitivity in animal models of type 2 diabetes. *Diabetes*. 2007;56:1210–1218.
51. Nagafuku M, et al. Control of homeostatic and pathogenic balance in adipose tissue by ganglioside GM3. *Glycobiology*. 2015;25:303–318.
52. Wentworth JM, et al. GM3 ganglioside and phosphatidylethanolamine-containing lipids are adipose tissue markers of insulin resistance in obese women. *Int J Obes*. 2016;40:706–713.
53. Kabayama K, et al. Dissociation of the insulin receptor and caveolin-1 complex by ganglioside GM3 in the state of insulin resistance. *Proc Natl Acad Sci USA*. 2007;104:13678–13683.
54. Ohashi M. A comparison of the ganglioside distributions of fat tissues in various animals by two-dimensional thin layer chromatography. *Lipids*. 1979;14:52–57.
55. Hakomori S. The glycosynapse. *Proc Natl Acad Sci USA*. 2002;99:225–232.
56. Sonnino S, Prinetti A, Mauri L, Chigorno V, Tettamanti G. Dynamic and structural properties of sphingolipids as driving forces for the formation of membrane domains. *Chem Rev*. 2006;106:2111–2125.
57. Chavez JA, et al. Ceramides and glucosylceramides are independent antagonists of insulin signaling. *J Biol Chem*. 2014;289:723–734.
58. Park JW, et al. Ablation of very long acyl chain sphingolipids causes hepatic insulin resistance in mice due to altered detergent-resistant membranes. *Hepatology*. 2013;57:525–532.
59. de Ferranti S, Mozaffarian D. The perfect storm: obesity, adipocyte dysfunction, and metabolic consequences. *Clin Chem*. 2008;54:945–955.
60. Matsuzawa Y. Pathophysiology and molecular mechanisms of visceral fat syndrome: the Japanese experience. *Diabetes Metab Rev*. 1997;13:3–13.
61. Saltiel AR. Insulin resistance in the defense against obesity. *Cell Metab*. 2012;15:798–804.
62. Sorisky A, Molgat AS, Gagnon A. Macrophage-induced adipose tissue dysfunction and the preadipocyte: should I stay (and differentiate) or should I go? *Adv Nutr*. 2013;4:67–75.
63. Xu H, et al. Chronic inflammation in fat plays a crucial role in the development of obesity-related insulin resistance. *J Clin Invest*. 2003;112:1821–1830.
64. Sato T, et al. Circulating levels of ganglioside GM3 in metabolic syndrome: A pilot study. *Obes Res Clin Pract*. 2008;2:I–II.
65. Shimizu K, et al. Newly developed primary culture of rat visceral adipocytes and their in vitro characteristics. *Cell Biol Int*. 2006;30:381–388.
66. Senn HJ, Orth M, Fitzke E, Wieland H, Gerok W. Gangliosides in normal human serum. Concentration, pattern and transport by lipoproteins. *Eur J Biochem*. 1989;181:657–662.
67. Bobryshev YV, et al. Phenotype determination of anti-GM3 positive cells in atherosclerotic lesions of the human aorta. Hypothetical role of ganglioside GM3 in foam cell formation. *Biochim Biophys Acta*. 2001;1535:87–99.

68. Bobryshev YV, et al. Incorporation and localisation of ganglioside GM3 in human intimal atherosclerotic lesions. *Biochim Biophys Acta*. 1997;1361:287–294.
69. Veillon L, et al. Identification of ganglioside GM3 molecular species in human serum associated with risk factors of metabolic syndrome. *PLoS One*. 2015;10:e0129645.
70. Konner AC, Bruning JC. Toll-like receptors: linking inflammation to metabolism. *Trends Endocrinol Metab*. 2011;22:16–23.
71. Martinez FO, Helming L, Gordon S. Alternative activation of macrophages: an immunologic functional perspective. *Annu Rev Immunol*. 2009;27:451–483.
72. Odegaard JI, Chawla A. Alternative macrophage activation and metabolism. *Annu Rev Pathol*. 2011;6:275–297.
73. Lumeng CN, Bodzin JL, Saltiel AR. Obesity induces a phenotypic switch in adipose tissue macrophage polarization. *J Clin Invest*. 2007;117:175–184.
74. Danforth Jr E. Failure of adipocyte differentiation causes type II diabetes mellitus? *Nat Genet*. 2000;26:13.
75. Torti FM, Dieckmann B, Beutler B, Cerami A, Ringold GM. A macrophage factor inhibits adipocyte gene expression: an in vitro model of cachexia. *Science*. 1985;229:867–869.
76. Suzawa M, et al. Cytokines suppress adipogenesis and PPAR- γ function through the TAK1/TAB1/NIK cascade. *Nat Cell Biol*. 2003;5:224–230.
77. Jager J, Gremeaux T, Cormont M, Le Marchand-Brustel Y, Tanti JF. Interleukin-1 β -induced insulin resistance in adipocytes through down-regulation of insulin receptor substrate-1 expression. *Endocrinology*. 2007;148:241–251.
78. Stephens JM, Butts MD, Pekala PH. Regulation of transcription factor mRNA accumulation during 3T3-L1 preadipocyte differentiation by tumour necrosis factor- α . *J Mol Endocrinol*. 1992;9:61–72.
79. Hotamisligil GS, Arner P, Caro JF, Atkinson RL, Spiegelman BM. Increased adipose tissue expression of tumor necrosis factor- α in human obesity and insulin resistance. *J Clin Invest*. 1995;95:2409–2415.
80. Weisberg SP, et al. Obesity is associated with macrophage accumulation in adipose tissue. *J Clin Invest*. 2003;112:1796–1808.
81. Kim JY, et al. Obesity-associated improvements in metabolic profile through expansion of adipose tissue. *J Clin Invest*. 2007;117:2621–2637.
82. Zhang Y, et al. Positional cloning of the mouse obese gene and its human homologue. *Nature*. 1994;372:425–432.
83. Friedman JM, Halaas JL. Leptin and the regulation of body weight in mammals. *Nature*. 1998;395:763–770.
84. Ollmann MM, et al. Antagonism of central melanocortin receptors in vitro and in vivo by agouti-related protein. *Science*. 1997;278:135–138.
85. Tartaglia LA, et al. Identification and expression cloning of a leptin receptor, OB-R. *Cell*. 1995;83:1263–1271.
86. Myers Jr MG, Munzberg H, Leininger GM, Leshan RL. The geometry of leptin action in the brain: more complicated than a simple ARC. *Cell Metab*. 2009;9:117–123.
87. Frederich RC, et al. Leptin levels reflect body lipid content in mice: evidence for diet-induced resistance to leptin action. *Nat Med*. 1995;1:1311–1314.
88. Schengrund CL. Gangliosides: glycosphingolipids essential for normal neural development and function. *Trends Biochem Sci*. 2015;40:397–406.
89. Schnaar RL, Gerardy-Schahn R, Hildebrandt H. Sialic acids in the brain: gangliosides and polysialic acid in nervous system development, stability, disease, and regeneration. *Physiol Rev*. 2014;94:461–518.
90. Scott MM, et al. Leptin targets in the mouse brain. *J Comp Neurol*. 2009;514:518–532.
91. Chua Jr SC et al. Fine structure of the murine leptin receptor gene: splice site suppression is required to form two alternatively spliced transcripts. *Genomics*. 1997;45:264–270.

92. Tartaglia LA. The leptin receptor. *J Biol Chem*. 1997;272:6093–6096.
93. Bates SH, Myers Jr MG. The role of leptin receptor signaling in feeding and neuroendocrine function. *Trends Endocrinol Metab*. 2003;14:447–452.
94. Taniguchi T. Cytokine signaling through nonreceptor protein tyrosine kinases. *Science*. 1995;268:251–255.
95. Couturier C, Jockers R. Activation of the leptin receptor by a ligand-induced conformational change of constitutive receptor dimers. *J Biol Chem*. 2003;278:26604–26611.
96. Zhou Y, Rui L. Leptin signaling and leptin resistance. *Front Med*. 2013;7:207–222.
97. Banks AS, Davis SM, Bates SH, Myers Jr MG. Activation of downstream signals by the long form of the leptin receptor. *J Biol Chem*. 2000;275:14563–14572.
98. Rahmouni K, Sigmund CD, Haynes WG, Mark AL. Hypothalamic ERK mediates the anorectic and thermogenic sympathetic effects of leptin. *Diabetes*. 2009;58:536–542.
99. You J, et al. Signaling through Tyr985 of leptin receptor as an age/diet-dependent switch in the regulation of energy balance. *Mol Cell Biol*. 2010;30:1650–1659.
100. Halaas JL, et al. Physiological response to long-term peripheral and central leptin infusion in lean and obese mice. *Proc Natl Acad Sci USA*. 1997;94:8878–8883.
101. Cui H, Lopez M, Rahmouni K. The cellular and molecular bases of leptin and ghrelin resistance in obesity. *Nat Rev Endocrinol*. 2017;13:338–351.
102. Banks WA, Farrell CL. Impaired transport of leptin across the blood-brain barrier in obesity is acquired and reversible. *Am J Physiol Endocrinol Metab*. 2003;285:E10–E15.
103. Pan W, et al. Astrocyte leptin receptor (ObR) and leptin transport in adult-onset obese mice. *Endocrinology*. 2008;149:2798–2806.
104. Banks WA. Leptin transport across the blood-brain barrier: implications for the cause and treatment of obesity. *Curr Pharm Des*. 2001;7:125–133.
105. Banks WA. The blood-brain barrier as a cause of obesity. *Curr Pharm Des*. 2008;14:1606–1614.
106. Balland E, et al. Hypothalamic tanycytes are an ERK-gated conduit for leptin into the brain. *Cell Metab*. 2014;19:293–301.
107. Starr R, et al. A family of cytokine-inducible inhibitors of signalling. *Nature*. 1997;387:917–921.
108. Bjorbaek C, El-Haschimi K, Frantz JD, Flier JS. The role of SOCS-3 in leptin signaling and leptin resistance. *J Biol Chem*. 1999;274:30059–30065.
109. Bjorbaek C, et al. SOCS3 mediates feedback inhibition of the leptin receptor via Tyr985. *J Biol Chem*. 2000;275:40649–40657.
110. Bjorbaek C, Elmquist JK, Frantz JD, Shoelson SE, Flier JS. Identification of SOCS-3 as a potential mediator of central leptin resistance. *Mol Cell*. 1998;1:619–625.
111. Howard JK, et al. Enhanced leptin sensitivity and attenuation of diet-induced obesity in mice with haploinsufficiency of Socs3. *Nat Med*. 2004;10:734–738.
112. Mori H, et al. Socs3 deficiency in the brain elevates leptin sensitivity and confers resistance to diet-induced obesity. *Nat Med*. 2004;10:739–743.
113. Zabolotny JM, et al. PTP1B regulates leptin signal transduction in vivo. *Dev Cell*. 2002;2:489–495.
114. Cheng A, et al. Attenuation of leptin action and regulation of obesity by protein tyrosine phosphatase 1B. *Dev Cell*. 2002;2:497–503.
115. Banno R, et al. PTP1B and SHP2 in POMC neurons reciprocally regulate energy balance in mice. *J Clin Invest*. 2010;120:720–734.
116. Bence KK, et al. Neuronal PTP1B regulates body weight, adiposity and leptin action. *Nat Med*. 2006;12:917–924.
117. Farooqi IS, et al. Clinical spectrum of obesity and mutations in the melanocortin 4 receptor gene. *N Engl J Med*. 2003;348:1085–1095.
118. Huszar D, et al. Targeted disruption of the melanocortin-4 receptor results in obesity in mice. *Cell*. 1997;88:131–141.

119. Marsh DJ, et al. Response of melanocortin-4 receptor-deficient mice to anorectic and orexigenic peptides. *Nat Genet.* 1999;21:119–122.
120. Fan W, Boston BA, Kesterson RA, Hrubby VJ, Cone RD. Role of melanocortinergic neurons in feeding and the agouti obesity syndrome. *Nature.* 1997;385:165–168.
121. Liao GY, et al. Dendritically targeted Bdnf mRNA is essential for energy balance and response to leptin. *Nat Med.* 2012;18:564–571.
122. Xu B, et al. Brain-derived neurotrophic factor regulates energy balance downstream of melanocortin-4 receptor. *Nat Neurosci.* 2003;6:736–742.
123. Liu Y, Li R, Ladisch S. Exogenous ganglioside GD1a enhances epidermal growth factor receptor binding and dimerization. *J Biol Chem.* 2004;279:36481–36489.
124. Nordstrom V, et al. Neuronal expression of glucosylceramide synthase in central nervous system regulates body weight and energy homeostasis. *PLoS Biol.* 2013;11:e1001506.
125. Ji S, et al. b-Series gangliosides crucially regulate leptin secretion in adipose tissues. *Biochem Biophys Res Commun.* 2015;459:189–195.
126. Ji S, et al. Increased a-series gangliosides positively regulate leptin/Ob receptor-mediated signals in hypothalamus of GD3 synthase-deficient mice. *Biochem Biophys Res Commun.* 2016;479:453–460.
127. Iwatsuka H, Shino A, Suzuoki Z. General survey of diabetic features of yellow KK mice. *Endocrinol Jpn.* 1970;17:23–35.
128. Jais A, Bruning JC. Hypothalamic inflammation in obesity and metabolic disease. *J Clin Invest.* 2017;127:24–32.
129. Dykstra M, Cherukuri A, Sohn HW, Tzeng SJ, Pierce SK. Location is everything: lipid rafts and immune cell signaling. *Annu Rev Immunol.* 2003;21:457–481.
130. Nagafuku M, et al. CD4 and CD8 T cells require different membrane gangliosides for activation. *Proc Natl Acad Sci USA.* 2012;109:E336–E342.
131. Hakomori S. Structure and function of glycosphingolipids and sphingolipids: recollections and future trends. *Biochim Biophys Acta.* 2008;1780:325–346.
132. Tidhar R, Futerman AH. The complexity of sphingolipid biosynthesis in the endoplasmic reticulum. *Biochim Biophys Acta.* 2013;1833:2511–2518.
133. Davis DM, Dustin ML. What is the importance of the immunological synapse? *Trends Immunol.* 2004;25:323–327.
134. Fooksman DR, et al. Functional anatomy of T cell activation and synapse formation. *Annu Rev Immunol.* 2010;28:79–105.
135. Harder T, Rentero C, Zech T, Gaus K. Plasma membrane segregation during T cell activation: probing the order of domains. *Curr Opin Immunol.* 2007;19:470–475.
136. Monks CR, Freiberg BA, Kupfer H, Sciaky N, Kupfer A. Three-dimensional segregation of supramolecular activation clusters in T cells. *Nature.* 1998;395:82–86.
137. Saito T, Yokosuka T. Immunological synapse and microclusters: the site for recognition and activation of T cells. *Curr Opin Immunol.* 2006;18:305–313.
138. Kovacs B, et al. Human CD8+ T cells do not require the polarization of lipid rafts for activation and proliferation. *Proc Natl Acad Sci USA.* 2002;99:15006–15011.
139. Gomez-Mouton C, et al. Segregation of leading-edge and uropod components into specific lipid rafts during T cell polarization. *Proc Natl Acad Sci USA.* 2001;98:9642–9647.
140. Marusic A, Markotic A, Kovacic N, Muthing J. Expression of glycosphingolipids in lymph nodes of mice lacking TNF receptor 1: biochemical and flow cytometry analysis. *Carbohydr Res.* 2004;339:77–86.
141. Nakamura K, Suzuki H, Hirabayashi Y, Suzuki A. IV3 alpha (NeuGc alpha 2-8NeuGc)-Gg4Cer is restricted to CD4+ T cells producing interleukin-2 and a small population of mature thymocytes in mice. *J Biol Chem.* 1995;270:3876–3881.

142. Simons K, Toomre D. Lipid rafts and signal transduction. *Nat Rev Mol Cell Biol.* 2000;1:31–39.
143. Pizzo P, et al. Lipid rafts and T cell receptor signaling: a critical re-evaluation. *Eur J Immunol.* 2002;32:3082–3091.
144. Greenwald RJ, Freeman GJ, Sharpe AH. The B7 family revisited. *Annu Rev Immunol.* 2005;23:515–548.
145. Kroczeck RA, Mages HW, Hutloff A. Emerging paradigms of T-cell co-stimulation. *Curr Opin Immunol.* 2004;16:321–327.
146. Leitenberg D, Balamuth F, Bottomly K. Changes in the T cell receptor macromolecular signaling complex and membrane microdomains during T cell development and activation. *Semin Immunol.* 2001;13:129–138.
147. Balamuth F, Leitenberg D, Unternaehrer J, Mellman I, Bottomly K. Distinct patterns of membrane microdomain partitioning in Th1 and th2 cells. *Immunity.* 2001;15:729–738.
148. Izsepi E, et al. Membrane microdomain organization, calcium signal, and NFAT activation as an important axis in polarized Th cell function. *Cytometry A.* 2013;83:185–196.
149. Sloan-Lancaster J, Steinberg TH, Allen PM. Selective loss of the calcium ion signaling pathway in T cells maturing toward a T helper 2 phenotype. *J Immunol.* 1997;159:1160–1168.
150. Smith JA, Tang Q, Bluestone JA. Partial TCR signals delivered by FcR-nonbinding anti-CD3 monoclonal antibodies differentially regulate individual Th subsets. *J Immunol.* 1998;160:4841–4849.
151. Holgate ST. Pathophysiology of asthma: what has our current understanding taught us about new therapeutic approaches? *J Allergy Clin Immunol.* 2011;128:495–505.
152. Orihara K, Dil N, Anaparti V, Moqbel R. What's new in asthma pathophysiology and immunopathology? *Expert Rev Respir Med.* 2010;4:605–629.
153. Hamid Q, Tulic M. Immunobiology of asthma. *Annu Rev Physiol.* 2009;71:489–507.
154. Levine SJ, Wenzel SE. Narrative review: the role of Th2 immune pathway modulation in the treatment of severe asthma and its phenotypes. *Ann Intern Med.* 2010;152:232–237.
155. Dong L, et al. Increased expression of ganglioside GM1 in peripheral CD4+ T cells correlates soluble form of CD30 in systemic lupus erythematosus patients. *J Biomed Biotechnol.* 2010;2010:569053.
156. Kabouridis PS, Jury EC. Lipid rafts and T-lymphocyte function: implications for autoimmunity. *FEBS Lett.* 2008;582:3711–3718.
157. Karman J, et al. Reducing glycosphingolipid biosynthesis in airway cells partially ameliorates disease manifestations in a mouse model of asthma. *Int Immunol.* 2010;22:593–603.
158. Shalaby KH, Martin JG. Overview of asthma; the place of the T cell. *Curr Opin Pharmacol.* 2010;10:218–225.
159. Lloyd CM, Hessel EM. Functions of T cells in asthma: more than just T(H)2 cells. *Nat Rev Immunol.* 2010;10:838–848.
160. Zhu Y, et al. Lowering glycosphingolipid levels in CD4+ T cells attenuates T cell receptor signaling, cytokine production, and differentiation to the Th17 lineage. *J Biol Chem.* 2011;286:14787–14794.
161. Rahman A, Isenberg DA. Systemic lupus erythematosus. *N Engl J Med.* 2008;358:929–939.
162. Tsokos GC. Systemic lupus erythematosus. *N Engl J Med.* 2011;365:2110–2121.
163. Jury EC, Kabouridis PS, Flores-Borja F, Mageed RA, Isenberg DA. Altered lipid raft-associated signaling and ganglioside expression in T lymphocytes from patients with systemic lupus erythematosus. *J Clin Invest.* 2004;113:1176–1187.

164. Krishnan S, et al. Alterations in lipid raft composition and dynamics contribute to abnormal T cell responses in systemic lupus erythematosus. *J Immunol.* 2004;172:7821–7831.
165. McDonald G, et al. Normalizing glycosphingolipids restores function in CD4+ T cells from lupus patients. *J Clin Invest.* 2014;124:712–724.
166. Tani-ichi S, et al. Structure and function of lipid rafts in human activated T cells. *Int Immunol.* 2005;17:749–758.
167. Tuosto L, et al. Organization of plasma membrane functional rafts upon T cell activation. *Eur J Immunol.* 2001;31:345–349.
168. Degroote S, Wolthoorn J, van Meer G. The cell biology of glycosphingolipids. *Semin Cell Dev Biol.* 2004;15:375–387.
169. Kidani Y, Bensinger SJ. Lipids rule: resetting lipid metabolism restores T cell function in systemic lupus erythematosus. *J Clin Invest.* 2014;124:482–485.
170. McInnes IB, Schett G. The pathogenesis of rheumatoid arthritis. *N Engl J Med.* 2011;365:2205–2219.
171. Gizinski AM, Fox DA. T cell subsets and their role in the pathogenesis of rheumatic disease. *Curr Opin Rheumatol.* 2014;26:204–210.
172. Kobezda T, Ghassemi-Nejad S, Mikecz K, Glant TT, Szekanecz Z. Of mice and men: how animal models advance our understanding of T-cell function in RA. *Nat Rev Rheumatol.* 2014;10:160–170.
173. Tsukuda Y, et al. Ganglioside GM3 has an essential role in the pathogenesis and progression of rheumatoid arthritis. *PLoS One.* 2012;7:e40136.
174. Farukhi F, Dakkouri C, Wang H, Wiznitzer M, Traboulsi EI. Etiology of vision loss in ganglioside GM3 synthase deficiency. *Ophthalmic Genet.* 2006;27:89–91.
175. Simpson MA, et al. Infantile-onset symptomatic epilepsy syndrome caused by a homozygous loss-of-function mutation of GM3 synthase. *Nat Genet.* 2004;36:1225–1229.
176. Fragaki K, et al. Refractory epilepsy and mitochondrial dysfunction due to GM3 synthase deficiency. *Eur J Hum Genet.* 2013;21:528–534.
177. Lee JS, et al. GM3 synthase deficiency due to ST3GAL5 variants in two Korean female siblings: Masquerading as Rett syndrome-like phenotype. *Am J Med Genet A.* 2016;170:2200–2205.
178. Boccutto L, et al. A mutation in a ganglioside biosynthetic enzyme, ST3GAL5, results in salt & pepper syndrome, a neurocutaneous disorder with altered glycolipid and glycoprotein glycosylation. *Hum Mol Genet.* 2014;23:418–433.
179. Wang H, Bright A, Xin B, Bockoven JR, Paller AS. Cutaneous dyspigmentation in patients with ganglioside GM3 synthase deficiency. *Am J Med Genet A.* 2013;161A:875–879.
180. Wang H, et al. Early growth and development impairments in patients with ganglioside GM3 synthase deficiency. *Clin Genet.* 2016;89:625–629.
181. Yoshikawa M, et al. Ganglioside GM3 is essential for the structural integrity and function of cochlear hair cells. *Hum Mol Genet.* 2015;24:2796–2807.
182. Yoshikawa M, et al. Mice lacking ganglioside GM3 synthase exhibit complete hearing loss due to selective degeneration of the organ of Corti. *Proc Natl Acad Sci USA.* 2009;106:9483–9488.
183. Luft JH. Ruthenium red and violet. II. Fine structural localization in animal tissues. *Anat Rec.* 1971;171:369–415.
184. de Groot JC, Hendriksen EG, Smoorenburg GF. Reduced expression of sialoglycoconjugates in the outer hair cell glycocalyx after systemic aminoglycoside administration. *Hear Res.* 2005;205:68–82.
185. Takumida M, Wersall J, Bagger-Sjoberg D, Harada Y. Observation of the glycocalyx of the organ of Corti: an investigation by electron microscopy in the normal and gentamicin-treated guinea pig. *J Laryngol Otol.* 1989;103:133–136.

186. Manor U, Kachar B. Dynamic length regulation of sensory stereocilia. *Semin Cell Dev Biol.* 2008;19:502–510.
187. Wright MB, Hugo C, Seifert R, Distèche CM, Bowen-Pope DF. Proliferating and migrating mesangial cells responding to injury express a novel receptor protein-tyrosine phosphatase in experimental mesangial proliferative glomerulonephritis. *J Biol Chem.* 1998;273:23929–23937.
188. Oganessian A, et al. Protein tyrosine phosphatase RQ is a phosphatidylinositol phosphatase that can regulate cell survival and proliferation. *Proc Natl Acad Sci USA.* 2003;100:7563–7568.
189. Nambiar R, McConnell RE, Tyska MJ. Myosin motor function: the ins and outs of actin-based membrane protrusions. *Cell Mol Life Sci.* 2010;67:1239–1254.
190. Sakaguchi H, et al. Dynamic compartmentalization of protein tyrosine phosphatase receptor Q at the proximal end of stereocilia: implication of myosin VI-based transport. *Cell Motil Cytoskeleton.* 2008;65:528–538.
191. Hertzano R, et al. A Myo6 mutation destroys coordination between the myosin heads, revealing new functions of myosin VI in the stereocilia of mammalian inner ear hair cells. *PLoS Genet.* 2008;4:e1000207.
192. Self T, et al. Role of myosin VI in the differentiation of cochlear hair cells. *Dev Biol.* 1999;214:331–341.
193. Zhao H, Williams DE, Shin JB, Brugger B, Gillespie PG. Large membrane domains in hair bundles specify spatially constricted radixin activation. *J Neurosci.* 2012;32:4600–4609.
194. Oshima K, et al. Mechanosensitive hair cell-like cells from embryonic and induced pluripotent stem cells. *Cell.* 2010;141:704–716.
195. Inokuchi J, Kabayama K. Modulation of growth factor receptors in membrane microdomains. *Trends in Glycosci Glycotech.* 2008;20:353–371.



Supplemental Material can be found at:
<http://www.jlr.org/content/suppl/2018/06/07/jlr.M085753.DC1.html>

Deficient ganglioside synthesis restores responsiveness to leptin and melanocortin signaling in obese KKAY mice[§]

Kei-ichiro Inamori,* Hideki Ito,* Yumi Tamura,* Takahiro Nitta,* Xiaohua Yang,* Wataru Nihei,* Fumi Shishido,* Susumu Imazu,[†] Sohei Tsukita,[§] Tetsuya Yamada,[§] Hideki Katagiri,[§] and Jin-ichi Inokuchi^{1,*}

Division of Glycopathology,* Institute of Molecular Biomembrane and Glycobiology, Tohoku Medical and Pharmaceutical University, Sendai, Miyagi 981-8558, Japan; Nippon Boehringer Ingelheim Company, Ltd.,[†] Shinagawa-Ku, Tokyo 141-6017, Japan; and Department of Metabolism and Diabetes,[§] Tohoku University Graduate School of Medicine, Sendai, Miyagi 980-8575, Japan

Abstract GM3, a precursor for synthesis of a- and b-series gangliosides, is elevated in adipocytes of obese model animals and in sera of obese human patients with type 2 diabetes and/or dyslipidemia. GM3 synthase (GM3S)-KO C57BL/6 mice display enhanced insulin sensitivity and reduced development of high-fat diet-induced insulin resistance. However, the pathophysiological roles of GM3 and related gangliosides in the central control of feeding and metabolism remain unclear. We found that a mouse model (KKAY GM3S KO) generated by KO of the *GM3S* gene in the yellow obese strain, KKAY, displayed significant amelioration of obese phenotype. Whereas KKAY mice were hyperphagic and developed severe obesity, KKAY GM3S KO mice had significantly lower body weight and food intake, and greater glucose and insulin tolerance. The hypothalamic response to intraperitoneal administration of leptin was greatly reduced in KKAY mice, but was retained in KKAY GM3S KO mice. In studies of a cultured mouse hypothalamic neuronal cell line, enhanced leptin-dependent phosphorylation of ERK was observed in GM3S-deficient cells. Furthermore, KKAY GM3S KO mice did show altered coat color, suggesting that GM3S is also involved in melanocortin signaling. Our findings, taken together, indicate that GM3-related gangliosides play key roles in leptin and melanocortin signaling.—Inamori, K-i., H. Ito, Y. Tamura, T. Nitta, X. Yang, W. Nihei, F. Shishido, S. Imazu, S. Tsukita, T. Yamada, H. Katagiri, and J-i. Inokuchi. Deficient ganglioside synthesis restores responsiveness to leptin and melanocortin signaling in obese KKAY mice. *J. Lipid Res.* 2018. 59: 1472–1481.

Supplementary key words animal models • diabetes • brain • receptors/hormone • GM3 • hypothalamus • leptin resistance • GM3 synthase knockout

This study was supported by Ministry of Education, Culture, Sports, Science and Technology Grants-in-Aid for Scientific Research 26440061 (K-i.I.); and 16H04767 (J-i.I.), the Uehara Memorial Foundation (K-i.I.), the Kato Memorial Bioscience Foundation (K-i.I.), the Novartis Foundation (Japan) for the Promotion of Science (K-i.I.), and the Suzuken Memorial Foundation (K-i.I.).

Manuscript received 5 April 2018 and in revised form 22 May 2018.

Published, JLR Papers in Press, June 7, 2018
DOI <https://doi.org/10.1194/jlr.M085753>

Gangliosides [glycosphingolipids (GSLs) that contain sialic acid] are key components of membrane microdomains, where they participate in a variety of biological processes, including cell growth, adhesion, and signal transduction (1). GM3, a precursor molecule in synthesis of a- and b-series gangliosides, shows increased levels in association with obesity, inflammation, and certain metabolic diseases (2–4). GM3 synthase (GM3S)-null mice display enhanced insulin sensitivity and reduced development of high-fat diet (HFD)-induced insulin resistance and chronic low-grade inflammatory states (4, 5). Our group observed associations between numerous metabolic disease risk factors and GM3 molecular species in human serum (6).

The mediobasal hypothalamus, which includes the arcuate nucleus (ARC) and paraventricular nucleus (PVH), plays essential roles in control of feeding, body weight, and energy expenditure. ARC contains two interconnected groups of neurons; one is orexigenic (appetite-stimulating) and releases agouti-related peptide (AgRP) and neuropeptide Y (NPY), while the other is anorexigenic (appetite-suppressing) and releases α -melanocyte-stimulating hormone (α -MSH) produced from proopiomelanocortin (POMC) precursors. α -MSH binds to melanocortin receptor 4 (MC4R) in PVH and other hypothalamic areas, and exerts anorectic effects. NPY binds to its cognate receptor, stimulates feeding, and reduces basal energy expenditure. AgRP acts on MC4R as an inverse agonist and inhibits α -MSH (7). AgRP/NPY neurons and POMC neurons thus regulate

Abbreviations: AgRP, agouti-related peptide; ARC, arcuate nucleus; ASP, agouti signaling protein; α -MSH, α -melanocyte-stimulating hormone; GM3S, GM3 synthase; GSL, glycosphingolipid; HFD, high-fat diet; JAK2-STAT3, Janus-activated kinase 2/signal transducers and activators of transcription 3; LepRb, leptin receptor long form; MC1R, melanocortin receptor 1; MC4R, melanocortin receptor 4; NPY, neuropeptide Y; POMC, proopiomelanocortin; PVH, paraventricular nucleus; TG, triglyceride.

¹To whom correspondence should be addressed.

e-mail: jin@tohoku-mpu.ac.jp

[§]The online version of this article (available at <http://www.jlr.org>) contains a supplement.

Copyright © 2018 Inamori et al. Published under exclusive license by The American Society for Biochemistry and Molecular Biology, Inc.

This article is available online at <http://www.jlr.org>

melanocortin signaling in a coordinated manner to maintain energy balance.

Leptin, an adipocyte-derived circulating hormone whose expression is correlated with adipose mass, is essential for maintenance of energy homeostasis and body weight. Increased levels of leptin lead to reduction of food intake and body weight through the long form of its receptor, LepRb (8), which is highly expressed in ARC, ventromedial hypothalamic nucleus, and other hypothalamic nuclei. LepRb is expressed in both AgRP/NPY neurons and POMC neurons. Leptin inhibits AgRP neuronal activity and NPY and AgRP expression in AgRP/NPY neurons, and stimulates POMC synthesis in POMC neurons (9).

Diet-induced obesity leads to a state of low-grade inflammation in peripheral insulin target tissues that is associated with development of insulin resistance and type 2 diabetes (10). Diet-induced activation of inflammatory pathways in the mediobasal hypothalamus has been reported (11). There is increasing evidence for an association between hypothalamic inflammation and development of leptin resistance and obesity (12), but the detailed molecular basis for such an association is unclear.

An obese diabetic mouse model, KKAY, was established by introducing *A^y* mutation into strain KK, resulting in ectopic expression of agouti signaling protein (ASP), which is homologous to AgRP. ASP acts as an antagonist at the melanocortin 1 receptor (MC1R) on hair follicular melanocytes to block α -MSH-induced eumelanin production, resulting in the subterminal band of pheomelanin (13). In the KKAY mouse, it is believed that the ectopic expression of ASP causes obesity due to disruption of melanocortin signaling outside the hair follicle. Onset of obesity and diabetic pathology appear earlier and are more severe in KKAY mice than in KK mice (14, 15). We and Proia's group observed previously that body weight following a HFD feeding regime did not differ significantly between GM3S-null C57BL/6 mice and WT mice (4, 5). In the present study, we generated GM3S-null mice in a KKAY genetic background (KKAY GM3S KO) to evaluate the pathophysiological roles of GM3 and related gangliosides in obesity. KKAY mice are hyperphagic and typically develop leptin resistance and morbid obesity. In contrast, KKAY GM3S KO mice were less likely to develop leptin resistance and had significantly lower body weight and food intake, comparable to values in control KK mice. The coat color was grayish in homozygous KKAY GM3S KO mice, but yellow in heterozygotes (similar to KKAY mice), suggesting that GM3 is involved in melanin synthesis, possibly through MC1R signaling. Our findings indicate that GM3 and/or related ganglioside species play an essential role in leptin and melanocortin signaling.

MATERIALS AND METHODS

Reagents

Phospho-STAT3 (Tyr705, D3A7), STAT3 (79D7), ERK1/2, and c-fos antibodies were from Cell Signaling Technology (Beverly,

MA). Phospho-ERK (E-4) antibody was from Santa Cruz Biotechnology (Santa Cruz, CA). Recombinant mouse leptin was from R&D Systems (Minneapolis, MN).

Generation of GM3S-deficient mice in KK/KKAY background

KK (*a/a*) and KKAY (*A^y/a*) mice were from CLEA Japan. GM3S (*St3gal5*)-deficient mice were generated from C57BL/6 mice as described previously (16). These mice were backcrossed over eight times into the KK background, and KK/GM3S^{+/-} or KK/GM3S^{-/-} females were crossed with KKAY males to obtain KKAY/GM3S^{+/-} mice. Genotyping for the *a/A^y* alleles was performed by PCR of ear DNA using primers 5'-GGCCACACTTAGGGAGTTCA-3' (forward primer for *a* 'nonagouti' and *A^y* 'lethal yellow' alleles), 5'-TGCCTTATTCTGTTTTTGTTC-3' (reverse primer for *a* allele), and 5'-GGTTGGCCACCATGTCTAGT-3' (reverse primer for *A^y* allele), according to the Jackson Laboratory website (KK, Cg-*A^y*/J 002468). Genotyping PCR for the GM3S gene was performed using the following primers: 5'-GGAATCCATCCCTTTCTCACAGAG-3' and 5'-TGAACCTCACTTGGCATTGCTGG-3' for WT allele, and 5'-ACTGGGCACAACAGACAATCGG-3' and 5'-TG-GATACTTTCTCGGCAGGAGC-3' for the KO allele (17). KK and KKAY mice with WT GM3S alleles were used as control for each experiment. Body weight and food consumption were measured once per week.

GSL analysis

Lyophilized brain tissue was extracted with chloroform/methanol 2:1, 1:1, 1:2 (v/v), in succession. Total lipids were purified, separated into acidic and neutral fractions, deesterified by methanolysis, and analyzed by HPTLC as described previously (18).

RNA isolation, reverse transcription, and quantitative PCR

Total RNA was extracted using the RNeasy Lipid Tissue Mini kit (Qiagen). cDNA was generated from 500 ng of RNA, and quantitative PCR was performed on a StepOnePlus real-time PCR system (Applied Biosystems) using SYBR Premix Ex Taq II (TaKaRa Shuzo, Kyoto, Japan). Relative mRNA levels were calculated either by a standard curve and normalized to peptidylprolyl isomerase B (*Ppib*) expression or as 2^{- $\Delta\Delta$ CT} with glyceraldehyde-3-phosphate dehydrogenase.

Glucose and insulin tolerance tests

Mice were either fasted for 16 h and administered glucose solution (1.5 g/kg body weight) orally or fasted for 6 h and injected intraperitoneally with insulin solution (0.75 U/kg body weight). Glucose levels in blood (from tail vein) at various time points before and after these treatments were measured with an Accu-Chek Aviva glucometer (Roche Applied Science).

Plasma parameters

Plasma levels of triglycerides (TGs), NEFAs, total cholesterol, and HDL cholesterol were determined using (respectively) the Triglyceride E-test kit, the NEFA C-test kit, the Cholesterol E-test kit, and the HDL-Cholesterol E-test kit (Wako Pure Chemical, Japan). Serum insulin and leptin levels were determined using ELISA kits (Morinaga Institute of Biological Science, Yokohama, Japan).

Generation of GM3S-deficient N41 cells

Exon 5 of the mouse *St3gal5* (GM3S) gene, which contains the coding sequence for sialyl motif L, was chosen to design targeting guide RNAs using the online CRISPR Design Tool (19). A primer pair (5'-CACCGCAGGTACGCGAAGACGGCTA-3' and 5'-AAAC-TAGCCGCTTCGCGTACCTGC-3') was cloned into plasmid

pSpCas9(BB)-2A-GFP (Addgene; #48138). The plasmid was introduced into embryonic mouse hypothalamic N41 cells (CELLutions Biosystems, Ontario, Canada) using a Nucleofector device with Cell Line Nucleofector Kit V (Amaxa), as per the manufacturer's protocol. The above plasmid without targeting sequence served as control. GFP+ cells were isolated using a FACSAria II flow cytometer (BD Biosciences); clonal cell lines were obtained by limiting dilution; and expression levels of gangliosides were evaluated by TLC.

Leptin administration and immunohistochemistry

Intraperitoneal injection of leptin and immunohistochemical detection of c-fos protein were performed as described previously (20, 21). In brief, mice were fasted for 24 h, intraperitoneally injected with either leptin (4 mg/kg body weight) or saline, anesthetized 2 h later with pentobarbital, and perfused transcardially with saline followed by 4% paraformaldehyde in PBS. Brains were removed, postfixed in the same fixative overnight, embedded in OCT compound (Sakura Finetek, Tokyo, Japan), frozen, and sectioned coronally (thickness 40 μ m). Floating sections were pretreated for 10 min with 3% hydrogen peroxide, blocked with 3% BSA for 1 h, incubated in c-fos antibody (dilution 1:2,000) for 72 h at 4°C, washed, incubated with Simple Stain MAX-PO (Nichirei Biosciences, Tokyo, Japan) for 1 h, washed, incubated in 0.05% DAB solution for 10 min (for visualization of c-fos protein), stained with hematoxylin, dehydrated, and mounted on coverslips. The c-fos-positive cells in ARC were counted at regular intervals in three sections for each animal.

Lentiviral construct and establishment of stably LepRb-expressing cells

To generate a lentiviral construct for stable expression of full-length mouse leptin receptor (mLepRb), a 3.5 kb mLepRb cDNA fragment was subcloned into CSII-EF-RfA vector (developed by Dr. H. Miyoshi, Keio University, Tokyo, Japan and provided by RIKEN BioResource Research Center, Tsukuba, Japan). HEK293T cells cultured in DMEM supplemented with 10% FBS were transfected with mLepRb/CSII-EF-RfA, pCAG-HIVgp, and pCMV-VSV-G-RSV-Rev plasmids using Lipofectamine 2000 (Invitrogen), and incubated for 24 h at 37°C. Medium was replaced by fresh medium containing 10 μ M forskolin, and cells were cultured for another 24 h at 32°C. Lentivirus-containing supernatant was harvested by centrifugation at 200 *g* for 3 min. For lentiviral transduction of cultured N41 cells, the supernatant was added; the cells were incubated for 24 h at 32°C; the temperature was increased to 37°C; the incubation was continued for 48 h; the medium was replaced; and the culture was continued for 1 week prior to experiments. Cells established by this procedure were designated as N41-LepRb cells.

Leptin treatment of N41 cells and immunoblotting

Phosphorylation assays of ERK and STAT3 were performed using N41 and N41-LepRb cells, respectively. Near-confluent cells were washed twice with DMEM, incubated for 2 h with DMEM containing 0.5% FBS, stimulated for various durations with 0.5 μ g/ml leptin, washed twice with ice-cold PBS, lysed, and analyzed by Western blotting with appropriate antibodies, as described previously (2).

Statistical analysis

Data were analyzed by Student's *t*-test and ANOVA followed by Tukey's post hoc test, using the GraphPad Prism software program.

RESULTS

Mouse strain KKAY was established in 1969 by *A*^Y mutation of strain KK, resulting in ectopic expression of ASP

and associated hyperphagia, obesity, and hyperglycemia (22). To investigate the roles of GM3 and/or related gangliosides in the pathogenesis of obesity, we knocked out the GM3S gene in KKAY to generate strain KKAY GM3S KO. These mice showed notable amelioration of obese phenotype in terms of reduced body weight, daily food intake, and blood glucose level (Fig. 1A–C). mRNA expression levels of *ASP*, *Pomc*, and *Mc4r* did not differ significantly in the hypothalami of KKAY versus KKAY GM3S KO mice (Fig. 1D). The coat color was grayish for KKAY GM3S KO homozygotes, but yellow (similar to KKAY) for heterozygotes (Fig. 1E). The *a/A*^Y genotype was confirmed by genotyping PCR (Fig. 1F) and it was found that whereas all the KKAY *GM3S*^{+/+} or *GM3S*^{+/-} mice had yellow coat color, only 6.1% of KKAY *GM3S*^{-/-} mice had yellow and all of the rest had gray coat color. Brain ganglioside expression patterns for KKAY GM3S KO were similar to those reported previously for GM3S-deficient mice in a C57BL/6 background (5, 17). Brains of KKAY GM3S KO animals lacked a- and b-series gangliosides (GM1, GD1a, GD1b, and GT1b), the major ganglioside species in WT brain; rather, they expressed predominantly o-series gangliosides, such as GM1b and GD1 α (Fig. 1H, I).

At age 14 weeks, the glucose tolerance of KKAY GM3S KO mice was significantly greater than that of KKAY mice (Fig. 2A). Even in the KK background, GM3S KO mice showed a slight improvement of glucose tolerance at age 24 weeks (Fig. 2B), similarly to our previous findings for HFD-fed C57BL/6 GM3S KO mice (4). KKAY GM3S KO mice also showed greatly increased insulin tolerance at age 24 weeks (Fig. 2C), and reduced expression levels of the gluconeogenesis genes, *G6pc* and *Pepck*, in liver (Fig. 2D). Plasma insulin levels at ages 16 and 24 weeks were low in KKAY mice, but significantly higher in KKAY GM3S KO mice, probably due to preserved insulin secretion (Fig. 3A). Plasma TG and non-HDL cholesterol levels at ages 10 and 16 weeks in KKAY mice were higher than in KK mice, while these levels in KKAY GM3S KO mice were lower than in KKAY mice (similar to those in KK) (Fig. 3B, D). Plasma leptin levels at age 8 weeks in KKAY GM3S KO mice were significantly higher than in KKAY mice (Fig. 3E). HDL cholesterol and NEFA levels did not differ notably between KKAY and KKAY GM3S KO mice (Fig. 3C, F).

KKAY mice develop obesity (associated with hyperglycemia and hyperinsulinemia), hyperleptinemia, and leptin resistance (23). We examined possible changes in central responsiveness to leptin in KKAY GM3S KO mice. In KKAY mice, intraperitoneal injection of leptin had only a slight effect on neuron activation, as assayed by c-fos expression in ARC (Fig. 4A), supporting the concept that development of obesity in these mice induces increased leptin resistance. In contrast, injection of leptin in KKAY GM3S KO mice caused a notable increase of c-fos expression (Fig. 4A, B), indicating that responsiveness to leptin is maintained in these mice.

To examine the possible effects of loss of GM3S activity on leptin receptor signaling, we established a GM3S-deficient mutant of mouse hypothalamic neuronal N41 cells. We used the CRISPR/Cas9 system to target exon 5,

Supplemental Material can be found at:
<http://www.jlr.org/content/suppl/2018/06/07/jlr.M085753.DC1.html>

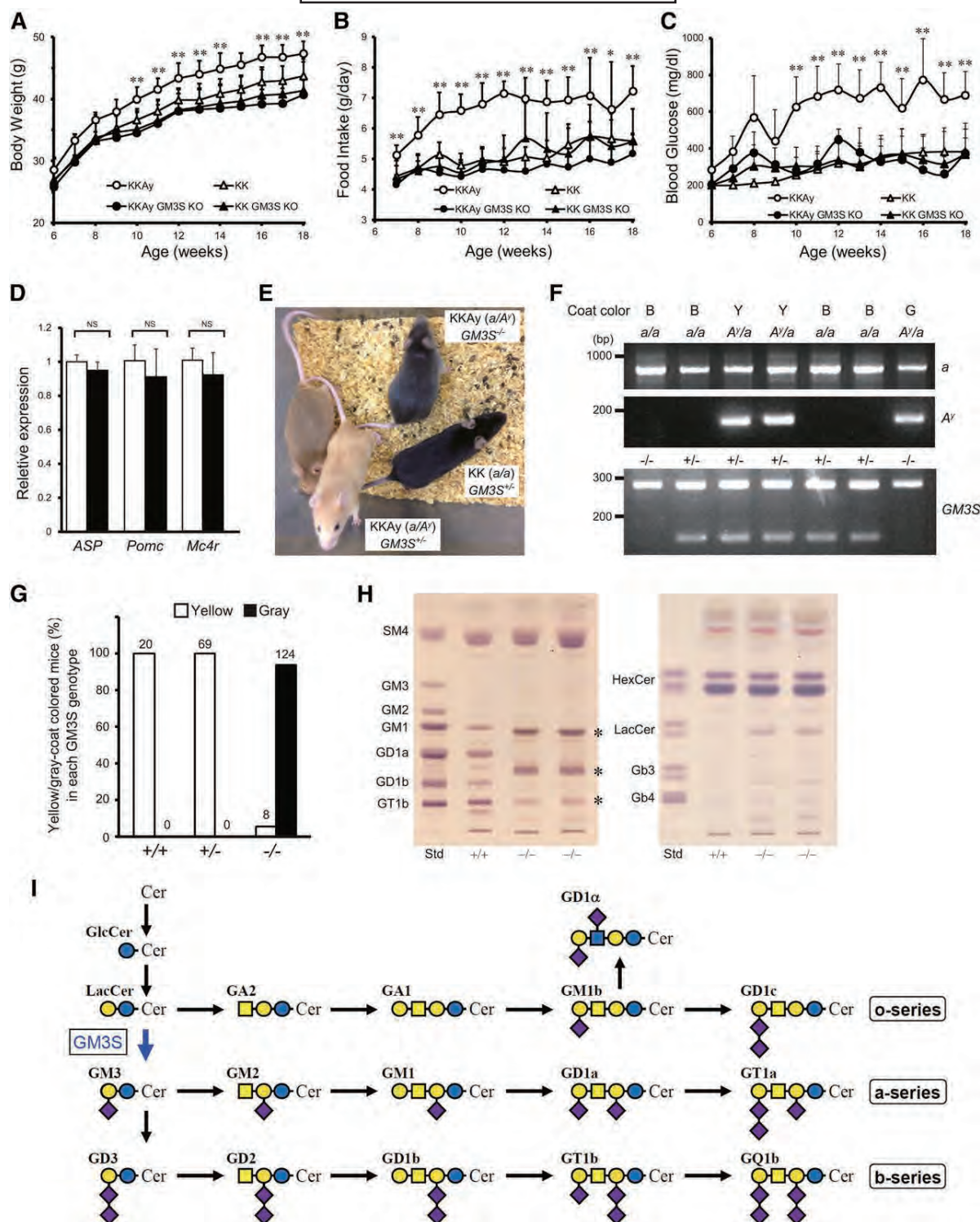


Fig. 1. *GM3S* KO prevented development of hyperphagia and obesity in KKAY mice. A–C: Body weight (A), food intake (B), and nonfasting blood glucose levels (C) of KKAY and KK mice with or without deletion of the *GM3S* gene (*GM3S* KO) ($n \geq 5$ for each group). * $P < 0.05$, ** $P < 0.01$ versus KKAY *GM3S* KO. D: Quantitative RT-PCR analysis of mRNA for *ASP*, *Pomc*, and *Mc4r* in KKAY and KKAY *GM3S* KO hypothalami. White bar, KKAY; black bar, KKAY *GM3S* KO ($n = 3$ for each group). * $P < 0.05$, ** $P < 0.01$ versus KKAY *GM3S* KO. E: Coat color phenotype of *GM3S* KO (*GM3S*^{-/-}) observed in the KKAY (*a/a'*) background. F: Representative genotyping PCR results for KKAY *GM3S* KO mice. Top panel: Genotyping results for the *a/a'* allele. The *a* and *A'* alleles generate PCR products of 839 bp and 163 bp, respectively. Coat color: B, black; Y, yellow; G, gray. Bottom panel: Genotyping results for *GM3S* KO. The WT and mutant alleles generate PCR products of 276 bp and 120 bp, respectively. G: The percentage of yellow- or gray-coat-colored offspring compared with the total number of *A'/a* offspring born with each *GM3S* genotype. The number of each group is indicated on the top of each bar. Because of the infertility of KKAY females, KKAY males (*A'/a*, *GM3S*^{+/-} or ^{-/-}) and KK females (*a/a*, *GM3S*^{+/-} or ^{-/-}) were used for breeding. Data of the *a/a* offspring (black coat

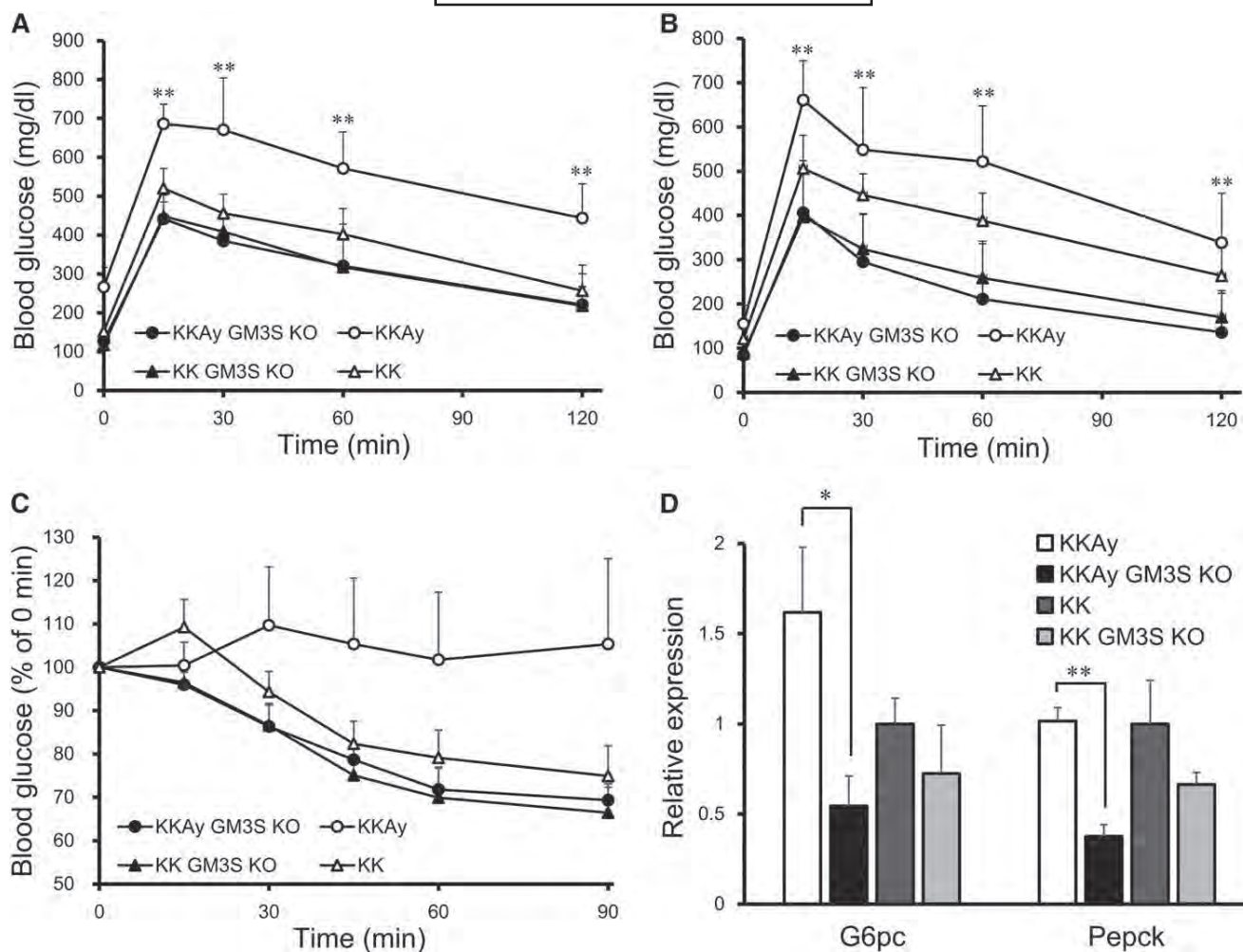


Fig. 2. GM3S KO-enhanced glucose and insulin tolerance in KKAY mice. A, B: Glucose tolerance tests at age 14 weeks (A) and 24 weeks (B). C: Insulin tolerance tests at age 24 weeks. D: Quantitative analysis of mRNA for *G6pc* and *Pepck* in liver at age 24 week ($n \geq 4$ for each group). * $P < 0.05$, ** $P < 0.01$ vs. KKAY GM3S KO.

which contains sialyl motif L, a conserved sequence motif essential for catalytic activity of mammalian sialyltransferases (24). GSL analysis showed that several obtained clones lacked GM3 and related gangliosides (Fig. 5A, left), but contained LacCer (Fig. 5A, right). A major GM1-like band (Fig. 5A, left) was found to be GM1 by LC/MS/MS multiple reaction monitoring (supplemental data), and most likely GM1b, an o-series ganglioside also observed in KKAY GM3S KO brain (Fig. 1D). *LepRb* is highly expressed in the mediobasal hypothalamus and mediates anti-obesity signaling by leptin via the Janus-activated kinase 2/signal transducers and activators of transcription 3 (JAK2-STAT3) pathway. The hypothalamic ERK pathway plays a key role in mediating control of food intake and thermogenesis by leptin (25). Leptin, at a concentration 0.5 $\mu\text{g/ml}$, greatly enhanced ERK phosphorylation in GM3S-deficient N41

cells (Fig. 5B). In contrast, we could not detect STAT3 phosphorylation by leptin, even at 1 $\mu\text{g/ml}$, in either parental or GM3S-deficient N41 cells (data not shown). To evaluate leptin-induced phosphorylation of STAT3, we established stable expression of *LepRb* by lentiviral transfer of the mouse *LepRb* gene. *LepRb*-expressing cells responded to leptin at 0.5 $\mu\text{g/ml}$, and STAT3 phosphorylation was slightly reduced in GM3S-deficient cells (Fig. 5C). These findings indicate that the leptin-dependent ERK pathway was enhanced by deficient ganglioside synthesis in KKAY GM3S KO.

The observed coat color change and reduction of food intake and body weight in KKAY GM3S KO mice suggested that GM3 and related gangliosides play an important role in melanocortin receptor signaling. We examined possible effects of GM3 deficiency on MC4R signaling in HEK293T

color) were excluded. H: TLC of acidic (left) and neutral (right) GSLs from KKAY (+/+) and KKAY GM3S KO (-/-) brains. GSLs were detected using orcinol-sulfuric acid reagent. The asterisks indicate o-series gangliosides whose biosynthesis is independent of GM3 [see text and references (5) and (17) for details]. (I): Biosynthetic pathway of ganglio-series gangliosides. GM3S is a sialyltransferase required for initiation of synthesis of a- and b-series gangliosides.

Supplemental Material can be found at:
<http://www.jlr.org/content/suppl/2018/06/07/jlr.M085753.DC1.html>

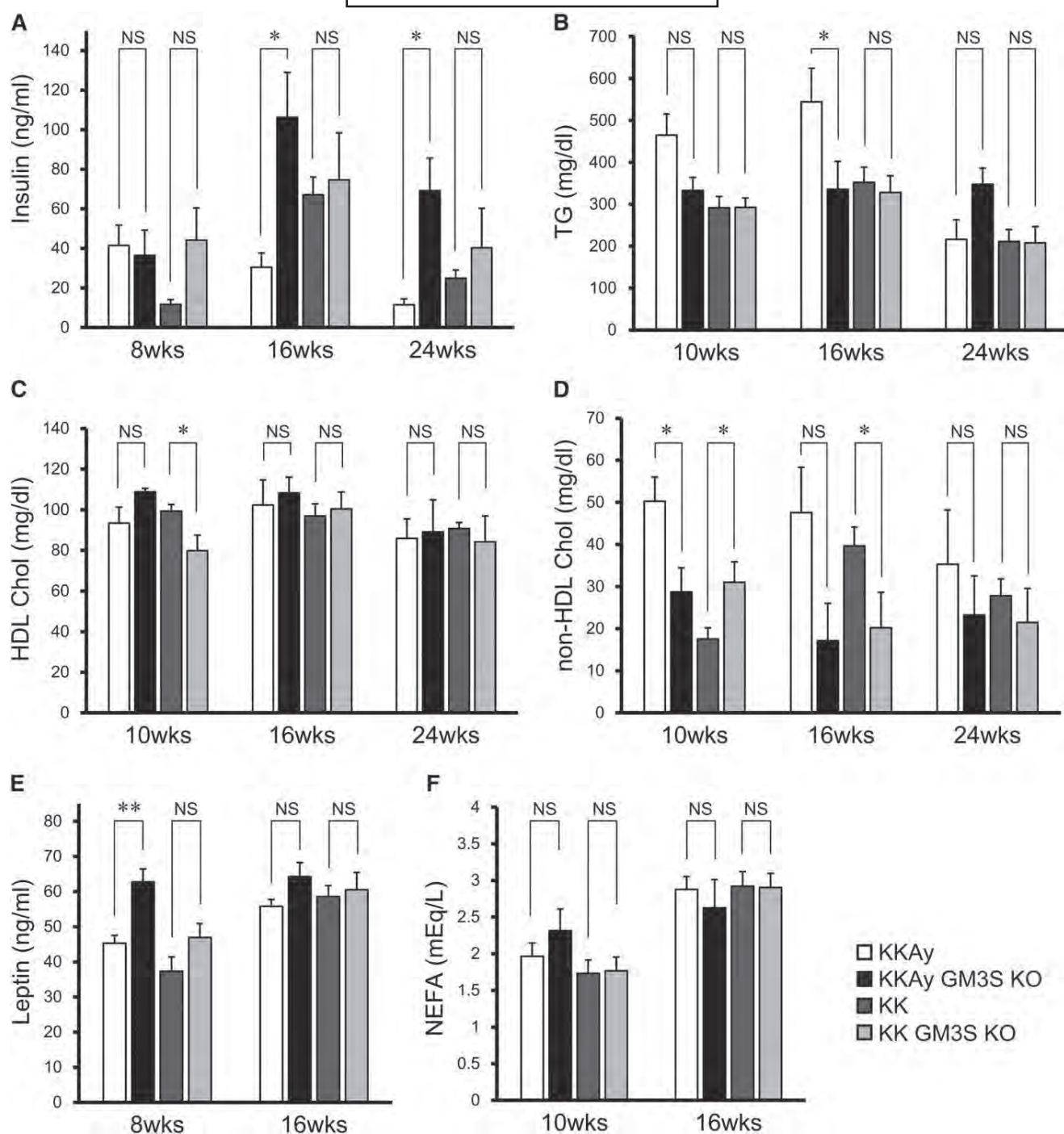


Fig. 3. Blood parameters in KKAY GM3S KO and control mice. Blood plasma or serum samples were collected from mice fed ad libitum at the indicated times. Insulin (A), TG (B), HDL cholesterol (HDL Chol) (C), non-HDL Chol (D), leptin (E), and NEFAs (F) ($n \geq 4$ for each group). * $P < 0.05$, ** $P < 0.01$.

cells. Parental and GM3-deficient cells were transfected with the mouse *Mchr* gene; intracellular cAMP production was evaluated; and G protein-coupled receptor activation was assayed by TGF- α shedding assay, as described previously (26), using α -MSH with or without synthetic mouse AgRP or ASP. No clear difference was observed between parental and GM3-deficient cells (data not shown; see Discussion).

DISCUSSION

Previous reports by our group and others have demonstrated the increased insulin sensitivity of GM3S KO mice in a C57BL/6 background relative to WT mice. KO mice developed HFD-induced obesity (as did WT mice), but exhibited reduced development of insulin resistance and chronic low-grade inflammatory states (4, 5). In the

Supplemental Material can be found at:
<http://www.jlr.org/content/suppl/2018/06/07/jlr.M085753.DC1.html>

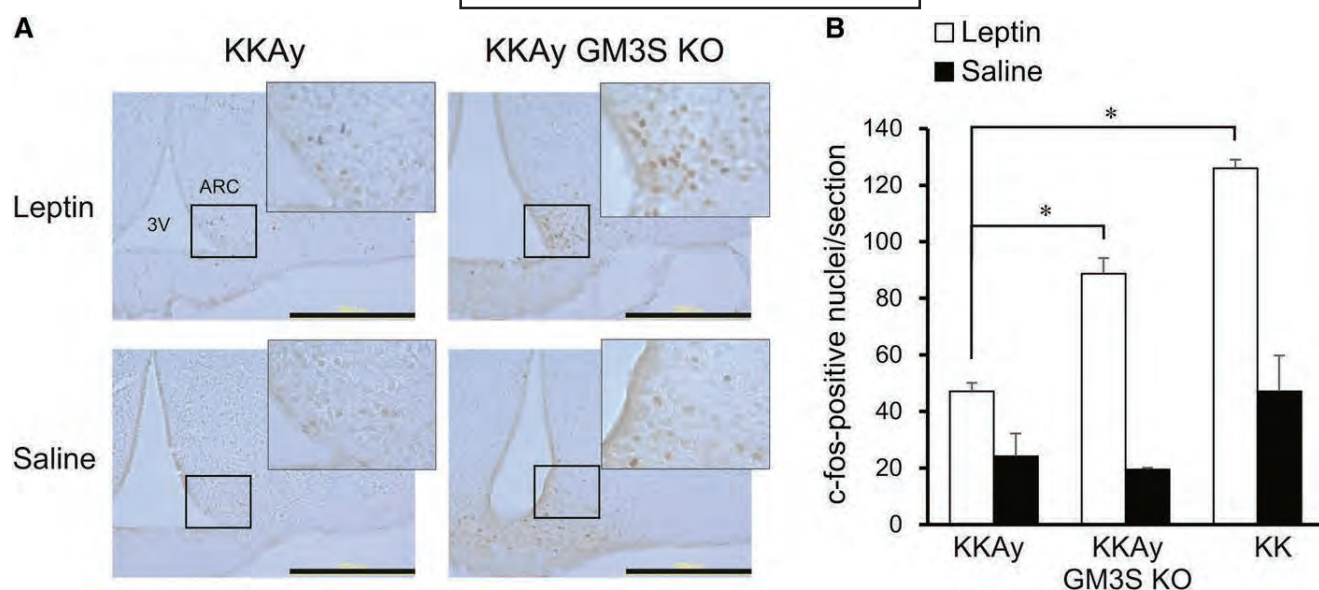


Fig. 4. KKAY GM3S KO mice retained leptin responsiveness in ARC. A: Representative images of basal (saline) and leptin-induced c-fos immunoreactivity in ARC of KKAY and KKAY GM3S KO mice (male, age 10 weeks). Fasted mice were injected intraperitoneally with either saline or leptin. ARC sections were stained with c-fos antibody. Scale bars: 300 μ m. B: The c-fos positive cells in ARC were counted (n = 3 for each group). * P < 0.05.

present study, we used a GM3S KO strain of obese mouse model KKAY to evaluate the pathophysiological effects of GM3 or related gangliosides in hyperphagic and obese phenotypes. The coat color was grayish in KKAY GM3S KO homozygotes, but yellow (similar to KKAY) in heterozygotes. The yellow A^y mutation (in the *agouti* gene) causes ectopic expression of the gene product, ASP, resulting in a switch of follicular melanocytes from synthesis of eumelanin (black) to pheomelanin (yellow) through inhibition of MC1R signaling as an endogenous antagonist, by blocking α -MSH (13). The observed coat color change of KKAY GM3S KO mice may suggest involvement of GM3/related gangliosides in MC1R signaling in melanocytes, possibly through direct effect on MC1R function (e.g., cell surface expression or α -MSH binding) or direct or indirect modulation of ASP binding to MC1R, although functional analysis will be required to establish this point. Mutations of the *GM3S* (*ST3GAL5*) gene were identified in patients with salt-and-pepper syndrome, an autosomal recessive neurocutaneous disorder characterized by altered skin pigmentation (27).

In contrast to the previous results from GM3S KO C57BL/6 mice, the obese model KKAY mice that have perturbed melanocortin signaling that thereby cause defects in the central control of feeding behavior, showed remarkable reductions of body weight and food intake by GM3S KO, suggesting that the anti-obese effects observed in the present study are mediated at least in part by the central defects in the synthesis of GM3/related gangliosides. Given that the reduced body weight and food intake in the KKAY GM3S KO mice were observed as early as 6 weeks of age, we believe that the food intake effects are central in origin. The observed food intake effects suggest that hypothalamic MC4R function may also be modulated by GM3/related gangliosides (Fig. 6, a schematic illustration of our current model). We used GM3-deficient HEK293T cells to

examine α -MSH-dependent MC4R activation in the presence/absence of ASP and AgRP. For this assay, we used commercially available synthetic mouse ASP(93-132)-NH₂ and AgRP(82-131)-NH₂, which are conserved Cys-rich C-terminal domains sufficient for melanocortin receptor antagonism (28). The synthetic ASP and AgRP both strongly inhibited MC4R activation, but the inhibitory effect did not differ notably in parental versus GM3S-deficient cells. (data not shown). However, we cannot exclude a possibility that the cell system may not reflect the conditions in neurons (e.g., intrinsic properties and ganglioside expression pattern) and thus, further investigation will be needed to conclude whether gangliosides are involved in the MC4R function.

Body weight and food intake were notably lower in KKAY GM3S KO mice than in KKAY mice, but no striking difference was observed between KK GM3S KO and KK mice (Fig. 1A, B). These findings suggest a function of GM3/related gangliosides in hyperphagia and obesity development, perhaps through altered ASP expression or function in KKAY mice. No significant changes were observed in *Asp*, *Pomc*, or *Mc4r* gene expression in KKAY GM3S KO hypothalamus at age 6 weeks (Fig. 1D).

In the leptin administration experiments, KKAY GM3S KO mice were less susceptible to central leptin resistance than were KKAY mice. In GM3S-deficient hypothalamic neuronal cells, leptin-dependent STAT3 phosphorylation was slightly reduced, whereas leptin-dependent ERK phosphorylation was greatly enhanced, suggesting differential roles of specific ganglioside(s) in LepRb signaling. Numerous studies have demonstrated an essential role of the JAK2-STAT3 pathway in the anorectic and metabolic effects of leptin. Leptin binding to LepRb activates JAK2, and JAK2 subsequently phosphorylates other Tyr residues within LepRb and JAK2 itself (29, 30). Phospho-Tyr¹¹³⁸ serves as a

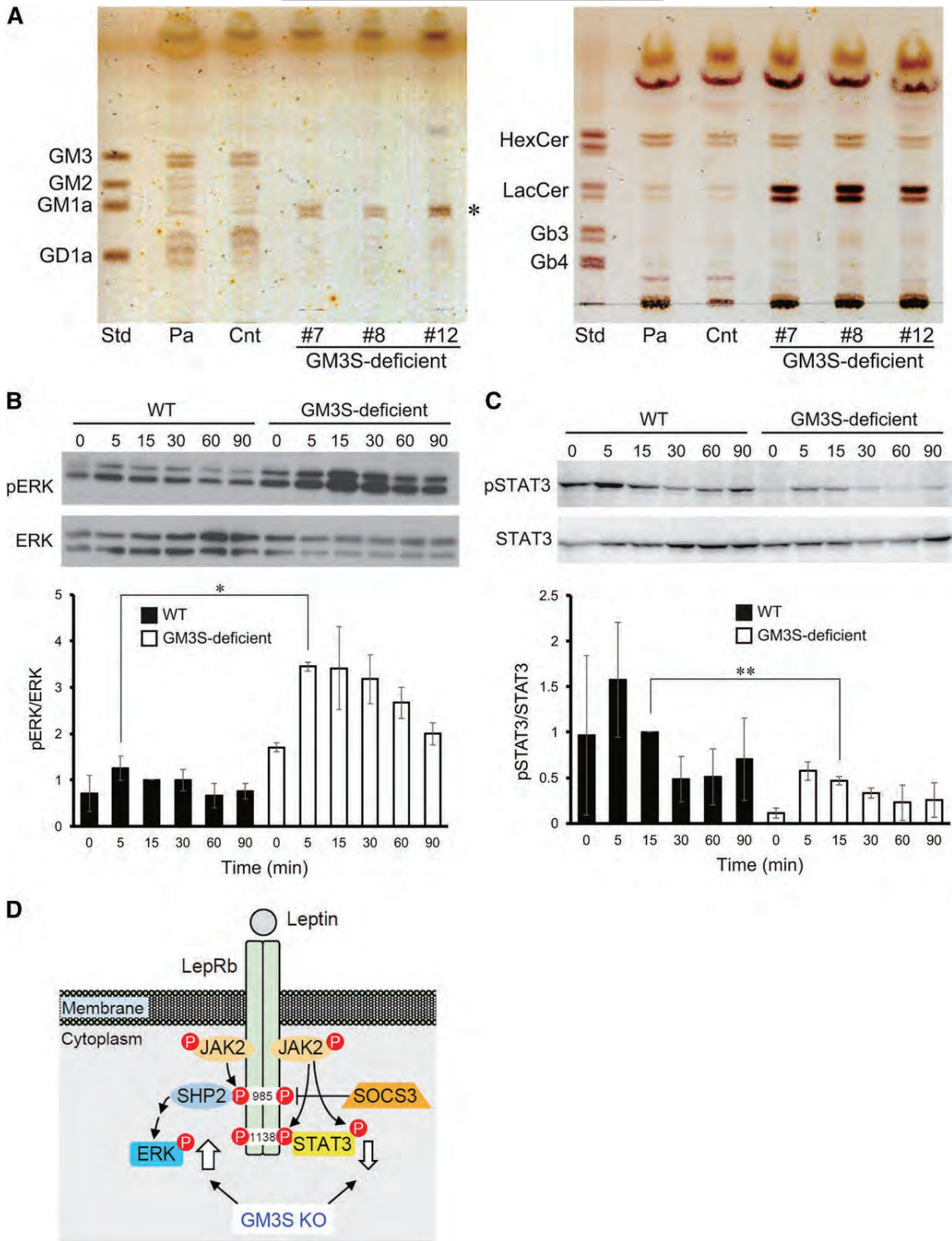


Fig. 5. Leptin-induced ERK phosphorylation was greatly enhanced in GM3S-deficient N41 cells. **A:** TLC of acidic (left) and neutral (right) GSLs from control and GM3S-deficient cell clones generated from N41 cells. Std, standard; Pa, parental cells; Cnt, control cells transfected with vector without targeting sequence. An asterisk indicates a GM1-like band, which is most likely GM1b, an o-series ganglioside. **B, C:** WT and GM3S-deficient cells were treated with leptin and then lysed at the indicated times. For pSTAT3 assay (**C**), the *LepRb* gene was introduced for stable expression (see text). The blots are representative of three independent experiments. Bottom: quantification of immunoblots ($n = 3$). * $P < 0.05$, ** $P < 0.01$. **D:** Leptin receptor signaling pathway. Thick arrows: increased and decreased phosphorylation of ERK and STAT3 (respectively) observed in GM3S-deficient cells.

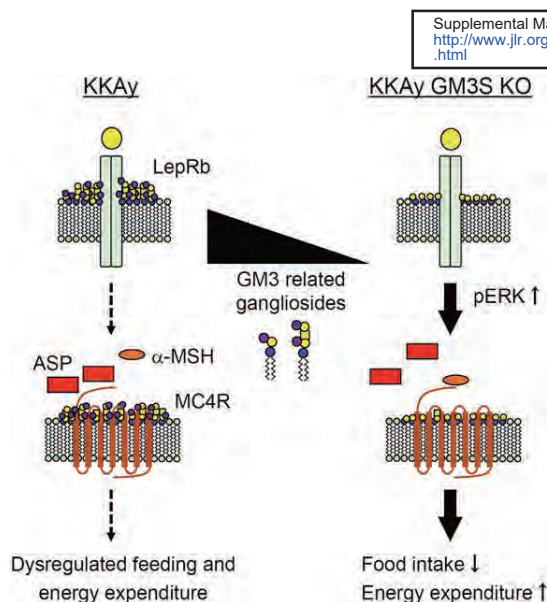


Fig. 6. A working hypothesis of the involvement of GM3/ related gangliosides in leptin and melanocortin receptor signaling. Elimination of GM3/related gangliosides ameliorated the obese phenotype of KKAY mice. Ectopic expression of ASP caused alteration of MC4R signaling and leptin resistance in hypothalamic neurons, resulting in dysregulated feeding and energy expenditure. Elimination of GM3/related gangliosides restored leptin sensitivity. These findings and the observed coat color change suggest that GM3/ related gangliosides are involved in MC1R/MC4R signaling (see Discussion).

binding site for STAT3, and STAT3 is subsequently phosphorylated by JAK2 and translocated to the nucleus to modulate expression of its target genes, which include POMC and suppressor of cytokine signaling 3 (SOCS3) (31). Protein tyrosine phosphatase 2 (SHP2) is recruited to phospho-Tyr⁹⁸⁵ in response to leptin, and phosphorylated by JAK2. Phosphorylated SHP2 can bind the adaptor protein, growth factor receptor-bound protein 2 (Grb2), which facilitates ERK activation. The SHP2/ERK pathway is involved in the anti-obesity effect of leptin (25, 32).

Nordstrom et al. (33) reported that loss of GlcCer synthase in hypothalamic neurons inhibited LepRb signaling, using mice with deletion of inducible neuron-specific *Ugcg*, the gene encoding GlcCer synthase. These mice developed progressive obesity, and the obese phenotype was significantly ameliorated by adeno-associated virus-mediated *Ugcg* delivery to ARC. GM1 and GD1a in N41 cells interacted with LepRb, suggesting that these a-series gangliosides enhance leptin signaling in hypothalamic neurons. In a study of GD3S-null mice, which lack all b-series gangliosides, Ji et al. (34) observed enhanced LepRb signaling in the hypothalamus, as indicated by phosphorylated STAT3 levels. Overexpression of GD3S in N41 cells reduced responsiveness to leptin, supporting the concept that certain a-series gangliosides positively regulate LepRb signaling. The GM3S KO mice used in the present study lacked all a-series gangliosides (Fig. 1F, G), but still retained hypothalamic responsiveness to leptin. Our findings in GM3S-deficient N41 cells (Fig. 5B, D) suggest that GM3S KO mice may be protected from central leptin resistance by enhancement of leptin-dependent ERK phosphorylation. We speculate

that there are at least two possibilities; that *i*) loss of GM3, GM1a, or GD1a or *ii*) increased GM1b, enhanced the ERK signaling. Future studies will address the detailed mechanism of this effect.

Increasing evidence indicates that hypothalamic inflammation contributes to the development of leptin resistance and obesity (11, 12). A HFD may result in activation of inflammatory pathways in the hypothalamus even in the absence of notable weight gain. In animal obesity models, GM3 and GM3S gene expression is upregulated in adipose tissues (2, 4). In obese human patients, serum GM3 levels are elevated and associated with metabolic risk factors (3, 6). It is conceivable that ganglioside expression in the hypothalamus is altered by HFD- and/or obesity-induced inflammation. Such alteration may play a pathophysiological role in the regulation of energy homeostasis through effects on receptor signaling involved in feeding behavior and energy expenditure. **BB**

The authors thank all members of the Inokuchi laboratory for fruitful discussions and technical assistance, Dr. S. Anderson for helpful comments and English editing of the manuscript, and Tohoku Medical and Pharmaceutical University Center for Laboratory Animal Science for their services.

REFERENCES

- Hakomori, S. 2002. The glycosynapse. *Proc. Natl. Acad. Sci. USA*. **99**: 225–232.
- Tagami, S., J. Inokuchi, K. Kabayama, H. Yoshimura, F. Kitamura, S. Uemura, C. Ogawa, A. Ishii, M. Saito, Y. Ohtsuka, et al. 2002. Ganglioside GM3 participates in the pathological conditions of insulin resistance. *J. Biol. Chem.* **277**: 3085–3092.
- Sato, T., Y. Nihei, M. Nagafuku, S. Tagami, R. Chin, M. Kawamura, S. Miyazaki, M. Suzuki, S. Sugahara, Y. Takahashi, et al. 2008. Circulating levels of ganglioside GM3 in metabolic syndrome: a pilot study. *Obes. Res. Clin. Pract.* **2**: I–II.
- Nagafuku, M., T. Sato, S. Sato, K. Shimizu, T. Taira, and J. Inokuchi. 2015. Control of homeostatic and pathogenic balance in adipose tissue by ganglioside GM3. *Glycobiology*. **25**: 303–318.
- Yamashita, T., A. Hashiramoto, M. Haluzik, H. Mizukami, S. Beck, A. Norton, M. Kono, S. Tsuji, J. L. Daniotti, N. Werth, et al. 2003. Enhanced insulin sensitivity in mice lacking ganglioside GM3. *Proc. Natl. Acad. Sci. USA*. **100**: 3445–3449.
- Veillon, L., S. Go, W. Matsuyama, A. Suzuki, M. Nagasaki, Y. Yatomi, and J. Inokuchi. 2015. Identification of ganglioside GM3 molecular species in human serum associated with risk factors of metabolic syndrome. *PLoS One*. **10**: e0129645.
- Ollmann, M. M., B. D. Wilson, Y. K. Yang, J. A. Kerns, Y. Chen, I. Gantz, and G. S. Barsh. 1997. Antagonism of central melanocortin receptors in vitro and in vivo by agouti-related protein. *Science*. **278**: 135–138.
- Tartaglia, L. A., M. Dembski, X. Weng, N. Deng, J. Culpepper, R. Devos, G. J. Richards, L. A. Campfield, F. T. Clark, J. Deeds, et al. 1995. Identification and expression cloning of a leptin receptor, OB-R. *Cell*. **83**: 1263–1271.
- Myers, M. G., Jr., H. Munzberg, G. M. Leininger, and R. L. Leshan. 2009. The geometry of leptin action in the brain: more complicated than a simple ARC. *Cell Metab.* **9**: 117–123.
- Wellen, K. E., and G. S. Hotamisligil. 2005. Inflammation, stress, and diabetes. *J. Clin. Invest.* **115**: 1111–1119.
- Valdearcos, M., A. W. Xu, and S. K. Koliwad. 2015. Hypothalamic inflammation in the control of metabolic function. *Annu. Rev. Physiol.* **77**: 131–160.
- Jais, A., and J. C. Bruning. 2017. Hypothalamic inflammation in obesity and metabolic disease. *J. Clin. Invest.* **127**: 24–32.
- Lu, D., D. Willard, I. R. Patel, S. Kadwell, L. Overton, T. Kost, M. Luther, W. Chen, R. P. Woychik, W. O. Wilkison, et al. 1994. Agouti

- protein is an antagonist of the melanocyte-stimulating-hormone receptor. *Nature*. **371**: 799–802.
14. Iwatsuka, H., A. Shino, and Z. Suzuoki. 1970. General survey of diabetic features of yellow KK mice. *Endocrinol. Jpn.* **17**: 23–35.
 15. Fan, W., B. A. Boston, R. A. Kesterson, V. J. Hruby, and R. D. Cone. 1997. Role of melanocortinergic neurons in feeding and the agouti obesity syndrome. *Nature*. **385**: 165–168.
 16. Tsukamoto, K., T. Kohda, M. Mukamoto, K. Takeuchi, H. Ihara, M. Saito, and S. Kozaki. 2005. Binding of Clostridium botulinum type C and D neurotoxins to ganglioside and phospholipid. Novel insights into the receptor for clostridial neurotoxins. *J. Biol. Chem.* **280**: 35164–35171.
 17. Yoshikawa, M., S. Go, K. Takasaki, Y. Kakazu, M. Ohashi, M. Nagafuku, K. Kabayama, J. Sekimoto, S. Suzuki, K. Takaiwa, et al. 2009. Mice lacking ganglioside GM3 synthase exhibit complete hearing loss due to selective degeneration of the organ of Corti. *Proc. Natl. Acad. Sci. USA*. **106**: 9483–9488.
 18. Inokuchi, J., K. Momosaki, H. Shimeno, A. Nagamatsu, and N. S. Radin. 1989. Effects of D-threo-PDMP, an inhibitor of glucosylceramide synthetase, on expression of cell surface glycolipid antigen and binding to adhesive proteins by B16 melanoma cells. *J. Cell. Physiol.* **141**: 573–583.
 19. Ran, F. A., P. D. Hsu, J. Wright, V. Agarwala, D. A. Scott, and F. Zhang. 2013. Genome engineering using the CRISPR-Cas9 system. *Nat. Protoc.* **8**: 2281–2308.
 20. Tsukita, S., T. Yamada, K. Uno, K. Takahashi, K. Kaneko, Y. Ishigaki, J. Imai, Y. Hasegawa, S. Sawada, H. Ishihara, et al. 2012. Hepatic glucokinase modulates obesity predisposition by regulating BAT thermogenesis via neural signals. *Cell Metab.* **16**: 825–832.
 21. Yamada, T., H. Katagiri, Y. Ishigaki, T. Ogihara, J. Imai, K. Uno, Y. Hasegawa, J. Gao, H. Ishihara, A. Nijima, et al. 2006. Signals from intra-abdominal fat modulate insulin and leptin sensitivity through different mechanisms: neuronal involvement in food-intake regulation. *Cell Metab.* **3**: 223–229.
 22. Nishimura, M. 1969. Breeding of mice strains for diabetes mellitus. *Exp. Anim.* **18**: 147–157.
 23. Masuzaki, H., Y. Ogawa, M. Aizawa-Abe, K. Hosoda, J. Suga, K. Ebihara, N. Satoh, H. Iwai, G. Inoue, H. Nishimura, et al. 1999. Glucose metabolism and insulin sensitivity in transgenic mice overexpressing leptin with lethal yellow agouti mutation: usefulness of leptin for the treatment of obesity-associated diabetes. *Diabetes*. **48**: 1615–1622.
 24. Datta, A. K., R. Chammass, and J. C. Paulson. 2001. Conserved cysteines in the sialyltransferase sialylmotifs form an essential disulfide bond. *J. Biol. Chem.* **276**: 15200–15207.
 25. Rahmouni, K., C. D. Sigmund, W. G. Haynes, and A. L. Mark. 2009. Hypothalamic ERK mediates the anorectic and thermogenic sympathetic effects of leptin. *Diabetes*. **58**: 536–542.
 26. Inoue, A., J. Ishiguro, H. Kitamura, N. Arima, M. Okutani, A. Shuto, S. Higashiyama, T. Ohwada, H. Arai, K. Makide, et al. 2012. TGF α shedding assay: an accurate and versatile method for detecting GPCR activation. *Nat. Methods*. **9**: 1021–1029.
 27. Boccuto, L., K. Aoki, H. Flanagan-Steet, C. F. Chen, X. Fan, F. Bartel, M. Petukh, A. Pittman, R. Saul, A. Chaubey, et al. 2014. A mutation in a ganglioside biosynthetic enzyme, ST3GAL5, results in salt & pepper syndrome, a neurocutaneous disorder with altered glycolipid and glycoprotein glycosylation. *Hum. Mol. Genet.* **23**: 418–433.
 28. Dinulescu, D. M., and R. D. Cone. 2000. Agouti and agouti-related protein: analogies and contrasts. *J. Biol. Chem.* **275**: 6695–6698.
 29. Couturier, C., and R. Jockers. 2003. Activation of the leptin receptor by a ligand-induced conformational change of constitutive receptor dimers. *J. Biol. Chem.* **278**: 26604–26611.
 30. Taniguchi, T. 1995. Cytokine signaling through nonreceptor protein tyrosine kinases. *Science*. **268**: 251–255.
 31. Banks, A. S., S. M. Davis, S. H. Bates, and M. G. Myers, Jr. 2000. Activation of downstream signals by the long form of the leptin receptor. *J. Biol. Chem.* **275**: 14563–14572.
 32. You, J., Y. Yu, L. Jiang, W. Li, X. Yu, L. Gonzalez, G. Yang, Z. Ke, W. Li, C. Li, et al. 2010. Signaling through Tyr985 of leptin receptor as an age/diet-dependent switch in the regulation of energy balance. *Mol. Cell. Biol.* **30**: 1650–1659.
 33. Nordström, V., M. Willershauser, S. Herzer, J. Rozman, O. von Bohlen Und Halbach, S. Meldner, U. Rothermel, S. Kaden, F. C. Roth, C. Waldeck, et al. 2013. Neuronal expression of glucosylceramide synthase in central nervous system regulates body weight and energy homeostasis. *PLoS Biol.* **11**: e1001506.
 34. Ji, S., K. Tokizane, Y. Ohkawa, Y. Ohmi, R. Banno, T. Okajima, H. Kiyama, K. Furukawa, and K. Furukawa. 2016. Increased α -series gangliosides positively regulate leptin/Ob receptor-mediated signals in hypothalamus of GD3 synthase-deficient mice. *Biochem. Biophys. Res. Commun.* **479**: 453–460.



NPC1L1-dependent intestinal cholesterol absorption requires ganglioside GM3 in membrane microdomains

Wataru Nihei,* Masakazu Nagafuku,* Hirotaka Hayamizu,* Yuta Odagiri,* Yumi Tamura,* Yui Kikuchi,* Lucas Veillon,*[†] Hirotaka Kanoh,* Kei-ichiro Inamori,* Kenta Arai,[§] Kazuya Kabayama,[§] Koichi Fukase,[§] and Jin-ichi Inokuchi^{1,*}

Division of Glycopathology,* Institute of Molecular Biomembrane and Glycobiology, Tohoku Medical and Pharmaceutical University, Sendai, Japan; Department of Bioinformatics and Computational Biology,[†] The University of Texas MD Anderson Cancer Center, Houston, TX; and Laboratory of Natural Product Chemistry,[§] Department of Chemistry, Osaka University, Toyonaka, Japan

Abstract Intestinal cholesterol absorption is a key regulator of systemic cholesterol homeostasis. Excessive dietary cholesterol and its intestinal uptake lead to hypercholesterolemia, a major risk factor for cardiovascular disease. Intestinal cholesterol uptake is mediated by Niemann-Pick C1-like 1 (NPC1L1), a transmembrane protein localized in membrane microdomains (lipid rafts) enriched in gangliosides and cholesterol. The roles of gangliosides, such as monosialodihexosylganglioside (GM3) and its synthesizing enzyme GM3 synthase (GM3S), in NPC1L1-dependent cholesterol uptake have not been examined previously. Here, we examined NPC1L1-dependent cholesterol uptake in a cell model as well as in wild-type and apoE-deficient mice fed normal or high-cholesterol diets. We showed that NPC1L1-dependent cholesterol uptake was impaired in GM3S-deficient cells and that GM3S deficiency promoted resistance to hypercholesterolemia in both wild-type and apoE-deficient mice fed the high-cholesterol but not the normal diet. Our findings suggest that GM3 and related gangliosides are essential for NPC1L1-mediated intestinal cholesterol absorption and are potential targets for hypercholesterolemia therapy.—Nihei, W., M. Nagafuku, H. Hayamizu, Y. Odagiri, Y. Tamura, Y. Kikuchi, L. Veillon, H. Kanoh, K-i. Inamori, K. Arai, K. Kabayama, K. Fukase, and J-i. Inokuchi. **NPC1L1-dependent intestinal cholesterol absorption requires ganglioside GM3 in membrane microdomains.** *J. Lipid Res.* 2018. 59: 2181–2187.

Supplementary key words gangliosides • monosialodihexosylganglioside • cholesterol absorption • hypercholesterolemia • lipid transport • Niemann-Pick C1-like 1

This study was supported by Ministry of Education, Culture, Sports, Science and Technology Research Grant-in-Aid 16H04767 (J.I.); grants-in-aid from the Mizutani Foundation for Glycoscience (J.I.), Takeda Science Foundation (J.I.), Fugaku Trust for Medicinal Research (J.I.), Naito Foundation (J.I.), Ono Medical Research Foundation (J.I.), and Uehara Memorial Foundation (J.I.); and the Ministry of Education, Culture, Sports, Science and Technology-supported Program for the Strategic Research Foundation at Private Universities.

Manuscript received 11 August 2018 and in revised form 14 September 2018.

Published, JLR Papers in Press, September 21, 2018

DOI <https://doi.org/10.1194/jlr.M089201>

Copyright © 2018 Nihei et al. Published under exclusive license by The American Society for Biochemistry and Molecular Biology, Inc.

This article is available online at <http://www.jlr.org>

Cholesterol is an important component of cell membranes. It is a precursor for biosynthesis of steroid hormones and bile acids and is present in the circulatory system. Lowering cholesterol levels in plasma reduces the risk of coronary heart disease, a major cause of death in developed countries (1, 2). The transmembrane protein Niemann-Pick C1-like 1 (NPC1L1) plays an essential role in dietary cholesterol absorption and biliary cholesterol reabsorption (3–5). NPC1L1 mediates cellular cholesterol uptake through vesicular endocytosis and is a target of the cholesterol absorption inhibitor ezetimibe (6–10). NPC1L1 is localized in ganglioside-enriched membrane domains and requires lipid raft proteins flotillin-1 and -2 to create cholesterol-enriched membrane microdomains for efficient cholesterol uptake (11, 12).

Gangliosides (glycosphingolipids [GSLs] that contain at least one sialic acid) are enriched in the outer leaflet of plasma membranes and concentrated in specialized membrane microdomains, termed lipid rafts, that function as platforms for cell-cell interaction and cell signaling (13, 14). The ganglioside monosialodihexosylganglioside (GM3), synthesized by GM3 synthase (GM3S), is a precursor of α -, β -, and γ -series gangliosides, interacts with transmembrane receptors such as the epidermal growth factor and insulin receptors, and regulates receptor functions by creating a specialized lipid environment (15, 16). There is often a close functional relationship between gangliosides and flotillins in membrane microdomain organization (17, 18); however, no study to date has addressed the role of gangliosides in NPC1L1-mediated cholesterol absorption. We demonstrate in the present study that *i)* NPC1L1-dependent cellular cholesterol uptake is inhibited in GM3S-deficient cells and *ii)* genetic hypercholesterolemia, diet-induced

Abbreviations: GM3, monosialodihexosylganglioside; GM3S, GM3 synthase; GSL, glycosphingolipid; NPC1L1, Niemann-Pick C1-like 1; M β CD, methyl- β -cyclodextrin.

¹To whom correspondence should be addressed.
e-mail: jin@tohoku-mpu.ac.jp

hypercholesterolemia, and the intestinal cholesterol absorption rate are reduced in GM3S-deficient mice. Our findings suggest that gangliosides, particularly GM3, are potential targets for hypercholesterolemia therapy.

MATERIALS AND METHODS

Animals

C57BL/6 mice and apoE-deficient mice (B6.KOR/stm Slc-*ApoE*^{shl}) were from Japan SLC, Inc. (Hamamatsu, Japan). GM3S (*St3gal5*)-deficient mice were generated in our lab as described previously (19). To generate *ApoE*^{shl}/*GM3S*^{-/-} mice, *ApoE*^{shl} mice were crossed with *GM3S*^{-/-} mice.

ApoE^{shl}/*GM3S*^{-/-} mice and littermate controls were generated by heterozygous mating. Mice were analyzed for the GM3S genotype by PCR and for apoE protein expression by immunoblotting as described previously (20, 21). Mice were fed a regular chow diet (CE-2; CLEA Japan, Tokyo, Japan) or high-cholesterol diet (Research Diets; New Brunswick, NJ) ad libitum. All animal experiments were approved by appropriate institutional review board committees at Tohoku Medical and Pharmaceutical University.

Materials, antibodies, and plasmid

Cholesterol and lipoprotein-deficient serum were from Sigma-Aldrich (St. Louis, MO), methyl- β -cyclodextrin (M β CD) and compactin were from Tokyo Chemical Industry (Tokyo, Japan), and ezetimibe was from AdooQ Bioscience (Irvine, CA). Rabbit anti-NPC1L1 antibody was from Novus Biologicals (Littleton, CO). Alexa 594-conjugated goat anti-rabbit IgG was from Thermo Fisher Scientific (Waltham, MA). pCMV6-hNPC1L1-turboGFP plasmid vector was from OriGene (Rockville, MD).

Cell culture

HEK293T cells were cultured in DMEM (Nacalai Tesque, Kyoto, Japan) supplemented with 10% FBS, 100 U/ml penicillin, and 100 μ g/ml streptomycin at 37°C in a 5% CO₂ atmosphere. Cholesterol-depleting medium was DMEM containing 5% lipoprotein-deficient serum, 2 μ M compactin, and 25 mM HEPES. Cholesterol-M β CD complex was prepared as described previously (22).

Generation of GM3S-deficient HEK293T cells

A single exon of the human *ST3GAL5* (*GM3S*) gene containing the coding sequence for sialyl motif L was selected for the design of targeting guide RNAs using an online CRISPR design tool (23). Guide oligos (5'-CACCCGAAGACCTGTCCGGCGCTGTG-3' and 5'-AAACCACAGCGCCGACAGGTCTTGC-3') were annealed and inserted into plasmid pSpCas9(BB) (Addgene, Cambridge, MA). The plasmid was introduced into HEK293T cells using Lipofectamine 2000 (Thermo Fisher) per the manufacturer's instructions, clonal cell lines were obtained by single-cell cloning, and expression levels of gangliosides were evaluated by TLC.

Measurement of cellular cholesterol

Cells were seeded in DMEM in 60-mm dishes at a density of 8×10^5 cells/dish and transfected at 24 h with the indicated plasmid using Lipofectamine LTX (Thermo Fisher) per the manufacturer's instructions. The medium was replaced by cholesterol-depleting medium at 48 h, cells were cultured overnight, and cholesterol-M β CD complex was added to the medium the next day. For ezetimibe treatment, cells were preincubated with 30 μ M ezetimibe for 30 min, incubated with cholesterol-M β CD complex for 60 min,

and washed with PBS, and total cellular lipids were extracted as described by Bligh and Dyer (24). Lipid extracts were dried by an N₂ stream and resuspended in 1 ml 1% Triton X-100 in chloroform, chloroform was evaporated by an N₂ stream, and detergent-solubilized lipids were resuspended in 1 ml distilled water. Total cholesterol and phospholipid concentrations were determined using LabAssayTM cholesterol and phospholipid test kits (Wako Pure Chemical Industries, Osaka, Japan).

Visualization of living cells and fluorescence quantification

For time-lapse fluorescence imaging, cells were seeded onto 35-mm glass-bottom dishes (Greiner Bio-One, Frickenhausen, Germany) coated with poly-L-lysine (Sigma-Aldrich) and transfected at 24 h. The medium was replaced by cholesterol-depleting medium at 48 h, and cells were cultured overnight. Cholesterol-M β CD complex was added to the medium the next day with or without 30 μ M ezetimibe. Living cells were visualized by confocal laser scanning microscopy (FluoView FV1000; Olympus, Tokyo, Japan) for 60 min. The relative intensity of plasma membrane-localized NPC1L1-GFP^{turbo} was quantified as described previously (6). The intensity at various time points was normalized relative to the intensity at time zero (defined as 100%). Fluorescence intensity was calculated using the FluoView software program (Olympus).

Blood cholesterol and lipoprotein analyses

Plasma total cholesterol was analyzed using the Cholesterol E-Test kit (Wako Pure Chemical Industries) per the manufacturer's instructions. Serum lipoproteins were analyzed by an HPLC system at Skylight Biotech (Akita, Japan) according to the procedure described by Usui et al. (25).

Lipid and LC/MS/MS analyses

Lipids were analyzed as described previously (26). Intestinal samples were obtained by perfusing mice with saline and scraping off small-intestinal mucosa with a plastic spatula. LC/MS/MS analysis was performed as described previously (27).

Intestinal cholesterol absorption rate

The fecal dual-isotope ratio method (28) was used to determine the intestinal cholesterol absorption rate in 6- to 8-week-old *ApoE*^{shl} mice and *ApoE*^{shl}/*GM3S*^{-/-} mice. Animals were orally gavaged with 100 μ L corn oil containing [¹⁴C]cholesterol (1 μ Ci) and [³H]sitostanol (2 μ Ci), feces were collected once per day for 3 days, and [¹⁴C]cholesterol and [³H]sitostanol levels were determined.

Cholesterol feeding and immunohistochemical analysis of NPC1L1

The mice were fasted for 16 h and then gavaged with 200 μ L corn oil containing 40 mg/ml cholesterol, anesthetized after 30 min, and perfused with saline. Intestinal tissues were removed, fixed in 4% paraformaldehyde in PBS, dehydrated in 30% sucrose overnight at 4°C, embedded in OCT compound (Sakura Finetek, Sendai, Japan), and frozen at -80°C. Sections (thickness: 8 μ m) were prepared by cryostat, blocked with 3% BSA for 1 h, incubated with anti-NPC1L1 primary antibody (1:200) for 24 h at 4°C, washed twice with PBS, incubated with Alexa 594-conjugated secondary antibody (1:500) for 30 min at room temperature, and viewed by fluorescence microscopy (Axioskop2; Carl Zeiss, Göttingen, Germany).

Statistical analysis

Data were expressed as mean \pm SD, and means were compared by Student's *t*-test or ANOVA followed by Tukey's post hoc test.

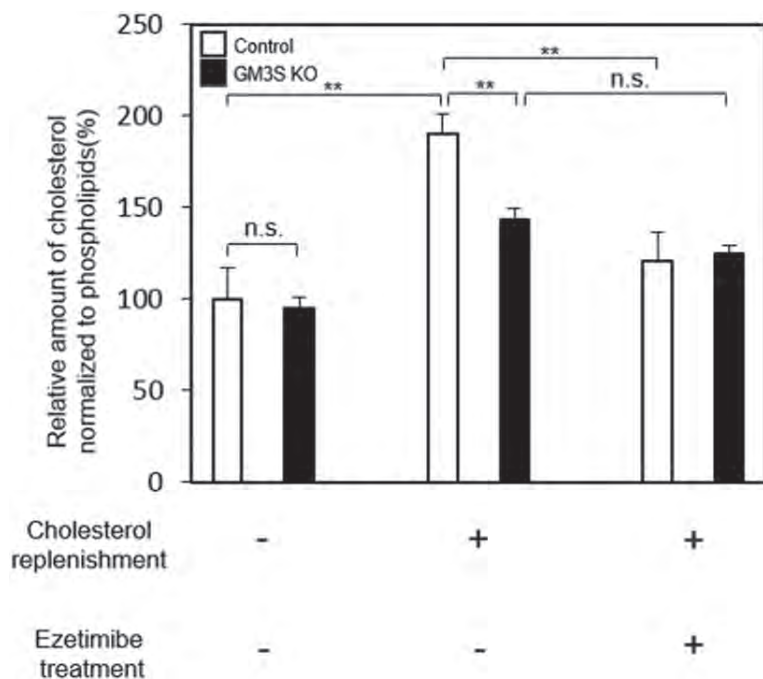


Fig. 1. GM3S deficiency inhibits cholesterol uptake via an NPC1L1-dependent pathway. NPC1L1-expressing control HEK293T cells and GM3S KO cells were incubated in cholesterol-depleting medium to reduce cellular cholesterol. For cholesterol replenishment, cholesterol-M β CD complex (30 μ g/ml) was added directly to the medium, and cells were cultured for 60 min with or without ezetimibe pretreatment. Total lipid extraction was performed, and cholesterol and phospholipid contents were measured. Cholesterol content was normalized relative to phospholipid content. ** $P < 0.01$.

RESULTS

To evaluate the possible involvement of gangliosides (GM3) in NPC1L1-mediated cholesterol absorption, we first examined cholesterol content in control HEK293T and GM3S-deficient (GM3S KO) cells. The two cell lines were

transfected with NPC1L1-GFP^{turbo}, and cellular cholesterol content was measured. GM3S deficiency had no effect on endogenous cholesterol levels (**Fig. 1**). In NPC1L1-expressing control cells, the cholesterol level was increased by cholesterol supplementation, and the increase was blocked by pretreatment with ezetimibe. In NPC1L1-expressing

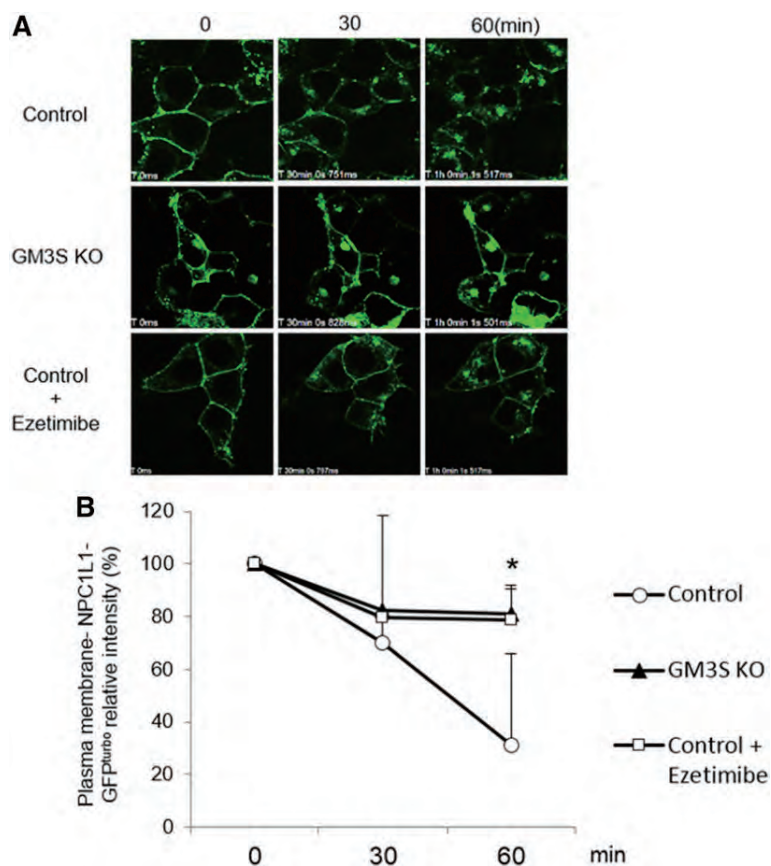


Fig. 2. Cholesterol-dependent internalization of NPC1L1-GFP^{turbo} is ameliorated by GM3S depletion. A: Control HEK293T and GM3S KO cells were seeded in 0.001% poly-L-lysine-coated 35-mm glass-bottom dishes on day 0 and transfected with NPC1L1-GFP^{turbo} on day 1. The medium was replaced with medium containing 5% lipoprotein-deficient serum and 2 μ M compactin on day 2 to deplete cellular cholesterol, and cells were supplemented with 60 μ g/ml cholesterol with or without ezetimibe treatment on day 3. Time-lapse images were taken by confocal microscopy. Representative images are shown. B: Quantification of plasma membrane-localized NPC1L1-GFP^{turbo} in the cells shown in panel A. Intensity at time zero was defined as 100%. * $P < 0.05$ for comparison of control versus GM3S KO.

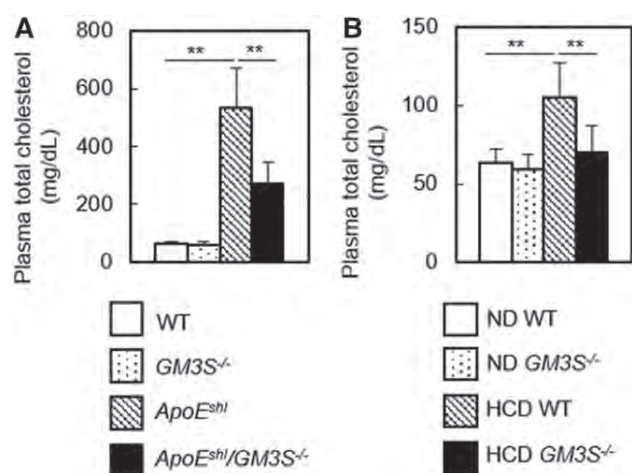


Fig. 3. Hypercholesterolemia is ameliorated in *GM3S* KO mice. A: Plasma total cholesterol was measured in four groups as indicated ($n = 18$ – 35 per group). B: Diet-induced hypercholesterolemia was normalized in *GM3S* KO mice. Plasma cholesterol levels were determined after 10 weeks of a normal diet (cholesterol-free; ND) or high-cholesterol diet (1.25% cholesterol; HCD) ($n = 10$ – 30 per group). $**P < 0.01$.

GM3S KO cells, cholesterol uptake was significantly lower than in control cells, and ezetimibe pretreatment had no notable effect (Fig. 1). Previous studies indicate that the dynamic translocation of NPC1L1 between the cell surface and intracellular region is essential for NPC1L1-mediated

cholesterol uptake and that cholesterol is required for the active endocytosis of NPC1L1 (6, 10).

Next, experiments were performed to evaluate the effect of *GM3S* deficiency on NPC1L1 translocation. In control cells, cholesterol supplementation following cholesterol depletion resulted in the translocation of NPC1L1 from the plasma membrane to the intracellular region. In contrast, NPC1L1 translocation was much lower in *GM3S* KO cells and at a level similar to that of ezetimibe-treated cells (Fig. 2). These findings indicate the involvement of *GM3* in NPC1L1-dependent cholesterol absorption.

We accordingly hypothesized that experimentally induced hypercholesterolemia in *GM3S* KO (*GM3S*^{-/-}) mice can be ameliorated by inhibiting NPC1L1-mediated intestinal cholesterol uptake. To test this hypothesis, we crossed apoE-deficient, spontaneously hyperlipidemic mice (*ApoE*^{shl}) with *GM3S*^{-/-} mice and examined plasma cholesterol levels. Plasma cholesterol was not significantly reduced in *GM3S*^{-/-} mice, whereas levels in *ApoE*^{shl}/*GM3S*^{-/-} mice were strikingly lower than the high levels in *ApoE*^{shl} mice (Fig. 3A). Next, we examined the possible resistance of *GM3S*^{-/-} mice to diet-induced hypercholesterolemia. Plasma cholesterol levels were increased by a high-cholesterol diet in WT mice but not in *GM3S*^{-/-} mice (Fig. 3B). These findings indicate that *GM3S*^{-/-} mice were resistant to hypercholesterolemia induced by either apoE deficiency or a high-cholesterol diet.

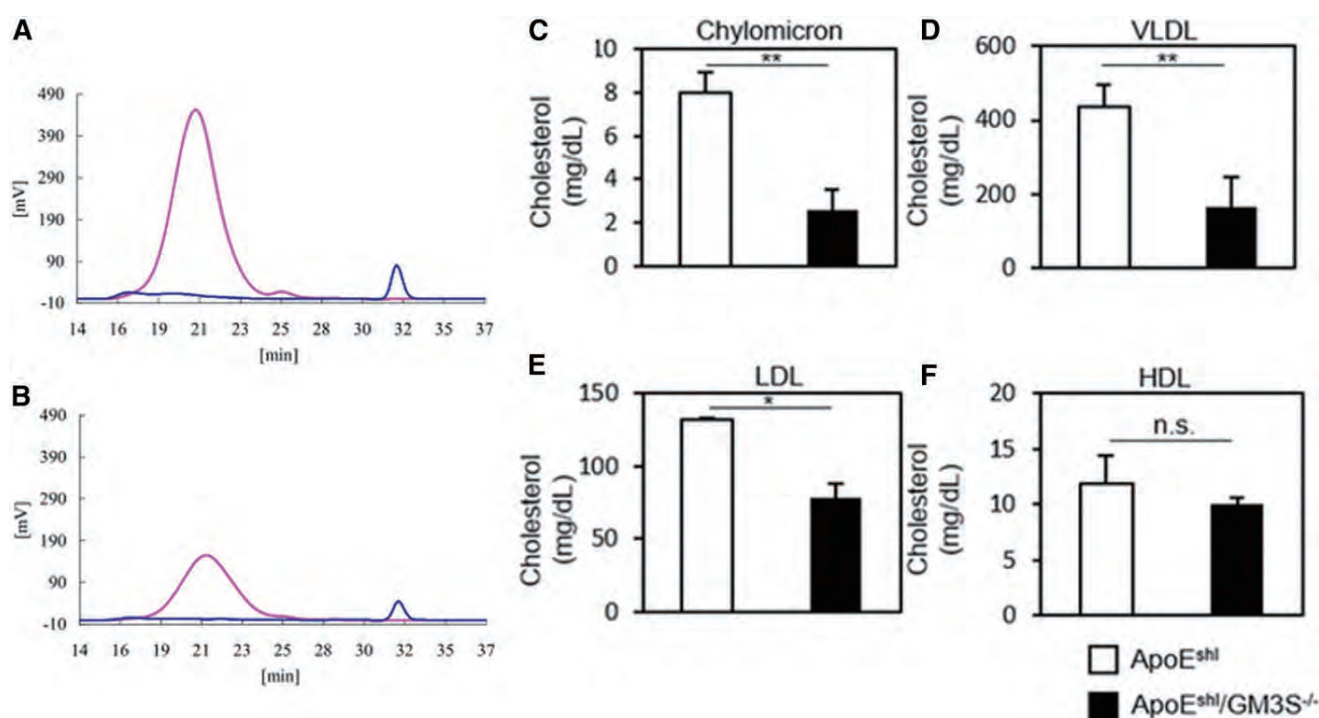


Fig. 4. Lipoprotein profiles of *ApoE*^{shl} and *ApoE*^{shl}/*GM3S*^{-/-} mice. Lipoprotein-associated cholesterol levels in 16- to 18-week-old male mice were determined by HPLC. A, B: Representative HPLC patterns of (A) *ApoE*^{shl} and (B) *ApoE*^{shl}/*GM3S*^{-/-} serum. A 5 μ l serum sample was injected onto two tandem gel permeation columns and eluted with TSK eluent LP-1 at a flow rate of 0.7 ml/min. Pink lines represent cholesterol, and blue lines represent triglyceride. Serum total cholesterol and total triglyceride levels are 587 ± 65 and 59 ± 33 mg/dl (A) and 259 ± 75 and 35 ± 11 mg/dl (B), respectively. Lipoprotein subclasses determined from observed elution times are presented. C–F: Chylomicron, VLDL, LDL, and HDL, respectively ($n = 3$ per group). $*P < 0.05$ and $**P < 0.01$.

Plasma lipoprotein profiles were obtained for *ApoE^{shl}* and *ApoE^{shl}/GM3S^{-/-}* mice. In *ApoE^{shl}/GM3S^{-/-}* mice, cholesterol content was significantly reduced in chylomicron, VLDL, and LDL fractions but not in the HDL fraction (Fig. 4). The reduction of cholesterol content was most striking for the chylomicron fraction (Fig. 4C), indicating defective intestinal cholesterol absorption in these mice.

We next examined the GSL composition of intestinal mucosa, where NPC1L1-mediated cholesterol absorption occurs. It has been reported that intestinal GM3S expression level is high in neonatal mice and declines during the course of development (29). We detected GM3 expression in WT and *ApoE^{shl}* mice by TLC and LC/MS/MS analyses. Trace amounts of GM3 molecular species were also detected in GM3S KO mice (Figs. 5A, 6), likely as the result of a newly identified transcriptional variant in *GM3S^{-/-}* mice generated by targeting exon 3 of the *GM3S* gene (30). Levels of neutral GSLs in intestinal mucosa were not notably altered in *GM3S^{-/-}* mice (Fig. 5B).

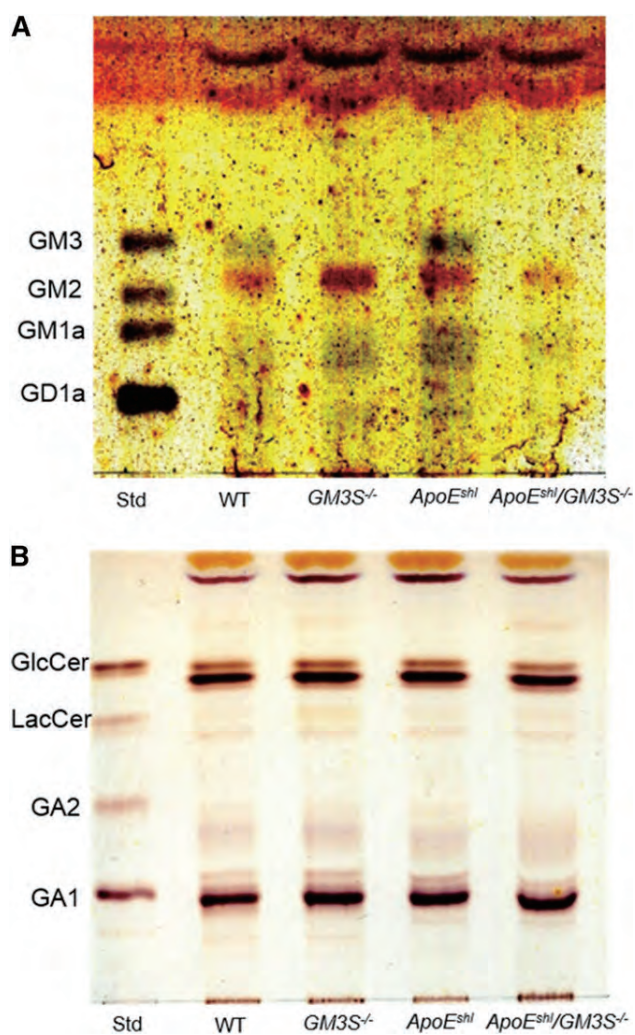


Fig. 5. TLC analysis of ganglioside composition in mouse intestinal mucosa. Acidic (A) and neutral (B) GSLs equivalent to 2 or 1 mg intestinal mucosa wet weight, respectively, were applied to plates.

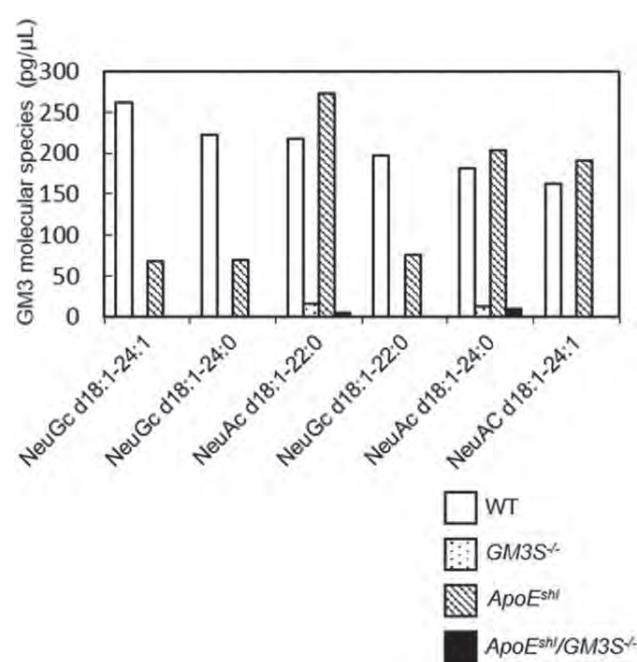


Fig. 6. LC/MS/MS analysis of GM3 molecular species in mouse intestinal mucosa. Six species were detected (arranged according to abundance in WT mice).

To test the hypothesis that resistance to hypercholesterolemia in *GM3S^{-/-}* mice is due to impaired NPC1L1 function, we compared the intestinal cholesterol absorption rates of *ApoE^{shl}* versus *ApoE^{shl}/GM3S^{-/-}* mice based on the oral administration of radiolabeled cholesterol. Uptake of cholesterol from the intestine was significantly lower in *ApoE^{shl}/GM3S^{-/-}* than in *ApoE^{shl}* mice (Fig. 7).

It has been demonstrated that the oral administration of cholesterol in mice induces the translocation of NPC1L1

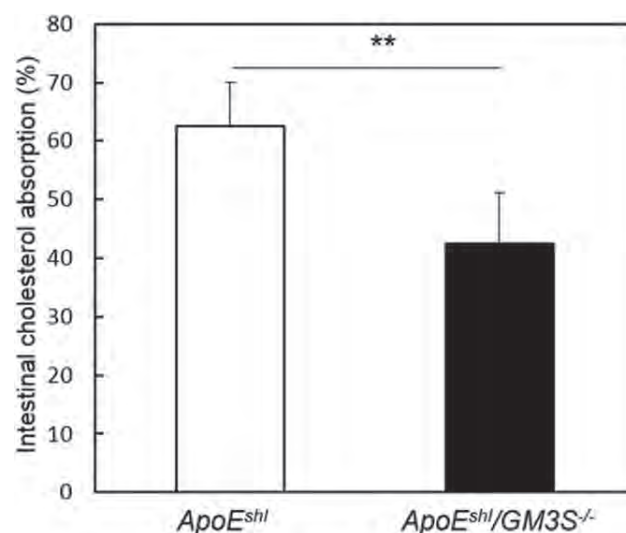


Fig. 7. GM3 plays an important role in intestinal cholesterol uptake. Mice ($n = 5-6$ per group) were orally gavaged with [^{14}C]cholesterol and [^3H]sitostanol, and the cholesterol absorption rate was determined by the fecal dual-isotope ratio method as described in Materials and Methods. $**P < 0.01$.

from the intestinal epithelial surface to the intracellular region (31, 32). We examined the possibility that GM3S deficiency impairs cholesterol-dependent NPC1L1 translocation *in vivo* by immunostaining of intestinal NPC1L1. In both *ApoE^{shl}* and *ApoE^{shl}/GM3S^{-/-}* mice, in the absence of cholesterol feeding, NPC1L1 localized mainly at the apical side of enterocytes (Fig. 8). Cholesterol feeding induced NPC1L1 internalization in *ApoE^{shl}* but not in *ApoE^{shl}/GM3S^{-/-}* mice. Taken together, these findings clearly indicate that GM3 and/or related gangliosides are essential for NPC1L1-dependent intestinal cholesterol absorption.

DISCUSSION

The protein NPC1L1 is known to be localized in detergent-resistant, ganglioside-enriched microdomains (11, 12, 32). The role of gangliosides in NPC1L1-dependent cholesterol absorption is unknown. Our previous studies have shown that GM3 plays key roles in certain metabolic disorders and that the inhibition of GM3 biosynthesis may help ameliorate metabolic imbalance (27, 33, 34). Results from the present study indicate that GM3S deficiency promotes resistance to hypercholesterolemia by inhibiting NPC1L1-mediated cholesterol uptake. NPC1L1-expressing GM3S KO cells displayed cholesterol uptake significantly lower than that of control cells (Fig. 1) and impairment of the cholesterol-dependent translocation of NPC1L1 from the plasma membrane to the intracellular region (Fig. 2). Consistent with these findings, *GM3S^{-/-}* mice showed reductions of intestinal cholesterol uptake and cholesterol-dependent translocation of NPC1L1 (Figs. 7, 8). Plasma

cholesterol levels in WT, *GM3S^{-/-}*, *ApoE^{shl}*, and *ApoE^{shl}/GM3^{-/-}* mice are summarized in Fig. 3A. GM3S-deficient mice were resistant to hypercholesterolemia induced by the high-cholesterol diet, and the hypercholesterolemia characteristic of *ApoE^{shl}* mice was significantly ameliorated in *ApoE^{shl}/GM3S^{-/-}* mice. On the other hand, plasma cholesterol levels were similar for WT and *GM3S^{-/-}* mice fed a normal diet. Taken together, these observations suggest functional involvement of GM3S in the exogenous pathways of cholesterol metabolism, including intestinal NPC1L1 activity.

Developmental changes in intestinal GSL composition have been found to be synchronized with expression levels of intestinal nutrient transporters (29). The knockdown of intestinal glucosylceramide synthase resulted in retarded growth and early death in mice because of defects in intestinal intracellular vesicular transport (35). These studies suggest that GSLs are physiologically important for intestinal nutrient absorption, but they did not address the role of GSLs in the NPC1L1 pathway. It has been shown that NPC1L1 requires a cholesterol-enriched membrane microdomain to function as a cholesterol transporter (11, 12, 32).

In the present study, cholesterol uptake by NPC1L1 was reduced in GM3S-deficient cells and mice. We therefore conclude that NPC1L1 requires not only cholesterol but also GM3 (or related gangliosides) to form functional membrane microdomains for cholesterol transport. Two possibilities can be considered: *i*) gangliosides interact directly with NPC1L1 via electrostatic interactions with multiple oligosaccharide chains to facilitate conformational change leading to translocation from lipid rafts to clathrin-coated pits, and *ii*) gangliosides are required for the association of NPC1L1 with proteins such as flotillins. The present findings provide novel insights into the mechanism of NPC1L1-mediated cholesterol absorption, which can be regulated by membrane lipid composition as well as by protein-protein interactions. The detailed mechanisms whereby GM3 and related gangliosides function in NPC1L1-mediated cholesterol absorption remain to be elucidated.

Gangliosides, particularly GM3, and its synthesizing enzyme GM3S appear to be potential targets for hypercholesterolemia therapy. Genetic variation in NPC1L1 is closely associated with interindividual variation in response to ezetimibe (36). Moreover, the loss of ezetimibe-binding mutations in the extracellular loop of NPC1L1 has been reported (9). Taken together, one can speculate that mutations in the region lead to unresponsiveness to the ezetimibe treatment. Membrane lipid modification such as GM3S inhibition can be used regardless of the binding affinity of compounds to the NPC1L1 and provide an alternative therapy for nonresponsive individuals. **■**

The authors are grateful to all members of the Inokuchi and Fukase laboratories for valuable scientific discussions and technical support, to the Tohoku Medical and Pharmaceutical University Center for Laboratory Animal Science for their services, and to S. Anderson for English editing of the manuscript.

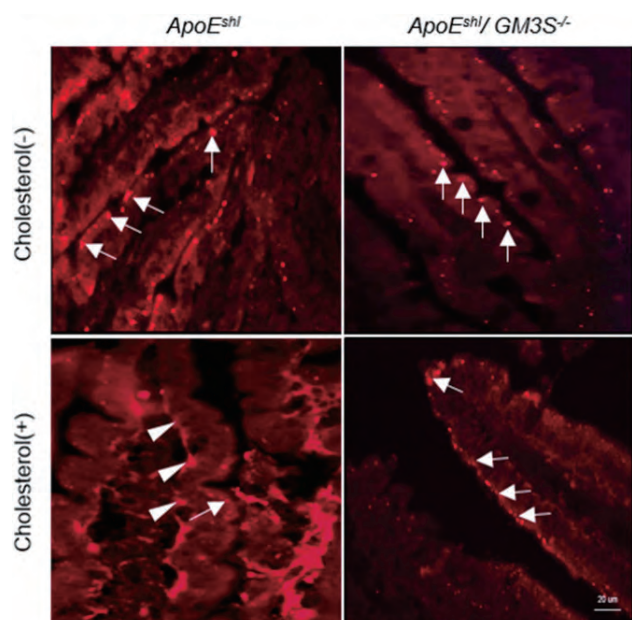


Fig. 8. Immunostaining of NPC1L1 in the small intestine of *ApoE^{shl}* and *ApoE^{shl}/GM3S^{-/-}* mice with or without oral cholesterol administration. Frozen sections were stained with anti-NPC1L1 antibodies. Arrows: plasma membrane-localized NPC1L1. Arrowheads: internalized NPC1L1.

REFERENCES

- Shepherd, J., S. M. Cobbe, I. Ford, C. G. Isles, A. R. Lorimer, P. W. Macfarlane, J. H. McKillop, and C. J. Packard. 1995. Prevention of coronary heart disease with pravastatin in men with hypercholesterolemia. *N. Engl. J. Med.* **333**: 1301–1307.
- Kreisberg, R. A., and A. Oberman. 2002. Clinical review 141: lipids and atherosclerosis: lessons learned from randomized controlled trials of lipid lowering and other relevant studies. *J. Clin. Endocrinol. Metab.* **87**: 423–437.
- Altmann, S. W., H. R. Davis, L.-J. Zhu, X. Yao, L. M. Hoos, G. Tetzloff, S. P. N. Iyer, M. Maguire, A. Golovko, M. Zeng, et al. 2004. Niemann-Pick C1 Like 1 protein is critical for intestinal cholesterol absorption. *Science*. **303**: 1201–1204.
- Davis, H. R., L.-J. Zhu, L. M. Hoos, G. Tetzloff, M. Maguire, J. Liu, X. Yao, S. P. N. Iyer, M.-H. Lam, E. G. Lund, et al. 2004. Niemann-Pick C1 Like 1 (NPC1L1) is the intestinal phytosterol and cholesterol transporter and a key modulator of whole-body cholesterol homeostasis. *J. Biol. Chem.* **279**: 33586–33592.
- Temel, R. E., W. Tang, Y. Ma, L. L. Rudel, M. C. Willingham, Y. A. Ioannou, J. P. Davies, L.-M. Nilsson, and L. Yu. 2007. Hepatic Niemann-Pick C1-like 1 regulates biliary cholesterol concentration and is a target of ezetimibe. *J. Clin. Invest.* **117**: 1968–1978.
- Ge, L., J. Wang, W. Qi, H.-H. Miao, J. Cao, Y.-X. Qu, B.-L. Li, and B.-L. Song. 2008. The cholesterol absorption inhibitor ezetimibe acts by blocking the sterol-induced internalization of NPC1L1. *Cell Metab.* **7**: 508–519.
- Chang, T.-Y., and C. Chang. 2008. Ezetimibe blocks internalization of the NPC1L1/cholesterol complex. *Cell Metab.* **7**: 469–471.
- Wang L.-J., B.-L. Song. 2012. Niemann-Pick C1-like 1 and cholesterol uptake. *Biochim. Biophys. Acta.* **1821**: 964–972.
- Weinglass, A. B., M. Kohler, U. Schulte, J. Liu, E. O. Nketiah, A. Thomas, W. Schmalhofer, B. Williams, W. Bildl, D. R. McMasters, et al. 2008. Extracellular loop C of NPC1L1 is important for binding to ezetimibe. *Proc. Natl. Acad. Sci. USA.* **105**: 11140–11145.
- Yu, L., S. Bharadwaj, J. M. Brown, Y. Ma, W. Du, M. A. Davis, P. Michaely, P. Liu, M. C. Willingham, and L. L. Rudel. 2006. Cholesterol-regulated translocation of NPC1L1 to the cell surface facilitates free cholesterol uptake. *J. Biol. Chem.* **281**: 6616–6624.
- Ge, L., W. Qi, L.-J. Wang, H.-H. Miao, Y.-X. Qu, B.-L. Li, and B.-L. Song. 2011. Flotillins play an essential role in Niemann-Pick C1-like 1-mediated cholesterol uptake. *Proc. Natl. Acad. Sci. USA.* **108**: 551–556.
- Zhang, J.-H., L. Ge, W. Qi, L. Zhang, H.-H. Miao, B.-L. Li, M. Yang, and B.-L. Song. 2011. The N-terminal domain of NPC1L1 protein binds cholesterol and plays essential roles in cholesterol uptake. *J. Biol. Chem.* **286**: 25088–25097.
- Hakomori, S. I. 2002. The glycosynapse. *Proc. Natl. Acad. Sci. USA.* **99**: 225–232.
- Simons, K., and M. J. Gerl. 2010. Revitalizing membrane rafts: new tools and insights. *Nat. Rev. Mol. Cell Biol.* **11**: 688–699.
- Wang, J., and R. K. Yu. 2007. Interaction of ganglioside GD3 with an EGF receptor sustains the self-renewal ability of mouse neural stem cells in vitro. *Proc. Natl. Acad. Sci. USA.* **110**: 19137–19142.
- Kabayama, K., T. Sato, K. Saito, N. Loberto, A. Prinetti, S. Sonnino, M. Kinjo, Y. Igarashi, and J. Inokuchi. 2007. Dissociation of the insulin receptor and caveolin-1 complex by ganglioside GM3 in the state of insulin resistance. *Proc. Natl. Acad. Sci. USA.* **104**: 13678–13683.
- Saslowsky, D. E., J. A. Cho, H. Chinnapan, R. H. Massol, D. J. F. Chinnapan, J. S. Wagner, H. E. De Luca, W. Kam, B. H. Paw, and W. I. Lencer. 2010. Intoxication of zebrafish and mammalian cells by cholera toxin depends on the flotillin/reggie proteins but not Derlin-1 or -2. *J. Clin. Invest.* **120**: 4399–4409.
- Ohmi, Y., O. Tajima, Y. Ohkawa, Y. Yamauchi, Y. Sugiura, K. Furukawa, and K. Furukawa. 2011. Gangliosides are essential in the protection of inflammation and neurodegeneration via maintenance of lipid rafts: Elucidation by a series of ganglioside-deficient mutant mice. *J. Neurochem.* **116**: 926–935.
- Yoshikawa, M., S. Go, K. Takasaki, Y. Kakazu, M. Ohashi, M. Nagafuku, K. Kabayama, J. Sekimoto, S. Suzuki, K. Takaiwa, et al. 2009. Mice lacking ganglioside GM3 synthase exhibit complete hearing loss due to selective degeneration of the organ of Corti. *Proc. Natl. Acad. Sci. USA.* **106**: 9483–9488.
- Nagafuku, M., K. Okuyama, Y. Onimaru, A. Suzuki, Y. Odagiri, T. Yamashita, K. Iwasaki, M. Fujiwara, M. Takayanagi, I. Ohno, et al. 2012. CD4 and CD8 T cells require different membrane gangliosides for activation. *Proc. Natl. Acad. Sci. USA.* **109**: E336–E342.
- Matsushima, Y., S. I. Hayashi, and M. Tachibana. 1999. Spontaneously hyperlipidemic (SHL) mice: Japanese wild mice with apolipoprotein E deficiency. *Mamm. Genome.* **10**: 352–357.
- Brown, A. J., L. Sun, J. D. Feramisco, M. S. Brown, and J. L. Goldstein. 2002. Cholesterol addition to ER membranes alters conformation of SCAP, the SREBP escort protein that regulates cholesterol metabolism. *Mol. Cell.* **10**: 237–245.
- Ran, F. A., P. D. Hsu, J. Wright, V. Agarwala, D. A. Scott, and F. Zhang. 2013. Genome engineering using the CRISPR-Cas9 system. *Nat. Protoc.* **8**: 2281–2308.
- Bligh, E. G., and W. G. Dyer. 1959. A rapid method of total lipid extraction and purification. *Can. J. Biochem. Physiol.* **37**: 911–917.
- Usui, S., Y. Hara, S. Hosaki, and M. Okazaki. 2002. A new on-line dual enzymatic method for simultaneous quantification of cholesterol and triglycerides in lipoproteins by HPLC. *J. Lipid Res.* **43**: 805–814.
- Inokuchi, J., K. Momosaki, H. Shimeno, A. Nagamatsu, and N. S. Radin. 1989. Effects of D-threo- PDMP, an inhibitor of glucosylceramide synthetase, on expression of cell surface glycolipid antigen and binding to adhesive proteins by B16 melanoma cells. *J. Cell. Physiol.* **141**: 573–583.
- Veillon, L., S. Go, W. Matsuyama, A. Suzuki, M. Nagasaki, Y. Yatomi, and J. Inokuchi. 2015. Identification of ganglioside GM3 molecular species in human serum associated with risk factors of metabolic syndrome. *PLoS One.* **10**: e0129645.
- Bietrix, F., E. Lombardo, C. P. A. Van Roomen, R. Ottenhoff, M. Vos, P. C. N. Rensen, A. J. Verhoeven, J. M. Aerts, and A. K. Groen. 2010. Inhibition of glycosphingolipid synthesis induces a profound reduction of plasma cholesterol and inhibits atherosclerosis development in APOE*3 leiden and low-density lipoprotein receptor^{-/-} mice. *Arterioscler. Thromb. Vasc. Biol.* **30**: 931–937.
- Yoneshige, A., A. Sasaki, M. Miyazaki, N. Kojima, A. Suzuki, and J. Matsuda. 2010. Developmental changes in glycolipids and synchronized expression of nutrient transporters in the mouse small intestine. *J. Nutr. Biochem.* **21**: 214–226.
- Shishido, F., S. Uemura, T. Nitta, and J. Inokuchi. 2017. Identification of a new liver-specific c-type mRNA transcriptional variant for mouse ST3GAL5 (GM3/GM4 synthase). *Glycoconj. J.* **34**: 651–659.
- Xie, C., Z. Zhou, N. Li, B. Li, and B.-L. Song. 2012. Ezetimibe blocks the internalization of NPC1L1 and cholesterol in mouse small intestine. *J. Lipid Res.* **53**: 2092–2101.
- Li, P.-S., Z.-Y. Fu, Y.-Y. Zhang, J.-H. Zhang, C.-Q. Xu, Y.-T. Ma, B.-L. Li, and B.-L. Song. 2014. The clathrin adaptor Numb regulates intestinal cholesterol absorption through dynamic interaction with NPC1L1. *Nat. Med.* **20**: 80–86.
- Nagafuku, M., T. Sato, S. Sato, K. Shimizu, T. Taira, and J. Inokuchi. 2015. Control of homeostatic and pathogenic balance in adipose tissue by ganglioside GM3. *Glycobiology.* **25**: 303–318.
- Inamori, K. I., H. Ito, Y. Tamura, T. Nitta, X. Yang, W. Nihei, F. Shishido, S. Imazu, S. Tsukita, T. Yamada, et al. 2018. Deficient ganglioside synthesis restores responsiveness to leptin and melanocortin signaling in obese KK^Y mice. *J. Lipid Res.* **59**: 1472–1481.
- Jennemann, R., S. Kaden, R. Sandhoff, V. Nordström, S. Wang, M. Volz, S. Robine, N. Amen, U. Rothermel, H. Wiegandt, et al. 2012. Glycosphingolipids are essential for intestinal endocytic function. *J. Biol. Chem.* **287**: 32598–32616.
- Hegele, R. A., J. Guy, M. R. Ban, J. Wang. 2005. NPC1L1 haplotype is associated with inter-individual variation in plasma low-density lipoprotein response to ezetimibe. *Lipids Health Dis.* **4**: 16.

Plasma membrane sphingomyelin modulates thymocyte development by inhibiting TCR-induced apoptosis

Kaoru Toshima^{1,*}, Masakazu Nagafuku^{1*}, Toshiro Okazaki², Toshihide Kobayashi³
and Jin-ichi Inokuchi¹

¹Division of Glycopathology, Institute of Molecular Biomembrane and Glycobiology, Tohoku Medical and Pharmaceutical University, 4-4-1 Komatsushima, Aoba-ku, Sendai, Miyagi 981-8558, Japan

²Department of Hematology and Immunology, Kanazawa Medical University, 1-1 Daigaku, Uchinada, Ishikawa 920-0293, Japan

³Faculté de Pharmacie, Université de Strasbourg, 74 route du Rhin, F-67401 Illkirch, France

Correspondence to: J.-i. Inokuchi; E-mail: jin@tohoku-mpu.ac.jp

*These authors equally contributed to this study.

Received 28 September 2018, editorial decision 4 December 2018, accepted 13 December 2018

Abstract

Sphingomyelin (SM) in combination with cholesterol forms specialized membrane lipid microdomains in which specific receptors and signaling molecules are localized or recruited to mediate intracellular signaling. SM-microdomain levels in mouse thymus were low in the early CD4⁺CD8⁺ double-positive (DP) stage prior to thymic selection and increased >10-fold during late selection. T-cell receptor (TCR) signal strength is a key factor determining whether DP thymocytes undergo positive or negative selection. We examined the role of SM-microdomains in thymocyte development and related TCR signaling, using SM synthase 1 (SMS1)-deficient (*SMS1*^{-/-}) mice which display low SM expression in all thymocyte populations. SMS1 deficiency caused reduced cell numbers after late DP stages in TCR transgenic models. TCR-dependent apoptosis induced by anti-CD3 treatment was enhanced in *SMS1*^{-/-} DP thymocytes both *in vivo* and *in vitro*. *SMS1*^{-/-} DP thymocytes, relative to controls, showed increased phosphorylation of TCR-proximal kinase ZAP-70 and increased expression of Bim and Nur77 proteins involved in negative selection following TCR stimulation. Addition of SM to cultured normal DP thymocytes led to greatly increased surface expression of SM-microdomains, with associated reduction of TCR signaling and TCR-induced apoptosis. Our findings indicate that SM-microdomains are increased in late DP stages, function as negative regulators of TCR signaling and modulate the efficiency of TCR-proximal signaling to promote thymic selection events leading to subsequent developmental stages.

Keywords: lipid raft, SM-microdomain, TCR signaling, thymic selection

Introduction

T-cell development in the thymus requires multiple stages to generate a T-cell population having a huge repertoire of antigen specificities but lacking autoreactivity determined by the T-cell receptor (TCR) (1–3). The early T-cell progenitors, CD4⁻CD8⁻ double-negative (DN) thymocytes, produce a functional pre-TCR which promotes further development into CD4⁺CD8⁺ double-positive (DP) thymocytes. During the DP thymocyte stage, developing cells rearrange their TCR α genes and express a mature TCR on their surface. Only cells that bear a TCR subsequently undergo both positive and negative selection to become mature CD4 or CD8

single-positive (SP) thymocytes, which then exit the thymus to enter the peripheral circulation.

DP thymocytes that recognize major histocompatibility complex (MHC) molecules are either positively or negatively selected, depending on the degrees of affinity and avidity of the TCR for MHC-peptide complexes, and the strength of intracellular signaling following TCR engagement (4, 5). Negative selecting ligands with high avidity induce stronger TCR signaling, leading to a variety of intracellular signaling cascades such as ERK5 and other MAPK activation pathways (6). These signaling pathways cooperatively trigger

overt expression of Nur77 family and proapoptotic Bim proteins, resulting ultimately in mitochondrial dysfunction and apoptosis (7, 8). Both loss- and gain-of-function studies of TCR signaling regulators have demonstrated that the threshold between positive and negative selection is defined by the balance between positive and negative signaling (9).

Studies during the past two decades have shown that the initial events of T-cell activation involve movement of the TCR into specialized membrane lipid microdomains, often termed 'lipid rafts', on the cell surface (10). The structure of such microdomains plays a crucial role in efficiency of TCR signaling; in both thymocytes and peripheral mature T cells, these microdomains are clearly involved in TCR signaling and in the localization and function of proximally located proteins (11, 12).

The term 'lipid raft' was introduced by K. Simons and E. Ikonen because of the close association of cholesterol and various sphingolipids, including glycosphingolipids (GSLs) and phosphocholine-containing sphingomyelin (SM), as components of the detergent-resistant complex of signaling molecules present in membrane lipid microdomains (13, 14). Ganglioside-microdomains on the cell surface are easily detected using cholera toxin B subunit (CTx-B), which binds with high sensitivity and specificity to gangliosides GM1 and extended-GM1b (15, 16), and the role of these microdomains in thymocyte development has been extensively studied (17). However, the role of lipid microdomains in thymocytes remains controversial because (i) thymocytes express far fewer GSLs including gangliosides than do peripheral mature CD4 and CD8 T cells and (ii) GM1 and extended-GM1b are extremely minor ganglioside species in thymus (18). Popovic *et al.* showed recently that conditional deletion very early in T-cell development of glucosylceramide synthase, a key enzyme in GSL biosynthesis, resulted in near-total absence of GSLs in DP thymocytes but had no effect on the development of conventional T-cell populations in the thymus (19).

Individual lipid species were recently shown to be localized in distinct, non-overlapping microdomains in plasma membrane; e.g. GM1-microdomains, GM3-microdomains and SM-microdomains (20). Lactosylceramide-microdomains are directly involved in phagocytosis mediated by the integrin CD11b/CD18 and chemotaxis induced by a kind of beta-glucan from *Candida albicans* (21, 22). SM is the most abundant sphingolipid in mammalian plasma membranes and is accumulated in TCR activation domains immunoisolated by anti-CD3 monoclonal antibody (mAb) from TCR-stimulated Jurkat cells (23); however, little is known regarding the involvement of SM-microdomains (in comparison with microdomains easily detected by CTx-B) in thymocyte TCR signaling events and thymic selection.

We investigated the role of SM-microdomains on TCR signaling and selection events in DP thymocytes. SM synthase 1 (SMS1)-deficient (*SMS1*^{-/-}) mice were used for this purpose because SMS1 is the enzyme responsible for *de novo* SM synthesis (24). In normal mouse thymocytes, levels of SM-microdomains and *SMS1* gene were low at the early DP stage but much higher in the late DP stages. Thymocytes of *SMS1*^{-/-} mice showed reduced DP populations and almost no SM expression. TCR-mediated signals involved in negative selection were strongly enhanced in *SMS1*^{-/-} DP

thymocytes, resulting in increased apoptosis induced by TCR stimulation. Normal DP thymocytes (which normally have no SM-microdomains), when treated with SM, acquired surface expression of SM-microdomains and became resistant to TCR-induced apoptosis. Our findings, taken together, indicate that (i) membrane SM lipids suppress apoptosis of DP thymocytes by reducing TCR signaling and (ii) SM-microdomains modulate the TCR signal intensity and the outcomes of thymic selection.

Methods

Mice

SMS1^{-/-} mice, from the C57BL/6 background, were established as described previously (25). OT-I and HY TCR transgenic mice were obtained from Dr K. Ikuta (Kyoto University, Japan) (26, 27). All mice were maintained under defined pathogen-free conditions in the animal facility of Tohoku Medical and Pharmaceutical University, in compliance with institutional guidelines. Animals used in experiments were usually aged 5–7 weeks. Gender- and age-matched littermates of wild-type and heterozygotes were used as controls.

Antibodies and FACS analysis

Thymus and spleen cells were stained with appropriate fluorochrome-conjugated antibodies. The following mAbs were from BioLegend (San Diego, CA, USA): CCR7 (4B12), CD4 (GK1.5), CD5 (53-7.3), CD8 α (53-6.7), CD11b (M1/70), CD24 (M1/69), CD25 (PC61), CD28 (E18), CD44 (IM7), CD62L (MEL-14), CD69 (H1.2F3), cKit (2B8), CD16/32 (93), Gr-1 (RB6-8C5), NK1.1 (PK136), TCR β (H57-597), TCR $\gamma\delta$ (GL3), TCRV α 2 (B20.1), TCRV β 5.1 5.2 (MR9-4), HY (MR14-1), Qa2 (695H1-9-9), TER119 (TER-119). For regulatory T-cell analysis, CD4SP thymocytes were identified by anti-CD4/CD8 surface staining, then fixed and permeabilized for intracellular staining with PE-conjugated anti-Foxp3 (MF-14, BioLegend) mAb. PE-conjugated, isotype-matched mAbs were used as controls. Stained cells were analyzed using a FACSAria II cell sorter (BD Biosciences, San Jose, CA, USA) and the FlowJo software program (Tree Star Inc., Ashland, OR, USA). Data shown are mean \pm SD.

Detection of SM using the specific probes

The physical status of SM present in biological membranes was assessed using two SM-binding proteins: lysenin (Lys) from *Eisenia fetida* (earthworm) and equinatoxin II (EqII) from *Actinia equina* (sea anemone) (28). These are pore-forming protein toxins that bind specifically to SM on target cell membranes, but their manners of binding are different: Lys binds to clusters of 5–6 SM molecules, whereas EqII binds to single SM molecules (Supplementary Figure S1A) (29, 30). A construct of non-toxic Lys fused with enhanced green fluorescent protein (EGFP-NT-Lys), pQE30/His₆-EGFP-NT-Lys containing EGFP at the N-terminus of the DNA fragment of Lys amino acids 161–297 was prepared as described previously (31). A construct of EqII fused with EGFP (EqII-EGFP), pET28/ EqII (8-69)-EGFP-His₆ containing EGFP at the C-terminus of EqII sequences was provided by the RIKEN BioResource Research Center (BRC) through the National Bio-Resource

Project of MEXT (Ministry of Education, Culture, Sports, Science and Technology), Japan. These lipid probes were prepared as described previously (32). To block hemolytic activity of EqtlI without disrupting its SM-binding activity, a disulfide bridge was introduced between Cys8 and Cys69 of EqtlI-EGFP by incubation with 0.5 mM 1,10-phenanthroline and 0.1 mM CuSO_4 for 1 h at 30°C (33). For FACS analysis, thymocytes were washed with phosphate-buffered saline (PBS) and labeled with EGFP-NT-Lys or EqtlI-EGFP in PBS, together with cell surface markers described in [Supplementary Figure S2](#). Stained cells were analyzed using a FACSAria II.

Immunohistochemistry

Whole thymic lobes were fixed in 4% paraformaldehyde–PBS, dehydrated in 20% sucrose, embedded in OCT compound (Sakura Finetek, Tokyo, Japan) and cut into 8- μm sections by cryostat (Microm HM560 MV, Thermo Scientific). For Lys staining, sections were blocked with 3% bovine serum albumin–PBS, and then serially incubated with Lys (Peptides International, Louisville, KY, USA) for 45 min, Lys anti-serum (1:500 dilution, Peptides International) or control rabbit polyclonal IgG (Santa Cruz Biotechnology, Santa Cruz, CA, USA) for 1 h, and Alexa594-conjugated anti-rabbit IgG antibody (1:200 dilution, Invitrogen) for 30 min at 20°C. Images were acquired with an Axioskop 2 Plus (Carl Zeiss, Inc., Thornwood, NY, USA).

Lipid analysis by thin-layer chromatography

Lipid analysis of plasma and thymocytes was performed as described previously (34, 35). Total lipids were extracted with chloroform/methanol and separated into neutral and acidic lipid fractions using DEAE-Sephadex A-25 columns (GE Healthcare, Chalfont St. Giles, UK). Fractions were dried, treated with 0.1 M NaOH in methanol for cleavage of phospholipids and neutralized. Solutions were desalted with Sep-Pak C18 reversed-phase cartridges (Waters Corp., Milford, MA, USA). Neutral lipid samples with equal protein content were separated on silica gel thin-layer chromatography (TLC) plates, half-developed with chloroform/methanol/water (60:25:4), dried and redeveloped with 1-butanol/acetic acid/water (3:1:1, for SM analysis) or with hexane/diethyl ether/acetic acid (50:50:1, for neutral sphingolipid analysis). Phosphorus-containing lipids such as SM were visualized by spraying plates with Dittmer reagent (36), and total lipids were visualized by spraying with 3% cupric acetate/8% phosphoric acid reagent.

In vitro thymocyte stimulation

Total thymocytes were incubated with various concentrations of immobilized anti-CD3 (2C11, BioLegend) plus anti-CD28 (PV-1, Southern Biotechnology, Birmingham, AL, USA) mAbs, with phorbol 12-myristate 13-acetate (PMA)/ionomycin (50 ng ml^{-1} /1 μM , BioLegend) or with dexamethasone (3 nM, Wako Pure Chemical, Osaka, Japan) at 37°C for various time periods. Apoptotic cells were determined by annexin-V and 7-AAD staining with a Vybrant Apoptosis Assay Kit 2 (Molecular Probes, Invitrogen). For Nur77 expression assay,

stimulated cells were stained with CD4 and CD8, fixed and permeabilized with a True-Nuclear Transcription Factor Buffer Set (BioLegend), and incubated with PE-conjugated anti-Nur77 (eBioscience) and mouse IgG1 control (BioLegend) mAbs. Total thymocytes were stimulated with soluble anti-CD3 plus anti-CD4 mAbs for 5 min at 37°C. DP thymocytes were identified by anti-CD4/CD8 surface staining, then fixed and permeabilized for intracellular staining with allophycocyanin (APC)-conjugated anti-phospho ZAP-70 (Y319) and FITC-conjugated ZAP-70 mAbs (BioLegend). Fluorochrome-conjugated, isotype-matched antibodies were used as controls. Labeled cells were analyzed using a FACSAria II.

Immunoblotting analysis

Thymocytes were stimulated with anti-CD3 plus anti-CD28 mAbs for 2 or 6 h at 37°C and lysed with ice-cold lysis buffer containing 25 mM Tris–HCl (pH 7.6), 120 mM NaCl, 5 mM ethylenediaminetetraacetic acid (pH 8.0), 5 mM Na_3VO_4 , 10 mM NaF, 1% TX-100, 1% deoxycholate-Na, 1 mM phenylmethylsulfonyl fluoride (PMSF) and the Complete Protease Inhibitor Cocktail (Roche) for 30 min. Cell lysates were resolved by sodium dodecyl sulfate–polyacrylamide gel electrophoresis, transferred onto PVDF membranes (Immobilon-P, Millipore, Bedford, MA, USA), and probed with the following mAbs: anti-phospho-ERK5 (T218/T220), anti-ERK5, anti-Bim (Cell Signaling Technology, Beverly, MA, USA) and anti- β -actin (Sigma-Aldrich).

Statistical analysis

Values presented are mean \pm SD. Homoscedasticity was verified by *F*-test. Means were compared by unpaired Student's *t*-test or Welch's *t*-test for two-group comparison. For data with non-Gaussian distribution, comparisons were made by Mann–Whitney *U*-test. For multigroup analysis, homoscedasticity was verified by Bartlett's test, and data were compared by the Tukey–Kramer test or Scheffe's *F*-test. Notations used to indicate significant differences were: **P* < 0.05, ***P* < 0.01, ****P* < 0.001.

Results

Expression of SM-microdomains in thymocytes increases greatly in late stages of thymic selection

SM is expressed ubiquitously in mammalian cell membranes and, in combination with cholesterol, forms specialized membrane lipid microdomains that regulate membrane fluidity, protein trafficking and signal transduction. To investigate the role of SM-microdomains in thymocyte development in our mouse model, we first examined SM expression profiles in thymocyte sub-populations. TLC analysis revealed that the SM content decreased sharply when DN thymocytes developed into DP thymocytes, and then increased when these developed into SP thymocytes (Fig. 1A). SM expression was higher in CD4SP than in CD8SP thymocytes.

Lys binds to clustered SM molecules, while EqtlI binds to single SM molecules (see Methods “Detection of SM using the specific probes”). We therefore presumed that Lys reactivity characterized SM-enriched membrane microdomains

(termed 'SM-microdomains'), whereas EqtlI reactivity characterized single SM molecules dispersed in membrane (termed 'dispersed-SM') (Supplementary Figure S1A) (19, 20). Consistent with this presumption, treatment of thymocytes with 4 mM methyl- β -cyclodextrin (M β CD), a cholesterol-depletion reagent commonly used for disruption of lipid rafts, completely eliminated Lys staining but not EqtlI staining (Supplementary Figure S1B). We therefore used these two probes to evaluate the physical status of SM present in plasma membranes at each stage of thymocyte development.

Expression patterns of SM-microdomains (detected by EGFP-NT-Lys) and of dispersed-SM (detected by EqtlI-EGFP) on the cell surface were similar to those of total SM analyzed by TLC (Fig. 1A and B). To assess SM-microdomain levels during thymocyte development, we labeled whole thymocytes with Lys and with several surface markers that identify various sub-populations during progression from DN to SP thymocytes and performed FACS analysis (Fig. 1C). Surface markers, and the hierarchical gating strategy used (37), are summarized in Supplementary Figure S2. SM-microdomain levels were lower in DP stages than in DN and SP stages in general, and particularly low at the small DP stage prior to thymic selection. After the small DP stage, the SM-microdomain level increased during progression from CD69⁺ DP to CD4⁺CD8^{int} thymocytes following thymic selection (Fig. 1C). There was a consequent >10-fold increase of cell surface SM-microdomains after versus before thymic selection. The dispersed-SM level was lowest at the small DP stage and nearly twice as high in the CD4⁺CD8^{int} stage (Fig. 1D). There was a striking difference in up-regulation of the SM-microdomain level (>10-fold) versus the dispersed-SM level (<2-fold) during DP thymocyte development (Fig. 1E). These findings suggest that *de novo* synthesized SM molecules are used almost entirely for microdomain formation rather than simply floating on the plasma membrane.

T-progenitor cells, after entry into the thymus, differentiate into DP thymocytes in the cortex (38, 39). DP thymocytes receive survival signals and undergo further differentiation into SP thymocytes. These signals also induce relocation of thymocytes from the cortex to the medulla; therefore, most thymocytes in the medulla are SP thymocytes (40). Staining intensity by Lys for SM-microdomains was much higher in the medulla than in the cortex, indicating high formation of SM-microdomains during DP-to-SP differentiation (Fig. 1F). To examine this process in more detail, we performed multicolor staining of thymocytes with Lys or EqtlI, in combination with the early activation marker CD69 and the chemokine receptor CCR7. CD69 and CCR7 are used to classify developing thymocytes into five stages in terms of selection, migration and maturation (41, 42). CD69⁺CCR7⁻ thymocytes are localized in the cortex and have not yet received TCR selection signals (stage I). CD69⁺CCR7⁻ thymocytes have received TCR signals and show increased CD69 expression (stage II). CD69⁺ thymocytes that receive continuous TCR signals begin to express CCR7 (stage III) and migrate to the medulla. CD69⁺CCR7^{hi} medullary thymocytes (stage IV) show reduced CD69 expression and then become competent to exit the thymus (stage V) (42). Lys^{hi} thymocytes, which show increased SM-microdomain expression, begin appearing in stage III, and are predominant in stage IV (Fig. 1G). Positively

selected thymocytes up-regulate surface TCR expression to become SP thymocytes (43). The time course of appearance of the TCR^{hi} population during stages I to V was similar to or slightly earlier than that of the Lys^{hi} population (Fig. 1G), even though thymocytes in stage II had already received TCR signals. These findings indicate that SM-microdomains are formed in the late stages of positive selection, up to or just before the DP-to-SP transition, probably as a consequence of TCR signals.

GSLs and SM form a variety of microdomains in plasma membranes, some of which are based on a physical association of cholesterol with SM (44–46). We used CTx-B (binds to GM1 and extended-GM1b) and filipin III (binds to cholesterol) to determine whether cell surface levels of GSLs and cholesterol fluctuate similarly to that of SM during thymocyte development. Levels of CTx-B-binding gangliosides did fluctuate, but (in contrast to SM-microdomain levels) did not increase from small DP to CD4⁺CD8^{int} stages (Supplementary Figure S3A). Cholesterol level increased in parallel with the SM-microdomain level from small DP to CD4⁺CD8^{int} stages (Supplementary Figure S3B). These findings suggest that the SM-microdomain level specifically increases after versus before thymic selection, because SM is able to form membrane microdomains in combination with cholesterol.

SM expression in mammalian cells is controlled by two SM synthases, SMS1 and SMS2 (Supplementary Figure S4) (24, 47). SMS1 is primarily responsible for *de novo* SM synthesis in the Golgi, while SMS2 is involved in regenerating SM from ceramide hydrolyzed by sphingomyelinases on the cell surface (24, 47, 48). We detected SMS1 mRNA, but not SMS2 mRNA, in thymocytes (Supplementary Figure S5A). In contrast, expression of SMS2 mRNA was much higher than that of SMS1 mRNA in liver, consistent with findings by Jiang's group (49, 50). Changes in SMS1 expression patterns among DN, DP and SP thymocytes as revealed by quantitative PCR analysis (Supplementary Figure S5B) were comparable to those of SM-microdomains (Fig. 1B). Thus, SMS1 but not SMS2 is evidently the enzyme primarily responsible for SM biosynthesis in mouse thymocytes.

To further evaluate the similarity of expression patterns of the SMS1 gene and SM-microdomains during DN-to-SP thymocyte development, we examined global microarray datasets from the Immunological Genome Project (www.immgen.org), which detail gene expression in >200 mouse immune cell populations (51). The pattern of SMS1 expression during DN-to-SP thymocyte development (Supplementary Figure S5C) was similar to that of Lys fluorescence intensity (Fig. 1C). Thus, cell surface SM-microdomain levels during thymocyte development appear to be strictly regulated by SMS1 gene expression levels.

SM-microdomains are essentially absent in SMS1-deficient thymocytes

The role of SM in thymocyte development was further evaluated using SMS1^{-/-} mice. Jiang *et al.* reported that serum SM levels in SMS1^{-/-} were ~50% of levels in controls (49). Similarly, our TLC analyses showed that in SMS1^{-/-}, 46% of SM remained in plasma. In SMS1^{-/-} thymocytes, cellular SM was present in <10% of thymocytes in control mice

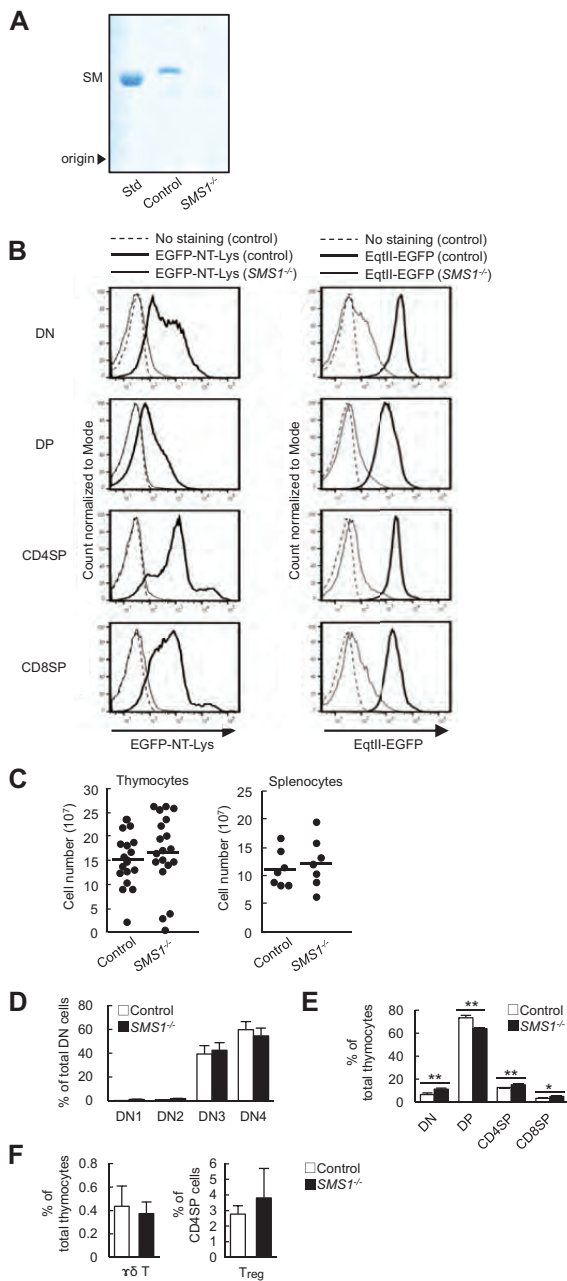


Fig. 2. *SMS1*^{-/-} thymocytes lack surface SM-microdomains. (A) Total cellular SM in *SMS1*^{-/-} thymocytes. Neutral lipids were purified from control and *SMS1*^{-/-} thymocytes and separated on TLC plates. SM was detected by Dittmer reagent. Std: standard lipid. Data shown are representative of three independent experiments. (B) Cell surface staining of gated DN, DP and SP sub-populations of control and *SMS1*^{-/-} thymocytes labeled with EGFP-NT-Lys (left) and EqtlI-EGFP (right). Data shown are representative of three independent experiments. Bold lines: littermate control thymocytes. Thin solid lines: *SMS1*^{-/-} thymocytes. Dashed lines: non-labeled control thymocytes. (C) Absolute numbers of total thymocytes and splenocytes. Dots: individual mice; *n* = 19 (left), *n* = 7 (right). Bars: means. (D) CD4⁺CD8⁻ DN thymocytes were subdivided into DN1 (CD25⁺cKit⁺), DN2 (CD25⁺cKit⁻) and DN4 (CD25⁺cKit⁻) subsets by multicolor FACS analysis. Data shown are ratios of cell numbers of sub-populations to total DN thymocytes. *n* = 3. (E) Ratios of numbers of DN, DP, CD4SP and CD8SP thymocytes to total thymocytes. *n* = 3. (F) Ratios of numbers $\gamma\delta$ T cells (TCR $\gamma\delta$ ⁺) to total thymocytes (left) and T_{reg} cells (CD25⁺Foxp3⁺) to CD4SP thymocytes (right). *n* = 3. **P* < 0.05, ***P* < 0.01.

(Fig. 2A and Supplementary Figure S6A). SM-microdomains were essentially absent in *SMS1*^{-/-} thymocytes, and a small amount of dispersed-SM was present (Fig. 2B), suggesting that the amount of cell surface SM was insufficient to cluster and form SM-microdomains. We next examined the effect of SMS1 deficiency on the content of ceramide, the precursor of numerous sphingolipids, including gangliosides and SM. Levels of ceramide on the cell surface and inside cells were not notably altered in *SMS1*^{-/-} thymocytes (Supplementary Figure S6A and B), indicating that SMS1 deficiency did not cause a compensatory increase of ceramide. In *SMS1*^{-/-} mice, levels of CTx-B-binding gangliosides were slightly increased in CD4SP thymocytes, and unchanged in other types of thymocytes (Supplementary Figure S6C).

Aberrant thymic selection in SMS1^{-/-} mice

Thymocyte cellularity was evaluated in *SMS1*^{-/-} mice. Total numbers of thymocytes and splenocytes were similar in *SMS1*^{-/-} versus control mice (Fig. 2C). The DP sub-population was smaller in *SMS1*^{-/-} versus control thymocytes (Fig. 2E), but DN sub-populations were similar (Fig. 2D). There are no significant differences in $\gamma\delta$ T and T_{reg} populations between control and *SMS1*^{-/-} mice (Fig. 2F).

Developmental defects associated with thymic selection can be masked by compensatory changes in the TCR repertoire. We therefore introduced single transgenes encoding $\alpha\beta$ TCRs into *SMS1*^{-/-} mice to limit compensation, and crossed HY and OT-I TCR transgenic mice with *SMS1*^{-/-} mice. Numbers of TCR transgenic positive thymocytes were much lower in OT-I *SMS1*^{-/-} and female HY *SMS1*^{-/-} mice than in TCR transgenic controls (Fig. 3A and B). Among both OT-I *SMS1*^{-/-} and female HY *SMS1*^{-/-} thymocytes, numbers of DP and CD8SP thymocytes were greatly reduced (Fig. 3C and D). In OT-I *SMS1*^{-/-} mice, numbers of stage II CD69^{hi}CCR7⁻ to stage IV CCR7^{hi}CD69^{hi} thymocytes were reduced (Fig. 3E). These findings demonstrate that SMS1 deficiency inhibits positive selection.

Finally, we examined the effect of SMS1 deficiency in male HY TCR transgenic mice. Total HY TCR⁺ cell number did not differ notably in *SMS1*^{-/-} versus control thymocytes (Fig. 4A). One possible explanation is that HY TCR recognizes a male-specific antigen, such that male HY mice undergo massive deletion of thymocytes by negative selection upon reaching the DP stage (52). On the other hand, the CD8SP population was reduced in *SMS1*^{-/-} thymocytes (Fig. 4B), suggesting that SMS1 deficiency promotes negative selection.

TCR stimulation in SMS1^{-/-} DP thymocytes induces up-regulation of apoptosis-related molecules involved in negative selection and apoptotic cell death

Thymic selection depends on TCR-mediated intracellular signaling. We examined the effect of SMS1 deficiency on thymocyte apoptosis induced by anti-CD3 mAb administration. Following *in vivo* anti-CD3 mAb treatment, annexin-V⁺ thymocytes were more numerous in *SMS1*^{-/-} versus control thymus (Fig. 5A). In *in vitro* culture, DP thymocyte apoptosis induced by anti-CD3 + anti-CD28 mAb treatment was also higher in *SMS1*^{-/-} versus control mice (Fig. 5B). SMS1 deficiency had no effect on apoptosis induced by PMA/ionomycin (which bypasses TCR-proximal signaling) or by dexamethasone (a synthetic glucocorticoid) (Fig. 5B). These findings, taken

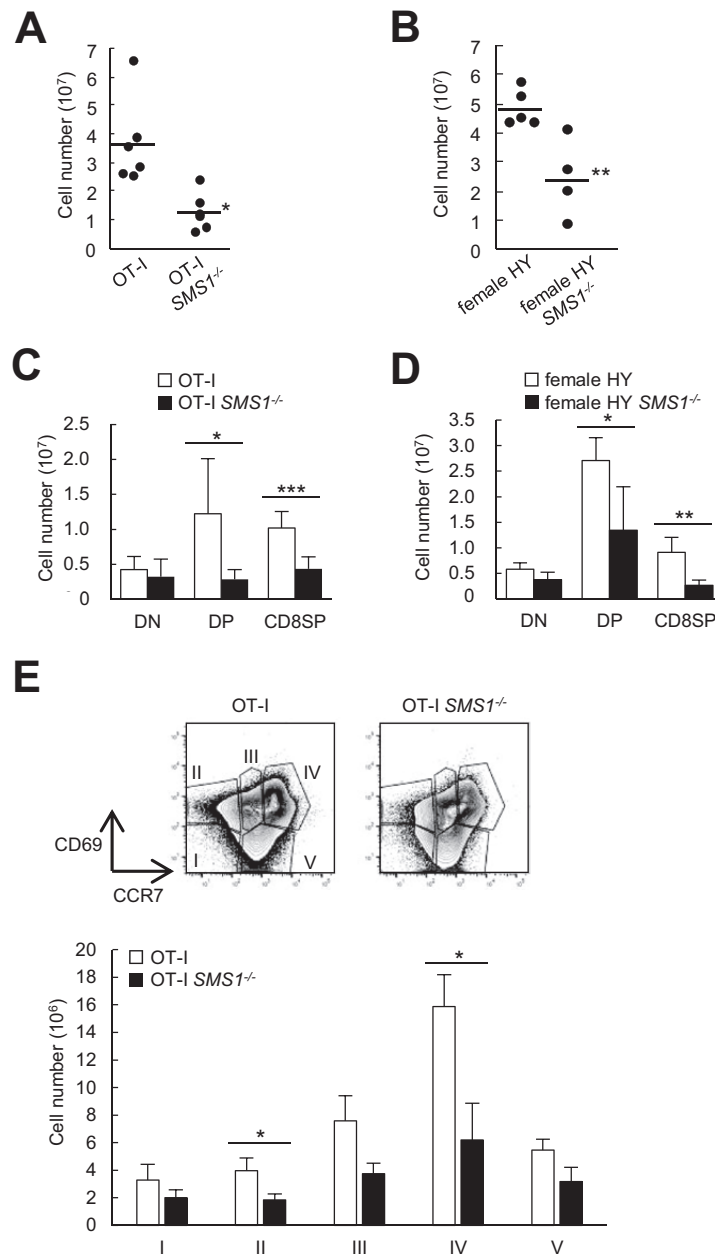


Fig. 3. Reduced positive selection in *SMS1*^{-/-} mice. (A, B) Absolute numbers of transgenic TCR-positive thymocytes gated on Vα2⁺Vβ5⁺ cells for OT-I mice (A), and on HY TCR⁺ cells for female HY mice (B). Dots: individual mice. Bars: means. Each group, *n* = 6 (A). Female HY mice, *n* = 5; female HY *SMS1*^{-/-} mice, *n* = 4 (B). (C, D) Absolute numbers of DN, DP and CD8SP thymocytes defined by CD4/CD8 expression in transgenic TCR-positive thymocytes as in A and B. Each group, *n* = 6. (C). Female HY mice, *n* = 5; female HY *SMS1*^{-/-} mice, *n* = 4 (D). (E) Absolute numbers of OT-I thymocytes, subdivided into five stages of thymocyte development (I through V) as in Fig. 1(G). Each group, *n* = 3. **P* < 0.05, ***P* < 0.01, ****P* < 0.001.

together, suggest that aberrant thymic selection in *SMS1*^{-/-} mice is a consequence of aberrant TCR signal intensity.

We next examined the role of TCR-mediated signaling in negative selection. ZAP-70, a Syk-family tyrosine kinase, plays a key role in both positive and negative selection (53). The amount of phosphorylated ZAP-70 recruited by a phosphorylated TCR complex affects the fate of DP thymocytes;

i.e. differentiation into SP thymocytes or elimination by apoptosis (54). ZAP-70 phosphorylation induced by anti-CD3 + anti-CD4 mAb treatment was higher in *SMS1*^{-/-} than in control DP thymocytes (Fig. 5C). TCR-proximal signaling, including ZAP-70, is divided into two cascades (ERK5 pathway and Bim pathway) in negative selection signals (55). ERK5 activity regulates the expression of proapoptotic Nur77 family members.

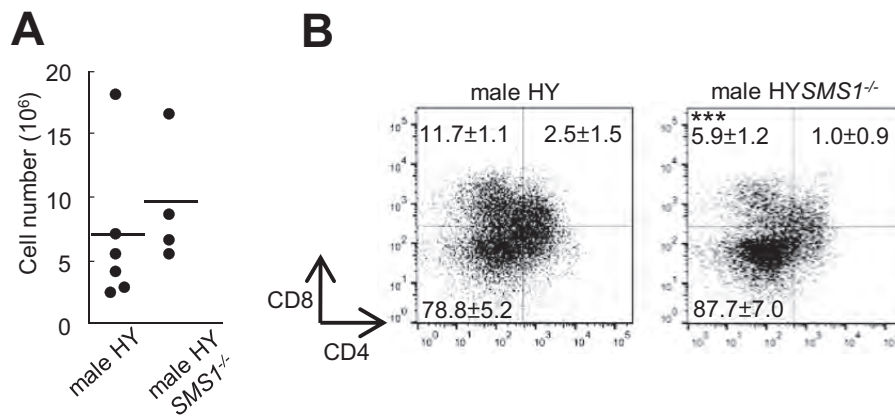


Fig. 4. Enhanced negative selection in *SMS1*^{-/-} mice. (A) Absolute numbers of transgenic TCR-positive thymocytes gated on HY TCR⁺ thymocytes for male HY and male HY *SMS1*^{-/-} mice. Dots: individual mice. Bars: means. Male HY mice, $n = 6$; male HY *SMS1*^{-/-} mice, $n = 4$. (B) Dot plots of CD4 versus CD8 α for HY TCR⁺ thymocytes. Numbers in quadrants: mean \pm SD of percentage of each thymocyte population defined by CD4 and CD8. Male HY mice, $n = 5$; male HY *SMS1*^{-/-} mice, $n = 3$. *** $P < 0.001$.

Proapoptotic Bim plays a key role in negative selection independently of the ERK5-Nur77 pathway (56, 57). TCR stimulation of *SMS1*^{-/-} thymocytes resulted in increases of ERK5 phosphorylation, Bim expression (Fig. 5D) and Nur77 induction (Fig. 5E). The CD5 expression level is developmentally regulated by TCR signaling and TCR avidity, and is therefore used as a marker of TCR signal intensity in thymocytes (58). CD5 expression in *SMS1*^{-/-} DP thymocytes was up-regulated by TCR stimulation (Fig. 5F). The enhancement of TCR signal intensity in *SMS1*^{-/-} DP thymocytes increased the sensitivity to TCR-mediated apoptosis.

SM-microdomains function as negative regulators of TCR signal intensity in normal DP thymocytes

The above-described findings suggest that SM-microdomains function as negative regulators of TCR signal intensity and thymocyte apoptosis during thymic selection. Expression of SM-microdomains in normal DP thymocytes was low prior to thymic selection, and increased greatly in the latter stage of positive selection (Fig. 1C and G). We examined the possibility that addition of SM to normal DP thymocytes leads to a reduction of TCR signaling and TCR-induced apoptosis. TCR stimulation of whole DP thymocytes resulted in a strong, dose-dependent increase of SM-microdomain formation in the latter stage of positive selection (Fig. 6A). By SM addition, TCR stimulation also significantly reduced CD5 expression and enhanced cell viability (Fig. 6B and C). These findings indicate that the SM content of normal DP thymocytes controls the formation of SM-microdomains, and consequent reduction of TCR signal intensity.

Discussion

We performed a comprehensive analysis of the expression and function of plasma membrane SM-microdomains as related to thymocyte development. Use of EGFP-NT-Lys, a probe that recognizes SM molecules clustered in microdomains as distinct from single SM molecules dispersed in the outer leaflet of the membrane lipid bilayer (Supplementary

Figure S1) (29, 30), allowed us to demonstrate for the first time a great increase in SM-microdomain levels during DP stages, particularly at the end of thymic selection events (Fig. 1). The process involved three stages: (i) the pre-selection stage, TCR β ^{low}CD69⁻ DP, characterized by the absence of SM-microdomains because of low SM expression levels; (ii) the CD69⁺ DP stage, with initiation of TCR signaling required for thymic selection, and an increase of SM-microdomain levels; and (iii) the post-selection stage, TCR β ^{hi}CD69⁺CD4⁺CD8^{low}, in which SM-microdomain levels are >10-fold higher than in the pre-selection stage. Levels of dispersed, single SM molecules increased only slightly during this process (Fig. 1). Up-regulation of the SM-microdomain level and TCR expression paralleled the course of thymic selection. TCR expression levels generally remain very low during thymic selection and are up-regulated only in successfully selected thymocytes (59, 60).

Cholesterol is physically associated with SM in membrane microdomains (46). The plasma membrane cholesterol content during pre- to post-selection stages increased in parallel with levels of SM but not of gangliosides (Supplementary Figure S3B). Expression levels of CTx-B-binding gangliosides were very low in the DP stage, increased upon differentiation into the CD8 SP stage, and then declined upon differentiation into the CD4SP stage, consistent with a report by de Mello Coelho *et al.* (61). Ganglioside-microdomains are polarized to TCR activation sites in response to TCR stimulation in mature peripheral T cells, but not in DP thymocytes (62). These findings, taken together, suggest that SM-microdomains (not ganglioside-microdomains) are formed preferentially in the plasma membrane during the course of selection events in DP thymocytes.

Analysis of SM-microdomains is necessary to elucidate the role of membrane lipid microdomains in thymocyte TCR signaling and its outcomes. We used *SMS1*^{-/-} mice for this purpose because they express only a trace amount of SM in thymocytes and have no Lys-positive DP thymocytes; i.e. DP thymocytes in these mice have no surface SM-microdomains (Fig. 2). *SMS1*^{-/-} mice show a slight (although significant)

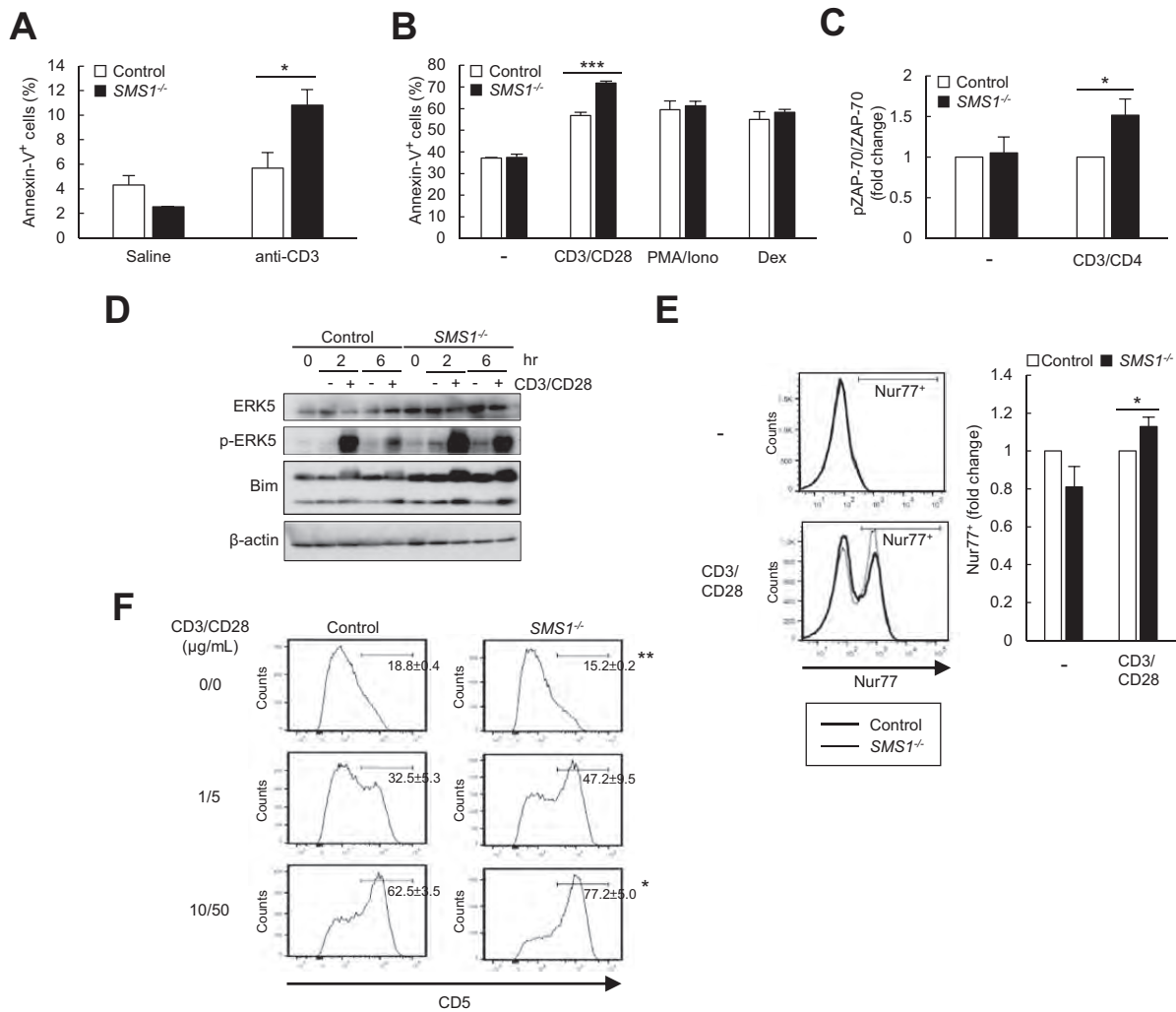


Fig. 5. Enhanced TCR signaling in *SMS1*^{-/-} DP thymocytes, accompanied by up-regulation of apoptosis-related molecules and of TCR-induced apoptotic cell death. (A) Thymocyte apoptosis induced by anti-CD3 mAb administration. Littermate control and *SMS1*^{-/-} mice were injected i.p. with 3 μg anti-CD3 mAb or saline twice, at 24-h intervals. Mice were killed 24 h after the last injection, thymocytes were isolated and stained with CD4, CD8 and annexin-V, and stained cells were analyzed by FACS. Data shown are percentages of annexin-V⁺ DP thymocytes. (B–F) *In vitro* assays with TCR stimulation. (B) Thymocytes were cultured in the absence (–) or presence of immobilized anti-CD3 (1 μg ml⁻¹) plus anti-CD28 (5 μg ml⁻¹) mAbs (CD3/CD28), 50 ng ml⁻¹ PMA plus 1 μM ionomycin (PMA/Iono) or 3 nM dexamethasone (Dex). Cells were cultured for 18 h, harvested and analyzed as in (A). Data shown are mean ± SD from three independent experiments. (C) Intracellular staining of phospho-ZAP-70. Thymocytes were unstimulated (–) or stimulated with anti-CD3 plus anti-CD4 mAbs (CD3/CD4) for 5 min, and analyzed as described in Methods. MFI values for phospho-ZAP-70 and total ZAP-70 were calculated in the DP-gated population. Relative phosphorylation of ZAP-70 in stimulated cells was normalized relative to total ZAP-70 protein for each group. Data shown are fold change values relative to unstimulated thymocytes of control mice, normalized to one. *n* = 4. (D) Thymocytes were unstimulated (–) or stimulated (+) with anti-CD3 (10 μg ml⁻¹) plus anti-CD28 (20 μg ml⁻¹) for the indicated periods. ERK5, phospho-ERK5, Bim and β-actin were detected by immunoblotting analysis. Data shown are from five independent experiments. (E) Thymocytes were cultured in the absence (–) or presence of immobilized anti-CD3 (1 μg ml⁻¹) plus anti-CD28 (5 μg ml⁻¹) mAbs (CD3/CD28) for 2 h, and analyzed as described in Methods. Histograms at left: intracellular Nur 77 expression on the gated DP population. Nur 77 MFI values in the Nur77⁺ cells were calculated for each group. Bar graphs at right: ratios of values to those of unstimulated cells of control mice, normalized to one. *n* = 3. (F) Thymocytes were cultured with immobilized anti-CD3 plus anti-CD28 mAbs for 16 h at the indicated concentrations, stained with anti-CD5 mAb and analyzed by FACS. Histograms: CD5 expression gated on the DP population. Horizontal lines: percent CD5⁺ cells. *n* = 4. **P* < 0.05, ***P* < 0.01, ****P* < 0.001.

reduction of DP thymocytes. Numbers of *SMS1*^{-/-} thymocytes bearing positively selected transgenic TCRs are relatively quite low (Fig. 3A and B). CD69⁺CCR7⁺ late developmental stages of thymic selection are particularly affected (Fig. 3E). Male *SMS1*^{-/-} mice bearing HY TCR transgenes show a significant decrease in the CD8SP compartment (Fig. 4C). Positive selection generally precedes negative

selection. In *SMS1*^{-/-} mice, positive selection was abolished at the end of selection stages, and negative selection was substantially enhanced.

A difference in ligand affinity for the TCR is essential for shifting the threshold from positive to negative selection signals via the TCR complex (63). Outcomes of positive and negative selection are determined by not only the affinity and

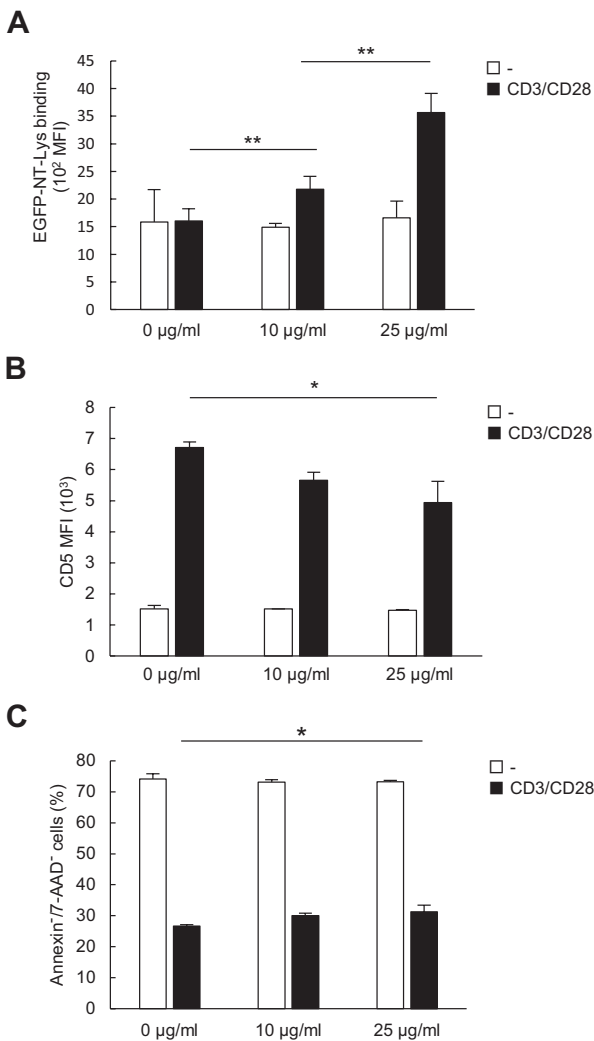


Fig. 6. Addition of SM to normal DP thymocytes lacking SM-microdomains reduces their TCR signal intensity. Thymocytes were cultured with or without immobilized anti-CD3 ($1 \mu\text{g ml}^{-1}$) plus anti-CD28 ($5 \mu\text{g ml}^{-1}$) mAbs (CD3/CD28) in the presence of indicated concentrations of SM. Cells were cultured for 16 h, harvested, stained with Lys (A), CD5 (B) or annexin-V plus 7-AAD (C), and analyzed by FACS. (A, B) Mean \pm SD of MFI of Lys and CD5 gated on DP thymocytes. (C) Percentage of annexin-V-7-AAD⁺ cells. $n = 3$. * $P < 0.05$, ** $P < 0.01$.

avidity of TCR-antigen engagement, but also the strength and duration of TCR signals (64). Induction of thymocyte apoptosis by *in vivo* administration of anti-CD3 mAb was enhanced in *SMS1*^{-/-} mice (Fig. 5A). In mature T cells, membrane lipid microdomains serve as a platform for TCR-proximal proteins, e.g. coreceptors CD4 and CD8, Src family kinases Lck and Fyn, ZAP-70, and the transmembrane adaptor LAT (65, 66). We demonstrated previously that splenic CD4⁺ T cells from *SMS1*^{-/-} mice showed impairment of clonal expansion, IL-2 and IFN γ production and phosphorylation of ZAP-70 and LAT upon CD3- and CD4-mediated activation (25). Protection of *SMS1*^{-/-} mice was observed in a ConA-induced hepatitis model (25). We therefore expected to find that

SM-microdomains are involved in TCR signaling associated with thymic selection in central tolerance.

Contrary to expectation, *SMS1*^{-/-} DP thymocytes showed enhanced ZAP-70 phosphorylation and increased expression of proapoptotic proteins and hyper-apoptotic phenotypes upon TCR ligation (Fig. 5). This finding may be attributable to two qualitative differences between immature thymocytes and mature T cells: (i) similar but not identical molecules involved in TCR-proximal signaling (67, 68) and (ii) formation patterns of the immunological synapse structure at the thymocyte/antigen-presenting cell interface are different from those observed during mature CD4⁺ T-cell activation (69–71). SM expression patterns vary greatly among T-cell developmental stages, e.g. DP, CD4SP and CD8SP thymocytes, and CD4⁺ and CD8⁺ T cells (Fig. 1; our unpublished data). The difference in need for SM-microdomains in thymocytes versus mature CD4⁺ T cells may be due to these factors.

Positive and negative selection, two contrasting developmental outcomes, depend completely on signals initiated from the TCR, even though the TCR signaling machinery is qualitatively similar in composition (67). Some key players in the TCR signaling network responsible for the induction of negative rather than positive selection have been identified (63, 72). Negative selecting ligands for the TCR induce stronger activation of TCR-proximal signaling in thymocytes, leading to ERK5 phosphorylation, induction of Nur77 family members, and up-regulation of proapoptotic Bim protein. ERK5-Nur77 and Bim cascades cooperatively develop mitochondrial dysfunction, resulting in apoptosis. Among the TCR-proximal signaling molecules, ZAP-70 is a well-known kinase essential for both positive and negative selection (53). Phosphorylation of ZAP-70 at Y319 after 5 min of TCR stimulation was significantly increased by *SMS1* deficiency (Fig. 5B). In a study by Daniels *et al.*, nearly all thymocytes stimulated by negative selecting ovalbumin peptides showed recruitment of phosphorylated ZAP-70 at Y319 to the plasma membrane within 2 min, while such recruitment was much lower for positive selecting ovalbumin peptides (9). Thus, SM-microdomains function as negative regulators of TCR-proximal signaling during thymic selection.

Expression of the proapoptotic protein Nur77 was correlated with the strength of TCR signaling, and particularly with ERK5 activation (55, 73, 74). Bim is an antagonist of Bcl-2 that promotes cellular survival by inhibiting the activities of the proapoptotic proteins Bax and Bak, thereby inducing mitochondrial dysfunction. These two major effector pathways of thymic deletion were promoted by *SMS1* deficiency (Fig. 5C and D). Enhanced TCR signaling in *SMS1*^{-/-} mice resulted in increased CD5 expression on DP thymocytes (Fig. 5F). The cell surface glycoprotein CD5 is used as a surrogate marker for TCR signal strength during thymic development; the degree of surface CD5 expression is correlated with the strength of TCR signaling generated by cells (58, 75). These findings suggest that SM-microdomains act as a platform to modulate TCR signaling during thymic selection events, and are involved in fine tuning of thresholds for positive and negative selection.

SMS1 deficiency inhibited the DP-to-SP differentiation in transgenic models of positive selection (Fig. 3), and greatly reduced (by 33–50%) the overall thymocyte cellularity,

particularly CD69⁺CCR7^{hi} medullary thymocytes (stage IV). CD69⁺ thymocytes up-regulate TCR surface expression during stages III and IV, when positively selected thymocytes migrate to the medulla to undergo negative selection, and develop very high surface expression of Lys-positive SM-microdomains (Fig. 1G). Evidently, expression of SM-microdomains is greatly increased when positively selected thymocytes are no longer able to generate intense intracellular signaling from mass-produced TCR molecules, perhaps causing a switch from a positive to a negative selection signal. Thus, SM-microdomains may reduce the TCR signal strength such that positive selection signals are shifted from a positive to a negative pathway in selecting thymocytes, whereas negative selection signals are enhanced.

The roles of lipid rafts in thymocyte development have been investigated by many groups. Positive selection signals occur during the recruitment of TCR signaling molecules to the raft fraction (11, 12). CD4 lineage commitment from DP is directed by raft-associated presentation of MHC class II molecules (76). Fluorescence-labeled CTx-B is often used for microscopic visualization of lipid rafts and immunological synapse structures; however, CTx-B reacts only with a few ganglioside species which comprise a minor proportion of raft-forming sphingolipids in DP thymocytes (18). Specific lipid species are presumed to be localized in distinct, non-overlapping microdomains in the plasma membrane. TCR signals did not cause polarization of lipid rafts visualized with CTx-B in DP thymocytes (62). Thus, the validity of the lipid microdomain concept in thymocytes is questionable. We demonstrate here that a reduction or increase of SM-microdomains in thymocytes causes, respectively, an increase or reduction of TCR signaling. Zech *et al.* found that SM lipids with cholesterol and saturated phosphatidylcholine were accumulated in TCR activation domains immunisolated by anti-CD3 mAb from Jurkat cells following TCR stimulation (23). These findings, taken together, suggest that SM-microdomains serve as a platform for TCR-proximal signaling, and that SM-microdomains (not ganglioside-microdomains) negatively modulate TCR responsiveness during thymic selection.

Several points remain unresolved. Do SM-microdomains contain TCR-associated signaling components and TCR *per se* following TCR ligation in selecting thymocytes, similarly to mature T cells? If so, is SM-microdomain clustering accompanied by immunological synapse formation on the surface of selecting thymocytes? The latter question is of great interest in view of the diversity of immunological synapse structures (77, 78). DP thymocytes interacting with thymic stromal cells did not form a central supramolecular activation cluster; i.e. a central area of immunological synapses observed between mature CD4⁺ T cells and B cells, where most of the TCR and CD28 are accumulated (70). Instead, the above cells, during positive selection, formed 'multifocal' immunological synapses in which small accumulated TCR clustered at multiple sites in the cell-cell interface (69). The formation of these multifocal synapses was the result of much lower TCR expression by DP thymocytes relative to peripheral T cells (79). In this way, pre-selected DP thymocytes inherently possess the ability to transduce the TCR signaling required for thymic selection, despite the low surface expression of

the TCR, SM-microdomains and cholesterol (Fig. 1C and Supplementary Figure S3B) (77, 80). Positively selected thymocytes multiply surface TCR levels, which potentially could lead to triggering stronger TCR signaling, and at this time they also up-regulate SM-microdomains and cholesterol on their surface (Fig. 1G and Supplementary Figure S3B). It was recently reported that cholesterol binding to the TCR β chain maintains the TCR in an inactive status and cholesterol removal causes it to switch to the active status (81). In contrast, other recent reports claim that cholesterol serves as a positive regulator of TCR activation because cholesterol extraction results in the disruption of TCR nanoclustering (82, 83). Other membrane lipids interacting with cholesterol may determine which of these opposing functions dominates; TCRs and associated signal molecules can perceive their microenvironment, such as the concentration of a specific lipid species and the presence of a specific lipid microdomain, and respond accordingly. In view of these findings, we hypothesize that initially low amounts of SM-microdomains are greatly increased to prevent the persistence of TCR signals in positively selected thymocytes, despite the fact that TCR expression is strongly up-regulated at the same time in these cells, which potentially could trigger a stronger TCR signaling to cause a switch from positive to negative selection.

SM-microdomains are shown in this study to negatively regulate TCR signal transduction in thymocyte development. Expression levels of CTx-B-binding gangliosides, in contrast to those of SM, are higher in CD8SP than CD4SP thymocytes (Supplementary Figure S6A). We demonstrated previously that these functions depend on distinct expression patterns of ganglioside species in CD4⁺ and CD8⁺ T cells (15). Optimal expression levels of specific sphingolipid species in specific types of immune cells are presumably necessary for proper functioning of the cells. We therefore need to elucidate the roles of specific lipid species in membrane microdomains. To understand how SM-microdomains reduce TCR signaling in the plasma membrane of positively selecting thymocytes, we require microscopic visualization of lipid microdomains and immunological synapse structures to clarify interactions between SM-microdomains and TCR-proximal signaling molecules during thymic selection. Confirmation that TCR signal transduction in thymic selection is controlled by 'fine tuning' of SM-microdomain levels will provide a basis for future therapy of autoimmune diseases by specific elimination of auto-reactive T cells to establish appropriate negative selection (central tolerance).

Funding

This work was supported by Grants-in-Aid for Scientific Research (16H04767 to J.-i. I.) from MEXT, Mizutani Foundation for Glycoscience (to J.-i. I.), Takeda Science Foundation (to J.-i. I.), Nagai Memorial Research Scholarship from the Pharmaceutical Society of Japan (to K.T.) and the MEXT-Supported Program for the Strategic Research Foundation at Private Universities.

Acknowledgements

The authors are grateful to Ms F. Shishido (Tohoku Medical and Pharmaceutical University) for experimental support, Ms M. Toyosawa (Tohoku Medical and Pharmaceutical University) for assistance with

mouse breeding and genotyping and Dr S. Anderson for English editing of the manuscript.

Conflicts of interest statement: The authors declared no conflicts of interest.

References

- Zúñiga-Pflücker, J. C. and Lenardo, M. J. 1996. Regulation of thymocyte development from immature progenitors. *Curr. Opin. Immunol.* 8:215.
- Marrack, P. and Kappler, J. 1997. Positive selection of thymocytes bearing alpha beta T cell receptors. *Curr. Opin. Immunol.* 9:250.
- Killeen, N., Irving, B. A., Pippig, S. and Zingler, K. 1998. Signaling checkpoints during the development of T lymphocytes. *Curr. Opin. Immunol.* 10:360.
- Ashton-Rickardt, P. G., Bandeira, A., Delaney, J. R. *et al.* 1994. Evidence for a differential avidity model of T cell selection in the thymus. *Cell* 76:651.
- Sebzda, E., Wallace, V. A., Mayer, J., Yeung, R. S., Mak, T. W. and Ohashi, P. S. 1994. Positive and negative thymocyte selection induced by different concentrations of a single peptide. *Science* 263:1615.
- Sohn, S. J., Rajpal, A. and Winoto, A. 2003. Apoptosis during lymphoid development. *Curr. Opin. Immunol.* 15:209.
- Liu, Z. G., Smith, S. W., McLaughlin, K. A., Schwartz, L. M. and Osborne, B. A. 1994. Apoptotic signals delivered through the T-cell receptor of a T-cell hybrid require the immediate-early gene *nur77*. *Nature* 367:281.
- Bouillet, P., Metcalf, D., Huang, D. C. *et al.* 1999. Proapoptotic Bcl-2 relative Bim required for certain apoptotic responses, leukocyte homeostasis, and to preclude autoimmunity. *Science* 286:1735.
- Daniels, M. A., Teixeira, E., Gill, J. *et al.* 2006. Thymic selection threshold defined by compartmentalization of Ras/MAPK signalling. *Nature* 444:724.
- Janes, P. W., Ley, S. C., Magee, A. I. and Kabouridis, P. S. 2000. The role of lipid rafts in T cell antigen receptor (TCR) signalling. *Semin. Immunol.* 12:23.
- Werlen, G., Hausmann, B. and Palmer, E. 2000. A motif in the alphabeta T-cell receptor controls positive selection by modulating ERK activity. *Nature* 406:422.
- Delgado, P., Fernández, E., Dave, V., Kappes, D. and Alarcón, B. 2000. CD3delta couples T-cell receptor signalling to ERK activation and thymocyte positive selection. *Nature* 406:426.
- Simons, K. and Ikonen, E. 1997. Functional rafts in cell membranes. *Nature* 387:569.
- Simons, K. and Vaz, W. L. 2004. Model systems, lipid rafts, and cell membranes. *Annu. Rev. Biophys. Biomol. Struct.* 33:269.
- Nagafuku, M., Okuyama, K., Onimaru, Y. *et al.* 2012. CD4 and CD8 T cells require different membrane gangliosides for activation. *Proc. Natl Acad. Sci. USA* 109:E336.
- Nakamura, K., Suzuki, M., Inagaki, F., Yamakawa, T. and Suzuki, A. 1987. A new ganglioside showing cholera toxin-binding activity in mouse spleen. *J. Biochem.* 101:825.
- Zhou, J., Cox, N. R., Ewald, S. J., Morrison, N. E. and Basker, H. J. 1998. Evaluation of GM1 ganglioside-mediated apoptosis in feline thymocytes. *Vet. Immunol. Immunopathol.* 66:25.
- Inokuchi, J., Nagafuku, M., Ohno, I. and Suzuki, A. 2013. Heterogeneity of gangliosides among T cell subsets. *Cell. Mol. Life Sci.* 70:3067.
- Popovic, Z. V., Rabionet, M., Jennemann, R. *et al.* 2017. Glucosylceramide synthase is involved in development of invariant natural killer T cells. *Front. Immunol.* 8:848.
- Gómez-Mouton, C., Abad, J. L., Mira, E. *et al.* 2001. Segregation of leading-edge and uropod components into specific lipid rafts during T cell polarization. *Proc. Natl Acad. Sci. USA* 98:9642.
- Sato, T., Iwabuchi, K., Nagaoka, I. *et al.* 2006. Induction of human neutrophil chemotaxis by *Candida albicans*-derived beta-1,6-long glycoside side-chain-branched beta-glucan. *J. Leukoc. Biol.* 80:204.
- Nakayama, H., Yoshizaki, F., Prinetti, A. *et al.* 2008. Lyn-coupled LacCer-enriched lipid rafts are required for CD11b/CD18-mediated neutrophil phagocytosis of nonopsonized microorganisms. *J. Leukoc. Biol.* 83:728.
- Zech, T., Ejsing, C. S., Gaus, K. *et al.* 2009. Accumulation of raft lipids in T-cell plasma membrane domains engaged in TCR signalling. *EMBO J.* 28:466.
- Huitema, K., van den Dikkenberg, J., Brouwers, J. F. and Holthuis, J. C. 2004. Identification of a family of animal sphingomyelin synthases. *EMBO J.* 23:33.
- Dong, L., Watanabe, K., Itoh, M. *et al.* 2012. CD4⁺ T-cell dysfunctions through the impaired lipid rafts ameliorate concanavalin A-induced hepatitis in sphingomyelin synthase 1-knockout mice. *Int. Immunol.* 24:327.
- Hogquist, K. A., Jameson, S. C., Heath, W. R., Howard, J. L., Bevan, M. J. and Carbone, F. R. 1994. T cell receptor antagonist peptides induce positive selection. *Cell* 76:17.
- Kisielow, P., Blüthmann, H., Staerz, U. D., Steinmetz, M. and von Boehmer, H. 1988. Tolerance in T-cell-receptor transgenic mice involves deletion of nonmature CD4⁺ thymocytes. *Nature* 333:742.
- Makino, A., Abe, M., Murate, M. *et al.* 2015. Visualization of the heterogeneous membrane distribution of sphingomyelin associated with cytokinesis, cell polarity, and sphingolipidosis. *FASEB J.* 29:477.
- Yamaji, A., Sekizawa, Y., Emoto, K. *et al.* 1998. Lysenin, a novel sphingomyelin-specific binding protein. *J. Biol. Chem.* 273:5300.
- Ishitsuka, R., Yamaji-Hasegawa, A., Makino, A., Hirabayashi, Y. and Kobayashi, T. 2004. A lipid-specific toxin reveals heterogeneity of sphingomyelin-containing membranes. *Biophys. J.* 86(1 Pt 1):296.
- Abe, M., Makino, A., Hulin-Matsuda, F. *et al.* 2012. A role for sphingomyelin-rich lipid domains in the accumulation of phosphatidylinositol-4,5-bisphosphate to the cleavage furrow during cytokinesis. *Mol. Cell. Biol.* 32:1396.
- Abe, M. and Kobayashi, T. 2017. Dynamics of sphingomyelin- and cholesterol-enriched lipid domains during cytokinesis. *Methods Cell Biol.* 137:15.
- Hong, Q., Gutierrez-Aguirre, I., Barlic, A. *et al.* 2002. Two-step membrane binding by Equinatoxin II, a pore-forming toxin from the sea anemone, involves an exposed aromatic cluster and a flexible helix. *J. Biol. Chem.* 277:41916.
- Inokuchi, J. I., Uemura, S., Kabayama, K. and Igarashi, Y. 2000. Glucosylphospholipid deficiency affects functional microdomain formation in Lewis lung carcinoma cells. *Glycoconj. J.* 17:239.
- Nagafuku, M., Kabayama, K., Oka, D. *et al.* 2003. Reduction of glucosylphospholipid levels in lipid rafts affects the expression state and function of glycosylphosphatidylinositol-anchored proteins but does not impair signal transduction via the T cell receptor. *J. Biol. Chem.* 278:51920.
- Dittmer, J. C. and Lester, R. L. 1964. A simple, specific spray for the detection of phospholipids on thin-layer chromatograms. *J. Lipid Res.* 5:126.
- Painter, M. W., Davis, S., Hardy, R. R., Mathis, D. and Benoist, C.; Immunological Genome Project Consortium. 2011. Transcriptomes of the B and T lineages compared by multiplatform microarray profiling. *J. Immunol.* 186:3047.
- Gill, J., Malin, M., Sutherland, J., Gray, D., Hollander, G. and Boyd, R. 2003. Thymic generation and regeneration. *Immunol. Rev.* 195:28.
- Petrie, H. T. 2003. Cell migration and the control of post-natal T-cell lymphopoiesis in the thymus. *Nat. Rev. Immunol.* 3:859.
- Kurd, N. and Robey, E. A. 2016. T-cell selection in the thymus: a spatial and temporal perspective. *Immunol. Rev.* 271:114.
- Van Laethem, F., Tikhonova, A. N., Pobezinsky, L. A. *et al.* 2013. Lck availability during thymic selection determines the recognition specificity of the T cell repertoire. *Cell* 154:1326.
- Takada, K., Van Laethem, F., Xing, Y. *et al.* 2015. TCR affinity for thymoproteasome-dependent positively selecting peptides conditions antigen responsiveness in CD8(+) T cells. *Nat. Immunol.* 16:1069.
- Suzuki, H., Punt, J. A., Granger, L. G. and Singer, A. 1995. Asymmetric signaling requirements for thymocyte commitment

- to the CD4⁺ versus CD8⁺ T cell lineages: a new perspective on thymic commitment and selection. *Immunity* 2:413.
- 44 Simons, K. and Toomre, D. 2000. Lipid rafts and signal transduction. *Nat. Rev. Mol. Cell Biol.* 1:31.
 - 45 Brown, D. A. and London, E. 2000. Structure and function of sphingolipid- and cholesterol-rich membrane rafts. *J. Biol. Chem.* 275:17221.
 - 46 van Erpecum, K. J. and Carey, M. C. 1997. Influence of bile salts on molecular interactions between sphingomyelin and cholesterol: relevance to bile formation and stability. *Biochim. Biophys. Acta.* 1345:269.
 - 47 Yamaoka, S., Miyaji, M., Kitano, T., Umehara, H. and Okazaki, T. 2004. Expression cloning of a human cDNA restoring sphingomyelin synthesis and cell growth in sphingomyelin synthase-defective lymphoid cells. *J. Biol. Chem.* 279:18688.
 - 48 Tafesse, F. G., Huitema, K., Hermansson, M. *et al.* 2007. Both sphingomyelin synthases SMS1 and SMS2 are required for sphingomyelin homeostasis and growth in human HeLa cells. *J. Biol. Chem.* 282:17537.
 - 49 Li, Z., Fan, Y., Liu, J. *et al.* 2012. Impact of sphingomyelin synthase 1 deficiency on sphingolipid metabolism and atherosclerosis in mice. *Arterioscler. Thromb. Vasc. Biol.* 32:1577.
 - 50 Liu, J., Zhang, H., Li, Z. *et al.* 2009. Sphingomyelin synthase 2 is one of the determinants for plasma and liver sphingomyelin levels in mice. *Arterioscler. Thromb. Vasc. Biol.* 29:850.
 - 51 Heng, T. S. and Painter, M. W.; Immunological Genome Project Consortium. 2008. The Immunological Genome Project: networks of gene expression in immune cells. *Nat. Immunol.* 9:1091.
 - 52 Swat, W., Ignatowicz, L., von Boehmer, H. and Kisielow, P. 1991. Clonal deletion of immature CD4⁺8⁺ thymocytes in suspension culture by extrathymic antigen-presenting cells. *Nature* 351:150.
 - 53 Negishi, I., Motoyama, N., Nakayama, K. *et al.* 1995. Essential role for ZAP-70 in both positive and negative selection of thymocytes. *Nature* 376:435.
 - 54 Mallaun, M., Zenke, G. and Palmer, E. 2010. A discrete affinity-driven elevation of ZAP-70 kinase activity initiates negative selection. *J. Recept. Signal Transduct. Res.* 30:430.
 - 55 Sohn, S. J., Lewis, G. M. and Winoto, A. 2008. Non-redundant function of the MEK5-ERK5 pathway in thymocyte apoptosis. *EMBO J.* 27:1896.
 - 56 Suen, A. Y. and Baldwin, T. A. 2012. Proapoptotic protein Bim is differentially required during thymic clonal deletion to ubiquitous versus tissue-restricted antigens. *Proc. Natl Acad. Sci. USA* 109:893.
 - 57 Bouillet, P., Purton, J. F., Godfrey, D. I. *et al.* 2002. BH3-only Bcl-2 family member Bim is required for apoptosis of autoreactive thymocytes. *Nature* 415:922.
 - 58 Azzam, H. S., Grinberg, A., Lui, K., Shen, H., Shores, E. W. and Love, P. E. 1998. CD5 expression is developmentally regulated by T cell receptor (TCR) signals and TCR avidity. *J. Exp. Med.* 188:2301.
 - 59 Starr, T. K., Jameson, S. C. and Hogquist, K. A. 2003. Positive and negative selection of T cells. *Annu. Rev. Immunol.* 21:139.
 - 60 Labrecque, N., Baldwin, T. and Lesage, S. 2011. Molecular and genetic parameters defining T-cell clonal selection. *Immunol. Cell Biol.* 89:16.
 - 61 de Mello Coelho, V., Nguyen, D., Giri, B., Bunbury, A., Schaffer, E. and Taub, D. D. 2004. Quantitative differences in lipid raft components between murine CD4⁺ and CD8⁺ T cells. *BMC Immunol.* 5:2.
 - 62 Ebert, P. J., Baker, J. F. and Punt, J. A. 2000. Immature CD4⁺CD8⁺ thymocytes do not polarize lipid rafts in response to TCR-mediated signals. *J. Immunol.* 165:5435.
 - 63 Sohn, S. J., Thompson, J. and Winoto, A. 2007. Apoptosis during negative selection of autoreactive thymocytes. *Curr. Opin. Immunol.* 19:510.
 - 64 Gascoigne, N. R., Rybakina, V., Acuto, O. and Brzostek, J. 2016. TCR signal strength and T cell development. *Annu. Rev. Cell Dev. Biol.* 32:327.
 - 65 Dykstra, M., Cherukuri, A., Sohn, H. W., Tzeng, S. J. and Pierce, S. K. 2003. Location is everything: lipid rafts and immune cell signaling. *Annu. Rev. Immunol.* 21:457.
 - 66 Harder, T., Rentero, C., Zech, T. and Gaus, K. 2007. Plasma membrane segregation during T cell activation: probing the order of domains. *Curr. Opin. Immunol.* 19:470.
 - 67 Morris, G. P. and Allen, P. M. 2012. How the TCR balances sensitivity and specificity for the recognition of self and pathogens. *Nat. Immunol.* 13:121.
 - 68 Fu, G., Rybakina, V., Brzostek, J., Paster, W., Acuto, O. and Gascoigne, N. R. 2014. Fine-tuning T cell receptor signaling to control T cell development. *Trends Immunol.* 35:311.
 - 69 Hailman, E., Burack, W. R., Shaw, A. S., Dustin, M. L. and Allen, P. M. 2002. Immature CD4⁺CD8⁺ thymocytes form a multifocal immunological synapse with sustained tyrosine phosphorylation. *Immunity* 16:839.
 - 70 Richie, L. I., Ebert, P. J., Wu, L. C., Krummel, M. F., Owen, J. J. and Davis, M. M. 2002. Imaging synapse formation during thymocyte selection: inability of CD3zeta to form a stable central accumulation during negative selection. *Immunity* 16:595.
 - 71 Bousso, P., Bhakta, N. R., Lewis, R. S. and Robey, E. 2002. Dynamics of thymocyte-stromal cell interactions visualized by two-photon microscopy. *Science* 296:1876.
 - 72 Hernandez, J. B., Newton, R. H. and Walsh, C. M. 2010. Life and death in the thymus—cell death signaling during T cell development. *Curr. Opin. Cell Biol.* 22:865.
 - 73 Moran, A. E., Holzapfel, K. L., Xing, Y. *et al.* 2011. T cell receptor signal strength in Treg and iNKT cell development demonstrated by a novel fluorescent reporter mouse. *J. Exp. Med.* 208:1279.
 - 74 Zikherman, J., Parameswaran, R. and Weiss, A. 2012. Endogenous antigen tunes the responsiveness of naive B cells but not T cells. *Nature* 489:160.
 - 75 Tarakhovskiy, A., Kanner, S. B., Hombach, J. *et al.* 1995. A role for CD5 in TCR-mediated signal transduction and thymocyte selection. *Science* 269:535.
 - 76 Komaniwa, S., Hayashi, H., Kawamoto, H. *et al.* 2009. Lipid-mediated presentation of MHC class II molecules guides thymocytes to the CD4 lineage. *Eur. J. Immunol.* 39:96.
 - 77 Thauland, T. J. and Parker, D. C. 2010. Diversity in immunological synapse structure. *Immunology* 131:466.
 - 78 Yokosuka, T. and Saito, T. 2010. The immunological synapse, TCR microclusters, and T cell activation. *Curr. Top. Microbiol. Immunol.* 340:81.
 - 79 Lee, S. J., Hori, Y. and Chakraborty, A. K. 2003. Low T cell receptor expression and thermal fluctuations contribute to formation of dynamic multifocal synapses in thymocytes. *Proc. Natl Acad. Sci. USA* 100:4383.
 - 80 Brumeanu, T. D., Preda-Pais, A., Stoica, C., Bona, C. and Casares, S. 2007. Differential partitioning and trafficking of GM gangliosides and cholesterol-rich lipid rafts in thymic and splenic CD4 T cells. *Mol. Immunol.* 44:530.
 - 81 Swamy, M., Beck-Garcia, K., Beck-Garcia, E. *et al.* 2016. A cholesterol-based allosteric model of T cell receptor phosphorylation. *Immunity* 44:1091.
 - 82 Wang, F., Beck-Garcia, K., Zorzin, C., Schamel, W. W. and Davis, M. M. 2016. Inhibition of T cell receptor signaling by cholesterol sulfate, a naturally occurring derivative of membrane cholesterol. *Nat. Immunol.* 17:844.
 - 83 Molnár, E., Swamy, M., Holzer, M. *et al.* 2012. Cholesterol and sphingomyelin drive ligand-independent T-cell antigen receptor nanoclustering. *J. Biol. Chem.* 287:42664.

The regulatory roles of glycosphingolipid-enriched lipid rafts in immune systems

Hitoshi Nakayama^{1,2}, Masakazu Nagafuku³, Akemi Suzuki³, Kazuhisa Iwabuchi^{1,2,4} and Jin-Ichi Inokuchi³

1 Laboratory of Biochemistry, Juntendo University Faculty of Health Care and Nursing, Urayasu, Japan

2 Institute for Environmental and Gender-specific Medicine, Juntendo University Graduate School of Medicine, Urayasu, Japan

3 Division of Glycopathology, Institute of Molecular Biomembrane and Glycobiology, Tohoku Medical and Pharmaceutical University, Sendai, Japan

4 Infection Control Nursing, Juntendo University Graduate School of Health Care and Nursing, Urayasu, Japan

Correspondence

K. Iwabuchi, Laboratory of Biochemistry, Juntendo University Faculty of Health Care and Nursing, Urayasu, Chiba 279-0023, Japan

Fax: +81 47 353 3178

Tel: +81 47 353 3171

E-mail: iwabuchi@juntendo.ac.jp

and

J. I. Inokuchi, Division of Glycopathology, Institute of Molecular Biomembrane and Glycobiology, Tohoku Medical and Pharmaceutical University, 4-4-1, Komatsushima, Aoba-ku, Miyagi 981-8558, Japan

Fax: +81 22 727 0076

Tel: +81 22 727 0117

E-mail: jin@tohoku-mpu.ac.jp

(Received 12 June 2018, revised 9 October 2018, accepted 10 October 2018, available online 27 October 2018)

doi:10.1002/1873-3468.13275

Edited by Sandro Sonnino

Lipid rafts formed by glycosphingolipids (GSLs) on cellular membranes play important roles in innate and adaptive immunity. Lactosylceramide (LacCer) forms lipid rafts on plasma and granular membranes of human neutrophils. These LacCer-enriched lipid rafts bind directly to pathogenic components, such as pathogenic fungi-derived β -glucan and *Mycobacteria*-derived lipoarabinomannan *via* carbohydrate-carbohydrate interactions, and mediate innate immune responses to these pathogens. In contrast, a-series and o-series gangliosides form distinct rafts on CD4⁺ and CD8⁺ T cell subsets, respectively, contributing to the respective functions of these cells and stimulating adaptive immune responses through T cell receptors. These findings suggest that gangliosides play indispensable roles in T cell selection and activation. This Review introduces the involvement of GSL-enriched lipid rafts in innate and adaptive immunity.

Keywords: acquired immunity; glycosphingolipid; innate immunity; intracellular parasitism; lipid raft; neutrophil; phagocytosis; T cell activation; T cell selection

Glycosphingolipids (GSLs) are composed of hydrophilic sugar structures and hydrophobic ceramide [1]. The ceramide moiety of GSLs interacts hydrophobically with

cholesterol sterol-ring systems *via* van der Waal's forces and hydrogen bonds [2]. Moreover, *cis* interactions between sugar moiety of GSLs facilitate lateral

Abbreviations

BCR, B cell antigen receptor; CSBG, *Candida* solubilized cell wall β -glucan; CTB, cholera toxin B subunit; EMRN, encephalomyeloradiculoneuropathy; Gb3, globotriaosyl ceramide; GM3S, GM3 synthase; GSLs, glycosphingolipids; LacCer, lactosylceramide; LAM, lipoarabinomannan; LPS, lipopolysaccharide; MAC, *Mycobacterium avium-intracellulare* complex; MAM, mitochondria-associated membranes; ManLAM, mannose capped LAM; MHC, major histocompatibility complex; M β CD, methyl- β -cyclodextrin; NKT, natural killer T; OVA, ovalbumin; PAMP, pathogen-associated molecular pattern; PILAM, phospho-myoinositol capped LAM; PRRs, pattern-recognition receptors; PtdGlc, phosphatidylglucoside; RA, rheumatoid arthritis; ROS, reactive oxygen species; SLE, systemic lupus erythematosus; SPR, surface plasmon resonance; Stx, Shiga toxin; SV40, simian virus 40; TCRs, T cell receptors; WT, wild-type.

interactions of these molecules with other membrane components. These interactions lead to the formation of cellular membrane microdomains, so called lipid rafts, which are rich domains in cholesterol, GSLs, sphingomyelin, glycosylphosphatidylinositol, and membrane-anchored molecules [3,4]. GSL-enriched lipid rafts contribute innate and adaptive immune systems [5–12]. The innate and adaptive immune systems are involved in resistance to invading pathogens, but the two systems are functionally distinct.

Innate immune responses are the initial step in resistance to invading pathogens, including viruses, bacteria, and fungi. Many viruses, bacteria, and bacterial toxins have been shown to bind to the carbohydrate components of GSLs on host cell surfaces [13]. Binding studies have revealed that several glycolipids are components of functional receptors for microorganisms and bacterial toxins [14]. For example, the neutral GSL, Lactosylceramide (LacCer, CDw17), forms LacCer-enriched lipid rafts on the plasma and granular membranes of human neutrophils. LacCer-enriched lipid rafts play essential roles in innate immune responses to bacterial pathogens, including *Candida* and *Mycobacteria*. Indeed, LacCer-enriched lipid rafts are capable of binding directly to bacterial components, such as *C. albicans*-derived β -glucan and *Mycobacteria*-derived lipoarabinomannan (LAM) through carbohydrate–carbohydrate interactions [15,16]. The binding of bacterial pathogens to LacCer-enriched lipid rafts activates signaling cascades involving Src family kinases, inducing chemotaxis, phagocytosis, and phagolysosome formation (phagosome maturation). Interestingly, pathogenic mycobacteria, such as *M. tuberculosis*, target LacCer-enriched lipid raft-dependent activation of the Src family kinase Hck on phagosomal membranes of neutrophils, thereby inhibiting phagolysosome formation [15]. These findings show that GSLs can act as direct and functional receptors for pathogen-derived ligands.

In addition to their roles as functional receptors, GSLs can act together with other receptors *via cis* interactions. Lipid rafts formed by the ganglioside (sialylated GSL) GM3 are associated with insulin receptor in adipocytes [17]. GM1 binds to TrkA protein and regulates the receptor function [18], and GM1-enriched lipid rafts work as signaling platforms for laminin-1-induced TrkA/ β_1 integrin-associated neurite outgrowth [19]. GM1 was also found to interact with the G protein-coupled receptor serotonin-1A receptor *via* the sphingolipid-binding domain of the latter [20], suggesting the involvement of GM1 in neurodegenerative diseases. In innate immune responses, the phagocytosis of non-opsonized microorganisms, such as *Mycobacteria*, in human neutrophils is regulated jointly by CD11b/

CD18 ($\alpha_M\beta_2$)-integrin and LacCer-enriched lipid rafts coupled with Src family kinase Lyn [15,21]. These observations suggest that GSL-enriched lipid rafts regulate receptor functions, resulting in various physiological activities.

In addition to modulating innate immune systems, GSLs have been found to play critical roles in adaptive immune systems. In adaptive immunity, a-series gangliosides (a-GMs) and o-series gangliosides are involved in the function and stimulation of T cell receptors (TCRs) on CD4-positive (CD4⁺) and CD8-positive (CD8⁺) T cells, respectively [22]. GQ1b and α -GalCer were shown to function as immunomodulators [23–25]. Moreover, α -GalCer, derived from a marine sponge, was found to act as a lipid antigen that activates natural killer T (NKT) cells [23], which control innate and adaptive immune responses [26]. α -Linked glycosylceramides were shown to be the major endogenous ligands of NKT cells [27]. These findings suggest that GSL-mediated NKT activation may be a potential immunotherapeutic target.

Although GSLs can mediate both innate and adaptive immune functions through a variety of pathways, the pathogenesis of autoimmune diseases likely involves immune system responses to GSL antigens. Interestingly, the anti-LacCer monoclonal antibodies (mAbs) T5A7 and Huly-m13 can recognize LacCer on human neutrophils, whereas T5A7 alone recognizes LacCer on mouse neutrophils [28]. Moreover, Huly-m13 can be used for immunoprecipitation, whereas T5A7 cannot [21]. These observations suggest that the specificities of antibodies against the same GSL antigens contribute to differences in the structural features of GSL-enriched lipid rafts.

This review describes the mechanisms by which GSLs and GSL-enriched lipid rafts recognize their ligands and receptors, as well as describing the regulatory roles of GSL-enriched lipid rafts in innate and adaptive immunity.

GSLs as immune modulators

Glycosphingolipids are abundantly expressed on the outer leaflets of cell membranes. In addition, some gangliosides are broadly distributed in body fluids of most vertebrates. Some GSLs have been demonstrated to function as unintentional binders of bacteria in specific tissues.

Binding of GSLs to microorganisms

Microorganisms and toxins target GSLs for the adhesion of microorganisms to specific tissues (Table 1).

Table 1. Binding of GSLs to pathogens and toxins.

GSLs	Pathogens or toxins	Ref. No.
GD1a, GT1b	Polyomavirus	[29]
GM1	Simian virus 40	[29]
	<i>Brucella suis</i>	[36]
	Cholera toxin B subunit	[37,38]
	<i>Escherichia coli</i> enterotoxin	[39]
	<i>Vibrio cholerae</i> enterotoxin	[42]
Gb3	Shiga toxin, Verotoxin B subunit	[30–33]
Asialo GM1	<i>Pseudomonas aeruginosa</i> , <i>Bifidobacterium bifidum</i> , <i>Lactobacillus</i>	[34,35]
LacCer	<i>Mycobacterium tuberculosis</i>	[15]
	<i>Mycobacterium avium-intracellulare</i> complex	[15]
	<i>Mycobacterium gordonae</i>	[15]
	<i>Mycobacterium smegmatis</i>	[15]
	<i>Mycobacterium tuberculosis</i> ManLAM	[15]
	<i>Mycobacterium avium-intracellulare</i> complex ManLAM	[15]
	<i>Mycobacterium smegmatis</i> PILAM	[15]
	<i>Candida albicans</i> β -glucan	[16]
	<i>Helicobacter pylori</i>	[44]
	<i>Pneumocystis carinii</i> β -glucan	[45]
	<i>Bacillus dysenteriae</i>	[46]
	<i>Bordetella pertussis</i>	[47]
	<i>Saccharomyces cerevisiae</i> PGG-glucan	[48]
	<i>Escherichia coli</i>	[50]
	<i>Propionibacterium granulosum</i>	[51]
	<i>Propionibacterium freudenreichii</i>	[52]
	<i>Yersinia pestis</i>	[53]
	<i>Escherichia coli</i> CFA/I protein	[54]
	<i>Neisseria gonorrhoeae</i>	[55]
	<i>Borrelia burgdorferi</i>	[56]
GM1, GM3	<i>Shigella</i> LPS	[58]

For instance, polyomavirus invades human erythrocyte through the binding to GD1a and GT1b [29]. Globotriaosyl ceramide (Gb3) binds to Shiga toxin (Stx) and verotoxin B subunit [30–33]. Human epithelial and endothelial cell surfaces contain binding sites for Stx [30–33], with cell surface Gb3 binding to the B subunit of Stx [30–32]. Epithelial cells-expressing asialo GM1 (GA1) binds to *Pseudomonas aeruginosa*, *Bifidobacterium bifidum*, and *Lactobacillus* [34,35]. Simian virus 40 (SV40) [29] and *Brucella suis* [36] were found to bind to GM1. Cholera toxin B subunit (CTB) also binds to GM1 [37,38]. GM1 expressing on epithelial cells also binds to CTB and *Escherichia coli* enterotoxin [39]. In addition to GM1, CTB binds to other gangliosides, especially fucosylated GM1 [40,41]. Gangliosides in human milk are thought to protect intestinal tissues from *Vibrio cholerae* and *E. coli* enterotoxins [42]. Ganglioside content and distribution of human milk individually alter by lactation period.

While GM3 is the main ganglioside in mature milk, GD3 is the most abundant in colostrum. Orally administered gangliosides are likely to catch microorganisms, resulting in the intestinal protection. Indeed, the dietary effects of ganglioside on the production of cytokines and IgA, which are involved in the development of the intestinal immunity, have been examined in animal models [7]. GD3 but not GM3 was shown to inhibit lipopolysaccharide (LPS)-induced murine dendritic cell maturation and to modulate LPS-induced inflammatory cytokine release [43]. However, the detailed mechanisms underlying the different activities of GM3 and GD3 remain to be elucidated.

Lactosylceramide is expressed not only on neutrophils but also on intestinal epithelial cells, and binds to various microorganisms, such as *Mycobacterium avium-intracellulare* complex (MAC), *M. tuberculosis*, *C. albicans*, *Bacillus dysenteriae*, *Bordetella pertussis*, *E. coli*, and *Propionibacterium freudenreichii* [15,16,44–56]. Human and bovine milk contain LacCer as a major GSL component [57], indicating that milk-derived LacCer is a putative trap and blocking pathogen binding in the intestines, and that milk-derived LacCer protects the host from invading pathogens. Interactions between the sugar moieties of gangliosides and the polysaccharide moieties of *Shigella* LPS were found to facilitate binding of bacteria to human CD4⁺ T cells [58]. Taken together, these observations suggest that specific carbohydrate-carbohydrate interactions between sugar moieties of GSL and of pathogen-associated molecular pattern (PAMP) may be related to various immune disorders.

Effects of GSL regulation on innate immunity

Innate-like T lymphocytes, such as NKT cells, recognize GSLs presented by CD1d and control innate and adaptive immune responses against not only some inflammatory diseases but also against cancers and infectious diseases [26]. It has been found that a marine sponge-derived α -GalCer is a lipid antigen molecule, which activates NKT cells [23]. Moreover, α -GalCer was found to enhance immune reactions to various infectious microorganisms and several cancers, as well as inhibiting autoimmune disorders, allograft rejection, and graft-versus-host disorders [59]. α -Linked glycosylceramides were determined to be the main endogenous ligands on NKT cells [27]. Macrophage inducible C-type lectin (Mincle) responds to β -GlcCer, which is an endogenous ligand and possess immunostimulatory activity [60]. These findings suggest that GSL-mediated NKT activation is a potential target for immunotherapy of several disorders.

However, the *in vivo* mechanism by which GSLs recognize their receptors is still unclear.

GSL regulation of adaptive immunity

The ganglioside GQ1b was shown to promote the production of cytokines from T cells, without altering cytokine productions in B cells and monocytes [24]. When B cells were cocultured with GQ1b pretreated T cells, B cells produced Ig. Addition of IL-6 or IL-10 to B cells increased Ig production, with the two together displaying additive effects. These findings indicate that GQ1b induces T cell production of IL-6 and IL-10, resulting in B cell production of Ig cells [24] and that extracellular or exogenously added gangliosides may modulate adaptive immune responses.

GSLs in innate immunity

Glycosphingolipids form lipid rafts on the plasma and granular membranes of host immune cells and act as functional pattern-recognition receptors (PRRs) for invading pathogens. LacCer and gangliosides recognize pathogen-specific carbohydrate structures. These GSLs mediate a variety of physiological activities, including chemotaxis, phagocytosis, cytokine production, apoptosis, and autophagy. In some cases, intracellular pathogens, such as *Mycobacteria*, alter GSL-enriched lipid raft-mediated innate immune functions, allowing these pathogens to escape killing by host phagocytes.

GSL-enriched lipid rafts as pattern-recognition receptors

Mammalian innate immune responses are initialized by binding of PAMPs, which are essential components required for the microbial survival and are not present on mammalian cells [61], to PRRs expressed on innate immune cells. PRRs are categorized according to their functions. Toll-like receptors [62,63], LPS-binding receptor CD14 [64], and C-type lectin receptor dectin-1 [65] are PRRs that sense a variety of PAMPs, and mainly mediate PAMPs-induced inflammatory signaling pathways. In contrast, macrophage mannose receptor CD206 [66], scavenger receptors [67,68], and $\alpha_M\beta_2$ -integrin [69] are phagocytic PRRs that directly recognize PAMPs covering microorganisms and induce phagocytosis of microorganisms. Not only glycoproteins but also GSLs such as LacCer [16,21,70] and GM1 [29,36], which form lipid rafts, are capable of binding and sensing PAMPs. As described above, LacCer has binding capacities for microbial PAMPs, including pathogenic fungi β -glucan *Candida*

solubilized cell wall β -glucan (CSBG) and mycobacterial LAM. In addition, LacCer-enriched lipid rafts serve as signaling platforms for both inflammatory responses and phagocytosis through $\alpha_M\beta_2$ -integrin that is devoid of signaling motif in the cytoplasm region. β -Glucan from *Pneumocystis carinii* has been shown to stimulate the production of large amounts of MIP-2 via LacCer on rat alveolar epithelial cells [45]. LacCer is expressed on the surfaces of human dendritic cells [71]. LacCer contained GSL-enriched lipid rafts have been reported to participate in the activation of human dendritic cells by *Pneumocystis* β -glucans [72]. These findings suggest that GSL-enriched rafts containing LacCer are involved in the initiation of β -glucan cellular responses and IL-23 release from dendritic cells. CSBG induces the migration of human neutrophils and this migration is completely inhibited by Src family kinase inhibitor PP1 or LacCer liposomes [70]. In contrast, capsular polysaccharide from *Streptococcus suis* inhibits LacCer-mediated macrophage phagocytosis [73]. We recently reported that both mannose capped LAM (ManLAM) from *M. tuberculosis* and phospho-myoinositol capped LAM (PILAM) from *Mycobacterium smegmatis* induce Lyn phosphorylation and subsequent $\alpha_M\beta_2$ -integrin-mediated phagocytosis by human neutrophils [15]. These observations suggest that LacCer-enriched lipid rafts act as not only a signaling PRR inducing inflammatory responses but also a phagocytic PRR inducing and supporting phagocytosis of microorganisms.

Organization and signal transduction by GSL-enriched lipid rafts

Biological membranes consist of various molecules, which form several kinds of clusters based on their physicochemical properties and cis interactions. These properties provide physical boundaries between outside and inside of the cells. Therefore, cell membrane components can undergo nonhomogeneous lateral distribution, leading to the formation of membrane domains with a highly distinguished molecular composition and supramolecular structures, which are stabilized by lateral interactions among membrane components. The physicochemical properties of GSLs suggest that they form defined clusters and that certain proteins cannot undergo free and continuous lateral diffusion, but rather are transiently confined to microdomains (lipid rafts) [74–76]. Several molecules can enter into these domains to form functional domains. In addition, palmitoylated proteins, such as Src family kinases and small G proteins, tend to enter GSL-enriched lipid rafts [77–80], suggesting that GSLs are involved in

signal transduction from outside into the cells. Many studies of the organization and immunological functions of GSL-enriched lipid rafts involve LacCer [3,15,16,21,28,70,71,81,82], a molecule that is selectively expressed on the plasma and granular membranes of human neutrophils, and that forms lipid rafts with other molecules [15,21,70]. The C24 fatty acid chain of LacCer on plasma membranes directly binds to Lyn and G α i [81], with ligand binding to these LacCer clusters mediating outside-in signaling (Fig. 1) [16,21,82]. Interestingly, immunoelectron microscopy found that only one-quarter of LacCer-enriched lipid rafts is coupled with Lyn on cellular membranes [82], indicating that different types of LacCer-enriched lipid rafts are present on individual membranes. Although two anti-LacCer monoclonal antibodies T5A7 and Huly-m13 bind to the lactose moiety of LacCer, the two were shown to recognize different areas of LacCer-enriched domains on artificial lipid layers [28]. Binding experiments suggested that Huly-m13 binds to lactose clusters in LacCer-enriched domains, while T5A7 binds to dispersed LacCer clusters in the phase boundary regions of LacCer-enriched domains. Two different LacCer-enriched lipid rafts, e.g., Lyn- and Hck-coupled LacCer-enriched lipid rafts are present on phagosomal membranes of neutrophils [15]. Among them, only Hck-associated LacCer-enriched lipid rafts can mediate phagolysosome formation. Interestingly, Hck is absent in LacCer-enriched lipid rafts of resting neutrophils. Thus, LacCer-mediated functions during phagocytosis require the reorganization of LacCer-enriched lipid rafts and the association with appropriate molecules during phagosome maturation. LacCer should gather with appropriate molecules to form several kinds of lipid rafts, each of which may express different molecular patterns and mediate different functions on the same membranes.

It is unclear, however, whether LacCer in LacCer-enriched lipid rafts can mediate outside-in signal transduction. The human acute myeloid leukemia cell line HL-60 can be induced to differentiate into neutrophilic lineage cells by treatment with dimethyl sulfoxide. The resulting D-HL-60 cells acquire superoxide generating activity, but cannot phagocytose microorganisms under non-opsonized conditions [21,70]. LacCer on plasma membranes of D-HL-60 cells consists primarily of C16:0-LacCer, with little C24-LacCer present [82]. In contrast, the main molecular species of LacCer on the plasma membranes of human neutrophils are C24:0-, C24:1-, and C16:0-LacCer. Importantly, Lyn is able to enter into LacCer-enriched lipid rafts of D-HL-60 cells that are loaded with C24:0- and C24:1-LacCer

molecules. On the other hand, the loading of C16:0- and C22:0-LacCer molecules hardly reconstruct Lyn-associated LacCer-enriched lipid rafts. LacCer-mediated immunological functions can be reconstructed in the C24:0- or C24:1-LacCer molecule-loaded D-HL-60 cells. Moreover, C24- but not C16-LacCer molecules have been demonstrated to be directly associated with Lyn and G α i by the crosslinking experiments with photoactivatable tritium-labeled LacCer analogues [81]. The interactions between C24 fatty acid chains of LacCer and palmitic chains of Lyn and G α i are thought to be indispensable for LacCer-enriched lipid rafts-mediated outside-in signaling (Fig. 1).

$\alpha_M\beta_2$ -Integrin mediates immunological functions of neutrophils and macrophages, such as adhesion, migration, chemotaxis, and phagocytosis of opsonized and non-opsonized microorganisms [83]. $\alpha_M\beta_2$ -Integrin does not possess a catalytic motif responsible for signaling inside of the cells [84,85]. Rather, Src family kinases are the responsible signal transduction molecules for $\alpha_M\beta_2$ -integrin-induced functions [86,87]. Thus, the $\alpha_M\beta_2$ -integrin requires adaptor molecules for connecting to Src kinases. $\alpha_M\beta_2$ -Integrin initiates innate immune responses through binding to several ligands. The α_M subunit can bind not only to C3bi but also to some kinds of PAMPs, including β -glucan and LPS [88,89]. In plasma membranes of resting neutrophils, $\alpha_M\beta_2$ -integrin and LacCer-enriched lipid rafts are close to but not colocalized with each other. Upon ligand binding to α_M integrin subunit, $\alpha_M\beta_2$ -integrins move to Lyn-associated LacCer-enriched lipid rafts (Fig. 1C). Anti-LacCer antibody Huly-m13 was shown to pull down the β_2 subunit from the detergent-resistant membrane fraction (DRM) of zymosan-containing phagosomes, whereas the β_2 subunit was not isolated from the plasma membrane DRM of resting neutrophils [21]. Gene-silencing experiments showed that $\alpha_M\beta_2$ -integrin-mediated activation by non-opsonized microorganisms depended on Lyn-associated LacCer-enriched lipid rafts in human neutrophils [15,21] (Table 2). These findings suggest that Lyn-associated LacCer-enriched lipid rafts act as signal transduction platforms for signaling motif-deficient molecules, such as $\alpha_M\beta_2$ -integrin.

Mechanism of the binding of LacCer-enriched lipid rafts to pathogens

As described in section I, several kinds of pathogenic microorganisms bind to LacCer, suggesting existence of the common pattern(s) on the membranes of these microorganisms, which can be recognized by LacCer clusters. Fungi express β -glucans, which are

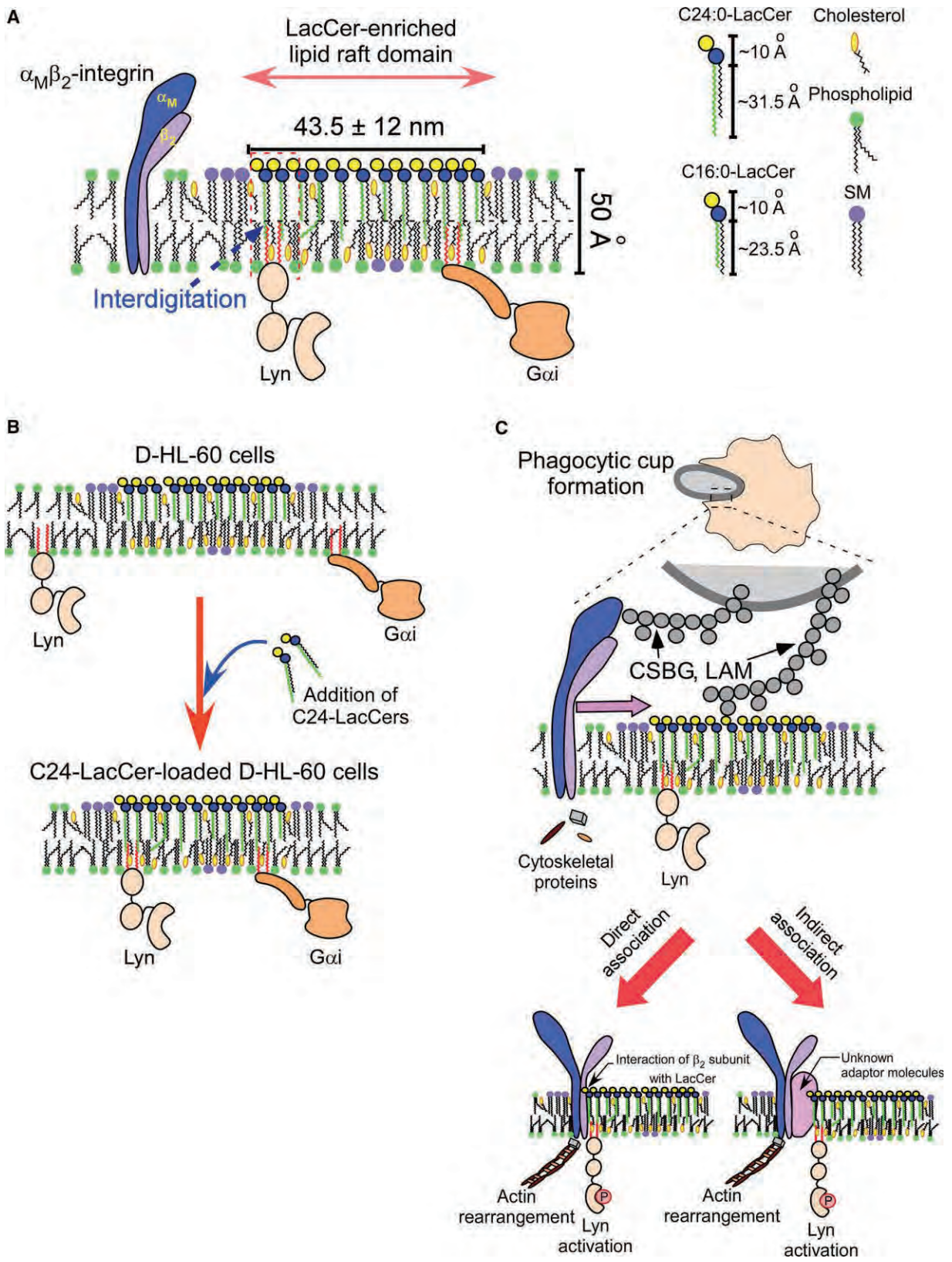


Fig. 1. LacCer-enriched lipid rafts. (A) Schematic image showing the direct association of C24-LacCer with Lyn and G α i. LacCer forms Lyn- and G α i-coupled lipid rafts on the plasma membrane of human neutrophils. The C24 fatty acid chains of LacCer interdigitate into the inner leaflet of plasma membranes and interact directly with the palmitic chains of Lyn and G α i. These interactions allow association of these signal transduction molecules with LacCer to mediate signaling from outside to inside, resulting in neutrophil functions, including chemotaxis, phagocytosis, and superoxide generation. In addition, LacCer-enriched lipid rafts also act as a signal transduction platform for $\alpha_M\beta_2$ -integrin (CD11b/CD18), which is devoid of a signaling motif in its cytoplasmic region. (B) Effect of C24-LacCer on the functions of D-HL-60 cells. Loading of C24-LacCer but not C16-LacCer into D-HL-60 cells reconstituted cellular functions, such as chemotaxis and phagocytosis, to almost the same levels as human neutrophils. (C) Schematic image showing the interactions of Lyn-associated LacCer-enriched lipid rafts with $\alpha_M\beta_2$ -integrin. Upon the binding of bacterial PAMPs, such as CSBG or LAM, to $\alpha_M\beta_2$ -integrin and LacCer-enriched lipid rafts on host cells, the α_M subunit is activated and undergoes a conformational change, inducing the accumulation of cytoskeletal proteins, including talin and α -actinin (actin rearrangement). $\alpha_M\beta_2$ -Integrin subsequently translocates into LacCer-enriched lipid rafts, stimulating Lyn by the direct or indirect interaction between LacCer and residues 514–553 in the C-terminal portion of the conserved domain of the β_2 subunit. These signaling cascades induce the formation of phagocytic cups, resulting in phagosome formation.

Table 2. Associations of GSLs with partner molecules to mediate immune responses.

GSLs	Partner molecules	Cell type	Phenotype	Ref. No.
LacCer	CD11b/CD18 ($\alpha_M\beta_2$)-integrin	Neutrophils (Human)	β -glucan- and LAM-induced phagocytosis of zymosan and mycobacterial species, respectively	[15,21]
GD1a	TLR2/TLR1	Monocytes (Human)	LT-IIb-B $_5$ -induced NF κ B activation	[169]
Asialo GM1	TLR5	Lung epithelial cells NCIH292 (Human)	Flagellin-induced autocrine release of ATP	[170]
GM1a	TrkA	Lung adenocarcinoma epithelial cell line A549 (Human)	<i>Clostridium perfringens</i> alpha-toxin-induced IL-8 release	[171]
GM1	PreTCR α	SCID thymocyte-derived cell line SCB.29 (Mouse)	PreTCR signaling	[114]
a-series gangliosides	CD4, TCR	T cells (Mouse)	Helper T cell activation	[22]
o-series gangliosides	CD8, TCR	T cells (Mouse)	Killer T cell activation	[22]
GM1	IgM-BCR	Immature B cells (Mouse)	Removal of autoreactive immature B cells (apoptosis)	[153]
GM3	Caspase-8 (upon CD95/Fas stimulation)	Lymphoblastoid T cells (Human)	Apoptosis	[157]

heterogeneous glucose polymers, consisting of β -1,3-linked β -D-glucopyranosyl units with or without β -1,6-linked side chains of various distributions and lengths [90,91]. CSBG consists of a β -1,3 glucopyranose glucan backbone, with β -1,6 long glucopyranose side chains and β -1,3 monoglucopyranose branches [91]. CSBG binds to GSLs having galactose as the terminal residue, such as GalCer, LacCer, and Gb3 [16]. The structure of yeast-derived PGG-glucan resembles that of CSBG [92]. PGG-glucan also binds to GSLs having galactose as the terminal residue [48].

Mycobacteria abundantly express glycolipid LAM on their cell wall [93]. Pathogenic mycobacteria, including *M. tuberculosis* and MAC, express a terminal Man-LAM, while nonpathogenic mycobacteria, including *M. smegmatis*, express a terminal PILAM or no capped LAM [94]. LAMs have the same mannan core structure, consisting of a linear chain of α -1,6

mannopyranose backbone with α -1,2 mannopyranose side branches [95]. Both *M. tuberculosis*-derived Man-LAM and *M. smegmatis*-derived PILAM bind to LacCer [15]. Surface plasmon resonance (SPR) experiments demonstrated that *M. tuberculosis*-derived ManLAM binds to LacCer but not to GM3 (Fig. 2B). *M. smegmatis* α -1,2 mannosyltransferase-deficient mutant (Δ MSMEG_4247) expresses mutated PILAM, which lacks α -1,2 monomannose side branches of the mannan core. Human neutrophils cannot phagocytose Δ MSMEG_4247 bacteria. Δ MSMEG_4247-derived LAM does not bind to LAM (Fig. 2C). Therefore, the α -1,2 monomannose side branches of mannan core in LAM of both nonpathogenic and pathogenic mycobacteria are important for phagocytosis of mycobacteria by neutrophils through the binding of LacCer to LAM and lipomannan. LacCer-enriched lipid rafts bind to β -1,6 long glucopyranose side chains with β -1,3

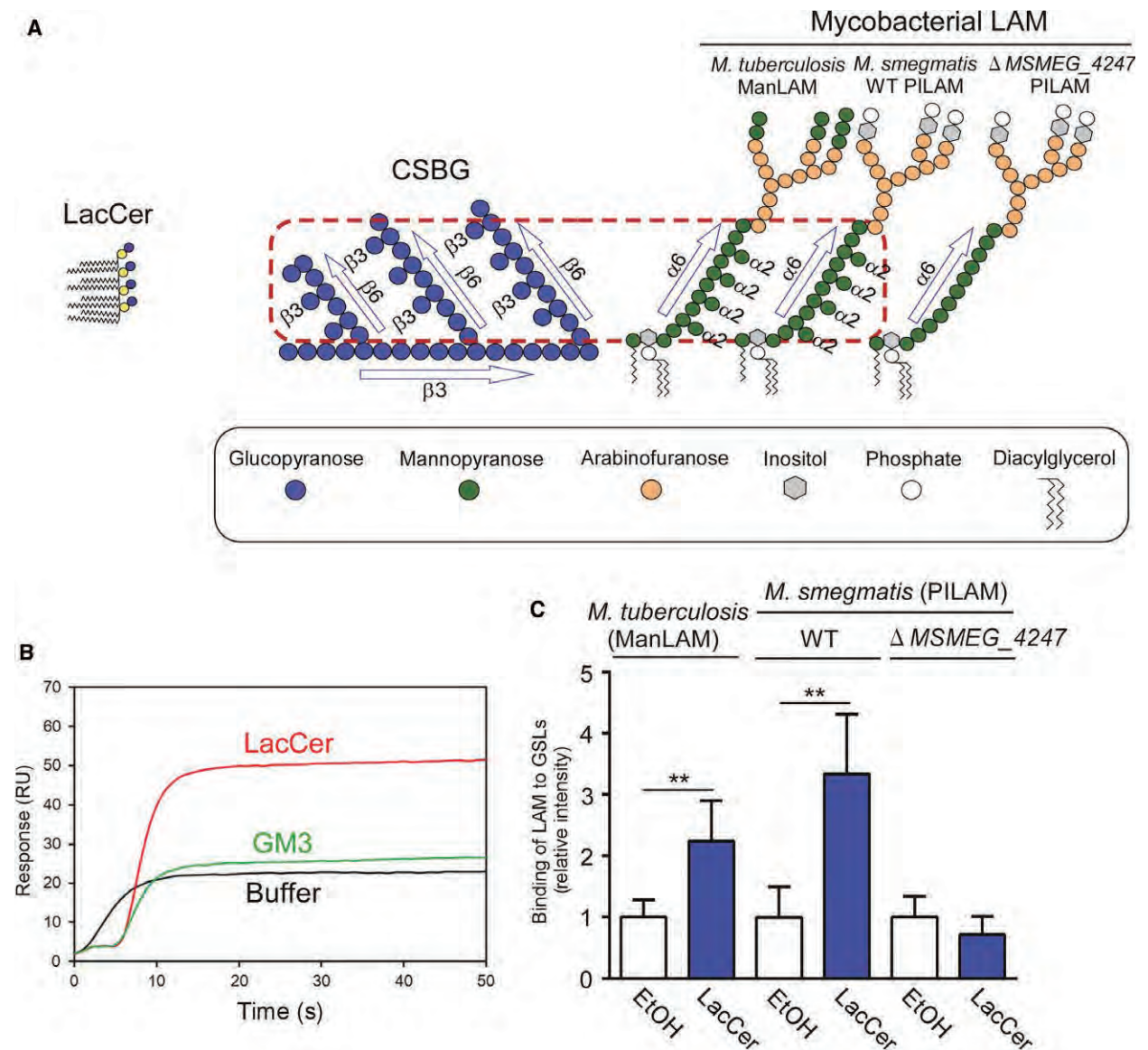


Fig. 2. Binding specificity of LacCer to the structures of β -glucans and LAM. (A) Schematic images showing binding specificities of β -glucans and LAMs to LacCer. β -Glucans are a heterogeneous group of glucose polymers, consisting of β -1,3-linked β -D-glucopyranosyl units with β -1,6-linked side chains of various distributions and lengths. LacCer does not bind to β -glucan, which lacks β -1,6-linked long β -D-glucopyranose side branches, such as curdlan. LAMs are major glycolipid components of all mycobacterial species. All mycobacterial LAMs have a mannan core structure, consisting of a 21–34 residue α -1,6-mannopyranose backbone and 5–10 α -1,2 mannopyranose side chains. LacCer recognizes the α -1,2-monomannose side branches of LAM, which are expressed by both pathogenic (*M. tuberculosis*) and nonpathogenic (*M. smegmatis*) mycobacteria. (B) SPR analysis of the binding specificity of LAMs to LacCer. SPR analysis indicated that *M. tuberculosis*-derived ManLAM binds specifically to LacCer, but not to GM3. RU, resonance unit. (C) Binding specificity of LAMs to LacCer. ManLAM and *M. smegmatis* LacCer bound to PILAM derived from WT, but not from the *M. smegmatis* α -1,2-mannosyltransferase deletion mutant (Δ MSMEG_4247), as the latter lacks the α -1,2-monomannose side branches of the LAM mannan core (reproduced from Science signaling 9, ra101 (2016)) with slight modifications. $**P < 0.01$. Thus, LacCer binds not only to β -1,6 long glucopyranose side chains with a β -1,3 glucopyranose branches of CSBG but also to α -1,2-monomannose side chain-containing mannan cores of LAM, suggesting that LacCer recognizes the common structural patterns of fungal β -glucans and mycobacterial LAMs.

glucopyranose branches of CSBG [16]. Therefore, these observations provide a novel mechanism that LacCer clusters bind to the comb-shaped common

three-dimensional structures between fungal β -glucans and mycobacterial LAMs through carbohydrate-carbohydrate interactions.

GSL-enriched lipid raft-mediated immune evasion by intracellular pathogens

The engulfment and killing of microorganisms by phagocytes are well-characterized functions of innate immunity. PRRs on phagocytes recognize microorganisms, either directly or indirectly, acting as direct sensors of non-opsonic infectious microorganisms in host phagocytes. Phagocytes efficiently engulf opsonized microorganisms through complement component C3b and IgG. Intracellular pathogens, including *Listeria*, *Salmonella*, and *Mycobacteria*, have been shown to target lipid rafts [96] as well as proteinaceous PRRs on host plasma membranes. Above all, pathogenic mycobacteria are known to exploit lipid rafts and PRRs to gain entry into phagocytes under non-opsonized conditions [97,98]. These intracellular pathogens are able to survive inside cells by manipulating a variety of signaling pathways. Once intracellular pathogens are engulfed by phagocytes, they inhibit the fusion of lysosomes to nascent microorganism-containing phagosomes or escape from phagocytic vesicles to reach the cytosol [98–105]. Lysosomes, which contain several kinds of digestive enzymes, effectively fuse to serum-opsonized *M. tuberculosis*-containing phagosomes, but do not fuse to non-opsonized bacteria-containing phagosomes [106,107], suggesting that signaling cascades differ under opsonized and non-opsonized conditions.

Although, regardless of pathogenicity, human neutrophils phagocytose mycobacteria through Lyn-associated LacCer-enriched lipid rafts and $\alpha_M\beta_2$ -integrin, the fates of these phagocytosed bacteria are distinct. Neutrophil phagocytosis of nonpathogenic mycobacteria results in the fusion of lysosomes to bacteria-containing phagosomes [108]. By contrast, phagocytosed pathogenic mycobacteria prevent lysosomal fusion to bacteria-containing phagosomes, resulting in the survival of mycobacteria inside phagocytes. Neutrophil granules highly express LacCer-enriched lipid rafts on their membrane [70,109]. LacCer-enriched lipid rafts are also expressed on bacteria-containing phagosome membranes [15,21]. The Src family kinase Hck, which localizes to the granular membranes [110], is essential for lysosomal fusion to phagosomes [111]. Along with phagosome formation, Hck associates with LacCer-enriched lipid rafts on membrane of phagosomes containing the nonpathogenic mycobacterium *M. goodii* but not the pathogenic mycobacterium MAC [15]. Furthermore, these molecular associations can be observed on phagosomes containing non-pathogenic *M. smegmatis*-derived PILAM- but not pathogenic *M. tuberculosis*-derived ManLAM-coated

beads. Therefore, the mannose cap motif of ManLAM is thought to abrogate the formation of Hck-associated LacCer-enriched lipid rafts on phagosomal membranes. ManLAMs derived from pathogenic mycobacteria may therefore affect the reorganization of phagosomal-membrane LacCer-enriched lipid rafts, disturbing Hck association with the LacCer domains, resulted in enhancing subsequent mycobacterial escape from neutrophil killing (Fig. 3).

Gangliosides in adaptive immunity

T cells are indispensable players in the cell-mediated immunity and differentiate into subsets with distinctive functions in the thymus which is a central organ for the education and maturation of T cells. T cell activation through T cell antigen receptors (TCRs) requires the recruitment of both membrane molecules including costimulatory receptors and intracellular molecules participating in signal transduction, into the lipid rafts [12]. T cells differentiate into helper T ($CD4^+$ T) cells, which are characterized with the expression of CD4 on their cell surface, and cytotoxic T ($CD8^+$ T) cells which are distinguished with the expression of CD8 on their cell membrane. $CD4^+$ and $CD8^+$ T cells achieve distinctive immunological functions, and have similar mechanisms of TCR-mediated signaling *via* particular intracellular signaling events. Th and Tc cells also express different types of gangliosides at different levels [22]. This section covers glycan structure-specific functions of gangliosides involved in the activation of $CD4^+$ and $CD8^+$ T cells and the roles of gangliosides in immune diseases.

Gangliosides in T cell development

Precursor cells migrating from bone marrow develop into conventional T cells in the thymus. Developing T cells in the thymus, usually called thymocytes, can be broadly divided into four subsets, based on their expression of the specific surface markers CD4 and CD8: DN ($CD4^-CD8^-$), DP ($CD4^+CD8^+$), CD4SP ($CD4^+CD8^-$), and CD8SP ($CD4^-CD8^+$). Cells in the DN subset, which are regarded as the least mature stage, can be further subdivided into four substages, DN1 to DN4. DN3 is a prominent stage in the course of thymocyte development. During this stage, TCR β chain genes undergo productive rearrangement, leading to the expression of a preTCR, which induces cell survival, proliferation and expression of both CD4 and CD8 coreceptors [112].

Unlike TCR signaling in mature T cells, preTCR signaling in DN3 cells does not require the recognition

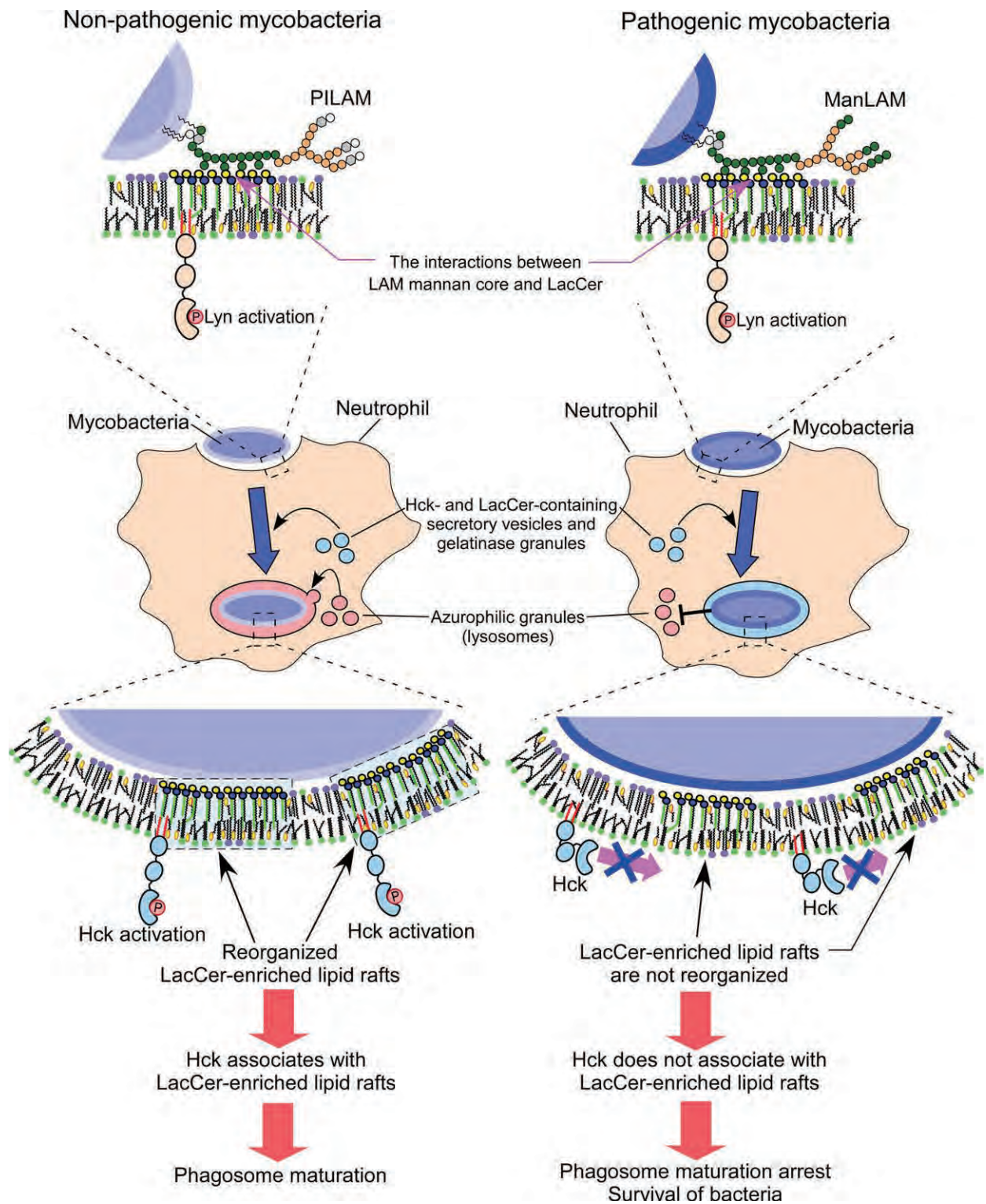


Fig. 3. The capping motif of LAM affects LacCer-enriched lipid raft-mediated phagosome maturation. Schematic images showing mycobacterial phagocytosis in human neutrophils. Human neutrophils engulf mycobacterial species through the binding of LacCer-enriched lipid rafts to the LAM mannan core region. Human neutrophils can therefore engulf both pathogenic and nonpathogenic mycobacteria using the same mechanism. In contrast, pathogenic mycobacteria, such as *M. tuberculosis* and MAC, disrupt the reorganization of Hck-coupled LacCer-enriched lipid rafts on phagosomal membranes through the mannose-capping motif of ManLAM, arresting phagosome maturation.

of major histocompatibility complex (MHC) plus antigen on antigen presenting cells. Rather, preTCR can mediate autonomous signaling, based on the ability of the preTCR component pT α to spontaneously form oligomers [113]. Patch formation by preTCR molecules can be assessed by fluorescence microscopy. PreTCR can be palmitoylated and is partially enriched in lipid rafts [114]. CTx staining, followed by fluorescent-activated cell sorting, showed that ganglioside expression is higher in the DN than in the DP and SP populations, with ganglioside expression being much higher at stages DN3 to DN4 than in other thymocyte populations. CTx-reacting ganglioside species (GM1 and extended-GM1b) were shown to colocalize with preTCR patches on DN cell surfaces [114] (Table 2). These findings suggest that CTx-reacting gangliosides can assist in preTCR clustering in lipid rafts enriched with gangliosides. Phosphorylation of ZAP-70 kinase following preTCR activation can be abolished by treatment with methyl- β -cyclodextrin (M β CD), which is widely used for lipid raft disruption. Forcibly targeting CD3 ζ , a signaling component of the preTCR complex, in lipid rafts by palmitoylation of the CD3 ζ -associated molecule calnexin in Rag recombinase null DN cells, which are defective in preTCR expression, allows the further development of DN cells [78]. However, mutated forms of preTCR, which lack putative palmitoylated sites or all intracellular domains, have normal preTCR signaling capacity [115,116]. Further research is necessary to better clarify the physiological functions of gangliosides in preTCR signaling and DN cell development.

PreTCR signaling has been associated with cell survival and proliferation and with expression of both CD4 and CD8 coreceptors. The resulting cells are termed DP thymocytes. After TCR rearrangement, DP cells express mature TCR and undergo positive and negative selection to become mature CD4 and CD8 SP cells, respectively. Because DP cells have fewer raft-forming lipids, GSLs, and sphingomyelin, than thymocytes of any other developmental stage, the profiles and functions of lipid rafts in DP cells remain unclear. TCR-mediated activation, such as the recruitment of signaling molecules into immunological synapses during positive selection of DP cells, does not involve the accumulation of CTx-reacting gangliosides [117]. DN4 cells in TCR-null mice exhibited greater Ca²⁺ responses than DP cells upon stimulation with an anti-TCR antibody. The forced expression on thymic epithelium of CD80, a costimulatory molecule that cooperates with CD28 on thymocytes, induces GM1 accumulation at the site of contact between thymocytes and thymic epithelium, as well as reducing

positive selection and increasing apoptosis like negative selection [118]. These results suggest that DP cells have a higher signal threshold for TCR activation and therefore require stronger stimulation than DN cells, as the structure and dynamics of lipid rafts on DP cells are limited by the reduced availability of gangliosides and sphingomyelin.

Although conditional targeted disruption of the GlcCer synthase (GlcCerS) gene in early DN stage thymocytes resulted in almost complete reduction of GSLs derived from GlcCer, conventional T cell development was not affected [119]. This was likely caused by the ability of trace amounts of GSLs to form specific microdomains and induce TCR-mediated signal transduction. Alternatively, it may have been due to the sphingomyelin microdomain essential for TCR-mediated DN thymocyte development, in that activation with anti-CD3 antibody induced the accumulation of sphingomyelin in a microdomain containing TCR [120].

Roles of gangliosides in TCR-dependent activation of T cells

Antigen-presenting cells carrying MHC-peptide complexes present peptide antigens to TCRs on the T cells, triggering T cell activation. CD4 and CD8 as costimulatory molecules on T cells bind to nonpolymorphic regions of the MHC and facilitate the signaling. During the activation, TCR and CD4 or CD8 on the cell membrane and intracellular signaling molecules need to be recruited into specific cell membrane region called lipid rafts.

The lipid rafts are composed of sphingomyelin and cholesterol as the major raft lipid components and GSLs or gangliosides as the minor but significant components. Cholesterol interacts with hydrocarbon chains of sphingolipids, holds the raft assembly together like a “glue”, and plays a critical role in maintaining membrane fluidity. The functions of cholesterol in the lipid rafts are very well documented on the basis of results obtained by M β CD treatment which depletes cholesterol from cell membranes and disrupts cellular functions [121]. Despite concerns about other effects produced by the treatment [122], experimental approaches using M β CD have been widely used. In contrast, fewer studies have addressed the role of gangliosides in raft functions due to the lack of convenient procedures manipulating the presence of GSLs and gangliosides in the cell membrane.

Important aspects of ganglioside expression of T cells can be seen in GM3 synthase knockout (GM3S^{-/-}) and GM2/GD2 synthase knockout (GM2/GD2S^{-/-}) mice [22]. GM3S transfers sialic acid to galactose residue of

LacCer for making GM3, which the simplest molecule of the “a-series” gangliosides. GM2/GD2S transfers GalNAc to LacCer, GM3 or GD3, and expressed GA2, GM3, and GD2. In wild-type (WT) mice, a-series GM1a expression of CD4⁺ T cells is higher than CD8⁺ T cells. In contrast, expressions of o-series GM1b, GalNAc-GM1b, and extended GM1b are higher in CD8⁺ T than in CD4⁺ T cells. TCR-induced proliferation and cytokine production were severely disordered in CD4⁺ T cells of GM3S^{-/-} mice, and these defects can be canceled by pretreatment of the cells with GM3 and GM1a, but not b-series, gangliosides. The severe disorder of TCR-dependent proliferation and cytokine production also can be seen in T cells of GM2/GD2S^{-/-} mice, and these defects were also canceled by pretreatment of the cells with o-series gangliosides or their precursor GSLs, GM1b and GA1, but not with a- or b-series gangliosides. These observations indicate that CD4⁺ and CD8⁺ T cell subsets have specific raft domains composed of distinct kinds of gangliosides, and this distinction is the basis of different function of TCR stimulation of these two subsets (Fig. 4; Table 2). An

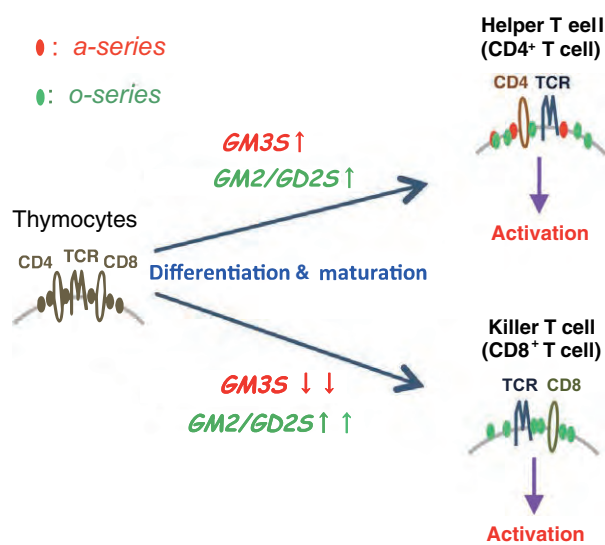


Fig. 4. Distinct expression signatures of ganglioside molecules during T cell development. The maturation of immature thymocytes (doubly positive for CD4⁺ and CD8⁺) to mature singly positive T cell subpopulations was accompanied by selective ganglioside expression. Gene expression patterns, together with ganglioside analysis, confirmed that CD8⁺ T cells exclusively express o-series gangliosides due to downregulation of *GM3S* and upregulation of *GM2/GD2S* expression. In contrast, GM1a expression was maintained in CD4⁺ T cells due to the upregulation of *GM3S*, suggesting that each T cell subset has unique rafts composed of different ganglioside molecules and that these rafts provide distinct functions during different intracellular events following receptor-mediated stimulation. This ganglioside selection process may be indispensable in the formation of distinct and functional lipid rafts in mature T cells.

interesting possibility is proposed as that CD4 may interact with the glycan structure common to GM3 and GM1a, Siaβ2-3Galβ1-4Glc, and CD8 with that of GM1b and GA1, Galβ1-3GalNAcβ1-4Galβ1-4Glc. Another possibility is the involvement of ceramide structures of these gangliosides. LC-MS analysis indicated GM1a and b, GD1, GalNAc-GM1b, and extended GM1b carry ceramides composed of d18:1-16:0, -18:0, -20:0, -22:0, -24:1, and -24:0. Ceramide structures of these gangliosides were not so much different between CD4⁺ and CD8⁺ cells except for higher content of d18:1-22:0 carrying gangliosides in CD8⁺ cells. Is this difference critical for the ganglioside preference by CD4 and CD8? These possibilities need to be addressed and, for doing this, further development of imaging mass spectrometry which is able to cover the m/z values of these gangliosides with much higher sensitivity would become an indispensable approach. CD4 and CD8 localize to lipid rafts by palmitoylation, a process during which acyl chains are attached to core proteins, but raft localization is not determined solely by this process [123,124]. To ensure the movement of CD4 and CD8 to specific and correct locations on the membrane, these molecules must likely interact with rafts carrying specific gangliosides. Taking these issues into consideration, the specific roles of individual gangliosides in regulating membrane microenvironments remain to be determined as critically important molecular mechanism for maintaining membrane functions.

Involvement of gangliosides in T cell-mediated autoimmune and allergic diseases

Negative selection of T cells is indispensable for the prevention of autoimmune diseases during T cell development in the thymus. Survival of self-reactive T cells could lead to autoimmune disorders and allergic diseases. There are several subsets of CD4⁺ T cells, e.g., Th1, Th2, Th17, and Treg cells. These CD4⁺ T cell subsets produce different kinds of cytokines and chemokines, and showing their specific functions. The functional specificity of CD4⁺ T cell subsets may be due to differences in the organization of TCR signaling complexes in lipid rafts [125].

Allergic asthma is defined as a type 1 hypersensitivity reaction, which is a manifestation of immediate and late-phase reactions in the lungs. Innate immune cells, including mast cells, basophils, and eosinophils, are effector cells during airway inflammation [126,127]. CD4⁺ T cells contribute to the initiation of allergic reactions by producing Th2 cytokines, such as IL-4 and IL-13, which initiate production of IgE antibodies against harmless antigen from B cells [128,129].

Administration of ovalbumin (OVA) induces allergic airway inflammation and airway hyperresponsiveness in OVA-sensitized mice [22]. The OVA-induced allergic airway inflammation includes OVA-specific IgE production, airway infiltration by inflammatory cells, mucus hypersecretion, and increased Th2 cytokine levels in serum. Importantly, these allergic airway responses markedly reduced in the OVA-sensitized GM3S^{-/-} mice (Fig. 5). The reduction of allergic responses in GM3S^{-/-} mice is thought to be due to a lack of GM1a in CD4⁺ T cells [22]. The expression of GM1a is enhanced in self-reactive CD4⁺ T cells, and this enhancement persists abnormal cell activation [130,131]. Administration of antisense oligonucleotides against the *GM3S* gene suppressed airway inflammation [132]. These findings indicate that the a-GMs such as GM1a are essential for T helper cell function

(Fig. 4). The balance between effector Th2 cells and suppressive Treg cells during allergic airway inflammation was skewed toward Th2 predominance [133]. The particular role of Th17 cells in asthma is still unknown. But, Th17 cells could be involved in neutrophilic, steroid-resistant severe asthma and enhance the airway inflammation caused by Th2 cells [134]. Th17 cells from GM3S^{-/-} mice reduced the number of Th17 cells *in vitro* [135].

One of the most common autoimmune diseases is systemic lupus erythematosus (SLE), which presents with multisystem clinical manifestations, including rash, arthritis, glomerulonephritis, hemolytic anemia, thrombocytopenia, and central nervous system involvement [136,137]. The pathogenesis of SLE involves the appearance of many types of autoantibodies and autoreactive T and B cells. T cells from patients with

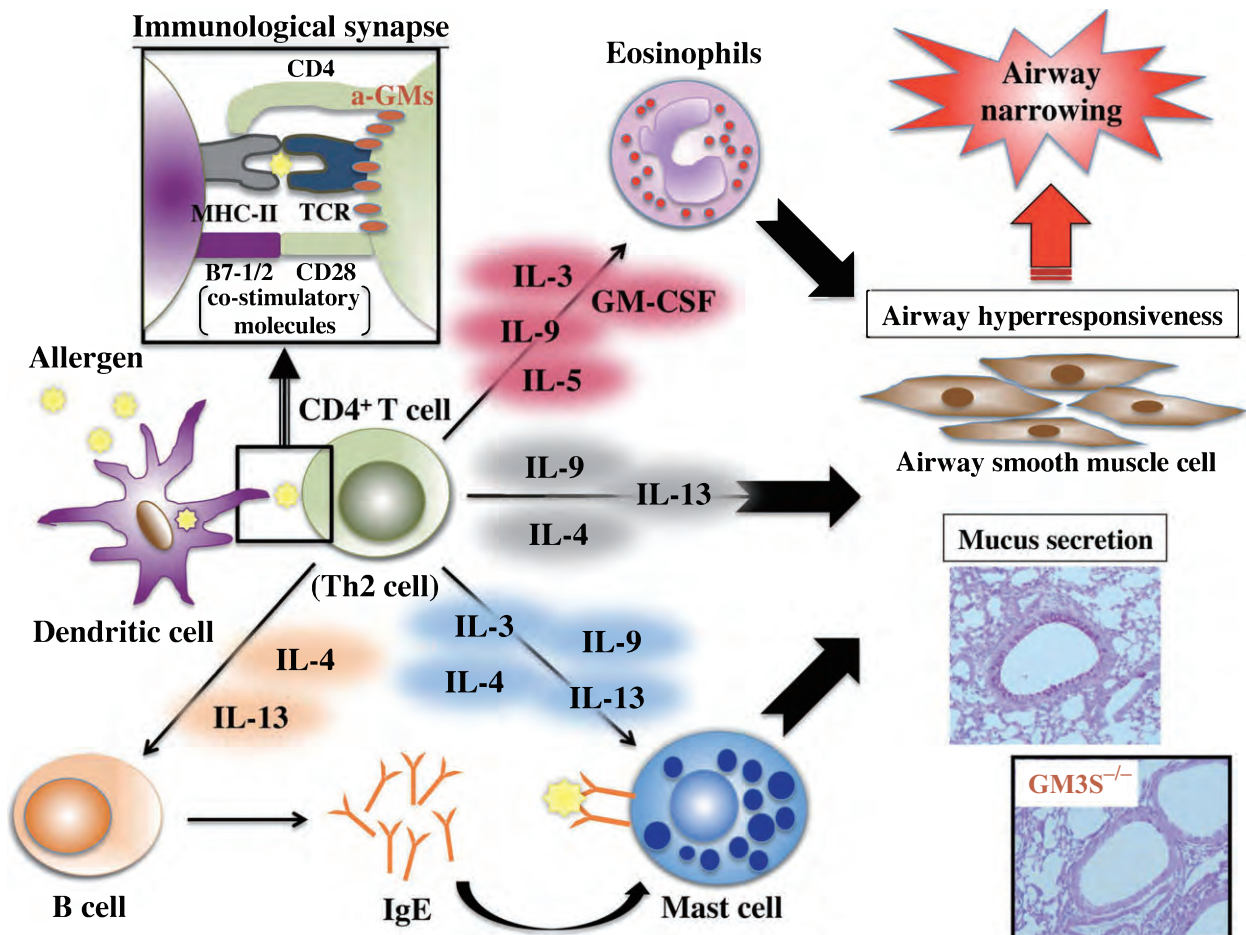


Fig. 5. The role of gangliosides in the pathogenesis of allergic asthma. a-GMs in CD4⁺ T cells are critical for signal transduction through immunological synapses, resulting in the synthesis and release of Th2 cytokines, such as IL-4, IL-5 and IL-13. These cytokines play a central role in the development of airway narrowing by activating eosinophils, B cells and mast cells, which cause mucus secretion and airway hyperresponsiveness.

SLE were reported to show intrinsic alterations in lipid components of lipid rafts [130,138,139]. The levels of expression of GM1a in CD4⁺, but not CD8⁺, T cells were significantly higher in SLE patients than in healthy controls. LacCer, GA2, Gb3, GM1a, and GD1a were also upregulated in SLE CD4⁺ T cells [140]. The increase in GM1a was greater in CD45RO-positive CD4⁺ memory T cells from patients with active than inactive SLE [130]. In addition, the expression of GM1a is enhanced in activated human T cells [130,139,141,142] and in self-reactive CD4⁺ T cells, resulting in the persistence of abnormal cell activation [130,131]. Taken together, these findings indicate that gangliosides are key factors in the pathogenesis and pathology of SLE. GlcCerS inhibitor normalized the increases in GM1a and LacCer levels in SLE CD4⁺ T cells after stimulation with anti-CD3 and anti-CD28 mAbs, as well as partially reversing the defects in TCR signaling [140]. The levels of expression of cellular GSLs are systematically controlled by *de novo* synthesis, turnover, and recycling [143]. The biosynthesis of GSLs and their trafficking to and from plasma membranes are increased in SLE T cells, leading to the aberrant accumulation of gangliosides in lipid rafts [144].

Rheumatoid arthritis (RA) is a typical autoimmune disease and typically results in warm, swollen, and painful joints, and adaptive immune systems are involved in RA development [145]. In RA patients, macrophages, Th1 cells, Th17 cells, and activated B cells migrates into inflamed tissues, and inflammatory cytokines, including IL-1, IL-6, IL-8, IL-17, TNF α , and interferon-gamma, can be detected in the fluids surrounding inflamed synovia and joints [146,147]. Moreover, the gene expression of *GM3S* and the GM3 expression levels were higher in the synovia of patients with RA than with osteoarthritis [148]. In *GM3S*^{-/-} mice, the progression of collagen-induced inflammatory arthritis, a mouse model of RA, was accelerated, and the induction of IL-17-producing cells in regional lymph nodes was enhanced by collagen immunization [148]. In contrast, *GM3S*^{-/-} mice exhibited a smaller number of Th17 cells after culture *in vitro* [135]. Further studies are needed to clarify the pathological significance of GM3 molecular species in RA development.

CD4⁺ T cells can be subclassified as GD1c-positive IL-2-producing Th1-like cells and GD1c-negative IL-4-producing Th2-like cells [149]. The lipid rafts of each of these subpopulations have a unique, characteristic ganglioside expression pattern, with these patterns being responsible for the specific functions of Th effector cells.

Role of GM1 in B cell antigen receptor (BCR) signaling

B cell antigen receptors (BCRs) are critical for the clonal selection of B cells and the differentiation of B cells into plasma cells. Mature B cells express not only IgM-type but also IgD-type BCRs. These IgM and IgD type BCRs possess identical antigen-binding sites, but differ in their membrane-bound heavy chain isoforms. GM1-enriched membrane lipid rafts involved in BCR signaling may be responsible for the ganglioside-related immune functions of B lymphocytes [150–153]. IgM-BCR is not closely localized to GM1-enriched lipid rafts in resting B cells, whereas IgD-BCR is located adjacent to these lipid domains [151]. BCR stimulation induces the translocation of IgM-BCRs into GM1-enriched lipid rafts in a caveolin-1-dependent manner, whereas IgD-BCRs are excluded from these lipid domains [153], resulting in the clustering of IgM- and IgD-BCR nanoclusters. The mechanisms by which IgM and IgD nanoclusters are organized in GM1-enriched lipid rafts and modulate BCR signaling remain unknown.

GSL-enriched lipid raft-mediated apoptosis and autophagy in immunity

Apoptosis is generally recognized as a principal mechanism that modulates cell death, occurring not only in cellular damages or stress but also in the normal development and morphogenesis [154]. In innate immunity, apoptosis is a significant mechanism for the elimination of neutrophils from inflamed tissues by tissue-resident macrophages, which are crucial for confining inflammatory tissue injury and subsequent resolution of inflammation [71]. Phosphatidylglucoside (PtdGlc) is a unique glycosphingolipid that forms PtdGlc-enriched raft-like domains on human neutrophil plasma membranes [71]. Furthermore, PtdGlc-enriched raft-like domains mediate the death receptor CD95/Fas-mediated apoptosis pathway. These findings suggest that lipid raft-mediated apoptosis regulation is essential in innate immune systems.

GM3 is the major component of lipid rafts in human lymphocytic cells [155]. Furthermore, the disialoganglioside GD3 is also abundant, and concentrated in lipid rafts [156]. Following treatment of human lymphoblastoid T cells with anti-CD95/Fas, GM3 was reported to associate with caspase-8, a component of the death-inducing signaling complex [157], suggesting that gangliosides are structural components of the membrane multi-molecular signaling complex involved in the apoptosis pathway mediated by CD95/

Fas receptor. In general, two different cascades are known to occur during apoptosis, the plasma membrane-associated death receptor-mediated cascade and the mitochondria-mediated cascade. GD3 permeabilizes mitochondria in MH1C1 rat hepatoma cells in a manner dependent on reactive oxygen species (ROS) and calcium [158]. TNF- α stimulation induces physical association and GD3 accumulation in mitochondria of rat hepatocytes [159]. Moreover, GD3-enriched raft-like domains have been reported present on the mitochondrial membranes that recruit Bcl-family proteins in human lymphoblastoid T cells [160]. Taken together, these findings suggest that GSLs play pivotal roles in apoptotic pathways of both innate and adaptive immune cells. In addition, GSLs form lipid rafts not only on plasma membranes but also on subcellular compartments, with these subcellular GSL-enriched lipid rafts mediating important signaling pathways involved in various physiological functions. Indeed, LacCer forms lipid rafts on both granular compartments and nascent microorganism-containing phagosomes [15], with the association of phagosomal LacCer-enriched lipid rafts with Hck, which facilitates lysosomal fusion, being indispensable for the maturation of microorganism-containing phagosomes.

Apoptosis and autophagy are well regulated and intertwined biological processes [154,161]. Under stress conditions, autophagy is unable to assist cell survival, and apoptosis pathways are activated in cells to ensure their effective elimination without triggering local inflammation [162]. Thus, efficient regulation of cross talk between apoptosis and autophagy is likely to be advantageous to cells [154]. Interestingly, GD3 was shown to associate with phosphatidylinositol(3)phosphate (PtdIns3P) and microtubule-associated protein light chain 3 in fibroblasts, indicating the important roles of GD3 in the timing of initiation of autophagy and autophagosome biogenesis [163]. Formation of autophagosomes at the endoplasmic reticulum–mitochondria contact site [mitochondria-associated membranes (MAM)] in mammalian cells has been suggested [164]. Recently, GD3 was shown to form lipid raft-like domains in MAM [165] and to interact with core-initiator proteins of autophagy. These observations suggest that lipid raft-like domains in MAM are important in the organelle scrambling activity that leads to autophagosome biogenesis. Detailed elucidation of the mechanisms by which GSLs interact with autophagy-related proteins and contribute to autophagosome biogenesis may suggest new treatments for many human diseases, because autophagy has been shown to be an important regulator not only of innate and adaptive immunity but also of other biological conditions,

including cellular responses to starvation, cell death, cancer, and neurodegenerative diseases [166].

Perspectives

Glycosphingolipids expressed on cells play essential roles in a variety of immunological functions. Neutral GSLs, such as LacCer and Gb3, are important in initializing host defense responses through binding to their ligands [15,30]. Exogenously added C24-LacCer can regulate cellular functions, such as chemotaxis and phagocytosis [21,81]. α -Linked glycosylceramides were identified as the major endogenous ligands of NKT cells [27], which control innate and adaptive immune responses. In addition, β -GlcCer was identified as an endogenous ligand for Mincle [60], suggesting that GSL-receptor trans-interactions may regulate immune responses. GSLs may play important roles in tuning the cross talk of signaling pathways in immune systems, by regulating their expression and release. Immune reactions to GSL antigens may be involved in the pathogenesis of autoimmune diseases, such as encephalomyeloneuropathy (EMRN), as autoantibodies against LacCer are present in patients with EMRN [167]. The binding sites of anti-LacCer antibody clones differ, even in LacCer-enriched rafts [28], suggesting that the antigenic specificity of GSLs is complicated on plasma membranes.

Recent studies have indicated that individual CD4⁺ T cell subsets express different ganglioside-enriched lipid rafts on plasma membranes, which affect the pathogenesis of allergic and autoimmune diseases. Thymus T cell differentiation is associated with differential expression patterns of gangliosides in individual T cell subsets. In peripheral lymphoid organs, the subpopulations of effector CD4⁺ T cells possess distinct lipid rafts with unique ganglioside patterns, which are responsible for specific Th functions. Therefore, the selective ganglioside expression is indispensable for the formation of distinct, functional lipid rafts of T cells during their maturation. Allergic reactions have some common features. However, these reactions are somehow reflected by greatly different molecular patterns responsible for antigens specificities. Reduction of a-GMs by suppression of GM3S causes changing of different ganglioside-enriched lipid rafts. Such kind of technique is a potentially powerful tool for the treatment of immune system disorders.

Glycosphingolipids having different types of sugar motifs and/or acyl chains are likely able to form distinct lipid domains [71,168]. Elucidating the functions of GSLs requires further technical advances to identify raft-associated molecules that maintain their

physiological status. These technical advances may lead to the development of new pharmacological agents for several types of disease, including infectious, inflammatory and autoimmune disorders.

Acknowledgements

The authors' studies described in this Review were supported in part by grants from Foundation of Strategic Research Projects in Private Universities (to HN and KI, S1201013 and S1311011; to JI, S1201031); MEXT KAKENHI (to KI, 16017293 and 24659293; to HN, 25860831 and 15K19592; to JI, 16H04767); AMED under Grant Number JP17g-m0910006 (to KI) and the Naito Foundation (to NH and JI), Mizutani Foundation for Glycoscience (JI and KI), ONO Medical Research Foundation (JI), Uehara Memorial Foundation (JI).

References

- Hakomori S (1981) Glycosphingolipids in cellular interaction, differentiation, and oncogenesis. *Annu Rev Biochem* **50**, 733–764.
- Mukherjee S and Maxfield FR (2004) Membrane domains. *Annu Rev Cell Dev Biol* **20**, 839–866.
- Murate M, Abe M, Kasahara K, Iwabuchi K, Umeda M and Kobayashi T (2015) Transbilayer distribution of lipids at nano scale. *J Cell Sci* **128**, 1627–1638.
- Pike LJ (2006) Rafts defined: a report on the keystone symposium on lipid rafts and cell function. *J Lipid Res* **47**, 1597–1598.
- Inokuchi J, Nagafuku M, Ohno I and Suzuki A (2015) Distinct selectivity of gangliosides required for CD4(+) T and CD8(+) T cell activation. *Biochim Biophys Acta* **1851**, 98–106.
- Nakayama H, Ogawa H, Takamori K and Iwabuchi K (2013) GSL-enriched membrane microdomains in innate immune responses. *Arch Immunol Ther Exp (Warsz)* **61**, 217–228.
- Rueda R (2007) The role of dietary gangliosides on immunity and the prevention of infection. *Br J Nutr* **98** (Suppl 1), S68–S73.
- Popa I and Portoukalian J (2003) Relationship between lipids and cutaneous immunity: example of the gangliosides. *Pathol Biol (Paris)* **51**, 253–255.
- Iwabuchi K, Nakayama H, Oizumi A, Suga Y, Ogawa H and Takamori K (2015) Role of ceramide from glycosphingolipids and its metabolites in immunological and inflammatory responses in humans. *Mediators Inflamm* **2015**, 120748.
- Anderson HA and Roche PA (2015) MHC class II association with lipid rafts on the antigen presenting cell surface. *Biochim Biophys Acta* **1853**, 775–780.
- Zuidsherwoude M, de Winde CM, Cambi A and van Spruiel AB (2014) Microdomains in the membrane landscape shape antigen-presenting cell function. *J Leukoc Biol* **95**, 251–263.
- Dykstra M, Cherukuri A, Sohn HW, Tzeng SJ and Pierce SK (2003) Location is everything: lipid rafts and immune cell signaling. *Annu Rev Immunol* **21**, 457–481.
- Schengrund CL (2003) “Multivalent” saccharides: development of new approaches for inhibiting the effects of glycosphingolipid-binding pathogens. *Biochem Pharmacol* **65**, 699–707.
- Yates AJ and Rampersaud A (1998) Sphingolipids as receptor modulators. An overview. *Ann N Y Acad Sci* **845**, 57–71.
- Nakayama H, Kurihara H, Morita YS, Kinoshita T, Mauri L, Prinetti A, Sonnino S, Yokoyama N, Ogawa H, Takamori K *et al.* (2016) Lipoarabinomannan binding to lactosylceramide in lipid rafts is essential for the phagocytosis of mycobacteria by human neutrophils. *Sci Signal* **9**, ra101.
- Sato T, Iwabuchi K, Nagaoka I, Adachi Y, Ohno N, Tamura H, Seyama K, Fukuchi Y, Nakayama H, Yoshizaki F *et al.* (2006) Induction of human neutrophil chemotaxis by *Candida albicans*-derived beta-1,6-long glycoside side-chain-branched beta-glucan. *J Leukoc Biol* **80**, 204–211.
- Kabayama K, Sato T, Saito K, Loberto N, Prinetti A, Sonnino S, Kinjo M, Igarashi Y and Inokuchi J (2007) Dissociation of the insulin receptor and caveolin-1 complex by ganglioside GM3 in the state of insulin resistance. *Proc Natl Acad Sci USA* **104**, 13678–13683.
- Mutoh T, Tokuda A, Miyadai T, Hamaguchi M and Fujiki N (1995) Ganglioside GM1 binds to the Trk protein and regulates receptor function. *Proc Natl Acad Sci USA* **92**, 5087–5091.
- Ichikawa N, Iwabuchi K, Kurihara H, Ishii K, Kobayashi T, Sasaki T, Hattori N, Mizuno Y, Hozumi K, Yamada Y *et al.* (2009) Binding of laminin-1 to monosialoganglioside GM1 in lipid rafts is crucial for neurite outgrowth. *J Cell Sci* **122**, 289–299.
- Prasanna X, Jafurulla M, Sengupta D and Chattopadhyay A (2016) The ganglioside GM1 interacts with the serotonin1A receptor via the sphingolipid binding domain. *Biochim Biophys Acta* **1858**, 2818–2826.
- Nakayama H, Yoshizaki F, Prinetti A, Sonnino S, Mauri L, Takamori K, Ogawa H and Iwabuchi K (2008) Lyn-coupled LacCer-enriched lipid rafts are required for CD11b/CD18-mediated neutrophil phagocytosis of nonopsonized microorganisms. *J Leukoc Biol* **83**, 728–741.

- 22 Nagafuku M, Okuyama K, Onimaru Y, Suzuki A, Odagiri Y, Yamashita T, Iwasaki K, Fujiwara M, Takayanagi M, Ohno I *et al.* (2012) CD4 and CD8 T cells require different membrane gangliosides for activation. *Proc Natl Acad Sci USA* **109**, E336–E342.
- 23 Kawano T, Cui J, Koezuka Y, Toura I, Kaneko Y, Sato H, Kondo E, Harada M, Koseki H, Nakayama T *et al.* (1998) Natural killer-like nonspecific tumor cell lysis mediated by specific ligand-activated Valpha14 NKT cells. *Proc Natl Acad Sci USA* **95**, 5690–5693.
- 24 Kanda N and Tamaki K (1998) Ganglioside GQ1b enhances Ig production by human PBMCs. *J Allergy Clin Immunol* **102**, 813–820.
- 25 Kawano T, Cui J, Koezuka Y, Toura I, Kaneko Y, Motoki K, Ueno H, Nakagawa R, Sato H, Kondo E *et al.* (1997) CD1d-restricted and TCR-mediated activation of valpha14 NKT cells by glycosylceramides. *Science* **278**, 1626–1629.
- 26 Kumar A, Suryadevara N, Hill TM, Bezbradica JS, Van Kaer L and Joyce S (2017) Natural killer T cells: an ecological evolutionary developmental biology perspective. *Front Immunol* **8**, 1858.
- 27 Kain L, Webb B, Anderson BL, Deng S, Holt M, Costanzo A, Zhao M, Self K, Teyton A, Everett C *et al.* (2014) The identification of the endogenous ligands of natural killer T cells reveals the presence of mammalian alpha-linked glycosylceramides. *Immunity* **41**, 543–554.
- 28 Iwabuchi K, Masuda H, Kaga N, Nakayama H, Matsumoto R, Iwahara C, Yoshizaki F, Tamaki Y, Kobayashi T, Hayakawa T *et al.* (2015) Properties and functions of lactosylceramide from mouse neutrophils. *Glycobiology* **25**, 655–668.
- 29 Tsai B, Gilbert JM, Stehle T, Lencer W, Benjamin TL and Rapoport TA (2003) Gangliosides are receptors for murine polyoma virus and SV40. *EMBO J* **22**, 4346–4355.
- 30 Lingwood CA (1996) Role of verotoxin receptors in pathogenesis. *Trends Microbiol* **4**, 147–153.
- 31 Louise CB, Kaye SA, Boyd B, Lingwood CA and Obrig TG (1995) Shiga toxin-associated hemolytic uremic syndrome: effect of sodium butyrate on sensitivity of human umbilical vein endothelial cells to Shiga toxin. *Infect Immun* **63**, 2766–2769.
- 32 Takenouchi H, Kiyokawa N, Taguchi T, Matsui J, Katagiri YU, Okita H, Okuda K and Fujimoto J (2004) Shiga toxin binding to globotriaosyl ceramide induces intracellular signals that mediate cytoskeleton remodeling in human renal carcinoma-derived cells. *J Cell Sci* **117**, 3911–3922.
- 33 Tyrrell GJ, Ramotar K, Toye B, Boyd B, Lingwood CA and Brunton JL (1992) Alteration of the carbohydrate binding specificity of verotoxins from Gal alpha 1-4Gal to GalNAc beta 1-3Gal alpha 1-4Gal and vice versa by site-directed mutagenesis of the binding subunit. *Proc Natl Acad Sci USA* **89**, 524–528.
- 34 Mukai T, Kaneko S, Matsumoto M and Ohori H (2004) Binding of *Bifidobacterium bifidum* and *Lactobacillus reuteri* to the carbohydrate moieties of intestinal glycolipids recognized by peanut agglutinin. *Int J Food Microbiol* **90**, 357–362.
- 35 de Bentzmann S, Roger P, Dupuit F, Bajolet-Laudinat O, Fuchey C, Plotkowski MC and Puchelle E (1996) Asialo GM1 is a receptor for *Pseudomonas aeruginosa* adherence to regenerating respiratory epithelial cells. *Infect Immun* **64**, 1582–1588.
- 36 Naroeni A and Porte F (2002) Role of cholesterol and the ganglioside GM(1) in entry and short-term survival of *Brucella suis* in murine macrophages. *Infect Immun* **70**, 1640–1644.
- 37 Cuatrecasas P (1973) *Vibrio cholerae* cholerae genoid. Mechanism of inhibition of cholera toxin action. *Biochemistry* **12**, 3577–3581.
- 38 Cuatrecasas P (1973) Gangliosides and membrane receptors for cholera toxin. *Biochemistry* **12**, 3558–3566.
- 39 Hyun CS and Kimmich GA (1984) Interaction of cholera toxin and *Escherichia coli* enterotoxin with isolated intestinal epithelial cells. *Am J Physiol* **247**, G623–G631.
- 40 Kuziemko GM, Stroh M and Stevens RC (1996) Cholera toxin binding affinity and specificity for gangliosides determined by surface plasmon resonance. *Biochemistry* **35**, 6375–6384.
- 41 Masserini M, Freire E, Palestini P, Calappi E and Tettamanti G (1992) Fuc-GM1 ganglioside mimics the receptor function of GM1 for cholera toxin. *Biochemistry* **31**, 2422–2426.
- 42 Otnaess AB, Laegreid A and Ertresvag K (1983) Inhibition of enterotoxin from *Escherichia coli* and *Vibrio cholerae* by gangliosides from human milk. *Infect Immun* **40**, 563–569.
- 43 Bronnum H, Seested T, Hellgren LI, Brix S and Frokiaer H (2005) Milk-derived GM(3) and GD(3) differentially inhibit dendritic cell maturation and effector functionalities. *Scand J Immunol* **61**, 551–557.
- 44 Angstrom J, Teneberg S, Milh MA, Larsson T, Leonardsson I, Olsson BM, Halvarsson MO, Danielsson D, Naslund I, Ljungh A *et al.* (1998) The lactosylceramide binding specificity of *Helicobacter pylori*. *Glycobiology* **8**, 297–309.
- 45 Hahn PY, Evans SE, Kottom TJ, Standing JE, Pagano RE and Limper AH (2003) *Pneumocystis carinii* cell wall beta-glucan induces release of macrophage inflammatory protein-2 from alveolar epithelial cells via a lactosylceramide-mediated mechanism. *J Biol Chem* **278**, 2043–2050.

- 46 Karlsson KA (1986) Animal glycolipids as attachment sites for microbes. *Chem Phys Lipid* **42**, 153–172.
- 47 Saukkonen K, Burnette WN, Mar VL, Masure HR and Tuomanen EI (1992) Pertussis toxin has eukaryotic-like carbohydrate recognition domains. *Proc Natl Acad Sci USA* **89**, 118–122.
- 48 Zimmerman JW, Lindermuth J, Fish PA, Palace GP, Stevenson TT and DeMong DE (1998) A novel carbohydrate-glycosphingolipid interaction between a beta-(1-3)-glucan immunomodulator, PGG-glucan, and lactosylceramide of human leukocytes. *J Biol Chem* **273**, 22014–22020.
- 49 Fukuda MN, Dell A, Oates JE, Wu P, Klock JC and Fukuda M (1985) Structures of glycosphingolipids isolated from human granulocytes. The presence of a series of linear poly-*N*-acetylglucosaminylceramide and its significance in glycolipids of whole blood cells. *J Biol Chem* **260**, 1067–1082.
- 50 Teneberg S, Angstrom J and Ljungh A (2004) Carbohydrate recognition by enterohemorrhagic *Escherichia coli*: characterization of a novel glycosphingolipid from cat small intestine. *Glycobiology* **14**, 187–196.
- 51 Stromberg N and Karlsson KA (1990) Characterization of the binding of *propionibacterium granulosum* to glycosphingolipids adsorbed on surfaces. An apparent recognition of lactose which is dependent on the ceramide structure. *J Biol Chem* **265**, 11244–11250.
- 52 Stromberg N, Ryd M, Lindberg AA and Karlsson KA (1988) Studies on the binding of bacteria to glycolipids. Two species of *Propionibacterium* apparently recognize separate epitopes on lactose of lactosylceramide. *FEBS Lett* **232**, 193–198.
- 53 Payne D, Tatham D, Williamson ED and Titball RW (1998) The pH 6 antigen of *Yersinia pestis* binds to beta1-linked galactosyl residues in glycosphingolipids. *Infect Immun* **66**, 4545–4548.
- 54 Jansson L, Tobias J, Lebens M, Svennerholm AM and Teneberg S (2006) The major subunit, CfaB, of colonization factor antigen i from enterotoxigenic *Escherichia coli* is a glycosphingolipid binding protein. *Infect Immun* **74**, 3488–3497.
- 55 Stromberg N, Deal C, Nyberg G, Normark S, So M and Karlsson KA (1988) Identification of carbohydrate structures that are possible receptors for *Neisseria gonorrhoeae*. *Proc Natl Acad Sci USA* **85**, 4902–4906.
- 56 Backenson PB, Coleman JL and Benach JL (1995) *Borrelia burgdorferi* shows specificity of binding to glycosphingolipids. *Infect Immun* **63**, 2811–2817.
- 57 Newburg DS and Chaturvedi P (1992) Neutral glycolipids of human and bovine milk. *Lipids* **27**, 923–927.
- 58 Belotserkovsky I, Brunner K, Pinaud L, Rouvinski A, Dellarole M, Baron B, Dubey G, Samassa F, Parsot C, Sansonetti P *et al.* (2018) Glycan-glycan interaction determines shigella tropism toward human T lymphocytes. *MBio* **9**, e02309–17.
- 59 Rossjohn J, Pellicci DG, Patel O, Gapin L and Godfrey DI (2012) Recognition of CD1d-restricted antigens by natural killer T cells. *Nat Rev Immunol* **12**, 845–857.
- 60 Nagata M, Izumi Y, Ishikawa E, Kiyotake R, Doi R, Iwai S, Omahdi Z, Yamaji T, Miyamoto T, Bamba T *et al.* (2017) Intracellular metabolite beta-glucosylceramide is an endogenous Mincle ligand possessing immunostimulatory activity. *Proc Natl Acad Sci USA* **114**, E3285–E3294.
- 61 Medzhitov R and Janeway C Jr (2000) Innate immune recognition: mechanisms and pathways. *Immunol Rev* **173**, 89–97.
- 62 Blander JM and Medzhitov R (2004) Regulation of phagosome maturation by signals from toll-like receptors. *Science* **304**, 1014–1018.
- 63 Doyle SE, O'Connell RM, Miranda GA, Vaidya SA, Chow EK, Liu PT, Suzuki S, Suzuki N, Modlin RL, Yeh WC *et al.* (2004) Toll-like receptors induce a phagocytic gene program through p38. *J Exp Med* **199**, 81–90.
- 64 Jiang Z, Georgel P, Du X, Shamel L, Sovath S, Mudd S, Huber M, Kalis C, Keck S, Galanos C *et al.* (2005) CD14 is required for MyD88-independent LPS signaling. *Nat Immunol* **6**, 565–570.
- 65 Herre J, Marshall AS, Caron E, Edwards AD, Williams DL, Schweighoffer E, Tybulewicz V, Reis e Sousa C, Gordon S and Brown GD (2004) Dectin-1 uses novel mechanisms for yeast phagocytosis in macrophages. *Blood* **104**, 4038–4045.
- 66 Ezekowitz RA, Sastry K, Bailly P and Warner A (1990) Molecular characterization of the human macrophage mannose receptor: demonstration of multiple carbohydrate recognition-like domains and phagocytosis of yeasts in Cos-1 cells. *J Exp Med* **172**, 1785–1794.
- 67 Elomaa O, Kangas M, Sahlberg C, Tuukkanen J, Sormunen R, Liakka A, Thesleff I, Kraal G and Tryggvason K (1995) Cloning of a novel bacteria-binding receptor structurally related to scavenger receptors and expressed in a subset of macrophages. *Cell* **80**, 603–609.
- 68 Peiser L, Gough PJ, Kodama T and Gordon S (2000) Macrophage class A scavenger receptor-mediated phagocytosis of *Escherichia coli*: role of cell heterogeneity, microbial strain, and culture conditions *in vitro*. *Infect Immun* **68**, 1953–1963.
- 69 Brown EJ (1991) Complement receptors and phagocytosis. *Curr Opin Immunol* **3**, 76–82.
- 70 Iwabuchi K and Nagaoka I (2002) Lactosylceramide-enriched glycosphingolipid signaling domain mediates

- superoxide generation from human neutrophils. *Blood* **100**, 1454–1464.
- 71 Kina K, Masuda H, Nakayama H, Nagatsuka Y, Nabetani T, Hirabayashi Y, Takahashi Y, Shimada K, Daida H, Ogawa H *et al.* (2011) The novel neutrophil differentiation marker phosphatidylglucoside mediates neutrophil apoptosis. *J Immunol* **186**, 5323–5332.
- 72 Carmona EM, Kottom TJ, Hebrink DM, Moua T, Singh RD, Pagano RE and Limper AH (2012) Glycosphingolipids mediate pneumocystis cell wall beta-glucan activation of the IL-23/IL-17 axis in human dendritic cells. *Am J Respir Cell Mol Biol* **47**, 50–59.
- 73 Houde M, Gottschalk M, Gagnon F, Van Calsteren MR and Segura M (2012) *Streptococcus suis* capsular polysaccharide inhibits phagocytosis through destabilization of lipid microdomains and prevents lactosylceramide-dependent recognition. *Infect Immun* **80**, 506–517.
- 74 Jacobson K, Sheets ED and Simson R (1995) Revisiting the fluid mosaic model of membranes. *Science* **268**, 1441–1442.
- 75 Hakomori S, Handa K, Iwabuchi K, Yamamura S and Prinetti A (1998) New insights in glycosphingolipid function: “glycosignaling domain”, a cell surface assembly of glycosphingolipids with signal transducer molecules, involved in cell adhesion coupled with signaling. *Glycobiology* **8**, xi–xix.
- 76 Hakomori S (2003) Structure, organization, and function of glycosphingolipids in membrane. *Curr Opin Hematol* **10**, 16–24.
- 77 Alvarez R, Lopez DJ, Casas J, Llado V, Higuera M, Nagy T, Barcelo M, Busquets X and Escriba PV (2015) G protein-membrane interactions I: Galphai1 myristoyl and palmitoyl modifications in protein-lipid interactions and its implications in membrane microdomain localization. *Biochem Biophys Acta* **1851**, 1511–1520.
- 78 Ferrera D, Panigada M, Porcellini S and Grassi F (2008) Recombinase-deficient T cell development by selective accumulation of CD3 into lipid rafts. *Eur J Immunol* **38**, 1148–1156.
- 79 Oddi S, Dainese E, Sandiford S, Fezza F, Lanuti M, Chiurciu V, Totaro A, Catanzaro G, Barcaroli D, De Laurenzi V *et al.* (2012) Effects of palmitoylation of Cys(415) in helix 8 of the CB(1) cannabinoid receptor on membrane localization and signalling. *Br J Pharmacol* **165**, 2635–2651.
- 80 Sonnino S, Prinetti A, Mauri L, Chigorno V and Tettamanti G (2006) Dynamic and structural properties of sphingolipids as driving forces for the formation of membrane domains. *Chem Rev* **106**, 2111–2125.
- 81 Chiricozzi E, Ciampa MG, Brasile G, Compostella F, Prinetti A, Nakayama H, Ekyalongo RC, Iwabuchi K, Sonnino S and Mauri L (2015) Direct interaction, instrumental for signaling processes, between LacCer and Lyn in the lipid rafts of neutrophil-like cells. *J Lipid Res* **56**, 129–141.
- 82 Iwabuchi K, Prinetti A, Sonnino S, Mauri L, Kobayashi T, Ishii K, Kaga N, Murayama K, Kurihara H, Nakayama H *et al.* (2008) Involvement of very long fatty acid-containing lactosylceramide in lactosylceramide-mediated superoxide generation and migration in neutrophils. *Glycoconj J* **25**, 357–374.
- 83 Arnaout MA (1990) Structure and function of the leukocyte adhesion molecules CD11/CD18. *Blood* **75**, 1037–1050.
- 84 Rabb H, Michishita M, Sharma CP, Brown D and Arnaout MA (1993) Cytoplasmic tails of human complement receptor type 3 (CR3, CD11b/CD18) regulate ligand avidity and the internalization of occupied receptors. *J Immunol* **151**, 990–1002.
- 85 Dedhar S and Hannigan GE (1996) Integrin cytoplasmic interactions and bidirectional transmembrane signalling. *Curr Opin Cell Biol* **8**, 657–669.
- 86 Evangelista V, Pamuklar Z, Piccoli A, Manarini S, Dell’elba G, Pecce R, Martelli N, Federico L, Rojas M, Berton G *et al.* (2007) Src family kinases mediate neutrophil adhesion to adherent platelets. *Blood* **109**, 2461–2469.
- 87 Piccardoni P, Manarini S, Federico L, Bagoly Z, Pecce R, Martelli N, Piccoli A, Totani L, Cerletti C and Evangelista V (2004) SRC-dependent outside-in signalling is a key step in the process of autoregulation of beta2 integrins in polymorphonuclear cells. *Biochem J* **380**, 57–65.
- 88 Vetvicka V, Thornton BP and Ross GD (1996) Soluble beta-glucan polysaccharide binding to the lectin site of neutrophil or natural killer cell complement receptor type 3 (CD11b/CD18) generates a primed state of the receptor capable of mediating cytotoxicity of iC3b-opsonized target cells. *J Clin Invest* **98**, 50–61.
- 89 Wright SD, Levin SM, Jong MT, Chad Z and Kabbash LG (1989) CR3 (CD11b/CD18) expresses one binding site for Arg-Gly-Asp-containing peptides and a second site for bacterial lipopolysaccharide. *J Exp Med* **169**, 175–183.
- 90 Liang J, Melican D, Cafro L, Palace G, Fiset L, Armstrong R and Patchen ML (1998) Enhanced clearance of a multiple antibiotic resistant *Staphylococcus aureus* in rats treated with PGG-glucan is associated with increased leukocyte counts and increased neutrophil oxidative burst activity. *Int J Immunopharmacol* **20**, 595–614.
- 91 Ohno N, Uchiyama M, Tsuzuki A, Tokunaka K, Miura NN, Adachi Y, Aizawa MW, Tamura H, Tanaka S and Yadomae T (1999) Solubilization of

- yeast cell-wall beta-(1→3)-D-glucan by sodium hypochlorite oxidation and dimethyl sulfoxide extraction. *Carbohydr Res* **316**, 161–172.
- 92 Brown GD and Gordon S (2001) Immune recognition. A new receptor for beta-glucans. *Nature* **413**, 36–37.
- 93 Briken V, Porcelli SA, Besra GS and Kremer L (2004) Mycobacterial lipoarabinomannan and related lipoglycans: from biogenesis to modulation of the immune response. *Mol Microbiol* **53**, 391–403.
- 94 Kaur D, Obregon-Henao A, Pham H, Chatterjee D, Brennan PJ and Jackson M (2008) Lipoarabinomannan of *Mycobacterium*: mannose capping by a multifunctional terminal mannosyltransferase. *Proc Natl Acad Sci USA* **105**, 17973–17977.
- 95 Mishra AK, Driessen NN, Appelmelk BJ and Besra GS (2011) Lipoarabinomannan and related glycoconjugates: structure, biogenesis and role in *Mycobacterium tuberculosis* physiology and host-pathogen interaction. *FEMS Microbiol Rev* **35**, 1126–1157.
- 96 Manes S, del Real G and Martinez AC (2003) Pathogens: raft hijackers. *Nat Rev Immunol* **3**, 557–568.
- 97 Peyron P, Bordier C, N'Diaye EN and Maridonneau-Parini I (2000) Nonopsonic phagocytosis of *Mycobacterium kansasii* by human neutrophils depends on cholesterol and is mediated by CR3 associated with glycosylphosphatidylinositol-anchored proteins. *J Immunol* **165**, 5186–5191.
- 98 Gatfield J and Pieters J (2000) Essential role for cholesterol in entry of mycobacteria into macrophages. *Science* **288**, 1647–1650.
- 99 Stuart ES, Webley WC and Norkin LC (2003) Lipid rafts, caveolae, caveolin-1, and entry by *Chlamydiae* into host cells. *Exp Cell Res* **287**, 67–78.
- 100 Baorto DM, Gao Z, Malaviya R, Dustin ML, van der Merwe A, Lublin DM and Abraham SN (1997) Survival of FimH-expressing enterobacteria in macrophages relies on glycolipid traffic. *Nature* **389**, 636–639.
- 101 Watarai M, Makino S, Fujii Y, Okamoto K and Shirahata T (2002) Modulation of *Brucella*-induced macropinocytosis by lipid rafts mediates intracellular replication. *Cell Microbiol* **4**, 341–355.
- 102 Tamilselvam B and Daefler S (2008) *Francisella* targets cholesterol-rich host cell membrane domains for entry into macrophages. *J Immunol* **180**, 8262–8271.
- 103 Harrison RE, Brumell JH, Khandani A, Bucci C, Scott CC, Jiang X, Finlay BB and Grinstein S (2004) *Salmonella* impairs RILP recruitment to Rab7 during maturation of invasion vacuoles. *Mol Biol Cell* **15**, 3146–3154.
- 104 Gekara NO and Weiss S (2004) Lipid rafts clustering and signalling by listeriolysin O. *Biochem Soc Trans* **32**, 712–714.
- 105 Brumell JH, Kujat-Choy S, Brown NF, Vallance BA, Knodler LA and Finlay BB (2003) SopD2 is a novel type III secreted effector of *Salmonella typhimurium* that targets late endocytic compartments upon delivery into host cells. *Traffic* **4**, 36–48.
- 106 Vieira OV, Botelho RJ and Grinstein S (2002) Phagosome maturation: aging gracefully. *Biochem J* **366**, 689–704.
- 107 Armstrong JA and Hart PD (1975) Phagosome-lysosome interactions in cultured macrophages infected with virulent tubercle bacilli. Reversal of the usual nonfusion pattern and observations on bacterial survival. *J Exp Med* **142**, 1–16.
- 108 Dell'Angelica EC, Mullins C, Caplan S and Bonifacino JS (2000) Lysosome-related organelles. *FASEB J* **14**, 1265–1278.
- 109 Kniep B and Skubitz KM (1998) Subcellular localization of glycosphingolipids in human neutrophils. *J Leukoc Biol* **63**, 83–88.
- 110 Mohn H, Le Cabec V, Fischer S and Maridonneau-Parini I (1995) The src-family protein-tyrosine kinase p59hck is located on the secretory granules in human neutrophils and translocates towards the phagosome during cell activation. *Biochem J* **309** (Pt 2), 657–665.
- 111 Peyron P, Maridonneau-Parini I and Stegmann T (2001) Fusion of human neutrophil phagosomes with lysosomes *in vitro*: involvement of tyrosine kinases of the Src family and inhibition by mycobacteria. *J Biol Chem* **276**, 35512–35517.
- 112 Rothenberg EV and Taghon T (2005) Molecular genetics of T cell development. *Annu Rev Immunol* **23**, 601–649.
- 113 Yamasaki S and Saito T (2007) Molecular basis for pre-TCR-mediated autonomous signaling. *Trends Immunol* **28**, 39–43.
- 114 Saint-Ruf C, Panigada M, Azogui O, Debey P, von Boehmer H and Grassi F (2000) Different initiation of pre-TCR and $\gamma\delta$ TCR signalling. *Nature* **406**, 524–527.
- 115 Aifantis I, Borowski C, Gounari F, Lacorazza HD, Nikolich-Zugich J and von Boehmer H (2002) A critical role for the cytoplasmic tail of pTalpha in T lymphocyte development. *Nat Immunol* **3**, 483–488.
- 116 Haks MC, Belkowski SM, Ciofani M, Rhodes M, Lefebvre JM, Trop S, Hugo P, Zuniga-Pflucker JC and Wiest DL (2003) Low activation threshold as a mechanism for ligand-independent signaling in pre-T cells. *J Immunol* **170**, 2853–2861.
- 117 Holdorf AD, Lee KH, Burack WR, Allen PM and Shaw AS (2002) Regulation of Lck activity by CD4 and CD28 in the immunological synapse. *Nat Immunol* **3**, 259–264.
- 118 Hare KJ, Pongracz J, Jenkinson EJ and Anderson G (2003) Modeling TCR signaling complex formation in positive selection. *J Immunol* **171**, 2825–2831.

- 119 Popovic ZV, Rabionet M, Jennemann R, Kronic D, Sandhoff R, Grone HJ and Porubsky S (2017) Glucosylceramide synthase is involved in development of invariant natural killer T cells. *Front Immunol* **8**, 848.
- 120 Zech T, Ejsing CS, Gaus K, de Wet B, Shevchenko A, Simons K and Harder T (2009) Accumulation of raft lipids in T-cell plasma membrane domains engaged in TCR signalling. *EMBO J* **28**, 466–476.
- 121 Simons K and Toomre D (2000) Lipid rafts and signal transduction. *Nat Rev Mol Cell Biol* **1**, 31–39.
- 122 Pizzo P, Giurisato E, Tassi M, Benedetti A, Pozzan T and Viola A (2002) Lipid rafts and T cell receptor signaling: a critical re-evaluation. *Eur J Immunol* **32**, 3082–3091.
- 123 Greenwald RJ, Freeman GJ and Sharpe AH (2005) The B7 family revisited. *Annu Rev Immunol* **23**, 515–548.
- 124 Kroczeck RA, Mages HW and Hutloff A (2004) Emerging paradigms of T-cell co-stimulation. *Curr Opin Immunol* **16**, 321–327.
- 125 Leitenberg D, Balamuth F and Bottomly K (2001) Changes in the T cell receptor macromolecular signaling complex and membrane microdomains during T cell development and activation. *Semin Immunol* **13**, 129–138.
- 126 Holgate ST (2011) Pathophysiology of asthma: what has our current understanding taught us about new therapeutic approaches? *J Allergy Clin Immunol* **128**, 495–505.
- 127 Orihara K, Dil N, Anaparti V and Moqbel R (2010) What's new in asthma pathophysiology and immunopathology? *Expert Rev Respir Med* **4**, 605–629.
- 128 Hamid Q and Tulic M (2009) Immunobiology of asthma. *Annu Rev Physiol* **71**, 489–507.
- 129 Levine SJ and Wenzel SE (2010) Narrative review: the role of Th2 immune pathway modulation in the treatment of severe asthma and its phenotypes. *Ann Intern Med* **152**, 232–237.
- 130 Dong L, Hu S, Chen F, Lei X, Tu W, Yu Y, Yang L, Sun W, Yamaguchi T, Masaki Y *et al.* (2010) Increased expression of ganglioside GM1 in peripheral CD4 + T cells correlates soluble form of CD30 in Systemic Lupus Erythematosus patients. *J Biomed Biotechnol* **2010**, 569053.
- 131 Kabouridis PS and Jury EC (2008) Lipid rafts and T-lymphocyte function: implications for autoimmunity. *FEBS Lett* **582**, 3711–3718.
- 132 Karman J, Tedstone JL, Gumlaw NK, Zhu Y, Yew N, Siegel C, Guo S, Siwkowski A, Ruzek M, Jiang C *et al.* (2010) Reducing glycosphingolipid biosynthesis in airway cells partially ameliorates disease manifestations in a mouse model of asthma. *Int Immunol* **22**, 593–603.
- 133 Shalaby KH and Martin JG (2010) Overview of asthma; the place of the T cell. *Curr Opin Pharmacol* **10**, 218–225.
- 134 Lloyd CM and Hessel EM (2010) Functions of T cells in asthma: more than just T(H)2 cells. *Nat Rev Immunol* **10**, 838–848.
- 135 Zhu Y, Gumlaw N, Karman J, Zhao H, Zhang J, Jiang JL, Maniatis P, Edling A, Chuang WL, Siegel C *et al.* (2011) Lowering glycosphingolipid levels in CD4 + T cells attenuates T cell receptor signaling, cytokine production, and differentiation to the Th17 lineage. *J Biol Chem* **286**, 14787–14794.
- 136 Rahman A and Isenberg DA (2008) Systemic lupus erythematosus. *N Engl J Med* **358**, 929–939.
- 137 Tsokos GC (2011) Systemic lupus erythematosus. *N Engl J Med* **365**, 2110–2121.
- 138 Jury EC, Kabouridis PS, Flores-Borja F, Mageed RA and Isenberg DA (2004) Altered lipid raft-associated signaling and ganglioside expression in T lymphocytes from patients with systemic lupus erythematosus. *J Clin Invest* **113**, 1176–1187.
- 139 Krishnan S, Nambiar MP, Warke VG, Fisher CU, Mitchell J, Delaney N and Tsokos GC (2004) Alterations in lipid raft composition and dynamics contribute to abnormal T cell responses in systemic lupus erythematosus. *J Immunol* **172**, 7821–7831.
- 140 McDonald G, Deepak S, Miguel L, Hall CJ, Isenberg DA, Magee AI, Butters T and Jury EC (2014) Normalizing glycosphingolipids restores function in CD4 + T cells from lupus patients. *J Clin Invest* **124**, 712–724.
- 141 Tani-ichi S, Maruyama K, Kondo N, Nagafuku M, Kabayama K, Inokuchi J, Shimada Y, Ohno-Iwashita Y, Yagita H, Kawano S *et al.* (2005) Structure and function of lipid rafts in human activated T cells. *Int Immunol* **17**, 749–758.
- 142 Tuosto L, Parolini I, Schroder S, Sargiacomo M, Lanzavecchia A and Viola A (2001) Organization of plasma membrane functional rafts upon T cell activation. *Eur J Immunol* **31**, 345–349.
- 143 Degroote S, Wolthoorn J and van Meer G (2004) The cell biology of glycosphingolipids. *Semin Cell Dev Biol* **15**, 375–387.
- 144 Kidani Y and Bensinger SJ (2014) Lipids rule: resetting lipid metabolism restores T cell function in systemic lupus erythematosus. *J Clin Invest* **124**, 482–485.
- 145 McInnes IB and Schett G (2011) The pathogenesis of rheumatoid arthritis. *N Engl J Med* **365**, 2205–2219.
- 146 Gizinski AM and Fox DA (2014) T cell subsets and their role in the pathogenesis of rheumatic disease. *Curr Opin Rheumatol* **26**, 204–210.
- 147 Kobezda T, Ghassemi-Nejad S, Mikecz K, Glant TT and Szekanecz Z (2014) Of mice and men: how animal models advance our understanding of T-cell function in RA. *Nat Rev Rheumatol* **10**, 160–170.
- 148 Tsukuda Y, Iwasaki N, Seito N, Kanayama M, Fujitani N, Shinohara Y, Kasahara Y, Onodera T,

- Suzuki K, Asano T *et al.* (2012) Ganglioside GM3 has an essential role in the pathogenesis and progression of rheumatoid arthritis. *PLoS ONE* **7**, e40136.
- 149 Nakamura K, Suzuki H, Hirabayashi Y and Suzuki A (1995) IV3 alpha (NeuGc alpha 2-8NeuGc)-Gg4Cer is restricted to CD4 + T cells producing interleukin-2 and a small population of mature thymocytes in mice. *J Biol Chem* **270**, 3876–3881.
- 150 Kimata H (1994) GM1, a ganglioside that specifically enhances immunoglobulin production and proliferation in human plasma cells. *Eur J Immunol* **24**, 2910–2913.
- 151 Klasener K, Maity PC, Hobeika E, Yang J and Reth M (2014) B cell activation involves nanoscale receptor reorganizations and inside-out signaling by Syk. *Elife* **3**, e02069.
- 152 Shrestha D, Exley MA, Vereb G, Szollosi J and Jenei A (2014) CD1d favors MHC neighborhood, GM1 ganglioside proximity and low detergent sensitive membrane regions on the surface of B lymphocytes. *Biochem Biophys Acta* **1840**, 667–680.
- 153 Minguet S, Klasener K, Schaffer AM, Fiala GJ, Osteso-Ibanez T, Raute K, Navarro-Lerida I, Hartl FA, Seidl M, Reth M *et al.* (2017) Caveolin-1-dependent nanoscale organization of the BCR regulates B cell tolerance. *Nat Immunol* **18**, 1150–1159.
- 154 Nikolettou V, Markaki M, Palikaras K and Tavernarakis N (2013) Crosstalk between apoptosis, necrosis and autophagy. *Biochem Biophys Acta* **1833**, 3448–3459.
- 155 Kiguchi K, Henning-Chubb CB and Huberman E (1990) Glycosphingolipid patterns of peripheral blood lymphocytes, monocytes, and granulocytes are cell specific. *J Biochem* **107**, 8–14.
- 156 Malorni W, Giammarioli AM, Garofalo T and Sorice M (2007) Dynamics of lipid raft components during lymphocyte apoptosis: the paradigmatic role of GD3. *Apoptosis* **12**, 941–949.
- 157 Garofalo T, Misasi R, Mattei V, Giammarioli AM, Malorni W, Pontieri GM, Pavan A and Sorice M (2003) Association of the death-inducing signaling complex with microdomains after triggering through CD95/Fas. Evidence for caspase-8-ganglioside interaction in T cells. *J Biol Chem* **278**, 8309–8315.
- 158 Scorrano L, Petronilli V, Di Lisa F and Bernardi P (1999) Commitment to apoptosis by GD3 ganglioside depends on opening of the mitochondrial permeability transition pore. *J Biol Chem* **274**, 22581–22585.
- 159 Garcia-Ruiz C, Colell A, Morales A, Calvo M, Enrich C and Fernandez-Checa JC (2002) Trafficking of ganglioside GD3 to mitochondria by tumor necrosis factor-alpha. *J Biol Chem* **277**, 36443–36448.
- 160 Garofalo T, Giammarioli AM, Misasi R, Tinari A, Manganelli V, Gambardella L, Pavan A, Malorni W and Sorice M (2005) Lipid microdomains contribute to apoptosis-associated modifications of mitochondria in T cells. *Cell Death Differ* **12**, 1378–1389.
- 161 Delgado ME, Dyck L, Laussmann MA and Rehm M (2014) Modulation of apoptosis sensitivity through the interplay with autophagic and proteasomal degradation pathways. *Cell Death Dis* **5**, e1011.
- 162 Booth LA, Tavallai S, Hamed HA, Cruickshanks N and Dent P (2014) The role of cell signalling in the crosstalk between autophagy and apoptosis. *Cell Signal* **26**, 549–555.
- 163 Matarrese P, Garofalo T, Manganelli V, Gambardella L, Marconi M, Grasso M, Tinari A, Misasi R, Malorni W and Sorice M (2014) Evidence for the involvement of GD3 ganglioside in autophagosome formation and maturation. *Autophagy* **10**, 750–765.
- 164 Hamasaki M, Furuta N, Matsuda A, Nezu A, Yamamoto A, Fujita N, Oomori H, Noda T, Haraguchi T, Hiraoka Y *et al.* (2013) Autophagosomes form at ER-mitochondria contact sites. *Nature* **495**, 389–393.
- 165 Garofalo T, Matarrese P, Manganelli V, Marconi M, Tinari A, Gambardella L, Faggioni A, Misasi R, Sorice M and Malorni W (2016) Evidence for the involvement of lipid rafts localized at the ER-mitochondria associated membranes in autophagosome formation. *Autophagy* **12**, 917–935.
- 166 Xu Y and Eissa NT (2010) Autophagy in innate and adaptive immunity. *Proc Am Thorac Soc* **7**, 22–28.
- 167 Shima S, Kawamura N, Ishikawa T, Masuda H, Iwahara C, Niimi Y, Ueda A, Iwabuchi K and Mutoh T (2014) Anti-neutral glycolipid antibodies in encephalomyeloneuropathy. *Neurology* **82**, 114–118.
- 168 Fujita A, Cheng J and Fujimoto T (2009) Segregation of GM1 and GM3 clusters in the cell membrane depends on the intact actin cytoskeleton. *Biochim Biophys Acta* **1791**, 388–396.
- 169 Liang S, Wang M, Tapping RI, Stepensky V, Nawar HF, Triantafilou M, Triantafilou K, Connell TD and Hajishengallis G (2007) Ganglioside GD1a is an essential coreceptor for Toll-like receptor 2 signaling in response to the B subunit of type IIb enterotoxin. *J Biol Chem* **282**, 7532–7542.
- 170 McNamara N, Gallup M, Sucher A, Maltseva I, McKemy D and Basbaum C (2006) AsialoGM1 and TLR5 cooperate in flagellin-induced nucleotide signaling to activate Erk1/2. *Am J Respir Cell Mol Biol* **34**, 653–660.
- 171 Oda M, Kabura M, Takagishi T, Suzue A, Tominaga K, Urano S, Nagahama M, Kobayashi K, Furukawa K, Furukawa K *et al.* (2012) Clostridium perfringens alpha-toxin recognizes the GM1a-TrkA complex. *J Biol Chem* **287**, 33070–33079.

Immunology

Globo-series glycosphingolipids enhance Toll-like receptor 4-mediated inflammation and play a pathophysiological role in diabetic nephropathy

Takahiro Nitta^{2,3}, Hirotaka Kanoh², Kei-ichiro Inamori², Akemi Suzuki², Tomoko Takahashi³, and Jin-ichi Inokuchi^{2,1}

²Division of Glycopathology, Institute of Molecular Biomembrane and Glycobiology and ³Division of Pathophysiology, Department of Pharmaceutical Sciences, Faculty of Pharmaceutical Sciences, Tohoku Medical and Pharmaceutical University, Sendai 981-8558, Japan

¹To whom correspondence should be addressed: Tel: +81-22-727-0117; Fax: +81-22-727-0076; e-mail: jin@tohoku-mpu.ac.jp

Received 4 October 2018; Revised 14 November 2018; Editorial decision 20 November 2018; Accepted 21 November 2018

Abstract

Alteration of glycosphingolipid (GSL) expression plays key roles in the pathogenesis and pathophysiology of many important human diseases, including cancer, diabetes and glycosphingolipidosis. Inflammatory processes are involved in development and progression of diabetic nephropathy, a major complication of type 2 diabetes mellitus. GSLs are known to play roles in inflammatory responses in various diseases, and levels of renal GSLs are elevated in mouse models of diabetic nephropathy; however, little is known regarding the pathophysiological role of these GSLs in this disease process. We studied proinflammatory activity of GSLs in diabetic nephropathy using spontaneously diabetic mouse strain KK. Mice were fed a high-fat diet (HFD) (60% kcal from fat) or normal diet (ND) (4.6% kcal from fat) for a period of 8 wk. HFD-feeding resulted in quantitative and qualitative changes of renal globo-series GSLs (particularly Gb3Cer), upregulation of TNF- α , and induction of renal inflammation. Gb3Cer/Gb4Cer treatment enhanced inflammatory responses via TLR4 in TLR4/MD-2 complex expressing cells, including HEK293T, mouse bone marrow-derived macrophages (BMDMs) and human monocytes. Our findings suggest that HFD-induced increase of Gb3Cer/Gb4Cer positively modulate TLR4-mediated inflammatory response, and that such GSLs play an important pathophysiological role in diabetic nephropathy.

Key words: diabetic nephropathy, Globo-series GSLs, renal inflammation, TLR4 ligands, Toll-like receptor 4

Introduction

Diabetic nephropathy, a major complication of type 2 diabetes mellitus (T2DM), is defined histologically by renal changes such as diffuse mesangial cell proliferation, mesangial matrix expansion, diffuse or nodular glomerulosclerosis, podocyte loss, glomerular basement membrane thickening, tubulointerstitial fibrosis and

atrophy, hyaline arteriosclerosis, and arterial sclerosis, and is associated with (micro)albuminuria and reduced glomerular filtration rate (Alsaad and Herzenberg 2007; Fioretto and Mauer 2007). Morphological changes as above involve genetic factors, and are based on biochemical and hemodynamic changes (Vardarli et al. 2002; Lee et al. 2005; Freedman et al. 2007; Kanwar et al. 2011).

Biochemical changes arise from immune cell-mediated inflammation, a key causative factor in pathogenesis of diabetic nephropathy. Inflammatory cytokines (e.g., TNF- α , IL-6, IL-1 β) are secreted from infiltrated and activated macrophages, and are enhanced by oxidative stress through increased levels of reactive oxygen species (ROS) (Pai et al. 1996; Das and Elbein 2006; Yoshida and Tsunawaki 2008; Elmarakby and Sullivan 2012; Badal and Danesh 2014).

Glycosphingolipids (GSLs) consist of hydrophilic oligosaccharides and hydrophobic ceramide (Figure 1A). Ceramide species are composed of sphingosine linked to a particular fatty acyl chain by amide bond (Figure 1B). Ceramide acyl chains vary in chain length, degree of saturation and presence/absence of α -hydroxylation (Figure 1B). GSLs containing a variety of ceramide structures are crucial components of plasma membranes. GSLs play key roles in fundamental biological processes such as development, cell adhesion, and signaling (Hakomori and Igarashi 1995; Hakomori et al. 1998; Tagami et al. 2002; Yu et al. 2009). Numerous previous reports have demonstrated pathophysiological involvement of GSLs in kidney diseases, including lupus nephritis, polycystic kidney disease, Fabry disease, renal cancer, hemolytic uremic syndrome and diabetic nephropathy (Obrig et al. 1993; Zador et al. 1993; Deshmukh et al. 1994; Biswas et al. 2006; Biancini et al. 2012; Grove et al. 2014; Nowling et al. 2015; Subathra et al. 2015). A 2015 study showed involvement of glucosylceramide (GlcCer) and lactosylceramide (LacCer) in fibrosis, extracellular matrix production, and hypertrophy of kidney cells (Subathra et al. 2015). Aside from this, little is known regarding roles of GSLs in pathophysiology of diabetic nephropathy. GSLs evidently play important roles in inflammatory responses contributing to various diseases (Kim et al. 2002; Ohmi et al. 2011; De Francesco et al. 2013), but no study to date has focused on such role of GSLs in diabetic nephropathy.

To test the hypothesis that GSLs play a pathophysiological role in inflammatory responses contributing to diabetic nephropathy, we used a mouse model of T2DM with high-fat diet (HFD). T2DM and diabetic nephropathy in humans are complex diseases that involve polygenic factors and environmental factors, such as obesity and sedentary lifestyle (Vardarli et al. 2002; Lee et al. 2005; Freedman et al. 2007; Kanwar et al. 2011; Wu et al. 2014). We analyzed associations between renal GSLs and renal inflammation using KK mice. This strain is a useful model for studies of T2DM and diabetic nephropathy because it displays correlations between polygenic factors and susceptibility to these disease processes (Shike et al. 2001; Fan et al. 2003). We fed KK mice with HFD to more closely simulate pathological conditions associated with human T2DM and

diabetic nephropathy, and observed for the first time increased levels of renal globo-series GSLs under such condition. Globo-series GSLs enhanced TLR4-mediated inflammation in both mouse bone marrow-derived macrophages (BMDMs) and human monocytes. Our findings indicate that globo-series GSLs act as a positive modulator on TLR4-mediated inflammatory response, and play a role in pathophysiology of diabetic nephropathy.

Results

HFD feeding induces obesity, hyperglycemia and renal inflammation in KK mice

Inbred mouse strain KK was established in 1957 from an inbred strain of native Japanese mice that spontaneously developed diabetes of polygenic origin. Many diabetic characteristics (glucose intolerance, insulin resistance, hyperinsulinemia, moderate hyperglycemia, hyperlipidemia, hypercholesterolemia, hyperleptinemia, histological changes of renal glomerulus) are associated with obesity in KK mice (Makino et al. 1985; Igel et al. 1998; Suto et al. 1998; Okazaki et al. 2002), and these mice are often used in studies of diabetes and diabetic complications. To elucidate the pathophysiological role of GSLs in diet-induced diabetic nephropathy, we introduced HFD at age 8 wk in one group of KK mice, while another group was maintained on normal diet (ND) as a control. Initial body weight (at age 8 wk) and final weight (at age 16 wk) for the two groups are shown in Figure 2A. Comparative values of three parameters at 16 wk in the two groups (hereafter referred to simply as "HFD" and "ND" for convenience) were: final body weight (ND, 35.4 \pm 2.5 g; HFD, 45.9 \pm 2.4 g; $P < 0.001$) (Figure 2A), weight gain (ND, 127 \pm 8.5%; HFD, 163 \pm 8.5%; $P < 0.001$) (Figure 2B), non-fasting blood glucose (ND, 214 \pm 51 mg/dL; HFD, 328 \pm 126 mg/dL; $P < 0.01$) (Figure 2C). Each of these parameters was significantly increased in HFD relative to ND. Blood glucose level in HFD was indicative of hyperglycemia. Renal inflammation was assessed by measuring TNF- α gene expression level by quantitative PCR. TNF- α level was significantly higher in HFD than in ND (Figure 2D). These findings indicate that HFD feeding induced nephritis in KK mice.

Increased levels of renal GSLs in HFD-fed KK mice

GSL levels are elevated in kidneys of mice with various renal diseases (diabetic nephropathy, lupus nephritis, polycystic kidney disease) (Deshmukh et al. 1994; Nowling et al. 2015; Subathra et al. 2015). We examined quantitative and qualitative changes of GSLs in kidneys of ND and HFD. HPTLC analysis revealed that levels of

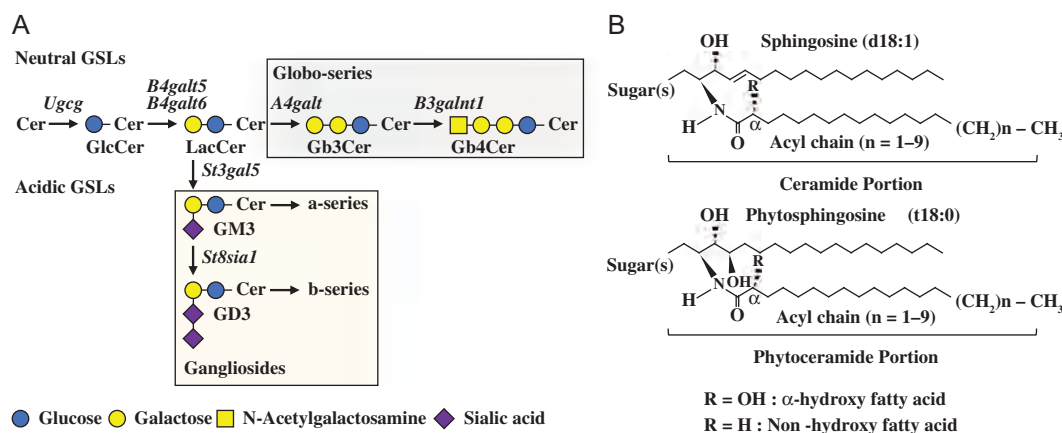


Fig. 1. Biosynthetic pathways and structural diversity of glycosphingolipids. (A) GSL biosynthetic pathways. (B) Structures of GSL molecular species.

neutral GSLs were significantly higher in HFD, whereas acidic GSL levels did not differ notably between the two groups (Figure 3A, B). Increase in HFD was particularly notable for globo-series GSLs (Gb3Cer and Gb4Cer) (Figure 3A). We further analyzed Gb3Cer level, which showed the greatest increase. Densitometric analysis of HPTLC data showed a 4.7-fold increase of Gb3Cer level in HFD (Figure 3C). Gb3Cer is synthesized from LacCer by A4GALT, and is then converted to Gb4Cer by B3GALNT1 (Figure 1A). In a search for possible causes of Gb3Cer metabolism abnormalities in HFD, we assessed renal expression levels of *A4galt* (Gb3Cer synthase gene) in HFD vs. ND. *A4galt* expression level was significantly higher in HFD (Figure 3D). The higher contents of Gb3Cer/Gb4Cer in HFD can therefore be explained, at least in part, by increased Gb3Cer synthase expression level. LC-ESI-MS/MS analysis detected 26 molecular species of Gb3Cer and 18 molecular species of Gb4Cer carrying ceramide (Figure 4A, B) or phytoceramide (phyto-Gb3Cer, phyto-Gb4Cer) (Figure S1). These species were increased significantly in HFD compared to ND. In particular, there were elevated levels of three species, d18:1-16:0, d18:1-22:0 and d18:1-

24:0, in Gb3Cer/Gb4Cer species (Figure 4A, B). Total Gb3Cer level (calculated as sum of values from the 26 molecular species) was 6.2-fold higher for HFD than for ND (Figure 4C), consistently with results from HPTLC/densitometry (Figure 3C). Total Gb4Cer level (calculated as sum of values from the 18 molecular species) was 2.8-fold higher for HFD than for ND (Figure 4D).

For our analyses, we define fatty acids (FAs) with chain length ≤ 20 carbons as long chain fatty acids (LCFAs) and those with chain length > 20 carbons as very long chain fatty acids (VLCFAs) according to previous report (Kihara 2012). In KK mouse kidney, the three most abundant species, d18:1-16:0, d18:1-22:0 and d18:1-24:0, accounted for more than half of the total in Gb3Cer (Figure S1E) or Gb4Cer (Figure S1F) species. Among these species, the proportion of d18:1-22:0 species, VLCFA, was increased markedly in HFD (Figure S1E, F). The elevated levels of renal Gb3Cer/Gb4Cer carrying VLCFAs (saturated FAs: 22:0, 23:0, 24:0; monounsaturated FAs: 24:1; α -hydroxy FAs: h22:0, h23:0, h24:0; monounsaturated and α -hydroxy FAs: h24:1) were higher than the elevated levels of Gb3Cer/Gb4Cer carrying LCFAs (saturated FAs: 16:0, 18:0, 20:0;

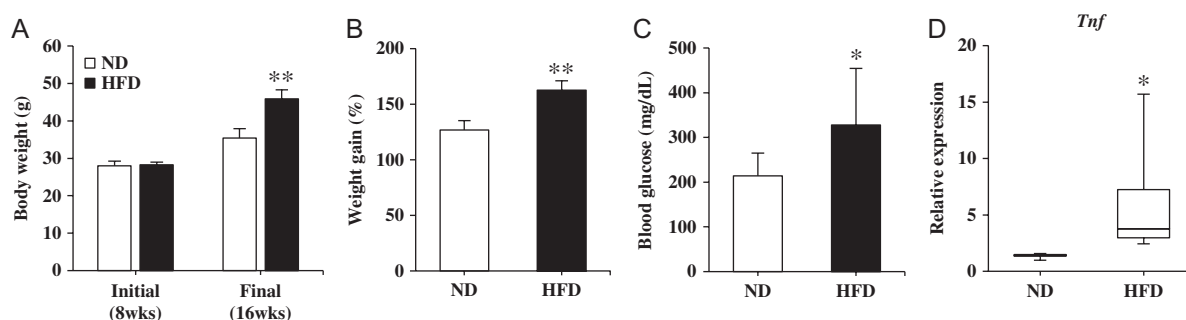


Fig. 2. Obesity, hyperglycemia, and renal inflammation in HFD-fed KK mice (hereafter referred to as “HFD”). (A) initial (age 8 wk) and final (age 16 wk) body weight ($n = 8$ for each group). (B) Weight gain ($n = 8$ for each group). (C) Non-fasting blood glucose of ND and HFD fed for 8 wk ($n = 13$ for each group). Data shown are mean \pm SD. * $P < 0.01$, ** $P < 0.001$ for comparison with ND (by Student’s t -test in A, B; Welch’s t -test in C). (D) mRNA expression level of TNF- α shown as box plot ($n = 4$ for each group). * $P < 0.05$ vs. ND, by Mann-Whitney unpaired test.

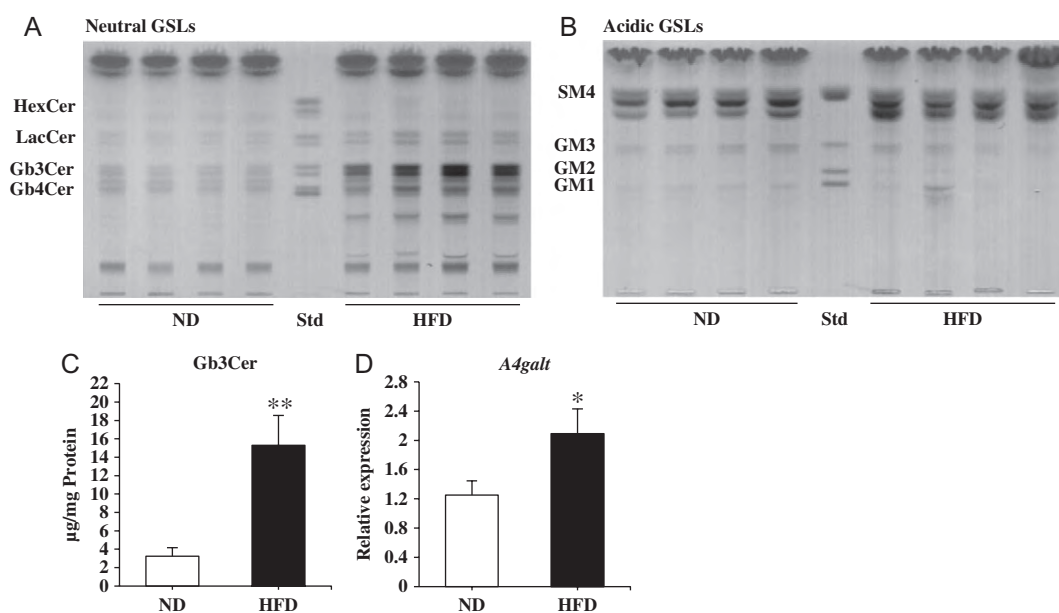


Fig. 3. Strong increase in renal globo-series GSL levels in HFD. (A, B) Neutral (A) and acidic (B) GSLs extracted from ND and HFD kidneys were spotted on HPTLC plates and developed as described in Materials and methods. (C) Comparison of kidney Gb3Cer levels under ND and HFD. (D) Quantitative RT-PCR analysis of Gb3Cer synthase gene *A4galt* in kidney. $n = 4$ for each group. * $P < 0.01$, ** $P < 0.001$ vs. ND, by Student’s t -test. Data shown are mean \pm SD.

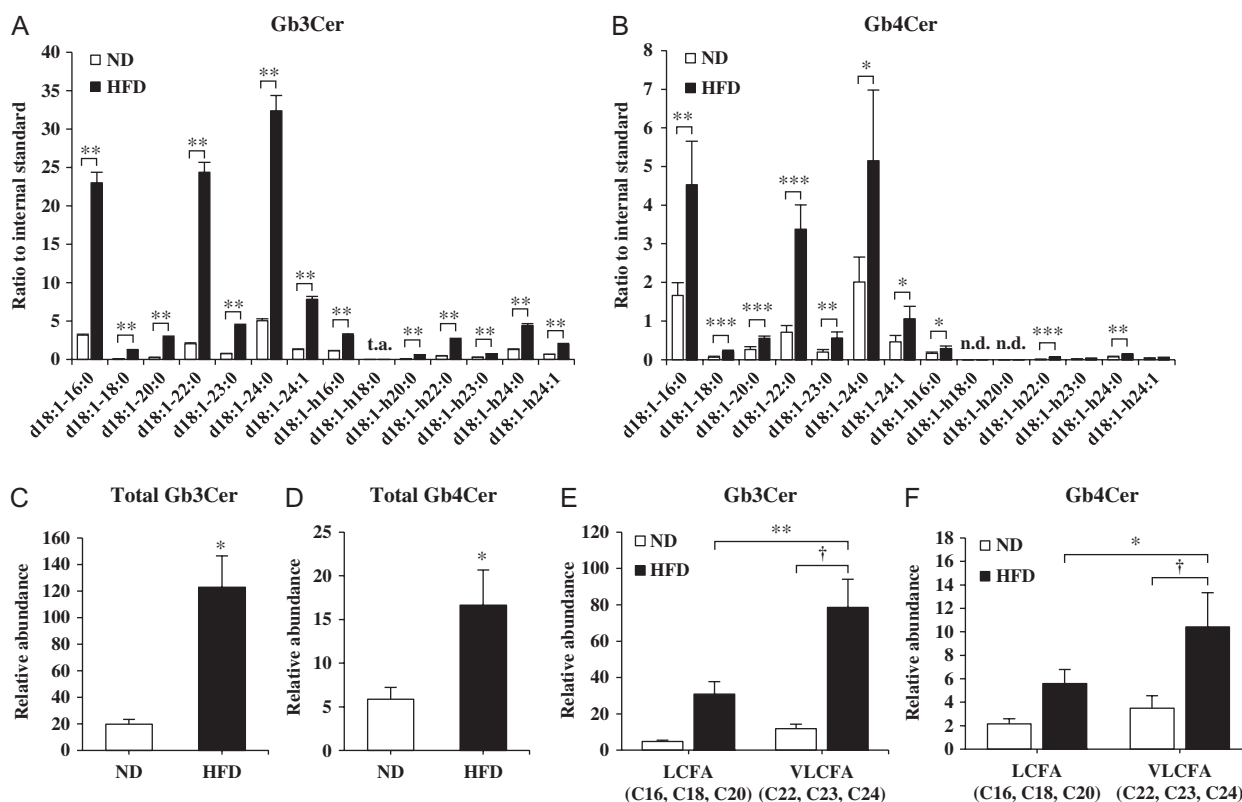


Fig. 4. LC-ESI-MS/MS analysis of renal Gb3Cer and Gb4Cer molecular species showing increased levels in HFD relative to ND. (A, B) 14 ceramide-carrying Gb3Cer species (A) and 12 ceramide-carrying Gb4Cer species (B) were detected, and are shown as relative abundance in bar graphs. $n = 4$ for each group. * $P < 0.05$, ** $P < 0.01$, *** $P < 0.001$ vs. ND, by Welch's t -test and Student's t -test. t.a., trace amount; n.d., not detected. (C, D) Total levels of Gb3Cer (C) and Gb4Cer (D), calculated as described in Materials and Methods, were compared in HFD vs. ND ($n = 4$ for each group). * $P < 0.01$ vs. ND, by Welch's t -test (C) and Student's t -test (D). (E, F) The levels of globo-series GSL molecular species (E, Gb3Cer; F, Gb4Cer) carrying VLCFAs (C22-C24) and LCFAs (C16-C20) and comparison between HFD and ND. $n = 4$ for each group. * $P < 0.05$, ** $P < 0.01$ vs. LCFAs, by Student's t -test; † $P < 0.01$ vs. ND (VLCFAs), by Welch's t -test (E) and Student's t -test (F). Data shown are mean \pm SD.

α -hydroxy FAs: h16:0, h18:0, h20:0) in comparison between ND and HFD (Figure 4E, F). These findings indicate that HFD feeding produces quantitative and qualitative changes of renal Gb3Cer and Gb4Cer, and suggest that these alterations of Gb3Cer and Gb4Cer molecular species plays a pathophysiological role in diet-induced diabetic nephropathy.

Involvement of globo-series GSLs in renal inflammatory responses

In view of the greatly altered renal Gb3Cer/Gb4Cer levels in HFD-induced diabetic nephropathy, we examined the roles of globo-series GSLs in inflammatory responses associated with diabetic nephropathy. Enzyme-linked immunosorbent assay (ELISA) was used to measure production of TNF- α by mouse BMDMs or human monocytes stimulated with LPS (0.25 ng/mL and 0.1 ng/mL, respectively) plus Gb3Cer or Gb4Cer (each 0, 2.5, 5, 10 μ M) (Figure 5A, B). We used commercially available Gb3Cer/Gb4Cer carrying VLCFAs (C22, C24) as major molecular species (Figure S2), and these molecular species were selectively increased in kidney by HFD feeding (Figure 4A, B). A higher TNF- α level was produced by co-stimulation with LPS and Gb3Cer/Gb4Cer than by stimulation with LPS alone (Figure 5A, B), but the degree of this effect declined as Gb3Cer/Gb4Cer concentration increased (Figure 5A). Human IL-6 and IL-12/23 levels also higher by co-stimulation with LPS and these GSLs than by stimulation with LPS alone (Fig. S4).

To determine the selectivity of Gb3Cer/Gb4Cer for TLR4, we assessed specificity of these GSLs for TLRs using TLR4/MD-2-overexpressing HEK293T cells or TLR ligands for TLR4, 1/2, 5, 7/8 and 2/6. We observed that a higher NF- κ B activity was induced in response to co-stimulation with LPS (20 ng/mL) and Gb3Cer/Gb4Cer (each 3, 10, 30 ng/mL) than by stimulation with LPS alone in TLR4/MD-2 overexpressing HEK293T (Figure 5C). The degree of NF- κ B activity declined as these GSLs increased, consistent with the result of co-stimulation of mouse BMDMs as shown in figure 5A. Gb3Cer/Gb4Cer also selectively enhanced human IL-6 (hIL-6) production induced by TLR4 ligands, LPS and HMGB1, but not by ligands for TLR1/2, 5, 7/8 and 2/6 (Figure 5D). However, these GSLs alone did not have the ability to produce hIL-6 via TLR4. These results indicated that Gb3Cer/Gb4Cer selectively and positively modulates TLR4-mediated inflammatory response in human and mouse monocytes/macrophages.

Discussion

Diabetic nephropathy is a major complication of T2DM arising from genetic factors and environmental factors. Associations between renal GSLs and diabetic nephropathy have been reported in several animal models (Masson et al. 2005; Grove et al. 2014; Subathra et al. 2015). The *db/db* mouse model used in the above studies has a diabetic phenotype resulting from a single gene

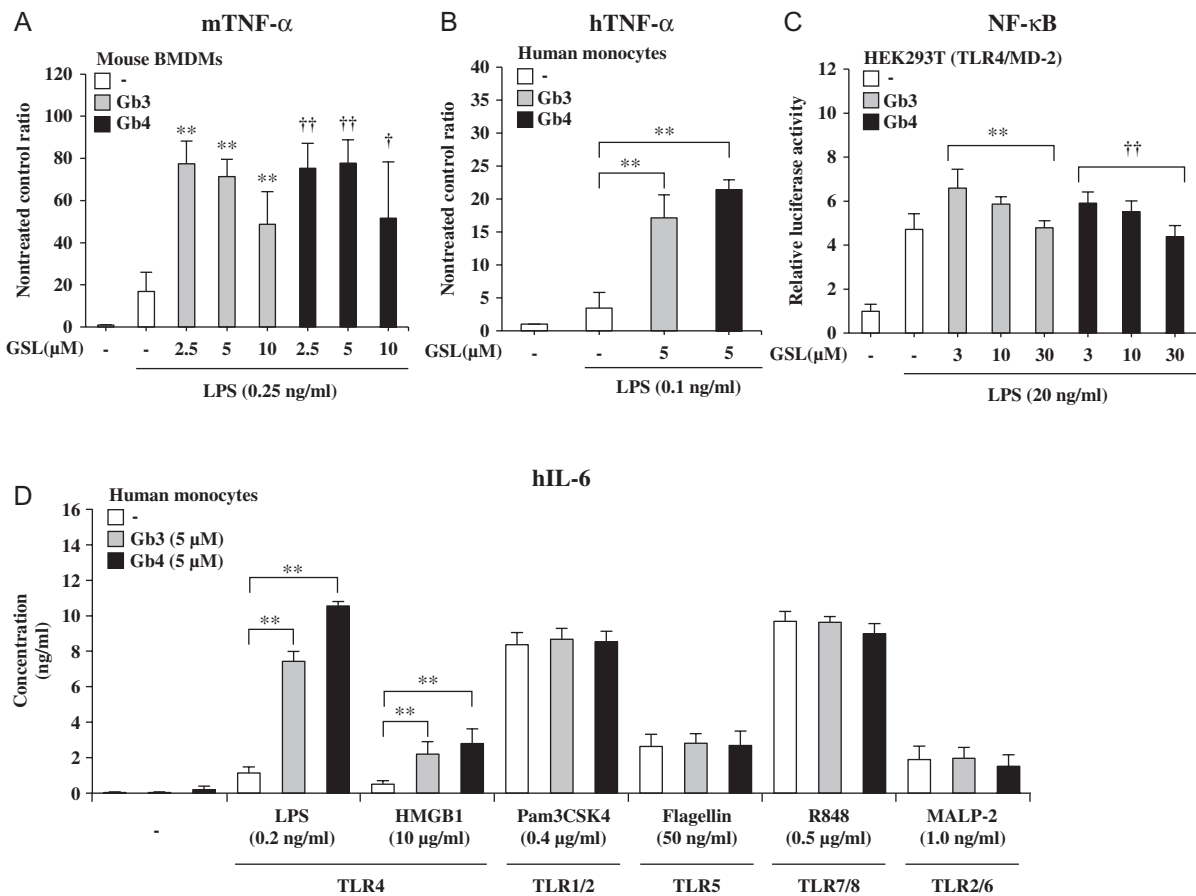


Fig. 5. Globo-series GSLs selectively affect inflammatory responses via TLR4. **A:** ELISAs for murine TNF- α in BMDM culture supernatant following treatment with LPS (0, 0.25 ng/mL) plus Gb3Cer or Gb4Cer (0, 2.5, 5, 10 μ M). TNF- α amount was normalized to nontreated control and expressed as ratio. $n = 4$ for each group. ** $p < 0.01$ vs. group treated with LPS only; † $p < 0.05$, †† $p < 0.01$ vs. group treated with LPS only, by Dunnett's test. **B:** ELISAs for human TNF- α in human monocyte culture supernatant following treatment with LPS (0, 0.1 ng/mL) plus 5 μ M Gb3Cer or Gb4Cer. TNF- α amount was normalized to nontreated control and expressed as ratio. $n = 3$ for each group. ** $p < 0.01$, by Dunnett's test. **C:** TLR4/MD-2-overexpressing HEK293T cells were transfected with NF- κ B luciferase construct and stimulated with LPS (0, 20 ng/mL) plus Gb3Cer or Gb4Cer (0, 3, 10, 30 μ M). Luciferase activity was normalized to nontreated control and expressed as relative luciferase activity. $n = 4$ for each group. ** $p < 0.01$ vs. group treated with LPS only; †† $p < 0.01$ vs. group treated with LPS only, by one-way ANOVA. **D:** ELISAs for human IL-6 in human monocyte culture supernatant following treatment with TLR ligands (TLR4: LPS, human recombinant HMGB1; TLR1/2: Pam3CSK4; TLR5: Flagellin; TLR7/8: R848; TLR2/6: MALP-2) plus 5 μ M Gb3Cer or Gb4Cer. $n = 4$ for each group. ** $p < 0.01$, by Dunnett's test. Data are shown as mean \pm SD.

mutation for leptin receptor. However, obesity, T2DM, and diabetic nephropathy in humans are polygenic diseases. We therefore used mouse strain KK, a polygenic disease model, for analysis of diabetic nephropathy. Levels of renal globo-series GSLs (Gb3Cer, Gb4Cer) were strikingly increased in HFD (Figure 3A). These GSLs were also increased by HFD feeding in nondiabetic C3H/HeN mice (Figure S3). L.J. Siskind's group (Subathra et al. 2015) and J.A. Shayman's group (Zador et al. 1993) reported increased levels of renal GSLs (HexCer, LacCer, GM3) in *db/db* mice with diabetic nephropathy and in Sprague-Dawley rats with streptozotocin-induced diabetes. Our findings and previous reports implicated the GSL species in pathophysiology of diabetic nephropathy.

In the present study, enhanced levels of globo-series GSLs resulted, at least in part, from increased gene expression of Gb3Cer synthase (Figure 3D). Increased Gb3Cer synthase expression has been observed in response to LPS and inflammatory cytokines such as IL-1 and TNF- α (van Setten et al. 1997; Hughes et al. 2000; Okuda et al. 2010; Kondo et al. 2013). Indeed, renal expression of

TNF- α gene was higher in HFD than in ND in the present study (Figure 2D).

We used LC-ESI-MS/MS to evaluate differential levels of renal Gb3Cer/Gb4Cer molecular species in HFD vs. ND. Contents of d18:1-16:0, 22:0, 24:0 species were significantly higher in HFD than in ND (Figure 4A, B). The proportion of d18:1-22:0, VLCFA, to the total Gb3Cer/Gb4Cer species was increased markedly in HFD compared to ND (Figure S1E, F). These results suggest that these species, specifically VLCFA species, are involved in pathophysiology of diabetic nephropathy. Hyperglycemia typically results in renal macrophage infiltration and renal inflammation, both of which contribute to pathogenesis and pathophysiology of diabetic nephropathy (Chow et al. 2004; Navarro-Gonzalez et al. 2011). Therefore, we assessed proinflammatory activity of Gb3Cer/Gb4Cer in TLR4/MD-2-overexpressing HEK293T cells, mouse BMDMs and human monocytes (Figure 5A–D). Gb3Cer/Gb4Cer enhanced inflammatory response in the presence of TLR4 ligands, LPS and HMGB1, but neither in the absence of the ligands nor in the presence of the other ligands (Figure 5D). The effects of Gb3Cer/Gb4Cer on TLR4-

mediated inflammatory response declined as concentration increased (Figure 5A, C). Furukawa's group has reported that Gb4Cer is an endogenous ligand of TLR4/MD-2, and that Gb4Cer negatively regulated TLR4/MD-2 complex at a dosage higher than the one we used for immune cells (Kondo et al. 2013). Therefore, Gb4Cer appears to be capable of enhancing inflammatory response at lower concentrations, and suppressing inflammatory response at higher concentrations (Figure 5A, C). These results indicated that Gb3Cer/Gb4Cer alone would not be able to induce inflammatory response via TLRs but selectively and positively modulate TLR4-mediated inflammatory response in presence of TLR4 ligands. However, the mechanism how Gb3Cer/Gb4Cer enhances TLR4-mediated inflammatory response remains unclear. Previous studies have been demonstrated that GSLs implicated in TLR4 signaling on the microdomain (Cai et al. 2013; Nikolaeva et al. 2015; Mobarak et al. 2018). However, our results support that Gb3Cer/Gb4Cer associates with TLR4 as a modulator, and induces TLR4 signaling through trans-interaction rather than *cis*-interaction between these GSLs and TLR4 on the microdomain because Gb3Cer/Gb4Cer did not enhance inflammatory response via TLR1/2, TLR5, and TLR2/6 that located on the plasma membranes. In addition, Furukawa's group has reported recently that Gb4Cer bind to MD-2 by binding assay using radiolabeled Gb4Cer (Kondo et al. 2013). Therefore, we propose the current model (Figure 6) whereby Gb3Cer/Gb4Cer modulates TLR4-mediated inflammatory response in the presence of TLR4 ligands by binding to TLR4/MD-2 complex. It is known that TLR4 signaling is required for the homo-dimerization composed of two units of TLR4/MD-2/LPS complex after LPS binding to TLR4/MD-2 units (Park et al. 2009). Interestingly, Saitoh et al. reported that, at least, a single TLR4 ligand could induce TLR4 dimerization (Figure 6A) (Saitoh et al. 2004), suggesting that there is still room for one more ligand to interact with dimeric TLR4/MD-2 complex. Therefore, Gb3Cer/Gb4Cer might bind to the empty side of TLR4/MD-2 units, and enhances TLR4 signaling mediated by LPS which

binds to the other side of TLR4/MD-2 units (Figure 6B). However, Gb3Cer/Gb4Cer alone would not be able to induce activation of TLR4/MD-2 complex (Figure 6C).

Previous reports (van Setten et al. 1997; Legros et al. 2017) showed that Gb3Cer and Gb4Cer are abundant in human renal glomerular cells, and that these cells and KK mouse kidney cells have similar expression patterns of certain molecular species. Gb3Cer in human renal glomerular cells is increased in response to proinflammatory cytokines (van Setten et al. 1997). Circulating endotoxin and HMGB1 levels, TLR4 ligands, are elevated in both humans and mice with T2DM (Brun et al. 2007; Creely et al. 2007; Al-Attas et al. 2009; Wang et al. 2015). HMGB1 is also up-regulated in mouse mesangial cells under high glucose levels (Chen et al. 2015). Given that Gb3Cer and Gb4Cer are up-regulated by proinflammatory cytokines and affect TLR4-expressing cells, such as macrophage and mesangial cells (Kaur et al. 2012), these GSLs might exacerbate and prolong renal inflammation in diabetic nephropathy.

Taken together, our findings suggest that the effect of Gb3Cer/Gb4Cer via TLR4 play an important role in the pathophysiology of diet-induced diabetic nephropathy.

Materials and methods

Animals and feeding conditions

Eight-week-old male KK/Ta mice (CLEA Japan; Tokyo, Japan) were divided randomly into two groups. The control group was fed normal diet (ND) (CE-2; CLEA Japan), while the HFD group was fed high-fat diet (HFD) (D12492; Research Diet; New Brunswick, NJ) ad lib for 8 wk. Kidneys and blood (from right ventricle) were harvested after sacrificing animals. Non-fasting blood glucose was measured using Accu-Chek Aviva strips (Roche DC; Japan).

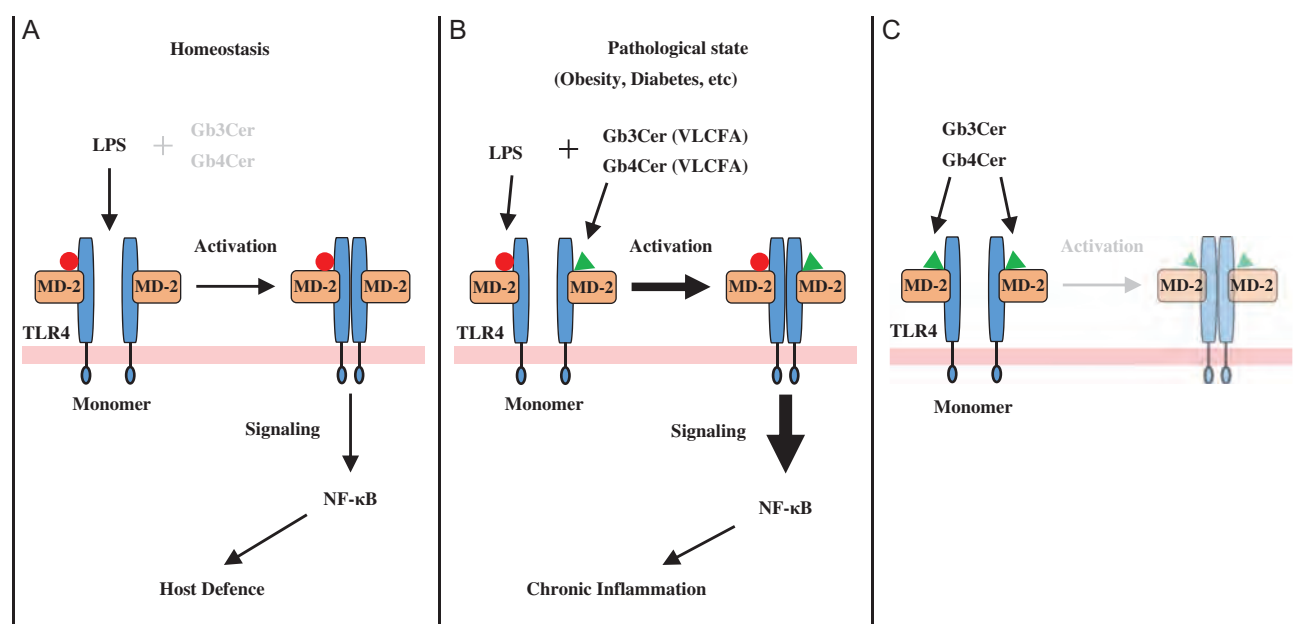


Fig. 6. Working hypothesis for the action of Gb3Cer/Gb4Cer on TLR4 signaling. (A) TLR4 signaling by LPS. Dimerization of TLR4/MD-2 units requires, at least, one molecule of LPS (Saitoh et al. 2004). (B) Synergistic activation of TLR4/MD-2 by LPS and Gb3Cer/Gb4Cer. Gb3Cer/Gb4Cer associates with TLR4/MD-2 complex as a modulator in presence of LPS, and enhances inflammatory response through trans-interaction. (C) Gb3Cer/Gb4Cer alone would not induce activation of TLR4/MD-2 complex.

Analysis of GSLs

Lyophilized kidney tissue was extracted with chloroform/methanol (2:1 and 1:1, v/v). Total lipids were separated into acidic and neutral fractions on DEAE-Sephadex A-25 anion-exchange columns (GE Healthcare Life Sciences). Acidic and neutral lipids were de-esterified by mild alkaline hydrolysis and desalted using a Sep-Pak C18 cartridge (Waters; Milford, MA). Acidic and neutral GSLs (respective protein equivalent 1000 μ g and 200 μ g) were spotted on HPTLC plates, developed respectively with chloroform/methanol/0.2% CaCl_2 (55:45:10, v/v/v) and chloroform/methanol/water (60:25:4, v/v/v), and visualized by orcinol/sulfuric acid staining.

RNA isolation, reverse transcription and quantitative PCR

Total RNA was extracted using Sepasol-RNA I super G (Nacalai Tesque; Kyoto, Japan) and Fast Gene RNA Premium Kit (Nippon Genetics; Tokyo). cDNA was generated from 500 ng total RNA using PrimeScript RT Reagent kit (Takara Bio). Primer-probe sets for mouse *A4galt* (Mm01307145_m1) and *Tnf* (Mm00443258_m1) were from Applied Biosystems (Foster City, CA) and mouse *Gapdh* (Mm.PT.39a.1) was from Integrated DNA Technologies (Coralville, IA). Quantitative PCR was performed on StepOnePlus Real-Time PCR System (Applied Biosystems) using these primer-probe sets and THUNDERBIRD Probe qPCR Mix (Toyobo Co.; Osaka, Japan). Relative mRNA levels were calculated from a standard curve and normalized to GAPDH expression.

Mass spectrometric (MS) analysis

Gb3Cer and Gb4Cer molecular species were quantified by HPLC coupled with electrospray ionization tandem MS (LC-ESI-MS/MS) in multiple reaction monitoring (MRM) positive ionization mode (Supplementary Table 1). A triple stage quadrupole (TSQ) Vantage AM instrument (Thermo Fisher; Waltham, MA) was calibrated by directly infusing a neutral GSL mixture containing Gb3Cer and Gb4Cer species. All ion source parameters and ionization conditions were optimized to improve sensitivity. Neutral GSLs from mouse kidney extract were dissolved in 100 μ L methanol, and 5 μ L of the solution was injected into an HPLC pump (model Accela 1250, Thermo Fisher) and separated on a Develosil C30 column (C30-UG-3-1 \times 50 mm; Nomura Chemical Co.; Japan).

Gradient program and parameters were as follow: start with 100% solvent A (20% H_2O /50% 2-propanol/30% methanol containing 0.1% acetic acid and 0.1% ammonia) for 5 min; ramp up to 100% solvent B (2% H_2O /50% 2-propanol/48% methanol containing 0.1% acetic acid and 0.1% ammonia) over 30 min; maintain 100% solvent B for 5 min; return to 100% solvent A over 1 min, hold there for 9 min; flow rate throughout chromatographic run: 60 μ L/min; +3000 V potential applied between ion source, electrospray needle, and nitrogen gas; collision energy 60 eV for Gb3Cer molecular species, 52 eV for Gb4Cer molecular species. Gb3Cer (d18:1-17:0) (Matreya, LLC; State College, PA) was added to neutral GSL samples from mouse kidney extract as internal standard and relative abundance of each Gb3Cer/Gb4Cer molecular species was determined based on ratio to internal standard. Total Gb3Cer/Gb4Cer value was calculated as sums of relative abundance for the 26 and 18 (respectively) molecular species detected. A caveat regarding interpretation of these MS data is that ionization efficiencies are not the same for all molecular species. In view of the limited availability of pure molecular species standards, we assumed that all

species have ionization efficiencies comparable to those of the internal standards used.

Purification of human monocytes

Heparinized fresh human peripheral blood was diluted to double the volume with cold PBS (4°C; endotoxin-free; Nacalai Tesque) containing 1 μ g/mL polymyxin B (Sigma-Aldrich; St. Louis, MO). Diluted blood was overlaid on cold lymphocyte separation solution (4°C, Nacalai Tesque) containing 1 μ g/mL polymyxin B, and centrifuged for 25 min at 4°C, 800 \times g. Peripheral blood mononuclear cell (PBMC) fraction was collected and diluted to double the volume of wash solution (PBS, 1% heat-inactivated FCS (Biosera), 5 mM EDTA, pH 7.5 (Nacalai Tesque), 1 μ g/mL polymyxin B). PBMCs were separated by centrifugation for 10 min at 4°C, 600 \times g, and washed twice. PBMCs were resuspended in 750 μ L wash solution and incubated with 120 μ L anti-human CD14 magnetic particles (BD Biosciences) for 30 min at room temperature. CD14-positive cells (monocytes) were separated by magnetic field and washed three times with wash solution. Purified cells were resuspended in cold low-glucose DMEM (Nacalai Tesque) with 0.75% FCS, left on ice for 45 min, counted, diluted to 2.0×10^5 /mL with culture medium (low-glucose DMEM, 0.75% FCS, 40 ng/mL recombinant human granulocyte-macrophage colony-stimulating factor (GM-CSF) (BioLegend; San Diego, CA), and cultured in 96-well plates (100 μ L/well) overnight at 37°C in 5% CO_2 atmosphere.

Differentiation of mouse bone marrow-derived macrophages (BMDMs)

Femoral and tibial bone marrows of 12- to 16-wk-old nondiabetic C3H/HeN mice (Japan SLC, Inc.) were collected in 1% FCS-supplemented low-glucose DMEM, and erythrocytes were lysed in RBC lysis buffer. Bone marrow cells were washed in 1% FCS DMEM, and then cultured for 5–7 days in 10% FCS DMEM supplemented with 40 ng/mL recombinant human macrophage colony-stimulating factor (M-CSF) (BioLegend). Non-adhesive cells were washed out with PBS. Differentiated macrophages were collected in ice-cold PBS (with 1% FCS, 5 mM EDTA) by scraping, washed, counted, diluted to 2.0×10^5 /mL in 1% FCS DMEM, and cultured in 96-well plates (100 μ L/well) overnight at 37°C in 5% CO_2 atmosphere.

Vector construction

Vector carrying murine MD-2 and TLR4 cDNA (pDUO-mMD2/TLR4) was from InvivoGen (San Diego, CA). cDNA fragments, fused with a KpnI site and one Kozak sequence (ACC) at 5'-end and a Sall site at 3'-end, were amplified by PCR (KOD-Plus-Neo; Toyobo), and inserted separately into pCDNA3 at KpnI and XhoI site (Invitrogen). A set of vectors for dual luciferase assay, NF- κ B reporter gene (pGL3-ELAM; a Firefly luciferase gene controlled by NF- κ B-dependent promoter of ELAM-1), and control reporter gene (pRL-TK; a Renilla luciferase gene controlled by constitutive active promoter of thymidine kinase) were gifts from Dr. Takayuki Kuraishi (Kanazawa University, Japan).

Cell culture and transfection

HEK293T cells were obtained from RIKEN Bioresource Center (Japan) and maintained in 10% FCS low-glucose DMEM at 37°C in 5% CO_2 atmosphere. Prior to transfection, cells were diluted to 2.0×10^5 /mL in 1% FCS DMEM and cultured in 96-well plates (100 μ L/well) overnight. Cells in each well were transfected with vectors

(20 ng pCDNA3-mMD-2, 0.1 ng pCDNA3-mTLR4, 40 ng pGL3-ELAM, 20 ng pRL-TK), complexed with 0.5 μ L Lipofectamine LTX and 0.25 μ L Plus reagent in 20 μ L Opti-MEM (Invitrogen), and subjected to stimulation 24 h after transfection.

Cell stimulation, enzyme-linked immunosorbent assay (ELISA) and luciferase assay

Gb3Cer (from pig RBCs; Nacalai Tesque) and Gb4Cer (from pig RBCs; Fuji-film Wako, Japan) were dissolved (1 mM) in DMSO, and diluted with low-glucose DMEM to 100 μ M just before experiments. Cells were incubated with Gb3Cer/Gb4Cer, and stimulated after 30 min with TLR ligands: LPS from *E. coli* O111:B4 (Sigma-Aldrich); human recombinant HMGB1 (Biolegend, San Diego, CA); Pam3CSK4 (Novus Biologicals, Littleton, CO); Flagellin from *S. Typhmuri* (ENZO Life science, Farmingdale, NY); R848 (Fuji-film wako, Japan); MALP-2 (Novus Biologicals, Littleton, CO). After 18 h culture, media were collected and subjected to ELISA. ELISA kits for human IL-6, human TNF-alpha, human IL-12/23 (p40), and murine TNF-alpha were from BioLegend. Firefly and Renilla luciferase activities were measured using Dual-Glo Luciferase Assay System (Promega; Australia) on a microplate reader (model Infinite 200 PRO; Tecan; Switzerland).

Statistical analysis

Data were analyzed by Student's *t*-test, Welch's *t*-test, Dunnett's multiple comparison test, one-way ANOVA, or Mann Whitney unpaired test as appropriate, using the Microsoft Excel.

Supplementary data

Supplementary data is available at *Glycobiology* online.

Funding

This study was supported by JSPS KAKENHI Grants-in-Aid for Scientific Research (B) (JP16H04767 to J.I.), Grants-in-Aid for Exploratory Research (JP17K19569 to J.I.), and Grants-in-Aid for Young Scientist (B) (JP17K15450 to H.K.), Takeda Science Foundation (J.I.), Fugaku Trust for Medicinal Research (J.I.), and Mizutani Foundation for Glycoscience (J.I.).

Acknowledgements

The authors are grateful to the Center for Laboratory Animal Science, Tohoku Medical and Pharmaceutical University, for their services, to Prof. Koichi Fukase at Osaka university for helpful suggestions, to K. Miyahara, N. Okajima, and M. Goto at Inokuchi laboratory for their skillful technical support, and to Dr. S. Anderson for English editing of the manuscript.

Conflict of interest statement

The authors declare that they have no conflict of interest.

Abbreviations

BMDMs, bone marrow-derived macrophages; ELISA, enzyme-linked immunosorbent assay; FAs, fatty acids; Gb3Cer, globotriaosylceramide; Gb4Cer, globotetraosylceramide; GlcCer, glucosylceramide; GSL(s), glycosphingolipid(s); HFD, high-fat diet; LacCer, lactosylceramide; LC-ESI-MS/MS, HPLC coupled with electrospray ionization tandem mass spectrometry; LCFAs, long chain fatty acids; LPS, lipopolysaccharide; ND,

normal diet; PBMC, peripheral blood mononuclear cell; T2DM, type 2 diabetes mellitus; TLR4, Toll-like receptor 4; TNF- α , tumor necrosis factor α ; VLCFAs, very long chain fatty acids.

References

- Al-Attas O, Al-Daghri N, Al-Rubeaan K, da Silva N, Sabico S, Kumar S, McTernan P, Harte A. 2009. Changes in endotoxin levels in T2DM subjects on anti-diabetic therapies. *Cardiovasc Diabetol.* 8:20.
- Alsaad K, Herzenberg A. 2007. Distinguishing diabetic nephropathy from other causes of glomerulosclerosis: an update. *J Clin Pathol.* 60:18–26.
- Badal S, Danesh F. 2014. New insights into molecular mechanisms of diabetic kidney disease. *Am J Kidney Dis.* 63:S63–S83.
- Biancini G, Vanzin C, Rodrigues D, Deon M, Ribas G, Barschak A, Manfredini V, Netto C, Jardim L, Giugliani R et al. 2012. Globotriaosylceramide is correlated with oxidative stress and inflammation in Fabry patients treated with enzyme replacement therapy. *Biochim Biophys Acta.* 1822:226–232.
- Biswas K, Richmond A, Rayman P, Biswas S, Thornton M, Sa G, Das T, Zhang R, Chahlavi A, Tannenbaum C et al. 2006. GM2 expression in renal cell carcinoma: potential role in tumor-induced T-cell dysfunction. *Cancer Res.* 66:6816–6825.
- Brun P, Castagliuolo I, Di Leo V, Buda A, Pinzani M, Palu G, Martines D. 2007. Increased intestinal permeability in obese mice: new evidence in the pathogenesis of nonalcoholic steatohepatitis. *Am J Physiol Gastrointest Liver Physiol.* 292:G518–G525.
- Cai W, Du A, Feng K, Zhao X, Qian L, Ostrom SR, Xu C. 2013. Adenylyl cyclase 6 activation negatively regulates TLR4 Signaling through lipid raft-mediated endocytosis. *J Immunol.* 191(12):6093–6100.
- Chen Y, Qiao F, Zhao Y, Wang Y, Liu G. 2015. HMGB1 is activated in type 2 diabetes mellitus patients and in mesangial cells in response to high glucose. *Int J Clin Exp Pathol.* 8(6):6683–6691.
- Chow F, Ozols E, Nikolic-Paterson D, Atkins R, Tesch G. 2004. Macrophages in mouse type 2 diabetic nephropathy: correlation with diabetic state and progressive renal injury. *Kidney Int.* 65:116–128.
- Creely S, McTernan P, Kusminski C, Fisher FM, Da Silva N, Khanolkar M, Evans M, Harte A, Kumar S. 2007. Lipopolysaccharide activates an innate immune system response in human adipose tissue in obesity and type 2 diabetes. *Am J Physiol Endocrinol Metab.* 292:E740–E747.
- Das SK, Elbein SC. 2006. The genetic basis of type 2 diabetes. *Cell Sci.* 2(4):100–131.
- De Francesco PN, Mucci JM, Ceci R, Fossati CA, Rozenfeld PA. 2013. Fabry disease peripheral blood immune cells release inflammatory cytokines: role of globotriaosylceramide. *Mol Genet Metab.* 109:93–99.
- Deshmukh GD, Radin NS, Gattone VH, Shayman JA. 1994. Abnormalities of glycosphingolipid, sulfate, and ceramide in the polycystic (cpwpcp) mouse. *J Lipid Res.* 35:1611–1618.
- Elmarakby A, Sullivan J. 2012. Relationship between oxidative stress and inflammatory cytokines in diabetic nephropathy. *Cardiovasc Ther.* 30:49–59.
- Fan Q, Shike T, Shigihara T, Tanimoto M, Gohda T, Makita Y, Wang L, Horikoshi S, Tomino Y. 2003. Gene expression profile in diabetic KK/Ta mice. *Kidney Int.* 64:1978–1985.
- Fioretto P, Mauer M. 2007. Histopathology of diabetic nephropathy. *Semin Nephrol.* 27:195–207.
- Freedman B, Bostrom M, Daeihagh P, Bowden D. 2007. Genetic factors in diabetic nephropathy. *Clin J Am Soc Nephrol.* 2:1306–1316.
- Grove K, Voziyan P, Spraggins J, Wang S, Pauksakon P, Harris R, Hudson B, Caprioli R. 2014. Diabetic nephropathy induces alterations in the glomerular and tubule lipid profiles. *J Lipid Res.* 55:1375–1385.
- Hakomori S, Handa K, Iwabuchi K, Yamamura S, Prinetti A. 1998. New insights in glycosphingolipid function glycosignaling domain a cell surface assembly of glycosphingolipids with signal transducer molecules, involved in cell adhesion coupled with signaling. *Glycobiology.* 8:xi–xix.
- Hakomori S, Igarashi Y. 1995. Functional role of glycosphingolipids and gangliosides in control of cell adhesion, motility, and growth, through glycosynaptic microdomains. *Biochim Biophys Acta.* 1780:421–433.

- Hughes A, Stricklett P, Schmid D, Kohan D. 2000. Cytotoxic effect of Shiga toxin-1 on human glomerular epithelial cells. *Kidney Int.* 57:2350–2359.
- Igel M, Taylor BA, Phillips SJ, Becker W, Herberg L, Joost H-G. 1998. Hyperleptinemia and leptin receptor variant Asp600Asn in the obese, hyperinsulinemic KK mouse strain. *J Mol Endocrinol.* 21:337–345.
- Kanwar Y, Sun L, Xie P, Liu F, Chen S. 2011. A glimpse of various pathogenetic mechanisms of diabetic nephropathy. *Annu Rev Pathol.* 6:395–423.
- Kaur H, Chien A, Jialal I. 2012. Hyperglycemia induces Toll like receptor 4 expression and activity in mouse mesangial cells: relevance to diabetic nephropathy. *Am J Physiol Renal Physiol.* 303:F1145–F1150.
- Kihara A. 2012. Very long-chain fatty acids: elongation, physiology and related disorders. *J Biochem.* 152:387–395.
- Kim OS, Park EJ, Joe E-h, Jou I. 2002. JAK-STAT signaling mediates gangliosides-induced inflammatory responses in brain microglial cells. *J Biol Chem.* 277:40594–40601.
- Kondo Y, Ikeda K, Tokuda N, Nishitani C, Ohto U, Akashi-Takamura S, Ito Y, Uchikawa M, Kuroki Y, Taguchi R et al. 2013. TLR4-MD-2 complex is negatively regulated by an endogenous ligand, globotetraosylceramide. *Proc Natl Acad Sci USA.* 110:4714–4719.
- Lee S, Lee T, Ihm C, Kim M, Woo J, Chung J. 2005. Genetics of diabetic nephropathy in type 2 DM: candidate gene analysis for the pathogenic role of inflammation. *Nephrology (Carlton).* 10(Suppl):S32–S36.
- Legros N, Pohlentz G, Runde J, Dusny S, Humpf H, Karch H, Muthing J. 2017. Colocalization of receptors for Shiga toxins with lipid rafts in primary human renal glomerular endothelial cells and influence of D-PDMP on synthesis and distribution of glycosphingolipid receptors. *Glycobiology.* 27:947–965.
- Makino H, Kanatsuka A, Suzuki T, Kuribayashi S, Hashimoto N, Yishida S, Nishimura M. 1985. Insulin resistance of fat cells from spontaneously diabetic KK mice. *Diabetes.* 34:844–849.
- Masson E, Troncy L, Ruggiero D, Wiernsperger N, Lagarde M, Bawab SE. 2005. a-series gangliosides mediate the effects of advanced glycation end products on pericyte and mesangial cell proliferation. *Diabetes.* 54:220–227.
- Mobarak E, Håversen L, Manna M, Rutberg M, Levin M, Perkins R, Rog T, Vattulainen I, Borén J. 2018. Glucosylceramide modifies the LPS-induced inflammatory response in macrophages and the orientation of the LPS/TLR4 complex in silico. *Sci Rep.* 8:1–11.
- Navarro-Gonzalez J, Mora-Fernandez C, Muros de Fuentes M, Garcia-Perez J. 2011. Inflammatory molecules and pathways in the pathogenesis of diabetic nephropathy. *Nat Rev Nephrol.* 7:327–340.
- Nikolaeva S, Bayunova L, Sokolova T, Vlasova Y, Bachtееva V, Avrova N, Parnova R. 2015. GM1 and GD1a gangliosides modulate toxic and inflammatory effects of E. coli lipopolysaccharide by preventing TLR4 translocation into lipid rafts. *Biochim Biophys Acta.* 1851(3):239–247.
- Nowling T, Mather A, Thiyagarajan T, Hernandez-Corbacho M, Powers T, Jones E, Snider A, Oates J, Drake R, Siskind L. 2015. Renal glycosphingolipid metabolism is dysfunctional in lupus nephritis. *J Am Soc Nephrol.* 26:1402–1413.
- Obrig TG, Louise CB, Lingwood CA, Boyd B, Barley-Maloney L, Daniel TO. 1993. Endothelial heterogeneity in Shiga toxin receptors and responses. *J Biol Chem.* 268:15484–15488.
- Ohmi Y, Tajima O, Ohkawa Y, Yamauchi Y, Sugiura Y, Furukawa K, Furukawa K. 2011. Gangliosides are essential in the protection of inflammation and neurodegeneration via maintenance of lipid rafts: elucidation by a series of ganglioside-deficient mutant mice. *J Neurochem.* 116:926–935.
- Okazaki M, Saito Y, Udaka Y, Maruyama M, Murakami H, Ota S, Kikuchi T, Oguchi K. 2002. Diabetic nephropathy in KK and KK-Ay mice. *Exp Anim.* 51(2):191–196.
- Okuda T, Nakakita S, Nakayama K. 2010. Structural characterization and dynamics of globotetraosylceramide in vascular endothelial cells under TNF-alpha stimulation. *Glycoconj J.* 27:287–296.
- Pai R, Bassa B, Kirschenbaum MA, Kamanna VS. 1996. TNF-a stimulates monocyte adhesion to glomerular mesangial cells. *J Immunol.* 156:2571–2579.
- Park SB, Song HD, Kim MH, Choi BS, Lee H, Lee JO. 2009. The structural basis of lipopolysaccharide recognition by the TLR4-MD-2 complex. *Nature.* 458:1191–1195.
- Saitoh S, Akashi S, Yamada T, Tanimura N, Kobayashi M, Konno K, Matsumoto F, Fukase K, Kusumoto S, Nagai Y et al. 2004. Lipid A antagonist, lipid IVA, is distinct from lipid A in interaction with Toll-like receptor 4 (TLR4)-MD-2 and ligand-induced TLR4 oligomerization. *Int Immunol.* 16(7):961–969.
- Shike T, Hirose S, Tomino Y, Kobayashi M, Funabiki K, Shirai T. 2001. Susceptibility and negative epistatic loci contributing to type 2 diabetes and related phenotypes in a KK/Ta mouse model. *Diabetes.* 50:1943–1948.
- Sonnino S, Prinetti A, Nakayama H, Yangida M, Ogawa H, Iwabuchi K. 2009. Role of very long fatty acid-containing glycosphingolipids in membrane organization and cell signaling: the model of lactosylceramide in neutrophils. *Glycoconj J.* 26:615–621.
- Subathra M, Korrapati M, Howell L, Arthur J, Shayman J, Schnellmann R, Siskind LJ. 2015. Kidney glycosphingolipids are elevated early in diabetic nephropathy and mediate hypertrophy of mesangial cells. *Am J Physiol Renal Physiol.* 309:F204–F215.
- Suto J, Matsuura S, Imamura K, Yamanaka H, Sekikawa K. 1998. Genetic analysis of non-insulin-dependent diabetes mellitus in KK and KKAY mice. *Eur J Endocrinol.* 139:654–661.
- Tagami S, Inokuchi J, Kabayama K, Yoshimura H, Kitamura F, Uemura S, Ogawa C, Ishii A, Saito M, Ohtsuka Y et al. 2002. Ganglioside GM3 participates in the pathological conditions of insulin resistance. *J Biol Chem.* 277:3085–3092.
- van Setten PA, van Hinsbergh VW, van der Velden TJ, van de Kar NC, Vermeer M, Mahan JD, Assmann KJ, van den Heuvel LP, Monnens LA. 1997. Effects of TNF- α on verocytotoxin cytotoxicity in purified human glomerular microvascular endothelial cells. *Kidney Int.* 51:1245–1256.
- Vardarli I, Baier L, Hanson R, Akkoyun I, Fischer C, Rohmeiss P, Basci A, Bartram C, Van Der Woude F, Janssen B. 2002. Gene for susceptibility to diabetic nephropathy in type 2 diabetes maps to 18q22.3-23. *Kidney Int.* 62:2176–2183.
- Wang H, Qu H, Deng H. 2015. Plasma HMGB-1 levels in subjects with obesity and Type 2 diabetes: a cross-sectional study in China. *PLoS One.* 10(8):1–10.
- Wu Y, Ding Y, Tanaka Y, Zhang W. 2014. Risk factors contributing to type 2 diabetes and recent advances in the treatment and prevention. *Int J Med Sci.* 11:1185–1200.
- Yoshida L, Tsunawaki S. 2008. Expression of NADPH oxidases and enhanced H₂O₂-generating activity in human coronary artery endothelial cells upon induction with tumor necrosis factor-alpha. *Int Immunopharmacol.* 8:1377–1385.
- Yu RK, Nakatani Y, Yanagisawa M. 2009. The role of glycosphingolipid metabolism in the developing brain. *J Lipid Res.* 50:S440–S445.
- Zador IZ, Deshmukh GD, Kunkel R, Johnson K, Radin NS, Shayman JA. 1993. A role for glycosphingolipid accumulation in the renal hypertrophy of streptozotocin-induced diabetes mellitus. *J Clin Invest.* 91:797–803.



Visual Function in Mice Lacking GM3 Synthase

Miki Hiraoka^a, Ei Ohkawa^b, Akira Abe^a, Masaki Murata^c, Shinji Go^{d,e}, Jin-ichi Inokuchi^d, and Hiroshi Ohguro^a

^aDepartment of Ophthalmology, School of Medicine, Sapporo Medical University, Sapporo, Japan; ^bOhkawa Eye Clinic, Iwamizawa, Japan; ^cDepartment of Pathology, School of Medicine, Sapporo Medical University, Sapporo, Japan; ^dDivision of Glycopathology, Institute of Molecular Biomembrane and Glycobiology, Tohoku Medical and Pharmaceutical University, Sendai, Japan; ^eDepartment of Pathophysiology and Metabolism, Kawasaki Medical University, Kurashiki, Japan

ABSTRACT

Purpose: Most complex gangliosides in vertebrates are formed from ganglioside GM3. GM3 deficiency in humans can result in epilepsy and visual impairment. To investigate whether a deficiency of GM3 is involved in visual function, ST3GAL5^{-/-} mice with mutations in the ST3GAL5 gene-coded GM3 synthase were employed.

Materials and Methods: Sixty mice were employed in this study. The glycosphingolipids of mice retinas were analyzed through high performance thin layer chromatography. The morphology of the optic nerves and retinas were evaluated by hematoxylin and eosin staining and immunohistochemical analysis using an anti-gial fibrillary acidic protein (GFAP) antibody. An electroretinogram (ERG) was applied on the eyes of 4, 9, 12, and 14-month-old mice. Also, visual evoked potential (VEP) was applied on 13-month-old mice.

Results: The GM3 in the retinas was detected in ST3GAL5^{+/+} mice but not ST3GAL5^{-/-} mice. Also, GM1b and GD1a expressions and lactosylceramide accumulation were found in the ST3GAL5^{-/-} mouse retinas. There was no significant difference in GFAP expression in the retinas or optic discs between ST3GAL5^{+/+} and ST3GAL5^{-/-} mice. Furthermore, the outcome of ERG and VEP analysis showed no disparity between the two strains in 13 and 14-month-old mice.

Conclusion: In the eye, neither histopathological abnormalities nor abnormal functions of the retina were found in GM3-deficient mice. Differing from the situation in patients with GM3 deficiency, the lack of GM3 in mice did not lead to optic nerve atrophy.

ARTICLE HISTORY

Received 8 May 2018
Revised 22 January 2019
Accepted 25 January 2019

KEYWORDS

Gangliosides; GM3; electroretinogram (ERG); visual evoked potential (VEP); anti-gial fibrillary acidic protein (GFAP); mice

Introduction

Gangliosides are a class of glycosphingolipids ubiquitously present in vertebrate plasma membranes. They are located in the outer leaflet of the cell membranes where they form microdomains and participate in transmembrane signaling and cell adhesion.¹ It is known that gangliosides are abundant in the central nervous system, and essential for neural development.² Among gangliosides, GM3 serves as a common precursor toward the formation of complex ganglioside species.³ Recent studies have shown some of the biological roles of GM3. For example, GM3 acts as an inducer for insulin resistance and is involved in the etiology of diabetes and obesity.⁴⁻⁶ Additionally, in the immune system, GM3 is essential for CD4⁺ T cell activation.⁷ In the auditory system, GM3 is necessary for the development of hair cells in the organ of Corti.^{8,9}

The ST3GAL5 gene encodes GM3 synthase, which is the first enzyme mediating the biosynthesis of complex a- and b-series gangliosides.^{3,10} The ST3GAL5^{-/-} mutant mice have no GM3 synthase activity. The deficiency of GM3 synthase leads to the a- and b-series gangliosides being replaced by o-series gangliosides. The ST3GAL5^{-/-} mice live normal life spans with fair fertile ability. The tissues from the brain, liver, and muscles of ST3GAL5^{-/-} mice do not show any

histological abnormalities.⁴ ST3GAL5^{-/-} mice have higher insulin sensitivity and a low response to a high-fat diet.⁴ These mice also express mild symptoms of experimental asthma induction through suppression of CD4⁺ T cells.⁷ In addition, studies indicate that the mice acquire deafness.^{8,9}

A 2004 study examines several patients in a family from the Old Order Amish community suffering from infantile onset epilepsy syndrome with hearing loss and vision loss.¹¹ They expressed an autosomal recessive inheritance pattern and the plasma samples from affected family members were GM3-deficient. The genetic screening of the patients revealed homozygous mutations in the ST3GAL5 gene. An additional report from France focuses on a family with two members suffering from early onset epilepsy, deafness, and blindness.¹² Those patients were identified to have homozygous mutations in the ST3GAL5 gene. Yet another report examines GM3-deficient patients with progressive epilepsy syndrome with visual impairment due to optic nerve atrophy.¹³

In the present study, we investigated ophthalmological differences between ST3GAL5^{+/+} mice and ST3GAL5^{-/-} mice with a C57BL/6 background to understand the role of GM3 in the visual system.

CONTACT Miki Hiraoka  mikihira@sapmed.ac.jp  Department of Ophthalmology, School of Medicine, Sapporo Medical University, S1W16 Chuo-ku, Sapporo, Hokkaido 060-8543, Japan

Color versions of one or more of the figures in the article can be found online at www.tandfonline.com/icey.

 Supplemental data for this article can be accessed here.

© 2019 Taylor & Francis Group, LLC

Materials and methods

Mice

The study protocols were approved by the Ethics Committee of the Sapporo Medical University School of Medicine. All procedures involving animals were performed in accordance with the ARVO Resolution on the Use of Animals in Research. ST3GAL5^{+/+} and ST3GAL5^{-/-} with a C57BL/6 background mice were generated as previously described.⁸ Mice colonies were maintained on a C57BL/6 background through heterozygous mating to generate a littermate control. Genotyping of ST3GAL5 alleles was performed by PCR as previously described.⁸ C57BL/6 mice were obtained from Hokudo (Sapporo, Japan), and bred in a pathogen-free condition in the animal resource center under 12-hour light and dark cycles. Before each experiment, mice were anesthetized with an intraperitoneal injection of a mixture of 0.75 mg/kg of medetomidine, 4 mg/kg of midazolam, and 5 mg/kg of butorphanol. Pupils were dilated with tropicamide and phenylephrine eye drops for electroretinogram (ERG) and visual evoked potential (VEP) study (0.5% each). No mice were used in more than one study.

Lipid extraction

Ten eyes were collected from ST3GAL5^{+/+} and ST3GAL5^{-/-} euthanized mice. The tissues (30–50 mg of wet weight) were transferred into a glass tube and homogenized with 800 μ l of 0.25 M sucrose/10 mM Hepes (pH 7.4)/1 mM EDTA on ice. The homogenate was subjected to a one-phase extraction in a chloroform/methanol/aqueous solution (1:2:0.8, v/v), sonicated for 5 min using a sonic bath, and then stood for 1 h at room temperature. The mixture was centrifuged at 2,330 g for 30 min at 25°C. The resultant supernatant was collected and the pellet was reextracted in 1 ml of chloroform/methanol (1:1, v/v) by a sonic bath for 2 min. After centrifugation at 2,330 g for 30 min at 25°C, the supernatant was combined with the first supernatant and kept at -30°C as a retina lipid extract. A part of the extract was used for the determination of phospholipid concentration.

Ganglioside analysis

Individual retina lipid extracts (containing 500 nmol of phospholipid) obtained from wild-type and GM3-deficient mice were dried down under a stream of N₂ gas using a water bath, dispersed with 2 ml of chloroform/methanol (1:1, v/v) using a sonic bath, and mixed with 0.45% (w/v) NaCl. After centrifugation at 1,000 g for 5 min at 25°C, the supernatant was collected and the organic phase was washed with 1 ml of chloroform, 2 ml of methanol, and 2 ml of water. After further centrifugation at 1,000 g for 5 min at 25°C, the supernatant was again collected and the organic phase was washed with 2 ml of methanol and 2 ml of water. After another process of centrifugation at 1,000 g for 5 min at 25°C, the resultant supernatant was collected and the organic phase was washed with 1 ml of methanol and 0.8 ml of water. After a final centrifugation at 1,000 g for 5 min at 25°C, the resultant organic phase was transferred into another tube, dried by N₂ gas and kept at -30°C as a neutral glycolipid fraction. The resultant supernatant was combined with other supernatants and loaded to a Sep-Pak C18 cartridge (Waters, Milford, MA), which had been prewashed

with methanol, chloroform/methanol (1:1, v/v), methanol, and methanol/water (1:1, v/v). After rinsing with water, gangliosides were eluted with methanol, dried by N₂ gas, and applied to a high performance thin layer chromatogram (HPTLC) plate (Merck, Darmstadt, Germany). The plate was developed in a solvent system consisting of chloroform/methanol/0.2% (w/v) CaCl₂·2H₂O (55:45:10, v/v). After drying the plate, it was soaked in an orcinol-sulfuric acid reagent to detect glycolipids. The uniformly wet plate was briefly dried by a hair dryer and baked for 15 min in a 100°C oven.

Neutral glycolipid analysis

The Individual neutral lipid fractions obtained in the ganglioside analysis section were dissolved with 500 μ l of chloroform and 1 ml of 0.21 N NaOH in methanol, and incubated for 1 h at 37°C. The reaction was terminated by the addition of 1 ml of 0.2 N HCl. After centrifugation at 1,000 g for 5 min at 25°C, the organic phase was transferred into a glass tube and mixed with 2 ml of methanol plus 800 μ l of 0.05 N HCl containing 25 mM HgCl₂. The reaction mixture was incubated for 20 min at 37°C and mixed with 1 ml of chloroform plus 1.2 ml of water. After centrifugation at 1,000 g for 5 min, the organic phase was washed with 1 ml of methanol and 800 μ l of 33.3 mM EDTA and then washed twice with 1 ml of methanol plus 800 μ l of 0.9% (w/v) of NaCl. The resultant organic phase was transferred into another glass tube, dried by N₂ gas and applied to an HPTLC plate. Glycolipids were detected as described in the ganglioside analysis section.

ERG recording

Two sets of experiments were performed. During the first set, mice aged 4, 9, and 12 months were employed and rod and dark-adapted maximal response ERG was performed. The number of eyes is listed in Supplementary data 1 and 2. During the second set, cone, rod, and dark-adapted maximal response ERG was performed using 14-month-old mice (five eyes for each genotype) (Figure 3).

Mice were dark-adapted overnight before the experiments. After anesthesia and mydriasis, the mice were placed on a heating pad for the duration of the ERG recordings. For each mouse, an active contact lens electrode (Mayo, Inazawa, Japan) was placed on the cornea. A reference electrode with a gold cup was placed in the mouth, and a ground electrode with a stainless clip was attached to the tail. The mice were placed in a Ganzfeld dome (LKC Technologies Inc., Gaithersburg, MD) and the response was obtained from one eye. The SG-2002 stimulator (LKC Technologies Inc., Gaithersburg, MD) was used, and analyzed with ERG-analysis software (PowerLab Scope version 3.7; ADInstruments Ltd., Castle Hill, NSW, Australia). According to the ISCEV standard,¹⁴ the a-wave amplitude was determined from the baseline to the negative peak of the a-wave (Figure 2). The b-wave amplitude was determined from the bottom of the a-wave to the top of the b-wave (Figure 2). For rod ERGs, four responses were averaged with an interstimulus interval of 2 s and stimulus strength of 0.008 cds/m². For dark-adapted maximal response ERGs, the single response was recorded with stimulus strength of 2.5 cds/m². After 10 min of light adaptation for mice,

cone ERGs were recorded. The responses to 16 flashes were averaged with an interstimulus interval of 0.5 s and stimulus strength of 2.5 cds/m² presented on a rod saturated background of 30 cd/m². Neutral density filters were used to reduce the stimulus strength.

VEP recording

Five mice for ST3GAL5^{+/+} and six mice for ST3GAL5^{-/-} mice, all 13 months old, were employed. One week prior to the experiment, under anesthesia, a stainless steel screw (1 mm diameter, 5 mm length) was inserted into the mice through the skull into the left visual cortex at the point of 1.5 mm lateral to the midline and 1.5 mm anterior to the lambda, penetrating the cortex to 1 mm in depth. For measurements, each screw was connected to the amplifier as a measuring electrode. The right eyes were stimulated in order to make the measurements. VEPs were recorded using the same equipment as for ERG under dark-adapted conditions. The responses to 128 flashes were averaged with an interstimulus interval of 1 s and stimulus strength of 2.5 cds/m². The N1 wave was defined as the initial negative deflection, and the P1 wave was defined as the positive deflection following the N1 wave. VEP was measured twice for each mouse, with the average taken as data.

Immunohistochemical analysis

After euthanasia, mouse eyes were immediately enucleated, fixed in Super Fix (Kurabo, Osaka, Japan), and embedded in paraffin. The 12-month-old mice were used for anti-gial fibrillary acidic protein (GFAP) study, and 9-month-old mice were used for PKC α study. Retinal sections were sagittally cut through the optic nerve head at 3 μ m thickness, mounted on slides, and dried. After the deparaffinization with graded ethanol and xylene solutions, sections were sequentially incubated with a blocking reagent, and then with an GFAP monoclonal antibody or anti-PKC α monoclonal antibody (clone MC5, Sigma Aldrich, St. Louis, USA). After washing the slides with PBS, the specific staining by the antibody was detected by the Histofine mouse stain kit (Nichirei, Tokyo, Japan) according to the manufacturer's protocol, and then developed with diaminobenzidine as a chromogen. Sections were counterstained with hematoxylin, dehydrated, and mounted. In the control sections, equivalent concentrations of irrelevant antibodies were substituted for the primary antibodies. The hematoxylin-eosin staining was also performed on each eye sample. All the sections were examined under a microscope equipped with a digital camera (Nikon, model ECLIPSE Ni, Tokyo, Japan). Three eyes for each genotype were examined for GFAP staining. The GFAP expression at the optic nerve was estimated by NIH-ImageJ 1.52a.

Statistical analysis

All results are expressed as mean \pm SD. The values were processed for statistical analyses (unpaired Student's *t*-test) and significant differences were considered at *p* < 0.05. Statistical analysis of multiple groups in ERG experiments was performed by using two-way ANOVA followed by the Tukey-Kramer test. *P* less than 0.05 was considered statistically significant.

Results

Glycosphingolipid expression in mouse retinas

The glycosphingolipid expression in mouse retinas from ST3GAL5^{+/+}, ST3GAL5^{+/-}, and ST3GAL5^{-/-} mice was examined. As shown in Figure 1, ST3GAL5^{-/-} mouse retinas had undetectable GM3, and expressed o-series gangliosides (GM1b and GD1 α) and a high content of lactosylceramide (LacCer), which is the proximate substrate of GM3 synthase.

ERG responses of mice

Representative ERG waveforms of 14-month-old mice (second set experiment), elicited by stimuli of different intensities recorded under cone, rod, and dark-adapted maximal response conditions are shown in Figure 2. From each strain 4, 9, 12, and 14-month-old mice were examined. The amplitudes and implicit times of the a-wave and b-wave in ST3GAL5^{+/+} and ST3GAL5^{-/-} mice were statistically analyzed. The results of 4, 9, and 12-month-old mice (first set experiment) are listed in Supplementary data 1 and 2, and those of 14-month-old mice are listed in Figure 3. In mice at the middle age of 4 and 9 months old, the implicit time of the b-wave was delayed in ST3GAL5^{-/-} mice in several instances. Those delays were not observed in 12- and 14-month-old mice.

VEP responses of mice

Representative VEP waveforms of 13-month-old mice are shown in Figure 2. The amplitudes and implicit times of the N1 peak and P1 peak in ST3GAL5^{+/+} and ST3GAL5^{-/-} mice were statistically analyzed. The results are listed in Table 1. There was no significant difference between the two strains at amplitude and implicit time.

Histological and immunohistological study of mouse eyes

Through hematoxylin-eosin staining, both ST3GAL5^{+/+} and ST3GAL5^{-/-} mice showed orderly formation of ocular tissues in the retinas and optic nerves (Figure 4). Optic nerve changes such as swelling or atrophy were not observed even in elderly mouse eyes of either strain.

GFAP is a marker of astrocytes and is also known as a marker of glial activation in response to neural injury.¹⁵ In the glaucoma model, the GFAP expression in the optic nerve is known to increase along with optic nerve damage. In the retina, GFAP expressions are limited in layers of ganglion cells (GCL) under normal conditions, but extend to the inner plexiform layer and inner nuclear layer (INL) under conditions such as uveoretinitis and retinal degeneration. In our study, the GFAP expression of the optic discs showed a similar intensity between 12-month-old ST3GAL5^{+/+} and ST3GAL5^{-/-} mice (Figure 4). The mean arbitrary unit of positive staining intensity in the optic nerve was $84.6 \pm 5.73 \times 10^6$ (bit/area) in ST3GAL5^{+/+} and $87.4 \pm 4.00 \times 10^6$ in ST3GAL5^{-/-} mice (*p* value = 0.52). In the retina, the GFAP expression was restricted in the GCL in both strains (Figure 5). In addition, immunohistochemical analysis

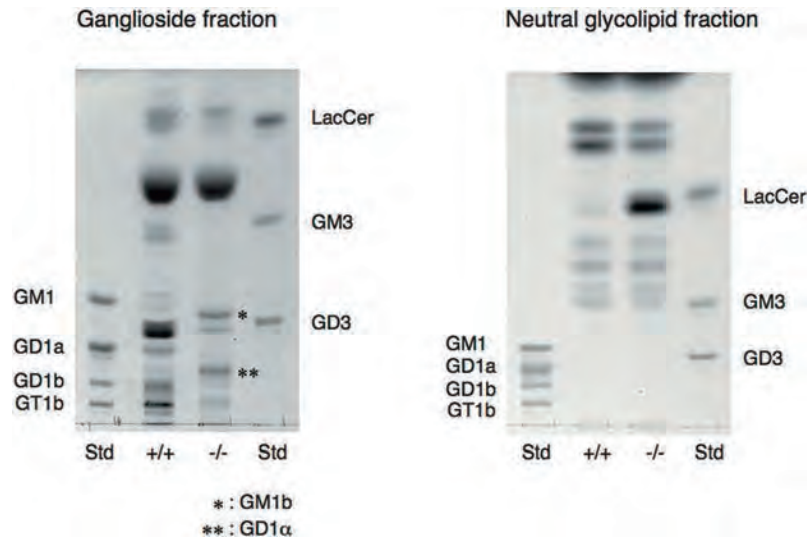


Figure 1. Glycosphingolipid expression in mice retinas.

HPTLCs of ganglioside fraction (left) and neutral lipid fraction (right) obtained from the retinas of ST3GAL5^{+/+} and ST3GAL5^{-/-} mice are presented. The ganglioside fraction and neutral lipid fraction were prepared and developed in HPTLC plates as described in the Materials and Methods. The amount of lipid spotted per lane was equivalent to 500 nmol retina phospholipid. Std, +/+, and -/- denote standard, ST3GAL5^{+/+}, and ST3GAL5^{-/-} mice, respectively.

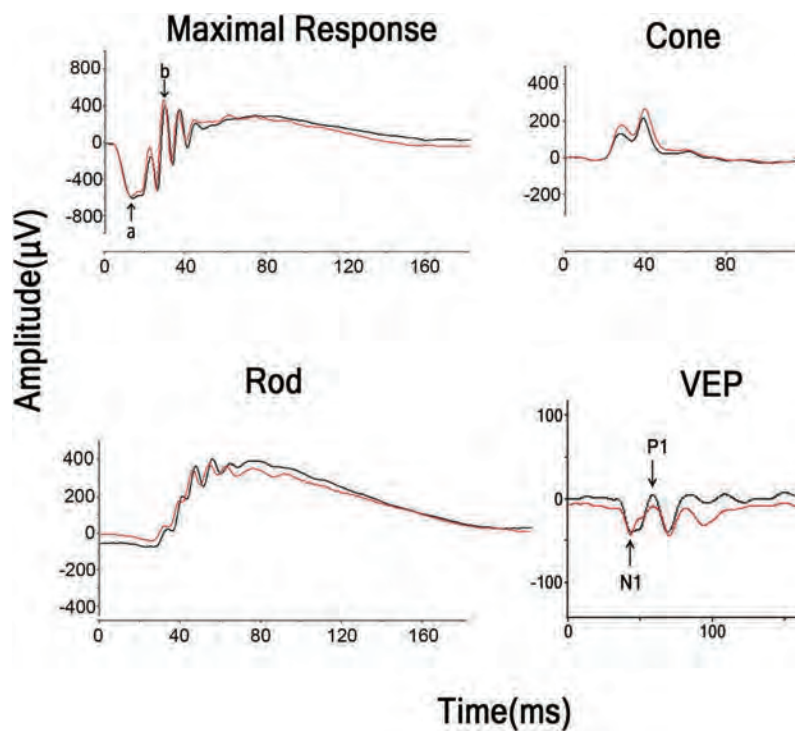


Figure 2. Representative ERGs of 14-month-old, and VEP of 13-month-old ST3GAL5^{+/+} and ST3GAL5^{-/-} mice.

The dark-adapted ERG responses to 2.5 and 0.008 cds/m² are shown in the upper and lower left panels, respectively. The light-adapted cone response is shown (2.5 cds/m²) in the upper right panel. Representative VEP responses are shown in the lower right panel. The waveform of ST3GAL5^{+/+} mice (black) and ST3GAL5^{-/-} mice (red) were plotted.

using an antibody against protein kinase C alpha subunit (PKC α), described in a previous study as being a marker on ON bipolar cells,¹⁶ was performed to examine the distribution of these cells in the retinas.¹⁶ The PKC α -positive cells were found at the side of the INL in the retinas of both strains of 12-month-old mice (Figure 5).

Discussion

In the present study, we investigated the ocular features of ST3GAL5^{-/-} mice. First, the glycosphingolipid profiles were examined. The retinas of ST3GAL5^{-/-} mice showed a complete lack of GM3 gangliosides and an increase in lactosylceramide, which is a precursor of GM3. In addition, GM1b

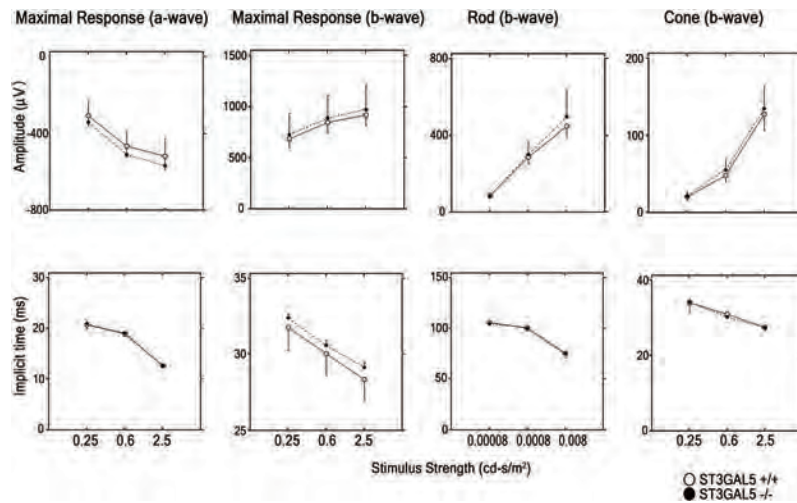


Figure 3. ERG intensity-response curves of the mean amplitude and implicit time of mice.

ERGs were elicited by three different stimulus intensities. The amplitudes are shown in the upper panel, and implicit times are shown in the lower panel. The mean amplitudes of ST3GAL5^{+/+} (open circles), and ST3GAL5^{-/-} mice (closed circles) were plotted with a SD bar. Five 14-month-old mice for each strain were employed. There was no difference between the two strains ($p > 0.05$).

Table 1. VEP amplitudes and implicit times in 13 months old ST3GAL5^{+/+} and ST3GAL5^{-/-} mice.

Strain	Eyes (n)	N1 wave		P1 wave	
		amp ¹ (µV)	I.T. ¹ (ms)	amp ¹ (µV)	I.T. ¹ (ms)
ST3GAL5 ^{+/+}	5	-51.3 ± 19.60	43.3 ± 2.50	42.2 ± 15.74	56.9 ± 3.20
ST3GAL5 ^{-/-}	6	-45.0 ± 20.74	42.5 ± 5.00	40.2 ± 5.34	57.2 ± 5.45
<i>p</i> Value		0.62	0.76	0.77	0.91

amp: amplitude; I.T: implicit time, ¹: Mean ± SD. *P* value: comparison with ST3GAL5^{+/+}.

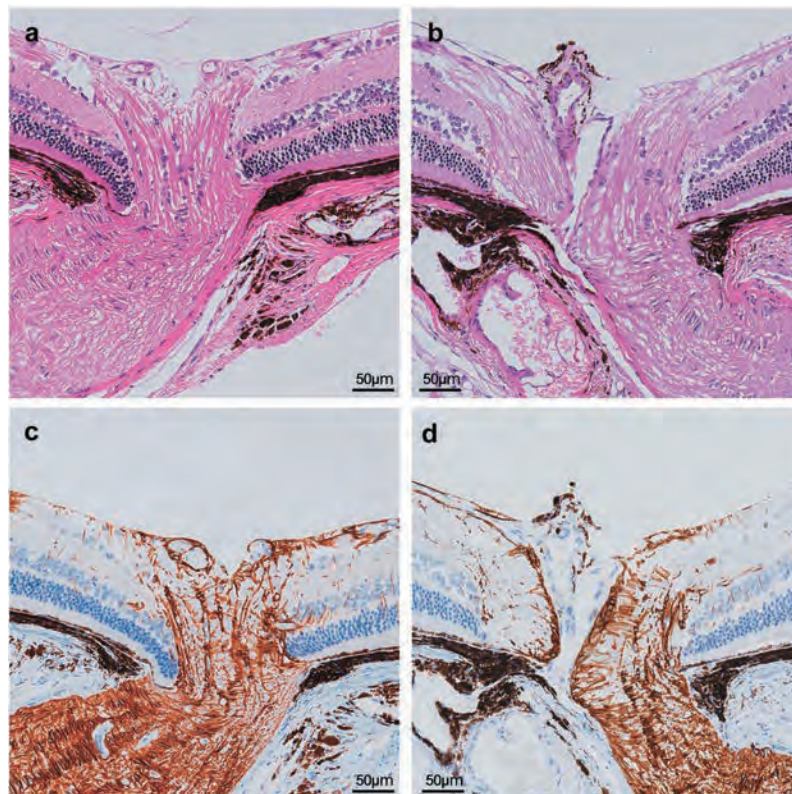


Figure 4. Histology of 12-month-old mouse eyes at optic disc area.

Panels A and C represent ST3GAL5^{+/+} mice and panels B and D represent ST3GAL5^{-/-} mice. Panels A and B show the optic disc area with hematoxylin-eosin staining. The GFAP expression of the optic disc area is shown in panels C and D.

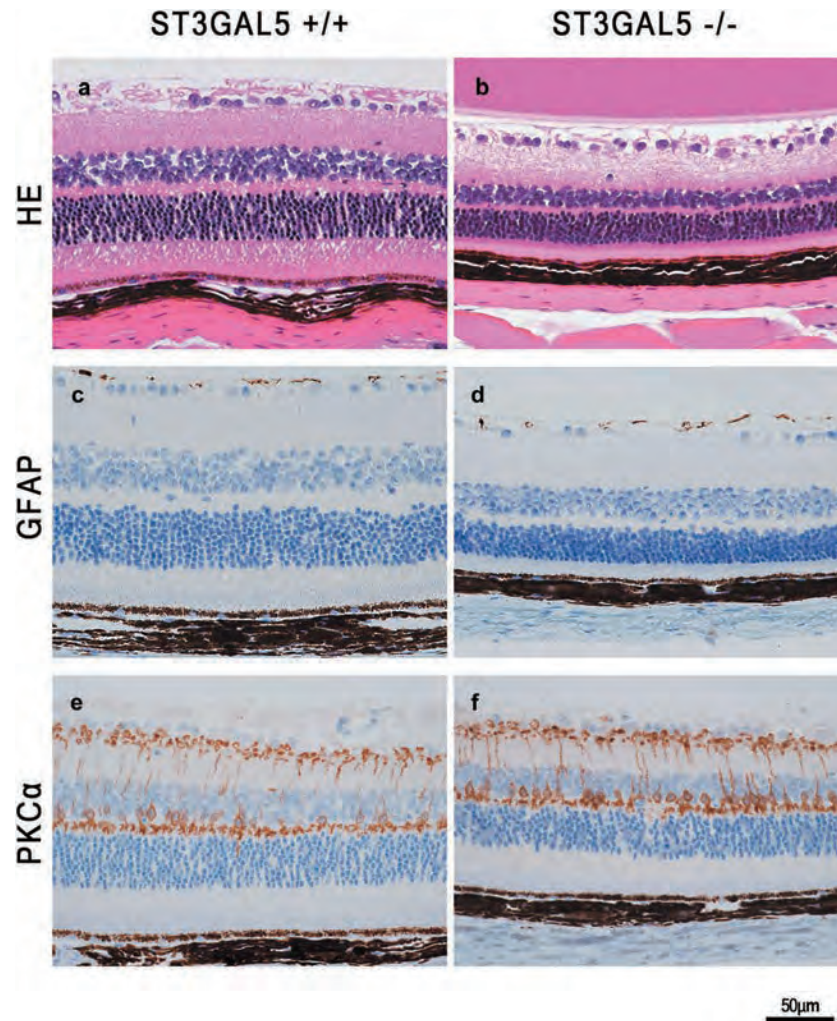


Figure 5. Histology of mouse eyes.

The retinal section of the central area between the peripapillary and peripheral areas are shown. Panels A, C, and E represent *ST3GAL5*^{+/+} mice and panels B, D, and F represent *ST3GAL5*^{-/-} mice. Panels A and B show images with hematoxylin-eosin staining. The GFAP expression is shown in panels C and D. The PKC α expression is shown in panels E and F. A scale bar represents 50 μ m.

and GD1 α were found to be upregulated in response to a deficiency of GM3, indicating that the deficiency of a- and b-series gangliosides are compensated by compensatory o-series gangliosides (GM1b and GD1 α) in the retinas of *ST3GAL5*^{-/-} mice. Although gangliosides are ubiquitously present in most tissues, the highest concentration is found in the gray matter of the brain.² Gangliosides are abundant in the central nervous system and essential for normal neural development and function. Most of the ganglio-series gangliosides in vertebrates are synthesized from GM3, and GM3 synthase catalyzes the primary step for the synthesis of complex gangliosides from lactosylceramide. GM3 is known to be involved in differentiation, proliferation, and signal transduction in cells. The antisense morpholino knockdown of *ST3GAL5* expression in zebrafish embryos results in neural apoptosis.¹⁷

Next, the pathophysiological manifestation of GM3-deficient mice was studied. It has been previously reported that the GM3 synthase deficiency caused by homozygous nonsense mutations in the *ST3GAL5* gene results in infant onset epilepsy syndrome.^{11,12} Some of those affected family members showed bilateral optic nerve pallor, but rod and cone ERG waveforms were found to be

normal.¹³ The brain magnetic resonance imaging of these patients showed diffuse cortical atrophy at older ages. In chick embryos, GM3 was detected in the retinal pigment epithelium and neural retina.¹⁸ It was assumed that blindness resulted from cortical atrophy in the visual cortex. In our study, we performed ERG on normal and GM3-deficient mice to clarify whether the deficiency of GM3 influences retinal development. In those the age of 4 and 9 months, the implicit time of the b-wave was delayed in GM3-deficient mice. Since the b-wave is generated by bipolar cells, the expression of PKC α in the retina was compared between two strains resulting in a similar outcome. There was no statistical difference in ERG results between *ST3GAL5*^{+/+} and *ST3GAL5*^{-/-} mice at ages 12 and 14 months. In addition, histological and immunohistological examinations were applied. Abnormalities or destruction of eyeball structure, either in the anterior or posterior segment of the eyes, were not found in GM3-deficient mice, even those aged 14 months. There was no evidence of GM3 involvement in retinal function in old age. Unlike results seen in trials with humans, optic nerve atrophy was not observed in GM3-deficient mice. Our VEP study did not show any influence due to lack of GM3. Additionally, the severe neurological phenotype of

GM3-deficient patients was not seen in ST3GAL5^{-/-} mice. These disparities might be due to species differences.

In conclusion, the absence of GM3 has no influence on the retinal or optic nerve function of mice.

Acknowledgments

We would like to express our appreciation to Dr. Kimura and Dr. Yamaguchi in the Division of Morphological Research at Sapporo Medical University for their histological work, and to Mr. Ito and Mr. Takeda in the Image and Media Support section at Sapporo Medical University Hospital for their technical support. Also, we would like to express our appreciation to Mr. Yoshikawa from the Mayo Corporation for his technical support on ERG measurements.

Disclosure statement

No potential conflict of interest was reported by the authors.

Funding

None.

References

- Hakomori S. Glycosynapses: microdomains controlling carbohydrate-dependent cell adhesion and signaling. *An Acad Bras Cienc*. 2004;76(3):553–72. doi:10.1590/S0001-37652004000300010.
- Schengrund CL. Gangliosides: glycosphingolipids essential for normal neural development and function. *Trends Biochem Sci*. 2015;40(7):397–406. doi:10.1016/j.tibs.2015.03.007.
- Kolter T, Proia RL, Sandhoff K. Combinatorial ganglioside biosynthesis. *J Biol Chem*. 2002;277(29):25859–62. doi:10.1074/jbc.R200001200.
- Yamashita T, Hashiramoto A, Haluzik M, Mizukami H, Beck S, Norton A, Kono M, Tsuji S, Daniotti JL, Werth N, et al. Enhanced insulin sensitivity in mice lacking ganglioside GM3. *Proc Natl Acad Sci U S A*. 2003;100(6):3445–49. doi:10.1073/pnas.0635898100.
- Inokuchi J. GM3 and diabetes. *Glycoconj J*. 2014;31(3):193–97. doi:10.1007/s10719-013-9516-4.
- Tagami S, Inokuchi Ji J, Kabayama K, Yoshimura H, Kitamura F, Uemura S, Ogawa C, Ishii A, Saito M, Ohtsuka Y, et al. Ganglioside GM3 participates in the pathological conditions of insulin resistance. *J Biol Chem*. 2002;277(5):3085–92. doi:10.1074/jbc.M103705200.
- Nagafuku M, Okuyama K, Onimaru Y, Suzuki A, Odagiri Y, Yamashita T, Iwasaki K, Fujiwara M, Takayanagi M, Ohno I, et al. CD4 and CD8 T cells require different membrane gangliosides for activation. *Proc Natl Acad Sci U S A*. 2012;109(6):E336–42. doi:10.1073/pnas.1114965109.
- Yoshikawa M, Go S, Takasaki K, Kakazu Y, Ohashi M, Nagafuku M, Kabayama K, Sekimoto J, Suzuki S, Takaiwa K, et al. Mice lacking ganglioside GM3 synthase exhibit complete hearing loss due to selective degeneration of the organ of Corti. *Proc Natl Acad Sci U S A*. 2009;106(23):9483–88. doi:10.1073/pnas.0903279106.
- Yoshikawa M, Go S, Suzuki S, Suzuki A, Katori Y, Morlet T, Gottlieb SM, Fujiwara M, Iwasaki K, Strauss KA, et al. Ganglioside GM3 is essential for the structural integrity and function of cochlear hair cells. *Hum Mol Genet*. 2015;24(10):2796–807. doi:10.1093/hmg/ddv041.
- Ishii A, Ohta M, Watanabe Y, Matsuda K, Ishiyama K, Sakoe K, Nakamura M, Inokuchi J, Sanai Y, Saito M. Expression cloning and functional characterization of human cDNA for ganglioside GM3 synthase. *J Biol Chem*. 1998;273(48):31652–55.
- Simpson MA, Cross H, Proukakis C, Priestman DA, Neville DC, Reinkensmeier G, Wang H, Wiznitzer M, Gurtz K, Verganelaki A, et al. Infantile-onset symptomatic epilepsy syndrome caused by a homozygous loss-of-function mutation of GM3 synthase. *Nat Genet*. 2004;36(11):1225–29. doi:10.1038/ng1460.
- Fragaki K, Ait-El-Mkadem S, Chaussonot A, Gire C, Mengual R, Bonesso L, Beneteau M, Ricci JE, Desquiret-Dumas V, Procaccio V, et al. Refractory epilepsy and mitochondrial dysfunction due to GM3 synthase deficiency. *Eur J Hum Genet*. 2013;21(5):528–34. doi:10.1038/ejhg.2012.202.
- Farukhi F, Dakkouri C, Wang H, Wiznitzer M, Traboulsi EI. Etiology of vision loss in ganglioside GM3 synthase deficiency. *Ophthalmic Genet*. 2006;27(3):89–91. doi:10.1080/13816810600862626.
- McCulloch DL, Marmor MF, Brigell MG, Hamilton R, Holder GE, Tzekov R, Bach M. ISCEV Standard for full-field clinical electroretinography (2015 update). *Doc Ophthalmol*. 2015;130(1):1–12. doi:10.1007/s10633-014-9473-7.
- Wang L, Cioffi GA, Cull G, Dong J, Fortune B. Immunohistologic evidence for retinal glial cell changes in human glaucoma. *Invest Ophthalmol Vis Sci*. 2002;43:1088–94.
- Grunert U, Martin PR, Wassle H. Immunocytochemical analysis of bipolar cells in the macaque monkey retina. *J Comp Neurol*. 1994;348(4):607–27. doi:10.1002/cne.903480410.
- Boccutto L, Aoki K, Flanagan-Steet H, Chen CF, Fan X, Bartel F, Petukh M, Pittman A, Saul R, Chaubey A, et al. A mutation in a ganglioside biosynthetic enzyme, ST3GAL5, results in salt & pepper syndrome, a neurocutaneous disorder with altered glycolipid and glycoprotein glycosylation. *Hum Mol Genet*. 2014;23(2):418–33. doi:10.1093/hmg/ddt434.
- Daniotti JL, Landa CA, Maccioni HJ. Regulation of ganglioside composition and synthesis is different in developing chick retinal pigment epithelium and neural retina. *J Neurochem*. 1994;62(3):1131–36.

原 著

スフィンゴミエリンマイクロドメインは
Jurkat 細胞の T 細胞抗原受容体依存性の活性化を負に制御する

永福 正和,¹ 豊島かおる,¹ 堀内 隼, 井ノ口仁一 *

Sphingomyelin Microdomains Negatively Regulate T Cell Receptor-Mediated
Activation in Human Jurkat T Cells

Masakazu NAGAFUKU,¹ Kaoru TOSHIMA,¹ Jun HORIUCHI, and Jin-ichi INOKUCHI *

Division of Glycopathology, Institute of Molecular Biomembrane and Glycobiology,
Faculty of Pharmaceutical Sciences, Tohoku Medical and Pharmaceutical University.

(Received November 20, 2018)

Sphingolipids, including sphingomyelin (SM) and glycosphingolipids (GSLs), associate with cholesterol to form membrane lipid microdomains in which specific receptors and signaling molecules are localized or recruited to mediate intracellular signaling. During T-cell activation, T cell antigen receptor (TCR) signaling clusters are formed in membrane lipid microdomains. In this study, we investigated the role of individual lipid microdomains constructed from SM and GSLs on TCR signaling. SM synthase 1 (SMS1) is primarily responsible for SM synthesis; glucosylceramide synthase (GlcCerS) is the enzyme responsible for the synthesis of GlcCer, which is the precursor for more complex GSLs such as gangliosides. We established SMS1 mutant and GlcCerS mutant Jurkat cells using the CRISPR/Cas9 system. In SMS1 mutant cells, SM-microdomain levels on the cell surface were nearly deficient, although cellular SM levels decreased by half compared with Jurkat cells. GlcCerS mutant cells did not express any kind of GSLs, while Jurkat cells expressed GlcCer and a-series gangliosides (such as GM3, GM2, GM1 and GD1a). We then examined the phosphorylation of ZAP-70 (a TCR-proximal kinase), intracellular calcium mobilization, and the expression of CD69 (an early activation marker of T cells) by TCR stimulation in the mutant cells; all these TCR-induced signaling events were greatly enhanced in SMS1 mutant cells, but not in GlcCerS mutant cells. The enhanced response to TCR stimulation in SMS1 mutant cells were restored by reintroduction of SMS1 gene. These findings indicate that SM-microdomains acts negative regulators of TCR signal transduction.

Key words — sphingomyelin, glycosphingolipid, lipid microdomain, lipid raft, TCR signaling

緒 論

スフィンゴ脂質に分類されるスフィンゴミエリン (sphingomyelin, SM) やスフィンゴ糖脂質 (glycosphingolipid, GSL) は、哺乳類細胞においてそのほとんどが形質膜二重層の外層に存在している。それらは形質膜上でコレステロールと共に特殊な微小領域 (“脂質マイクロドメイン”あるいは“脂質ラフト”と呼ばれる) を形成すると考えられている。^{1,2)} SM は形質膜に最も多く存在するスフィンゴ脂質であり、セラミドから SM 合成酵素 (SM synthase, SMS) によって合成される。de novo の SM 合成には 2 種類の SMS (SMS1, SMS2) が関与

している。SMS1 はゴルジ体に局在して SM の主たる生合成を担うのに対し、SMS2 はゴルジ体の他に形質膜にも存在して膜上でセラミドと SM の間の交換反応に関与するとされる。^{3,4)} 一方、GSL もセラミドを起点とし、種々の糖転移酵素によって数百に及ぶ分子種を形成する。セラミドからグルコシルセラミド合成酵素 (glucosylceramide synthase, GlcCerS) によって GlcCer が合成され、そこからラクトシルセラミド (lactosylceramide, LacCer) やガングリオシドなど多様な GSL 分子群が生合成される (Fig. 1A)。

脂質マイクロドメインには膜受容体やシグナル伝達分子が恒常的あるいはリガンド刺激依存的に集積し、そこは受容体シグナル伝達などの場として機能している。^{1,5,8)} T 細胞においても脂質マイクロドメインは T 細胞抗原受容体 (T cell receptor, TCR) シグナル伝達に重要な役割を持つと考えら

東北医科薬科大学薬学部分子生体膜研究所機能病態分子学教室

*e-mail: jin@tohoku-mpu.ac.jp

¹ 共同筆頭著者

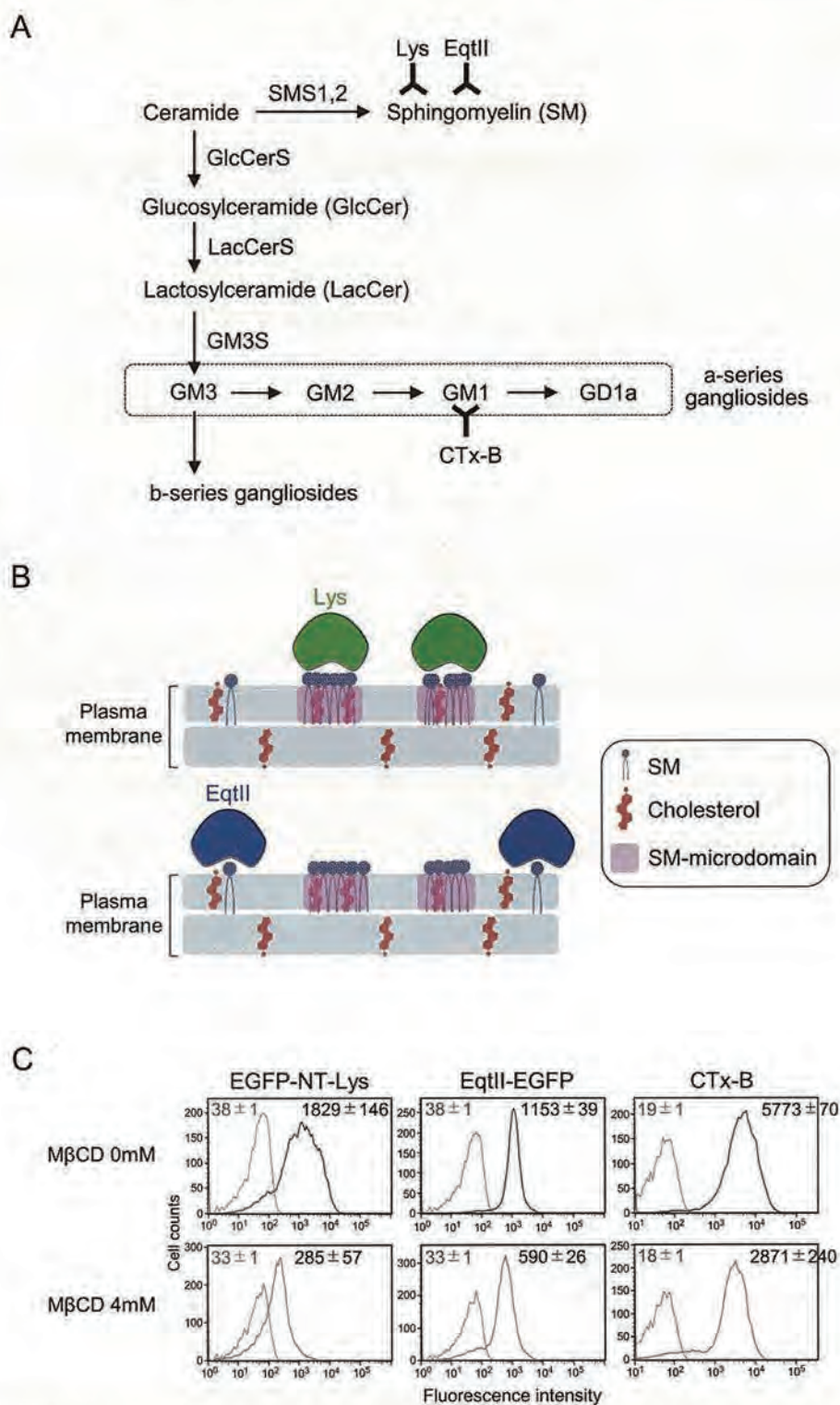


Fig. 1. Lys is a probe for SM-enriched membrane microdomains on the cell surface. (A) SM and GSL biosynthetic pathways. SM is synthesized by SM synthases (SMS1, SMS2), which transfer phosphorylcholine moiety onto ceramide. GSLs, including gangliosides, are also enzymatically synthesized from ceramide. Gangliosides are subclassified as a- and b-series gangliosides. Both lysenin (Lys) and equinatoxin II (EqtII) target SM but they have differing binding modes, as described in Methods and Figure 1B. Cholera toxin B subunit (CTx-B) targets a-series GM1. GlcCerS: glucosylceramide synthase. LacCerS: lactosylceramide synthase. GM3S: GM3 synthase. (B) Schematic representation of SM recognition modes by Lys and EqtII (refs 20, 21). Lys specifically binds clusters composed of 5-6 SM molecules, which are regarded as SM-microdomains present in plasma membrane. EqtII binds preferentially to single SM molecules, which are regarded as dispersed in plasma membrane. (C) Effect of lipid raft disruption on the lipid probe binding to the cell surface. Jurkat cells were untreated (0 mM) or treated with the MβCD (4 mM), and stained with EGFP-NT-Lys (left panels), EqtII-EGFP (middle panels) and CF640R-conjugated CTx-B (right panels). Each number indicates the MFI ± SD of triplicate assays. Black and red lines: with staining. Light gray lines: without staining.

れている。実際、膜からコレステロールを除去する薬剤 methyl- β -cyclodextrin (M β CD) を T 細胞に添加すると、形質膜のコレステロールが減少して脂質マイクロドメインは破壊され、TCR シグナル伝達に影響が及ぶことが知られている。^{9,10)} この10年余りの間に、脂質マイクロドメイン構成脂質 (SM, GSL) の分子種ごとに多様なドメインが存在するという知見が続いている。藤本らは、マウス繊維芽細胞の界面活性剤処理凍結割断レプリカを作製して形質膜を免疫染色することにより、GM1 と GM3 とがそれぞれ異なった脂質マイクロドメインを形成すると報告している。¹¹⁾ また、好中球では LacCer で構成されるマイクロドメインが存在してその機能に重要な役割を果たす。^{12,13)} T 細胞では、TCR 刺激に伴い形成される TCR 活性化ドメインは SM やコレステロールを含むマイクロドメインであるという報告がされた。¹⁴⁾ このように、細胞の種類あるいは活性化状態などに応じて、ある特定のスフィンゴ脂質で構成された脂質マイクロドメインが機能すると考えられている。

これまでに我々は、マウスの未熟 T 細胞 (胸腺細胞) の分化過程において、SM 発現量は分化に伴って大きく変動し、それは *SMS1* mRNA の発現と相関することを見いだした。¹⁵⁾ さらに、*SMS1* 欠損マウスの胸腺細胞では TCR 刺激に伴う細胞内シグナル伝達が増強し、強い刺激依存的な細胞死である負の選択が亢進していた。しかし、ヒト T 細胞白血病株である Jurkat 細胞の *SMS1* 遺伝子の発現をノックダウンした実験では、細胞の SM 量の2割減少で SM マイクロドメインは消滅するのに付随して、TCR シグナル伝達が増強することが報告されている。¹⁶⁾ 一方、*GlcCerS* の T 細胞特異的欠損マウスでは通常の T 細胞分化には影響がないことが示されている。¹⁷⁾ また、*GlcCerS* 阻害剤 D-threo-1-phenyl-2-decanoylamino-3-morpholino-1-propanol (D-PDMP) 処理によって Jurkat 細胞の GSL 量を 90%低下させた場合でも TCR シグナル伝達に影響はなかった。¹⁸⁾ 以上より、マイクロドメイン構成脂質の中で SM が T 細胞の分化・活性化および TCR シグナル伝達に関与すると考えられるが、TCR シグナル伝達における脂質マイクロドメインの機能には議論の余地がある。

そこで本研究では、SM マイクロドメインが TCR シグナル伝達および T 細胞の活性化に対して抑制的と促進的のどちらに寄与するかを再検証す

るとともに、GSL マイクロドメインとの比較を行った。そのために、CRISPR/Cas9 システムを用いて、Jurkat 細胞の *SMS1* および *GlcCerS* 遺伝子に変異を導入して、それぞれ SM および GSLs の欠損細胞の作製を試みた。その結果、親株の Jurkat 細胞と比べて *SMS1* 変異導入細胞では、SM 発現は約半分の低下であったが、このとき SM マイクロドメインはほとんど消失していた。*GlcCerS* 変異導入細胞では *GlcCer* やガングリオシド発現が欠損していた。*SMS1* 変異細胞で特異的に TCR 刺激に伴う細胞内シグナルおよび T 細胞活性化が総じて増強されていることが判明した。先のマウスでの結果と合わせて、SM マイクロドメインは TCR シグナル伝達を負に制御することにより、適切な強さのシグナル伝達の誘導に寄与するものと考えられる。

実験材料および実験方法

細胞培養

Jurkat 細胞 (クローン E6.1) は、最終濃度 10% (v/v) 非働化牛胎児血清 (fetal bovine serum, FBS)、2-メルカプトエタノール (50 μ M)、ペニシリン (100 U/mL) およびストレプトマイシン (100 μ g/mL) を添加した RPMI 1640 培地 (ナカライテスク社) を用いて 37°C、5% CO₂ 条件下で培養した。¹⁸⁾ FBS には SM が含まれているため、Jurkat 変異細胞樹立後、親株 Jurkat 細胞も含めてすべての細胞を SM 不含有の無血清培地 AIM-V (Invitrogen 社) を用いて培養した。

形質膜 SM の検出

形質膜上の SM の存在状態を明らかにするため、シマミズ由来のライセニン (lysenin, Lys) およびウメボシイソギンチャク由来のエキナトキシン II (equinatoxin II, EqtII) の2種類の SM 結合性タンパク質毒素を用いた。¹⁹⁾ これら2つの毒素は形質膜上の SM を特異的に認識し、膜に孔を形成することで毒性を示すが、認識する SM の存在形態がそれぞれ異なる (Fig. 1B)。^{20,21)} Lys は 5-6 分子の SM がクラスター化している状態 (SM マイクロドメインとみなされる構造) でのみ SM に結合することができる。一方、EqtII は 1 分子単位の分散した SM を優位に認識して結合する。N 末端のアミノ酸 161-297 残基のみの無毒性型 Lys (NT-Lys) に緑色蛍光タンパク質 EGFP を融合させた EGFP-NT-Lys のコンストラクトである pQE30/His6-

EGFP-NT-Lys は既に報告した通りに用意した。²²⁾ EqtII の C 末端に EGFP を融合した EqtII-EGFP のコンストラクトである pET28/EqtII (8-69)-EGFP-His6 は理化学研究所バイオリソース研究センターより供与された。これらの SM 結合性プローブは既報の方法により精製した。²³⁾ EqtII の溶血活性を阻害するため、EqtII-EGFP を 0.5 mM 1,10-フェナントロリン酸溶液と 0.1 mM 硫酸銅水溶液で 30°C, 1 時間インキュベートすることによって、Cys8 と Cys69 に分子内ジスルフィド結合を形成させた。²⁴⁾ **FACS による細胞表面脂質の検出**

細胞表面 SM の検出のため前述の EGFP-NT-Lys または EqtII-EGFP を用いた。細胞表面ガングリオシド GM1 の検出のため、フルオレセインイソチオシアネート (fluorescein isothiocyanate, FITC) 標識 (Sigma 社) あるいは CF640R 標識 (Invitrogen 社) のコレラトキシン B サブユニット (cholera toxin B subunit, CTx-B) を用いた。CTx-B は膜上での GM1 の存在状態に依存せず GM1 に結合すると考えられている。²⁵⁾ Jurkat 細胞をリン酸緩衝生理食塩水 PBS で洗浄した後、EGFP-NT-Lys, EqtII-EGFP および FITC 標識 CTx-B を用いて細胞を染色した。細胞表面セラミド発現は、細胞を 4%パラホルムアルデヒドにて室温で 15 分間固定し、0.1%ウシ血清アルブミン (bovine serum albumin, BSA) 含 PBS にて室温で 15 分間ブロッキングをし、10%正常ヤギ血清含 PBS に抗セラミド抗体 (マウス IgM, Enzo Life Sciences 社) あるいはコントロールマウス IgM を加えた染色液にて 37°C で 1 時間インキュベートし、10%正常ヤギ血清含 PBS にフィコエリスリン (phycoerythrin, PE) 標識ヤギ抗マウス IgM 抗体にて室温で 1 時間インキュベートした後、FACS [FACS AriaII (BD Biosciences 社) あるいは Attune NxT Flow Cytometer (Thermo Fisher Scientific 社)] にてデータを採取し、FlowJo ソフトウェア (Tree Star 社) を用いて解析した。

Methyl- β -cyclodextrin (M β CD) 処理

M β CD はコレステロールをキレートして膜から除去する薬剤であり、マイクロドメインの破壊のために広く利用されている。Jurkat 細胞への M β CD 処理は既報に従った。⁹⁾ 細胞を RPMI 1640 培地のみあるいは 4 mM M β CD (Sigma 社) を含む RPMI 1640 培地にて 37°C で 40 分間インキュベートした後、EGFP-NT-Lys, EqtII-EGFP または FITC 標識

CTx-B にて標識して、FACS 解析を行った。

CRISPR/Cas9 システムを用いた遺伝子変異 Jurkat 細胞の樹立

CRISPR/Cas9 システムを用いた SMSI および *GlcCerS* 変異 Jurkat 細胞の作製は既報に従った。²⁶⁾ CRISPR デザインツールを用いて、オフターゲット効果の可能性が低いガイドオリゴを設計した。²⁷⁾ ガイドオリゴの配列は以下の通り。SMSI (センス鎖, 5'-CACCGCTTCATTATTCTTCGCAGT-3'; アンチセンス鎖, 5'-AAACACTGCGAAGAATAATGAAGC-3'), *GlcCerS* (センス鎖, 5'-CACCGAAGAGGACGAACCCGAAGA-3'; アンチセンス鎖, 5'-AAACTCTTCGGTTCGTCCTCTTC-3')。ガイドオリゴを pSpCas9(BB)-2A-GFP(PX458) プラスミドに導入した。Amaza Human T Cell Nucleofector Kit と Nucleofector I Device (Lonza 社) を用いて、Jurkat 細胞にプラスミドを導入した。本プラスミドには GFP が含まれているため、遺伝子導入の 2 日後、GFP 陽性 Jurkat 細胞を遺伝子導入に成功した細胞として FACS AriaII を用いてソートした。

SMSI 変異 Jurkat 細胞および *GlcCerS* 変異 Jurkat 細胞の樹立

一過性の GFP 発現が消失するまでソートした細胞を数日間培養した後、変異細胞の樹立を行った。SMSI 変異細胞の樹立のため、溶血活性を有する全長の Lys (400 ng/ml, ペプチド研究所) にて細胞を処理することにより、SM マイクロドメインを発現する細胞を除去した。Lys 処理後、生き残った細胞を SMSI 変異細胞とした。このとき、Jurkat 細胞に Lys 処理を行うとすべて死滅することを確認している (データ非表示)。*GlcCerS* 変異 Jurkat 細胞の樹立のため、細胞を FITC 標識 CTx-B で標識し、FITC 陰性の細胞集団を *GlcCerS* 変異 Jurkat 細胞として FACS AriaII で再ソートした。Jurkat 細胞および各変異細胞の TCR 発現レベルが均一であることを、PE/Cy7 標識抗 TCR α/β 抗体 (BioLegend 社) にて細胞を染色して FACS 解析にて確認した。

ヒト SMSI 遺伝子のクローニングおよび SMSI 遺伝子再構成細胞の樹立

レンチウイルス発現用ベクターの作製およびレンチウイルスの調製は既報に従った。²⁸⁾ ヒト SMSI のオープンリーディングフレームを Jurkat 細胞の cDNA より増幅した。増幅産物を pGEM-T Easy ベ

クター (Promega 社) に組み込み pKT1 を作製した。pKT1 を鋳型とし、プライマー (5'-CACCATGAAGGAAGTGGTTTATTGGTCACC-3', 5'-TTATGTGTCATTCACCAGCCGGCTG-3') で増幅した産物を pENTR/D-TOPO ベクター (Life Technologies 社) に組み込み、pKT2 を作製した。レンチウイルス作製のため、Gateway vector conversion system (Life Technologies 社) を用いて、pKT2 の SMS1 配列をレンチウイルス発現ベクター CSII-CMV-RfA に LR クロナーゼ反応により導入し、pKT4 (SMS1/CSII-CMV-RfA) を作製した。HEK293T 細胞に Lipofectamine 2000 を用いて pKT4 あるいは CSII-CMV-RfA (mock) を遺伝子導入した。16 時間培養後、フォルスコリン (10 μ M) を添加した高グルコース DMEM 培地に培地交換し、37°C で 24 時間培養し、32°C に移しさらに 24 時間培養した後、ウイルスを含む上清を回収した。Jurkat 細胞および各変異 Jurkat 細胞を DMEM/RPMI 1640=1/1 の培地で 37°C、24 時間培養後、ウイルス含有培地に交換して 32°C で 1 日培養し、通常の RPIM 1640 に培地交換して 32°C で 1 日培養した後、37°C に移した。Lys, EqtII 染色と FACS 解析によって、SMS1 遺伝子再構成細胞の樹立を確認した。

薄層クロマトグラフィー (thin-layer chromatography, TLC) による脂質解析

Jurkat 細胞の脂質解析方法は既報の通りである。^{18,29)} クロロホルム/メタノールを用いて細胞の総脂質を抽出し、DEAE-Sephadex A-25 カラム (GE Healthcare 社) を用いて中性脂質画分と酸性脂質画分とに分離した。各画分を窒素乾固した後、0.1 M 水酸化ナトリウム含メタノール溶液を加えて 37°C で 2 時間アルカリ加水分解をすることにより、グリセリン脂質を除去した。中和後、Sep-Pak C18 (Waters 社) を用いて脱塩処理を行った。中性および酸性の脂質画分を TLC 用シリカゲルプレートにスポットした。中性脂質画分のプレートは、クロロホルム/メタノール/水 (60:25:4) にてプレートの下半分まで展開し、乾燥させた後、SM の解析のために 1-ブタノール/酢酸/水 (3:1:1)、中性スフィンゴ脂質全体の解析のためヘキサン/ジエチルエーテル/酢酸 (50:50:1) にて再度展開した。酸性脂質画分のプレートはクロロホルム/メタノール/0.2%塩化カルシウム水溶液 (55:45:10) にて展開した。SM の検出のためリン酸基を含む脂質で青

色を呈する Dittmer 試薬をプレートに噴霧した。³⁰⁾ すべての脂質の検出のため銅リン酸試薬を噴霧した後、180°C で発色するまで加熱した。スフィンゴ糖脂質の検出のため糖を検出するオルシノール硫酸液を噴霧した後、110°C で発色するまで加熱した。発色後のプレートの画像をスキャナーで取り込んで、ImageJ を用いてデンシティーを計測した。

TCR 刺激後の ZAP-70 リン酸化

TCR 刺激には TCR 複合体の構成分子である CD3 ϵ に対する刺激抗体 (クローン OKT3, BioLegend 社) を用いた。細胞を抗 CD3 ϵ 抗体 (3 μ g/ml) にて 37°C で 5 分間刺激した。その後、4%パラホルムアルデヒドによる固定、90%メタノールによる膜透過処理、および 0.1% BSA によるブロッキングを行った後、アロフィコシアニン (allophycocyanin, APC) 標識抗リン酸化 ZAP-70 (Y319) および FITC 標識抗 ZAP-70 抗体 (BioLegend 社) を用いて細胞内染色を行った。蛍光標識アイソタイプコントロール抗体をネガティブコントロールとして用いた。標識した細胞を FACS 解析した。得られた平均蛍光強度 (MFI) から以下の式を用いて、細胞間における ZAP-70 のリン酸化の比較を行った。

(“APC 標識抗 ZAP-70 抗体の MFI” - “APC 標識コントロール抗体の MFI”) / (“FITC 標識抗 ZAP-70 抗体の MFI” - “FITC 標識コントロール抗体の MFI”)

TCR 刺激後の細胞内 Ca²⁺ 応答の測定

Fluo-4 Calcium Assay Kit (Molecular Probes 社) を用い、製品に添付のプロトコルに従って行った。Ca²⁺ インジケータ Fluo-4 を含む溶液にて細胞を 37°C で 40 分間インキュベートした。FACS AriaII を用いて定常状態の Ca²⁺ レベルを 15 秒間測定し、それを蛍光のベースラインとして設定した後、CD3 抗体 (3 μ g/mL) を加え、引き続き 360 秒間測定を継続した。FlowJo ソフトウェアを用いて、刺激後における細胞内 Ca²⁺ のピークの蛍光値 (Peak) および AUC (area under the curve, 毎秒のカルシウム応答の平均値を結んでカーブを描いたときのカーブより下の部分の面積) を算出した。

TCR 刺激後の T 細胞活性化マーカー CD69 発現量

抗 CD3 抗体 (1 μ g/ml) を固相化した培養プレートに細胞を播種した。また、TCR をバイパスして細胞を直接刺激することで知られるホルボールエステル Phorboll2-myristate13-acetate (PMA,

100 ng/ml) による刺激も行った. いずれも 37°C で 18 時間培養した. 細胞を回収し, APC 標識抗 CD69 抗体 (BioLegend 社) にて標識して FACS 解析を行った.

統計処理

実験結果はいずれも平均値と標準偏差で示した. 2 群間の比較には t -検定を, 多群間の比較には Tukey-Kramer 法を用いた. 危険率 5% 以下を有意差ありとして判定した. なお, 危険率に関しては, * $p < 0.05$, ** $p < 0.01$, *** $p < 0.001$ で示した.

結 果

SMS1 変異および *GlcCerS* 変異導入 Jurkat 細胞におけるスフィンゴ脂質の発現

形質膜において, SM や GSL はコレステロール

の存在下でその物理化学的性質により自発的に脂質マイクロドメインを形成するが, ドメインは安定的ではなく可逆的に形成と分散とを繰り返している. 小林らのグループは, Lys と EqtII を用いてドメイン化した SM と分散した SM とが識別できることを示している (Fig. 2A) (“実験材料および実験方法” 参照).¹⁹⁾ 我々はこのことを Jurkat 細胞において確認するため, M β CD によりマイクロドメインを破壊したときの Lys および EqtII の結合能を解析した (Fig. 1C). Jurkat 細胞を 4 mM M β CD にて処理すると EGFP-NT-Lys の結合は未処理の約 10% まで低下していたが, EqtII-EGFP および CTx-B の結合は半分程度が維持されていた. M β CD 処理により Lys の結合が 90% 近く抑制されたということは, Jurkat 細胞においても Lys を用いることで SM マイクロドメインを選択的に検出

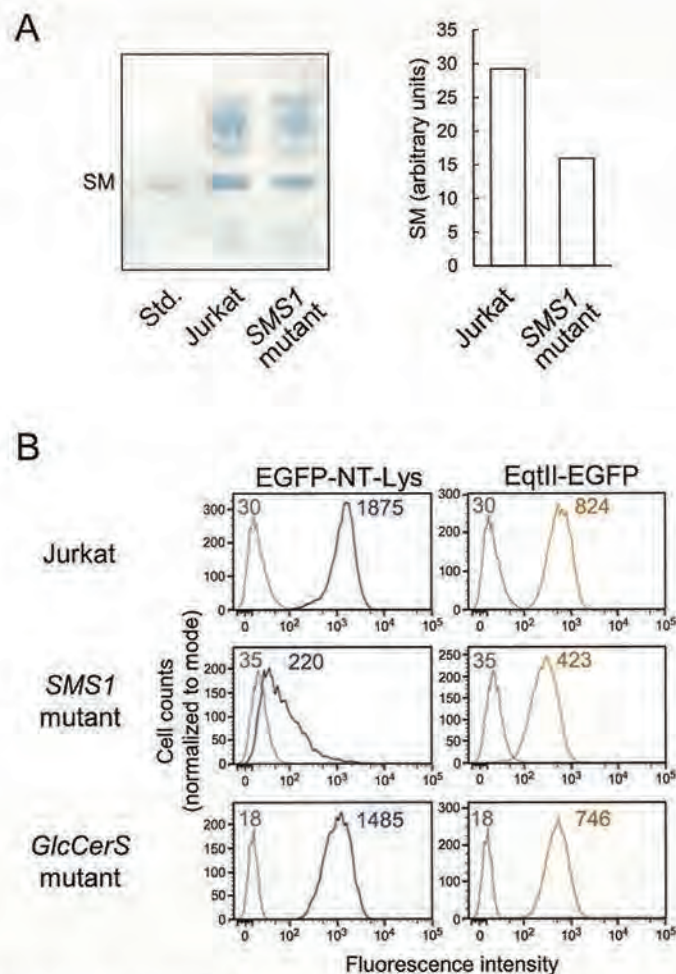


Fig. 2. SM-microdomain levels were reduced in SMS1 mutant Jurkat cells. (A) Total SM expression. Neutral lipids purified from Jurkat cells and SMS1 mutant Jurkat cells were separated on TLC plates, and phosphorus-containing lipids such as SM was detected by Dittmer reagent. SM contents were determined by densitometric analysis using ImageJ software program. Std: standard SM. (B) Cell surface staining with EGFP-NT-Lys (left panels) and EqtII-EGFP (right panels). Cell counts are normalized to mode. Each number indicates MFI. Blue and orange lines: with staining. Light gray lines: without staining.

できることを示している。コレステロールはマイクロドメイン以外の形質膜にも存在し、M β CD によってコレステロールがキレートされる際には近傍の分子も引き抜かれる非特異的な作用が報告されていることから、分散した SM (Eq β II が認識) や GM1 (CTx-B が認識) にも多少影響が及んだものと考えられる。

T 細胞の活性化における脂質マイクロドメイン構成脂質の役割を解析するために、Jurkat 細胞の SM および GSL が欠損した細胞の作製を試みた。今回、Jurkat において SM 合成を担う SMS1 お

よび GSL 合成の初発段階 GlcCer の生合成を担う GlcCerS を標的とした、SMS1 変異導入 Jurkat 細胞の SM 発現を調べた。細胞全体の SM 量を TLC 解析により調べたところ、SMS1 変異細胞では Jurkat 細胞の約半分ほどに低下していた (Fig. 2A)。EGFP-NT-Lys と Eq β II-EGFP を用いた FACS 解析により形質膜上の SM マイクロドメインと分散した SM の発現量を調べた (Fig. 2B)。SMS1 変異細胞では、形質膜上の SM マイクロドメインの発現量 (EGFP-NT-Lys による検出量) は親株の Jurkat 細胞の約 12% にまで減少しており、これは M β CD

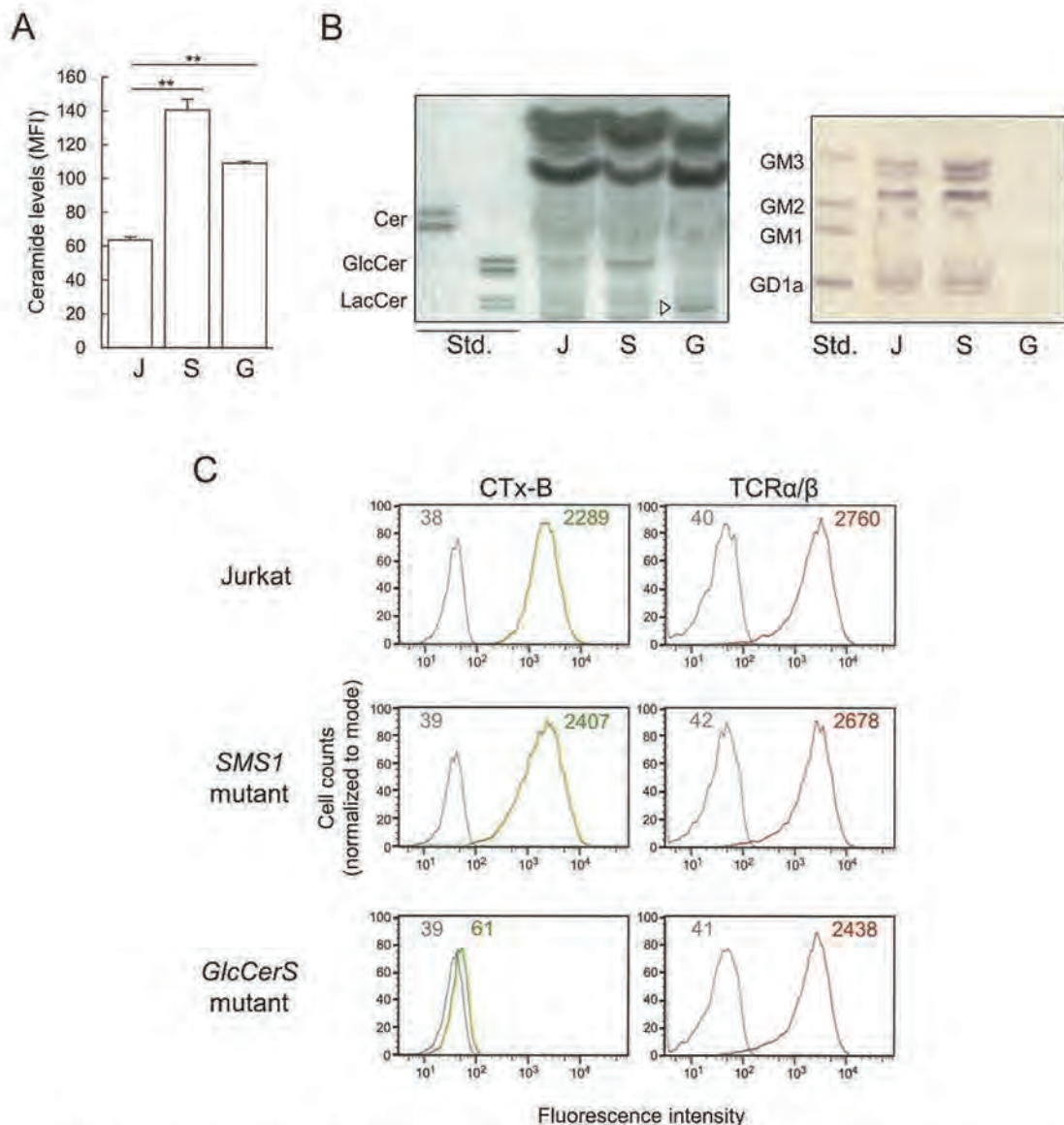


Fig. 3. Sphingolipid expression patterns were altered in mutant Jurkat cells. (A) Surface ceramide expression levels in Jurkat cells (J), SMS1 mutant cells (S), and GlcCerS mutant cells (G) analyzed by FACS. Values presented are MFI \pm SD of triplicate assays. ** $p < 0.01$. (B) Neutral sphingolipid fractions (left) or acidic GSL fractions (right) purified from Jurkat and the mutant cells were analyzed by TLC. All lipids were detected using cupric phosphate reagent (left) or sugar-containing lipids such as GSLs were detected using orcinol-sulfuric acid (right). The arrow head is an unknown band. Std: standard lipids. Cer: ceramide. GlcCer: glucosylceramide. LacCer: lactosylceramide. (C) Cell surface staining with FITC-conjugated CTx-B (left panels) and PE-conjugated TCR α/β (right panels). Cell counts are normalized to mode. Each number indicates MFI. Green and red lines: with staining. Light gray lines: without staining.

によるマイクロドメイン破壊のときと同程度の著しく減少であった (Fig. 1C, Fig. 2B). 一方, 分散したSMの発現量 (Eq2II-EGFPによる検出) 低下は約半分程度であった. 以上より, *SMS1* 変異細胞ではSMは発現するものの, マイクロドメインを形成するには不十分なレベルであることが判明した. *GlcCerS* 変異導入 Jurkat 細胞では, 形質膜上のSMマイクロドメインおよび分散したSMのどちらの発現量も *SMS1* 変異細胞で認めたような大きな変化は認められなかった.

セラミドはSMやGSLなどの前駆体である (Fig. 1A). FACS解析により形質膜上のセラミド発現量を解析したところ, いずれの変異導入細胞でも Jurkat 細胞に比べて有意に増加していた (Fig. 3A). Jurkat 細胞ではGSLの中でGlcCerおよびa系列 ganglioside (GM3, GM2, GD1a) の発現量が優位であることが知られている.¹⁸⁾ *SMS1* 変異細胞では, TLCを用いた脂質解析よりGlcCer, GM3およびGM2の増加が認められたが, GD1a量には変化がなかった (Fig. 3B). さらに, CTx-BのFACS解析よりGM1の発現に変化は認められなかった (Fig. 3C). *GlcCerS* 変異細胞では, GlcCer以下すべてのGSLの発現が欠損していた (Fig. 3B, C).

以上より, *SMS1* 変異細胞では, SMの半減により, 代償的に前駆物質 (セラミド) およびGSLの増加が起こっていることが判明した. 一方, *GlcCerS* 変異細胞ではセラミドの上昇は起こるが, SMマイクロドメインおよび分散したSMの発現量に変化はないことが判明した.

SMS1 変異 Jurkat 細胞では TCR シグナル伝達が増強する

T細胞の活性化はTCRを介した種々の細胞内シグナル伝達により生じる. TCR刺激に伴いTCRは脂質マイクロドメインに局在化し, そこに種々のシグナル伝達分子が動員されて, 十分な活性化が惹起される.³¹⁾ *SMS1* 変異細胞と *GlcCerS* 変異細胞を用いて, TCRシグナル伝達における脂質マイクロドメインの機能を解析した. はじめに, いずれの変異細胞でも形質膜上のTCR発現量にほとんど変化はないことを確認した (Fig. 3C).

ZAP-70はSyk型チロシンキナーゼの一種で, TCR刺激に伴いリン酸化を受けてTCR複合体に会合して活性化し, アダプタータンパク質LATのリン酸化を起こすことで下流のシグナル伝達分子

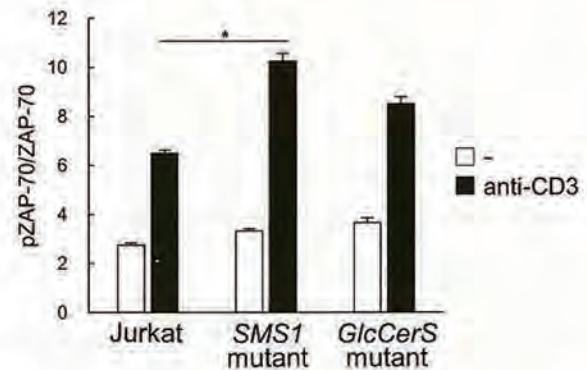


Fig. 4. ZAP-70 phosphorylation was increased in *SMS1* mutant Jurkat cells. Cells were unstimulated (-) or stimulated with anti-CD3 mAb for 5 min, and analyzed as described in Methods. Relative phosphorylation of ZAP-70 in stimulated cells was normalized relative to total ZAP-70 protein for each group. * $p < 0.05$.

をTCR直下に動員する.³²⁾ 抗CD3抗体によるTCR刺激を行った細胞におけるリン酸化ZAP-70 (pZAP-70) 量および総ZAP-70発現量をFACS解析し, そこで得られたMFIを用いて, “実験材料および実験方法”で示す方法でZAP-70のリン酸化の程度を比較した. *SMS1* 変異細胞ではJurkat細胞と比べてZAP-70のリン酸化が有意に増加していたが, *GlcCerS* 変異細胞ではリン酸化の程度に有意な変化は認められなかった (Fig. 4).

ZAP-70によるLATのリン酸化によりホスホリパーゼPLC γ 1が動員され, この活性により小胞体プールからのCa²⁺放出が誘導され細胞内Ca²⁺濃度が上昇する. Ca²⁺濃度上昇は, カルシニューリンの活性化, 転写因子NF-ATの核内移行を介してT細胞活性化に重要なサイトカインなどの転写に関与する.³¹⁾ Fig. 5Aのように, TCR刺激に伴う細胞内Ca²⁺濃度の上昇は刺激後数秒で認められ, 数分間持続することがわかっている.¹⁸⁾ このCa²⁺濃度の時間変化データを解析したところ, *SMS1* 変異細胞ではCa²⁺応答のピーク値 (Fig. 5B) およびCa²⁺上昇量 (Fig. 5C) の増強が認められた. 一方, *GlcCerS* 変異 Jurkat 細胞ではCa²⁺上昇量は有意に増加していたが, ピーク値に有意な差は認められなかった (Fig. 5B, C).

Ca²⁺シグナルとは別の経路として, ZAP-70活性化の下流ではMAPキナーゼ系の活性化も起こり, その結果としてCD69 (T細胞の早期活性化マーカー分子) の発現が誘導される. TCR依存的なCD69発現上昇においてJurkat細胞と各変異細胞

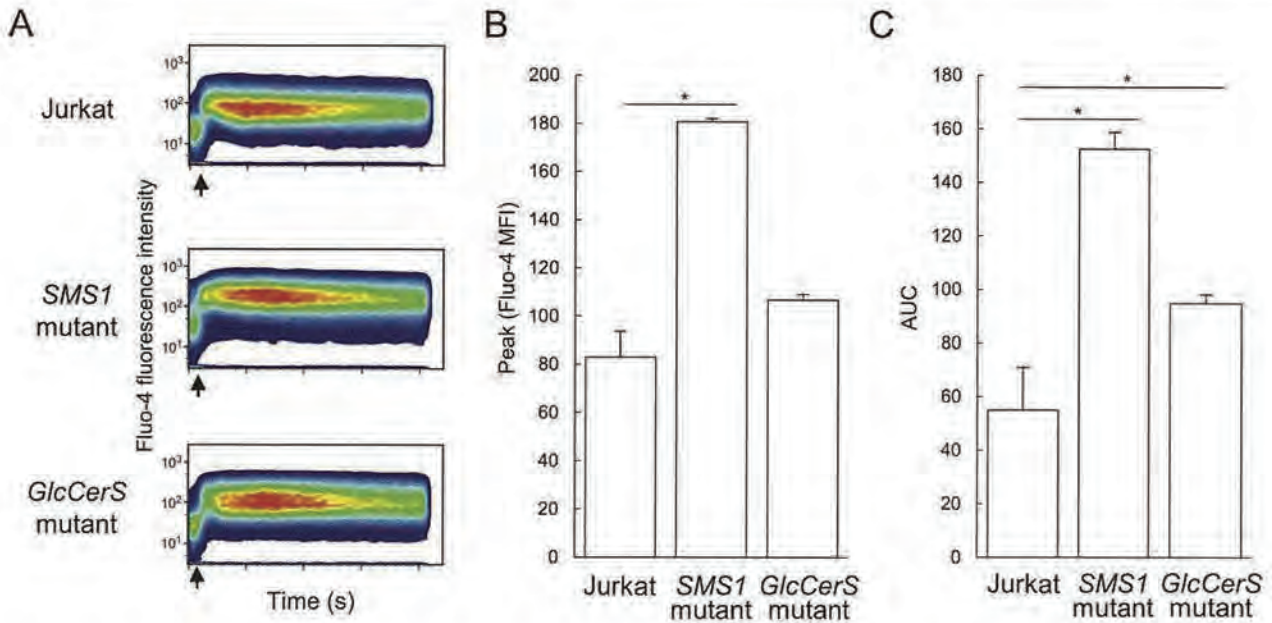


Fig. 5. *SMS1* mutant Jurkat cells exhibited increased Ca^{2+} influx. Cells were loaded with the calcium indicators Fluo-4, and intracellular Ca^{2+} levels were analyzed by FACS. (A) Ca^{2+} influx, represented by Fluo-4 intensity. Anti-CD3 mAb was added 15s after baseline acquisition (arrows). Plots shown are representative of three experiments with similar results. (B, C) Summary of experiments as peak increase of intracellular Ca^{2+} levels with respect to baseline (B) or as area under the curve (AUC) of the calcium response induced by anti-CD3 treatment (C). $n = 3$. $*p < 0.05$.

との間に違いがあるか否かを解析した。Jurkat 細胞と変異細胞を 1 対 1 で混和してプレートに播種することにより両細胞に同一の条件で TCR 刺激を行った。刺激後の細胞に CD69 と Lys あるいは CD69 と CTx-B の共染色を行って FACS によって解析した。Jurkat 細胞と *SMS1* 変異細胞の混合細胞の解析にあたっては、Lys の染色強度に基づいて強陽性と陰性~弱陽性とにゲーティングし、それぞれを Jurkat 細胞と変異細胞とみなして CD69 の発現量を調べた。また、Jurkat 細胞と *GlcCerS* 変異細胞の混合細胞では、CTx-B の染色強度に基づいて強陽性と陰性とにゲーティングして同様に解析した。その結果、*SMS1* 変異細胞では TCR 刺激に伴う CD69 発現の有意な上昇が認められたが、*GlcCerS* 変異細胞では有意な低下が認められた (Fig. 6)。このとき、TCR をバイパスして PKC-MAP キナーゼ経路を直接活性化する薬剤である PMA 刺激では、いずれの変異細胞も CD69 の発現量は Jurkat 細胞と同程度であった。

以上の TCR シグナル伝達の解析結果より、Jurkat 細胞の TCR シグナル伝達には SM マイクロドメインが強く関与しており、GSL が形成するマイクロドメインの寄与は小さいと考えられる。また、*SMS1* 変異細胞では TCR シグナル伝達が亢進する

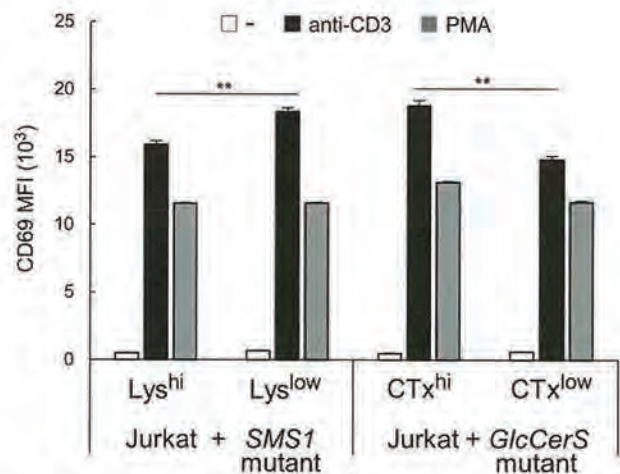


Fig. 6. TCR-induced CD69 expression was upregulated in *SMS1* mutant Jurkat cells. Jurkat cells were mixed with *SMS1* mutant cells or *GlcCerS* mutant cells in ratio 1 : 1, and cultured without (-) or with anti-CD3 mAb (1 $\mu\text{g}/\text{ml}$) or PMA (100 ng/ml) for 18 h. Cells were harvested, stained with APC-conjugated anti-CD69 mAb and lipid probes (EGFP-NT-Lys and CF640R-conjugated CTx-B), and analyzed by FACS. To distinguish mutant cells from Jurkat cells for quantification of CD69 MFI, cells were gated according to the staining intensity of lipid probes: Lys^{hi} and CTx^{hi} cells are Jurkat cells identified by the strong intensity of Lys and CTx staining, respectively, Lys^{low} cells are *SMS1* mutant cells with the weak intensity of Lys staining, and CTx^{low} cells are *GlcCerS* mutant cells with the weak intensity of CTx-B staining. Results were expressed as mean \pm SD of triplicate assays. $**p < 0.01$.

ことから, SM マイクロドメインには TCR シグナルを負に調節する役割があることが示唆される。

SMS1 遺伝子再構成 SMS1 変異 Jurkat 細胞では TCR シグナル伝達が回復する

CRISPR/Cas9 を用いた遺伝子変異導入にはオフターゲット効果が知られている。³³⁾ SMS1 変異細胞の表現型の原因として, TCR シグナルに関与する他の分子の遺伝子に変異が導入されたということも考えうる。そこで, その可能性を検討するために, TCR シグナルにおける SMS1 変異細胞の変化が SMS1 遺伝子の再導入によって回復するか否か解析したところ, SMS1 遺伝子導入 SMS1 変異細胞では Lys および EqtII 結合能が完全に回復した (Fig. 7)。そこで, TCR 刺激に伴う Ca^{2+} 応答を解析したところ, mock 導入 SMS1 変異細胞では, Fig. 6 同様, Ca^{2+} 応答が増強したのに対し, SMS1 遺伝子導入 SMS1 変異細胞では mock 導入 Jurkat 細胞と同程度にまで低下した (Fig. 8A, B)。次に, TCR 刺激後の CD69 発現上昇を解析したところ, mock 導入 SMS1 変異細胞では, Fig. 7 同様, CD69 発現上昇が著明に増強しているのに対し, SMS1 遺伝子導入 SMS1 変異細胞では mock 導入 Jurkat 細胞と同程度にまで低下した (Fig. 8C)。以上の結果より, SMS1 変異細胞における SM マイクロドメインの喪失と TCR シグナルの増強は SMS1 の変異によって生じていることが明らかとなった。

考 察

今回我々は, SM マイクロドメインまたは GSL マイクロドメインを欠損した変異 Jurkat 細胞を構築することによって, TCR 依存性の T 細胞活性化におけるマイクログドメイン構成脂質の役割を検討した。CRISPR/Cas9 システムを用いて Jurkat 細胞に SMS1 および *GlcCerS* の変異を導入した細胞を作製した。*GlcCerS* 変異細胞では GlcCer 以下の全ての GSL の発現が欠損していた (Fig. 3B, C)。一方, SMS1 変異細胞では SM 発現量は親細胞の約 5 割の低下であったにもかかわらず, 形質膜上の SM マイクロドメインの発現は M β CD 処理によるマイクログドメイン破壊と同レベルの著明な減少を示した (Fig. 2)。M β CD 処理により, マイクログドメインの破壊が起こり, TCR 刺激に伴うマイクログドメイン局在分子の集積が起こらないということが生化学的あるいは形態学的に示されていることから, SMS1 変異細胞において SM マイクロドメインはほとんど消失したと考えられる。実際, 既報の SMS1 ノックダウン細胞においても, SM の 2 割の低下で形質膜上の Lys 陽性の SM マイクロドメインは消失することが報告されている。¹⁶⁾ 形質膜における SM 密度の低下は形質膜の流動性および脂質の側方拡散速度を高めるので, 効率的な SM マイクロド

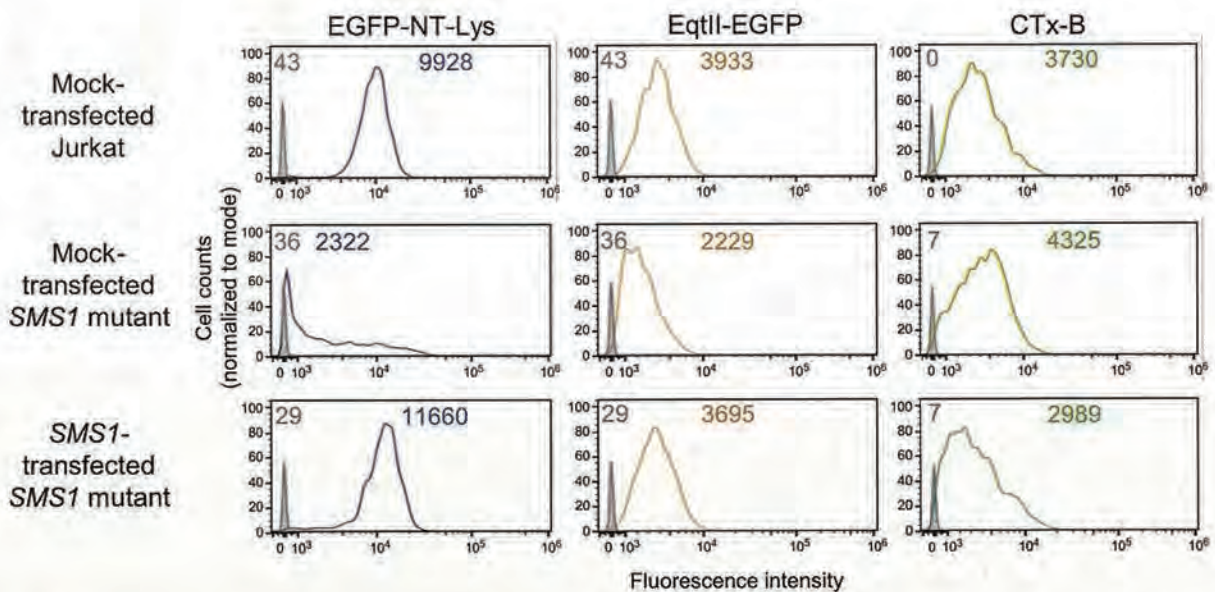


Fig. 7. SMS1 mutant Jurkat cells reconstituted with SMS1 gene completely restored SM-microdomain levels. Mock-transfected Jurkat cells and mock- or SMS1-transfected SMS1 mutant cells were stained with EGFP-NT-Lys (left panels), EqtII-EGFP (middle panels) and CF640R-conjugated CTx-B (right panels), and analyzed by FACS. Cell counts are normalized to mode. Each number indicates MFI. Blue, orange and green lines: with staining. Light gray lines: without staining.

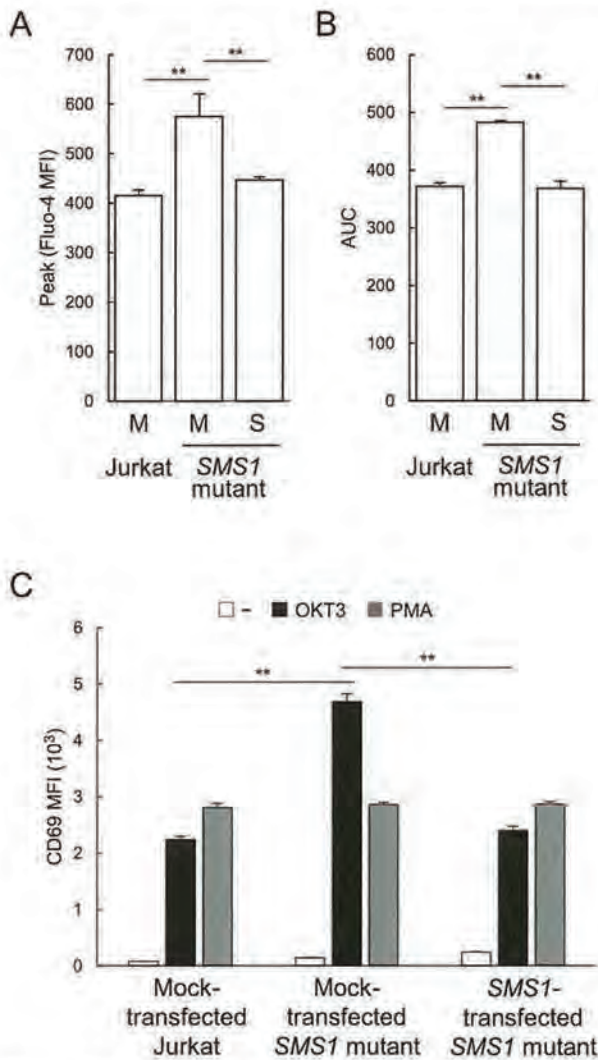


Fig. 8. Enhanced TCR signaling in *SMS1* mutant cells is reversed by reintroducing *SMS1* gene. (A, B) Ca^{2+} influx assay under similar conditions of Fig. 5. Summary of experiments as peak increase of intracellular Ca^{2+} levels with respect to baseline (A) or as area under the curve (AUC) of the calcium response induced by anti-CD3 treatment (B). M: mock-transfected, S: *SMS1*-transfected, n = 3. (C) Cells were cultured without (-) or with anti-CD3 mAb (1 $\mu\text{g}/\text{ml}$) or PMA (100 ng/ml) for 18 h, stained with APC-conjugated anti-CD69 mAb and analyzed by FACS. Results were expressed as mean \pm SD of triplicated assays. **p < 0.01.

メインの形成あるいはその維持にとって不都合であるのかもしれない。^{34,35)} 形質膜中のコレステロール量が20%程度減るだけでマイクロドメインは存在しなくなり、受容体シグナル伝達が抑制されることが報告されていることから、形質膜の脂質濃度はマイクロドメイン形成に重要な要素であることが窺える。^{36,37)} また、今回我々は、*SMS1*の酵素活性部位付近を標的として変異細胞の樹立を試みたが、SMそのものが完全に欠損した細胞を樹立

できなかった。花田らが樹立したCHO細胞(チャイニーズハムスター卵巣由来繊維芽細胞)のLys耐性変異株もLys結合性は喪失しているがSM発現は完全に欠損していない。³⁸⁾ また、2種類のSMS合成酵素(*SMS1*と*SMS2*)を同時に欠損させたマウス胎児由来繊維芽細胞ではSM合成能がほぼ欠損しており、ダブル欠損マウスは胎生致死のようである。^{39,40)} SMは哺乳類細胞におけるスフィンゴ脂質の約85%を占めていることも含めて考えると、SMが完全に欠損したJurkat細胞は細胞死を起こすか増殖能が極めて低いため、結果として*SMS1*酵素活性が低下した変異細胞が選択されてきたのかもしれない。*SMS1*変異細胞でSMが完全に欠損しない別の理由として、*SMS2*はJurkat細胞では発現していないとされているが、¹⁶⁾ この特殊な条件下で*SMS2*が代償的に発現しているのかもしれない。

また、どちらの変異細胞もセラミドの代償的な蓄積が認められた(Fig. 3A)。*SMS1*遺伝子変異または欠損によるセラミド量への影響は細胞株やマウスを用いて検討されているが、セラミドが増加するケースや不変なケースなどさまざまである。⁴¹⁾ SM分解酵素を介したセラミドの増加はアポトーシスの誘導に関与することが知られているが、⁴²⁾ 我々の変異細胞では細胞死が亢進することはなかった(データ非表示)。

TCR刺激に伴い、TCRは脂質マイクロドメインに局在化し、そこに種々のシグナル伝達分子がリクルートされる。ZAP-70キナーゼのリン酸化には脂質マイクロドメインの存在が重要であることが知られている。⁴³⁾ *SMS1*変異細胞ではZAP-70のリン酸化は亢進したが、*GlcCerS*変異細胞ではそれに有意な変化はなかった(Fig. 4)。スフィンゴ脂質の分子種ごとに多様な脂質マイクロドメインが存在するが、⁴⁴⁾ Jurkat細胞においてはGSLが形成するマイクロドメインよりもSMマイクロドメインの方がTCR近傍シグナルにとって重要であることが実証された。ZAP-70の活性化はその下流のTCRシグナル伝達に大きな影響を及ぼす。活性亢進型の変異ZAP-70遺伝子をJurkat細胞に導入すると、TCR刺激依存的に Ca^{2+} 応答やMAPキナーゼのERK活性化などが亢進するという報告がある。⁴⁵⁾ *SMS1*変異Jurkat細胞ではTCR刺激に伴い、 Ca^{2+} 応答が増強するとともに、ERK経路依存的に誘導される活性化マーカーCD69の発現も亢

進した (Fig. 5, Fig. 6). SM マイクロドメイン欠損における初期の TCR シグナル伝達 (ZAP-70 のリン酸化) の亢進は, 下流のシグナル伝達および T 細胞の活性化にまで影響していることが実証された。

既報の SMS1 遺伝子ノックダウンを利用した Jurkat 細胞の SM 発現抑制では, 今回の我々の結果と反して, TCR 刺激に伴う TCR シグナル伝達の低下が示された.¹⁶⁾ ただ, その実験では細胞培養の培地として FBS を添加したものを使用したが, 一般的に血清中にはリポタンパク質などに多量の SM が含まれているため, 培地由来の SM が細胞に取り込まれた可能性は高い。また, SMS1 ノックダウン Jurkat 細胞の実験ではモノクローン化が行われていることから, TCR シグナルの反応性が弱いクローンが選択されていたのかもしれない。我々の作製した SMS1 変異 Jurkat 細胞は, 無血清培地で継代および実験を行った。また, クローン化も行わず, 親株の Jurkat 細胞と TCR 発現量が変わらないことを確認して使用したため, Jurkat 細胞の平均的な TCR の反応性をみていると考えられる。さらに, 既報のノックダウン Jurkat 細胞では, 我々が実施したような SMS1 遺伝子の再導入の実験を行っていない。以上のように既報と我々の実験とでは異なる点が多いため比較は難しいと考えている。

SMS1 変異細胞に SMS1 遺伝子を再導入すると, SM マイクロドメイン発現量は完全に回復し, このとき Ca^{2+} 応答と CD69 発現が Jurkat 細胞レベルに低下した (Fig. 7, Fig. 8)。SMS1 変異細胞では代償的なセラミドや GSL の増加が確認されたことから, この細胞の表現型が SM マイクロドメイン欠損に起因するのか, 代償的なセラミドや GSL の増加に起因するのかを考察する必要がある。GlcCerS 変異細胞でもセラミドの有意な増加が起こるが, SMS1 変異細胞のような全般的な TCR シグナルの亢進は認められなかった。したがって, TCR シグナルの場として機能するマイクログドメインはセラミドによって構成されていないことが示唆される。

全身性エリテマトーデス (systemic lupus erythematosus, SLE) 患者の T 細胞では, 形質膜の GSL (特に, LacCer, GM1, グロボ系 GSL の Gb3) の発現増加が報告されている。SLE 患者由来 T 細胞に GlcCerS 阻害剤である *N*-butyldeoxy-nojirimycin (NB-DNJ) を処理することにより,

CTx-B 陽性ガングリオシド (GM1) と LacCer の発現量を健常人由来 T 細胞と同程度に戻すと, TCR シグナル伝達が回復するとともに炎症性サイトカインの産生が抑制される。⁴⁶⁾ これは過剰な GSL の発現が TCR シグナルに対して抑制的な効果があることを示している。我々は, SMS1 欠損マウスの胸腺未熟 T 細胞において SMS1 変異細胞と同様の傾向を示す結果を得ている。この胸腺細胞ではセラミドや GSL の増加はみられない。¹⁵⁾ 以上より, SM が形質膜上で特異的に TCR シグナルを抑制的に制御しているものと考えられる。

自己免疫疾患患者の T 細胞では, マイクロドメイン構成脂質の質的・量的な変化が起こることがいくつも報告されている。⁴⁷⁾ SLE 患者の T 細胞では, 形質膜のコレステロールや GSL が増加している。⁴⁶⁻⁴⁸⁾ SLE 患者由来 T 細胞では TCR 複合体を形成する CD3 ζ 鎖の発現低下により TCR シグナル伝達が低下しているが, これはコレステロール生合成阻害剤 (アトルバスタチン) を添加することによって回復する。⁴⁹⁻⁵¹⁾ T 細胞において形質膜のコレステロールが増加すると, TCR の膜上での流動性が低下した結果, TCR の活性化が抑制されるということが近年相次いで報告されている。⁵²⁻⁵⁴⁾ Jurkat 細胞では SM はコレステロールと共に TCR を含むマイクログドメインを形成することから,¹⁴⁾ コレステロールが増加している病態では SM マイクロドメイン発現量も増加し, TCR シグナル伝達の抑制に寄与している可能性がある。自己免疫疾患患者の T 細胞における SM 発現量はいまだ報告されていないが, 炎症が関与するような肥満病態では血清中の SM の質的变化 (脂肪酸のアシル鎖長の変化) が起きることが知られている。⁵⁵⁾ 今後, 正常人と自己免疫疾患患者のヒト T 細胞における SM マイクロドメインの質的・量的関係を解明することが肝要である。SM 発現を微調整することで TCR シグナル伝達を制御することができれば, T 細胞の機能異常に起因する自己免疫疾患の発症メカニズムの解明や新たな治療法の開発につながることを期待される。

謝辞 本研究を行うにあたり, CRISPR/Cas9 システムによる遺伝子変異導入細胞の樹立に多大なご協力を賜りました。東北医科薬科大学機能病態分子学教室の稲森啓一郎准教授, 宍戸史女史, 山本博之氏, 齋藤恵梨香女史, 南條真央女史, 高

橋沙織女史に深く感謝いたします。本研究は、文部科学省による科研費 16H04767 と水谷糖質科学振興財団、武田科学振興財団、長井記念薬学研究奨励支援、私立大学戦略的研究基盤形成支援事業の助成を受けて行われました。

利益相反

著者全てにおいて、開示すべき利益相反はありません。

REFERENCES

- 1) Rietveld A., Simons K., *Biochim. Biophys. Acta Rev. Biomembr.*, **1376**, 467–479 (1998).
- 2) Pike L. J., *J. Lipid Res.*, **47**, 1597–1598 (2006).
- 3) Huitema K., van den Dikkenberg J., Brouwers J. F. H. M., Holthuis J. C. M., *EMBO J.*, **23**, 33–44 (2004).
- 4) Yamaoka S., Miyaji M., Kitano T., Umehara H., Okazaki T., *J. Biol. Chem.*, **279**, 18688–18693 (2004).
- 5) Helms J. B., Zurzolo C., *Traffic*, **5**, 247–254 (2004).
- 6) Munro S., *Cell*, **115**, 377–388 (2003).
- 7) Mukherjee S., Maxfield F. R., *Annu. Rev. Cell Dev. Biol.*, **20**, 839–866 (2004).
- 8) Hancock J. F., *Nat. Rev. Mol. Cell Biol.*, **7**, 456–462 (2006).
- 9) Tanimura N., Nagafuku M., Minaki Y., Umeda Y., Hayashi F., Sakakura J., Kato A., Liddicoat D. R., Ogata M., Hamaoka T., Kosugi A., *J. Cell Biol.*, **160**, 125–135 (2003).
- 10) Kabouridis P. S., Janzen J., Magee A. L., Ley S. C., *Eur. J. Immunol.*, **30**, 954–963 (2000).
- 11) Fujita A., Cheng J., Hirakawa M., Furukawa K., Kusunoki S., Fujimoto T., *Mol. Biol. Cell*, **18**, 2112–2122 (2007).
- 12) Sato T., Iwabuchi K., Nagaoka I., Adachi Y., Ohno N., Tamura H., Seyama K., Fukuchi Y., Nakayama H., Yoshizaki F., Takamori K., Ogawa H., *J. Leukoc. Biol.*, **80**, 204–211 (2006).
- 13) Nakayama H., Yoshizaki F., Prinetti A., Sonnino S., Mauri L., Takamori K., Ogawa H., Iwabuchi K., *J. Leukoc. Biol.*, **83**, 728–741 (2008).
- 14) Zech T., Ejsing C. S., Gaus K., de Wet B., Shevchenko A., Simons K., Harder T., *EMBO J.*, **28**, 466–476 (2009).
- 15) Toshima K., Nagafuku M., Okazaki T., Kobayashi T., Inokuchi J., *Int. Immunol.*, (in revised)
- 16) Jin Z. X., Huang C. R., Dong L., Goda S., Kawanami T., Sawaki T., Sakai T., Tong X. P., Masaki Y., Fukushima T., Tanaka M., Mimori T., Tojo H., Bloom E. T., Okazaki T., Umehara H., *Int. Immunol.*, **20**, 1427–1437 (2008).
- 17) Popovic Z. V., Rabionet M., Jennemann R., Krunic D., Sandhoff R., Gröne H. J., Porubsky S., *Front. Immunol.*, **8**, 1–16 (2017).
- 18) Nagafuku M., Kabayama K., Oka D., Kato A., Tani-ichi S., Shimada Y., Ohno-Iwashita Y., Yamasaki S., Saito T., Iwabuchi K., Hamaoka T., Inokuchi J., Kosugi A., *J. Biol. Chem.*, **278**, 51920–51927 (2003).
- 19) Makino A., Abe M., Murate M., Inaba T., Yilmaz N., Hullin-Matsuda F., Kishimoto T., Schieber N. L., Taguchi T., Arai H., Anderluh G., Parton R. G., Kobayashi T., *FASEB J.*, **29**, 477–493 (2014).
- 20) Yamaji A., Sekizawa Y., Emoto K., Sakuraba H., Inoue K., Kobayashi H., Umeda M., *J. Biol. Chem.*, **273**, 5300–5306 (1998).
- 21) Ishitsuka R., Yamaji-Hasegawa A., Makino A., Hirabayashi Y., Kobayashi T., *Biophys. J.*, **86**, 296–307 (2004).
- 22) Abe M., Makino A., Hullin-Matsuda F., Kamiyo K., Ohno-Iwashita Y., Hanada K., Mizuno H., Miyawaki A., Kobayashi T., *Mol. Cell. Biol.*, **32**, 1396–407 (2012).
- 23) Abe M., Kobayashi T., *Methods Cell Biol.*, **137**, 15–24 (2017).
- 24) Hong Q., Gutiérrez-Aguirre I., Barli A., Malovrh P., Kristan K., Podlesek Z., Maek P., Turk D., González-Mañas J. M., Lakey J. H., Anderluh G., *J. Biol. Chem.*, **277**, 41916–41924 (2002).
- 25) Kiyokawa E., Baba T., Otsuka N., Makino A., Ohno S., Kobayashi T., *J. Biol. Chem.*, **280**, 24072–24084 (2005).
- 26) Inamori K., Ito H., Tamura Y., Nitta T., Yang X., Nihei W., Shishido F., Imazu S., Tsukita S., Yamada T., Katagiri H., Inokuchi J., *J. Lipid Res.*, **59**, 1472–1481 (2018).
- 27) Ran F. A., Hsu P. D., Wright J., Agarwala V., Scott D. A., Zhang F., *Nat. Protoc.*, **8**, 2281–2308 (2013).
- 28) Uemura S., Go S., Shishido F., Inokuchi J., *Glycoconj. J.*, **31**, 101–108 (2014).
- 29) Inokuchi J., Uemura S., Kabayama K., Igarashi Y.,

- Glycoconj. J.*, **17**, 239–245 (2000).
- 30) Dittmer J. C., Lester R. L., *J. Lipid Res.*, **5**, 126–127 (1964).
- 31) Horejsi V., Hrdinka M., *FEBS Lett.*, **588**, 2392–2397 (2014).
- 32) Gaud G., Lesourne R., Love P. E., *Nat. Rev. Immunol.*, 485–497 (2018).
- 33) Fu Y., Foden J. a., Khayter C., Maeder M. L., Reyon D., Joung K., Sander J. D., *Nat. Biotechnol.*, **31**, 822–826 (2013).
- 34) London E. *Biochim. Biophys. Acta - Mol. Cell Res.*, **1746**, 203–220 (2005).
- 35) Sengupta P., Baird B., Holowka D., *Semin. Cell Dev. Biol.*, **18**, 583–590 (2007).
- 36) Kusumi A., Fujiwara T. K., Morone N., Yoshida K. J., Chadda R., Xie M., Kasai R. S., Suzuki K. G. N., *Semin. Cell Dev. Biol.*, **23**, 126–144 (2012).
- 37) Kusumi A., Suzuki K. G. N., Kasai R. S., Ritchie K., Fujiwara T. K., *Trends Biochem. Sci.*, **36**, 604–615 (2011).
- 38) Hanada K., Hara T., Fukasawa M., Yamaji A., Umeda M., Nishijima M., *J. Biol. Chem.*, **273**, 33787–33794 (1998).
- 39) Mitsutake S., Zama K., Yokota H., Yoshida T., Tanaka M., Mitsui M., Ikawa M., Okabe M., Tanaka Y., Yamashita T., Takemoto H., Okazaki T., Watanabe K., Igarashi Y., *J. Biol. Chem.*, **286**, 28544–28555 (2011).
- 40) Hussain M. M., Jin W., Jiang X. C., *Nutr. Metab.*, **9**, 71–77 (2012).
- 41) Taniguchi M., Okazaki T., *Biochim. Biophys. Acta*, **1841**, 692–703 (2014).
- 42) Hannun Y. A., Obeid L. M., *Nat. Rev. Mol. Cell Biol.*, **9**, 139–150 (2008).
- 43) Dykstra M., Cherukuri A., Sohn H. W., Tzeng S.-J., Pierce S. K., *Annu. Rev. Immunol.*, **21**, 457–481 (2003).
- 44) Gómez-Mouton C., Abad J. L., Mira E., Lacalle R. A., Gallardo E., Jiménez-Baranda S., Illa I., Bernad A., Mañes S., Martínez-A C., *Proc. Natl. Acad. Sci. U. S. A.*, **98**, 9642–9647 (2001).
- 45) Deindl S., Kadlecsek T. A., Cao X., Kuriyan J., Weiss A., *Proc. Natl. Acad. Sci. U. S. A.*, **106**, 20699–20704 (2009).
- 46) McDonald G., Deepak S., Miguel L., Hall C. J., Isenberg D. A., Magee A. I., Butters T., Jury E. C., *J. Clin. Invest.*, **124**, 712–724 (2014).
- 47) Jury E. C., Flores-Borja F., Kabouridis P. S., *Semin. Cell Dev. Biol.*, **18**, 608–615 (2007).
- 48) Dong L., Hu S., Chen F., Lei X., Tu W., Yu Y., Yang L., Sun W., Yamaguchi T., Masaki Y., Umehara H., *J. Biomed. Biotechnol.*, **2010**, 931018 (2010).
- 49) Baniyash M., *Nat. Rev. Immunol.*, **4**, 675–687 (2004).
- 50) Liossis S. N., Ding X. Z., Dennis G. J., Tsokos G. C., *J. Clin. Invest.*, **101**, 1448–1457 (1998).
- 51) Jury E. C., Isenberg D. A., Mauri C., Ehrenstein M. R., *J. Immunol.*, **177**, 7416–7422 (2006).
- 52) Swamy M., Beck-Garcia K., Beck-Garcia E., Hartl F. A., Morath A., Yousefi O. S., Dopfer E. P., Molnár E., Schulze A. K., Blanco R., Borroto A., Martín-Blanco N., Alarcon B., Höfer T., Minguet S., Schamel W. W. A., *Immunity*, **44**, 1091–1101 (2016).
- 53) Molnár E., Swamy M., Holzer M., Beck-García K., Worch R., Thiele C., Guigas G., Boye K., Luescher I. F., Schwille P., Schubert R., Schamel W. W. A., *J. Biol. Chem.*, **287**, 42664–42674 (2012).
- 54) Wang F., Beck-García K., Zorzín C., Schamel W. W. A., Davis M. M., *Nat. Immunol.*, **17**, 844–850 (2016).
- 55) Hanamatsu H., Ohnishi S., Sakai S., Yuyama K., Mitsutake S., Takeda H., Hashino S., Igarashi Y., *Nutr. Diabetes*, **4**, e141–147 (2014).



Regulation of membrane raft recruitment of the bradykinin B2 receptor by close association with the ATP/UTP receptor P2Y₂

Tetsuto Nakagawa, Chihiro Takahashi, Hitomi Matsuzaki, Yoshiyuki Kuroda, Hideyoshi Higashi*

Division of Glyco-Signal Research, Institute of Molecular Biomembrane and Glycobiology, Tohoku Medical and Pharmaceutical University, Sendai, Miyagi, 981-8558, Japan

ARTICLE INFO

Article history:

Received 4 September 2018
Accepted 12 September 2018
Available online 17 September 2018

Keywords:

GPCR-GPCR interaction
Lipid rafts
N-linked glycosylation
B2 receptor
P2Y₂ receptor

ABSTRACT

Several G protein-coupled receptors are present in lipid rafts. We have shown that most of the P2Y₂ receptor (P2Y₂R) protein is fractionated into lipid rafts in COS 7 cells. In the same cells, about 25–30% of the bradykinin B2 receptor (B2R) protein is also fractionated into lipid rafts. When both P2Y₂R and B2R are co-expressed, the distribution of P2Y₂R remained unchanged, but more B2R shifted into the raft fraction. This indicates that the interaction between both receptors recruited B2R into the lipid rafts. After 15 min of UTP stimulation, both receptors almost completely disappeared from the cell surface by endocytosis as observed with a confocal fluorescence microscope. Furthermore, with bradykinin stimulation for 15 min, portions of both receptors disappeared from the cell surface and were endocytosed. As we reported previously with both CHO-K1 cells and HEK 293 cells, continuous stimulation of COS7 cells with GT1b and CSC resulted in the disappearance of both P2Y₂R and B2R from the cell membrane surface. Thus, both P2Y₂R and B2R migrate into membrane rafts and are endocytosed in parallel with signal crosstalk, clearly indicating that both closely interact on membrane rafts. The P2Y₂R N-glycosylation deficient mutant does not migrate to the cell surface. It remains predominantly in the endoplasmic reticulum and is fractionated into raft fractions. In the presence of this glycosylation mutant, most of B2R remains in the endoplasmic reticulum, and is fractionated into the raft fraction. These findings demonstrate that in the membrane rafts of the endoplasmic reticulum, both receptors are already closely associated, and B2R shifts into the rafts by affinity with P2Y₂R.

© 2018 Elsevier Inc. All rights reserved.

1. Introduction

P2Y₂R, which uses ATP/UTP as a ligand, and B2R, which uses bradykinin as a ligand, are G protein-coupled receptors (GPCRs). Both receptors are coupled with Gαq/11 and are involved in physiological functions, such as blood pressure reduction, inflammation, and pain. In our previous studies using both Ca²⁺ imaging and the β-galactosidase α-complementation assay, we showed that both receptors are associated closely in desensitization and internalization, are co-immunoprecipitated, and are involved in signal cross talk with each other [1].

A lipid raft, a membrane microdomain on the cell membrane, is rich in both sphingolipids and cholesterol. Lipid rafts have characteristic receptor proteins and signaling molecules and play

important roles in signal transduction through membranes, bacterial and viral infections, cell adhesion, intracellular vesicular trafficking, and intracellular polarity [2,3]. Experimentally, lipid rafts are insoluble in nonionic surfactants at low temperature, and thus can be distinguished from other membrane regions. We recently showed that most P2Y₂R molecules localize to lipid rafts in COS 7 cells [4]. On the other hand, B2R was distributed in both raft and non-raft fractions. Therefore, we examined whether the interaction between the two receptors affects their distribution into rafts. The co-endocytosis of both receptors was observed by immunofluorescence microscopy even when both molecules were separately stimulated.

2. Materials and methods

Preparation of Plasmids. Plasmids encoding human P2Y₂R and human short variant B2R, starting at the third initiating ATG were

* Corresponding author.

E-mail address: hhigashi@tohoku-mpu.ac.jp (H. Higashi).

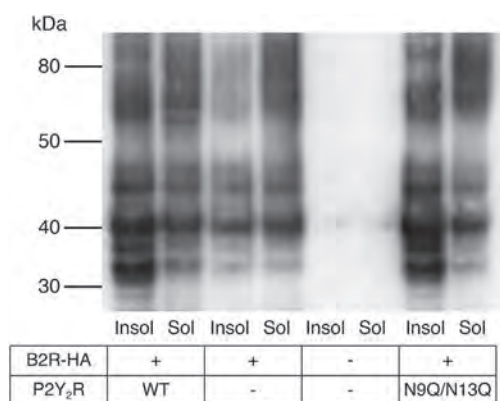


Fig. 1. Effects of co-expression on B2R distribution in the lipid raft fraction of both wild type (WT) and *N*-linked sugar chain-deficient mutant P2Y₂R (N9Q/N13Q). HA-tagged B2R was expressed either alone or with P2Y₂R, and the detergent insoluble (Insol) membrane fraction and the detergent soluble (Sol) membrane fraction were analyzed by Western blotting using an anti-HA antibody.

prepared by insertion of each cDNA between the EcoRI and BamHI sites of pIRES2-EGFP (Clontech). The *N*-glycan deficient N9Q/N13Q P2Y₂R mutant was prepared as described previously [4]. Human P2Y₂R genes with a C-terminal c-Myc epitope tag and human B2R genes with a C-terminal HA epitope tag were prepared as described previously [1,4].

Cell culture. COS-7 cells were grown in D-MEM supplemented with 10% fetal calf serum and kept in a humidified incubator with 5% CO₂ at 37 °C. COS-7 cells were transiently transfected using Viafect transfection reagent (Promega).

SDS-PAGE and Western blotting. Membrane fractions and protein samples for SDS-PAGE was prepared as described previously [4]. SDS-PAGE was performed using the Novex NuPAGE SDS-Gel system with 4–12% Bis-Tris gels (Thermo Fisher Scientific), and proteins were electrophoretically transferred to an Immobilon PVDF membrane (Merck Millipore) using a semi-dry blotting system. After blocking with 5% skim milk in PBS, P2Y₂R-Myc was stained using anti-Myc mouse mAb 9E10 (Roche Diagnostics) followed by horseradish peroxidase-conjugated anti-mouse IgG (PIERCE). B2R-HA was stained using anti-HA rat mAb 3F10 antibody (Roche Diagnostics), followed by horseradish peroxidase-conjugated anti-rat IgG (#16549, Invitrogen). Then, the bound peroxidase was detected with Luminata Forte Western HRP Substrate (Merck Millipore).

Immunocytochemistry. After one day of culture, COS-7 cells were transfected and cultured for an additional day on glass coverslips in 24-well culture plates. The cells were exposed to the following stimulants: either 100 μM UTP for 15 min, 1 μM bradykinin (BK) for 15 min, or 100 ng/mL GT1b ganglioside for 15 min followed by 10 μg/mL chondroitin sulfate C (CSC) for 15 min. After removing the medium, the cells were fixed with 3% paraformaldehyde. After blocking with 5% skim milk in PBS, P2Y₂R-Myc and B2R-HA were detected using anti-Myc monoclonal antibody (71D10 rabbit mAb; Cell Signaling Technology) and anti-HA monoclonal antibody 3F10, respectively, followed by Alexa Fluor 546 conjugated goat anti-rabbit IgG and Alexa Fluor 488 conjugated goat anti-rat IgG (Thermo Fisher Scientific), respectively. The cells were observed using confocal laser scanning microscopy (FV1000; Olympus).

3. Results

3.1. Effect of P2Y₂R on B2R membrane microdomain distribution

Since B2R and P2Y₂R interact and P2Y₂R localizes in lipid rafts, the interaction between both receptors was expected on lipid rafts. When B2R-HA was expressed in COS7 cells and immunoblotted with anti-HA antibody after SDS-PAGE, about 25–30% of the protein was localized to the lipid rafts and the remainder of the protein fractionated to non-raft fractions. When P2Y₂R was co-expressed, 80% or more of B2R was fractionated into the raft fraction (Fig. 1). This result shows that the interaction between the two receptors promotes the transition of B2R into lipid rafts by P2Y₂R. The same finding was also observed when an *N*-linked sugar chain deletion mutant of P2Y₂R (N9Q/N13Q) was co-expressed. This indicated that the *N*-linked sugar chain of P2Y₂R was not involved in association with B2R. In addition, the N9Q/N13Q mutant is not expressed on the cell surface and remains in the endoplasmic reticulum [4] despite its association with B2R. The intracellular localization of both receptors was observed with a confocal fluorescence microscope. The staining of N9Q/N13Q-P2Y₂R in the endoplasmic reticulum was consistent with some of the B2R staining (Fig. 2). Therefore, it was demonstrated that both receptors were already associated in the endoplasmic reticulum.

Almost all of P2Y₂R is fractionated into raft fractions in both wild type and the N9Q/N13Q mutant. The influence of B2R co-expression on the raft distribution of these P2Y₂R molecules was investigated. Both P2Y₂R and its mutant fractionated into raft fractions, and no migration to non-raft fractions was observed

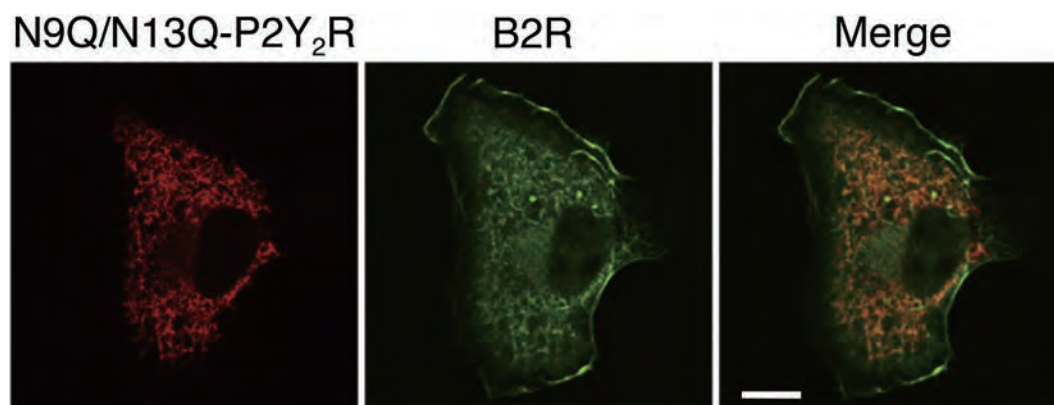


Fig. 2. Confocal fluorescence microscopic images of N9Q/N13Q-P2Y₂R and B2R. Myc-tagged P2Y₂R mutant and HA-tagged B2R were expressed in COS 7 cells and observed with a confocal microscope. Anti-Myc rabbit mAb and anti-HA rat mAb were used as the primary antibodies, respectively, and Alexa Fluor 546 goat anti-rabbit IgG and Alexa Fluor 488 goat anti-rat IgG were used as the secondary antibodies, respectively. "P2Y₂R" is the fluorescence (red) of the secondary antibody bound to the anti-Myc antibody and "B2R" is the fluorescence (green) of the secondary antibody bound to the anti-HA antibody. "Merge" is both fluorescent images superimposed. Scale bar indicates 10 μm.

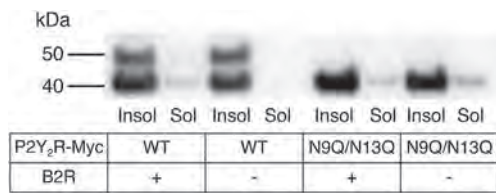


Fig. 3. Distribution of wild type (WT) and N9Q/N13Q-P2Y₂R into lipid rafts during B2R co-expression. Wild type and mutant of Myc-tagged P2Y₂R was co-expressed either individually or with B2R, and the detergent insoluble (Insol) membrane fraction and the detergent soluble (Sol) membrane fraction were analyzed by Western blotting using an anti-Myc antibody.

(Fig. 3). These data demonstrate that P2Y₂R was fractionated into lipid rafts with or without B2R co-expression.

3.2. Intracellular dynamics of P2Y₂R and B2R

The data suggest that B2R and P2Y₂R directly interact and function together. The effects of stimulants on the localization of both receptors were investigated with a confocal fluorescence microscope in cells co-expressing both P2Y₂R and B2R (Fig. 4). When stimulated with 100 μM UTP for 15 min, most of P2Y₂R disappeared from the cell membrane surface by endocytosis. B2R was involved in the endocytosis of P2Y₂R, and most of the B2R disappeared from the cell membrane surface. On the other hand, when the cells were stimulated with 1 μM BK for 15 min, only a portion of both B2R and P2Y₂R was endocytosed (Fig. 4). When the stained images after UTP stimulation were merged, it was shown that P2Y₂R and B2R were

present in different granules, suggesting that these receptors did not interact with each other after endocytosis.

Since we have found that desensitization of B2R is caused by continuous stimulation of both GT1b and CSC [5] and that P2Y₂R is also desensitized at that time [1], we investigated the intracellular localization of both receptors. After incubation with 100 ng/mL GT1b for 15 min followed by incubation with 10 μg/mL CSC for 15 min, most of both receptors disappeared from the cell membrane surface. In this case too, it was shown that many of the both receptors were present in different granules (Fig. 4).

4. Discussion

We have previously demonstrated signal crosstalk between P2Y₂R and B2R. Both receptors have a close relationship and agonist stimulation of one receptor results in activation of both receptors [1]. Since most of the P2Y₂R protein is fractionated into lipid rafts [4], interaction between both receptors was expected to occur in the lipid rafts. P2Y₂R fractionated into lipid rafts regardless of either the presence or absence of its component *N*-linked sugar chain or of co-expression with B2R. B2R was fractionated into lipid rafts when co-expressed with P2Y₂R, but when B2R was not co-expressed with P2Y₂R, more of the B2R protein was localized in non-raft fractions. Since the localization of B2R into lipid rafts was affected by the expression of P2Y₂R, additional evidence was obtained that a portion of the B2R protein was associated with P2Y₂R. These findings demonstrate that B2R localizes to lipid rafts due to its affinity for P2Y₂R. Both receptors signal cross talk probably by forming a hetero-oligomer [1] in the rafts. Moreover, this association also occurred between B2R and the *N*-linked sugar chain-deficient

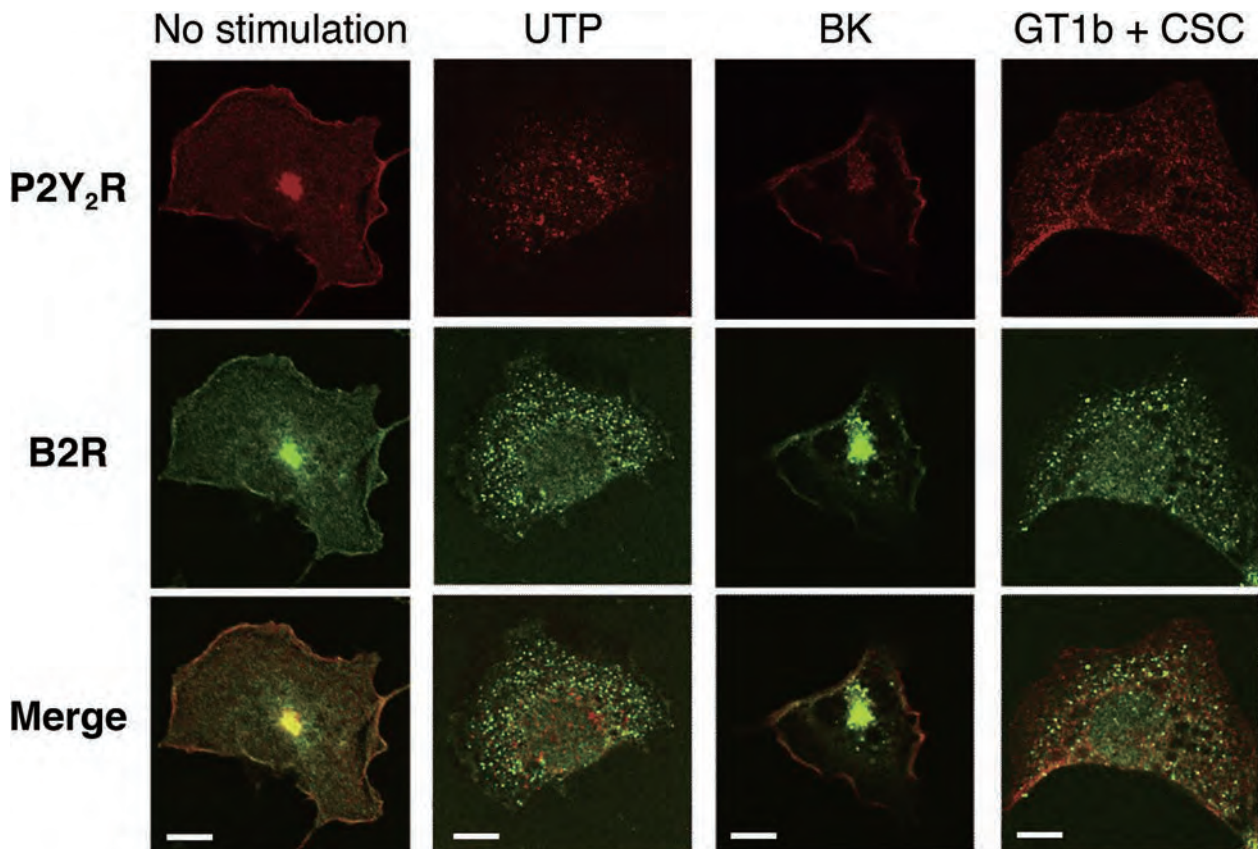


Fig. 4. Confocal fluorescence micrograph of wild-type P2Y₂R and B2R. Myc-tagged wild-type P2Y₂R and HA-tagged B2R were expressed in COS7 cells and observed with a confocal microscope as in Fig. 2. Scale bar indicates 10 μm.

P2Y₂R mutant that is not expressed on the cell surface [4]. In this case, both receptors remained in the endoplasmic reticulum.

After a 15 min stimulation with UTP, P2Y₂R is endocytosed, and B2R was also endocytosed (Fig. 4). In addition, after continuous stimulation with GT1b/CSC, B2R is desensitized, and co-existing P2Y₂R is also desensitized [1,5]. Thus, after desensitization of either receptor, both receptors disappeared from the cell membrane surface (Fig. 4). With both UTP and continuous GT1b/CSC stimulation, many of the receptors were localized in different granules. This may be due to the fact that either P2Y₂R and B2R cooperate and follow different routes after being transported into the cell or the two receptors have different transport speeds from the early endosome to the recycling endosome.

A membrane raft is a signaling domain in the cell membrane, and the signals of some GPCRs, such as P2Y₂R [6,7] and gonadotropin-releasing hormone (GnRH) [8] are transmitted downstream by localizing into rafts. Also, B2R is transferred by activation in smooth muscle cells by caveolae, a type of raft [9]. In both adrenal chromaffin cells and PC 12 cells, a raft is involved in sensitization of the EGFR-inducing signal by B2R [10]. In smooth muscle cells, P2Y₂R also shifts into rafts by agonist stimulation [11]. In addition, there are chemokine receptor GPCRs that transmit different signals through inside or outside rafts [12]. Kaiser et al. [7] reported that whereas lipid rafts are required for the activation of P2Y₂R, it is not necessary for the activation of B2R. However, lipid rafts are required for both receptors to exert the relaxing action on guinea pig endothelium. Our data demonstrate that the downstream B2R signal is regulated by the presence of P2Y₂R since B2R associates with P2Y₂R and enters into the rafts.

In summary, we demonstrated that P2Y₂R recruits B2R into lipid rafts due to the close interaction between these molecules. Both receptors disappear from the cell membrane surface after stimulation of either receptor. In the future, it should be determined whether this process after endocytosis is carried out independently or not.

Transparency document

Transparency document related to this article can be found online at <https://doi.org/10.1016/j.bbrc.2018.09.072>.

Acknowledgements

Funding

This study was supported by the Strategic Study Base Formation Support Project for Private Universities (S1201031), Japan.

References

- [1] S. Yashima, A. Shimazaki, J. Mitoma, T. Nakagawa, M. Abe, H. Yamada, H. Higashi, Close association of B2 bradykinin receptors with P2Y₂ ATP receptors, *J. Biochem., Tokyo* 158 (2015) 155–163.
- [2] K. Simons, E. Ikonen, Functional rafts in cell membranes, *Nature* 387 (1997) 569–572.
- [3] G. van Meer, Cell biology. The different hues of lipid rafts, *Science* 296 (2002) 855–857.
- [4] T. Nakagawa, C. Takahashi, H. Matsuzaki, S. Takeyama, S. Sato, A. Sato, Y. Kuroda, H. Higashi, N-glycan-dependent cell-surface expression of the P2Y₂ receptor and N-glycan-independent distribution to lipid rafts, *Biochem. Biophys. Res. Commun.* 485 (2017) 427–431.
- [5] A. Shimazaki, T. Nakagawa, J. Mitoma, H. Higashi, Gangliosides and chondroitin sulfate desensitize and internalize B2 bradykinin receptors, *Biochem. Biophys. Res. Commun.* 420 (2012) 193–198.
- [6] K. Ando, Y. Obara, J. Sugama, A. Kotani, N. Koike, S. Ohkubo, N. Nakahata, P2Y₂ receptor-Gq/11 signaling at lipid rafts is required for UTP-induced cell migration in NG 108–15 cells, *J. Pharmacol. Exp. Ther.* 334 (2010) 809–819.
- [7] R.A. Kaiser, B.C. Oxhorn, G. Andrews, I.L. Buxton, Functional compartmentation of endothelial P2Y receptor signaling, *Circ. Res.* 91 (2002) 292–299.
- [8] A.M. Navratil, S.P. Bliss, K.A. Berghorn, J.M. Haughian, T.A. Farmerie, J.K. Graham, C.M. Clay, M.S. Roberson, Constitutive localization of the gonadotropin-releasing hormone (GnRH) receptor to low density membrane microdomains is necessary for GnRH signaling to ERK, *J. Biol. Chem.* 278 (2003) 31593–31602.
- [9] W.F. de Weerd, L.M. Leeb-Lundberg, Bradykinin sequesters B2 bradykinin receptors and the receptor-coupled Galpha subunits Galphaq and Galphai in caveolae in DDT1 MF-2 smooth muscle cells, *J. Biol. Chem.* 272 (1997) 17858–17866.
- [10] E.M. Hur, Y.S. Park, B.D. Lee, I.H. Jang, H.S. Kim, T.D. Kim, P.G. Suh, S.H. Ryu, K.T. Kim, Sensitization of epidermal growth factor-induced signaling by bradykinin is mediated by c-Src. Implications for a role of lipid microdomains, *J. Biol. Chem.* 279 (2004) 5852–5860.
- [11] A. Norambuena, F. Palma, M.I. Poblete, M.V. Donoso, E. Pardo, A. Gonzalez, J.P. Huidobro-Toro, UTP controls cell surface distribution and vasomotor activity of the human P2Y₂ receptor through an epidermal growth factor receptor-transregulated mechanism, *J. Biol. Chem.* 285 (2010) 2940–2950.
- [12] R. Shamri, V. Grabovsky, S.W. Feigelson, O. Dvir, Y. Van Kooyk, R. Alon, Chemokine stimulation of lymphocyte alpha 4 integrin avidity but not of leukocyte function-associated antigen-1 avidity to endothelial ligands under shear flow requires cholesterol membrane rafts, *J. Biol. Chem.* 277 (2002) 40027–40035.

Homodimer formation by the ATP/UTP receptor P2Y₂ via disulfide bridges

Received September 20, 2017; accepted December 20, 2017; published online January 18, 2018

Maya Abe, Kanae Watanabe,
Yoshiyuki Kuroda, Tetsuto Nakagawa and
Hideyoshi Higashi*

Division of Glyco-Signal Research, Institute of Molecular Biomembrane and Glycobiology, Tohoku Medical and Pharmaceutical University, Sendai, Miyagi 981-8558, Japan

*Hideyoshi Higashi, Division of Glyco-Signal Research, Institute of Molecular Biomembrane and Glycobiology, Tohoku Medical and Pharmaceutical University, Sendai, Miyagi 981-8558, Japan.
Tel: +81-22-727-0119, Fax: +81-22-727-0077,
email: hhigashi@tohoku-mpu.ac.jp

Many class C G-protein coupled receptors (GPCRs) function as homo- or heterodimers and several class A GPCRs have also been shown to form a homodimer. We expressed human P2Y₂ receptor (P2Y₂R) in cultured cells and compared SDS-PAGE patterns under reducing and non-reducing conditions. Under non-reducing conditions, approximately half of the P2Y₂Rs were electrophoresed as a dimer. We then produced Cys to Ser mutants at four sites (Cys25, Cys106, Cys183 and Cys278) in the extracellular domains of P2Y₂R and examined the effect on dimer formation and receptor activity. All single mutants formed dimers similarly to the wild-type protein, but C25S, C106S and C183S P2Y₂R lost activity, while C278S P2Y₂R maintained weak activity. Coexpression with wild-type P2Y₂R recovered the activity of the C25S mutant. These results show that Cys106 and Cys183 are required for monomer or homodimer activity; Cys25 is required for monomer activity, but it is not needed in one protomer for homodimer activity; and Cys278 can be replaced in the monomer and homodimer. Approximately, half of C25S/C278S double mutants were electrophoresed as a dimer, similarly to the wild-type and single mutants, and dimers with the wild-type protein were active. These results suggest involvement of Cys106 and Cys183 in disulfide bonding between protomers in homodimer formation.

Keywords: α -complementation assay; arrestin recruitment; disulfide bond; GPCR homodimer; GPCR signal cross-talk.

Abbreviations: A1R, adenosine A₁ receptor; B2R, bradykinin receptor B2; BSS, balanced salt solution; GPCR, G-protein coupled receptor; HEPES, 4-(2-hydroxyethyl)-1-piperazineethanesulfonic acid; P2Y₂R, P2Y₂ receptor; PBS, phosphate buffered saline; PCR, polymerase chain reaction; SDS-PAGE, sodium dodecyl sulphate polyacrylamide gel electrophoresis.

Some G-protein coupled receptors (GPCRs) form homodimer or heteromers. Among the many class A GPCRs, rhodopsin (1), bradykinin receptor B2 (B2R) (2), purinergic adenosine A₁ receptor (A₁R) and P2Y₂ receptors (P2Y₂R) (3) form homodimers. Disulfide bridges are present in B2R (4), but the bridging details are unknown and the quaternary structure has not been determined. All class A GPCRs except S1P₁ have preserved Cys residues in the first and second extracellular loops and disulfide bridges are formed between two Cys residues in monomers, as shown by structural analysis of several GPCRs, including rhodopsin (5), and this structural motif is presumed to be similar in other GPCRs.

P2Y₂R is a GPCR activated by ATP/UTP that couples to G α q/11 (G protein) and is involved in induction of inflammation, hypotension and pain. P2Y₂R forms hetero-oligomers or has cross-talk with other class A GPCRs, such as β 2-adrenergic receptor (6), CXC chemokine receptor 2 (7), A₁R (8) and B2R (9). Given that homodimer formation by disulfide bridges was found in SDS-PAGE, we examined how four extracellular Cys residues in P2Y₂R (Cys25, Cys106, Cys183 and Cys278) form bridges in the monomer and dimer. Hillmann *et al.* proposed Cys25–Cys278 and Cys106–Cys183 disulfide bridges based on the effects of mutation of Cys106 and Cys278 to Ser, homologous residues in rhodopsin, and a similar structure to P2Y₁ receptor (10), in which there is a disulfide bond between Cys residues in N terminal domain and third extracellular loop (11). In the current study, we produced point mutants with each of the four Cys residues replaced with Ser. These proteins were used to examine disulfide bridge formation using SDS-PAGE under reducing and nonreducing conditions, and formation of functional homodimers based on UTP-induced activation. Our results show that P2Y₂R can function as a monomer or homodimer and that disulfide bonds contribute to homodimer formation.

Materials and Methods

Cell culture

HEK293T and 1321N1 cells were grown in Dulbecco's Modified Eagle's Medium with 25 mM glucose supplemented with 10% (v/v) fetal calf serum and kept in a humidified 10% CO₂/90% air atmosphere at 37°C. The cells were transiently transfected with plasmids using Lipofectamine 2000 (Invitrogen) for western blotting and Ca²⁺ imaging. Cell membranes for western blotting were prepared from cells 48 h after transfection.

Plasmids and constructs

Plasmids encoding human P2Y₂R were prepared by inserting P2Y₂R cDNA between the EcoRI and BamHI sites of pIRES2-EGFP (Clontech). P2Y₂Rs with Ser substitution at Cys25, Cys106, Cys183, Cys278 and Cys25/278 were prepared by PCR. The C-terminal of P2Y₂R was fused to the H31R-substituted α donor peptide

of a LacZ β -galactosidase reporter enzyme (P2Y₂R- α) or Myc epitope. The C-terminal of β -arrestin-2 was fused to the M15 acceptor deletion mutant of β -galactosidase (the ω peptide, arrestin- ω). Plasmids encoding fusion proteins were generated by subcloning PCR products into pAlpha-N1 or pOmega-N1 vectors, which were constructed from pAcGFP-N1 vector (Clontech) (9).

Preparation of membrane fractions, SDS-PAGE and western blotting

Preparation of membrane fractions (12), SDS-PAGE and western blotting (9) were performed as described previously.

β -galactosidase complementation assay

The interaction between activated GPCR and β -arrestin (arrestin recruitment) was measured using complementation between the α and ω domains of LacZ β -galactosidase (9, 13). Since P2Y₂R was activated with autocrine ATP generated by physical stimulus during cell cultivation in our original method (9), we modified the procedure to avoid autocrine effects by cultivating the cells 24 h before the assay, as described below. HEK293T or 1321N1 cells were cultured in 10 cm ϕ cell culture dishes to 80% confluence. Cells were washed once with phosphate buffered saline (PBS; 137 mM NaCl, 2.7 mM KCl, 1.5 mM KH₂PO₄, and 8.1 mM Na₂HPO₄) and harvested by digestion with 2 mL of 0.05% trypsin/EDTA for 30 s at room temperature. Digestion was stopped by adding 2.5 mL of culture medium. The harvested cells were spun down (700 g, 5 min) and washed with 3 mL of PBS. The pelleted cells were suspended in 36 mL of culture medium and dispensed as 3 mL aliquots. Cell suspensions were mixed with transfection reagents, 0.4 μ g of each plasmid DNA coding for GPCR- α and arrestin- ω in 200 μ L Opti-MEM, and 1.6 μ L of Lipofectamine 2000 (Invitrogen) in 200 μ L of Opti-MEM. Then, a 180 μ L aliquot of the mixture was seeded on a white tissue culture 96-well plate (Corning 3917) and cultured at 37°C for 24 h. After stimulation of the cells with 20 μ L of 10 \times concentrated UTP for 1 h at 37°C, 150 μ L of the supernatant was discarded and 50 μ L of Gal Screen (B, Applied Biosystems) was added, followed by incubation at room temperature. Luminescence of the wells was read after about 40 min.

Ca²⁺ imaging

Cells cultured on glass-bottom dishes were loaded with the Ca²⁺ indicator Fura-2 and exposed to stimulants using the bath application method. Images were acquired and analyzed using balanced salt solution (pH 7.3; 130 mM NaCl, 5.4 mM KCl, 20 mM HEPES, 5.5 mM glucose, 0.8 mM MgSO₄, and 1.8 mM CaCl₂) as the extracellular media (14–16).

Statistical analysis

Results are presented as means \pm SEM. Differences between groups were assessed by two-way ANOVA followed by a Dunnett's multiple comparison test, using GraphPad software (San Diego, CA). $P < 0.05$ was considered significant.

Results

Homodimer formation by P2Y₂R and effect of mutation of Cys residues

P2Y₂R with a C-terminal Myc tag was expressed in HEK293T cells. Western blotting was performed after SDS-PAGE under reducing and non-reducing conditions. Under non-reducing conditions, western blot analysis showed bands at the monomer position and at a position consistent with a dimer (Fig. 1B). Cys to Ser mutants were examined similarly, and all mutants, including the C25S/C278S double mutant, formed bands with molecular masses consistent with the monomer and dimer. However, most dimer bands transferred to the monomer position under reducing conditions (Fig. 1A), which suggests that P2Y₂R forms a homodimer with disulfide bonds. The ratios of monomer and dimer forms of wild-type and mutant P2Y₂R were estimated from Fig. 1B. About 60% of

wild-type P2Y₂R formed a dimer, while less than 40% of the C278S mutant formed a dimer (Table I). We previously showed that most P2Y₂R molecules in COS7 cells are present in lipid rafts (12), and a similar result was found in HEK293T cells, with most wild-type and mutant P2Y₂R in raft component fractions.

Effect on arrestin recruitment of homodimer formation by wild-type and Cys-mutant P2Y₂R

Using P2Y₂R with the C-terminal attached to the LacZ α -domain, UTP-stimulated arrestin recruitment was determined based on reactivity to the arrestin attached to the LacZ ω -domain. In HEK293T cells, C25S, C278S and C25S/C278S mutants had weaker activity than the wild-type protein but were activated by UTP, whereas C106S and C183S mutants were not activated (Fig. 2A). Since endogenous P2Y₂R is expressed in HEK293T cells, the assay was also conducted in 1321N1 cells, which do not have endogenous expression of P2Y₂R. In these cells, the activity of the C25S and C25S/C278S mutants disappeared (Fig. 2B). The C278S mutant maintained some activity, but this was weaker than that of wild-type P2Y₂R. To confirm the effect of dimers, both wild-type P2Y₂R and P2Y₂R mutant- α proteins were expressed in 1321N1 cells. Under these conditions, results similar to those observed in HEK293T cells were obtained (Fig. 2C). Combination of wild-type P2Y₂R with C25S, C278S or C25S/S278S mutants gave activity of approximately 25% that of the wild-type homodimer. C25S- α was activated in the presence of wild-type or C278S P2Y₂R but was not activated in the presence of C25S/C278S mutant (Fig. 2D). This result implies that the activation signal from wild-type or the C278S mutant was transmitted to C25S- α and shows that activation signals from wild-type are not transmitted to C106S- α or C183S- α .

Examination of G-protein activation

The above results show that Cys25, Cys106 and Cys183 are required for recruitment of arrestin. Further assays were conducted to examine whether mutation of these Cys residues inhibited G-protein activity, an upstream reaction in 1321N1 cells, using intracellular Ca²⁺ imaging. None of the C25S, C106S and C183S mutants caused an increase in Ca²⁺, in contrast to wild-type P2Y₂R (Fig. 3; results for C106S and C183S P2Y₂R are not shown but were similar to those for C25S P2Y₂R). Expression of the three mutants with pIRES2-EGFP resulted in less expression of EGFP than with wild-type P2Y₂R, for a reason that is unclear.

Discussion

Extracellular Cys residues in proteins located on the surface of cell membranes maintain protein structure via disulfide bridging. Among GPCRs, rhodopsin has four extracellular Cys residues that form disulfide crosslinks between two central and two terminal residues (cf. Fig. 4A). The activity of GPCRs is regulated by formation of homodimers and heterooligomers, which leads to signaling cross-talk. Many class C GPCRs form homo- or heterodimers, and mGluRs

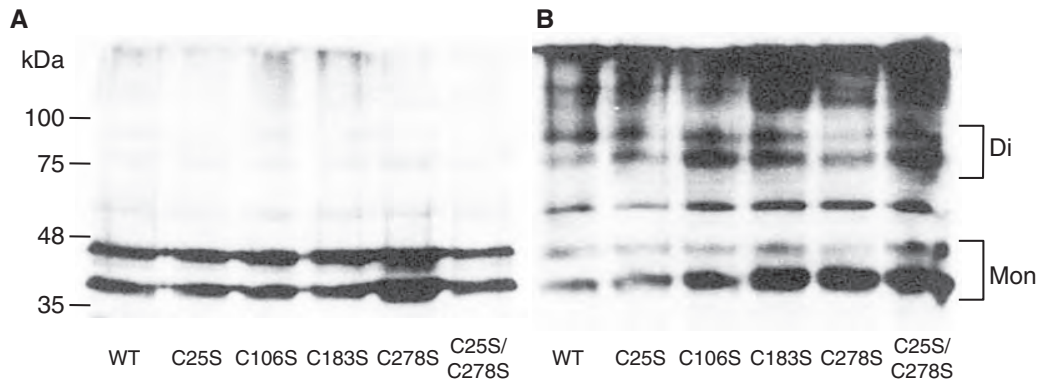


Fig. 1 Wild-type (WT) P2Y₂R-Myc and Cys to Ser mutants were expressed in HEK293T cells and detected by Western blotting. Results are shown for detergent-resistant membrane fractions under reducing (**A**) and nonreducing (**B**) conditions. Almost no expressed protein was fractionated in the detergent-soluble fraction. Di, dimer; Mon, monomer.

Table I. Ratio of monomer and dimer forms of P2Y₂R and its Cys to Ser mutants^a

P2Y ₂ R	Monomer (%)	Dimer (%)
Wild type	38	62
C25S	48	52
C106S	42	58
C183S	53	47
C278S	69	31
C25S/C278S	62	38

^aRatios were calculated from scanned image of western blot in Fig. 1B.

(17) and Ca²⁺ sensing receptor (18) have disulfide bonds that contribute to dimer formation. In mGluRs, Cys residues in the long N terminal extracellular domain contribute to homodimer formation (19). Several class A GPCRs also form homodimers, including rhodopsin (1), A₁R and P2Y₂R (3), B2R (2, 4), D2R (20), β₂AR (21) and 5-HT_{2C} (22). Many class A GPCRs have Cys residues in N terminal domain and the first, second and third extracellular loops, but the majority view is that homodimer formation depends on interactions between transmembrane domains. Only B2R (4) and P2Y₂R in this study have been shown to have disulfide bonds involved in homodimer formation and it is still unclear how these Cys residues are bridged.

Fusion of a GPCR with an α domain to facilitate a LacZ α complementary reaction permits evaluation of signaling cross-talk by GPCR homodimers and heterooligomers (9). In this study, we found that some P2Y₂Rs formed dimers under non-reducing conditions (Fig. 1). The dimers were formed with all of the mutants examined. We examined whether extracellular Cys residues at four sites contributed to 'functional' dimer formation by evaluating signaling cross-talk of Cys to Ser mutants expressed alone or with wild-type P2Y₂R (Fig. 2). All mutants formed dimers with each other or with wild type. The C25S mutant received active signal from wild type revealing arrestin recruitment activity. That is, it formed a 'functional' dimer capable of cross-talk. The C106S and C183S mutants were able to form dimers, but they were not activated alone and could not engage in signal cross-talk from

wild type. This indicates that these mutants cannot form a 'functional' dimer, even though they were able to form a dimer with wild type. The C278S mutant showed somewhat diminished dimer formation but had activity itself and was able to transfer a signal to the C25S mutant. Based on these results, a disulfide bridge pattern can be proposed for P2Y₂R (Fig. 4).

Cys106 and Cys183 are positioned in the first and second extracellular loops, and mutation of either of these residues to Ser eliminated receptor activity when expressed alone and in coexpression with wild-type P2Y₂R. This suggests that a disulfide bond is formed between these two residues, as Hillmann *et al.* proposed based on homology to rhodopsin (11). Hillmann *et al.* indicated that C106S P2Y₂R was not expressed on the cell surface in 1321N1 cells, as the binding of antibodies to the HA-tag added to the N-terminus is undetectable (11). In our observation, the level of protein expression did not differ between wild-type and mutant proteins in both HEK293T (Fig. 1) and 1321N1 cells (unpublished observation). Thus, C106S mutant protein is expressed but its sorting to the cell surface is prohibited. It is probable that bridging with an appropriate disulfide bond between Cys106 and Cys183 is sufficient for the cell surface expression of the receptor.

Cys106 and Cys183 are also probably involved in a disulfide bridge between protomers in homodimer formation (Fig. 4C). Ser mutations at each of these sites formed dimers in SDS-PAGE under nonreducing conditions. In the C25S/C278S double mutant, dimer bands also occurred and were changed to monomers by reduction. Therefore, an inter-protomer disulfide bridge between Cys106 and Cys183 is also involved in homodimer formation (Fig. 4C).

Mutation of Cys25 in N terminal domain to Ser did not prevent activation in coexpression with wild-type P2Y₂R. If molecules forming homodimers are equivalently expressed, the ratio of homodimer formation with wild-type P2Y₂R is approximately half; however, the activity was less than half. Mutation of Cys278 in the third extracellular loop to Ser attenuated activity, but some was maintained. Therefore, Cys278 seems to be less important for monomer and homodimer formation. The C25S/C278S double mutant lost

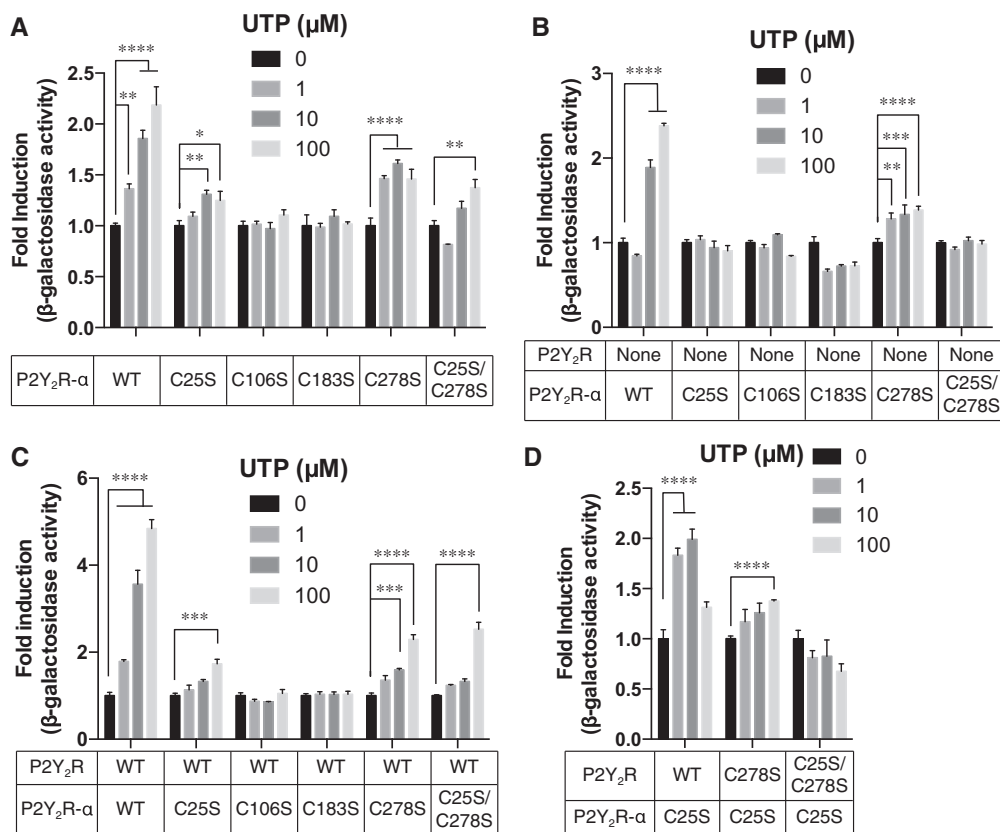


Fig. 2 Difference in reaction of Cys to Ser mutants with and without wild-type P2Y₂R. P2Y₂R-α or mutant-α in HEK293T cells with endogenous wild-type P2Y₂R (A) and in 1321N1 cells that do not express wild-type P2Y₂R (B–D). Wild-type or mutant P2Y₂R was coexpressed with arrestin-α and stimulated by UTP, after which arrestin recruitment activity was determined by an α complementary reaction. Activity is expressed as a multiple of the control activity measured without the reagents. n = 3. ****P < 0.0001; ***P < 0.001; **P < 0.01; *P < 0.05.

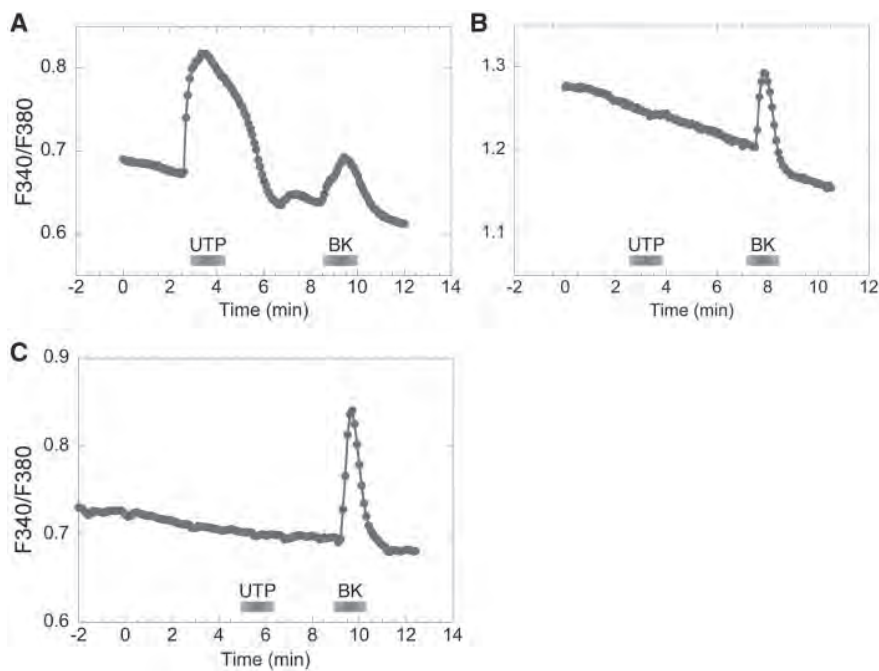


Fig. 3 Intracellular Ca²⁺ changes for wild-type and C25S P2Y₂R in 1321N1 cells after UTP addition. Wild-type (A) or C25S (B) P2Y₂R was expressed in 1321N1 cells and 15 cells each were stimulated by 10 μM UTP, followed by stimulation with 1 μM BK. C106S and C183S mutants gave similar results to those for C25S P2Y₂R. (C) Non-transfected 1321N1 cells were stimulated as above and served as controls (n = 21).

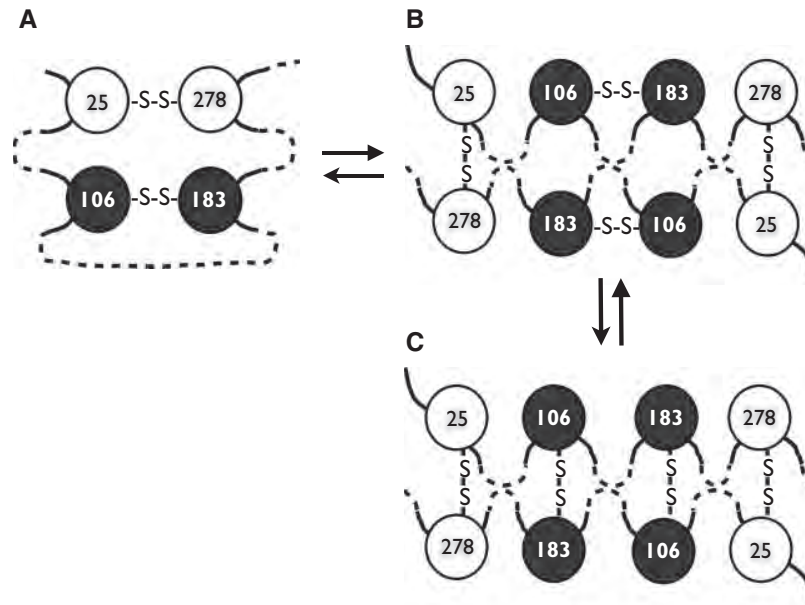


Fig. 4 Proposed disulfide bridges in P2Y₂R monomers and homodimers. In monomers, similarly to rhodopsin, Cys25 and Cys278, and Cys106 and Cys183 are likely to be bridged (A). When homodimers are formed, Cys25 is bridged with Cys278 in the other protomer. Consequently, it is possible that bridges between Cys106 and Cys183 occur within one protomer (B) and between two protomers (C).

activity, but this was recovered in coexpression with wild-type P2Y₂R. These results are likely to be due to homodimer formation and thus support the conclusion that Cys106 and Cys183 are involved in disulfide bridges with wild-type P2Y₂R; i.e. they are involved in bridging between molecules. Therefore, a Cys106-Cys183 intra- or interprotomer disulfide bond is essential for receptor expression on the cell surface and activation (Fig. 4). This hypothesis is also supported by the activation of C25S- α in the presence of C278S P2Y₂R (Fig. 2D). Signals were transduced from C278S to C25S P2Y₂R but not from C25S/C278S P2Y₂R (Fig. 2D). This suggests that Cys25 and Cys278 form a disulfide bond, but that this disulfide bond is not essential for homodimer formation, given that signals were transduced from wild-type P2Y₂R to the C25S/C278S mutant (Fig. 2A and C).

In COS7 cells, most P2Y₂R molecules are found in fractions corresponding to lipid raft components (12). The results of this study showed that most P2Y₂R molecules also fractionated to lipid raft components in HEK293T cells. Only some of these molecules formed dimers, which shows that dimer formation has no relationship with distribution of P2Y₂R to raft fractions. Also, in the presence of wild-type P2Y₂R, Cys mutants had no effect on raft distribution.

Formation of B2R homodimers with disulfide bonds is promoted by agonist binding (2). However, no agonist was necessary for P2Y₂R to form homodimers. P2Y₂R shows cross-reaction with B2R (9) and cross-talk with β -adrenergic receptor (6), CXC chemokine receptor 2 (7), and A₁R (8). Thus, P2Y₂R may form heteromers with other GPCRs, but it is unknown how homodimer formation is related to the occurrence of heteromers. There were many smear bands up to 100 kDa in non-reducing SDS-PAGE (Fig. 1B). Bands above 100 kDa often appear in non-reducing

SDS-PAGE, and some of those seen in Fig. 1B may be homo-oligomers or hetero-oligomers with other GPCRs.

Formation of a dimer or oligomer greatly affects the binding kinetics, signal enhancement and termination thereof, as it regulates the density of molecules involved in GPCR signal transduction (1). The monomer and dimer are rapidly interconvertible (23), and involvement of a disulfide bridge is likely to prolong the presence of the dimer.

Funding

This study was supported by the Strategic Study Base Formation Support Project for Private Universities, Japan.

Conflict of Interest

None declared.

References

1. Fotiadis, D., Liang, Y., Filipek, S., Saperstein, D.A., Engel, A., and Palczewski, K. (2003) Atomic-force microscopy: rhodopsin dimers in native disc membranes. *Nature* **421**, 127–128
2. AbdAlla, S., Zaki, E., Lothar, H., and Quitterer, U. (1999) Involvement of the amino terminus of the B2 receptor in agonist-induced receptor dimerization. *J. Biol. Chem.* **274**, 26079–26084
3. Namba, K., Suzuki, T., and Nakata, H. (2010) Immunogold electron microscopic evidence of in situ formation of homo- and heteromeric purinergic adenosine A₁ and P2Y₂ receptors in rat brain. *BMC Res. Notes* **3**, 323
4. Michineau, S., Alhenc-Gelas, F., and Rajerison, R.M. (2006) Human bradykinin B2 receptor sialylation and

- N-glycosylation participate with disulfide bonding in surface receptor dimerization. *Biochemistry* **45**, 2699–2707
5. Palczewski, K., Kumasaka, T., Hori, T., Behnke, C.A., Motoshima, H., Fox, B.A., Le Trong, I., Teller, D.C., Okada, T., Stenkamp, R.E., Yamamoto, M., and Miyano, M. (2000) Crystal structure of rhodopsin: a G protein-coupled receptor. *Science* **289**, 739–745
 6. Suh, B.C., Kim, J.S., Namgung, U., Han, S., and Kim, K.T. (2001) Selective inhibition of β_2 -adrenergic receptor-mediated cAMP generation by activation of the P2Y₂ receptor in mouse pineal gland tumor cells. *J. Neurochem* **77**, 1475–1485
 7. Werry, T.D., Wilkinson, G.F., and Willars, G.B. (2003) Cross talk between P2Y₂ nucleotide receptors and CXC chemokine receptor 2 resulting in enhanced Ca²⁺ signaling involves enhancement of phospholipase C activity and is enabled by incremental Ca²⁺ release in human embryonic kidney cells. *J. Pharmacol. Exp. Ther.* **307**, 661–669
 8. Suzuki, T., Namba, K., Tsuga, H., and Nakata, H. (2006) Regulation of pharmacology by hetero-oligomerization between A₁ adenosine receptor and P2Y₂ receptor. *Biochem. Biophys. Res. Commun.* **351**, 559–565
 9. Yashima, S., Shimazaki, A., Mitoma, J., Nakagawa, T., Abe, M., Yamada, H., and Higashi, H. (2015) Close association of B2 bradykinin receptors with P2Y₂ ATP receptors. *J. Biochem.* **158**, 155–163
 10. Hoffmann, C., Moro, S., Nicholas, R.A., Harden, T.K., and Jacobson, K.A. (1999) The role of amino acids in extracellular loops of the human P2Y₁ receptor in surface expression and activation processes. *J. Biol. Chem.* **274**, 14639–14647
 11. Hillmann, P., Ko, G.-Y., Spinrath, A., Raulf, A., von Kügelgen, I., Wolff, S.C., Nicholas, R.A., Kostenis, E., Höltje, H.-D., and Müller, C.E., (2009) Key determinants of nucleotide-activated G protein-coupled P2Y₂ receptor function revealed by chemical and pharmacological experiments, mutagenesis and homology modeling. *J. Med. Chem.* **52**, 2762–2775
 12. Nakagawa, T., Takahashi, C., Matsuzaki, H., Takeyama, S., Sato, S., Sato, A., Kuroda, Y., and Higashi, H. (2017) N-glycan-dependent cell-surface expression of the P2Y₂ receptor and N-glycan-independent distribution to lipid rafts. *Biochem. Biophys. Res. Commun.* **485**, 427–431
 13. Hammer, M.M., Wehrman, T.S., and Blau, H.M. (2007) A novel enzyme complementation-based assay for monitoring G-protein-coupled receptor internalization. *FASEB J.* **21**, 3827–3834
 14. Kudo, Y. and Ogura, A. (1986) Glutamate-induced increase in intracellular Ca²⁺ concentration in isolated hippocampal neurons. *Br. J. Pharmacol.* **89**, 191–198
 15. Chadborn, N., Eickholt, B., Doherty, P., and Bolsover, S. (2002) Direct measurement of local raised subplasmalemmal calcium concentrations in growth cones advancing on an N-cadherin substrate. *Eur. J. Neurosci.* **15**, 1891–1898
 16. Shimazaki, A., Nakagawa, T., Mitoma, J., and Higashi, H. (2012) Gangliosides and chondroitin sulfate desensitize and internalize B2 bradykinin receptors. *Biochem. Biophys. Res. Commun.* **420**, 193–198
 17. Romano, C., Yang, W.L., and O'Malley, K.L. (1996) Metabotropic glutamate receptor 5 is a disulfide-linked dimer. *J. Biol. Chem.* **271**, 28612–28616
 18. Pace, A.J., Gama, L., and Breitwieser, G.E. (1999) Dimerization of the calcium-sensing receptor occurs within the extracellular domain and is eliminated by Cys → Ser mutations at Cys101 and Cys236. *J. Biol. Chem.* **274**, 11629–11634
 19. Kunishima, N., Shimada, Y., Tsuji, Y., Sato, T., Yamamoto, M., Kumasaka, T., Nakanishi, S., Jingami, H., and Morikawa, K. (2000) Structural basis of glutamate recognition by a dimeric metabotropic glutamate receptor. *Nature* **407**, 971–977
 20. Ng, G.Y., O'Dowd, B.F., Lee, S.P., Chung, H.T., Brann, M.R., Seeman, P., and George, S.R. (1996) Dopamine D2 receptor dimers and receptor-blocking peptides. *Biochem. Biophys. Res. Commun.* **227**, 200–204
 21. Hebert, T.E., Moffett, S., Morello, J.P., Loisel, T.P., Bichet, D.G., Barret, C., and Bouvier, M. (1996) A peptide derived from a beta2-adrenergic receptor transmembrane domain inhibits both receptor dimerization and activation. *J. Biol. Chem.* **271**, 16384–16392
 22. Herrick-Davis, K., Grinde, E., and Mazurkiewicz, J.E. (2004) Biochemical and biophysical characterization of serotonin 5-HT_{2C} receptor homodimers on the plasma membrane of living cells. *Biochemistry* **43**, 13963–13971
 23. Kasai, R.S., Suzuki, K.G., Prossnitz, E.R., Koyama-Honda, I., Nakada, C., Fujiwara, T.K., and Kusumi, A. (2011) Full characterization of GPCR monomer-dimer dynamic equilibrium by single molecule imaging. *J. Cell Biol.* **192**, 463–480



A complex between phosphatidylinositol 4-kinase II α and integrin α 3 β 1 is required for *N*-glycan sialylation in cancer cells

Received for publication, August 19, 2018, and in revised form, January 8, 2019. Published, Papers in Press, January 18, 2019, DOI 10.1074/jbc.RA118.005208

Tomoya Isaji^{†1}, Sanghun Im^{†1}, Akihiko Kameyama[§], Yuqin Wang[¶], Tomohiko Fukuda[‡], and Jianguo Gu^{‡2}

From the [†]Division of Regulatory Glycobiology, Institute of Molecular Biomembrane and Glycobiology, Tohoku Medical and Pharmaceutical University, 4-4-1 Komatsushima, Aoba-ku, Sendai Miyagi 981-8558, Japan, the [§]Department of Life Science and Biotechnology, National Institute of Advanced Industrial Science and Technology, 1-1-1 Umezono, Tsukuba, Ibaraki 305-8568, Japan, and the [¶]Department of Pharmacology, Pharmacy College, Nantong University, Nantong, Jiangsu 226001, China

Edited by Gerald W. Hart

Aberrant *N*-glycan sialylation of glycoproteins is closely associated with malignant phenotypes of cancer cells and metastatic potential, which includes cell adhesion, migration, and growth. Recently, phosphatidylinositol 4-kinase II α (PI4KII α), which is localized to the trans-Golgi network, was identified as a regulator of Golgi phosphoprotein 3 (GOLPH3) and of vesicle transport in the Golgi apparatus. GOLPH3 is a target of PI4KII α and helps anchor sialyltransferases and thereby regulates sialylation of cell surface receptors. However, how PI4KII α -mediated sialylation of cell surface proteins is regulated remains unclear. In this study, using several cell lines, CRISPR/Cas9-based gene knockout and short hairpin RNA-mediated silencing, RT-PCR, lentivirus-mediated overexpression, and immunoblotting methods, we confirmed that PI4KII α knockdown suppresses the sialylation of *N*-glycans on the cell surface, in Akt phosphorylation and activation, and integrin α 3-mediated cell migration of MDA-MB-231 breast cancer cells. Interestingly, both integrin α 3 β 1 and PI4KII α co-localized to the trans-Golgi network, where they physically interacted with each other, and PI4KII α specifically associated with integrin α 3 but not α 5. Furthermore, overexpression of both integrin α 3 β 1 and PI4KII α induced hypersialylation. Conversely, integrin α 3 knockout significantly inhibited the sialylation of membrane proteins, such as the epidermal growth factor receptor, as well as in total cell lysates. These findings suggest that the malignant phenotype of cancer cells is affected by a sialylation mechanism that is regulated by a complex between PI4KII α and integrin α 3 β 1.

Alteration of the sialylation of glycoproteins has often been observed in several types of malignant tumors, such as those found in breast, ovary, and colorectal cancers (1–3). Sialylation is linked via either an α 2,3 or an α 2,6 bond to Gal/GalNAc and

via an α 2,8 bond to sialic acid in glycoproteins through a group of sialyltransferases. The up-regulation of cell surface sialic acid is thought to control cell phenotypes such as cell adhesion, migration, immune response, apoptosis, and cell epithelial–mesenchymal transition (EMT).³ Sialylation is also believed to be essential for the differentiation potential of human mesenchymal stem cells (4, 5). The sialylation levels of glycoproteins on the cell surface are mainly determined by sialyltransferase, sialidase, and substrate expression (6, 7). Some transcription factors are critical for transcriptional activation of sialyltransferases in cancer cells. For example, the expression level of α 2,6-galactoside sialyltransferase 1 (ST6GAL1) is up-regulated by the *RAS* oncogene and increases the α 2,6 sialylation of β 1 integrins, which promotes integrin-mediated cell migration, adhesion, and cell proliferation (8, 9).

As described above, sialylation levels are mainly dependent on their gene expression levels, whereas other mechanisms for regulation are usually neglected. However, Popoff and co-workers (10) and our group (11) independently reported that Golgi phosphoprotein 3 (GOLPH3), which has been identified as an oncogenic protein and is increased in several human solid tumors (12), could anchor sialyltransferases to regulate sialylation on cell surface receptors without regulating the gene expression levels of sialyltransferases. In particular, suppression of GOLPH3 attenuated the levels of cellular sialylation and integrin-dependent cell migration. Furthermore, tumor formation was significantly reduced in mice implanted with GOLPH3 shRNA-expressing cells (11–13). GOLPH3 has multiple cellular functions in vesicle trafficking and in support of Golgi apparatus structure, which has specific affinity for phosphatidylinositol 4 (PI4P) (14, 15). PI4P is mainly catalyzed by phosphatidylinositol 4-kinase II α (PI4KII α), which is localized to the trans-Golgi network (TGN) (16). Given the importance of

This work was supported in part by Grants-in-Aid for Scientific Research 15H04354 (to J. G.) and JP17H03808 (to A. K.) from the Japan Society for the Promotion of Science, National Natural Science Foundation of China Grant 31670807, and Grant-in-Aid for Scientific Research on Innovative Areas 18H04868 (to J. G.) from the Ministry of Education, Culture, Sports, Science, and Technology of Japan. The authors declare that they have no conflicts of interest with the contents of this article.

¹ These authors contributed equally to this work.

² To whom correspondence should be addressed. Tel.: 81-22-727-0216; Fax: 81-22-727-007; E-mail: jgu@tohoku-mpu.ac.jp.

³ The abbreviations used are: EMT, epithelial–mesenchymal transition; shRNA, short hairpin RNA; PI4P, phosphatidylinositol 4-phosphate; PI4K, phosphatidylinositol 4-kinase; TGN, trans-Golgi network; ECM, extracellular matrix; EGF, epidermal growth factor; PH, pleckstrin homology; DOX, doxycycline; KD, knockdown; SNA, *Sambucus nigra* agglutinin; WGA, wheat germ agglutinin; PA, pyridilaminated; SSA, *Sambucus sieboldiana* agglutinin; MAM, *Maackia amurensis* mitogen; ConA, concanavalin A; KO, knockout; EGFR, epidermal growth factor receptor; DMEM, Dulbecco's modified Eagle's medium; FBS, fetal bovine serum; cDNA, complementary DNA; mRFP, monomeric red fluorescent protein; SALSA, sialic acid linkage-specific alkylamidation; Ctrl, control.

Importance of the PI4K-integrin $\alpha 3\beta 1$ complex for sialylation

GOLPH3 in sialylation and cell functions, it is plausible that PI4P expression at the TGN may influence sialylation.

Integrins are heterodimeric cell surface adhesion receptors and major carriers of sialylation. The interaction between integrin and the extracellular matrix (ECM) is essential for cell adhesion, migration, viability, and proliferation (17, 18). In fact, glycosylation is a key regulator that plays important roles in modulating integrin functions. For example, integrin $\alpha 5\beta 1$ binding to fibronectin and integrin-mediated cell spreading and migration are modulated by overexpression of glycosyltransferase genes such as *N*-acetylglucosaminyltransferase III and V or ST6GAL1 (19–21). In addition, sialylated *N*-glycans on the membrane-proximal domain of integrin $\beta 1$ play crucial roles in integrin activation and in complex formation between integrin and EGF receptors and syndecan-4 to regulate cell migration and proliferation (22).

In contrast to the regulation of integrin functions from the extracellular domain, it is well known that integrin function is regulated by its association with cytoplasmic molecules such as focal adhesion kinase and phosphatidylinositol 3-kinase (23, 24). Other studies have detected PI4K activity in the immune complex with integrin $\beta 1$, suggesting that integrin might also regulate the biosynthesis of PI4P (25–27). Mammalian PI4Ks are classified as types II and III (28). PI4KII α plays important roles in clathrin-dependent molecular sorting and associates with TGN membranes (29–31), whereas PI4KIII β is enriched in the cis-medial Golgi in breast cancer cells (32).

In this study, to further understand the underlying mechanism for GOLPH3 expression on sialylation and cell functions, we investigated the effects of PI4KII α , which is one of the regulators of GOLPH3 in breast cancer MDA-MB-231 cells. We found that the sialylation on integrins, Akt phosphorylation, and integrin $\alpha 3$ -mediated cell migration all were significantly inhibited in PI4KII α knockdown cells. It was interesting that overexpression of both PI4KII α and integrin $\alpha 3$ greatly increased sialylation. Conversely, knockout of integrin $\alpha 3$ significantly inhibited sialylation in membrane proteins. These findings suggest a novel mechanism for sialylation, which suggests a new concept for the regulation of glycosylation in cell biology.

Results

We recently reported that the expression of GOLPH3 up-regulated cell surface sialylation and cell migration (11). However, the molecular mechanism of posttranslational modification of sialylation on the cell surface remains unclear. Considering that GOLPH3 exhibits a highly selective affinity for PI4P that is similar to the canonical pleckstrin homology (PH) domain in the TGN (33), we hypothesized that the expression of PI4P in the TGN could affect sialylation and cell properties. PI4P is produced mainly by PI4Ks, which are classified as type II and III according to their sensitivity to inhibitors (30). PI4KIII β is enriched in early Golgi compartments, whereas PI4KII α is localized mainly in the TGN and in the endosome (16), where sialyltransferases also are localized (34). Furthermore, PI4KII α is a dominant PI4K in mammalian cells (35). Therefore, we chose PI4KII α for functional analysis,

and established a line of doxycycline (DOX)-controlled PI4KII α silencing in MDA-MB-231 breast cancer cells.

Knockdown of PI4KII α affected the sialylation of *N*-glycans

First, we verified the expression levels of PI4KII α and sialyltransferases (ST3GAL3, ST3GAL4, and ST6GAL1) that involve major sialylated *N*-glycans (36). RT-PCR analysis showed that the expression levels of PI4KII α mRNA were significantly decreased in knockdown cells, whereas the expression levels of ST6GAL1 for $\alpha 2,6$ sialylation and those of ST3GAL3 and ST3GAL4 for $\alpha 2,3$ sialylation were all similar in both cells (Fig. 1A). Second, we verified the expression levels and the distributions of PI4P in KD cells. The PH domain of four-phosphate adaptor protein 1 (FAPP1), which preferentially recognizes PI4P, is known for its use as a monitor for PI4P distribution (37). In control cells, PI4P was localized near the medial Golgi marker GM130, as expected (Fig. 1B). In contrast, PI4P staining was significantly decreased in knockdown (KD) cells (Fig. 1B). These data confirmed that PI4KII α is mainly involved in the synthesis and localization of PI4P in the TGN, which agrees with previous reports (35).

Next, we tested whether decreased PI4P affects sialylation expression on the cell surface. As shown in Fig. 1C, top panels, the intensities of the staining in KD cells with *Sambucus nigra* agglutinin (SNA) lectin, which preferentially recognizes $\alpha 2,6$ sialylation of glycoproteins, was weaker than that in control cells. However, the intensities of staining with WGA lectin, which preferentially recognizes GlcNAc residues and hybrid-type and lactohexose *N*-glycans (38), were almost equal in both cells (Fig. 1C, bottom panels). These data suggested that the expression levels of sialylated glycans were decreased in KD cells. Furthermore, the decrease was confirmed by quantitative analysis using HPLC. Total pyridylaminated (PA) *N*-glycans of cells were examined via anion exchange chromatography, and the ratios of sialylated *N*-glycans versus total *N*-glycans were calculated. The expression levels of sialylated *N*-glycans were significantly suppressed in KD cells (Fig. 1D). A similar change in $\alpha 2,6$ sialylation on specific membrane proteins such as integrin $\beta 1$ was also consistently observed (Fig. 1E) using *Sambucus sieboldiana* agglutinin (SSA)-agarose. These data suggest that the expression levels of PI4P in the TGN are important for sialylation.

Knockdown of PI4KII α significantly inhibited cell migration and Akt phosphorylation

Alterations in *N*-glycosylation affect many cellular events involved in cellular signaling and cell migration. Here we examined the effects of PI4KII α KD on cell migration and Akt activation. As shown in Fig. 2A, cell migration on laminin-332 in a Transwell assay was significantly reduced in KD cells compared with control cells. The expression levels of integrin $\alpha 3\beta 1$, a major receptor for laminin-332 and $\alpha 5\beta 1$ on the cell surface were similar in both cells (Fig. 2B). Activation of Akt is required for integrin-mediated cell migration (39). As shown in Fig. 2C, the level of phosphorylated Akt was apparently decreased in KD cells compared with control cells. These data suggest that PI4P in the TGN plays an important role in Akt activation and in integrin $\alpha 3$ -mediated cell migration.

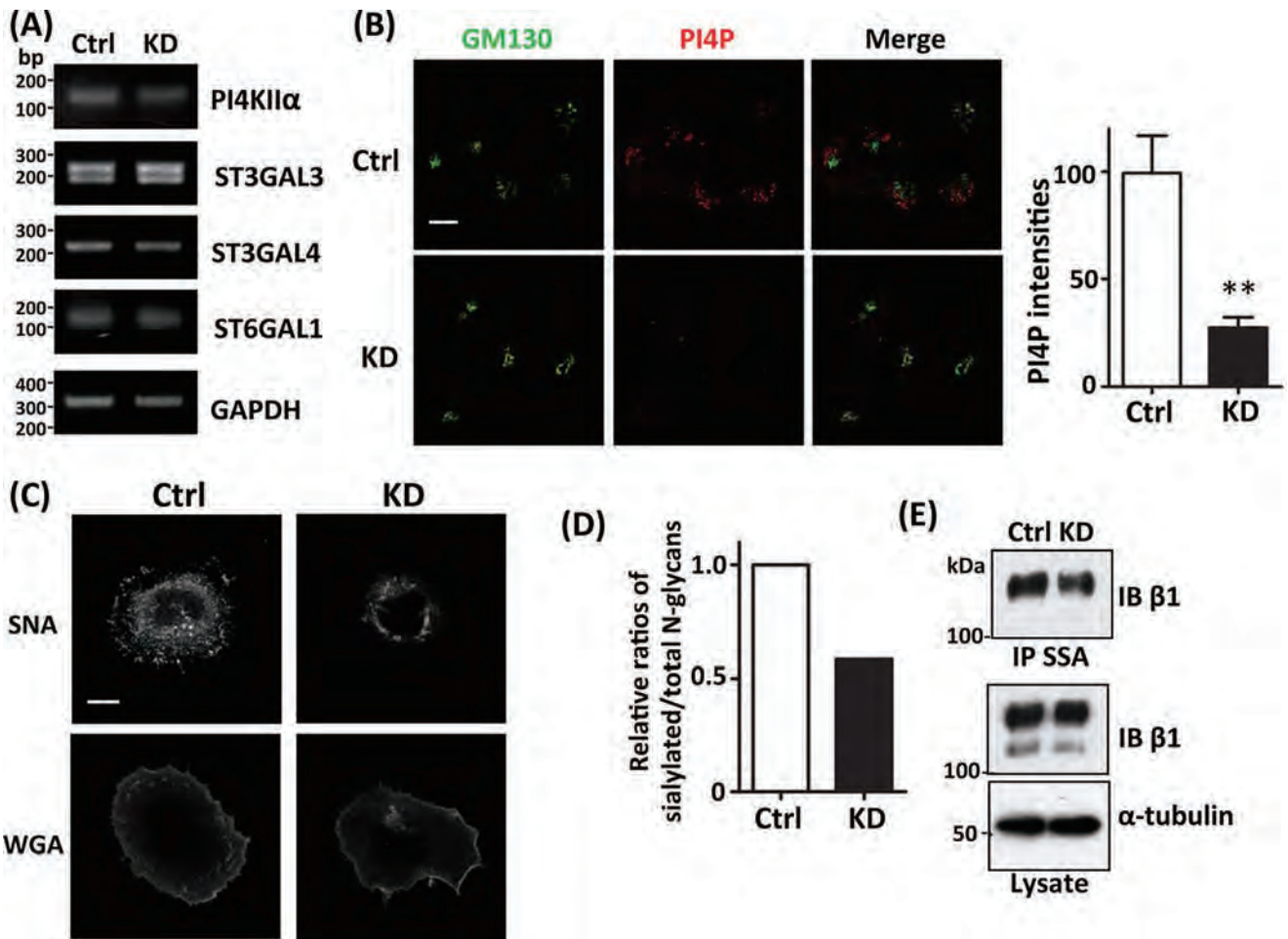


Figure 1. Effects of PI4KII α gene knockdown on the sialylation of N-glycans. A, RT-PCR using total RNA extracted from the control (Ctrl) and PI4KII α KD of MDA-MB-231 cells were carried out to examine the expression levels of PI4KII α and sialyltransferases that involve sialylated N-glycans. The expression level of glyceraldehyde-3-phosphate dehydrogenase (GAPDH) was used as a loading control. ST3GAL, β -galactoside $\alpha 2,3$ -sialyltransferase. B, the amounts and distribution of PI4P in KD and Ctrl cells were examined by expressing mRFP-FAPP, which specifically binds to PI4P. These cells were also immunostained with anti-GM130 antibody, which is a medial Golgi marker. The immunostaining intensities for PI4P were quantified using ImageJ software, averaged by cell numbers, and normalized to the control values (percent). Values represent the means \pm S.E. ($n = 10$). **, $p < 0.01$ (Welch's t test). Scale bar = 10 μ m. C, Cells were incubated with biotin-conjugated SNA or WGA and then fixed and visualized by Alexa Fluor-streptavidin conjugates. Scale bar = 20 μ m. D, preparation of PA oligosaccharides and calculation of ratios of sialylated N-glycans versus total N-glycans as described under "Experimental procedures." Data were normalized to the control. E, equal amounts of cell lysates from Ctrl and KD cells were precipitated by SSA-agarose (preferentially recognizes the $\alpha 2,6$ sialylation) and probed with anti- $\beta 1$ antibody (top panel). The expression levels of integrin $\beta 1$ in total cell lysates were verified by Western blotting with anti- $\beta 1$ antibody (center panel). α -Tubulin was used as a loading control. KD and Ctrl cells refer to transfectants with DOX-inducible knockdown of PI4KII α cultured with or without DOX, respectively. IB, immunoblot.

Complex formation between integrin $\alpha 3$ and PI4KII α is important for sialylation

As described above, PI4KII α regulated sialylation and the integrin $\alpha 3$ -mediated phenotype. Therefore, we examined the interaction between PI4KII α and integrin $\alpha 3$ in the Golgi apparatus. First, we used immunostaining to assess the intracellular distributions of PI4KII α and $\alpha 3$. Immunostaining showed that PI4KII α was localized in the vicinity of GM130 and that it was extensively co-localized with integrin $\alpha 3$ (Fig. 3A). Notably, co-immunoprecipitation with anti-integrin $\beta 1$ showed that it was $\alpha 3$, rather than $\alpha 5$, that interacted with PI4KII α in 293T cell stable expression of PI4KII α and/or either integrin $\alpha 3$ or $\alpha 5$ (Fig. 3B). The interaction between PI4KII α and $\alpha 3$ was further reciprocally confirmed by immunoprecipitation with either anti- $\alpha 3$ antibody (Fig. 3C) or anti-GFP antibody (Fig. 3D).

Next we wondered whether this interaction was required for efficient sialylation. To address this question, we precipitated

those cell lysates with SSA or *Maackia amurensis* mitogen (MAM) agarose, which preferentially recognize $\alpha 2,6$ -sialylated and $\alpha 2,3$ -sialylated N-glycans, respectively, and then performed Western blotting against integrin $\beta 1$. Interestingly, both sialylated N-glycans were up-regulated on integrin $\beta 1$ in cells that expressed both PI4KII α and integrin $\alpha 3$ but not in those that expressed PI4KII α and $\alpha 5$ (Fig. 3E, top and center panels). In contrast to SSA or MAM lectin blotting, ConA lectin blots showed a similar level in both integrin $\alpha 3$ - and $\alpha 5$ -expressing cells (Fig. 3E, bottom panel). ConA lectin equally recognized both mature and immature forms of integrin $\beta 1$ in $\alpha 3$ -expressing cells but only the most immature form of $\beta 1$ in $\alpha 5$ -expressing cells. These data further suggest the importance of $\alpha 3$ for sialylation. Data obtained from flow cytometry analysis via MAM lectin consistently supported this observation, although SSA lectin showed no significant changes in these cells (Fig. 3F). Therefore, these results clearly suggest that intracellular com-

Importance of the PI4K-integrin $\alpha 3\beta 1$ complex for sialylation

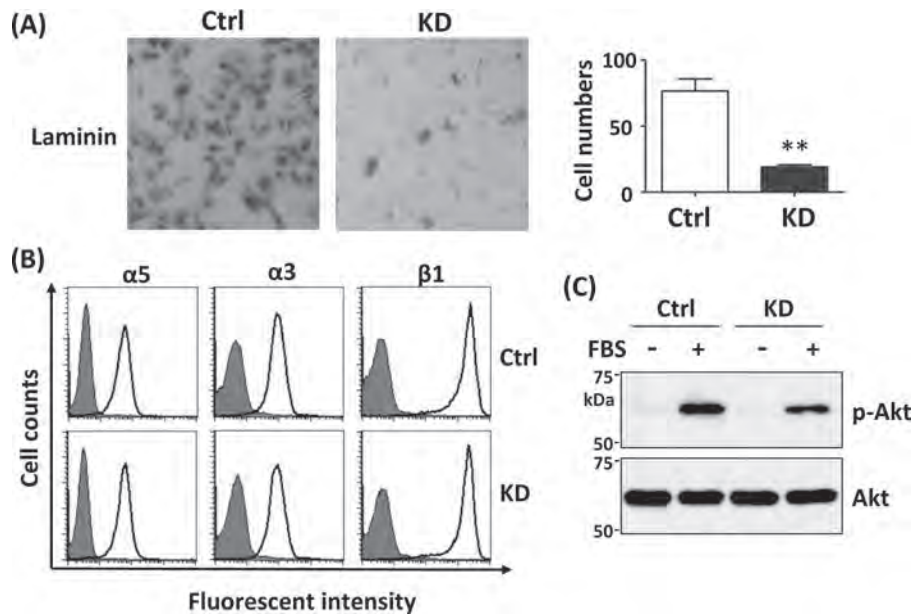


Figure 2. Comparison of cell migration and cellular signaling between Ctrl and KD cells. A, cell migration toward laminin-332 was determined by a Transwell assay as described under "Experimental procedures." The quantitative data were obtained by counting the cell number of five random fields. The p values were calculated using Welch's t test. Values represent the means \pm S.E. **, $p < 0.01$. B, comparison of the expression levels of $\alpha 3\beta 1$ and $\alpha 5\beta 1$ integrins on the cell surface between Ctrl and KD cells. Both Ctrl and PI4KII α KD cells were incubated with (bold line) or without (gray shadow) antibodies against integrin $\alpha 3$, $\alpha 5$, or $\beta 1$ and subjected to FACS analysis. C, comparison of Akt activation upon FBS stimulation between Ctrl and KD cells. After starvation, cells were supplied with fresh medium with (+) or without (-) 3% FBS. The cell lysates were then analyzed by Western blotting with anti-p-Akt or total Akt antibody.

plex formation between PI4KII α and $\alpha 3$ regulates the biosynthesis of sialylated N -glycans.

Expression of integrin $\alpha 3$ is important for efficient sialylation

To further verify the importance of complex formation between PI4KII α and integrin $\alpha 3$ for cellular sialylation, we used the CRISPR/Cas9 system to construct an integrin $\alpha 3$ knockout (KO) MDA-MB-231 cell line. Flow cytometric analysis revealed a KO efficiency of more than 95% (Fig. 4A), which also was confirmed by Western blotting with anti-integrin $\alpha 3$ (Fig. 4B). Notably, the band mobility of integrin $\beta 1$ on SDS-PAGE in KO cells was faster than in the control cells, suggesting that integrin $\alpha 3$ deficiency leads to an accumulation of the immature $\beta 1$ form without sialylation. It is well known that integrin $\alpha 3$ is important for laminin-mediated cell adhesion, migration, and several forms of cellular signaling (40–42). Consistent with previous reports (42, 43), expression of $\alpha 3\beta 1$ regulated cell morphology and that of the actin cytoskeleton by promoting lamellipodium and filopodium formation on laminin-332, a specific ligand for integrin $\alpha 3$, whereas lack of $\alpha 3$ blocked their formation (Fig. 4C). There were no significant differences between two cells spread on collagen, which is a specific ligand for integrin $\alpha 1$ and $\alpha 2$. Furthermore, cell spreading and migration on laminin-332 were inhibited in KO cells compared with control cells (Fig. 4, D and E).

Next, we compared total sialylated N -glycan levels between KO and control cells, which were quantified using HPLC. Consistent with the data from PI4KII α KD cells, the ratios of sialylated N -glycans versus total N -glycans were greatly suppressed in KO cells (Fig. 5A). Because N -glycans of integrin $\beta 1$ could be directly influenced by $\alpha 3$ knockout (Fig. 4B, center panel), here we also analyzed sialylation on the EGF receptor, which has been reported to affect receptor activation (44). As expected,

sialylation of EGF receptors obtained from KO cells was also decreased compared with control cells (Fig. 5B). To investigate whether the phenomenon also occurred in other cell lines, we examined HeLa cells. The knockout efficiency of $\alpha 3$ was assessed via flow cytometry analysis (Fig. 5C). Interestingly, a similar tendency of sialylation decline was observed in $\alpha 3$ KO HeLa cells compared with control cells (Fig. 5D). To thoroughly examine the glycosylation states caused by knockout of integrin $\alpha 3$ or knockdown of PI4KII α , we utilized MS-based approaches to identify the N -glycan and O -glycan structures (Fig. 6, A and B). Consistently, hyposialylation in N -glycans was observed by attenuation of either integrin $\alpha 3$ or PI4KII α (Fig. 6A), which further suggests the importance of this pathway in the biosynthesis of sialylated N -glycans. In contrast to N -glycans, there were no significant changes in the sialylation of O -glycans among these cells (Fig. 6B). It was also notable that a decrease in $\alpha 2,3$ sialylation in N -glycans could slightly increase $\alpha 2,6$ sialylation in total cell lysates of $\alpha 3$ KO and PI4KII α KD cells (Fig. 6A), which seems contrary to the observation for integrin $\beta 1$ (Fig. 3E). Further study is needed to fully elucidate the mechanism. Nevertheless, these data suggest that complex formation of $\alpha 3$ and PI4KII α could act as a novel regulator for the sialylation of N -glycans.

Discussion

In this study, we found that PI4KII α expression played an important role in $\alpha 3\beta 1$ integrin-mediated cell migration, cellular signaling, and the expression of sialylation; PI4KII α could specifically associate with $\alpha 3$ but not $\alpha 5$, and complex formation between PI4KII α and $\alpha 3$ enhanced sialylation; and deletion of integrin $\alpha 3$ significantly inhibited not only cell adhesion and migration but also sialylation. These observations are the first to directly demonstrate a novel regulatory mechanism for sia-

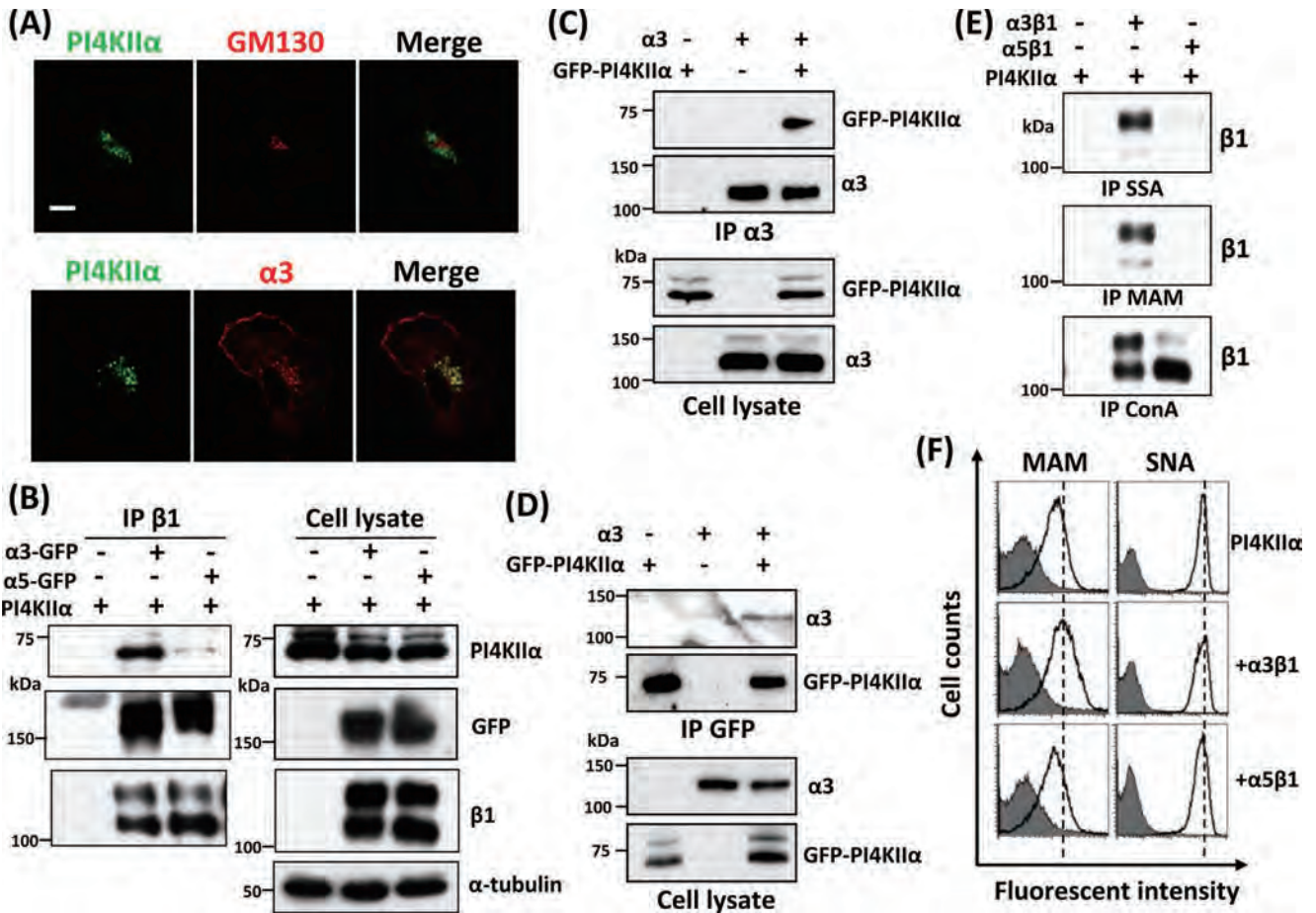


Figure 3. Interaction between integrin $\alpha 3\beta 1$ and PI4KII α and the effect on sialylation. A, MDA-MB-231 cells overexpressed with GFP-PI4KII α were fixed and then stained with either anti-GM130 (top panel) or anti-integrin $\alpha 3$ (bottom panel) antibody, followed by detection using anti-mouse Alexa 647 conjugates. Scale bar = 20 μ m. B, three overexpressed 293T cells were established by lentivirus infection: PI4KII α alone; PI4KII α , GFP-tagged $\alpha 3$ and $\beta 1$; and PI4KII α , GFP-tagged $\alpha 5$ and $\beta 1$ integrin. Equal amounts of cell lysates were immunoprecipitated (IP) with anti-integrin $\beta 1$ antibody, followed by detection with the indicated antibodies. The cell lysates were used as input to show similar expression levels of PI4KII α , integrin $\alpha 3\beta 1$, or $\alpha 5\beta 1$ among these cells. C and D, reciprocal immunoprecipitation was performed using either anti- $\alpha 3$ antibody (C) or anti-GFP for tagged PI4KII α (D) using cell lysates from 293T cells stably overexpressed with or without GFP tagged PI4KII α , which were further transiently transfected with or without $\alpha 3$ and $\beta 1$ integrin. The cell lysates were used as input to show similar expression levels of integrin $\alpha 3$ and GFP-PI4KII α . E, equal amounts of cell lysates were precipitated with either SSA-, MAM-, or ConA-conjugated agarose, followed by detection with antibody against integrin $\beta 1$. F, 293T cells expressing the indicated genes were incubated with (bold line) or without (gray shading) biotin-conjugated MAM or SNA and subjected to FACS analysis.

lylation, which may also partially explain the previous observation that GOLPH3 is a special regulator in the sialylation of *N*-glycans and a part of the signaling events that could influence mTOR signaling and tumor progression (11).

Many cancers are associated with sialylated structures such as sialyl Tn, sialyl Lewis antigen (sLe), $\alpha 2,6$ -sialylated lactosamine, polysialic acid, and gangliosides (45–48). The altered expression of these structures in cancer cells could be the result of multiple mechanisms. Loss of expression or excessive expression of certain sialyltransferases is frequently observed. For example, up-regulated expression of $\alpha 2,3$ and $\alpha 2,6$ sialyltransferases has been observed in many cancers, such as colon cancer, breast cancer, liver cancer, cervical cancer, choriocarcinomas, acute myeloid leukemias, and some malignancies of the brain (49), and this type of change can affect the structures and functions of some important target *N*-glycoproteins such as integrin $\beta 1$ (50), EGFR (44), and platelet endothelial cell adhesion molecule (51).

Recent studies have suggested that activation of the EMT programs serves as a major mechanism for generating cancer

stem cells (52). Interestingly, high expression of ST6GAL1 has been correlated with human-induced pluripotent stem cells and cancer stem cells, indicating that sialylation may be involved in maintaining some aspects of stem cell behavior (4, 5, 53). In fact, ST6GAL1 expression is required for transforming growth factor β -induced EMT. Knockdown of ST6GAL1 prevented a transforming growth factor β -induced increase in cell migration (54).

Given the accumulating evidence of the importance of sialylation in cancer progression, much attention has been paid to elucidating the regulatory mechanisms of its expression. The expression of sialylation on a tumor cell surface can be modulated at different levels (49). The most frequently observed mechanism is modulation of transcription. For example, ST6GAL1 expression is induced by the *ras* oncogene in NIH3T3 cells via its promoter (8). Beyond its promoter activity, in this study, we clearly showed that sialylation could also be regulated by complex formation of PI4KII α and integrin $\alpha 3\beta 1$ on a posttranscriptional level. In fact, the PI4P-binding Golgi protein GOLPH3, which functions in secretory trafficking in

Importance of the PI4K-integrin $\alpha 3\beta 1$ complex for sialylation

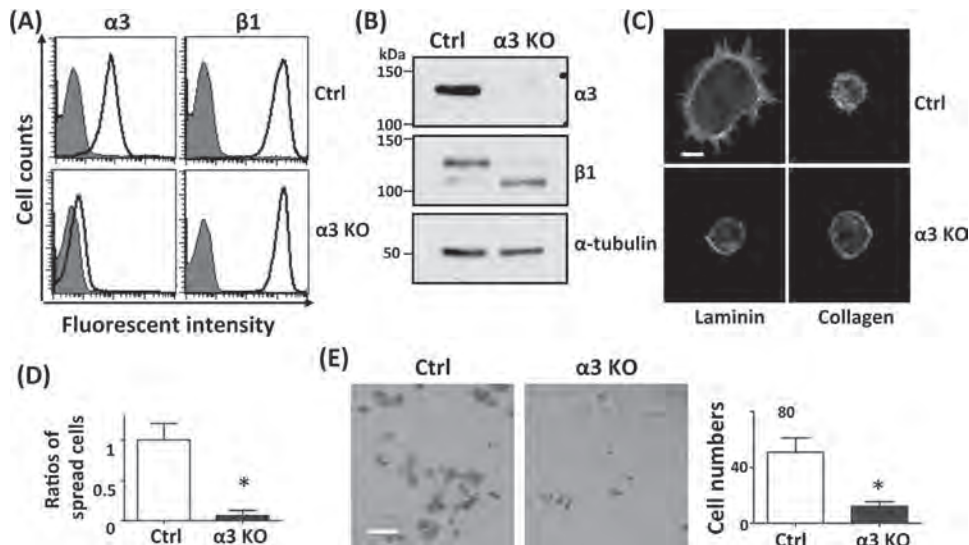


Figure 4. Effects of integrin $\alpha 3$ deficiency on cell spreading and migration. Establishment of integrin $\alpha 3$ KO MDA-MB-231 cells using the CRISPR/Cas9 system is described under “Experimental procedures.” The efficiency of $\alpha 3$ KO was assessed via flow cytometric analysis (A) and Western blotting (B). A, Both $\alpha 3$ KO and Ctrl cells were stained with (bold line) or without (gray shading) anti- $\alpha 3$ or $\beta 1$ integrin antibody and subjected to FACS analysis. B, the same amount of cell lysate was subjected to Western blotting to detect the indicated antibodies. C, cells were replated on coverslips coated with the indicated ECM, followed by incubation for 30 min, and were then fixed and stained with Alexa Fluor–conjugated phalloidin. Representative images are shown. Scale bar = 10 μm . D, cells were detached and then replated on laminin 332-coated dishes. After incubation for 15 min, the cells were fixed. The ratios of cell spreading were calculated. Cell spreading was defined as a cell spread of more than 0.025 μm^2 . Values represent the means \pm S.E. ($n = 5$). *, $p < 0.05$ (Welch’s t test). E, cell migration toward laminin-332 was determined using a Transwell assay. Scale bar = 100 μm . The quantitative data were obtained from three independent experiments. Values represent the means \pm S.E. ($n = 6$). *, $p < 0.05$ (Welch’s t test).

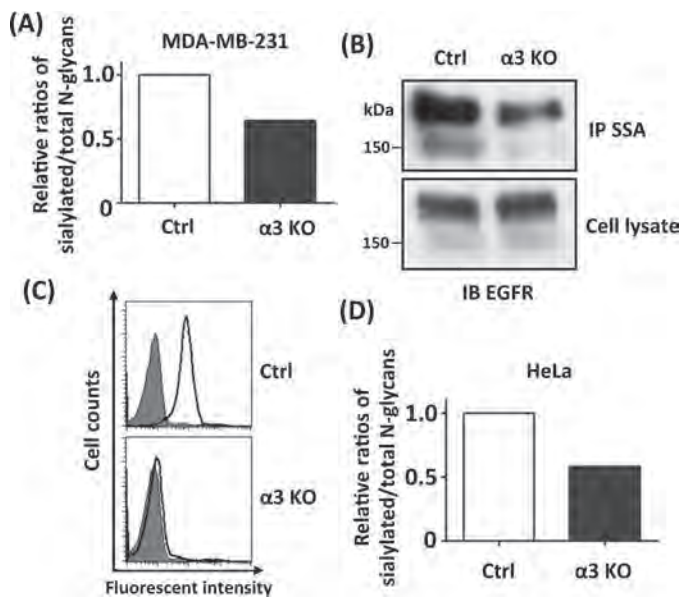


Figure 5. Deficiency of integrin $\alpha 3$ decreased sialylation of N -glycans in different cell lines. A, N -glycans released from both Ctrl and $\alpha 3$ KO MDA-MB-231 cells were pyridylaminated and verified as populations of sialylated N -glycans. The relative ratios of sialylated N -glycans versus total N -glycans were calculated by subtracting the neutral portions from the total and then dividing by the total. The control data were set as 1. B, equal amounts of cell lysates for control and $\alpha 3$ knockout cells were precipitated via SSA-agarose and probed with anti-SSA antibody (top panel). The same cell lysates were also probed with anti-EGFR antibody as a loading control (bottom panel). IP, immunoprecipitation. C, $\alpha 3$ KO of HeLa cells was established using the CRISPR/Cas9 system and verified via flow cytometric analysis. D, the ratios of sialylated N -glycans were analyzed as described in A.

the Golgi, is also important for the localization of several glycosyltransferases (10, 55, 56). Our previous study showed that knockdown of GOLPH3 leads to down-regulation of both $\alpha 2,3$ and $\alpha 2,6$ sialylation but has no effect on the transcription of

sialyltransferases. Therefore, regulation of biosynthetic glycan is not only dependent on the expression levels of glycosyltransferases but also on those of substrates, chaperones, and on the environment of the Golgi apparatus.

Considering that PI4P is a relatively abundant phosphoinositide that is required for the maintenance and function of the Golgi apparatus, which includes intracellular trafficking, it is plausible that PI4K could be involved in membrane transport from the trans-Golgi network to the plasma membrane. In fact, PI4KII α is known to associate with several cellular receptors such as EGFR, E-cadherin, LDL receptor-related protein, and the Fas receptor (57–60). In addition, alteration of the N -glycosylation of such receptors also regulates the functions of these receptors. For example, N -glycosylation is required for EGFR trafficking and has an effect on its endocytosis (61, 62). N -glycans of the LRP ectodomain also regulate the conformation and bending angle of the receptor (63). Cell surface sialylation protects Fas ligand-induced apoptosis by modification of the Fas ligand receptor (64), which could partially explain why enhancement of apoptosis has been observed in PI4KII α knockdown cells (60). Thus, the various phenotypes associated with PI4P and membrane proteins might be partially due to alteration of glycosylation.

The expression level of integrin $\beta 1$ is negatively correlated with the survival rates of patients with invasive breast cancer (65, 66), particularly $\alpha 3\beta 1$ expression in breast carcinoma associated with metastasis (41). During tumor progression, PI4KII α is also significantly up-regulated along with tumor growth compared with corresponding normal tissue (67). Given the importance of sialylation as described here, it is reasonable to expect up-regulation of both $\alpha 3\beta 1$ and PI4KII α in cancer cells.

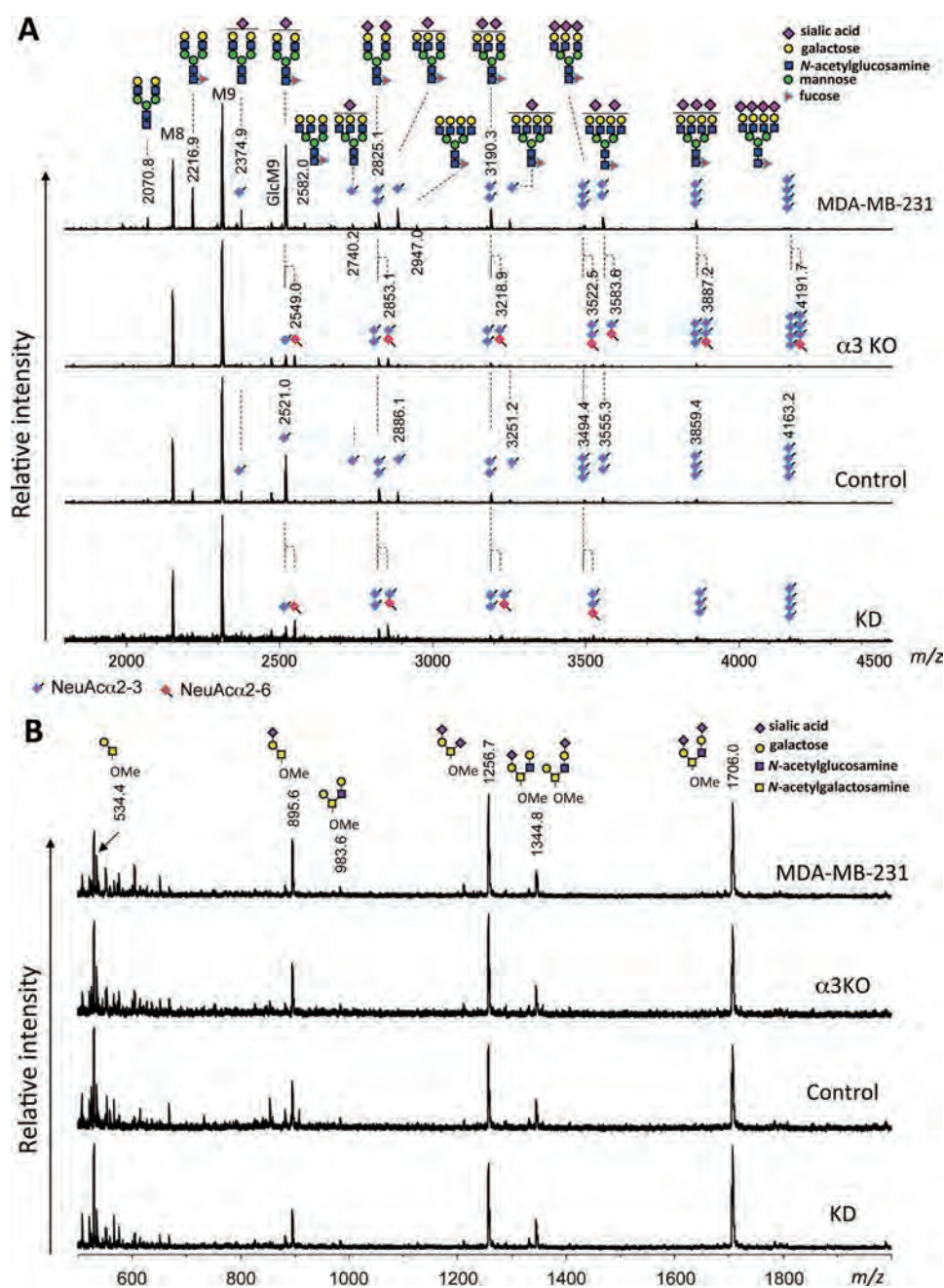


Figure 6. MS spectra of glycans obtained from cultured cells. *A*, MS spectra of *N*-linked glycans. The reducing ends of the *N*-linked glycans were derivatized with aWR (86). The sialic acids of the *N*-linked glycans were differentially amidated with methylamine (+13.0 Da) for $\alpha 2,3$ -sialic acids and isopropylamine (+41.1 Da) for $\alpha 2,6$ -sialic acids via the SALSA method (87). MDA-MB-231 and $\alpha 3$ KO cells refer to parent and $\alpha 3$ knockout cells, respectively. KD and control cells of MDA-MB-231 cell line refer to transfectants with DOX-inducible knockdown of PI4KII α cultured with or without DOX, respectively. *B*, MS spectra of *O*-linked glycans. The *O*-linked glycans were obtained as the corresponding alditols and then permethylated.

These facts raise the question of why the interaction of PI4KII α with integrin $\alpha 3\beta 1$ but not of $\alpha 5\beta 1$ regulates sialylation. So far, the association underlying the mechanism between $\alpha 3\beta 1$ and PI4KII α remains unclear. However, the specificity of $\alpha 3\beta 1$ could be due to its interaction with the tetraspanin family, such as CD151, CD63, and CD9. In fact, other studies have reported that integrin $\alpha 3\beta 1$ and the tetraspanin family can interact with type II of PI4K (25–27). In addition, palmitoylation could also be a plausible factor because PI4Ks are proteins with membrane association and activity that are highly dependent on such a modification (68, 69), and palmitoylation also

plays an important role in the association between integrin and several molecules, such as tetraspanin and c-Met (70, 71). We assume that the association between PI4KII α and $\alpha 3$, but $\alpha 5$, might also relate to tetraspanin or palmitoylation.

It is noteworthy that both cell spreading and migration on laminin 332 of integrin $\alpha 3$ KO cells were significantly suppressed (Fig. 4), which further supports the notion that $\alpha 3\beta 1$ is a major receptor of lamin-332 compared with integrin $\alpha 6\beta 1$ and $\alpha 6\beta 4$ in epithelial cells (43, 72). Accumulating evidence shows that integrin $\alpha 3\beta 1$ is important for tumor metastasis in human breast and prostate cancer cell lines (40, 41) and sialy-

Importance of the PI4K-integrin $\alpha 3\beta 1$ complex for sialylation

lation of adhesive molecules such as integrin $\beta 1$, which, in turn, contributes to tumorigenesis (73). In this study, $\alpha 3$ deficiency significantly inhibited sialylation, indicating a novel link between sialylation and this integrin, which demonstrated the importance for both forms of functional expression. Although the MS analysis clearly showed that the complex between PI4KII α and integrin $\alpha 3$ regulates the biosynthesis of sialylation on *N*-glycans but not *O*-glycans, we could not completely exclude other possibilities for the regulation of *N*-glycan structures other than sialylation or gangliosides. In addition, it has been reported that GOLPH3 containing a PI4P binding domain could control Golgi localization of core 2 *N*-acetylglucosaminyltransferase 1 for the biosynthesis of *O*-glycans (74). Thus, further studies are required to explain the underlying mechanism for different influences, such as localization of glycosyltransferase, pH environment (75), and cholesterol homeostasis (76) through this system. Taken together, this study may provide a new concept for the regulation of glycosylation and could suggest insights for the development of cancer treatment.

Experimental procedures

Cell lines and cell culture

The HeLa and 293T cells were obtained from the RIKEN Bioresource Research Center (Japan). The MDA-MB-231 cells were purchased from the ATCC. All cell lines were maintained at 37 °C in DMEM containing 10% FBS in a humidified atmosphere of 5% CO₂.

PCR for mRNA expression analysis

Total RNA was prepared with TRIzol (Invitrogen), and 1.0 μ g of RNA was reverse-transcribed using the PrimeScript RT reagent kit (Takara Bio Inc.) according to the manufacturer's instructions. PCR primers against ST3GAL3, ST3GAL4, ST6GAL1, and GAPDH have been described previously (54). The following primers were used for PI4KII α : 5'-CTCCAGCGGAAGCTACTTCG-3' and 5'-TCCACTTAGGATTAAGATGCCCA-3'.

shRNA-mediated silencing of PI4KII α in MDA-MB-231 cells

Conditional knockdown of the target gene was achieved using the DOX-inducible CS-RfA-ETBsd lentivirus vector (RIKEN) with minor modifications (11, 54). The following oligonucleotides were inserted into pENTR/H1/TO (Invitrogen): 5'-CACCAGAAGCAGAACCTCTTCCTGATGATATGTGCATCAGGAAGAGGTTCTGCTTCT-3' and 5'-AAAAAGAAGCAGAACCTCTTCCTGATGCACATATCATCAGGAAGAGGTTCTGCTTCT-3' (29). The use of LR Clonase allowed the inserted oligo to be transferred to CS-RfA-ETBsd, which is an encoding DOX-dependent transactivator for shRNA expression. The resultant vector was then transfected into 293T cells with packaging plasmids of calcium phosphate for the preparation of viruses. MDA-MB-231 cells were then infected with the obtained viruses and selected for stable integration with 1 μ g/ml blasticidin. shRNA-mediated silencing of PI4KII α was induced by addition of 1 μ g/ml DOX for 72 h in the established cell line, and cells cultured in DOX-free medium were used as a control.

Gene introduction using the lentivirus system

The cDNA sequences for the PH domain of human FAPP1, PI4KII α , and integrin $\alpha 3$ were cloned from HeLa cells and inserted into pENTR vectors (pENTR/D-TOPO cloning kit, Invitrogen). To obtain the *N*-terminal GFP-tagged PI4KII α , C-terminal mRFP-tagged FAPP1 and a C-terminal GFP-tagged integrin $\alpha 3$, in-fusion enzyme (Clontech) was used with standard PCR protocols. The linkers for GFP-PI4KII α , mRFP-FAPP1, and $\alpha 3$ -GFP were 5'-GGGGS-3', 5'-KNPPVAT-3' (37), and 5'-LELKLRLQSTVPRARDPPVAT-3', respectively. The resultant cDNAs were confirmed by DNA sequencing using an ABI Prism 3130 sequencer (Applied Biosystems Japan Ltd., Tokyo, Japan). The subcloned cDNAs were transferred into CSII-EF-Rfa (11) via LR Clonase (Invitrogen) for lentivirus production. The resultant vectors (CSII-EF-GFP-PI4KII α /mRFP-FAPP1/ $\alpha 3$ -GFP) and the previously constructed integrins of either $\alpha 5$ -GFP- or $\beta 1$ -overexpressed lentiviral vectors (CSII-EF- $\alpha 5$ GFP (77)/ $\beta 1$ (78)) were then transfected into 293T cells with packaging plasmids via calcium phosphate during the preparation of viruses. Either MDA-MB-231 or 293T cells were then infected with the obtained viruses for further experiments.

Cell migration (Boyden chamber assay)

Cell Migration was performed as described previously with minor modifications (11, 79). Each Transwell (BD BioCoat control inserts, 8.0- μ m inserts; BD Biosciences) was coated only on the bottom side with 1 μ g/ml laminin-332 (Oriental Yeast Co., Ltd.) in PBS containing 0.1% BSA at 4 °C for 24 h and then blocked with 5% BSA in DMEM at 37 °C for 1 h. Cells were trypsinized and suspended in DMEM containing 1% FBS. The suspended cells were centrifuged, and the cell pellets were resuspended in an assay medium (0.1% BSA in DMEM containing 1% FBS) and diluted to 3 $\times 10^5$ cells/ml; cell viability was confirmed by trypan blue staining. Cell suspensions were then added to the Transwell. Following incubation, the membranes were fixed with 4% paraformaldehyde and stained with 0.5% crystal violet solution (Merck) for 24 h. After washing the Transwells with PBS, cells that migrated to the lower side were counted using a phase-contrast microscope.

Immunostaining

Cells (1 $\times 10^5$) were plated on glass coverslips (MatTek), precoated with or without ECM for 24 h, fixed with 4% paraformaldehyde for 15 min, permeabilized with 0.1% Triton X-100 for 10 min, and blocked with PBS containing 3% BSA and 0.01% Tween 20 (PBSBT) for 1 h. Cells were then incubated with the indicated primary antibodies (GM130, BD Biosciences, 610822; $\alpha 3$, Millipore, P1B5) at 4 °C overnight, followed by incubation with Alexa Fluor 647-conjugated secondary antibodies (Molecular Probes) for 1 h. For lectin staining, cells on coverslips were incubated with either biotinylated SNA lectin (Vector Laboratories, B-1305) or wheat germ agglutinin (WGA) lectin (J-Oil Mills, J220) at 4 °C for 30 min in DMEM, fixed and blocked with PBSBT for 1 h, followed by incubation with streptavidin-conjugated Alexa Fluor 647 at 4 °C for 1 h in the dark. All samples were mounted using Prolong Diamond Antifade mounting medium (Molecular Probes). Images were acquired by sequential excitation using an Olympus FV1000 laser-scanning confo-

cal microscope with an UPlanSApo $\times 60/1.35$ oil objective operated with F10-ASW version 4.02 software.

Cell spreading and adhesion experiment

Coverslips were coated with 1 $\mu\text{g}/\text{ml}$ laminin-332 or 2 mg/ml gelatin in PBS containing 0.1% BSA at 4 °C for 24 h and then blocked with 5% BSA in DMEM at 37 °C for 1 h. Cells were replated on the coverslips in DMEM with 0.1% BSA. After incubation for 10 min, the areas of adherent cells were measured using ImageJ. We defined cells spread at more than 0.025 μm^2 as adherent cells. After incubation for 30 min, the cells were fixed with 4% paraformaldehyde and stained with phalloidin–Alexa Fluor 647 (Molecular Probes).

Immunoprecipitation and Western blotting

Immunoprecipitation was performed as described previously with minor modifications (11, 80). Briefly, cells were gently rinsed three times with PBS at room temperature and solubilized in cold lysis buffer A (20 mM Tris-HCl (pH 7.4), 150 mM NaCl, and 1% Brij98), which included protease inhibitors. Protein concentrations of lysates were determined via BCA assay (Pierce). The lysates were immunoprecipitated using either anti-GFP-agarose (MBL), anti-integrin $\alpha 3$ antibody (Millipore, P1B5), or anti-integrin $\beta 1$ (P5D2, DSHB) with Ab-Capcher Protein A-R28 (Protenova, Tokushima, Japan) for 1 h at 4 °C and gentle rotation. After washing with lysis buffer, the immunoprecipitates were subjected to SDS-PAGE. The proteins were probed with anti-integrin $\alpha 3$ (Santa Cruz Biotechnology, sc-6592) or anti-GFP antibody (Rockland, 600-101-215) and then detected using anti-goat IgG-conjugated horseradish peroxidase (Santa Cruz Biotechnology) with an Immobilon Western chemiluminescent horseradish peroxidase substrate (Millipore). For analysis of the lectin precipitates, we used lysis buffer B (20 mM Tris-HCl (pH 7.4), 150 mM NaCl, and 1% Triton X-100). Cell lysates were precipitated with either SSA-agarose (J-Oil Mills, J318), MAM (also called MAL-1)–agarose (J-Oil Mills, J310) or concanavalin A (ConA)–agarose (J-Oil Mills, J303), which specifically recognize either $\alpha 2,6$ - and $\alpha 2,3$ -sialylation or total *N*-glycans, respectively. The precipitants were detected using either anti-integrin $\beta 1$ (BD Biosciences, 610468) or anti-EGFR (Cell Signaling Technology, 4267). Antibody agents against Akt (9272) and p-Akt (4060) were purchased from Cell Signaling Technology. α -Tubulin (Sigma, T6199) was used as a loading control.

Flow cytometric analysis

Flow cytometric analysis was performed as described previously with minor modifications (11, 79, 80). Briefly, semiconfluent cells were detached from the culture dishes using trypsin containing 1 mM EDTA. The cells were subsequently stained with or without primary mouse anti- $\alpha 3$ (P1B5), anti- $\beta 1$ (P5D2), and anti- $\alpha 5$ integrin (Millipore, HA5) in PBS, followed by incubation with Alexa Fluor 647–conjugated secondary antibodies. For staining cells with biotin-conjugated lectins (MAM and SNA), we used PBS buffer containing 0.5 mM CaCl_2 and MgCl_2 . Flow cytometric analysis was performed using a FACSCalibur flow cytometer and Cell Quest Pro software (BD Biosciences).

PA oligosaccharide preparation of *N*-glycosylation and quantitative analysis of sialylated *N*-glycans by anion exchange HPLC

To release *N*-glycans from glycoproteins, the lyophilized cell pellets (1–2 mg) were heated with 200 μl of anhydrous hydrazine at 100 °C for 10 h using an oil bath. Removal of hydrazine and acetylation of *N*-glycans were carried out with a graphite carbon column (81). The released *N*-glycans were then 2-pyridylaminated using the Pyridylation Manual Kit (Takara Bio Inc.), and then the excess 2-aminopyridine was removed via phenol–chloroform extraction (81) with a gel filtration column (82). The prepared PA oligosaccharides treated with or without neuraminidases were subjected to a HPLC system (JASCO) equipped with a TSKgel DEAE-5PW column (7.5 \times 75 mm, Tosoh) and analyzed as described previously (19). HPLC chromatogram data were analyzed using chromNAV software (JASCO). The amounts of total and neutral *N*-glycans were calculated based on the peak area of neutral fraction with or without neuraminidase treatment. Relative ratios of sialylated *N*-glycans versus total *N*-glycans were calculated by subtracting the neutral portions from the total and then dividing by the total. The data were normalized to the control as 1.

Generation of CRISPR/Cas9-based integrin $\alpha 3$ KO cells

CRISPR/Cas9-based integrin $\alpha 3$ cells were established as described previously (83, 84). Briefly, the single guide RNA-specifying oligo sequences spanning human integrin $\alpha 3$ (forward, 5'-CACCGCATCGGGCACAGCGAGCTCC-3'; reverse, 5'-AAACGGAGCTCGCTGTGCCCGATGC-3) were chosen from the human KO library (85). Then the oligos were cloned into pSpCas9 (BB)-2A-GFP, which was a kind gift from Dr. Feng Zhang (Addgene plasmid ID 48138). The plasmid was transfected into cells according to the manufacturer's instructions (Amaya Cell Line Nucleofector kitV). After 4 days of transfection, GFP-positive cells were sorted using a FACSAria II (BD Bioscience). Following 10-day culture, $\alpha 3$ -negative and GFP-negative cells were sorted, and the procedure was repeated twice. The KO cells were defined by flow cytometry and Western blot analysis as described above.

Mass spectrometry of glycans

Total plasma membrane proteins of cells were prepared using a plasma membrane protein extraction kit (101Bio). For *N*-glycan analysis, a previous report (86) suggests that the pellets are dissolved and denatured and then digested by glycopeptidase F (Takara Bio Inc.). The released *N*-glycans were captured on hydrazide beads (BlotGlyco, 5 mg, Sumitomo Bakelite Co., Ltd.) using a process recommended by the manufacturer. Sialic acids of the *N*-glycans on the beads were then differentially amidated with methylamine for $\alpha 2,3$ -sialic acids and isopropylamine for $\alpha 2,6$ -sialic acids using the sialic acid linkage-specific alkylamidation (SALSA) method (87). The derivatized *N*-glycans were liberated, labeled with aoWR (a component of BlotGlyco, Sumitomo Bakelite Co., Ltd.) (86), and purified according to the manufacturer's instructions. The obtained glycan solutions were mixed with a 2,5-dihydroxybenzoic acid solution (10 mg/ml in 30% acetonitrile) at a ratio of 1:10. Aliquots (0.5 μl) of the mixed solutions were deposited onto a

Importance of the PI4K-integrin $\alpha 3\beta 1$ complex for sialylation

MALDI target plate and dried. MS spectra were acquired with a MALDI quadrupole ion trap TOF mass spectrometer (AXIMA-QIT, Shimadzu Corp.). For O-glycan analysis, pellets of the membrane fractions were dissolved in a 1% SDS solution. Aliquots (10 μ l) of the solution were transferred into 90 μ l of 0.6 M sodium borohydride containing 60 mM NaOH and incubated at 45 °C for 16 h. Then the mixtures were neutralized, diluted to 1 ml, and applied onto a solid-phase extraction cartridge (Sep-Pak C18 Vac 1cc, 50 mg, Waters Corp.), and then the cartridge was washed with distilled water (1 ml). The eluents and washings were combined and lyophilized. The obtained residues were dissolved in 1% acetic acid in methanol (100 μ l) and evaporated using a centrifuge evaporator. The procedure of dissolution and evaporation was repeated. The obtained residues were permethylated according to previous reports (88). The permethylated glycans were dissolved in a 2,5-dihydroxybenzoic acid solution (20 μ l, 10 mg/ml in 30% acetonitrile), and aliquots (0.5 μ l) of the mixed solutions were deposited onto a MALDI target plate and dried. MS spectra were acquired with a MALDI-TOF mass spectrometer (Ultraflex, Bruker Daltonik).

Author contributions—T. I., T. F., and J. G. conceptualization; T. I., S. I., A. K., Y. W., and J. G. data curation; T. I., S. I., A. K., Y. W., and J. G. formal analysis; T. I. and J. G. supervision; T. I., S. I., A. K., Y. W., T. F., and J. G. validation; T. I., S. I., A. K., and Y. W. investigation; T. I., S. I., A. K., Y. W., T. F., and J. G. methodology; T. I. and S. I. writing-original draft; T. I., S. I., A. K., Y. W., T. F., and J. G. writing-review and editing; S. I. visualization; A. K. and J. G. funding acquisition.

Acknowledgments—We thank Dr. Takashi Nishikaze for informative suggestions regarding the SALSA method and Dr. Wai Wai The Tin for technical assistance with glycan analysis.

References

- Christie, D. R., Shaikh, F. M., Lucas, J. A., 4th, Lucas, J. A., 3rd, and Bellis, S. L. (2008) ST6Gal-I expression in ovarian cancer cells promotes an invasive phenotype by altering integrin glycosylation and function. *J. Ovarian Res.* **1**, 3 [CrossRef Medline](#)
- Lin, S., Kemmer, W., Grigull, S., and Schlag, P. M. (2002) Cell surface $\alpha 2,6$ sialylation affects adhesion of breast carcinoma cells. *Exp. Cell Res.* **276**, 101–110 [CrossRef Medline](#)
- Zhuo, Y., Chammas, R., and Bellis, S. L. (2008) Sialylation of $\beta 1$ integrins blocks cell adhesion to galectin-3 and protects cells against galectin-3-induced apoptosis. *J. Biol. Chem.* **283**, 22177–22185 [CrossRef Medline](#)
- Hasehira, K., Hirabayashi, J., and Tatenno, H. (2017) Structural and quantitative evidence of $\alpha 2-6$ -sialylated N-glycans as markers of the differentiation potential of human mesenchymal stem cells. *Glycoconj. J.* **34**, 797–806 [Medline](#)
- Wang, Y. C., Stein, J. W., Lynch, C. L., Tran, H. T., Lee, C. Y., Coleman, R., Hatch, A., Antontsev, V. G., Chy, H. S., O'Brien, C. M., Murthy, S. K., Laslett, A. L., Peterson, S. E., and Loring, J. F. (2015) Glycosyltransferase ST6GAL1 contributes to the regulation of pluripotency in human pluripotent stem cells. *Sci. Rep.* **5**, 13317 [CrossRef Medline](#)
- Kornfeld, R., and Kornfeld, S. (1985) Assembly of asparagine-linked oligosaccharides. *Annu. Rev. Biochem.* **54**, 631–664 [CrossRef Medline](#)
- Grabenhorst, E., and Conradt, H. S. (1999) The cytoplasmic, transmembrane, and stem regions of glycosyltransferases specify their *in vivo* functional sublocalization and stability in the Golgi. *J. Biol. Chem.* **274**, 36107–36116 [CrossRef Medline](#)
- Dalziel, M., Dall'Olio, F., Mungul, A., Piller, V., and Piller, F. (2004) Ras oncogene induces beta-galactoside $\alpha 2,6$ -sialyltransferase (ST6Gal I) via a RalGEF-mediated signal to its housekeeping promoter. *Eur. J. Biochem.* **271**, 3623–3634 [CrossRef Medline](#)
- Seales, E. C., Jurado, G. A., Singhal, A., and Bellis, S. L. (2003) Ras oncogene directs expression of a differentially sialylated, functionally altered $\beta 1$ integrin. *Oncogene* **22**, 7137–7145 [CrossRef Medline](#)
- Eckert, E. S., Reckmann, I., Hellwig, A., Röhling, S., El-Battari, A., Wieland, F. T., and Popoff, V. (2014) Golgi phosphoprotein 3 triggers signal-mediated incorporation of glycosyltransferases into coatamer-coated (COPI) vesicles. *J. Biol. Chem.* **289**, 31319–31329 [CrossRef Medline](#)
- Isaji, T., Im, S., Gu, W., Wang, Y., Hang, Q., Lu, J., Fukuda, T., Hashii, N., Takakura, D., Kawasaki, N., Miyoshi, H., and Gu, J. (2014) An oncogenic protein Golgi phosphoprotein 3 up-regulates cell migration via sialylation. *J. Biol. Chem.* **289**, 20694–20705 [CrossRef Medline](#)
- Scott, K. L., Kabbarah, O., Liang, M. C., Ivanova, E., Anagnostou, V., Wu, J., Dhakal, S., Wu, M., Chen, S., Feinberg, T., Huang, J., Saci, A., Widlund, H. R., Fisher, D. E., Xiao, Y., et al. (2009) GOLPH3 modulates mTOR signalling and rapamycin sensitivity in cancer. *Nature* **459**, 1085–11068 [CrossRef Medline](#)
- Zeng, Z., Lin, H., Zhao, X., Liu, G., Wang, X., Xu, R., Chen, K., Li, J., and Song, L. (2012) Overexpression of GOLPH3 promotes proliferation and tumorigenicity in breast cancer via suppression of the FOXO1 transcription factor. *Clin. Cancer Res.* **18**, 4059–4069 [CrossRef Medline](#)
- Dippold, H. C., Ng, M. M., Farber-Katz, S. E., Lee, S. K., Kerr, M. L., Peterman, M. C., Sim, R., Wiharto, P. A., Galbraith, K. A., Madhavarapu, S., Fuchs, G. J., Meerloo, T., Farquhar, M. G., Zhou, H., and Field, S. J. (2009) GOLPH3 bridges phosphatidylinositol-4-phosphate and actomyosin to stretch and shape the Golgi to promote budding. *Cell* **139**, 337–351 [CrossRef Medline](#)
- Ng, M. M., Dippold, H. C., Buschman, M. D., Noakes, C. J., and Field, S. J. (2013) GOLPH3L antagonizes GOLPH3 to determine Golgi morphology. *Mol. Biol. Cell* **24**, 796–808 [CrossRef Medline](#)
- Clayton, E. L., Minogue, S., and Waugh, M. G. (2013) Mammalian phosphatidylinositol 4-kinases as modulators of membrane trafficking and lipid signaling networks. *Prog. Lipid Res.* **52**, 294–304 [CrossRef Medline](#)
- Park, C. C., Zhang, H., Pallavicini, M., Gray, J. W., Baehner, F., Park, C. J., and Bissell, M. J. (2006) $\beta 1$ integrin inhibitory antibody induces apoptosis of breast cancer cells, inhibits growth, and distinguishes malignant from normal phenotype in three dimensional cultures and *in vivo*. *Cancer Res.* **66**, 1526–1535 [CrossRef Medline](#)
- Takada, Y., Ye, X., and Simon, S. (2007) The integrins. *Genome Biol.* **8**, 215 [CrossRef Medline](#)
- Lu, J., Isaji, T., Im, S., Fukuda, T., Kameyama, A., and Gu, J. (2016) Expression of N-acetylglucosaminyltransferase III suppresses $\alpha 2,3$ -sialylation, and its distinctive functions in cell migration are attributed to $\alpha 2,6$ -sialylation levels. *J. Biol. Chem.* **291**, 5708–5720 [CrossRef Medline](#)
- Isaji, T., Gu, J., Nishiuchi, R., Zhao, Y., Takahashi, M., Miyoshi, E., Honke, K., Sekiguchi, K., and Taniguchi, N. (2004) Introduction of bisecting GlcNAc into integrin $\alpha 5\beta 1$ reduces ligand binding and down-regulates cell adhesion and cell migration. *J. Biol. Chem.* **279**, 19747–19754 [CrossRef Medline](#)
- Guo, H. B., Lee, I., Kamar, M., Akiyama, S. K., and Pierce, M. (2002) Aberrant N-glycosylation of $\beta 1$ integrin causes reduced $\alpha 5\beta 1$ integrin clustering and stimulates cell migration. *Cancer Res.* **62**, 6837–6845 [Medline](#)
- Hou, S., Hang, Q., Isaji, T., Lu, J., Fukuda, T., and Gu, J. (2016) Importance of membrane-proximal N-glycosylation on integrin $\beta 1$ in its activation and complex formation. *FASEB J.* **30**, 4120–4131 [CrossRef Medline](#)
- Hynes, R. O. (2002) Integrins: bidirectional, allosteric signaling machines. *Cell* **110**, 673–687 [CrossRef Medline](#)
- Mitra, S. K., Hanson, D. A., and Schlaepfer, D. D. (2005) Focal adhesion kinase: in command and control of cell motility. *Nat. Rev. Mol. Cell Biol.* **6**, 56–68 [CrossRef Medline](#)
- Yauch, R. L., Berditchevski, F., Harler, M. B., Reichner, J., and Hemler, M. E. (1998) Highly stoichiometric, stable, and specific association of integrin $\alpha 3\beta 1$ with CD151 provides a major link to phosphatidylinositol 4

- kinase, and may regulate cell migration. *Mol. Biol. Cell* **9**, 2751–2765 [CrossRef Medline](#)
26. Berditchevski, F., Toliás, K. F., Wong, K., Carpenter, C. L., and Hemler, M. E. (1997) A novel link between integrins, transmembrane-4 superfamily proteins (CD63 and CD81), and phosphatidylinositol 4-kinase. *J. Biol. Chem.* **272**, 2595–2598 [CrossRef Medline](#)
 27. Yauch, R. L., and Hemler, M. E. (2000) Specific interactions among transmembrane 4 superfamily (TM4SF) proteins and phosphoinositide 4-kinase. *Biochem. J.* **351**, 629–637 [CrossRef Medline](#)
 28. Boura, E., and Nencka, R. (2015) Phosphatidylinositol 4-kinases: function, structure, and inhibition. *Exp. Cell Res.* **337**, 136–145 [CrossRef Medline](#)
 29. Wang, Y. J., Wang, J., Sun, H. Q., Martinez, M., Sun, Y. X., Macia, E., Kirchhausen, T., Albanesi, J. P., Roth, M. G., and Yin, H. L. (2003) Phosphatidylinositol 4 phosphate regulates targeting of clathrin adaptor AP-1 complexes to the Golgi. *Cell* **114**, 299–310 [CrossRef Medline](#)
 30. D'Angelo, G., Vicinanza, M., Di Campli, A., and De Matteis, M. A. (2008) The multiple roles of PtdIns₄P: not just the precursor of PtdIns_{4,5}P-2. *J. Cell Sci.* **121**, 1955–1963 [CrossRef Medline](#)
 31. Weixel, K. M., Blumental-Perry, A., Watkins, S. C., Aridor, M., and Weisz, O. A. (2005) Distinct Golgi populations of phosphatidylinositol 4-phosphate regulated by phosphatidylinositol 4-kinases. *J. Biol. Chem.* **280**, 10501–10508 [CrossRef Medline](#)
 32. Morrow, A. A., Alipour, M. A., Bridges, D., Yao, Z., Saltiel, A. R., and Lee, J. M. (2014) The lipid kinase PI4KIII β is highly expressed in breast tumors and activates Akt in cooperation with Rab11a. *Mol. Cancer Res.* **12**, 1492–1508 [CrossRef Medline](#)
 33. Moravcevic, K., Oxley, C. L., and Lemmon, M. A. (2012) Conditional peripheral membrane proteins: facing up to limited specificity. *Structure* **20**, 15–27 [CrossRef Medline](#)
 34. Rabouille, C., Hui, N., Hunte, F., Kieckbusch, R., Berger, E. G., Warren, G., and Nilsson, T. (1995) Mapping the distribution of Golgi enzymes involved in the construction of complex oligosaccharides. *J. Cell Sci.* **108**, 1617–1627 [Medline](#)
 35. Lu, D., Sun, H. Q., Wang, H., Barylko, B., Fukata, Y., Fukata, M., Albanesi, J. P., and Yin, H. L. (2012) Phosphatidylinositol 4-kinase II α is palmitoylated by Golgi-localized palmitoyltransferases in cholesterol-dependent manner. *J. Biol. Chem.* **287**, 21856–21865 [CrossRef Medline](#)
 36. Bhide, G. P., and Colley, K. J. (2017) Sialylation of N-glycans: mechanism, cellular compartmentalization and function. *Histochem. Cell Biol.* **147**, 149–174 [CrossRef Medline](#)
 37. Balla, A., Tuymetova, G., Tsiomenko, A., Várnai, P., and Balla, T. (2005) A plasma membrane pool of phosphatidylinositol 4-phosphate is generated by phosphatidylinositol 4-kinase type-III α : studies with the PH domains of the oxysterol binding protein and FAPP1. *Mol. Biol. Cell* **16**, 1282–1295 [CrossRef Medline](#)
 38. Itakura, Y., Nakamura-Tsuruta, S., Kominami, J., Tateno, H., and Hirabayashi, J. (2017) Sugar-binding profiles of chitin-binding lectins from the hevein family: a comprehensive study. *Int. J. Mol. Sci.* **18**, E1160 [CrossRef Medline](#)
 39. Grottke, A., Ewald, F., Lange, T., Nörz, D., Herzberger, C., Bach, J., Grabski, N., Gräser, L., Höppner, F., Nashan, B., Schumacher, U., and Jücker, M. (2016) Downregulation of AKT3 Increases migration and metastasis in triple negative breast cancer cells by upregulating S100A4. *PLoS ONE* **11**, e0146370 [CrossRef Medline](#)
 40. Mitchell, K., Svenson, K. B., Longmate, W. M., Gkirtzimanaki, K., Sadej, R., Wang, X., Zhao, J., Eliopoulos, A. G., Berditchevski, F., and Dipersio, C. M. (2010) Suppression of Integrin $\alpha 3\beta 1$ in breast cancer cells reduces cyclooxygenase-2 gene expression and inhibits tumorigenesis, invasion, and cross-talk to endothelial cells. *Cancer Res.* **70**, 6359–6367 [CrossRef Medline](#)
 41. Morini, M., Mottolise, M., Ferrari, N., Ghiorzo, F., Buglioni, S., Mortarini, R., Noonan, D. M., Natali, P. G., and Albini, A. (2000) The $\alpha 3\beta 1$ integrin is associated with mammary carcinoma cell metastasis, invasion, and gelatinase B (MMP-9) activity. *Int. J. Cancer* **87**, 336–342 [CrossRef Medline](#)
 42. Cagnet, S., Faraldo, M. M., Kreft, M., Sonnenberg, A., Raymond, K., and Glukhova, M. A. (2014) Signaling events mediated by $\alpha 3\beta 1$ integrin are essential for mammary tumorigenesis. *Oncogene* **33**, 4286–4295 [CrossRef Medline](#)
 43. Dogic, D., Rousselle, P., and Aumailley, M. (1998) Cell adhesion to laminin 1 or 5 induces isoform-specific clustering of integrins and other focal adhesion components. *J. Cell Sci.* **111**, 793–802 [Medline](#)
 44. Liu, Y. C., Yen, H. Y., Chen, C. Y., Chen, C. H., Cheng, P. F., Juan, Y. H., Chen, C. H., Khoo, K. H., Yu, C. J., Yang, P. C., Hsu, T. L., and Wong, C. H. (2011) Sialylation and fucosylation of epidermal growth factor receptor suppress its dimerization and activation in lung cancer cells. *Proc. Natl. Acad. Sci. U.S.A.* **108**, 11332–11337 [CrossRef Medline](#)
 45. Varki, A., Kannagi, R., Toole, B., and Stanley, P. (2015) in *Essentials of Glycobiology* (Varki, A., Cummings, R. D., Esko, J. D., Stanley, P., Hart, G. W., Aebi, M., Darvill, A. G., Kinoshita, T., Packer, N. H., Prestegard, J. H., Schnaar, R. L., and Seeberger, P. H., eds.) pp. 597–609, Cold Spring Harbor Laboratory Press, Cold Spring Harbor, NY
 46. Brockhausen, I. (2006) Mucin-type O-glycans in human colon and breast cancer: glycodynamics and functions. *EMBO Rep.* **7**, 599–604 [CrossRef Medline](#)
 47. Dall'Olio, F., Malagolini, N., Trinchera, M., and Chiricolo, M. (2014) Sialosignaling: sialyltransferases as engines of self-fueling loops in cancer progression. *Biochim. Biophys. Acta* **1840**, 2752–2764 [CrossRef Medline](#)
 48. Schultz, M. J., Swindall, A. F., and Bellis, S. L. (2012) Regulation of the metastatic cell phenotype by sialylated glycans. *Cancer Metastasis Rev.* **31**, 501–518 [CrossRef Medline](#)
 49. Lu, J., and Gu, J. (2015) Significance of β -galactoside $\alpha 2,6$ sialyltransferase 1 in cancers. *Molecules* **20**, 7509–7527 [CrossRef Medline](#)
 50. Woodard-Grice, A. V., McBrayer, A. C., Wakefield, J. K., Zhuo, Y., and Bellis, S. L. (2008) Proteolytic shedding of ST6Gal-I by BACE1 regulates the glycosylation and function of $\alpha 4\beta 1$ integrins. *J. Biol. Chem.* **283**, 26364–26373 [CrossRef Medline](#)
 51. Kitazume, S., Imamaki, R., Ogawa, K., Komi, Y., Futakawa, S., Kojima, S., Hashimoto, Y., Marth, J. D., Paulson, J. C., and Taniguchi, N. (2010) $\alpha 2,6$ -sialic acid on platelet endothelial cell adhesion molecule (PECAM) regulates its homophilic interactions and correlates with antiapoptotic signaling. *J. Biol. Chem.* **285**, 6515–6521 [CrossRef Medline](#)
 52. Ye, X., and Weinberg, R. A. (2015) Epithelial-mesenchymal plasticity: a central regulator of cancer progression. *Trends Cell Biol.* **25**, 675–686 [CrossRef Medline](#)
 53. Swindall, A. F., Londoño-Joshi, A. I., Schultz, M. J., Fineberg, N., Buchsbaum, D. J., and Bellis, S. L. (2013) ST6Gal-I protein expression is upregulated in human epithelial tumors and correlates with stem cell markers in normal tissues and colon cancer cell lines. *Cancer Res.* **73**, 2368–2378 [CrossRef Medline](#)
 54. Lu, J., Isaji, T., Im, S., Fukuda, T., Hashii, N., Takakura, D., Kawasaki, N., and Gu, J. (2014) β -Galactoside $\alpha 2,6$ -sialyltransferase 1 promotes transforming growth factor β -mediated epithelial-mesenchymal transition. *J. Biol. Chem.* **289**, 34627–34641 [CrossRef Medline](#)
 55. Schmitz, K. R., Liu, J., Li, S., Setty, T. G., Wood, C. S., Burd, C. G., and Ferguson, K. M. (2008) Golgi localization of glycosyltransferases requires a Vps74p oligomer. *Dev. Cell* **14**, 523–534 [CrossRef Medline](#)
 56. Pereira, N. A., Pu, H. X., Goh, H., and Song, Z. (2014) Golgi phosphoprotein 3 mediates the Golgi localization and function of protein O-linked mannose β -1,2-N-acetylglucosaminyltransferase 1. *J. Biol. Chem.* **289**, 14762–14770 [CrossRef Medline](#)
 57. Minogue, S., Waugh, M. G., De Matteis, M. A., Stephens, D. J., Berditchevski, F., and Hsuan, J. J. (2006) Phosphatidylinositol 4-kinase is required for endosomal trafficking and degradation of the EGF receptor. *J. Cell Sci.* **119**, 571–581 [CrossRef Medline](#)
 58. Tokuda, E., Itoh, T., Hasegawa, J., Ijuin, T., Takeuchi, Y., Fukumoto, M., and Takenawa, T. (2014) Phosphatidylinositol 4-phosphate in the Golgi apparatus regulates cell-cell adhesion and invasive cell migration in human breast cancer. *Cancer Res.* **74**, 3054–3066 [CrossRef Medline](#)
 59. Qin, Y., Li, L., Pan, W., and Wu, D. (2009) Regulation of phosphatidylinositol kinases and metabolism by Wnt3a and Dvl. *J. Biol. Chem.* **284**, 22544–22548 [CrossRef Medline](#)
 60. Chu, K. M., Minogue, S., Hsuan, J. J., and Waugh, M. G. (2010) Differential effects of the phosphatidylinositol 4-kinases, PI4KII α and PI4KIII β , on Akt activation and apoptosis. *Cell Death Dis.* **1**, e106 [CrossRef Medline](#)

Importance of the PI4K-integrin $\alpha 3\beta 1$ complex for sialylation

61. Yamabhai, M., and Anderson, R. G. (2002) Second cysteine-rich region of epidermal growth factor receptor contains targeting information for caveolae/rafts. *J. Biol. Chem.* **277**, 24843–24846 [CrossRef Medline](#)
62. Sato, Y., Takahashi, M., Shibukawa, Y., Jain, S. K., Hamaoka, R., Miyagawa, J., Yaginuma, Y., Honke, K., Ishikawa, M., and Taniguchi, N. (2001) Over-expression of *N*-acetylglucosaminyltransferase III enhances the epidermal growth factor-induced phosphorylation of ERK in HeLaS3 cells by up-regulation of the internalization rate of the receptors. *J. Biol. Chem.* **276**, 11956–11962 [CrossRef Medline](#)
63. Matoba, K., Mihara, E., Tamura-Kawakami, K., Miyazaki, N., Maeda, S., Hirai, H., Thompson, S., Iwasaki, K., and Takagi, J. (2017) Conformational freedom of the LRP6 ectodomain is regulated by *N*-glycosylation and the binding of the Wnt antagonist Dkk1. *Cell Rep.* **18**, 32–40 [CrossRef Medline](#)
64. Swindall, A. F., and Bellis, S. L. (2011) Sialylation of the Fas death receptor by ST6Gal-I provides protection against Fas-mediated apoptosis in colon carcinoma cells. *J. Biol. Chem.* **286**, 22982–22990 [CrossRef Medline](#)
65. Jonjić, N., Lucin, K., Krstulja, M., Iternicka, Z., and Mustać, E. (1993) Expression of β -1 integrins on tumor-cells of invasive ductal breast-carcinoma. *Pathol. Res. Pract.* **189**, 979–984 [CrossRef Medline](#)
66. Yao, E. S., Zhang, H., Chen, Y. Y., Lee, B., Chew, K., Moore, D., and Park, C. (2007) Increased $\beta 1$ integrin is associated with decreased survival in invasive breast cancer. *Cancer Res.* **67**, 659–664 [CrossRef Medline](#)
67. Li, J., Lu, Y., Zhang, J., Kang, H., Qin, Z., and Chen, C. (2010) PI4KII α is a novel regulator of tumor growth by its action on angiogenesis and HIF-1 α regulation. *Oncogene* **29**, 2550–2559 [CrossRef Medline](#)
68. Zhou, Q., Li, J., Yu, H., Zhai, Y., Gao, Z., Liu, Y., Pang, X., Zhang, L., Schulten, K., Sun, F., and Chen, C. (2014) Molecular insights into the membrane-associated phosphatidylinositol 4-kinase II α . *Nat. Commun.* **5**, 3552 [CrossRef Medline](#)
69. Baumlova, A., Chalupska, D., Różycki, B., Jovic, M., Wisniewski, E., Klima, M., Dubankova, A., Kloer, D. P., Nencka, R., Balla, T., and Boura, E. (2014) The crystal structure of the phosphatidylinositol 4-kinase II α . *EMBO Rep.* **15**, 1085–1092 [CrossRef Medline](#)
70. Yang, X., Kovalenko, O. V., Tang, W., Claas, C., Stipp, C. S., and Hemler, M. E. (2004) Palmitoylation supports assembly and function of integrin-tetraspanin complexes. *J. Cell Biol.* **167**, 1231–1240 [CrossRef Medline](#)
71. Coleman, D. T., Gray, A. L., Kridel, S. J., and Cardelli, J. A. (2016) Palmitoylation regulates the intracellular trafficking and stability of c-Met. *Oncotarget* **7**, 32664–32677 [Medline](#)
72. Goldfinger, L. E., Hopkinson, S. B., deHart, G. W., Collawn, S., Couchman, J. R., and Jones, J. C. (1999) The $\alpha 3$ laminin subunit, $\alpha 6\beta 4$ and $\alpha 3 \beta 1$ integrin coordinately regulate wound healing in cultured epithelial cells and in the skin. *J. Cell Sci.* **112**, 2615–2629 [Medline](#)
73. Hedlund, M., Ng, E., Varki, A., and Varki, N. M. (2008) $\alpha 2$ -6-linked sialic acids on *N*-glycans modulate carcinoma differentiation *in vivo*. *Cancer Res.* **68**, 388–394 [CrossRef Medline](#)
74. Ali, M. F., Chachadi, V. B., Petrosyan, A., and Cheng, P. W. (2012) Golgi phosphoprotein 3 determines cell binding properties under dynamic flow by controlling Golgi localization of core 2 *N*-acetylglucosaminyltransferase 1. *J. Biol. Chem.* **287**, 39564–39577 [CrossRef Medline](#)
75. Maeda, Y., Ide, T., Koike, M., Uchiyama, Y., and Kinoshita, T. (2008) GPHR is a novel anion channel critical for acidification and functions of the Golgi apparatus. *Nat. Cell Biol.* **10**, 1135–1145 [CrossRef Medline](#)
76. Mesmin, B., Bigay, J., Moser von Filseck, J., Lacas-Gervais, S., Drin, G., and Antonny, B. (2013) A four-step cycle driven by PI(4)P hydrolysis directs sterol/PI $_4$ P exchange by the ER-Golgi tether OSBP. *Cell* **155**, 830–843 [CrossRef Medline](#)
77. Hang, Q., Isaji, T., Hou, S., Zhou, Y., Fukuda, T., and Gu, J. (2016) *N*-Glycosylation of integrin $\alpha 5$ acts as a switch for EGFR-mediated complex formation of integrin $\alpha 5\beta 1$ to $\alpha 6\beta 4$. *Sci. Rep.* **6**, 33507 [CrossRef Medline](#)
78. Hou, S., Isaji, T., Hang, Q., Im, S., Fukuda, T., and Gu, J. (2016) Distinct effects of $\beta 1$ integrin on cell proliferation and cellular signaling in MDA-MB-231 breast cancer cells. *Sci. Rep.* **6**, 18430 [CrossRef Medline](#)
79. Isaji, T., Sato, Y., Zhao, Y., Miyoshi, E., Wada, Y., Taniguchi, N., and Gu, J. (2006) *N*-glycosylation of the beta-propeller domain of the integrin $\alpha 5$ subunit is essential for $\alpha 5\beta 1$ heterodimerization, expression on the cell surface, and its biological function. *J. Biol. Chem.* **281**, 33258–33267 [CrossRef Medline](#)
80. Sato, Y., Isaji, T., Tajiri, M., Yoshida-Yamamoto, S., Yoshinaka, T., Somehara, T., Fukuda, T., Wada, Y., and Gu, J. (2009) An *N*-glycosylation site on the β -propeller domain of the integrin $\alpha 5$ subunit plays key roles in both its function and site-specific modification by $\beta 1,4$ -*N*-acetylglucosaminyltransferase III. *J. Biol. Chem.* **284**, 11873–11881 [CrossRef Medline](#)
81. Tanabe, K., and Ikenaka, K. (2006) In-column removal of hydrazine and *N*-acetylation of oligosaccharides released by hydrazinolysis. *Anal. Biochem.* **348**, 324–326 [CrossRef Medline](#)
82. Yanagida, K., Natsuka, S., and Hase, S. (1999) A pyridylamination method aimed at automatic oligosaccharide analysis of *N*-linked sugar chains. *Anal. Biochem.* **274**, 229–234 [CrossRef Medline](#)
83. Ran, F. A., Hsu, P. D., Lin, C. Y., Gootenberg, J. S., Konermann, S., Trevino, A. E., Scott, D. A., Inoue, A., Matoba, S., Zhang, Y., and Zhang, F. (2013) Double nicking by RNA-guided CRISPR Cas9 for enhanced genome editing specificity. *Cell* **154**, 1380–1389 [CrossRef Medline](#)
84. Ran, F. A., Hsu, P. D., Wright, J., Agarwala, V., Scott, D. A., and Zhang, F. (2013) Genome engineering using the CRISPR-Cas9 system. *Nat. Protoc.* **8**, 2281–2308 [CrossRef Medline](#)
85. Shalem, O., Sanjana, N. E., Hartenian, E., Shi, X., Scott, D. A., Mikkelsen, T., Heckl, D., Ebert, B. L., Root, D. E., Doench, J. G., and Zhang, F. (2014) Genome-scale CRISPR-Cas9 knockout screening in human cells. *Science* **343**, 84–87 [CrossRef Medline](#)
86. Toyoda, M., Kaji, H., Sawaki, H., Togayachi, A., Angata, T., Narimatsu, H., and Kameyama, A. (2016) Identification and characterization of sulfated glycoproteins from small cell lung carcinoma cells assisted by management of molecular charges. *Glycoconj. J.* **33**, 917–926 [CrossRef Medline](#)
87. Nishikaze, T., Tsumoto, H., Sekiya, S., Iwamoto, S., Miura, Y., and Tanaka, K. (2017) Differentiation of sialyl linkage isomers by one-pot sialic acid derivatization for mass spectrometry-based glycan profiling. *Anal. Chem.* **89**, 2353–2360 [CrossRef Medline](#)
88. Kameyama, A., Yamakoshi, K., and Watanabe, A. (2019) A rapid separation and characterization of mucins from mouse submandibular glands by supported molecular matrix electrophoresis. *Biochim. Biophys. Acta Proteins Proteom.* **1867**, 76–81 [CrossRef Medline](#)

N-acetylglucosaminyltransferase-I as a novel regulator of epithelial-mesenchymal transition

Guowei Zhang, Tomoya Isaji, Zhiwei Xu, Xu Lu, Tomohiko Fukuda, and Jianguo Gu¹

Division of Regulatory Glycobiology, Institute of Molecular Biomembrane and Glycobiology, Tohoku Medical and Pharmaceutical University, Sendai, Japan

ABSTRACT: *N*-Glycans are involved in numerous biologic processes, such as cell adhesion, migration, and invasion. To distinguish the functions of complex high-mannose types of *N*-glycans, we used the clustered, regularly interspaced, short palindromic repeats/Cas9 system to establish *N*-acetylglucosaminyltransferase (GnT)-I-knockout (KO) cells. Loss of GnT-I greatly induced cell-cell adhesion and decreased cell migration. In addition, the expression levels of epithelial-mesenchymal transition (EMT) markers such as α -SMA, vimentin, and N-cadherin were suppressed, whereas the expression of claudin-1 was promoted, suggesting a mesenchymal-epithelial transition-like phenotype, an opposite process to the EMT, was occurred in the KO cells. The phosphorylation levels of Smad-2, epidermal growth factor receptor, and integrin-mediated focal adhesion kinase (FAK) were consistently suppressed. Furthermore, the restoration of GnT-I in the KO cells suppressed the cell-cell adhesion and augmented the expression of EMT markers as well as that of FAK activation. The expression levels of integrins were upregulated in the KO cells, although their functions were decreased, whereas their expression levels were downregulated in the rescued cells, which suggests a negative feedback loop between function and expression. Finally, we also found that the expression of GnT-I was important for cell survival, resistance to cancer drugs, and increased colony formation. The results of the present study demonstrate that GnT-I works as a switch to turn on/off EMT, which further supports the notion that on most surface receptors, the *N*-glycans differentially play essential roles in biologic functions.—Zhang, G., Isaji, T., Xu, Z., Lu, X., Fukuda, T., Gu, J. *N*-acetylglucosaminyltransferase-I as a novel regulator of epithelial-mesenchymal transition. *FASEB J.* 33, 000–000 (2019). www.fasebj.org

KEY WORDS: cell adhesion · *N*-glycosylation · integrins

Epithelial-to-mesenchymal transition (EMT) is a cellular *trans*-differentiation process that allows polarized epithelial cells to undergo multiple biochemical changes and enables them to acquire a mesenchymal identity that results in a loss of cell-cell adhesion. EMT is integral in cell adhesion, migration, and wound healing and pathologically contributes to cancer metastasis and resistance to therapy (1). This switch in cell behavior is executed mainly

by specific transcription factors [*e.g.*, the Snail, Twist-related protein, and zinc-finger E-box-binding homeobox (ZEB) families] at transcriptional levels (2). Mesenchymal-epithelial transition (MET) is a reversible biologic process that involves the transition from motile, spindle-shaped mesenchymal cells to planar arrays of polarized cells that acquire cell-cell adhesion. Recent studies have shown that MET participates in the establishment and stabilization of distant metastases by allowing cancerous cells to regain epithelial properties and integrate into distant organs (3). Several studies have focused on the sequential EMT-MET process that underlies the fate of cells (4, 5), and the flexible transitions are related to different stages of metastasis (6). Details of the mechanism involved in this process, however, await elucidation.

An important hallmark of EMT is the attenuation of the epithelial marker E-cadherin and the enhancement of mesenchymal markers such as N-cadherin (7). E-cadherin is a central component of cell-cell adhesion junctions, the loss of which facilitates cell migration and alters integrin-mediated cell adhesion (8). Integrins control cell interactions with the extracellular matrix (ECM), which is critical to EMT progression (9, 10). In fact, TGF- β -induced EMT enhances the expressions of α V β 6 and α V β 3 integrins,

ABBREVIATIONS: AAL, *Aleuria aurantia* lectin; BSA, bovine serum albumin; ConA, concanavalin A; CRISPR/Cas-9, clustered regularly interspaced short palindromic repeats/caspase-9; DSA, *Datura stramonium* agglutinin; ECM, extracellular matrix; EGFR, epidermal growth factor receptor; EMT, epithelial-mesenchymal transition; E-PHA, *Phaseolus vulgaris* erythroagglutinin; FAK, focal adhesion kinase; FBS, fetal bovine serum; FN, fibronectin; GlcNAc, *N*-acetylglucosamine; GnT, *N*-acetylglucosaminyltransferase; KO, knockout; L-PHA, *Phaseolus vulgaris* leucoagglutinin; MAA, *Maackia amurensis* agglutinin; MET, mesenchymal-epithelial transition; PHA, phytohemagglutinin; PNGase, peptide-*N*-glycosidase; Res, rescued; SW, swainsonine; T β RII, TGF- β receptor type II; WT, wild type; ZEB, zinc-finger E-box-binding homeobox

¹ Correspondence: Division of Regulatory Glycobiology, Institute of Molecular Biomembrane and Glycobiology, Tohoku Medical and Pharmaceutical University, 4-4-1 Komatushima, Aobaku, Sendai, Miyagi 981-8558, Japan. E-mail: jgu@tohoku-mpu.ac.jp

doi: 10.1096/fj.201801478R

Establishment of GnT-I-Res HeLa cells

The full open reading frame of human GnT-I was cloned into the pENTR/D-TOPO vector and then transferred into the CSII-EF-Rfa destination vector by LR recombination, according to the manufacturer's instructions (Thermo Fisher Scientific). To prepare lentivirus, 293T cells were cotransfected with CSII-EF-Rfa-GnT-I and lentiviral packaging vectors (pCAG-HIVgp and pCMV-VSV-G-RSV-Rev). The culture supernatants were collected 48 h after infection, and the virus was introduced into GnT-I-KO HeLa cells *via* addition of the supernatant to the culture medium. The cells that highly reacted with L-PHA were selected by using FACS Aria II for GnT-I-Res cells, and the stable GnT-I-Res cell line was used for subsequent studies.

Western blot analysis

Total cell lysates were prepared with lysis buffer containing 20 mM Tris-HCl (pH 7.4), 100 mM NaCl, 1% Triton X-100, protease inhibitors, and phosphatase inhibitors (Nacalai Tesque, Kyoto, Japan) and normalized by protein concentrations with a bicinchoninic acid protein assay kit (Thermo Fisher Scientific). An equal amount of protein from each sample was subjected to SDS-PAGE and transferred to PVDF membranes (MilliporeSigma). The membranes were detected with primary and secondary antibodies and visualized by chemiluminescence (MilliporeSigma).

For peptide-*N*-glycosidase F (PNGase F) treatment, the indicated cell lysates were treated with PNGase F at 37°C for 1 h according to the manufacturer's instruction and then subjected to Western blot analysis.

Flow cytometric analysis

After detachment, cells were washed with ice-cold PBS and stained with primary antibodies or lectins in PBS containing 1 mM EDTA and 0.1% bovine serum albumin (BSA) (m/v) at 4°C for 20 min, followed by incubation with Alexa Fluor 647-conjugated secondary antibodies according to the primary antibodies or lectins (Thermo Fisher Scientific) for 20 min at 4°C. Nonstained cells were included as controls, and dead cells and debris were excluded from the analysis, based on scatter characteristics. Data for at least 10,000 live events per sample were acquired *via* FACSCalibur flow cytometry (BD Biosciences). After incubation with doxorubicin for 1 d, the identified cells were detached and washed with ice-cold PBS and then subjected to flow cytometry. The fluorescence was measured with an FL2 (phycoerythrin) band-pass filter to monitor doxorubicin cellular uptake. Untreated cells were used as controls, and dead cells and debris were excluded from the analysis, based on scatter characteristics.

Cell migration assay

For the *in vitro* wound-healing assay, cells were seeded in 6-well plates precoated with 10 µg/ml FN (MilliporeSigma) and grown into a confluent monolayer. Then the cells were scratched *via* a pipette tip. Images of the wound area were photographed after 8 h, and the distance of cell migration was measured by QCapture Pro 7 software (QImaging, Surrey, BC, Canada). Another cell migration test was performed with a 24-well Transwell chamber system (8-µm pore control inserts; BD BioCoat; BD Biosciences). The bottom side of the chamber was coated with 10 µg/ml FN, and blocked with 1% BSA. Cells were seeded in the upper FN-pretreated chamber at 4×10^4 cells in 0.2 ml serum-free DMEM. Then, 0.6 ml complete medium containing 10% FBS was placed in the bottom well. After incubation for 8 h, the migrated cells on the lower surface were fixed, stained with crystal violet, and counted

under a light microscope. Three independent experiments were performed for each assay.

Soft agar assay

Cells were suspended in DMEM containing 0.3% agarose and layered onto solidified 0.6% agarose containing DMEM at a density of 1×10^4 per dish. After incubating for 20 d, the plates were stained with 0.005% crystal violet, and the colonies were identified randomly by stereo microscope (Stemi 2000-CS; Zeiss, Oberkochen, Germany) and counted. Three independent experiments were performed for each assay.

Cell growth assay

Cells (5×10^4) were seeded into 6-well culture dishes overnight. Cells in the same area were photographed by phase contrast on 4 consecutive days and counted, and the fold change in number of cells was normalized to the number on d 0.

Cell aggregation assay

Cells were harvested and resuspended in DMEM containing 1% BSA at a concentration of 2×10^5 cells/ml. For each condition, 1 ml of the cell suspension was added to a 15-ml tube, with or without 2 mM EDTA. The cells were incubated on a rotator (MACSmix Tube Rotator; Miltenyi Biotec, Bergisch-Gladbach, Germany) at 12 rpm for 6 h at 37°C, and images of random fields were obtained with a microscope. Cell aggregation assays were performed in triplicate.

Cell-spreading assay

A cell-spreading assay was performed as previously described with minor modifications (41). In brief, cells were harvested and suspended in DMEM containing 0.1% BSA at 2×10^4 cells/ml. After seeding on the FN (10 µg/ml)-pretreated dishes for 30 min, the cells were washed with PBS to remove the nonadherent ones, and the attached cells were fixed with 4% paraformaldehyde in PBS. The representative images were photographed by phase-contrast microscopy (Olympus, Tokyo, Japan).

Cell surface biotinylation

Cells cultured on dishes were gently washed with PBS and incubated with ice-cold PBS that contained 0.2 mg/ml Sulfo-NHS-SS Biotin for 1 h at 4°C. After incubation, the cells were washed 3 times with ice-cold PBS and harvested with lysis buffer. Biotinylated proteins were immunoprecipitated with anti-β1 integrin mAb (P5D2) and Ab-Capcher Mag (ProteNova, Higashikagawa, Japan) and subjected to SDS-PAGE. The biotinylated proteins were visualized with a Vectastain ABC Kit (Vector Laboratories, Burlingame, CA, USA) and an ECL kit.

Cell viability assays

Cells were cultured at 5×10^3 cells per well in 96-well plates and exposed to the indicated concentrations of paclitaxel for 3 d or doxorubicin for 2 d. Cell viability was detected by adding 10 µl of 5 mg/ml 3-[4,5-dimethylthiazol-2-yl]-2,5-diphenyltetrazolium bromide (MTT; Dojindo, Kumamoto, Japan) to 100 µl culture medium and incubating the mixture for an additional 3 h at 37°C. The medium was then removed, and DMSO (MilliporeSigma) was added to dissolve the resultant formazan crystals within the cells. The optical absorbance was assessed at 570 nm with a microplate reader (BioTek Instruments, Winooski, VT, USA).

Statistical analysis

All data are expressed as means \pm SEM. Prism, v.5.0, was used to perform statistical analyses (GraphPad Software, La Jolla, CA, USA). Significant differences were analyzed with Welch's *t* test. Values of *P* < 0.05 were considered statistically significant.

RESULTS

Knockout of the GnT-I gene blocked complex types of *N*-glycans

To distinguish the functions of only high-mannose *N*-glycans and mixed *N*-glycans including high-mannose, hybrid, and complex types, we established GnT-I-KO cells using CRISPR/Cas9-based technology. As expected, the expression of GnT-I was not at detectable levels (Fig. 1A). Flow cytometric analysis and lectin blots using different kinds of lectins were performed to confirm the efficiency of GnT-I-KO in HeLa cells (Fig. 1B, C) and in MDA-MB-231

cells (data not shown). The reactive abilities of L-PHA, E-PHA, and MAA lectins preferentially recognized branched GlcNAc *N*-glycans, bisected *N*-glycans, and α 2,3 sialylated *N*-glycans, respectively. Those reactive abilities, however, were greatly suppressed in the KO cells compared with those in wild-type (WT) cells (Fig. 1B). Lectin blots using DSA and AAL lectins preferentially recognized branched GlcNAc *N*-glycans and fucosylated *N*-glycans, respectively, which showed that the reactive abilities were almost totally blocked. The binding ability with ConA lectin, however, preferentially recognized high-mannose types of *N*-glycans that were augmented in the KO cells (Fig. 1C). These results show that the GnT-I gene knockout was successful.

Deletion of GnT-I-induced cell aggregation and a MET-like phenotype

Next, we used these cell lines to compare the cell biologic functions of GnT-I. First, during cell passages we noticed

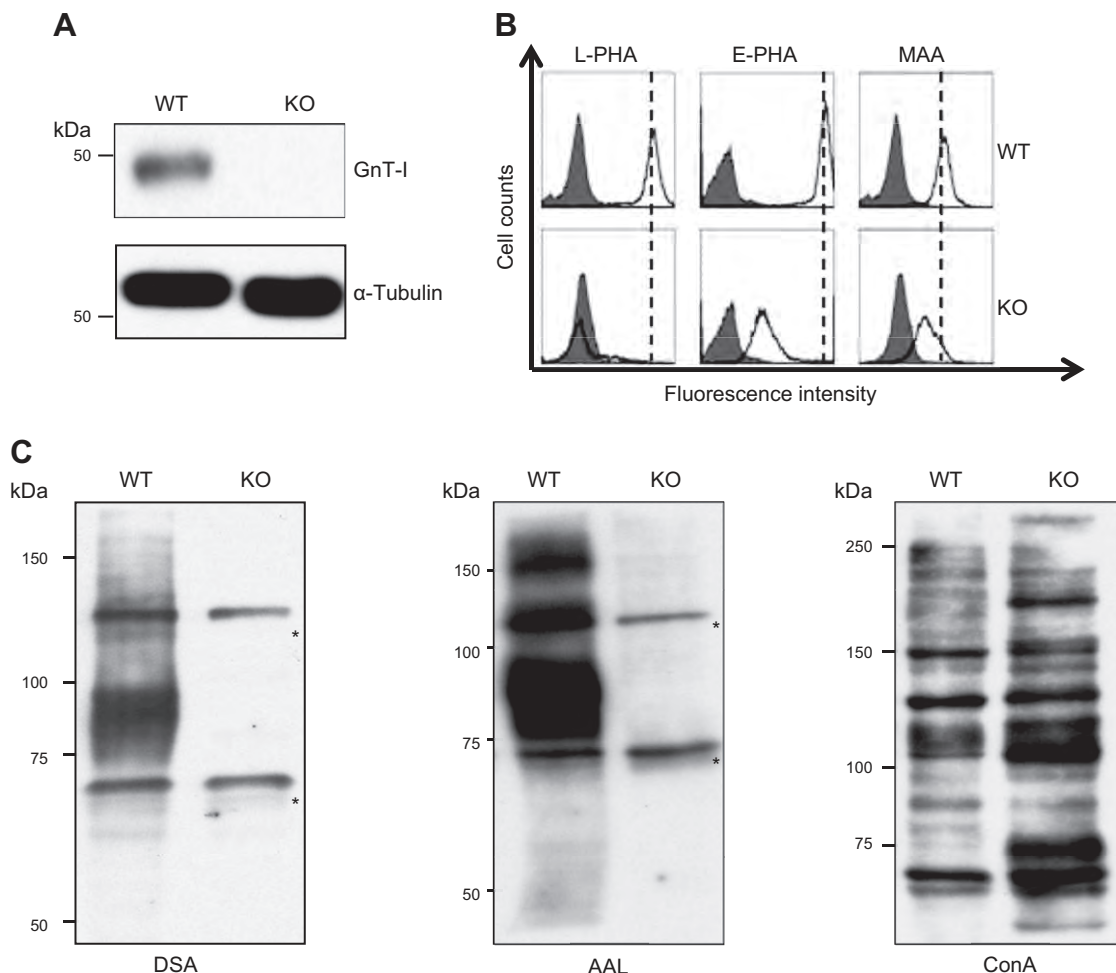


Figure 1. Deficiency of complex types of *N*-glycans in GnT-I-KO cells. **A)** Equal amounts of cell lysates from WT and KO HeLa cells were analyzed by immunoblot with an anti-GnT-I antibody; α -tubulin served as the loading control. **B)** The WT and KO cells were collected and incubated with (bold line) or without (gray shadow) the lectins LL-PHA, E-PHA, and MAA, which preferentially recognize branched GlcNAc *N*-glycans, bisected *N*-glycans, and α 2,3 sialylated *N*-glycans, respectively, followed by incubation with Alexa Fluor 647 streptavidin and flow cytometric analysis. The vertical dashed lines indicate the peaks of lectin expressions in WT cells. **C)** The same amounts of cell lysates from WT and KO cells were analyzed by immunoblot with the lectins DSA, AAL, and ConA, which preferentially recognize branched GlcNAc *N*-glycans, fucosylated *N*-glycans, and high-mannose *N*-glycans, respectively. Asterisks denote no specific bands.

that the KO cells tended to form islands, which was not observed in the WT cells (Fig. 2A), suggesting that knockout of GnT-I may induce cell-cell adhesion. We performed a cell adhesion assay in the suspension. Both the WT and KO cells were incubated with rotation for 6 h. The KO cells tended to form many aggregates that resulted in larger sizes, whereas the WT cells remained as either single cells or smaller aggregates (Fig. 2B). The cell aggregates disappeared in the presence of EDTA, suggesting that the cell-cell adhesion had proceeded in a calcium-dependent manner. A similar phenomenon was observed in the MDA-MB-231 cells (data not shown). Of particular interest, the expression levels of mesenchymal markers such as α -SMA, vimentin, ZEB-1, N-cadherin, and Snail were greatly suppressed in the KO cells, whereas epithelial markers such as claudin-1, which is a tight junction protein, were increased, compared with those in WT cells (Fig. 2C). It is noteworthy that the expression levels of E-cadherin in both WT and KO cells were undetectable. These results suggest that the deletion of GnT-I induces cell aggregation and MET-like phenotypes.

Deletion of GnT-I inhibited cell spreading and migration, but did not affect cell proliferation

As previously described, the expression of GnT-I was essential for cell-cell adhesion, and, therefore, we next

explored whether GnT-I is also necessary for integrin-mediated cell-ECM adhesion. By using a cell-spreading assay, we found that the WT cells had already begun to spread after the cells were replated on FN-coated dishes for 30 min, whereas the KO cells continued to exhibit a rounded shape with white dots under phase-contrast photography (Fig. 3A, B). Unexpectedly, there were no significant changes in the proliferation of these 2 types of cells (Fig. 3C). However, we investigated some related cellular signaling pathways and found that p-Smad-2, p-FAK, and p-EGFR, which corresponds with TGF- β receptor-, integrin- and EGFR-mediated signaling, respectively, were decreased in the KO cells compared with those in the WT cells (Fig. 3D), which confirmed the notion that a complex type of N-glycans on these signal receptors plays an important role in cellular signaling.

Cell migration is considered a crucial step in the metastatic cascade (42), and we examined the effects of GnT-I on cell migration by using wound healing and Transwell assays. Wound closure capability was significantly suppressed in the KO cells compared with that in the WT cells (Fig. 4A, B). The integrin-mediated Transwell migration was also greatly inhibited (Fig. 4C, D). These data clearly show that the expression of GnT-I is essential for integrin-mediated functions.

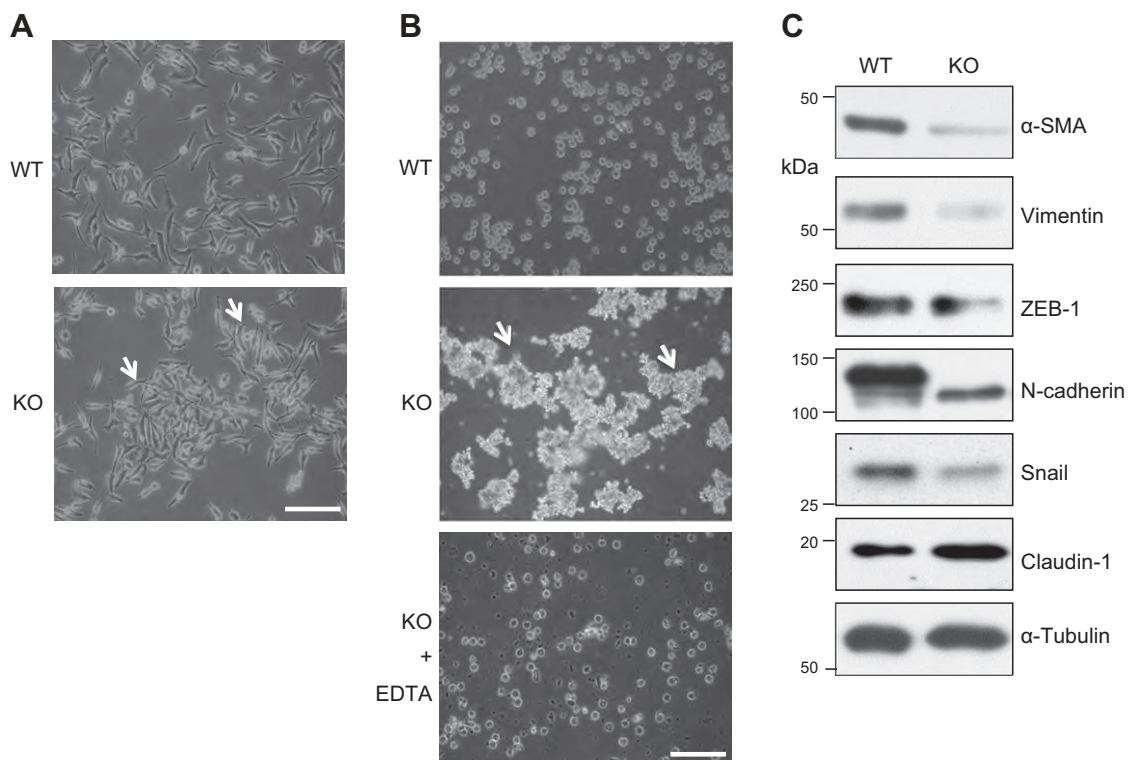


Figure 2. Comparison of the cell-cell adhesion and expression levels of EMT markers between WT and KO cells. A) The WT and KO cells were cultured in normal culture dishes for 1 d and were photographed with a phase-contrast microscope. B) The WT and KO cells were detached from culture dishes and separated into single cells in 10% FBS culture medium at 2×10^5 cells/ml, with or without EDTA, followed by a constant rotation (12 rpm) at 37°C for 6 h. An aliquot of each of these cell suspensions was photographed with a phase-contrast microscope. C) The same amounts of cell lysates from the WT and KO cells were analyzed by immunoblot with the anti- α -SMA, vimentin, ZEB-1, N-cadherin, snail, and claudin-1 antibodies, and α -tubulin was used as the loading control. Arrows: cell aggregation. Scale bars, 50 μ m.

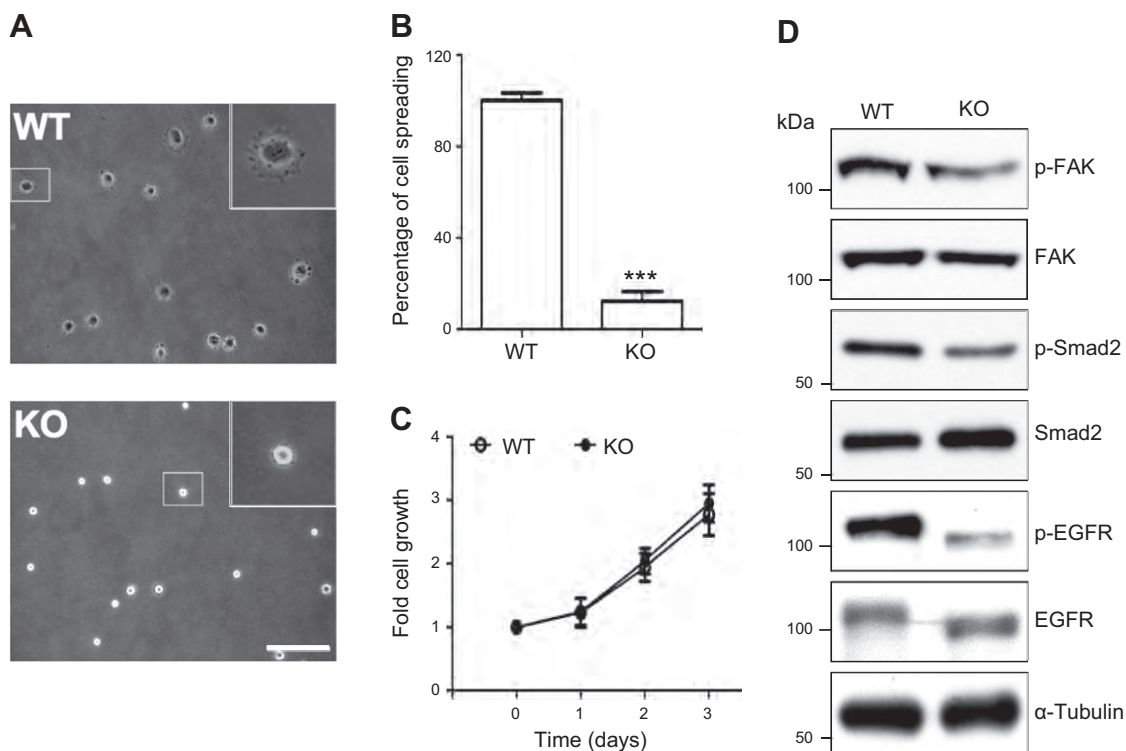


Figure 3. Effects of GnT-I deficiency on cell spreading, cell proliferation, and cellular signaling. *A*) The WT and KO cells were detached and then replated onto FN-coated plates. After incubation for 30 min, cells were fixed, and representative images were taken *via* a phase-contrast microscope. Insert: a magnified view of the area indicated by the box. Scale bar, 50 μ m. *B*) The percentages of spread cells were statistically analyzed. *C*) The WT and KO cells were starved with serum-free DMEM for 24 h and then cultured in DMEM containing 10% FBS. The number of cells was counted on the indicated days, and the counts were normalized to that of each group at 0 h. Data are means \pm SEM ($n = 3$). *D*) The same amounts of cell lysates from the WT and KO cells were analyzed by immunoblot with anti-p-FAK, FAK, p-Smad-2, Smad-2, p-EGFR, and EGFR antibodies. α -Tubulin was used as the internal control. *** $P < 0.001$.

The expression levels of integrins were up-regulated in the KO cells

Because integrin-mediated cell adhesion was inhibited in the KO cells, we next sought to determine whether the expression of integrin was also suppressed. Flow cytometric analysis and Western blot were performed to evaluate the expression levels of different integrins. The expression levels on the cell surface of integrins, such as $\alpha 3$, $\alpha 5$, αV , $\beta 1$, $\beta 3$, $\beta 4$, and $\beta 5$, were increased in the KO cells, compared with their expression levels in the WT cells (Fig. 5A). Because of the lack of complex *N*-glycans on integrin $\alpha 3$ and $\beta 1$ in the KO cells, the bands of those integrins shifted on SDS-PAGE much faster than in the WT cells (Fig. 5B). In the WT cells, the so-called immature band of $\beta 1$ was similar to that in the KO cells, confirming that immature $\beta 1$ carries a high-mannose type of *N*-glycan. These differences dissipated after the removal of *N*-glycans by PNGase F. Treatment with PNGase F showed enhanced expression levels of $\alpha 3$ and $\beta 1$ in the KO cells. These results suggest a negative feedback loop from integrin function to expression.

Restoration of GnT-I in KO cells restored cell behavior and induced an EMT-like phenotype

Given the observation that the KO cells exhibited aberrant behavior, we restored GnT-I expression in the KO cells

(Res) to determine whether it would rescue these phenotypes. The efficiencies of Res cells were confirmed by Western blot with the anti-GnT-I antibody (Fig. 6A) and flow cytometric analysis of L-PHA lectin (Fig. 6B). Integrin-mediated FAK phosphorylation (Fig. 6A) increased, whereas the expression levels of $\alpha 5$ and $\beta 1$ (Fig. 6B) decreased in the Res cells, further supporting the notion of a negative feedback loop from function to expression, as previously described. The expression levels of mesenchymal markers, such as vimentin, ZEB-1, and N-cadherin, were increased in the Res cells, compared with those in the KO cells (Fig. 6C). Furthermore, the cell islands caused by cell-cell adhesion, which could be observed in the KO cells, disappeared in the Res cells (Fig. 6D). Integrin-mediated cell migration increased significantly in the Res cells (Fig. 6E, F). These results showed the importance of GnT-I switching by the EMT process.

Influences of integrin and GnT-I on cell-cell adhesion

As previously described, deletion of GnT-I induced integrin expression, which indicated that complex *N*-glycans are not essential for integrin expression. We used biotinylation to further compare the expression levels of $\beta 1$ among the WT, KO, and Res cells. The expression levels of $\beta 1$ and the associated α -subunits on the cell surface were

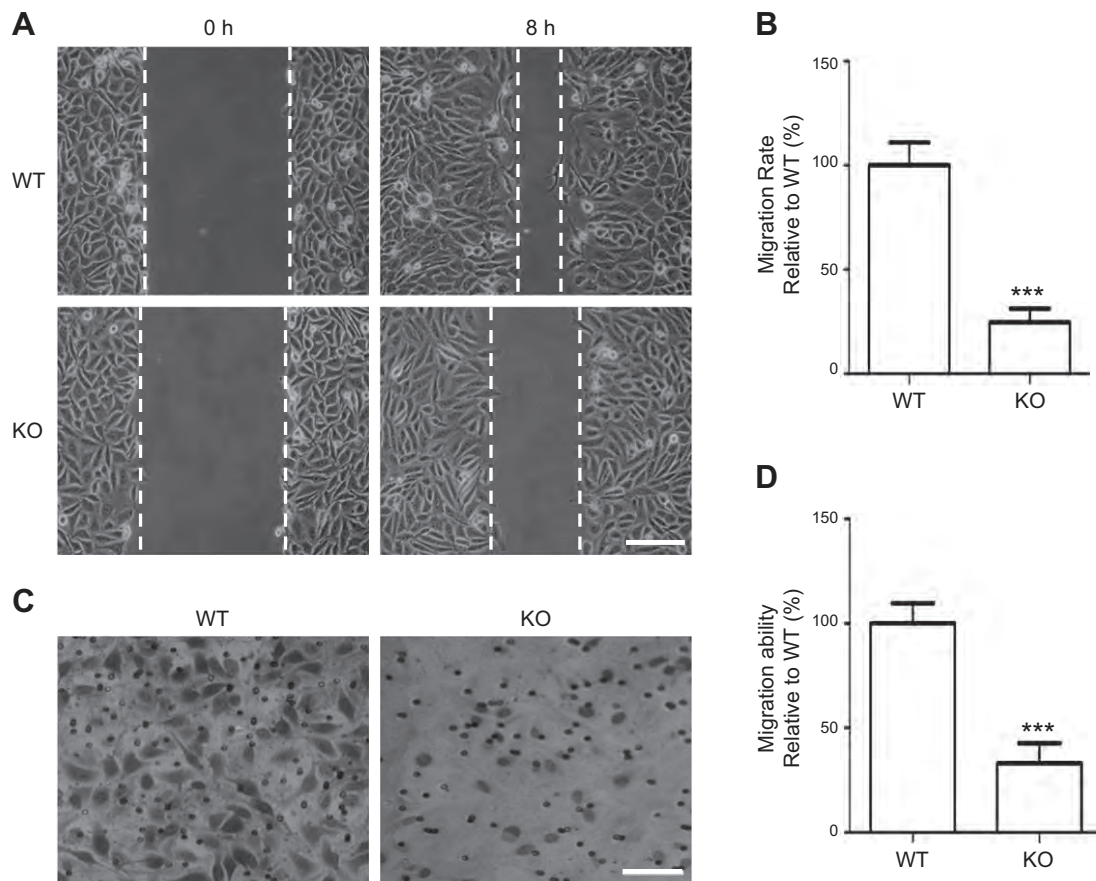


Figure 4. Comparison of cell migration between the WT and KO cells. *A*) Cells were grown to more than 90% confluence, and the monolayers were incised with a pipette in each well. Photographs were taken by phase-contrast microscopy at 0 and 8 h. *B*) The quantification of cell migration rate relative to the WT (100%) was expressed as means \pm SEM of results in 3 independent experiments. *C*) A cell migration chamber was used to examine the migration capacity of WT and KO cells. Migrated cells were stained and photographed. *D*) Relative cell migration was expressed as the percentage of migrating cells compared with that of WT cells (100%). Results are representative of at least 3 independent experiments. Scale bars: 50 μ m (*A*); 100 μ m (*C*). *** $P < 0.001$, WT *vs.* KO.

enhanced in KO cells, but restored to the levels of WT in the Res cells (Fig. 7A). The deletion of GnT-I enhanced the expression levels of integrins, but the integrin-mediated cell-ECM adhesion including FAK phosphorylation and cell adhesion and migration, all were down-regulated. We speculated as to whether the suppression of cell-ECM adhesion *via* blocking the process for complex-type *N*-glycans on integrins could induce cell-cell adhesion, as observed in the KO cells. To test the hypothesis, we added a functional blocking β 1 antibody (P5D2) (43), to attenuate cell-matrix adhesion in the cell culture. All 3 types of cells clearly exhibited cell aggregation in the presence of anti- β 1 integrin antibody (Fig. 7B). These data may partly explain why cell aggregation occurred in the KO cells and could further suggest that the modification of complex types of *N*-glycans on β 1 integrin is very important for its ability to function.

Deletion of GnT-I increased drug sensitivity

Because recent studies revealed the involvement of EMT on the efficacy of cancer drug responses (44, 45), we evaluated whether GnT-I deficiency affects drug sensitivities in HeLa cells. The 3 cell groups were incubated with the

cancer drugs paclitaxel for 3 d (Fig. 8A) and doxorubicin for 2 d (Fig. 8B) at the indicated concentrations. The KO cells were more sensitive to both drugs, compared with the WT and Res cells. When we used fluorescence-activated cell sorting to monitor the cellular uptake of doxorubicin, we consistently observed higher fluorescence intensities in KO cells (Fig. 8C).

The ability of tumor cells to form colonies from a single cell is a well-known feature of metastatic potential (46). Cells that undergo EMT are also known to form more colonies (47), and, therefore, we evaluated the effects of GnT-I on colony formation in HeLa cells. As shown in Fig. 8D, the colony formation in soft agar was significantly suppressed in the KO cells, compared with the WT and the Res cells. These data suggest that the expression of GnT-I greatly contributes to tumor survival and formation.

DISCUSSION

In the present study, we found that GnT-I works as a switch to activate EMT, based on the following observations: 1) deletion of GnT-I suppressed the expression of mesenchymal markers and cell-ECM adhesion and induced

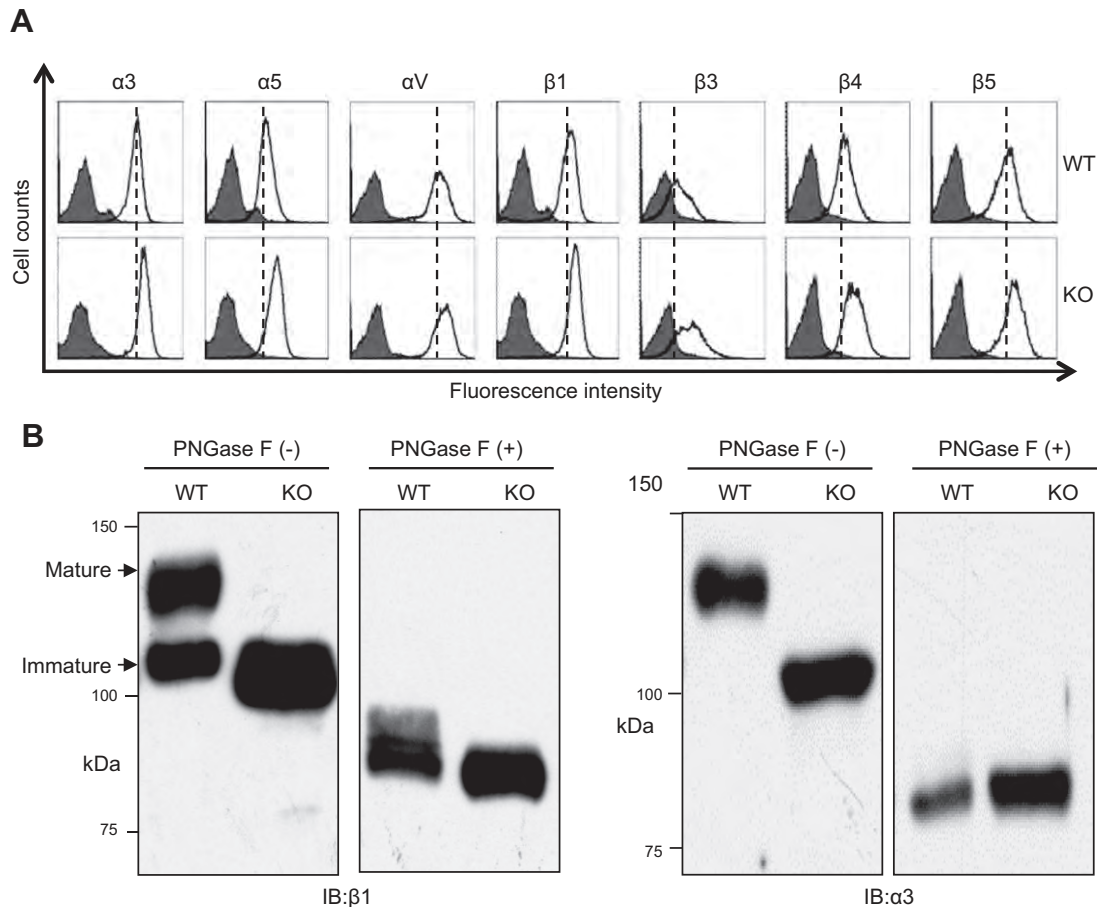


Figure 5. Effects of GnT-I deficiency on the expression levels of integrins and the effects of *N*-glycosylation on $\alpha 3\beta 1$ integrin. *A*) The WT and KO cells were collected and incubated with (bold line) or without (gray shadow) the indicated integrins, followed by incubation with Alexa Fluor 647 conjugated with goat anti-mouse antibody, and then subjected to flow cytometry. The vertical dashed lines indicate the peaks of integrins expressions in WT cells. *B*) The same amounts of cell lysates (20 μ g) obtained from the WT and KO cells were treated with (+) or without (-) peptide: *N*-glycosidase F (PNGase F), and then immunoblot analysis was performed with anti- $\beta 1$ and - $\alpha 3$ antibodies.

cell-cell adhesion; 2) loss of GnT-I decreased integrin-mediated cell migration; and 3) restoration of GnT-I efficiently rescued the expression of mesenchymal markers and cell migration, and decreased cell-cell adhesion. In addition, the expression of GnT-I was important for cell survival against anticancer drugs.

One study has shown that mice lacking GnT-I die at midgestation (37). Biochemical and morphologic analyses of embryos have revealed GnT-I-null embryos that are developmentally retarded, particularly in neural tissue. The neural crest is known to be a transient embryonic cell population that migrates long distances through the vertebrate embryo during development, wherein the integrin family of cell adhesion receptors are necessary for proper cell migration, proliferation, survival, and differentiation. In fact, both major ECM molecules, laminin and FN, have receptors that include the $\alpha 3\beta 1$ and $\alpha 5\beta 1$ integrins and are abundantly expressed in neural crest migration pathways (48, 49). Furthermore, a loss of function of the murine $\alpha 5$ integrin by gene targeting posed a recessive embryonic lethal threat at midgestation that was related to defects in the development of the cardiac neural crest, mesoderm formation, and cell movement and function (50, 51). In our study, GnT-I deficiency greatly suppressed

integrin-mediated cellular signaling (FAK phosphorylation), cell-ECM adhesion, and migration, which may partly explain some of the important phenotypes shown in the GnT-I-null embryos. We speculate that the defect in integrin functions is one of the main causes of the embryonic lethality at midgestation of GnT-I-KO mice. In fact, there is an increasing body of evidence implicating *N*-glycans in integrin function (52). For example, alterations in the oligosaccharide portion of integrins that are modulated by glycosyltransferases, such as GnT-III, GnT-V, and $\alpha 2,6$ sialyltransferase, differentiate in the regulation of cell malignant phenotypes, such as in integrin-mediated cell migration and cell spreading. The expression of GnT-V stimulates $\alpha 3\beta 1$ integrin-mediated cell migration, whereas the overexpression of GnT-III inhibits GnT-V-induced cell migration (19). Therefore, the lack of GnT-I may result in the loss of the dynamic and precise post-translational regulation that plays a crucial role in embryo development. It is intriguing that GnT-I deficiency increased the expression levels of many types of integrins, although integrin functions were suppressed, whereas the restoration of GnT-I decreased integrin expression and enhanced integrin-mediated cell adhesion and cellular signaling. These findings suggest

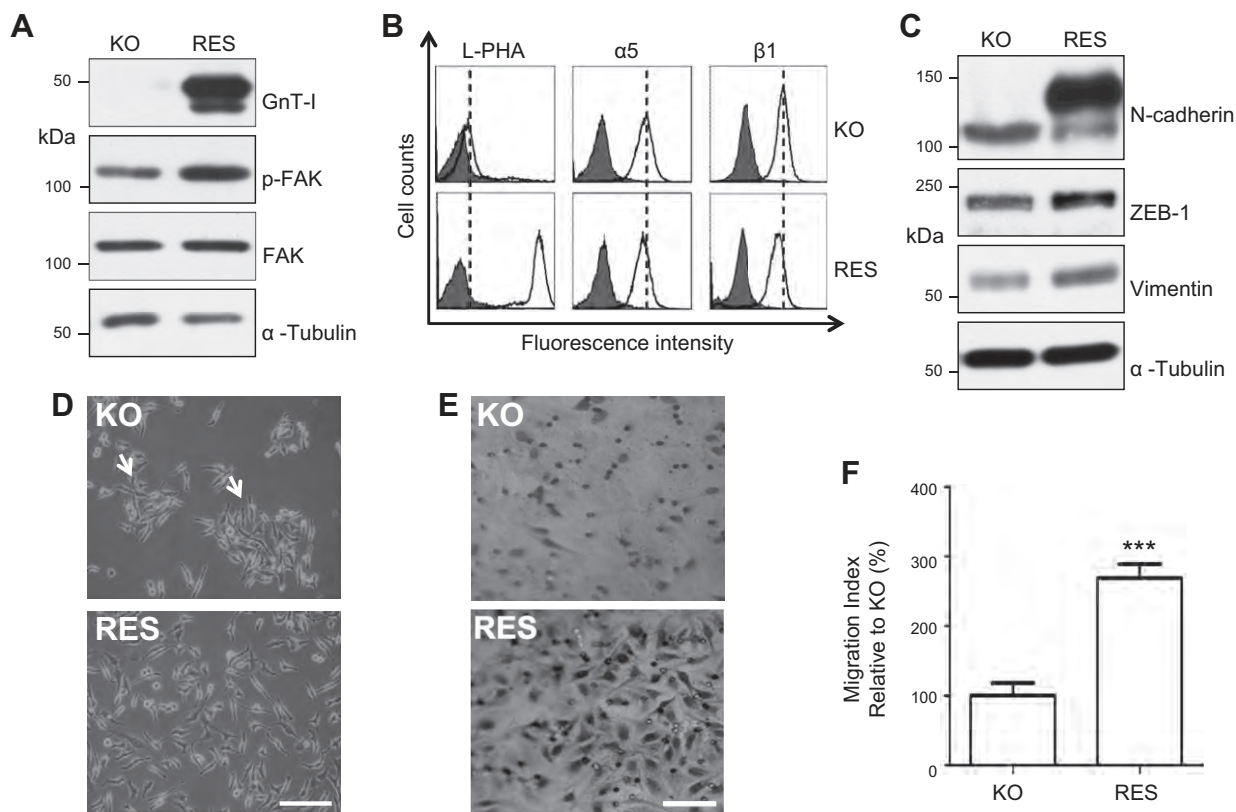


Figure 6. Forced expression of the GnT-I in KO cells Res cell behavior and induced EMT-like phenotypes. *A*) Equal amounts of cell lysates from the KO and restoration of GnT-I in the KO cells (Res cells) were analyzed by immunoblot with anti-GnT-I, -p-FAK, and -FAK antibodies. α -Tubulin was used as an internal control. *B*) The KO and Res cells were collected and incubated with (bold line) or without (gray shadow) anti-GnT-I antibody, followed by incubation with Alexa Fluor 647 conjugated with goat anti-mouse antibody and counting by flow cytometry. The vertical dashed lines indicate the peaks of the indicated expressions in KO cells. *C*) The expression levels of EMT markers such as N-cadherin, ZEB-1, and vimentin were examined by Western blot analysis. *D*) Images were taken with a phase-contrast microscope to show representative cell morphologies of the KO and Res cells. Arrows: cell aggregations. Scale bar, 50 μ m. *E, F*) Photographs (*E*) and quantitative analysis (*F*) of the cell migration assays were used to determine migration capabilities of the KO and Res cells. Scale bar, 100 μ m. *** $P < 0.001$, KO *vs.* Res.

the existence of a negative feedback loop from the function to the expression of integrins. Furthermore, the results support the notion that *N*-glycans closely regulate integrin function.

EMT is an important phenotype characterized by a loss of the cell-cell junction and the acquisition of cell migration, which plays crucial roles, not only in physiologic processes, such as embryo implantation, embryogenesis and organ development, but also in tissue repair and pathologic processes such as tissue fibrosis, tumor invasiveness, and metastasis (53). Different signaling pathways—for example, receptor tyrosine kinase, Notch, Wnt, and TGF- β —are known to provide the necessary stimuli that modulate gene expression and trigger EMT and cell migration (54). The regulation of EMT by GnT-I may have crosstalk with those signaling pathways. In fact, glycosylation and signaling mutually regulate and affect cell behavior. Inhibition of GnT-V-mediated *N*-glycosylation suppresses PI3K and MAPK signaling (55, 56), but the inverse is true of the PI3K/Akt (55) and ras/raf/ets2 (57) signaling pathways, which regulate GnT-V expression. In addition, core fucosylation is critical to the activation of the TGF- β receptor type II (T β RII) and Smad-2 signaling pathways (58), and high-mannose type T β RII

decreases TGF- β -induced Smad-2 activation (59), whereas TGF- β receptor-mediated signaling promotes GnT-V expression (60). Our data show that GnT-I deficiency exhibited a MET-like phenotype and that restoration of GnT-I efficiently reversed MET to an EMT-like phenotype, which may also partly explain why the formation of neural tissue was delayed in the GnT-I-null embryos. The inhibition of complex types of *N*-glycans by SW efficiently and consistently inhibit cell invasion and EMT processes in esophageal carcinoma cells (30). In addition, the deletion of GnT-I suppressed the phosphorylation of both EGFR and Smad-2, which further confirmed the switching function of GnT-I toward EMT. Thus, high-mannose types of *N*-glycans may maintain MET-like phenotypes, whereas GnT-I initiates the EMT process.

We also demonstrated how the deletion of GnT-I augmented cell-cell adhesion, which may have 2 explanations. The first concerns a weakening of the cell-ECM adhesion in KO cells, as previously described. It is reasonable to speculate that the cell-cell adhesion and cell-ECM adhesion regulate each other in an opposing manner. Indeed, treatment with a blocking β 1 integrin antibody (P5D2) greatly induced cell-cell adhesion in the WT and Res HeLa cells, which was observed in the KO cells without this

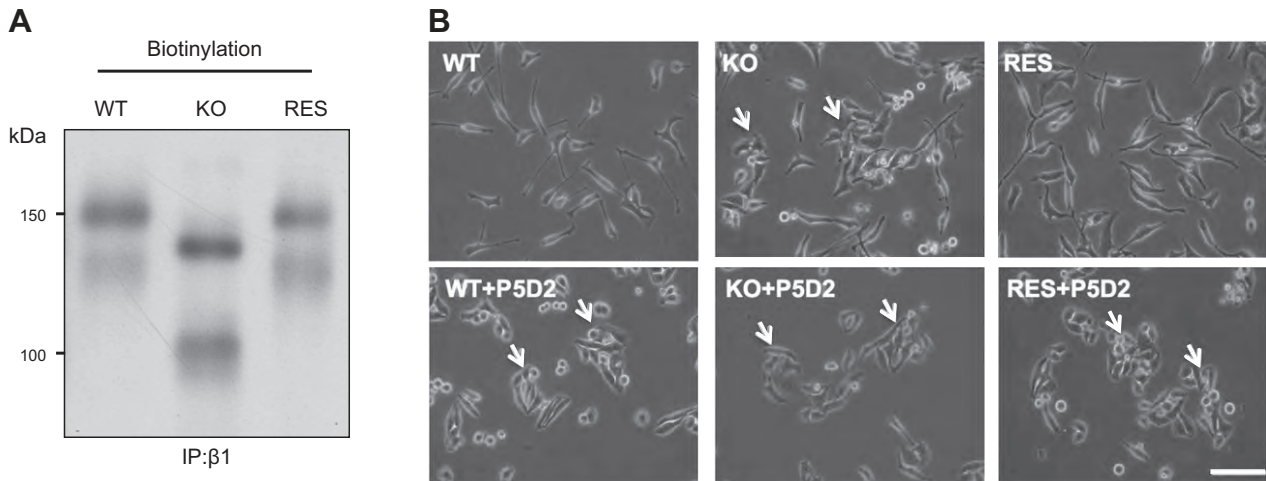


Figure 7. Effects of GnT-I on integrin $\beta 1$ maturation and the cell-cell adhesion induced by a blocking anti- $\beta 1$ integrin antibody. *A*) The indicated cells were incubated with Sulfo-NHS-SS biotin for 1 h, and then the cell lysates were immunoprecipitated with anti- $\beta 1$ integrin mAb (P5D2) and the biotinylated proteins were detected. *B*) The indicated cells were replated in 6-well culture dishes in normal culture medium, with or without a blocking anti- $\beta 1$ integrin antibody (P5D2, 10 $\mu\text{g}/\text{ml}$). After incubation for 16 h, phase-contrast photographs were taken. Arrows: cell aggregation. Scale bar, 75 μm .

treatment. Consistently, the KO of $\beta 1$ integrin resulted in cell-cell adhesion and in the suppression of FAK phosphorylation and cell migration (61). The second

explanation involves the possibility that high-mannose types of *N*-glycans may enhance cell-cell adhesion. E-cadherin is the core transmembrane glycoprotein of

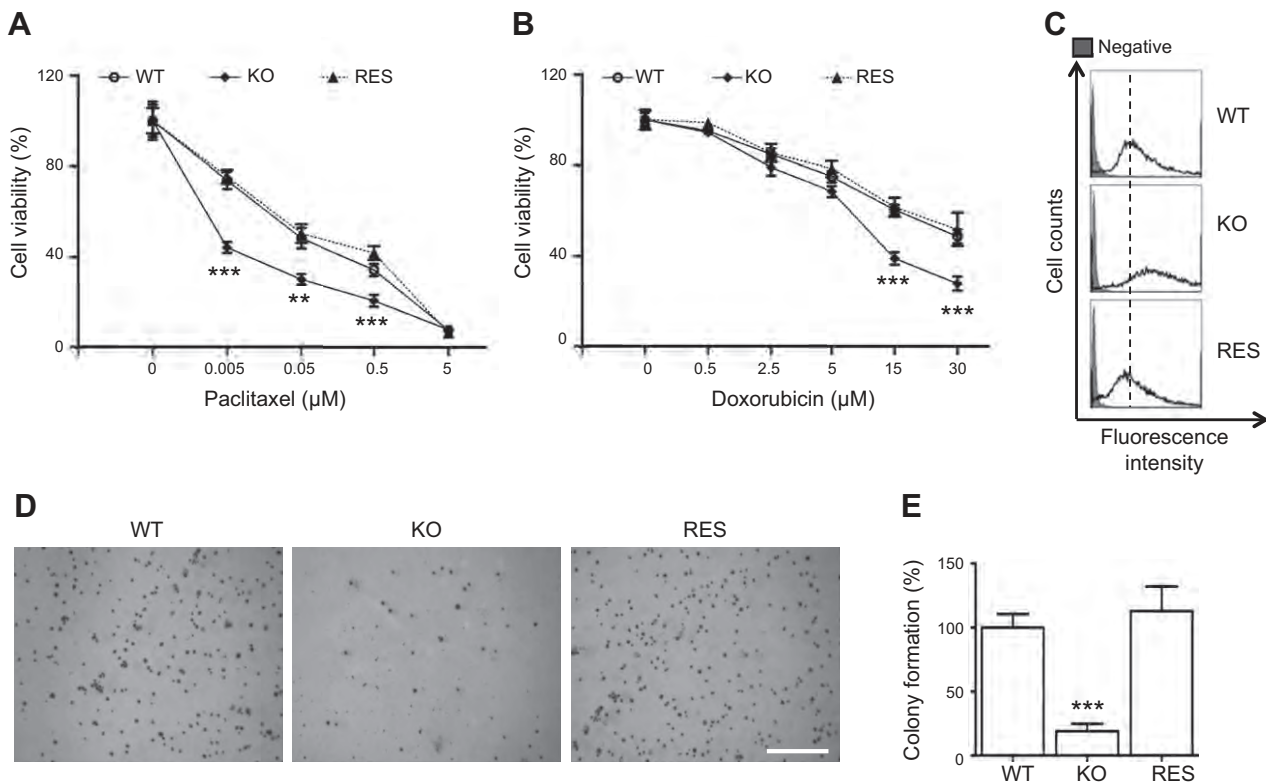


Figure 8. Loss of GnT-I chemosensitized the cells to cancer drugs. *A–B*) The cells were cultured in normal culture medium containing paclitaxel (*A*) and doxorubicin (*B*) at the indicated concentrations. Percentages of cell viability were measured *via* MTT assay. $**P < 0.01$, $***P < 0.001$ *vs.* paclitaxel- or doxorubicin-treated WT cells, which was set as 100%. *C*) After incubation with (bold line) or without (gray shadow) doxorubicin for 1 d, the indicated cells were collected and then subjected to flow cytometry *via* the FL2 (phycoerythrin) channel. *D*) The indicated cells (1×10^4 /per well) were cultured in soft-agar plates for 20 d, the colonies were stained with crystal violet, and images were taken by light microscope. *E*) The stained colonies were counted, and the quantitative data are presented as means \pm SEM of results in 3 independent experiments. Scale bar, 5 mm. $***P < 0.001$ compared to the WT group, which was set as 100%.

the adherens-junction, although the expression level of E-cadherin in HeLa cells is marginal. The modification of E-cadherin with complex *N*-glycans has been associated with the formation of dynamic and weak adherens junctions, whereas E-cadherin, modified by high-mannose types or fewer *N*-glycans, is known to promote the establishment of stable adherens junctions (62). E-cadherin was modified by *N*-glycans containing β 1,6 branched and sialylated structures during acquisition of the malignant phenotype (63), whereas overexpression of GnT-III prolonged the turnover of E-cadherin on the cell surface by suppression of extensive branched complex *N*-glycan formation by the action of GnT-V and then enhanced homophilic adhesion (15). Up-regulation of GnT-V expression was observed in TGF- β -induced EMT (60), and overexpression of GnT-V promoted EMT and keratinocyte migration in GnT-V-transgenic mice (64). Therefore, smaller *N*-glycans, such as the high-mannose or bisected types, may promote cell-cell adhesion.

It is also worth noting why GnT-I deficiency did not affect cell proliferation (Fig. 3B). Studies have shown that lost or reduced branched-complex *N*-glycans catalyzed by GnT-IV and -V lead to a reduction in the retention time of glycoprotein receptors on the cell surface related to a weakening of their interactions with a galectin lattice (65, 66). Thus, it could be more plausible to speculate that deletion of GnT-I inhibits cell proliferation. However, our results showed there was no significant difference in cell growth between WT and KO cells, although the level of phosphorylated EGFR was decreased in the KO cells compared with that in the WT cells (Fig. 3). In fact, a study showed that the proliferation of CHO cells is not affected by the genetic disruption of multiple α 1,2-mannosidases and induced to generate high-mannose types of *N*-glycans in HEK293 cells (67). Knockdown of GnT-I by short hairpin RNA consistently did not alter cell proliferation rates in a human PC-3 prostate tumor cell line (38). These results indicate that complex types of *N*-glycans remodeled by glycosyltransferases on glycoprotein receptors may positively or negatively regulate cellular signaling for cell proliferation. For instance, the lack of α 1,6-fucosylation in T β RII reduced its binding with ligands, and subsequently suppressed intracellular signaling by phospho-Smad-2, which suggests that α 1,6-fucosylation positively regulates TGF- β downstream signaling (58). In contrast to TGF- β -mediated signaling, α 1,6-fucosylation on an activin receptor, a member of the TGF- β superfamily, negatively regulates phospho-Smad-2 signaling (68). In addition, cells expressing high levels of GnT-V increase migration (69) and EMT behavior by up-regulating EGFR signaling (64). However, lower expression of GnT-V is found in lung cancer, and GnT-V inversely regulates EMT behavior by suppressing Smad activation in human lung cancer cells (70). Therefore, even the same types of *N*-glycans on different receptors may play distinctive roles in their cellular signaling.

Inhibition of *N*-linked glycosylation has generated interest in its potential use as an anticancer agent (71, 72), because aberrant *N*-glycosylation is implicated in cancer growth and metastasis. In our study, we found that the KO cells were more sensitive to cancer drugs than WT and Res

cells, and more drugs were detected in the KO cells. The treatment with SW promoted cell apoptosis induced by paclitaxel (73). Inhibition of *N*-glycosylation treated with tunicamycin also greatly increased the sensitivity to doxorubicin (74). These results indicate that the functions of some membrane glycoproteins such as ABC transporters and P-glycoprotein (75), which are involved in the export and import of drugs, may be regulated by *N*-glycans. *N*-glycosylation of ABC transporters has been associated with functional activity in rat hepatocytes (76), and the inhibition of protein glycosylation has enhanced the effect of chemotherapy by interfering with the localization and function of transporter proteins in several cancer cell lines (77). In addition, the decrease in the functions of integrin in KO cells suggests an increase in the sensitivity to drugs, given that β 1 deficiency increases the inhibitory effects of AG1478, an EGFR tyrosine kinase inhibitor (61). The underlying mechanisms for drug sensitivity must be studied further.

In summary, our findings indicate that GnT-I plays a pivotal role in the regulation of key processes in cancer cells, such as EMT, cell adhesion, migration, and chemoresistance. Thus, we believe that GnT-I is a promising therapeutic target for cancer. FJ

ACKNOWLEDGMENTS

This work was supported, in part, by Grant-in-Aid for Scientific Research 15H04354 (to J.G.) from the Japanese Society for the Promotion of Science, and by Grant-in-Aid for Scientific Research on Innovative Areas 18H04868 (to J.G.) from the Ministry of Education, Culture, Sports, Science, and Technology of Japan. The authors declare no conflicts of interest.

AUTHOR CONTRIBUTIONS

G. Zhang, T. Isaji, and J. Gu designed the research; G. Zhang performed all the experiments; Z. Xu, X. Lu, and T. Fukuda assisted with the experiments; G. Zhang, T. Isaji, T. Fukuda, and J. Gu analyzed and interpreted the data; G. Zhang, T. Isaji, and J. Gu wrote and revised the manuscript; and all authors approved the final version of the manuscript.

REFERENCES

1. Nieto, M. A., Huang, R. Y., Jackson, R. A., and Thiery, J. P. (2016) EMT: 2016. *Cell* **166**, 21–45
2. Lamouille, S., Xu, J., and Derynck, R. (2014) Molecular mechanisms of epithelial-mesenchymal transition. *Nat. Rev. Mol. Cell Biol.* **15**, 178–196
3. Yang, J., and Weinberg, R. A. (2008) Epithelial-mesenchymal transition: at the crossroads of development and tumor metastasis. *Dev. Cell* **14**, 818–829
4. Li, Q., Hutchins, A. P., Chen, Y., Li, S., Shan, Y., Liao, B., Zheng, D., Shi, X., Li, Y., Chan, W. Y., Pan, G., Wei, S., Shu, X., and Pei, D. (2017) A sequential EMT-MET mechanism drives the differentiation of human embryonic stem cells towards hepatocytes. *Nat. Commun.* **8**, 15166
5. Jolly, M. K., Ware, K. E., Gilja, S., Somarelli, J. A., and Levine, H. (2017) EMT and MET: necessary or permissive for metastasis? *Mol. Oncol.* **11**, 755–769

6. Thompson, E. W., and Haviv, I. (2011) The social aspects of EMT-MET plasticity. *Nat. Med.* **17**, 1048–1049
7. Adhikary, A., Chakraborty, S., Mazumdar, M., Ghosh, S., Mukherjee, S., Manna, A., Mohanty, S., Nakka, K. K., Joshi, S., De, A., Chattopadhyay, S., Sa, G., and Das, T. (2014) Inhibition of epithelial to mesenchymal transition by E-cadherin up-regulation via repression of slug transcription and inhibition of E-cadherin degradation: dual role of scaffold/matrix attachment region-binding protein 1 (SMAR1) in breast cancer cells. *J. Biol. Chem.* **289**, 25431–25444
8. Cai, D., Chen, S. C., Prasad, M., He, L., Wang, X., Choemsel-Cadamuro, V., Sawyer, J. K., Danuser, G., and Montell, D. J. (2014) Mechanical feedback through E-cadherin promotes direction sensing during collective cell migration. *Cell* **157**, 1146–1159
9. Chen, Q. K., Lee, K., Radisky, D. C., and Nelson, C. M. (2013) Extracellular matrix proteins regulate epithelial-mesenchymal transition in mammary epithelial cells. *Differentiation* **86**, 126–132
10. Ganguly, K. K., Pal, S., Moulik, S., and Chatterjee, A. (2013) Integrins and metastasis. *Cell Adhes. Migr.* **7**, 251–261
11. Bates, R. C., Bellovin, D. I., Brown, C., Maynard, E., Wu, B., Kawakatsu, H., Sheppard, D., Oettgen, P., and Mercurio, A. M. (2005) Transcriptional activation of integrin beta6 during the epithelial-mesenchymal transition defines a novel prognostic indicator of aggressive colon carcinoma. *J. Clin. Invest.* **115**, 339–347
12. Mori, S., Kodaira, M., Ito, A., Okazaki, M., Kawaguchi, N., Hamada, Y., Takada, Y., and Matsuura, N. (2015) Enhanced expression of integrin $\alpha 5 \beta 3$ induced by TGF- β is required for the enhancing effect of fibroblast growth factor 1 (FGF1) in TGF- β -induced epithelial-mesenchymal transition (EMT) in mammary epithelial cells. *PLoS One* **10**, e0137486
13. Li, X. L., Liu, L., Li, D. D., He, Y. P., Guo, L. H., Sun, L. P., Liu, L. N., Xu, H. X., and Zhang, X. P. (2017) Integrin $\beta 4$ promotes cell invasion and epithelial-mesenchymal transition through the modulation of Slug expression in hepatocellular carcinoma. *Sci. Rep.* **7**, 40464
14. Li, X., Wang, X., Tan, Z., Chen, S., and Guan, F. (2016) Role of glycans in cancer cells undergoing epithelial-mesenchymal transition. *Front. Oncol.* **6**, 33
15. Pinho, S. S., Figueiredo, J., Cabral, J., Carvalho, S., Dourado, J., Magalhães, A., Gärtner, F., Mendonça, A. M., Isaji, T., Gu, J., Carneiro, F., Seruca, R., Taniguchi, N., and Reis, C. A. (2013) E-cadherin and adherens-junctions stability in gastric carcinoma: functional implications of glycosyltransferases involving N-glycan branching biosynthesis, N-acetylglucosaminyltransferases III and V. *Biochim. Biophys. Acta* **1830**, 2690–2700
16. Tu, C. F., Wu, M. Y., Lin, Y. C., Kannagi, R., and Yang, R. B. (2017) FUT8 promotes breast cancer cell invasiveness by remodeling TGF- β receptor core fucosylation. *Breast Cancer Res.* **19**, 111
17. Shao, K., Chen, Z. Y., Gautam, S., Deng, N. H., Zhou, Y., and Wu, X. Z. (2016) Posttranslational modification of E-cadherin by core fucosylation regulates Src activation and induces epithelial-mesenchymal transition-like process in lung cancer cells. *Glycobiology* **26**, 142–154
18. Pocheč, E., Lityńska, A., Amoresano, A., and Casbarra, A. (2003) Glycosylation profile of integrin alpha 3 beta 1 changes with melanoma progression. *Biochim. Biophys. Acta* **1643**, 113–123
19. Zhao, Y., Nakagawa, T., Itoh, S., Inamori, K., Isaji, T., Kariya, Y., Kondo, A., Miyoshi, E., Miyazaki, K., Kawasaki, N., Taniguchi, N., and Gu, J. (2006) N-acetylglucosaminyltransferase III antagonizes the effect of N-acetylglucosaminyltransferase V on alpha3beta1 integrin-mediated cell migration. *J. Biol. Chem.* **281**, 32122–32130
20. Isaji, T., Gu, J., Nishiuchi, R., Zhao, Y., Takahashi, M., Miyoshi, E., Honke, K., Sekiguchi, K., and Taniguchi, N. (2004) Introduction of bisecting GlcNAc into integrin alpha5beta1 reduces ligand binding and down-regulates cell adhesion and cell migration. *J. Biol. Chem.* **279**, 19747–19754
21. Taniguchi, N., and Kizuka, Y. (2015) Glycans and cancer: role of N-glycans in cancer biomarker, progression and metastasis, and therapeutics. *Adv. Cancer Res.* **126**, 11–51
22. Ho, W. L., Hsu, W. M., Huang, M. C., Kadomatsu, K., and Nakagawara, A. (2016) Protein glycosylation in cancers and its potential therapeutic applications in neuroblastoma. *J. Hematol. Oncol.* **9**, 100
23. Kanda, Y., Yamada, T., Mori, K., Okazaki, A., Inoue, M., Kitajima-Miyama, K., Kuni-Kamochi, R., Nakano, R., Yano, K., Kakita, S., Shitara, K., and Satoh, M. (2007) Comparison of biological activity among nonfucosylated therapeutic IgG1 antibodies with three different N-linked Fc oligosaccharides: the high-mannose, hybrid, and complex types. *Glycobiology* **17**, 104–118
24. Porwoll, S., Loch, N., Kannicht, C., Nuck, R., Grunow, D., Reutter, W., and Tauber, R. (1998) Cell surface glycoproteins undergo postbiosynthetic modification of their N-glycans by stepwise demannosylation. *J. Biol. Chem.* **273**, 1075–1085
25. De Leoz, M. L., Young, L. J., An, H. J., Kronewitter, S. R., Kim, J., Miyamoto, S., Borowsky, A. D., Chew, H. K., and Lebrilla, C. B. (2011) High-mannose glycans are elevated during breast cancer progression. *Mol. Cell. Proteomics* **10**, M110.002717
26. Ozcan, S., Barkauskas, D. A., Renee Ruhaak, L., Torres, J., Cooke, C. L., An, H. J., Hua, S., Williams, C. C., Dimapasoc, L. M., Han Kim, J., Camorlinga-Ponce, M., Rocke, D., Lebrilla, C. B., and Solnick, J. V. (2014) Serum glycan signatures of gastric cancer. *Cancer Prev. Res. (Phila.)* **7**, 226–235
27. Pocheč, E., Bocian, K., Zabczyńska, M., Korczak-Kowalska, G., and Lityńska, A. (2015) Immunosuppressive drugs affect high-mannose/hybrid N-glycans on human allostimulated leukocytes. *Anal. Cell. Pathol. (Amst.)* **2015**, 324980
28. Chang, V. T., Crispin, M., Aricescu, A. R., Harvey, D. J., Nettleship, J. E., Fennelly, J. A., Yu, C., Boles, K. S., Evans, E. J., Stuart, D. I., Dwek, R. A., Jones, E. Y., Owens, R. J., and Davis, S. J. (2007) Glycoprotein structural genomics: solving the glycosylation problem. *Structure* **15**, 267–273
29. Olden, K., Breton, P., Grzegorzewski, K., Yasuda, Y., Gause, B. L., Oredipe, O. A., Newton, S. A., and White, S. L. (1991) The potential importance of swainsonine in therapy for cancers and immunology. *Pharmacol. Ther.* **50**, 285–290
30. Ma, J., Wang, L., Li, J., Zhang, G., Tao, H., Li, X., Sun, D., and Hu, Y. (2017) Swainsonine inhibits invasion and the EMT process in esophageal carcinoma cells by targeting Twist1. *Oncol. Res.* **26**, 1207–1213
31. Shaheen, P. E., Stadler, W., Elson, P., Knox, J., Winquist, E., and Bukowski, R. M. (2005) Phase II study of the efficacy and safety of oral GD0039 in patients with locally advanced or metastatic renal cell carcinoma. *Invest. New Drugs* **23**, 577–581
32. Helenius, A., and Aebi, M. (2001) Intracellular functions of N-linked glycans. *Science* **291**, 2364–2369
33. Stanley, P., Taniguchi, N., and Aebi, M. (2015) N-glycans. In *Essentials of Glycobiology* (Varki, A., Cummings, R. D., Esko, J. D., Stanley, P., Hart, G. W., Aebi, M., Darvill, A. G., Kinoshita, T., Packer, N. H., Prestegard, J. H., Schnaar, R. L., and Seeberger, P. H., eds.), pp. 99–111, Cold Spring Harbor Laboratory Press, Cold Spring Harbor, New York
34. Fanata, W. I., Lee, K. H., Son, B. H., Yoo, J. Y., Harmoko, R., Ko, K. S., Ramasamy, N. K., Kim, K. H., Oh, D. B., Jung, H. S., Kim, J. Y., Lee, S. Y., and Lee, K. O. (2013) N-glycan maturation is crucial for cytokinin-mediated development and cellulose synthesis in *Oryza sativa*. *Plant J.* **73**, 966–979
35. He, X., Galpin, J. D., Tropak, M. B., Mahuran, D., Haselhorst, T., von Itzstein, M., Kolarich, D., Packer, N. H., Miao, Y., Jiang, L., Grabowski, G. A., Clarke, L. A., and Kermode, A. R. (2012) Production of active human glucocerebrosidase in seeds of *Arabidopsis thaliana* complex-glycan-deficient (cgl) plants. *Glycobiology* **22**, 492–503
36. Strasser, R., Stadlmann, J., Schähs, M., Stiegler, G., Quendler, H., Mach, L., Glössl, J., Weterings, K., Pabst, M., and Steinkellner, H. (2008) Generation of glyco-engineered *Nicotiana benthamiana* for the production of monoclonal antibodies with a homogeneous human-like N-glycan structure. *Plant Biotechnol. J.* **6**, 392–402
37. Ioffe, E., and Stanley, P. (1994) Mice lacking N-acetylglucosaminyltransferase I activity die at mid-gestation, revealing an essential role for complex or hybrid N-linked carbohydrates. *Proc. Natl. Acad. Sci. USA* **91**, 728–732
38. Beheshti Zavareh, R., Sukhai, M. A., Hurren, R., Gronda, M., Wang, X., Simpson, C. D., Maclean, N., Zih, F., Ketela, T., Swallow, C. J., Moffat, J., Rose, D. R., Schachter, H., Schimmer, A. D., and Dennis, J. W. (2012) Suppression of cancer progression by MGAT1 shRNA knockdown. *PLoS One* **7**, e43721
39. Ran, F. A., Hsu, P. D., Wright, J., Agarwala, V., Scott, D. A., and Zhang, F. (2013) Genome engineering using the CRISPR-Cas9 system. *Nat. Protoc.* **8**, 2281–2308
40. Shalem, O., Sanjana, N. E., Hartenian, E., Shi, X., Scott, D. A., Mikkelsen, T., Heckl, D., Ebert, B. L., Root, D. E., Doench, J. G., and Zhang, F. (2014) Genome-scale CRISPR-Cas9 knockout screening in human cells. *Science* **343**, 84–87
41. Isaji, T., Sato, Y., Zhao, Y., Miyoshi, E., Wada, Y., Taniguchi, N., and Gu, J. (2006) N-glycosylation of the beta-propeller domain of the integrin alpha5 subunit is essential for alpha5beta1 heterodimerization, expression on the cell surface, and its biological function. *J. Biol. Chem.* **281**, 33258–33267

42. Li, W., Ng, J. M., Wong, C. C., Ng, E. K. W., and Yu, J. (2018) Molecular alterations of cancer cell and tumour microenvironment in metastatic gastric cancer. *Oncogene* **37**, 4903–4920
43. Isaji, T., Sato, Y., Fukuda, T., and Gu, J. (2009) N-glycosylation of the I-like domain of beta1 integrin is essential for beta1 integrin expression and biological function: identification of the minimal N-glycosylation requirement for alpha5beta1. *J. Biol. Chem.* **284**, 12207–12216
44. Du, B., and Shim, J. S. (2016) Targeting epithelial-mesenchymal transition (EMT) to overcome drug resistance in cancer. *Molecules* **21**, 965
45. Davis, F. M., Stewart, T. A., Thompson, E. W., and Monteith, G. R. (2014) Targeting EMT in cancer: opportunities for pharmacological intervention. *Trends Pharmacol. Sci.* **35**, 479–488
46. Quintana, E., Shackleton, M., Sabel, M. S., Fullen, D. R., Johnson, T. M., and Morrison, S. J. (2008) Efficient tumour formation by single human melanoma cells. *Nature* **456**, 593–598
47. Mani, S. A., Guo, W., Liao, M. J., Eaton, E. N., Ayyanan, A., Zhou, A. Y., Brooks, M., Reinhard, F., Zhang, C. C., Shipitsin, M., Campbell, L. L., Polyak, K., Brisken, C., Yang, J., and Weinberg, R. A. (2008) The epithelial-mesenchymal transition generates cells with properties of stem cells. *Cell* **133**, 704–715
48. Duband, J. L., and Thiery, J. P. (1987) Distribution of laminin and collagens during avian neural crest development. *Development* **101**, 461–478
49. Newgreen, D., and Thiery, J. P. (1980) Fibronectin in early avian embryos: synthesis and distribution along the migration pathways of neural crest cells. *Cell Tissue Res.* **211**, 269–291
50. Goh, K. L., Yang, J. T., and Hynes, R. O. (1997) Mesodermal defects and cranial neural crest apoptosis in alpha5 integrin-null embryos. *Development* **124**, 4309–4319
51. Mittal, A., Pulina, M., Hou, S. Y., and Astrof, S. (2010) Fibronectin and integrin alpha 5 play essential roles in the development of the cardiac neural crest. *Mech. Dev.* **127**, 472–484
52. Gu, J., Isaji, T., Xu, Q., Kariya, Y., Gu, W., Fukuda, T., and Du, Y. (2012) Potential roles of N-glycosylation in cell adhesion. *Glycoconj. J.* **29**, 599–607
53. Kalluri, R., and Weinberg, R. A. (2009) The basics of epithelial-mesenchymal transition. *J. Clin. Invest.* **119**, 1420–1428
54. Moustakas, A., and Heldin, C. H. (2007) Signaling networks guiding epithelial-mesenchymal transitions during embryogenesis and cancer progression. *Cancer Sci.* **98**, 1512–1520
55. Cui, J., Huang, W., Wu, B., Jin, J., Jing, L., Shi, W. P., Liu, Z. Y., Yuan, L., Luo, D., Li, L., Chen, Z. N., and Jiang, J. L. (2018) N-glycosylation by N-acetylglucosaminyltransferase V enhances the interaction of CD147/basigin with integrin beta1 and promotes HCC metastasis. *J. Pathol.* **245**, 41–52
56. Guo, P., Wang, Q. Y., Guo, H. B., Shen, Z. H., and Chen, H. L. (2004) N-acetylglucosaminyltransferase V modifies the signaling pathway of epidermal growth factor receptor. *Cell. Mol. Life Sci.* **61**, 1795–1804
57. Buckhaults, P., Chen, L., Fregien, N., and Pierce, M. (1997) Transcriptional regulation of N-acetylglucosaminyltransferase V by the src oncogene. *J. Biol. Chem.* **272**, 19575–19581
58. Wang, X., Inoue, S., Gu, J., Miyoshi, E., Noda, K., Li, W., Mizuno-Horikawa, Y., Nakano, M., Asahi, M., Takahashi, M., Uozumi, N., Ihara, S., Lee, S. H., Ikeda, Y., Yamaguchi, Y., Aze, Y., Tomiyama, Y., Fujii, J., Suzuki, K., Kondo, A., Shapiro, S. D., Lopez-Otin, C., Kuwaki, T., Okabe, M., Honke, K., and Taniguchi, N. (2005) Dysregulation of TGF-beta1 receptor activation leads to abnormal lung development and emphysema-like phenotype in core fucose-deficient mice. *Proc. Natl. Acad. Sci. USA* **102**, 15791–15796
59. Kim, Y. W., Park, J., Lee, H. J., Lee, S. Y., and Kim, S. J. (2012) TGF-beta sensitivity is determined by N-linked glycosylation of the type II TGF-beta receptor. *Biochem. J.* **445**, 403–411
60. Xu, Q., Isaji, T., Lu, Y., Gu, W., Kondo, M., Fukuda, T., Du, Y., and Gu, J. (2012) Roles of N-acetylglucosaminyltransferase III in epithelial-to-mesenchymal transition induced by transforming growth factor beta1 (TGF-beta1) in epithelial cell lines. *J. Biol. Chem.* **287**, 16563–16574
61. Hou, S., Isaji, T., Hang, Q., Im, S., Fukuda, T., and Gu, J. (2016) Distinct effects of beta1 integrin on cell proliferation and cellular signaling in MDA-MB-231 breast cancer cells. *Sci. Rep.* **6**, 18430
62. Liwosz, A., Lei, T., and Kukuruzinska, M. A. (2006) N-glycosylation affects the molecular organization and stability of E-cadherin junctions. *J. Biol. Chem.* **281**, 23138–23149
63. Pinho, S. S., Osório, H., Nita-Lazar, M., Gomes, J., Lopes, C., Gärtner, F., and Reis, C. A. (2009) Role of E-cadherin N-glycosylation profile in a mammary tumor model. *Biochem. Biophys. Res. Commun.* **379**, 1091–1096
64. Terao, M., Ishikawa, A., Nakahara, S., Kimura, A., Kato, A., Moriwaki, K., Kamada, Y., Murota, H., Taniguchi, N., Katayama, I., and Miyoshi, E. (2011) Enhanced epithelial-mesenchymal transition-like phenotype in N-acetylglucosaminyltransferase V transgenic mouse skin promotes wound healing. *J. Biol. Chem.* **286**, 28303–28311
65. Ohtsubo, K., Takamatsu, S., Minowa, M. T., Yoshida, A., Takeuchi, M., and Marth, J. D. (2005) Dietary and genetic control of glucose transporter 2 glycosylation promotes insulin secretion in suppressing diabetes. *Cell* **123**, 1307–1321
66. Partridge, E. A., Le Roy, C., Di Guglielmo, G. M., Pawling, J., Cheung, P., Granovsky, M., Nabi, I. R., Wrana, J. L., and Dennis, J. W. (2004) Regulation of cytokine receptors by Golgi N-glycan processing and endocytosis. *Science* **306**, 120–124
67. Jin, Z. C., Kitajima, T., Dong, W., Huang, Y. F., Ren, W. W., Guan, F., Chiba, Y., Gao, X. D., and Fujita, M. (2018) Genetic disruption of multiple alpha1,2-mannosidases generates mammalian cells producing recombinant proteins with high-mannose-type N-glycans. *J. Biol. Chem.* **293**, 5572–5584
68. Gu, W., Fukuda, T., Isaji, T., Hashimoto, H., Wang, Y., and Gu, J. (2013) alpha1,6-Fucosylation regulates neurite formation via the activin/phospho-Smad2 pathway in PC12 cells: the implicated dual effects of Fut8 for TGF-beta/activin-mediated signaling. *FASEB J.* **27**, 3947–3958
69. Huang, C., Huang, M., Chen, W., Zhu, W., Meng, H., Guo, L., Wei, T., and Zhang, J. (2015) N-acetylglucosaminyltransferase V modulates radiosensitivity and migration of small cell lung cancer through epithelial-mesenchymal transition. *FEBS J.* **282**, 4295–4306
70. Li, N., Xu, H., Fan, K., Liu, X., Qi, J., Zhao, C., Yin, P., Wang, L., Li, Z., and Zha, X. (2014) Altered beta1,6-GlcNAc branched N-glycans impair TGF-beta-mediated epithelial-to-mesenchymal transition through Smad signalling pathway in human lung cancer. *J. Cell. Mol. Med.* **18**, 1975–1991
71. Goss, P. E., Reid, C. L., Bailey, D., and Dennis, J. W. (1997) Phase IB clinical trial of the oligosaccharide processing inhibitor swainsonine in patients with advanced malignancies. *Clin. Cancer Res.* **3**, 1077–1086
72. Banerjee, A., Martinez, J. A., Longas, M. O., Zhang, Z., Santiago, J., Baksi, K., and Banerjee, D. K. (2015) N-acetylglucosaminyl 1-phosphate transferase: an excellent target for developing new generation breast cancer therapeutic. *Adv. Exp. Med. Biol.* **842**, 355–374
73. You, N., Liu, W., Wang, T., Ji, R., Wang, X., Gong, Z., Dou, K., and Tao, K. (2012) Swainsonine inhibits growth and potentiates the cytotoxic effect of paclitaxel in hepatocellular carcinoma in vitro and in vivo. *Oncol. Rep.* **28**, 2091–2100
74. Peiris, D., Spector, A. F., Lomax-Browne, H., Azimi, T., Ramesh, B., Loizidou, M., Welch, H., and Dwek, M. V. (2017) Cellular glycosylation affects Herceptin binding and sensitivity of breast cancer cells to doxorubicin and growth factors. *Sci. Rep.* **7**, 43006
75. Sereš, M., Cholujová, D., Bubenčikova, T., Breier, A., and Sulová, Z. (2011) Tunicamycin depresses P-glycoprotein glycosylation without an effect on its membrane localization and drug efflux activity in L1210 cells. *Int. J. Mol. Sci.* **12**, 7772–7784
76. Draheim, V., Reichel, A., Weitschies, W., and Moenning, U. (2010) N-glycosylation of ABC transporters is associated with functional activity in sandwich-cultured rat hepatocytes. *Eur. J. Pharm. Sci.* **41**, 201–209
77. Wojtowicz, K., Januchowski, R., Nowicki, M., and Zabel, M. (2015) Inhibition of protein glycosylation reverses the MDR phenotype of cancer cell lines. *Biomed. Pharmacother.* **74**, 49–56

Received for publication July 18, 2018.
Accepted for publication September 17, 2018.



O-GlcNAcylation regulates integrin-mediated cell adhesion and migration via formation of focal adhesion complexes

Received for publication, September 19, 2018, and in revised form, December 2, 2018. Published, Papers in Press, December 26, 2018, DOI 10.1074/jbc.RA118.005923

Zhiwei Xu⁺¹, Tomoya Isaji⁺¹, Tomohiko Fukuda⁺, Yuqin Wang⁵, and Jianguo Gu⁺²

From the ⁺Division of Regulatory Glycobiology, Institute of Molecular Biomembrane and Glycobiology, Tohoku Medical and Pharmaceutical University, 4-4-1 Komatsushima, Aoba-ku, Sendai Miyagi 981-8558, Japan and the ⁵Department of Pharmacology, Pharmacy College, Nantong University, Nantong, Jiangsu Province 226001, China

Edited by Qi-Qun Tang

O-GlcNAcylation is a post-translational modification of a protein serine or threonine residue catalyzed by O-GlcNAc transferase (OGT) in the nucleus and cytoplasm. O-GlcNAcylation plays important roles in the cellular signaling that affect the different biological functions of cells, depending upon cell type. However, whether or not O-GlcNAcylation regulates cell adhesion and migration remains unclear. Here, we used the doxycycline-inducible short hairpin RNA (shRNA) system to establish an OGT knockdown (KD) HeLa cell line and found that O-GlcNAcylation is a key regulator for cell adhesion, migration, and focal adhesion (FA) complex formation. The expression levels of OGT and O-GlcNAcylation were remarkably suppressed 24 h after induction of doxycycline. Knockdown of OGT significantly promoted cell adhesion, but it suppressed the cell migration on fibronectin. The immunostaining with paxillin, a marker for FA plaque, clearly showed that the number of FAs was increased in the KD cells compared with that in the control cells. The O-GlcNAcylation levels of paxillin, talin, and focal adhesion kinase were down-regulated in KD cells. Interestingly, the complex formation between integrin $\beta 1$, focal adhesion kinase, paxillin, and talin was greatly increased in KD cells. Consistently, levels of active integrin $\beta 1$ were significantly enhanced in KD cells, whereas they were decreased in cells overexpressing OGT. The data suggest a novel regulatory mechanism for O-GlcNAcylation during FA complex formation, which thereby affects integrin activation and integrin-mediated functions such as cell adhesion and migration.

O-GlcNAcylation is controlled by OGT³ and is a specific type of post-translational modification that consists of the covalent attachment of single GlcNAc to the nucleus and cytoplasm of the serine or threonine residue of an extremely large family of target proteins (1, 2). This post-translational modification is essential for cell survival and division (3), and aberrant

O-GlcNAcylation provokes tumorigenesis, diabetes, and Alzheimer's disease by regulating cell signaling, transcription, metabolism, and cytoskeletal formation (4–7). The increased O-GlcNAcylation seems to be a general characteristic of cancer cells. For example, higher levels of O-GlcNAcylation expression have been observed in cancers of the liver (8), lung, colon (9), and breast (10). Furthermore, numerous breast cancer cell lines have shown higher levels of O-GlcNAcylation, and the levels of OGT expression in aggressive breast cancer cell lines are much higher than those seen in less aggressive breast cancer cell lines (11). O-GlcNAc modifications have also been observed in important target proteins, such as p53 (12), HIF-1 α (13), β -catenin (10), and G6PD (14), which are involved in the regulation of malignant cancer characteristics by controlling cellular metabolism and proliferation. On the other hand, the suppression of OGT expression in breast or liver cancer cell lines decreases cell motility, which suggests that O-GlcNAcylation could be involved in cell migration (10, 15).

Cell migration is a highly integrated multistep process that includes the development of cytoplasmic protrusions, attachment, and spreading (16). The migratory capacity of cancer cells is initially mediated by alterations in the expression of cell surface molecules known as integrins (17). It is becoming increasingly clear that integrins are crucial for cell migration in the tumor microenvironment (18). Following ligand binding, integrins cluster into focal contacts that contain different focal adhesion (FA)-associated proteins, such as α -actinin, vinculin, talin, FAK, and paxillin, which link the integrins to the actin cytoskeleton (19). The processes of adhesion formation and disassembly drive the migration cycle through ligand binding, which in turn regulates integrin activity and cytoskeletal complex formation as well as adhesion dynamics (20). O-GlcNAcylation appears to occur in actin cytoskeletal regulatory proteins, such as paxillin (21) and talin (22), as well as in microtubule assembly proteins, such as tubulin (23), and in microtubule-associated proteins (24). However, whether and how O-GlcNAcylation impacts cell migration remains unclear.

In the present study, we used the doxycycline shRNA-inducible system to knock down the OGT gene to identify the biological functions of O-GlcNAcylation and its regulatory mechanisms in cell adhesion and migration. We found that the knockdown of OGT aberrantly increased cell adhesion, FA formation, and integrin $\beta 1$ activation, which in turn decreased cell migration. Thus, our findings may provide

This work was supported in part by Japan Society for the Promotion of Science Grant-in-Aid for Scientific Research 15H04354; National Natural Science Foundation of China Grant 31670807; and Grant-in-Aid for Scientific Research on Innovative Areas 18H04868 from the Ministry of Education, Culture, Sports, Science, and Technology of Japan. The authors declare that they have no conflicts of interest with the contents of this article.

¹ Both authors contributed equally to this work.

² To whom correspondence should be addressed. Tel.: 81-22-727-0216; Fax: 81-22-727-007; E-mail: jgu@tohoku-mpu.ac.jp.

³ The abbreviations used are: OGT, O-GlcNAc transferase; KD, knockdown; DOX, doxycycline; shRNA, short hairpin RNA; FAK, focal adhesion kinase; FA, focal adhesion; ECM, extracellular matrix; VSV, vesicular stomatitis virus glycoprotein; DMEM, Dulbecco's modified Eagle's medium.

FAK was modified by O-GlcNAc

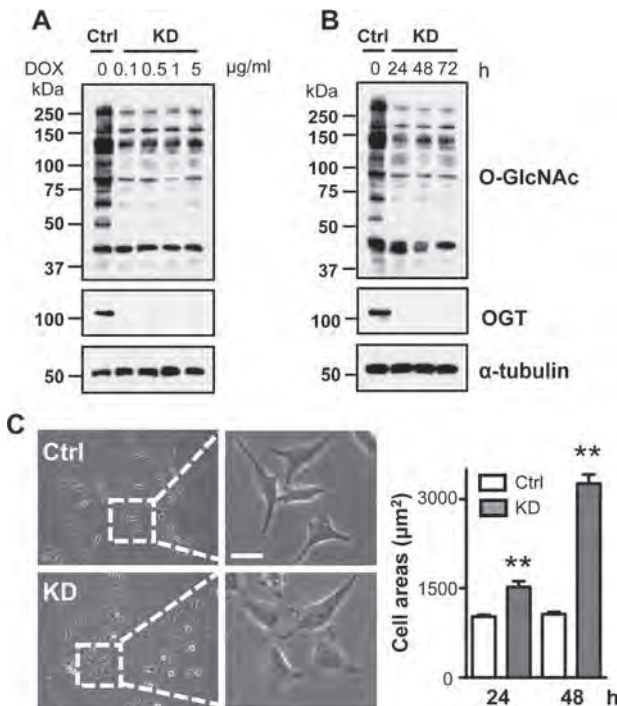


Figure 1. Knockdown of OGT suppressed O-GlcNAcylation and enhanced cell spreading in HeLa cells. A and B, the expression levels of OGT and O-GlcNAcylation from cell lysates of DOX-controlled OGT KD HeLa cells were verified with concentrations of DOX at 0, 0.1, 0.5, 1.0, and 5.0 $\mu\text{g/ml}$ for 72 h (A) or at the indicated time with 0.1 $\mu\text{g/ml}$ DOX (B). The control (Ctrl) indicates the cells treated without DOX. Cell lysates from the indicated cells were subjected to Western blotting with the O-GlcNAc (CTD110.6), OGT, and α -tubulin antibodies. C, representative images of cell spreading are shown after incubation for 48 h. Cells were incubated with (KD) or without (Ctrl) 0.1 $\mu\text{g/ml}$ DOX for 24 or 48 h on a normal culture dish, after which the cell areas were measured. Values represent the mean \pm S.E. (error bars) ($n = 50$). **, $p < 0.01$ (Welch's correction t test). Scale bars, 15 μm . Experiments were independently repeated at least two times.

new insight into integrin-mediated cell migration and explain why O-GlcNAcylation is usually highly expressed in some malignant cancers.

Results

Established OGT knockdown (KD) cells

A growing number of studies have shown that O-GlcNAcylation plays a critical role in the regulation of tumor cell growth (11) and cancer metastasis (25, 26). To investigate the effects of O-GlcNAc expression on cell adhesion and migration, we used the DOX-dependent inducible shRNA KD system to establish OGT KD HeLa cells. In this cellular system, OGT and O-GlcNAc were expressed at normal levels in the absence of DOX, whereas both expressions were drastically suppressed in the presence of DOX in the culture medium at the indicated concentrations, as shown in Fig. 1A. Furthermore, similar suppression levels were observed even following incubation at the lowest concentration of 0.1 $\mu\text{g/ml}$ after 24 h (Fig. 1B), suggesting an effective KD of OGT and a rapid turnover of O-GlcNAc levels in HeLa cells. After culture for 48 h, elongated cell shapes were converted to a more-rounded morphology, and the KD cells showed significantly increased cell spreading areas compared with those in the control cells (Fig. 1C). These observations suggest the impact that O-GlcNAcylation exerts on cell morphology.

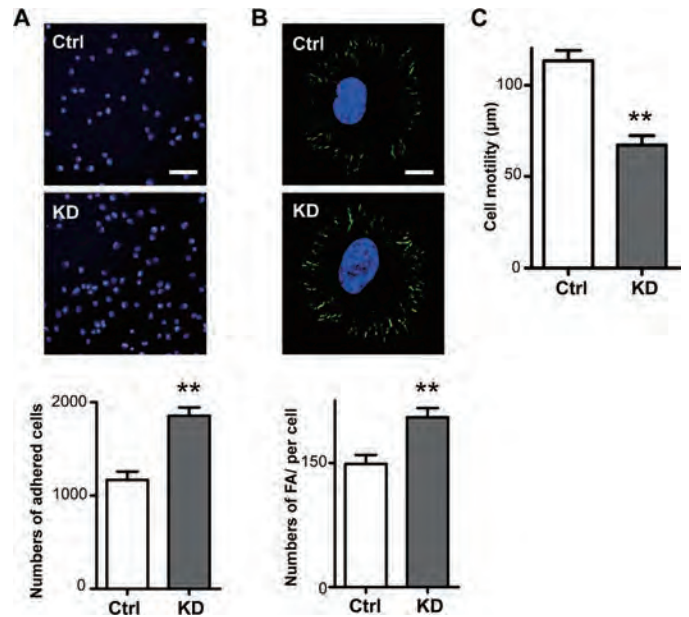


Figure 2. Reduced O-GlcNAcylation promoted cell adhesion and FA formation but decreased cell migration. HeLa cells were cultured in the presence (KD) or absence (Ctrl) of DOX for 24 h. A, 20 min after replating cells onto FN-coated 96-well plates, the attached cells were fixed, and then the nuclei were stained and counted. Representative fields were photographed via fluorescent microscopy. Scale bars, 30 μm . Values represent the mean \pm S.E. (error bars) ($n = 11$). **, $p < 0.01$ (Welch's correction t test). B, cells were allowed to spread on FN-coated coverslips for 1 h. Cells were then stained with anti-paxillin antibody (green) and TO-PRO-3 (blue). The numbers of focal adhesions were quantified by ImageJ software. Scale bars, 5 μm . Values represent the mean \pm S.E. ($n = 11$). **, $p < 0.01$ (Welch's correction t test). C, cell motility was observed by time-lapse video microscopy. Values represent the mean \pm S.E. ($n = 30$). **, $p < 0.01$ (Welch's correction t test). Experiments were independently repeated at least two times.

Knockdown of O-GlcNAcylation enhanced cell adhesion and FA formation and suppressed cell motility

Next, we used a fibronectin (FN)-coated dish to investigate the effects of OGT KD on cell adhesion, FA formation, and cell motility. To verify the initial stage of cell adhesion, we performed a 20-min cell adhesion assay on FN. Interestingly, the number of adhered cells was drastically increased in the KD cells compared with that in the control cells (Fig. 2A). During cell adhesion, integrins and cytoplasmic proteins such as paxillin, talin, and FAK become clustered in the plane of the cell membrane and in well-developed aggregates, the so-called FA plaque, which can be detected by immunofluorescence microscopy (27). Consistent with their enhancement of cell adhesion, in the present study, OGT KD cells also promoted an increase in FA formation, by comparison with the activity in control cells (Fig. 2B). By contrast, the KD cells showed a significant reduction in cell motility, as observed by video microscopy (Fig. 2C). These data indicate that a loss of O-GlcNAcylation promotes cell adhesion and focal contact formation while suppressing cell migration.

Talin, FAK, and paxillin were O-GlcNAc-modified proteins

Previous studies have revealed that some forms of protein FA plaque, such as paxillin and talin, are modified by O-GlcNAc (21, 22). In the present study, we investigated whether O-GlcNAc modification of those target proteins also occurred in HeLa cells in this system. Consistent with previous studies,

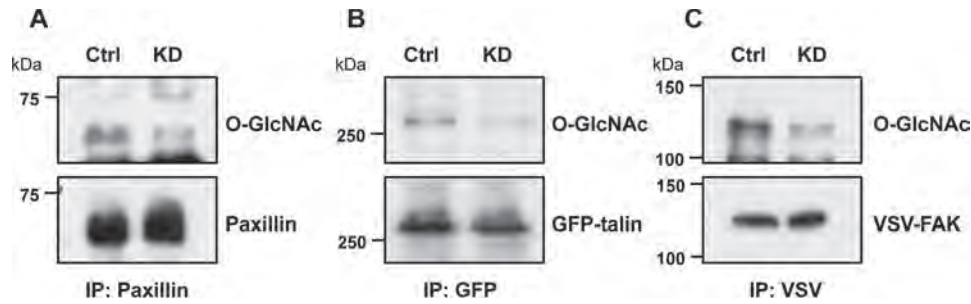


Figure 3. Decreased O-GlcNAcylation levels of paxillin, talin, and FAK in OGT-KD cells. HeLa cells (A) or cells transfected with talin (B) or FAK (C) were incubated without (Ctrl) or with (KD) DOX. The cell extracts were immunoprecipitated (IP) with the indicated antibodies and Western blotted with anti-O-GlcNAc or the indicated antibodies, respectively. Experiments were independently repeated at least three times.

O-GlcNAc modifications were detected on both paxillin and talin, whereas O-GlcNAcylation levels for both proteins were significantly decreased in KD cells, compared with that seen in control cells (Fig. 3, A and B). Importantly, we also found that FAK, a key molecule for integrin-mediated signaling, was also a target protein for O-GlcNAcylation, which was decreased in the KD cells (Fig. 3C). The suppression of O-GlcNAcylation on FAK and talin was also confirmed in DOX-induced OGT KD 293T cells (data not shown). To further establish the occurrence of O-GlcNAcylation in these proteins, we conducted a chemoenzymatic labeling assay using an azido-GalNAc sugar, as described under “Experimental procedures.” Clearly, talin, FAK, and paxillin were labeled, which proved that they are O-GlcNAcylated proteins (Fig. 4, A–C). These results suggest that O-GlcNAcylation may affect both integrin $\beta 1$ -mediated complex formation and FA formation, which confirms this process as a regulator of cell adhesion and migration.

Reduction of O-GlcNAcylation promoted complex formation

FAK is a key component of the signal transduction pathways triggered by integrins. When cells bind to the extracellular matrix (ECM), FAK is usually recruited to integrin-mediated nascent FA, because it interacts directly through the cytoskeletal proteins talin and paxillin, with the cytoplasmic tail of integrin $\beta 1$ (28). Therefore, we compared the ability of control and KD cells to form FA complexes. As shown in Fig. 5A, the complexes immunoprecipitated with anti-FAK antibody showed higher levels of paxillin in KD cells than in control cells. Consistently, KD cells demonstrated a greater number of complex formations composed of both $\beta 1$ integrin and talin (Fig. 5B) and talin and FAK (Fig. 5C). A similar phenomenon was also confirmed in OGT-KD 293T cells (data not shown).

Knockdown of O-GlcNAcylation activated integrin $\beta 1$

Given the increase in FA complex formation in KD cells, it is reasonable to speculate that OGT-KD may affect integrin activation. Integrin-mediated adhesion can recruit FA proteins to form FA plaque and then trigger conformational activation, so-called inside-out signaling, of integrin $\beta 1$ in the ectodomain, which then can be recognized by a specific antibody (29, 30) that we used to examine the expression levels of active integrin $\beta 1$ in both control and KD cells. The expression levels of active $\beta 1$ in immunostaining (Fig. 6A) or cell lysates (Fig. 6B) were clearly up-regulated in the KD cells compared with control cells. In contrast to KD cells, the expression levels of active $\beta 1$

were suppressed in the OGT-overexpressing HeLa cells, which further suggested that O-GlcNAcylation negatively regulates integrin-mediated inside-out signaling. Thus, we were convinced that OGT could be a novel regulator for FA complex formation and integrin activation by dynamically regulating cell adhesion and migration.

Discussion

In the present study, we clearly showed that O-GlcNAcylation negatively regulates integrin-mediated cell adhesion and FA complex formation as well as integrin activation, which results in the control of cell migration on the ECM (Fig. 7). Our findings are the first to demonstrate that OGT may function as a key regulator of FA complex formation during cell–ECM adhesion. These results provide clues to understanding the roles of O-GlcNAcylation in cell migration.

Cell migration is a central process in the development and maintenance of multicellular organisms (16). Although the detailed mechanisms underlying cell migration remain unclear, it is reasonable to postulate that integrin-mediated cell adhesion could regulate migration, which would allow communication between cell–ECM contact and the actin cytoskeleton through focal adhesions (31). The dynamic balance between adhesion receptors and the binding of ECM ligands provides FA turnover that regulates adhesion formation and disassembly (32). In the framework of this model, an imbalance in the processes of attachment and detachment leads to conformational changes that mediate abnormal adhesion (19). In the present study, we clearly demonstrated that the suppression of O-GlcNAcylation inhibited HeLa cell migration, whereas it enhanced cell–ECM adhesion (Fig. 2), which indicated that O-GlcNAcylation is involved in the regulation of integrin-mediated cell adhesion. Consistently, FAK serves as a key regulator of FA assembly and disassembly processes that are fundamental for efficient cell migration (33). Indeed, there were more stress fibers and focal adhesions in FAK-deficient cells, whereas cell motility was inhibited (34). Aberrant cell–ECM adhesiveness is likely to suppress cell migration, and proper cell adhesion is an important determinant for cell migration (35). Thus, our data are reasonable in that the knockdown of O-GlcNAcylation aberrantly increased cell adhesion, as well as spreading and FA complex formation, which in turn decreased cell migration. Consistently, a loss of paxillin phosphorylation at Ser-250 markedly inhibits focal adhesion turnover and cell migration (36).

FAK was modified by O-GlcNAc

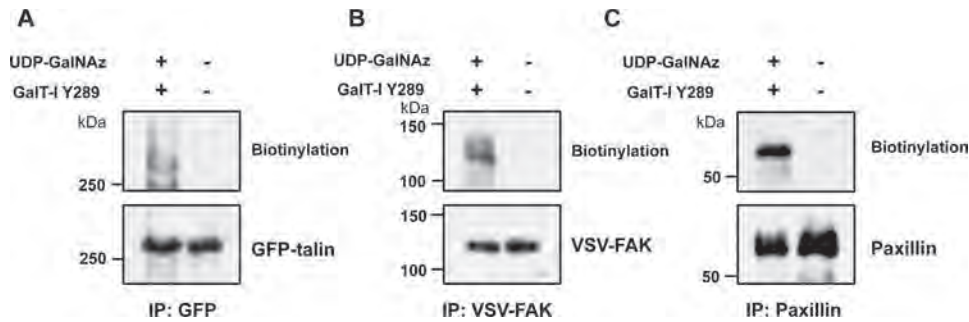


Figure 4. Confirmation of O-GlcNAcylation on talin, FAK, and paxillin. Cell lysates of 293T cells transfected with talin (A), FAK (B), or WT HeLa cells (C) were immunoprecipitated (IP) with anti-GFP, anti-VSV, or anti-paxillin antibodies, respectively, followed by click chemistry labeling of O-GlcNAc residues with (+) or without (–) GalT and UDP-GalNAz, and were detected using an ABC kit, as described under “Experimental procedures.” Experiments were independently repeated at least two times.

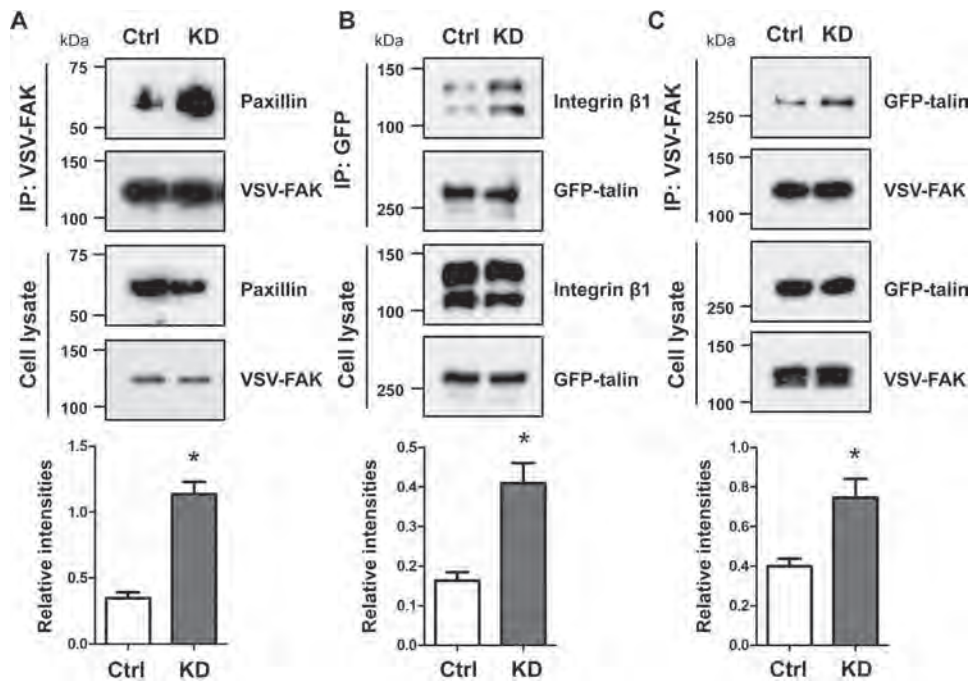


Figure 5. Increased focal adhesion complex formation in OGT KD cells. Cell lysates from the control (Ctrl) and KD HeLa cells that were transfected with expression plasmids of FAK (A), talin (B), or both FAK and talin (C) were immunoprecipitated (IP) by the indicated antibodies and then subjected to Western blotting as described under “Experimental procedures.” The relative ratios are shown at the bottom ($n = 3$ individual experiments). Values represent the mean \pm S.E. (error bars). *, $p < 0.05$ (Welch’s correction t test). Cell lysates were used as input. Experiments were independently repeated at least three times.

We were intrigued as to why a knockdown of OGT would enhance integrin activation. Integrins are the major cell surface receptors used to assemble and recognize a functional ECM and to facilitate cell signaling and migration (37). The organization of cell adhesions is complex and includes a number of cytoplasmic proteins, such as paxillin, talin, FAK, vinculin, and α -actinin (29). Integrin activation is associated with an array of biological and pathological conditions involving both outside-in and inside-out signaling (38). Accumulating data have indicated that the cytoplasmic domain of the integrin $\beta 1$ subunit cooperatively promotes integrin activation through the binding of talin (39). Consequently, our results clearly showed the interaction of integrin $\beta 1$ with talin, and the association of FAK, paxillin, and/or talin both were greatly increased in the KD cells, which suggests that the KD of OGT promotes inside-out signaling (Fig. 5). A reciprocal relationship between O-GlcNAcylation and O-phosphorylation has been observed in the specific serine or threonine residue of particular proteins

(40,41), and, therefore, how O-GlcNAcylation affects the O-phosphorylation of FA complex proteins is worthy of clarification.

The O-GlcNAcylation of FAK is noteworthy. Integrins do not possess enzymatic activity; rather, they associate with a number of cytoplasmic protein kinases, such as FAK and Src. Tyrosine-phosphorylated FAK is well-known to be a promoter of interactions with various Src homology 2- and 3- containing proteins and to initiate enzymatic cascades via these associated kinases that ultimately lead to changes in cell behavior (42). By contrast, serine or threonine phosphorylation on FAK is not well-understood. FAK phosphorylation at either Ser-732 or Ser-722 has recently been recognized as important for microtubule organization, nuclear movement, and neuronal migration during cell adhesion (43, 44). Interestingly, phosphorylation of both Ser-843 and Ser-910 on FAK exhibited synchronized phosphorylation during cell mitosis (45), which may be related to O-GlcNAcylation because expression levels of OGT change during mitosis (46). Furthermore, a cluster of ser-

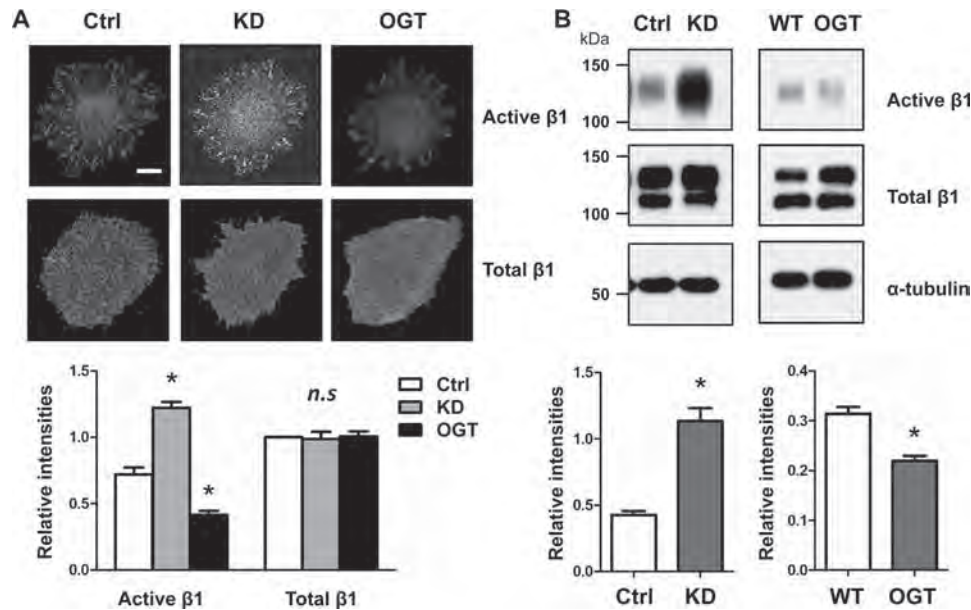


Figure 6. Comparison of the expression levels of active integrin $\beta 1$ among the control (Ctrl), KD, and OGT-overexpressing cells. A, a representative immunostaining pattern with anti-active $\beta 1$ or anti- $\beta 1$ antibodies in the control, KD, and OGT-overexpressing (OGT) HeLa cells. Cells were cultured on FN-coated coverslips for 1 h and then subjected to immunostaining analyses. The relative fluorescence intensities of KD and OGT-overexpressing cells were compared with the control, and relative fluorescence intensity was 1.0 for the control cells. Scale bar, 5 μm . B, the expression levels of active and total integrin $\beta 1$ were verified by immunoblotting with the indicated antibodies in control and KD HeLa cells or parent (WT) or transiently OGT-overexpressing HeLa cells. The relative ratios are shown at the bottom ($n = 10$ random fields of view). Values represent the mean \pm S.E. (error bars). *, $p < 0.05$ (Welch's correction t test); n.s., not significant ($p > 0.05$). Experiments were independently repeated at least two times.

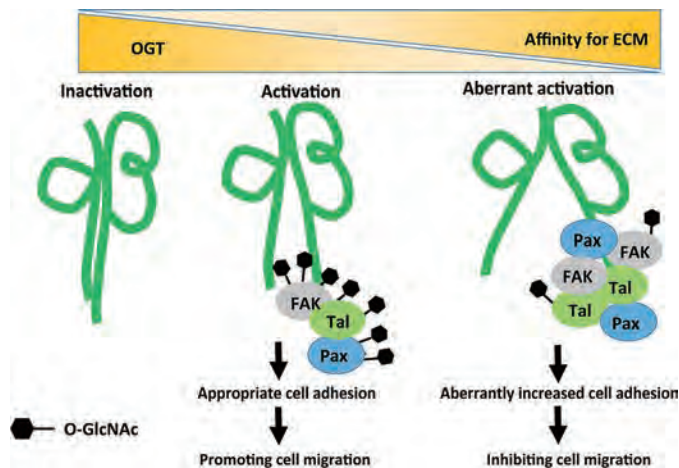


Figure 7. Proposed molecular mechanism for the regulation of cell adhesion and migration by O-GlcNAcylation. During cell adhesion, integrin may form a complex with focal adhesion proteins, such as FAK, talin, and paxillin, to connect with an actin cytoskeleton, which mediates appropriate cell adhesion to promote cell migration. It is well-known that focal adhesion assembly and disassembly processes are fundamental for efficient cell migration. Most focal adhesion proteins can be modified by O-GlcNAc and O-phosphate on serine or threonine residues. In the present study, suppression of the O-GlcNAcylation of paxillin, talin, and FAK aberrantly enhanced integrin activation, integrin-mediated cell adhesion, and complex formation, which in turn led to an inhibition of cell migration, which strongly suggests that OGT functions as a key regulator for cell adhesion.

ine phosphorylation sites was recently identified at the initiation of the FA-targeting domain in FAK (47), which may suggest that some of those sites could be modified by O-GlcNAcylation. Thus, to elucidate the roles of OGT in cell biology, it is necessary to identify the specific sites and functions of O-GlcNAcylation in FAK.

Our results indicate that O-GlcNAcylation plays important roles in regulating cell adhesion, FA complex formation, and

cell migration. Emerging data have already established that O-GlcNAc modification has a critical role in the progress of human diseases, and particularly diseases such as cancer, diabetes, and Alzheimer's (7). Intriguingly, FAK has been associated with insulin resistance in adipocytes in the early stages of type II diabetes (48, 49) and has also been implicated in the deposition of β -amyloid plaque (50, 51). It would be reasonable to assume that dynamic regulation of FAK O-GlcNAcylation with phosphorylation may partially serve as a possible explanation for a number of diseases.

Experimental procedures

Antibodies and reagents

Experiments were performed using the following antibodies: mAb against O-GlcNAc (CTD110.6, 9875S) and peroxidase-conjugated secondary antibody against rabbit (7074S) from Cell Signaling Technology; the rabbit polyclonal antibody against OGT (O0164) and mAb against α -tubulin (T6199) and VSV (V5507) from Sigma; mAb against integrin $\beta 1$ (610468) and paxillin (610052) from BD Biosciences; mAb against active integrin $\beta 1$ (HUTS-4; 2079Z) and peroxidase-conjugated secondary antibodies against mouse (AP124P) and goat (AB324P) from Millipore; Alexa Fluor 488-conjugated anti-mouse (A11029) from Invitrogen; TO-PRO-3 (T3605) from Molecular Probes, Inc.; and GFP-agarose (MBL, D153-8) and goat antibody against GFP (Rockland, 600-101-215). The mAb against human $\beta 1$ (P5D2) was obtained from the Developmental Studies Hybridoma Bank, University of Iowa. Human FN and doxycycline hyclate (D9891) were from Sigma-Aldrich. An ABC kit was acquired from Vector Laboratories, and Ab-Capcher Mag was from ProteNova (Takamatsu, Japan).

FAK was modified by O-GlcNAc

Cell culture and expression plasmids

HeLa and 293T cell lines (RIKEN, Japan) were maintained at 37 °C in DMEM high-glucose (Invitrogen) supplemented with 10% fetal bovine serum under a humidified atmosphere that contained 5% CO₂. To express GFP-tagged talin (52) and 2× VSV-tagged FAK, expression vector pEGFP-N1-talin-GFP (Addgene 26724) and pRKVSV-FAK were kindly provided by Dr. Anna Huttenlocher (52) and Dr. Kenneth Yamada (53), respectively. The pcDNA3.1/myc-his expression vector containing human OGT was kindly provided by Dr. Yuanyuan Ruan (School of Basic Medical Sciences, Fudan University, Shanghai, China). Transfection was performed using PEI MAX (molecular mass, 40 kDa; Polysciences Inc.) and following the dictates of the United States patent application (number US20110020927A1) with minor modifications. Briefly, 24 h prior to transfections, cells were seeded on a 10-cm dish, and expression vectors with PEI MAX (1 mg/ml in 0.2 M hydrochloric acid) were preincubated for 15 min at a 1:3 ratio in 2,000 μl of a solution that contained 20 mM CH₃COONa buffer, pH 4.0, and 150 mM NaCl. Cells and DNA complexes were further incubated for 24 h with 10 ml of normal culture medium to promote expression.

Establishment of doxycycline-inducible OGT knockdown cells

We used CS-Rfa-ETBsd DOX-dependent inducible RNAi mediated by a single lentivirus vector (RIKEN) for the knockdown experiment (54). The following oligonucleotides were inserted into pENTR/H1/TO (sense, CACCGCTGAGCAGT-ATTCGAGAACTCGAGTTTCTCGGAATACTGCTCAGCC; antisense, AAAAGGCTGAGCAGTATTCGAGAACTCGAGTTTCTCGGAATACTGCTCAGC) with minor modification from a procedure established in a previous report (13). Using LR clonase, inserted oligonucleotide was then transferred to CS-Rfa-ETBsd, which encodes tetracycline-dependent transactivators for shRNA expression. To prepare the viruses, PEI MAX was used to transfect the resultant vector into 293T cells with packaging plasmids. HeLa and 293T cells were then infected by the obtained viruses and selected for stable integration with 10 μg/ml blasticidin. The shRNA-mediated silencing of OGT was induced by the addition of DOX in the established cell line, and the cells cultured by DOX-free medium were used as the control in the present study.

Immunoprecipitation and Western blotting

The cells were washed with PBS, and lysed in lysis buffer (20 mM Tris-HCl, pH 7.4, 150 mM NaCl, 0.1% Triton X-100) with protease and phosphatase inhibitors (Nacalai Tesque, Kyoto, Japan). The supernatants were collected, and the protein concentrations were determined using a bicinchoninic acid protein assay kit (Pierce). Equal amounts of proteins were subjected to SDS-PAGE and then transferred to polyvinylidene difluoride membranes. To detect active integrin β1, we prepared samples under nonreducing conditions. The membranes were blocked either with 5% nonfat milk in TBST or with 3% BSA for 2 h at room temperature, and then the proteins were probed with antibodies against O-GlcNAc, OGT, α-tubulin, active integrin β1 (HUTS-4) (55, 56), integrin β1 (Millipore), paxillin, VSV, and GFP. After being washed, the membranes were incubated

with horseradish peroxidase-conjugated secondary antibodies. Detection was accomplished using a horseradish peroxidase substrate (Millipore) according to the manufacturer's instructions. For immunoprecipitation, the supernatant (500 μg of protein) was incubated with an anti-VSV or an anti-paxillin with an Ab-Capcher Mag. GFP-talin was immunoprecipitated with GFP-conjugated beads. The immunoprecipitates were washed with lysis buffer and subjected to SDS-PAGE. The immunocomplexes then were detected using the indicated antibodies. An mAb against α-tubulin was used as the loading control.

Cell adhesion assay

Cell adhesion assays were performed in a 96-well CellCarrier (PerkinElmer Life Sciences) coated with FN (5 μg/ml) overnight. HeLa cells were pretreated with or without DOX (0.1 μg/ml) for 24 h. Cells were replated at a density of 10⁴ cells/well in plates using serum-free DMEM with 0.1% BSA, followed by incubation at 37 °C for 20 min. Nonadherent cells were removed by washing three times with PBS. Cells were fixed with 4% formaldehyde and stained 4',6-diamidino-2-phenylindole (Invitrogen) and were then imaged by fluorescent microscopy using an Operetta CLS (PerkinElmer Life Sciences). To count the number of nuclei in the each well, images were analyzed using Harmony software (PerkinElmer Life Sciences).

Immunofluorescence

Cells were plated onto FN-coated glass coverslips (MatTek Corp., Ashland, MA) for 1 h, washed with PBS, and fixed with 4% paraformaldehyde. For permeabilization, the cells were treated with 0.1% Triton X-100 in PBS. The cells were blocked with 0.1% Tween 20 and 3% BSA in PBS and then stained with paxillin, active β1 (HUTS-4), total β1 (P5D2), and OGT antibodies overnight at 4 °C. The samples were followed by incubation with anti-mouse Alexa Fluor 488-conjugated secondary antibody and were then incubated with TO-PRO-3. Images were acquired by sequential excitation using an Olympus FV1000 laser-scanning confocal microscope with an UPlanSApo ×60/1.35 oil objective and high-sensitivity gallium arsenide phosphide detector units operated by F10-ASW version 4.02 software. To count the number of FAs, we followed a protocol previously described using ImageJ (57), excluding focal adhesions that were less than 0.2 μm², because these disappeared quickly (58). OGT-overexpressing cells were identified via co-immunostaining with OGT. The relative fluorescence intensities of active integrin β1 and total integrin β1 were quantified using ImageJ software.

Video microscopy

Glass-bottom dishes (Asahi Glass, Shizuoka, Japan) were precoated with FN (10 μg/ml) in PBS, let stand at 4 °C overnight, and were then blocked with 1% BSA. Ten thousand cells were suspended in 2 ml of DMEM containing 3% fetal bovine serum medium, which was then added to each FN-coated glass-bottom dish and monitored for 12 h using AxioVision equipment (Carl Zeiss, Oberkochen, Germany). Images were acquired using an inverted microscope (Axio Observer.D1, Carl Zeiss) every 10 min with 5% CO₂ at 37 °C in a heated chamber equipped with temperature and CO₂ controllers

(Onpu-4 and CO₂; AR BROWN, Tokyo, Japan) during time-lapse imaging. Cell motility was evaluated using an AxioVision Tracking module (Carl Zeiss).

Chemoenzymatic labeling assay

Chemoenzymatic labeling and biotinylation of proteins in cell lysates was carried out using the Click-iT O-GlcNAc enzymatic labeling system (Invitrogen). Briefly, the whole-cell lysate of 293T cells transfected with an expression plasmid for VSV-FAK or GFP-talin (500 μ g) and HeLa cells were immunoprecipitated and then labeled with labeling enzyme GalT and UDP-GalNAz according to the Click-iT O-GlcNAc enzymatic labeling system protocol (Invitrogen). Labeled proteins were conjugated with an alkyne-biotin compound following the Click-iT protein analysis detection kit protocol (Invitrogen). Control experiments were performed in the absence of GalT and UDP-GalNAz. Biotinylated and control samples were then subjected to SDS-PAGE and transferred to a polyvinylidene difluoride membrane for further detection using an ABC kit (Vector Laboratories).

Statistics

All results shown are the results of at least two independent experiments and are shown as representative data. The values represent the mean \pm S.E. *p* values were calculated using Welch's correction *t* test using GraphPad Prism version 5 (*, *p* < 0.05; **, *p* < 0.01).

Author contributions—T. I. and J. G. designed the research; Z. X. and T. I. performed all experiments; T. F. and Y. W. assisted with experiments; T. I., T. F., Y. W., and J. G. analyzed and interpreted the data; Z. X., T. I., Y. W., and J. G. wrote and revised the manuscript; and all authors approved the final version of the manuscript.

References

- Zachara, N. E., and Hart, G. W. (2006) Cell signaling, the essential role of O-GlcNAc! *Biochim. Biophys. Acta* **1761**, 599–617 [CrossRef Medline](#)
- Vosseller, K., Sakabe, K., Wells, L., and Hart, G. W. (2002) Diverse regulation of protein function by O-GlcNAc: a nuclear and cytoplasmic carbohydrate post-translational modification. *Curr. Opin. Chem. Biol.* **6**, 851–857 [CrossRef Medline](#)
- Tan, E. P., Duncan, F. E., and Slawson, C. (2017) The sweet side of the cell cycle. *Biochem. Soc. Trans.* **45**, 313–322 [CrossRef Medline](#)
- Singh, J. P., Zhang, K., Wu, J., and Yang, X. (2015) O-GlcNAc signaling in cancer metabolism and epigenetics. *Cancer Lett.* **356**, 244–250 [CrossRef Medline](#)
- Itkonen, H. M., Minner, S., Guldvik, I. J., Sandmann, M. J., Tsourlakis, M. C., Berge, V., Svindland, A., Schlomm, T., and Mills, I. G. (2013) O-GlcNAc transferase integrates metabolic pathways to regulate the stability of c-MYC in human prostate cancer cells. *Cancer Res.* **73**, 5277–5287 [CrossRef Medline](#)
- Slawson, C., and Hart, G. W. (2011) O-GlcNAc signalling: implications for cancer cell biology. *Nat. Rev. Cancer* **11**, 678–684 [CrossRef Medline](#)
- Copeland, R. J., Han, G., and Hart, G. W. (2013) O-GlcNAcomics: revealing roles of O-GlcNAcylation in disease mechanisms and development of potential diagnostics. *Proteomics Clin. Appl.* **7**, 597–606 [CrossRef Medline](#)
- Zhang, X., Qiao, Y., Wu, Q., Chen, Y., Zou, S., Liu, X., Zhu, G., Zhao, Y., Chen, Y., Yu, Y., Pan, Q., Wang, J., and Sun, F. (2017) The essential role of YAP O-GlcNAcylation in high-glucose-stimulated liver tumorigenesis. *Nat. Commun.* **8**, 15280 [CrossRef Medline](#)
- Mi, W., Gu, Y., Han, C., Liu, H., Fan, Q., Zhang, X., Cong, Q., and Yu, W. (2011) O-GlcNAcylation is a novel regulator of lung and colon cancer malignancy. *Biochim. Biophys. Acta* **1812**, 514–519 [CrossRef Medline](#)
- Gu, Y., Mi, W., Ge, Y., Liu, H., Fan, Q., Han, C., Yang, J., Han, F., Lu, X., and Yu, W. (2010) GlcNAcylation plays an essential role in breast cancer metastasis. *Cancer Res.* **70**, 6344–6351 [CrossRef Medline](#)
- Caldwell, S. A., Jackson, S. R., Shahriari, K. S., Lynch, T. P., Sethi, G., Walker, S., Vosseller, K., and Reginato, M. J. (2010) Nutrient sensor O-GlcNAc transferase regulates breast cancer tumorigenesis through targeting of the oncogenic transcription factor FoxM1. *Oncogene* **29**, 2831–2842 [CrossRef Medline](#)
- Yang, W. H., Kim, J. E., Nam, H. W., Ju, J. W., Kim, H. S., Kim, Y. S., and Cho, J. W. (2006) Modification of p53 with O-linked N-acetylglucosamine regulates p53 activity and stability. *Nat. Cell Biol.* **8**, 1074–1083 [CrossRef Medline](#)
- Ferrer, C. M., Lynch, T. P., Sodi, V. L., Falcone, J. N., Schwab, L. P., Peacock, D. L., Vocadlo, D. J., Seagroves, T. N., and Reginato, M. J. (2014) O-GlcNAcylation regulates cancer metabolism and survival stress signaling via regulation of the HIF-1 pathway. *Mol. Cell* **54**, 820–831 [CrossRef Medline](#)
- Rao, X., Duan, X., Mao, W., Li, X., Li, Z., Li, Q., Zheng, Z., Xu, H., Chen, M., Wang, P. G., Wang, Y., Shen, B., and Yi, W. (2015) O-GlcNAcylation of G6PD promotes the pentose phosphate pathway and tumor growth. *Nat. Commun.* **6**, 8468 [CrossRef Medline](#)
- Xu, W., Zhang, X., Wu, J. L., Fu, L., Liu, K., Liu, D., Chen, G. G., Lai, P. B., Wong, N., and Yu, J. (2017) O-GlcNAc transferase promotes fatty liver-associated liver cancer through inducing palmitic acid and activating endoplasmic reticulum stress. *J. Hepatol.* **67**, 310–320 [CrossRef Medline](#)
- Franz, C. M., Jones, G. E., and Ridley, A. J. (2002) Cell migration in development and disease. *Dev. Cell* **2**, 153–158 [CrossRef Medline](#)
- Hood, J. D., and Cheresch, D. A. (2002) Role of integrins in cell invasion and migration. *Nat. Rev. Cancer* **2**, 91–100 [CrossRef Medline](#)
- Guo, W., and Giancotti, F. G. (2004) Integrin signalling during tumour progression. *Nat. Rev. Mol. Cell Biol.* **5**, 816–826 [CrossRef Medline](#)
- Parsons, J. T., Horwitz, A. R., and Schwartz, M. A. (2010) Cell adhesion: integrating cytoskeletal dynamics and cellular tension. *Nat. Rev. Mol. Cell Biol.* **11**, 633–643 [CrossRef Medline](#)
- Webb, D. J., Parsons, J. T., and Horwitz, A. F. (2002) Adhesion assembly, disassembly and turnover in migrating cells: over and over and over again. *Nat. Cell Biol.* **4**, E97–E100 [CrossRef Medline](#)
- Kwak, T. K., Kim, H., Jung, O., Lee, S. A., Kang, M., Kim, H. J., Park, J. M., Kim, S. H., and Lee, J. W. (2010) Glucosamine treatment-mediated O-GlcNAc modification of paxillin depends on adhesion state of rat insulinoma INS-1 cells. *J. Biol. Chem.* **285**, 36021–36031 [CrossRef Medline](#)
- Hagmann, J., Grob, M., and Burger, M. M. (1992) The cytoskeletal protein talin is O-glycosylated. *J. Biol. Chem.* **267**, 14424–14428 [Medline](#)
- Ji, S., Kang, J. G., Park, S. Y., Lee, J., Oh, Y. J., and Cho, J. W. (2011) O-GlcNAcylation of tubulin inhibits its polymerization. *Amino Acids* **40**, 809–818 [CrossRef Medline](#)
- Ding, M., and Vandré, D. D. (1996) High molecular weight microtubule-associated proteins contain O-linked-N-acetylglucosamine. *J. Biol. Chem.* **271**, 12555–12561 [CrossRef Medline](#)
- Ferrer, C. M., Lu, T. Y., Bacigalupa, Z. A., Katsetos, C. D., Sinclair, D. A., and Reginato, M. J. (2017) O-GlcNAcylation regulates breast cancer metastasis via SIRT1 modulation of FOXM1 pathway. *Oncogene* **36**, 559–569 [CrossRef Medline](#)
- Jiang, M., Xu, B., Li, X., Shang, Y., Chu, Y., Wang, W., Chen, D., Wu, N., Hu, S., Zhang, S., Li, M., Wu, K., Yang, X., Liang, J., Nie, Y., and Fan, D. (2018) O-GlcNAcylation promotes colorectal cancer metastasis via the miR-101-O-GlcNAc/EZH2 regulatory feedback circuit. *Oncogene*, in press [CrossRef Medline](#)
- Giancotti, F. G., and Ruoslahti, E. (1999) Integrin signaling. *Science* **285**, 1028–1032 [CrossRef Medline](#)
- Chen, H. C., Appeddu, P. A., Parsons, J. T., Hildebrand, J. D., Schaller, M. D., and Guan, J. L. (1995) Interaction of focal adhesion kinase with cytoskeletal protein talin. *J. Biol. Chem.* **270**, 16995–16999 [CrossRef Medline](#)

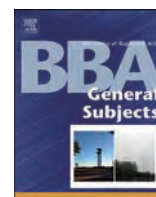
FAK was modified by O-GlcNAc

29. Valdembrì, D., and Serini, G. (2012) Regulation of adhesion site dynamics by integrin traffic. *Curr. Opin. Cell Biol.* **24**, 582–591 [CrossRef Medline](#)
30. Askari, J. A., Tynan, C. J., Webb, S. E., Martin-Fernandez, M. L., Balles-trem, C., and Humphries, M. J. (2010) Focal adhesions are sites of integrin extension. *J. Cell Biol.* **188**, 891–903 [CrossRef Medline](#)
31. Collins, C., and Nelson, W. J. (2015) Running with neighbors: coordinat-ing cell migration and cell-cell adhesion. *Curr. Opin. Cell Biol.* **36**, 62–70 [CrossRef Medline](#)
32. Wolfram, T., Spatz, J. P., and Burgess, R. W. (2008) Cell adhesion to agrin presented as a nanopatterned substrate is consistent with an interaction with the extracellular matrix and not transmembrane adhesion molecules. *BMC Cell Biol.* **9**, 64 [CrossRef Medline](#)
33. Parsons, J. T., Martin, K. H., Slack, J. K., Taylor, J. M., and Weed, S. A. (2000) Focal adhesion kinase: a regulator of focal adhesion dynamics and cell movement. *Oncogene* **19**, 5606–5613 [CrossRef Medline](#)
34. Ilić, D., Furuta, Y., Kanazawa, S., Takeda, N., Sobue, K., Nakatsuji, N., Nomura, S., Fujimoto, J., Okada, M., and Yamamoto, T. (1995) Reduced cell motility and enhanced focal adhesion contact formation in cells from FAK-deficient mice. *Nature* **377**, 539–544 [CrossRef Medline](#)
35. Hang, Q., Isaji, T., Hou, S., Wang, Y., Fukuda, T., and Gu, J. (2017) A key regulator of cell adhesion: identification and characterization of impor-tant N-glycosylation sites on integrin $\alpha 5$ for cell migration. *Mol. Cell Biol.* **37**, e00558-16 [CrossRef Medline](#)
36. Quizi, J. L., Baron, K., Al-Zahrani, K. N., O'Reilly, P., Sriram, R. K., Conway, J., Laurin, A. A., and Sabourin, L. A. (2013) SLK-mediated phosphoryla-tion of paxillin is required for focal adhesion turnover and cell migration. *Oncogene* **32**, 4656–4663 [CrossRef Medline](#)
37. Anthis, N. J., and Campbell, I. D. (2011) The tail of integrin activation. *Trends Biochem. Sci.* **36**, 191–198 [CrossRef Medline](#)
38. Wolfenson, H., Lavelin, I., and Geiger, B. (2013) Dynamic regulation of the structure and functions of integrin adhesions. *Dev. Cell* **24**, 447–458 [CrossRef Medline](#)
39. Shattil, S. J., Kim, C., and Ginsberg, M. H. (2010) The final steps of integrin activation: the end game. *Nat. Rev. Mol. Cell Biol.* **11**, 288–300 [CrossRef Medline](#)
40. Comer, F. I., and Hart, G. W. (2000) O-Glycosylation of nuclear and cyto-solic proteins: dynamic interplay between O-GlcNAc and O-phosphate. *J. Biol. Chem.* **275**, 29179–29182 [CrossRef Medline](#)
41. Yang, X., and Qian, K. (2017) Protein O-GlcNAcylation: emerging mech-anisms and functions. *Nat. Rev. Mol. Cell Biol.* **18**, 452–465 [CrossRef Medline](#)
42. Mitra, S. K., Hanson, D. A., and Schlaepfer, D. D. (2005) Focal adhesion kinase: in command and control of cell motility. *Nat. Rev. Mol. Cell Biol.* **6**, 56–68 [CrossRef Medline](#)
43. Xie, Z., Sanada, K., Samuels, B. A., Shih, H., and Tsai, L. H. (2003) Serine 732 phosphorylation of FAK by Cdk5 is important for microtubule orga-nization, nuclear movement, and neuronal migration. *Cell* **114**, 469–482 [CrossRef Medline](#)
44. Bianchi, M., De Lucchini, S., Marin, O., Turner, D. L., Hanks, S. K., and Villa-Moruzzi, E. (2005) Regulation of FAK Ser-722 phosphorylation and kinase activity by GSK3 and PP1 during cell spreading and migration. *Biochem. J.* **391**, 359–370 [CrossRef Medline](#)
45. Ma, A., Richardson, A., Schaefer, E. M., and Parsons, J. T. (2001) Serine phosphorylation of focal adhesion kinase in interphase and mitosis: a pos-sible role in modulating binding to p130^{Cas}. *Mol. Biol. Cell* **12**, 1–12 [CrossRef Medline](#)
46. Sakabe, K., and Hart, G. W. (2010) O-GlcNAc transferase regulates mit-otic chromatin dynamics. *J. Biol. Chem.* **285**, 34460–34468 [CrossRef Medline](#)
47. Grigera, P. R., Jeffery, E. D., Martin, K. H., Shabanowitz, J., Hunt, D. F., and Parsons, J. T. (2005) FAK phosphorylation sites mapped by mass spec-trometry. *J. Cell Sci.* **118**, 4931–4935 [CrossRef Medline](#)
48. Luk, C. T., Shi, S. Y., Cai, E. P., Sivasubramaniam, T., Krishnamurthy, M., Brunt, J. J., Schroer, S. A., Winer, D. A., and Woo, M. (2017) FAK signalling controls insulin sensitivity through regulation of adipocyte survival. *Nat. Commun.* **8**, 14360 [CrossRef Medline](#)
49. Rondas, D., Tomas, A., and Halban, P. A. (2011) Focal adhesion remodel-ing is crucial for glucose-stimulated insulin secretion and involves activa-tion of focal adhesion kinase and paxillin. *Diabetes* **60**, 1146–1157 [CrossRef Medline](#)
50. Lachén-Montes, M., González-Morales, A., de Morentin, X. M., Pérez-Valderrama, E., Ausín, K., Zelaya, M. V., Serna, A., Aso, E., Ferrer, I., Fernández-Irigoyen, J., and Santamaría, E. (2016) An early dysregulation of FAK and MEK/ERK signaling pathways precedes the β -amyloid deposi-tion in the olfactory bulb of APP/PS1 mouse model of Alzheimer's dis-ease. *J. Proteomics* **148**, 149–158 [CrossRef Medline](#)
51. Grace, E. A., and Busciglio, J. (2003) Aberrant activation of focal adhesion proteins mediates fibrillar amyloid β -induced neuronal dystrophy. *J. Neu-rosci.* **23**, 493–502 [CrossRef Medline](#)
52. Franco, S. J., Rodgers, M. A., Perrin, B. J., Han, J., Bennin, D. A., Critchley, D. R., and Huttenlocher, A. (2004) Calpain-mediated proteolysis of talin regulates adhesion dynamics. *Nat. Cell Biol.* **6**, 977–983 [CrossRef Medline](#)
53. Segarra, M., Vilardell, C., Matsumoto, K., Esparza, J., Lozano, E., Serra-Pages, C., Urbano-Márquez, A., Yamada, K. M., and Cid, M. C. (2005) Dual function of focal adhesion kinase in regulating integrin-induced MMP-2 and MMP-9 release by human T lymphoid cells. *FASEB J.* **19**, 1875–1877 [CrossRef Medline](#)
54. Isaji, T., Im, S., Gu, W., Wang, Y., Hang, Q., Lu, J., Fukuda, T., Hashii, N., Takakura, D., Kawasaki, N., Miyoshi, H., and Gu, J. (2014) An oncogenic protein Golgi phosphoprotein 3 up-regulates cell migration via sialylation. *J. Biol. Chem.* **289**, 20694–20705 [CrossRef Medline](#)
55. Du, J., Chen, X., Liang, X., Zhang, G., Xu, J., He, L., Zhan, Q., Feng, X. Q., Chien, S., and Yang, C. (2011) Integrin activation and internalization on soft ECM as a mechanism of induction of stem cell differentiation by ECM elasticity. *Proc. Natl. Acad. Sci. U.S.A.* **108**, 9466–9471 [CrossRef Medline](#)
56. McFarlane, S., McFarlane, C., Montgomery, N., Hill, A., and Waugh, D. J. (2015) CD44-mediated activation of $\alpha 5 \beta 1$ -integrin, cortactin and paxillin signaling underpins adhesion of basal-like breast cancer cells to endothe-lium and fibronectin-enriched matrices. *Oncotarget* **6**, 36762–36773 [Medline](#)
57. Horzum, U., Ozdil, B., and Pesen-Okvur, D. (2014) Step-by-step quanti-tative analysis of focal adhesions. *MethodsX* **1**, 56–59 [CrossRef Medline](#)
58. Berginski, M. E., Vitriol, E. A., Hahn, K. M., and Gomez, S. M. (2011) High-resolution quantification of focal adhesion spatiotemporal dynam-ics in living cells. *PLoS One* **6**, e22025 [CrossRef Medline](#)



Contents lists available at ScienceDirect

BBA - General Subjects

journal homepage: www.elsevier.com/locate/bbagen

Deficiency of α 1,6-fucosyltransferase promotes neuroinflammation by increasing the sensitivity of glial cells to inflammatory mediators

Xu Lu^{a,b}, Dongmei Zhang^{a,c}, Hayato Shoji^a, Chengwei Duan^a, Guowei Zhang^a, Tomoya Isaji^a, Yuqin Wang^b, Tomohiko Fukuda^{a,*}, Jianguo Gu^{a,*}

^a Division of Regulatory Glycobiology, Tohoku Medical and Pharmaceutical University, Institute of Molecular Biomembrane and Glycobiology, 4-4-1 Komatsushima, Aoba-ku, Sendai, Miyagi 981-8558, Japan

^b Department of Pharmacology, Pharmacy College, Nantong University, Nantong, Jiangsu Province 226001, China

^c Clinical Medical Research Center, The Second Affiliated Hospital of Nantong University, Nantong, Jiangsu Province 226001, China



ARTICLE INFO

Keywords:

Core fucosylation
Cytokines
Fut8
Glial cell
Neuroinflammation

ABSTRACT

Background: α 1,6-Fucosyltransferase-deficient (Fut8^{-/-}) mice displayed increased locomotion and schizophrenia-like behaviors. Since neuroinflammation is a common pathological change in most brain diseases, this study was focused on investigating the effects of Fut8 in microglia and astrocytes.

Methods: Brain tissues were analyzed using immunohistochemical staining. Core fucosylation and protein expression were analyzed using lectin blot and western blot, respectively. Fut8-knockout (KO) cells were established by the CRISPR/Cas9 system.

Results: The number of Iba-1 positive cells and GFAP positive cells were significantly increased in both untreated and lipopolysaccharide stimulated inflammatory conditional Fut8^{-/-} mice by comparison with both wild-type (Fut8^{+/+}) and hetero (Fut8^{+/-}) mice. Stimulation with pro-inflammatory factors, such as IFN- γ and IL-6, induced expression levels of fucosylation in primary microglia and astrocytes, as well as in glial cell lines. Cell motility and iNOS expression were easily induced by IFN- γ in Fut8-KO BV-2 cells compared with wild-type (WT) cells. In a similar manner, both Fut8-KO C6 cells and primary astrocytes treated with 2-fluoro-L-fucose, a specific inhibitor for fucosylation, showed a higher response to IL-6-stimulated phospho-STAT3 signaling, compared with WT cells.

Conclusions: Core fucosylation negatively regulates the states of neuroinflammation by modulating the sensitivity of microglia and astrocytes to inflammatory mediators. The disorders of Fut8^{-/-} mice are caused not only by neurons but also by glial cell dysfunction.

General significance: Core fucose is a novel regulator for neuroinflammation in the central nervous system.

1. Introduction

α 1,6-Fucosyltransferase (Fut8) transfers a fucose residue from GDP-fucose to the innermost *N*-acetylglucosamine (GlcNAc) residue via α 1,6-linkage to form α 1,6-fucosylation [1], which is referred to as core fucosylation in mammals [2,3]. In fact, *N*-glycans with core fucosylation are widely distributed in a variety of glycoproteins, and differently regulate their functions. Accumulating data suggests that Fut8 and its products play important roles in various physiological and pathological

processes, such as tumor formation [4,5], inflammation and immune response [6–9], and central nervous system (CNS) diseases [10,11].

Fut8-deficient (Fut8^{-/-}) mice exhibit a schizophrenia-like phenotype with a decrease in working memory [10] and long-term potentiation [12]. Very recently, a complete loss of core fucosylation in patients was reported [13]. Those patients showed growth retardation, severe developmental and growth delays and also including neurological impairment, which was quite similar to that seen in the phenotypes of Fut8^{-/-} mice [10,14]. These data suggested core fucosylation

Abbreviations: Fut8, α 1,6-Fucosyltransferase; CNS, central nervous system; IL-6, interleukin-6; IFN- γ , interferon gamma; LPS, lipopolysaccharide; 2FF, 2-fluoro-L-fucose; Iba-1, ionized calcium binding adaptor molecule 1; GFAP, glial fibrillary acidic protein; AAL, Aleuria Aurantia Lectin; PhoSL, Pholiota Squarrosa Lectin; ConA, concanavalin A; SNA, *Sambucus nigra* lectin; MAA, *Maackia amurensis* lectin; iNOS, inducible nitric oxide synthase; NO, nitric oxide; TGF- β , transforming growth factor β ; GAPDH, glyceraldehyde-3-phosphate dehydrogenase; DAPI, 4',6-Diamidino-2-phenylindole Dihydrochloride n-Hydrate; STAT1, signal transducer and activator of transcription 1; STAT3, signal transducer and activator of transcription 3; gp130, glycoprotein 130

* Corresponding authors.

E-mail addresses: tfukuda@tohoku-mpu.ac.jp (T. Fukuda), jgu@tohoku-mpu.ac.jp (J. Gu).

<https://doi.org/10.1016/j.bbagen.2018.12.008>

Received 14 September 2018; Received in revised form 5 December 2018; Accepted 13 December 2018

Available online 17 December 2018

0304-4165/ © 2018 Published by Elsevier B.V.

plays important roles in the CNS.

The pathophysiology of schizophrenia has not yet been fully elucidated. Studies involving *in vivo* imaging suggest that neuroinflammation may contribute to the pathogenesis of schizophrenia, which could be due to a dysfunction in glial cells [15,16]. In the CNS, glial cells are made up mostly of microglia, astrocytes, and oligodendrocytes. For several decades, many researchers believed that glial cells outnumbered neurons at a ratio of 10:1 [17], but recently researchers used isotropic fractionators to demonstrate that the ratio of glial cells to neurons is actually about 1:1 [18]. Anyway, glial cells are known to play crucial roles in neuronal functions [19,20]. As the only resident macrophage-like cells in the CNS, microglia are the pre-eminent form of active immune defense [21], even though they only account for 10–15% of all glial cells [22]. In addition to their surveillance role, microglia participates in maintaining synapses and homeostasis in the CNS [23,24]. Astrocytes are the most abundant glial type, and make up ~20–40% [25]. They provide trophic support for neurons [26], and also participate in the maintenance of synapses and in the process of neuroinflammation [27,28].

Microglial cells play a key role in neuroinflammation. After activation, microglia quickly release several pro-inflammatory mediators such as interleukin-1 β (IL-1 β), interleukin-6 (IL-6), and interferon gamma (IFN- γ), and induce reactive astrocytes, which leads to the further injury of neurons [28]. In fact, postmortem studies have discovered a higher level of activation and increased microglia density in schizophrenia [29]. Gene-set analyses have also shown that genetic alterations of astrocytes could increase the risk for schizophrenia [30]. These results suggest the potential role of microglia and astrocytes in this disorder.

Recently, several studies have also demonstrated that *N*-glycosylation might play important roles in schizophrenia. Postmortem examinations of the cortex of schizophrenia patients have shown alterations in the *N*-glycosylation of α -amino-3-hydroxy-5-methyl-4-isoxazolepropionate receptor (AMPA), *N*-methyl-D-aspartate receptor (NMDAR) and γ -aminobutyric acid type A (GABA_A) receptors [31–33]. Furthermore, in the superior temporal gyrus of elderly patients with schizophrenia, the expression levels of Fut8 were decreased [34].

The present study was focused on glial cells to explore the underlying mechanisms of the disorders found in the brains of Fut8^{-/-} mice. We found that the initial status of microglia and astrocytes activation and the neuroinflammation model induced by lipopolysaccharide (LPS) both were significantly enhanced in Fut8^{-/-} mice, compared with wild-type (Fut8^{+/+}) mice. In accordance with the *in vivo* data, the sensitivities to inflammatory stimulators such as IFN- γ or IL-6 were greatly increased in glial cell lines lacking Fut8 (Fut8 KO cells) or primary astrocyte cells treated with 2-fluoro-L-fucose (2FF) [35–37], a fluorinated analog of fucose, which could dramatically inhibit fucosylation in cells, compared with those in wild-type (WT) cells. Along with previous results [10–12], these data clearly demonstrate the importance of Fut8 in microglia and astrocytes, and the disorders of Fut8^{-/-} mice are caused not only by neurons but also by glial cell dysfunction.

2. Materials and methods

2.1. Materials

The experiments were performed using the following antibodies: mouse mAb against inducible nitric oxide synthase (iNOS) (ab49999) and goat pAb against ionized calcium binding adaptor molecule 1 (Iba-1) (ab5076) were purchased from Abcam; rabbit pAb against Iba-1 (019–19,741) was from Wako, Japan; mouse mAb against glial fibrillary acidic protein (GFAP) (MAB360) was from Millipore Corporation; mouse mAb against signal transducer and activator of transcription 3 (STAT3) (9139S), rabbit mAb against p-STAT3 Tyr705 (9145S), mouse mAb against Smad2 (3103S), rabbit mAb against p-

Smad2 Ser465/467 (3108S), rabbit mAb against signal transducer and activator of transcription 1 (STAT1) (14994S), and rabbit mAb against p-STAT1 Tyr701 (9167S) were purchased from Cell Signaling Technology; mouse mAb against gp130 (MAB5029) was from R&D Systems; mouse mAb against α -tubulin (T6199) was from Sigma and rabbit pAb against glyceraldehyde-3-phosphate dehydrogenase (GAPDH) (sc-25,778) was from Santa Cruz.

Biotinylated *Aleuria Aurantia Lectin* (AAL), *concanavalin A* (ConA), *sambucus nigra lectin* (SNA) and *maackia amurensis lectin* (MAA) were obtained from J-oil Mills (Tokyo, Japan). Biotinylated *Pholiota Squarrosa Lectin* (PhoSL), which specifically recognizes core fucosylated *N*-glycans, was a generous gift from Dr. Yuka Kobayashi (J-oil Mills, Tokyo, Japan).

The peroxidase-conjugated goat against mouse and rabbit IgG antibodies, and donkey against sheep/goat IgG antibody were obtained from Promega, Cell Signaling Technology and Millipore Corporation, respectively. Goat anti-mouse IgG Alexa Fluor 568, goat anti-rabbit IgG Alexa Fluor 488, streptavidin-conjugate Alexa Fluor 647 were purchased from Invitrogen. 4',6-Diamidino-2-phenylindole Dihydrochloride n-Hydrate (DAPI) was obtained from Wako, Japan.

LPS purified from *Escherichia coli* 0111:B4 was the product of Sigma, recombinant mouse IFN- γ was purchased from Prospec Bio, recombinant rat IL-6 was purchased from PEPROTECH, and 2FF was purchased from Synchem, Inc., IL, USA.

2.2. Animals

The generation of Fut8^{-/-} mice by a gene-targeting technique has been described previously [10]. ICR genetic background F1 heterozygous mice were mated with JF1/Ms. (Japanese fancy mouse 1, M. m. molossinus-derived inbred strains) [38] mice to produce F2 generation mice, and the F2 generation mice were paired with other F2 generation mice to generate the Fut8^{-/-} mice. All experiments were conducted with male and female mice 5–6 weeks old. Mice were housed in groups in each cage under conditions of constant temperature (22 \pm 2 $^{\circ}$ C) and humidity (55 \pm 5%) on a 12-h light-dark cycle (lights on: 07:00–19:00) with free access to food and water. All animal experiments were performed in accordance with protocols approved by the Animal Care and Use Committee of the Graduate School of Pharmaceutical Sciences, Tohoku Medical and Pharmaceutical University.

2.3. Cell culture

Mouse microglia cell line BV-2 was kindly provided by Professor Elisabetta Blasi (University of Modena and Reggio Emilia, Modena, Italy). Rat glioma cell line C6 was purchased from American Type Culture Collection (Rockville, MD, USA). Cells were cultured in Dulbecco's modified Eagle Medium (DMEM) containing 10% fetal bovine serum (FBS) and incubated at 37 $^{\circ}$ C in a humidified atmosphere with 5% CO₂. The medium was replaced every 3 days.

Mouse primary cells from brain tissues were prepared as previously reported with some modifications [39]. Briefly, newborn (day 0–1) ICR Fut8^{+/+} mice were euthanized by decapitation using scissors, the cortex was removed, and cut into pieces on ice, and then digested with 0.125% trypsin for 20 min at 37 $^{\circ}$ C. A 100 μ m Nylon (Falcon) cell strainer was used to filter the undigested tissue. This procedure was followed by centrifugation at 300g for 5 min, and then the cells were resuspended and plated on poly-D-lysine (PDL, 50 μ g/mL)-coated culture flasks. Single-cell suspensions were cultured in DMEM/F12 supplemented with 10% FBS and 1% penicillin-streptomycin (100 U/mL). The medium was replaced with fresh medium after 24 h and changed every 3 days. In order to isolate the primary microglia, after 14 days, the mixed cells were shaken gently at 180 rpm for 2 h at 37 $^{\circ}$ C, and then the supernatants containing microglia were collected and plated on the new PDL-coated culture dishes. The remaining cells were washed with phosphate buffered saline (PBS), and then detached with 0.25% trypsin

to obtain the primary astrocytes. After centrifuge, the primary astrocytes were also cultured in PDL-coated culture dishes. All cells were maintained in a 37 °C incubator containing 95% air and 5% CO₂. Immunofluorescent staining with Iba-1 and GFAP antibodies was used to differentiate the microglia and astrocytes. The purity of both the microglia and astrocytes was > 90%.

2.4. Immunofluorescence

After intraperitoneal injection with LPS (1 mg/kg) for 24 h, animals were deeply anesthetized with sodium pentobarbital and intracardially perfused with 50 ml of PBS, followed by 50 ml of 4% paraformaldehyde (PFA; Sigma-Aldrich) in 0.1 M PBS. Brains were post-fixed in 4% PFA-0.1 M PBS at 4 °C overnight, followed by immersion in 20% sucrose-0.1 M PBS for 48 h. The brains were cut into 40 μm sections that included the dorsal dentate gyrus from bregma –1.60 mm to –2.60 mm using a cryostat (MICROM HM560, Microm International GmbH, Walldorf, Germany). Frozen sections were mounted on glass slides (Matsunami Glass, Japan). The sections were incubated with PBS containing 1% normal goat serum and 0.3% Triton X-100 (PBSGT) at room temperature for 2 h. The sections were incubated overnight at 4 °C with rabbit anti-Iba1 (1:200) and mouse anti-GFAP (1:200) antibodies. Sections were washed 3 times with PBS every 10 min, then incubated with goat anti-mouse IgG Alexa Fluor 568 (1:500) and goat anti-rabbit IgG Alexa Fluor 488 (1:500) in PBSGT for 2 h at room temperature. Finally, sections were washed 3 times with PBS every 10 min and coverslipped with fluorescent mounting medium (Dako, Carpinteria, CA, USA). Immunofluorescent images were analyzed using a confocal laser-scanning microscope (A1Rsi; Nikon, Tokyo, Japan). The number of Iba-1 positive cells in the images (0.04 cm²) and the length of each soma radius were measured using NIS-Elements AR Analysis (Nikon, Tokyo, Japan), the area of superficial somas was then calculated by following the equation (4πR²).

2.5. Generation of CRISPR/Cas9-based Fut8- KO Cells

The CRISPR/Cas9-based Fut8-KO cells were established, as described previously [40]. Briefly, the sgRNA-specifying oligo sequences (sequences one: 5'-CACCGCAGAATTGGCGCTATGCTAC-3' and 5'-AAACGTCATAGCGCCAATTCTGC-3'; sequences two: 5'-CACCGATTTCGTCACAACCTTGGC-3' and 5'-AAACGCCAAGGTTGTGGACGAATC-3') spanning *Mus musculus fucosyltransferase 8* (NM_001252614) and the sgRNA-specifying oligo sequences (sequences one: 5'-CACCGGAGATAAGTTATTCTCCGC-3' and 5'-AAACGCGGAGAATAACTTATCTCC-3'; sequences two: 5'-CACCGATTTGATTCGTCACAACCT-3' and 5'-AAACAGGTTGTGACGAATCAAATC-3') spanning *Rattus norvegicus fucosyltransferase 8* (NM_001002289.1) were cloned into the pSpCas9 (BB)-2A-GFP (Addgene plasmid ID: 48138) vector [40], which was a kind gift from Dr. Feng Zhang. The plasmid was electroincorporated into the BV-2 and C6 cells according to the manufacturer's instructions (Amaya® cell line Nucleofector R kit V). After 72 h of transfection, GFP-positive cells were sorted using the FACS Aria II (BD Bioscience). Cells that were Fut8 positive and GFP negative were sorted approximately three times using PhoSL during the following 3-week culture. The Fut8-KO cells were confirmed by flow cytometric and lectin blotting analyses, as described in the following section.

2.6. Flow cytometric analysis

Cells were grown to ~80% confluency, then detached from culture dishes, washed with ice-cold PBS, and subsequently stained with biotinylated PhoSL for 1 h on ice, followed by incubation with streptavidin-conjugate Alexa Fluor 647 for 1 h on ice in the dark. A negative control was prepared only with streptavidin-conjugate Alexa Fluor 647. During incubation, the cells were gently mixed every 10 min by flicking. Finally, cells were washed 3 times with ice-cold PBS and

analyzed via FACSCalibur flow cytometer (BD Biosciences).

2.7. Western blot and lectin blot analyses

The mice were euthanized by decapitation after 24 h of LPS (1 mg/kg) administration. Brain hippocampi were rapidly removed, placed on ice, and then homogenized in 4 volumes of TBS (20 mM Tris-HCl, pH 7.4, 150 mM NaCl, 1% protease) with φ2.0 Zirconia Beads by Micro Smash MS-100 (Digital Biology), according to the manufacturer's instructions. After centrifugation at 8000 rpm for 15 min, the supernatants were collected and used for analysis.

Cells cultured under different conditions were washed with PBS and lysed with lysis buffer that contained 20 mM Tris-HCl (pH 7.4), 150 mM NaCl, 1% Triton-X100, and 1% protease and phosphatase inhibitor cocktail (Nacalai Tesque, Japan). Protein concentrations were measured using a bicinchoninic acid protein assay kit (Thermo Fisher Scientific, Wilmington, DE, USA).

Equal amounts of proteins were separated by sodium dodecyl sulfate-polyacrylamide gel electrophoresis (SDS-PAGE) and then transferred to PVDF (Millipore, Billerica, MA, USA) membranes for future detection. For western blot, after blocking with 5% skim milk or 3% bovine serum albumin (BSA) for 2 h at room temperature, the membranes were incubated with specific primary antibodies at 4 °C overnight, followed by incubation with appropriate horseradish peroxidase (HRP)-conjugated secondary antibody. For lectin blot, the membranes were blocked in 3% BSA overnight at 4 °C, followed by incubation with biotinylated AAL, ConA, SNA or MAA lectin for 2 h at room temperature, and then the immunoreactive bands were probed with a Vectastain ABC kit (Vector Laboratories, Burlingame, CA, USA). Finally, specific proteins were visualized using an ECL select™ reagent (Amersham, Piscataway, NJ, USA).

2.8. Video microscope

BV-2 Cells were plated at a density of 1 × 10⁴ in a glass-bottom dish (Asahi Glass, Shizuoka, Japan). After the cells attached over night, the culture media were replaced with fresh media without phenol red but with IFN-γ (20 ng/ml), and then cell motility was monitored for 12 h using Axio Vision (Carl Zeiss, Jena, Germany). Images were acquired using an inverted microscope (AxioObserver.D1; Carl Zeiss) every 10 min with 5% CO₂ at 37 °C in a heated chamber equipped with temperature and CO₂ controllers (Onpu-4 and CO₂; AR Brown, Tokyo, Japan) during time-lapse imaging. Cell migration was evaluated using an AxioVision Tracking module (Carl Zeiss).

2.9. Immunoprecipitation

After being washed with PBS, cells were treated with lysis buffer, as previously described. Anti-gp130 antibody and Ab-Capcher Protein A-R28 agarose (Protenova, Tokushima, Japan) were first mixed together for 1 h on ice, and then gently mixed again every 10 min. The cell lysates were then immunoprecipitated with the antibody-agarose solution for 1 h at 4 °C with rotation. The immunoprecipitates were then washed twice with TBS and subjected to SDS-PAGE.

2.10. Statistical analysis

Results are reported as the means ± S.E.M. Statistical analyses were performed using an unpaired Student's *t*-test with Welch's correction or a one-way analysis of variance (ANOVA) with Tukey's *post hoc* test by GraphPad Prism version 5. Statistical significance was defined as *p* < .05.

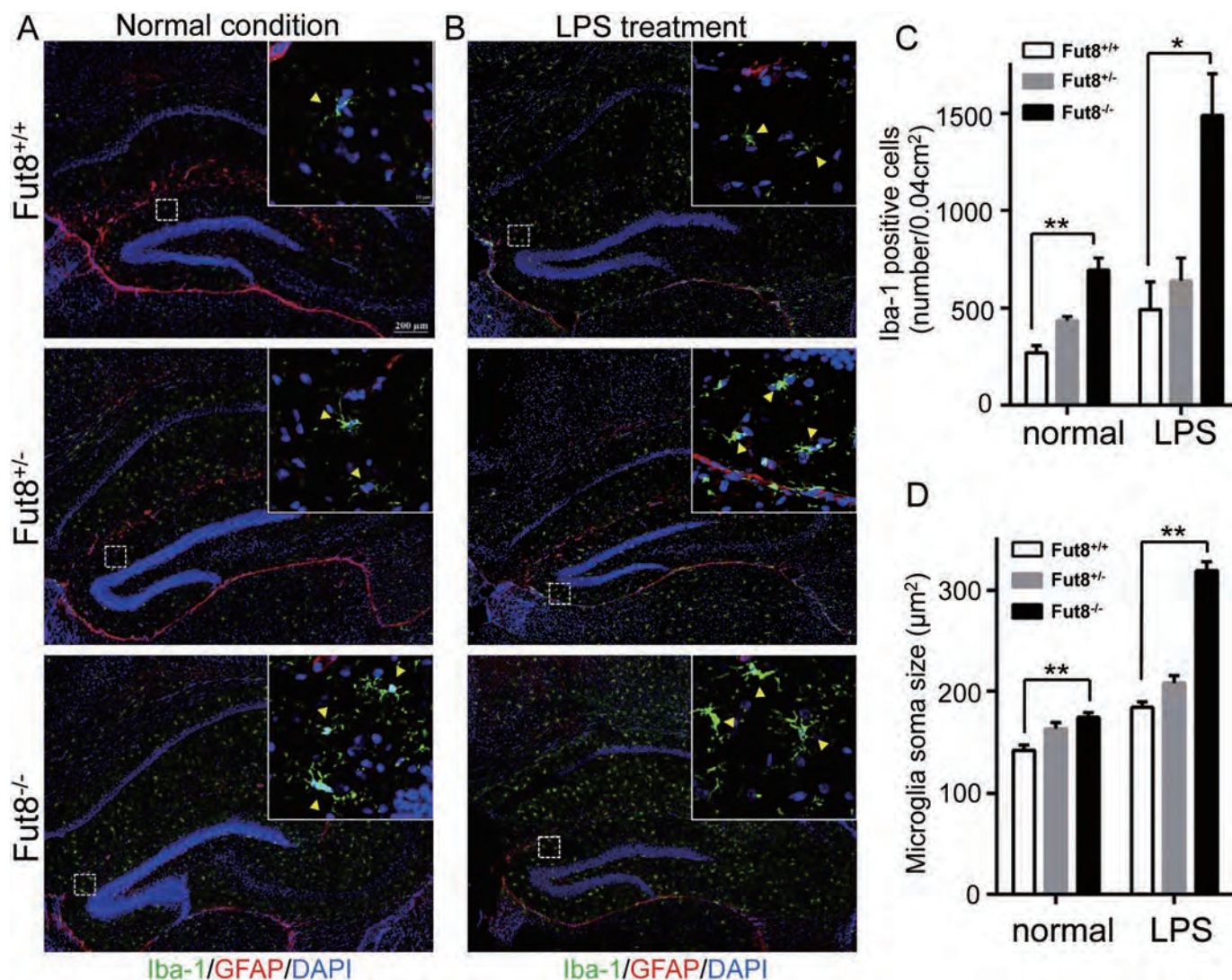


Fig. 1. Effects of core fucosylation on the activation of glial cells in mice brain tissues. Brain sections of mice were prepared and analyzed, as described in “Experimental procedures”. (A) The representative microscopy images immunostained with anti-Iba1 (green) antibodies, anti-GFAP (red) antibodies, and DAPI (blue) in the hippocampus of brain tissues of mice under normal conditions; (B) The representative microscopy images after the administration of LPS by intraperitoneal injection (i.p. 1 mg/kg, 24 h). (C) Quantification of Iba-1 positive cells using representative tissue sections stained with anti-Iba1 antibody. Data represent the mean \pm S.E.M.; *p* values were calculated using one-way ANOVA with Tukey’s multiple comparison test. **p* < .05 vs. Fut8^{+/+} mice (*n* = 3, *n*: number of slices; *N* = 3, *N*: number of the mice per group). (D) Quantification of microglia soma size using representative tissue sections stained with anti-Iba1 antibody. Data represent the mean \pm S.E.M.; *p* values were calculated using one-way ANOVA with Tukey’s multiple comparison test. ***p* < .01 vs. Fut8^{+/+} mice (*n* = 96, *n*: number of recordings; *N* = 3, *N*: number of the mice per group).

3. Results

3.1. The basal status of microglia activation was increased in Fut8^{-/-} mice

First, we checked the basal status of glial cell activation by detecting Iba-1 and GFAP, which are markers for microglia and astrocytes, respectively, in the hippocampus regions *in vivo*. The immunohistochemical staining with anti-Iba-1 antibody clearly showed that the Iba-1-positive cells were significantly increased in Fut8^{-/-} mice under normal conditions without treatment, compared with that of the Fut8^{+/+} mice (Fig. 1A and C). Interestingly, the number of Iba-1-positive cells in the Fut8^{+/-} mice fell between those of both the Fut8^{+/+} and Fut8^{-/-} mice, which may have been due to the lower enzyme activity of Fut8. Furthermore, the sizes of the microglia, evaluated by the superficial area of the central soma, in Fut8^{-/-} mice were larger than those in the Fut8^{+/+} mice, while the sizes in the Fut8^{+/-} mice fell between those of both the Fut8^{+/+} and Fut8^{-/-} mice (Fig. 1A and D). These results suggest that the deficiency of Fut8 could have spontaneously increased

the basal level of microglia activation *in vivo*.

3.2. Microglia and astrocytes of Fut8^{-/-} showed a greater level of sensitivity to LPS

It is well known that neuroinflammation is a common pathological change in many disorders of the CNS such as Alzheimer’s disease [41] and Parkinson’s disease [42], and that it also could participate in the pathology of schizophrenia [43]. Here, we established a systemic inflammatory model induced by a low dose of LPS at 1 mg/kg *via* intraperitoneal injection, as described in “Experimental procedures”. The immunohistochemical staining of brain tissues with anti-Iba-1 antibody showed greater increase in microglia activation, which included both numbers and sizes in Fut8^{-/-} mice, compared with those in Fut8^{+/-} and Fut8^{+/+} mice (Fig. 1B, C and D). Consistent with the immunohistochemical analysis, western blot analysis has shown that without LPS treatment the basal expression levels of Iba-1 are increased in both Fut8^{-/-} and Fut8^{+/-} mice, compared with that in Fut8^{+/+}

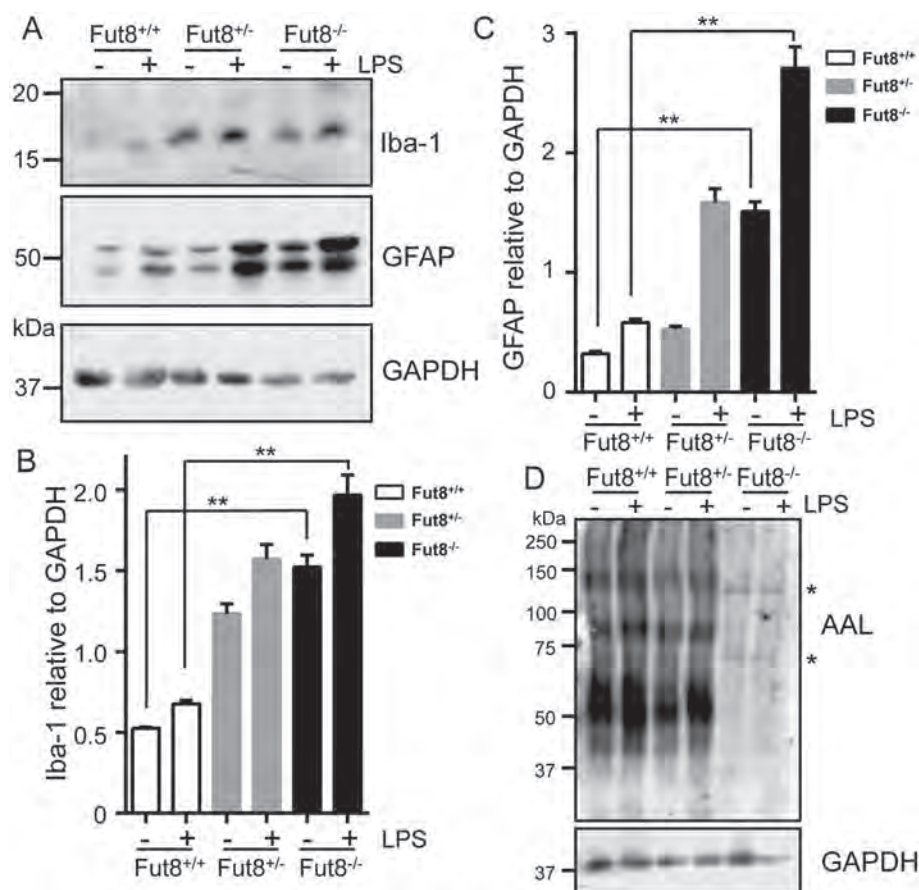


Fig. 2. Effects of LPS on fucosylation, and expression of Iba-1 and GFAP in mice brain tissues. Tissue lysates from mice hippocampi were prepared as described in “Experimental procedures”. (A) The expression levels of Iba-1 and GFAP were examined by western blotting with anti-Iba-1 and anti-GFAP antibodies. GAPDH was used as a loading control. (B) Quantitative analysis of Iba-1 protein expression in normal and LPS-stimulated Fut8^{+/+} and Fut8^{-/-} mice. Data represent the mean \pm S.E.M; *p* values were calculated using unpaired *t*-test with Welch's correction. ***p* < .01 vs. Fut8^{+/+} mice (*n* = 3). (C) Quantitative analysis of GFAP protein expression in normal and LPS-stimulated Fut8^{+/+} and Fut8^{-/-} mice. Data represent the mean \pm S.E.M; *p* values were calculated using unpaired *t*-test with Welch's correction. ***p* < .01 vs. Fut8^{+/+} mice (*n* = 3). (D) The expression levels of fucosylation were detected by AAL lectin blot. Asterisks indicate nonspecific bands.

mice (Fig. 2A, B), and the injection of LPS greatly increased the expression levels of Iba-1 in the Fut8^{-/-} and Fut8^{+/-} mice, but only modestly increased the levels in Fut8^{+/+} mice (Fig. 2A, B). Western blot analysis also showed a significantly increased expression of GFAP in both untreated and LPS-treated Fut8^{-/-} and Fut8^{+/-} mice, compared with Fut8^{+/+} mice (Fig. 2A, C). These results indicated that Fut8 may negatively regulate microglia and astrocytes responses to extrinsic stimuli during the process of neuroinflammation.

It is worth mentioning that the inflammation induced by LPS increased the expression of fucosylation. The lectin blotting with AAL, which preferentially recognizes core fucose [44], showed an increase in both Fut8^{+/-} and Fut8^{+/+} mice brain tissues for 24 h following an injection of LPS. It is reasonable to speculate that specific reactive bands simply could not be detected in the Fut8^{-/-} mice (Fig. 2D).

3.3. Neuroinflammation upregulated fucosylation expression in microglia

We isolated primary microglial cells from Fut8^{+/+} mice brain tissues and stimulated them with a commonly used stimuli for inflammation, IFN- γ [45], which also shows an increased expression in schizophrenia patients [46]. The IFN- γ stimulation consistently increased the expression of fucosylation detected by lectin blotting with AAL (Fig. 3A), and induced the expression of iNOS, which is an enzyme responsible for the inflammation-induced production of nitric oxide (NO) [47]. To further confirm the effects of neuroinflammation on fucosylation expression in microglia, we used BV-2, a microglial cell line, as a cell model. The reactivity with AAL was also enhanced in a dose- (Fig. 3B) and time-dependent manner (Fig. 3C). The expression of iNOS induced by IFN- γ was observed at a final concentration at 10 ng/ml, and remarkably appeared at 20 ng/ml (Fig. 3B). In addition, iNOS expression reached a peak at 24 h, after which it diminished (Fig. 3C). These data showed that neuroinflammation might upregulate the

expression of fucosylation in microglia.

3.4. Effects of Fut8 on neuroinflammation in BV-2 cells

To explore the roles of core fucosylation in microglia-mediated neuroinflammation, we established a core fucosylation-deficient BV-2 cell line using the CRISPR/Cas9 system described in “Experimental procedures”. The efficiency of Fut8 KO was confirmed by AAL blot analysis (Fig. 4A) and flow cytometric analysis stained with PhoSL (Fig. 4E). These results clearly showed that core fucosylation was completely abolished in Fut8 KO cells. The results of ConA, SNA and MAA lectin blotting showed no significant differences between WT and KO cells (Fig. 4B, C and D), which suggested that only core fucosylation was specifically blocked. Here, we chose KO2 cells for the following experiments.

Western blot assay revealed that IFN- γ induced iNOS expression with a dose-dependent manner in both the WT and KO cells. However, the induction of iNOS expression by IFN- γ at doses of both 10 ng/ml and 20 ng/ml was much higher in the KO cells, compared with that in WT cells (Fig. 5A, B). The time-course effects of IFN- γ at 20 ng/ml also clearly showed that the iNOS expression levels were higher in the KO cells, compared with those in WT cells (Fig. 5C, D). In addition, we used time-lapse microscopy to detect cell motility, which is known to indicate the activation of microglia after inflammatory stimulation. We found that those cells did not move under normal culture condition, while after IFN- γ stimulation, the cell motility was significantly increased in the KO cells (Fig. 5E).

Consistently, the IFN- γ -induced phosphorylation levels of STAT1 in the KO cells were slightly higher than those in the WT cells (Fig. 5F, G). While examining the involvement of crosstalk between IFN- γ - and transforming growth factor β (TGF- β)-mediated signaling, a common anti-inflammatory cytokine [48,49], we detected phosphorylation

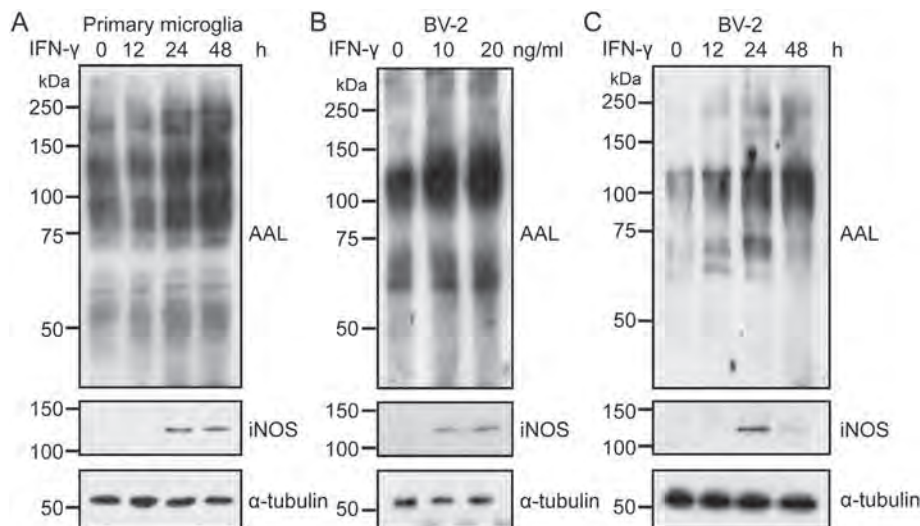


Fig. 3. Changes in fucosylation and iNOS expression in primary microglia cells and in BV-2 cells treated with IFN- γ . (A) Primary microglia cells were prepared as described in “Experimental procedures”, and were then treated with IFN- γ (20 ng/ml) at the indicated times. Equal amounts of cell lysates were detected via AAL lectin blot (upper panel) and anti-iNOS antibody (middle panel). (B) BV-2 cells were treated with IFN- γ for 24 h at the indicated concentrations, and then harvested. The cell lysates were detected via AAL lectin blot (upper panel) and anti-iNOS antibody (middle panel). (C) BV-2 cells were treated with IFN- γ (20 ng/ml) at the indicated times, and then harvested for AAL lectin blot (upper panel) and anti-iNOS antibody (middle panel) testing. α -tubulin was used as a loading control.

levels of Smad2, which is a specific TGF- β downstream signaling molecule. As shown in Fig. 5H and I, the expression of p-Smad2 was detected under stimulation with IFN- γ at 12 and 24 h in the WT cells, while it was undetectable in the KO cells. These data indicated that a deficiency in Fut8 could increase the sensitivity of microglia to inflammatory stimulators and increase the inflammatory reaction while decrease the anti-inflammatory reaction.

3.5. Effects of Fut8 expression on cellular signaling in astrocytes

It is well known that astrocytes also participate in neuroinflammation [50]. Thus, we isolated the primary astrocytes from the Fut8^{+/+} mice brain tissues, and treated them with or without 2FF. After treatment for 3 days, the inhibitory effects of 2FF were observed at a final concentration at 30 μ M, and remarkably appeared at 100 μ M (Fig. 6A). IL-6 is an important inflammatory cytokine in schizophrenia [46], and the responses which it stimulates were compared between the cells. As shown in Fig. 6B and C, IL-6-mediated phosphorylation levels of STAT3 were higher in the 2FF-pretreated cells, compared with those in the control cells.

To further explore the effect of Fut8 in astrocytes during

neuroinflammation, we used glioma C6 cells as an astrocyte cell model. We established the Fut8-KO cells via the CRISPR/Cas9 system, which was confirmed by AAL lectin blotting (Fig. 7A) and flow cytometric analysis (Fig. 7B). We chose the KO2 cells for further experiments. Consistent with data obtained from primary astrocytes (Fig. 6), the responses stimulated by IL-6 in KO cells were sharper and stronger than those in the WT (Fig. 7C, D). When considering the core fucosylation influence on the functions of glycoproteins expressed on the cell surface, we attempted to detect whether these receptors were modified by core fucosylation. We found that glycoprotein 130 (gp130), one subunit of IL-6 receptor, contained core fucosylation as detected by AAL lectin in the WT cells, and the reactivity with AAL was abolished in the KO cells (Fig. 7E). Unfortunately, at the present time, we could not conclude whether IFN- γ and IL-6 receptors are also modified by core fucosylation, since the appropriate antibodies for immunoprecipitation were unavailable.

4. Discussion

In the present study, we investigated the potential roles of core fucosylation involved in neuroinflammation, and found that a higher

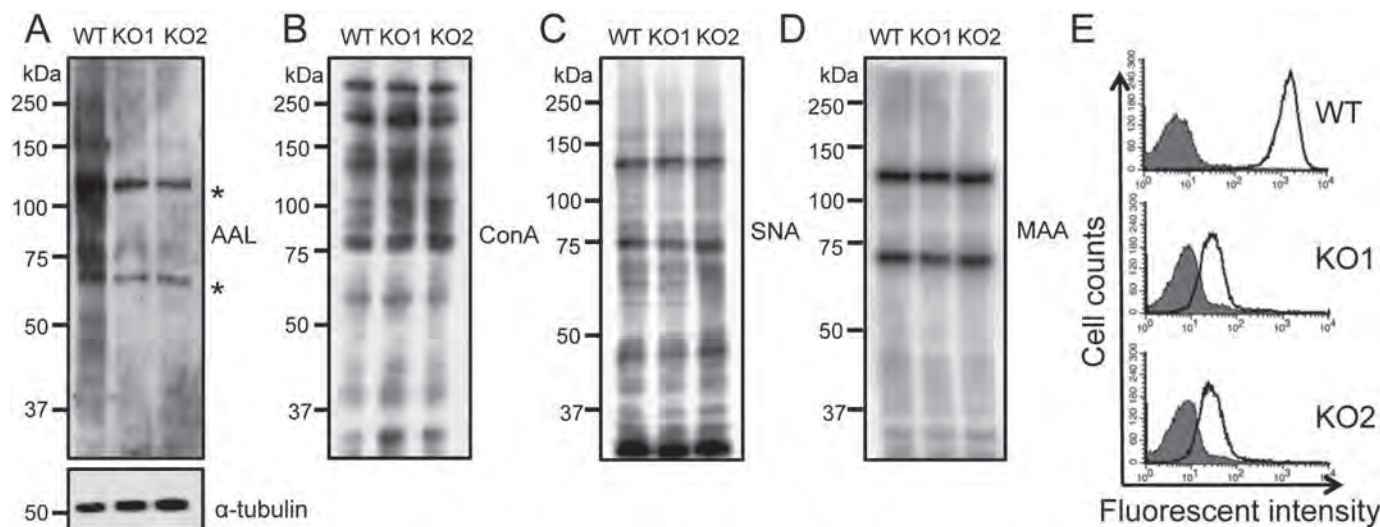


Fig. 4. Established the Fut8 KO BV-2 cell line. The Fut8-deficient BV-2 cells were established using the CRISPR/Cas9 system, as described in “Experimental procedures”. (A) Equal amounts of cell lysates were detected by AAL lectin blot with α -tubulin used as the loading control. Asterisks indicate nonspecific bands. Equal amounts of cell lysates were detected by ConA lectin blot (B), SNA lectin blot (C), and MAA lectin blot (D). (E) The expression level of core fucosylation on the cell surface recognized by PhoSL, was analyzed via flow cytometry.

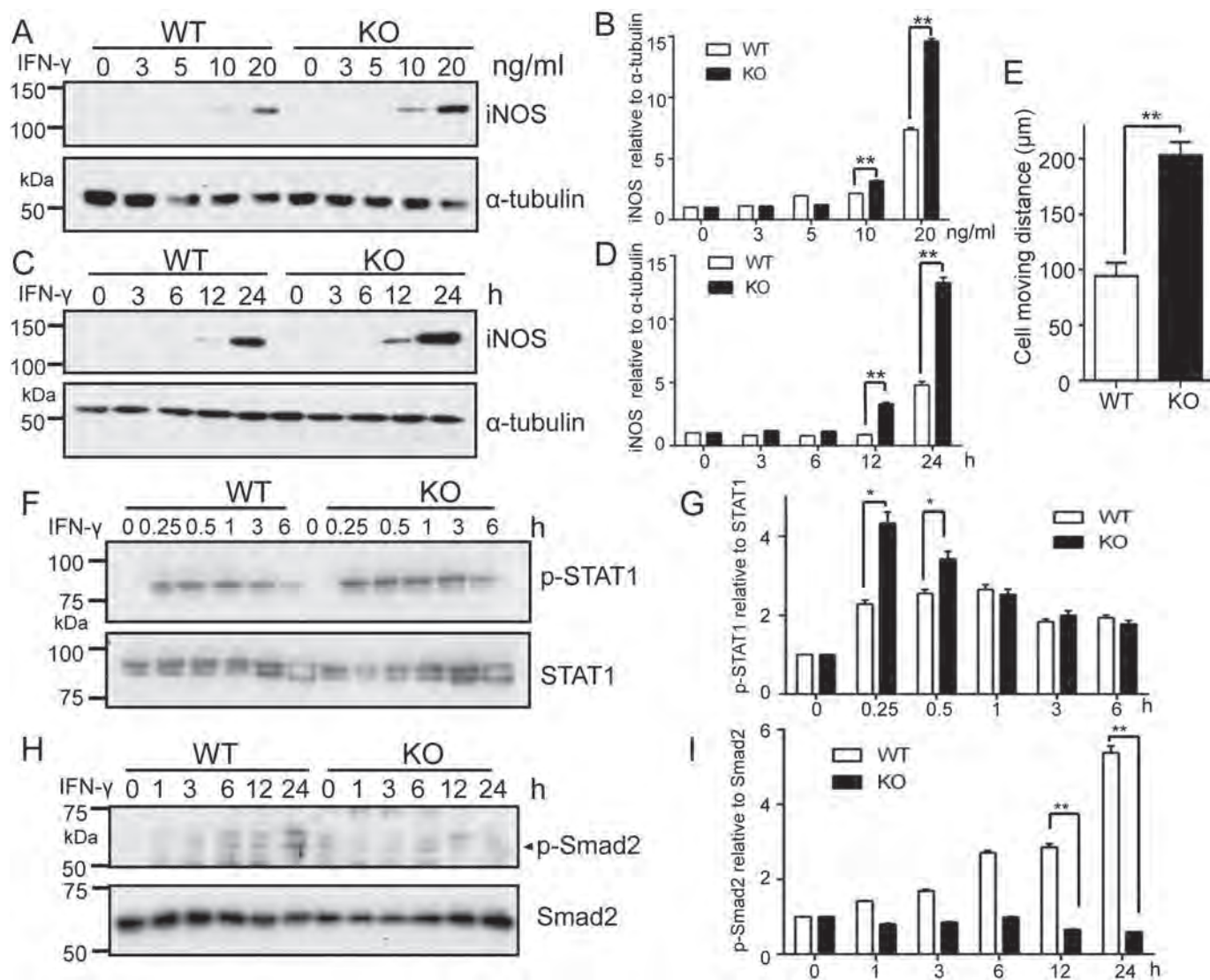


Fig. 5. Effects of core fucosylation on cellular signaling and cell motility in BV-2 cells treated with IFN-γ. (A) After cells were stimulated with IFN-γ at the indicated doses for 24 h, the expression levels of iNOS in both WT and KO cells were examined by western blotting with anti-iNOS antibody. (B) Quantitative analysis of iNOS protein expression in IFN-γ-stimulated WT and KO cells. Data represent the mean ± S.E.M; *p* values were calculated using unpaired *t*-test with Welch's correction. **p* < .05 vs. WT cells (*n* = 3). (C) After cells were stimulated with IFN-γ at 20 ng/ml for the indicated time, the expression levels of iNOS in both WT and KO cells were examined by western blotting with anti-iNOS antibody. (D) Quantitative analysis of iNOS protein expression in IFN-γ-stimulated WT and KO cells. Data represent the mean ± S.E.M; *p* values were calculated using unpaired *t*-test with Welch's correction. **p* < .05 vs. WT cells (*n* = 3). (E) Cell motility of BV-2 cells was examined via video microscope, as described in "Experimental procedures". The cell moving distances of both WT and KO cells were recorded during the stimulation with IFN-γ (20 ng/ml) for 12 h. Data represent the mean ± S.E.M; *p* values were calculated using unpaired *t*-test with Welch's correction. ***p* < .01 vs. WT cells (*n* = 33, *n*: numbers of recording). (F) After cells were stimulated with IFN-γ (20 ng/ml) at the indicated times, the expression levels of phosphorylation for STAT1, a downstream signaling of IFN-γ, in both WT and KO cells were examined by western blotting with anti-phospho-STAT1 antibody. Total STAT1 was used as a loading control. (G) Quantitative analysis of p-STAT1 protein expression in IFN-γ-stimulated WT and KO cells. Data represent the mean ± S.E.M; *p* values were calculated using unpaired *t*-test with Welch's correction. **p* < .05 vs. WT cells (*n* = 3). (H) After cells were stimulated with IFN-γ (20 ng/ml) at indicated times, the expression levels of the phosphorylation of Smad2, a specific signaling of TGF-β, were examined by western blotting in both WT and KO cells with anti-phospho-Smad2 antibody. Total Smad2 was used as a loading control. (I) Quantitative analysis of p-Smad2 protein expression in IFN-γ-stimulated WT and KO cells. Data represent the mean ± S.E.M; *p* values were calculated using unpaired *t*-test with Welch's correction. ***p* < .01 vs. WT cells (*n* = 3).

activation of microglia and astrocytes was observed in *Fut8*^{-/-} mice, compared with that in *Fut8*^{+/+} mice. The experiments using primary cells and cell models of microglia and astrocytes suggested that suppression of core fucosylation resulted in an increase in sensitivity for pro-inflammatory cytokines such as IFN-γ and IL-6. Furthermore, the results of mouse inflammatory models induced by LPS also showed that the response for LPS was greatly increased in the *Fut8*^{-/-} mice, compared with that in *Fut8*^{+/+} mice, although the responses were different from results obtained from mouse embryonic fibroblasts [51], which may be due to different cell types and the existence of blood-brain barrier. It is also worth noting that those responses in the *Fut8*^{+/-} mice

always occurred on a level that fell between that of *Fut8*^{-/-} and *Fut8*^{+/+} mice. These results clearly suggest that core fucosylation negatively regulates the functions of microglia and astrocytes in neuroinflammation.

Neuroinflammation could protect the CNS from harmful stimuli arising from both endogenous and exogenous substances in physiological conditions. However, uncontrolled or persistent neuroinflammation is potentially harmful and can result in cellular damage, which is particularly relevant to neurodegenerative diseases [52]. Our data clearly showed that the microglia cells in *Fut8*^{-/-} mice exist in a spontaneously activated state, while those in *Fut8*^{+/+} mice are in a

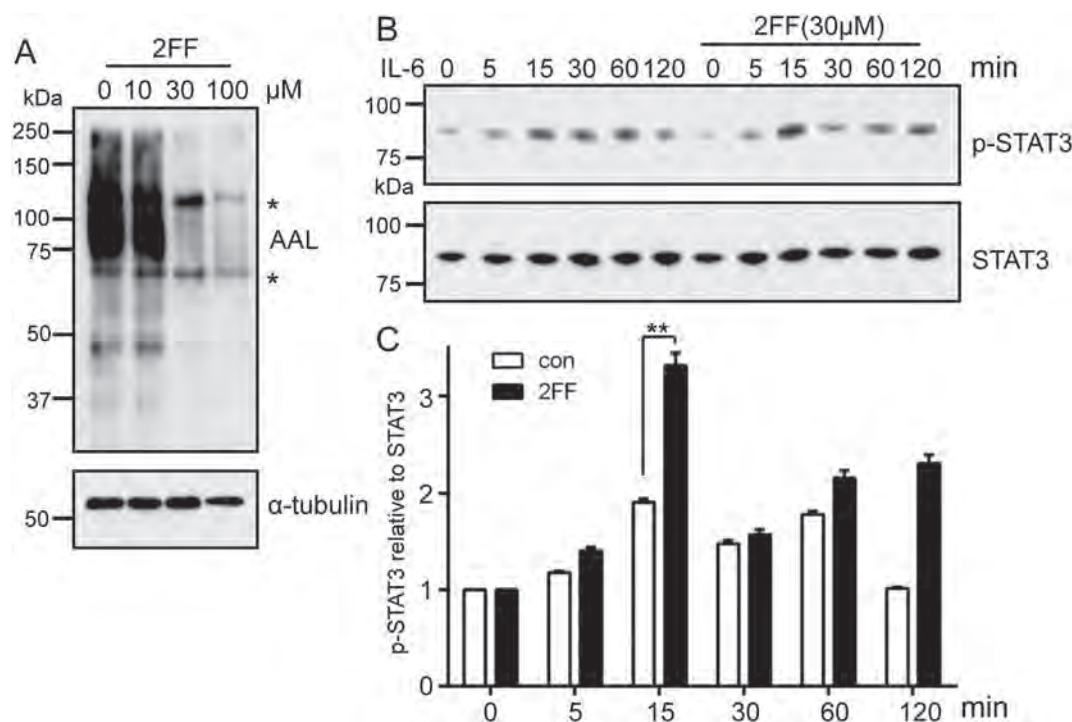


Fig. 6. Effects of 2FF on fucosylation and cellular signaling in primary astrocytes. (A) Primary astrocytes were prepared as described in “Experimental procedures”, and were cultured with 2FF, an inhibitor of fucosylation, for 3 days at the indicated concentrations. Equal amounts of cell lysates were detected by AAL lectin blot. α -Tubulin was used as a loading control. Asterisks indicate the nonspecific bands. (B) The primary astrocytes were pretreated with or without 2FF at 30 μ M for 3 days, and then were further stimulated with or without IL-6 at the indicated times. The expression levels of phosphorylated STAT3 in those cells were examined by western blotting with anti-phospho-STAT3 antibody. Total STAT3 was used as a loading control. (C) Quantitative analysis of the effects of 2FF on p-STAT3 protein expression in IL-6-stimulated primary cells. Data represent the mean \pm S.E.M.; p values were calculated using unpaired t-test with Welch’s correction. ** $p < .01$ vs. control cells ($n = 3$).

resting state under normal conditions (Fig. 1), which suggests the occurrence of persistent neuroinflammation in the *Fut8*^{-/-} mice. Further *in vitro* experiments have shown that a lack of core fucosylation could increase the response of the microglia cell line BV-2 to IFN- γ (Fig. 5), and the IL-6-mediated cellular signaling was greatly promoted by primary astrocytes treated with 2FF, an inhibitor of fucosylation, which was also confirmed by the deletion of *Fut8* in glioma C6 cells (Figs. 6,7). All these data indicated that deficiency of core fucosylation might increase the sensitivity of microglia and astrocytes to stimuli. It is also worth mentioning that both *in vivo* and *in vitro* experiments showed the increased expression of AAL after long-time inflammatory stimulation. This interesting phenotype may be due to a negative feedback of inflammation.

We wondered why the sensitivity of microglia and astrocytes increases with a lack of core fucosylation. Although the underlying molecular mechanism remains unclear, the following scenario is plausible. First, a lack of core fucosylation on these cytokine receptors might enhance the interaction between a receptor and its ligand, and could promote several pro-inflammatory signaling (Fig. 8). Previous studies by our group and by those of other groups have indicated that many receptors expressed on the cell surface contain core fucose: TGF- β 1 receptors [14,53], epidermal growth factor (EGF) receptors [54,55], T cell receptors (TCR) [6,9], and integrin α 3 β 1 [56]. The present study found that gp130, an important transmembrane protein of IL-6 signaling complexes, also contain core fucose (Fig. 7). Loss of core fucose on activin receptors [11] and AMPARs, one type of ionotropic glutamate receptor, enhanced the formation of receptor complexes [12], which constitutively activated intracellular signaling. The results of the present study showed an enhancement of the IL-6-induced p-STAT3 signal pathway in *Fut8* KO C6 cells (Fig. 7) as well as in the *Fut8* KO BV-2 cells (data not shown), and the IFN- γ -induced p-STAT1 signaling in *Fut8* KO BV-2 cells (Fig. 5) as well as in the *Fut8* KO C6 cells (data not

shown), all of which could share similar mechanisms. The detailed molecular mechanisms require further studies.

Second, core fucosylation deficiency could down-regulate anti-inflammatory signaling (Fig. 8). It is known that microglia can exist in two different states: one is an activated state (M1), which is typified by the expression of inflammatory cytokines and reactive oxygen species such as NO produced by iNOS; the other is a state of alternative activation (M2), which exhibits the properties of an anti-inflammatory phenotype involved in the production of interleukin 4 (IL-4), interleukin 10 (IL-10), and TGF- β etc., that are implicated in inhibiting inflammation and restoring homeostasis in the CNS [57]. As described above, the TGF- β -induced Smad2/3 signaling pathway is also one of the important anti-inflammatory signaling pathways. Core fucosylation differentially regulates the biological functions of receptors. Our previous study showed that a lack of core fucose led to a marked reduction in the ligand-binding ability and the downstream signaling of several receptors [8,14,53]. A lack of core fucose in TGF- β receptors suppressed its binding with TGF- β and subsequently inhibited its downstream signaling such as in the phosphorylation of Smad2/3, which resulted in the development of an emphysema-like phenotype in *Fut8*^{-/-} mice [14,53]. Furthermore, in a cigarette smoke-induced emphysema model, the *Fut8*^{+/-} mice showed a higher inflammatory response than that of *Fut8*^{+/+} mice [8]. In this study, coincidentally, we observed a modest expression of phosphorylated Smad2 following stimulation with IFN- γ in WT BV-2 cells, but this expression was below the detection level in the KO cells (Fig. 5). These data suggested that the anti-inflammatory signaling pathways, at least TGF- β signaling pathway, could be down-regulated in *Fut8* deficient cells.

In summary, results from the present study clearly showed that core fucosylation exerts dual effects in microglia and astrocytes. Deficiency of *Fut8* enhanced the pro-inflammatory signaling pathways, while inhibited the anti-inflammatory signaling pathways (Fig. 8). It should be

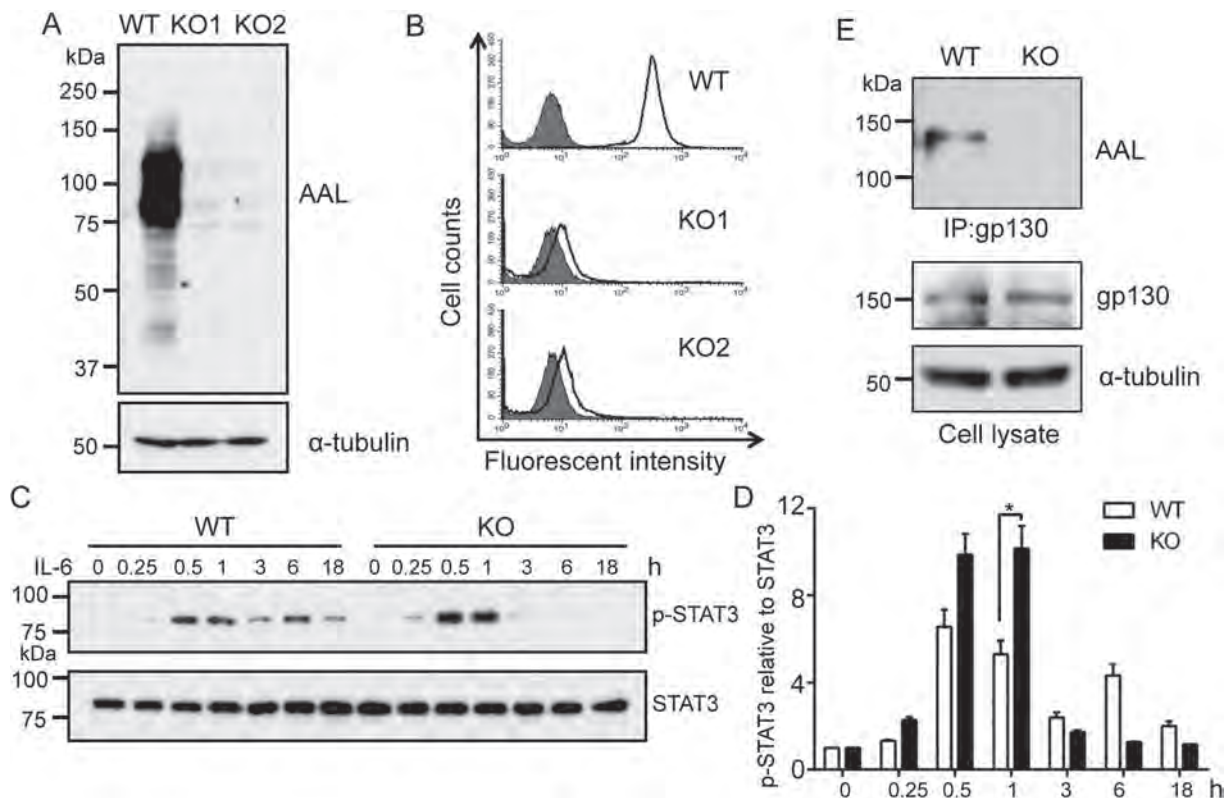


Fig. 7. Effects of core fucosylation on cellular signaling in C6 cells. Establishment of the Fut8 KO C6 cells was performed via a CRISPR/Cas9 system, as described in “Experimental procedures”. (A) Equal amounts of cell lysates were detected by AAL lectin blot. (B) The expression level of core fucosylation recognized by PhoSL on the cell surfaces was subjected to flow cytometric analysis. (C) The expression levels of phosphorylated STAT3 in both WT and KO cells treated with or without IL-6 stimulation at indicated times, were examined by western blotting with anti-phospho-STAT3 antibody. Total STAT3 was used as a loading control. (D) Quantitative analysis of p-STAT3 protein expression in IL-6-stimulated C6 WT and KO cells. Data represent the mean \pm S.E.M; *p* values were calculated using unpaired t-test with Welch's correction. **p* < .05 vs. WT cells (*n* = 3). (E) Equal amounts of cell lysates were immunoprecipitated (IP) with anti-gp130 antibody, which was followed by AAL lectin blot (upper panel). Whole cell lysates were directly blotted with anti-gp130 (as an input, middle panel) and α -tubulin (as a loading control, lower panel) antibodies.

noted that only modest changes in the pro-inflammatory and anti-inflammatory signaling could be detected between WT and Fut8 KO cells in this study, but in concerted responses these small effects may result in a big impact *in vivo*, as shown in Fig. 1. Considering the important roles of microglia during brain development [58] and the participation

of glial cells in schizophrenia [16], and the schizophrenia-like phenotype [10] as well as the high rate of mortality [14] found in Fut8^{-/-} mice, we concluded that the disorders in CNS with deficient core fucosylation may be caused by not only neurons but also by glial cells.

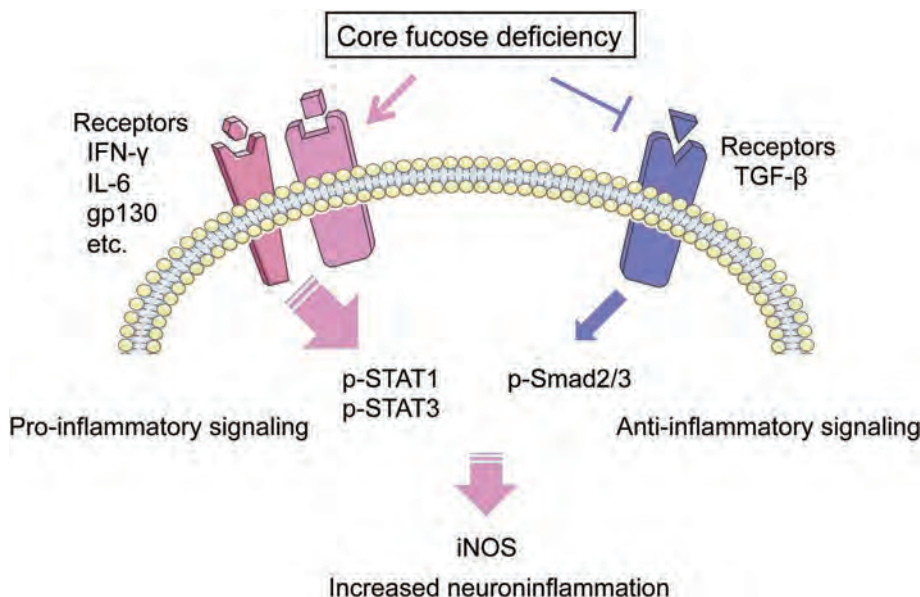


Fig. 8. A simplified model for core fucosylation on a neuroinflammation model. Based on our observations in the present study, loss of core fucosylation could cause differences in the regulation of the sensitivities of microglia and astrocytes to stimuli. Core fucose deficiency seemed to enhance the pro-inflammatory signaling, such as IFN- γ /p-STAT1 and IL-6/p-STAT3 signaling pathways, while decrease the anti-inflammatory signaling, such as in the TGF- β /p-Smad2 signaling pathway, which has been also observed in lung tissues as well as in fibroblast cells [14]. It should be noted that only modest changes could be detected in the pro-inflammatory and anti-inflammatory signaling levels between WT and Fut8 KO glial cells. Considering most cytokine receptors, such as TGF- β receptor and gp130, could be core fucosylated, we believe that the concerted responses of these small effects could result in a significant impact *in vivo*, as observed in Fut8 KO mice as well as in Fut8-deficient patients [10,12,13].

Author contributions

X. Lu, T. Fukuda and J. Gu designed the research; X. Lu performed the mice *in vivo* experiments, primary microglia and BV-2 related experiments; H. Shoji performed the primary astrocytes experiments; D. Zhang performed the C6 cell-related experiments; C. Duan, G. Zhang and Y. Wang assisted with experiments; X. Lu, T. Isaji, T. Fukuda, and J. Gu analyzed and interpreted the data; X. Lu, D. Zhang, T. Isaji, T. Fukuda, and J. Gu wrote and revised the manuscript; and, all authors approved the final version of the manuscript.

Funding sources

This work was supported in part by a Grant-in-Aid for Scientific Research (15H04354 to J.G.; 17 K08284 to T.F.) from the Japan Society for the Promotion of Science; grant from National Natural Science Foundation of China (No. 31670807); and by a Grant-in-Aid for Scientific Research on Innovative Areas (18H04868 to J.G.) from the Ministry of Education, Culture, Sports, Science, and Technology of Japan.

Acknowledgments

We thank Dr. Kohei Takahashi, Dr. Osamu Nakagawasai and Dr. Koichi Tan-No (Department of Pharmacology, Tohoku Medical and Pharmaceutical University) for technical support.

Conflicts of interest

The authors declare that they have no conflicts of interest with the contents of this article.

References

- M.P. Kotzler, S. Blank, F.I. Bantleon, E. Spillner, B. Meyer, Donor substrate binding and enzymatic mechanism of human core alpha1,6-fucosyltransferase (FUT8), *Biochim. Biophys. Acta* 1820 (2012) 1915–1925.
- J.R. Wilson, D. Williams, H. Schachter, The control of glycoprotein synthesis: N-acetylglucosamine linkage to a mannose residue as a signal for the attachment of L-fucose to the asparagine-linked N-acetylglucosamine residue of glycopeptide from alpha1-acid glycoprotein, *Biochem. Biophys. Res. Commun.* 72 (1976) 909–916.
- M. Schneider, E. Al-Shareffi, R.S. Haltiwanger, Biological functions of fucose in mammals, *Glycobiology* 27 (2017) 601–618.
- Y. Zhou, T. Fukuda, Q. Hang, S. Hou, T. Isaji, A. Kameyama, J. Gu, Inhibition of fucosylation by 2-fluorofucose suppresses human liver cancer HepG2 cell proliferation and migration as well as tumor formation, *Sci. Rep.* 7 (2017) 11563.
- Y. Wang, T. Fukuda, T. Isaji, J. Lu, S. Im, Q. Hang, W. Gu, S. Hou, K. Ohtsubo, J. Gu, Loss of alpha1,6-fucosyltransferase inhibits chemical-induced hepatocellular carcinoma and tumorigenesis by down-regulating several cell signaling pathways, *FASEB J.* 29 (2015) 3217–3227.
- H. Fujii, S. Shinzaki, H. Iijima, K. Wakamatsu, C. Iwamoto, T. Sobajima, R. Kuwahara, S. Hiyama, Y. Hayashi, S. Takamatsu, N. Uozumi, Y. Kamada, M. Tsujii, N. Taniguchi, T. Takehara, E. Miyoshi, Core Fucosylation on T Cells, required for activation of T-cell receptor signaling and induction of colitis in mice, is increased in patients with inflammatory bowel disease, *Gastroenterology* 150 (2016) 1620–1632.
- W. Li, R. Yu, B. Ma, Y. Yang, X. Jiao, Y. Liu, H. Cao, W. Dong, L. Liu, K. Ma, T. Fukuda, Q. Liu, T. Ma, Z. Wang, J. Gu, J. Zhang, N. Taniguchi, Core fucosylation of IgG B cell receptor is required for antigen recognition and antibody production, *J. Immunol.* 194 (2015) 2596–2606.
- C. Gao, T. Maeno, F. Ota, M. Ueno, H. Korekane, S. Takamatsu, K. Shirato, A. Matsumoto, S. Kobayashi, K. Yoshida, S. Kitazume, K. Ohtsubo, T. Betsuyaku, N. Taniguchi, Sensitivity of heterozygous alpha1,6-fucosyltransferase knock-out mice to cigarette smoke-induced emphysema: implication of aberrant transforming growth factor-beta signaling and matrix metalloproteinase gene expression, *J. Biol. Chem.* 287 (2012) 16699–16708.
- W. Liang, S. Mao, S. Sun, M. Li, Z. Li, R. Yu, T. Ma, J. Gu, J. Zhang, N. Taniguchi, W. Li, Core Fucosylation of the T cell receptor is required for T cell activation, *Front. Immunol.* 9 (2018) 78.
- T. Fukuda, H. Hashimoto, N. Okayasu, A. Kameyama, H. Onogi, O. Nakagawasai, T. Nakazawa, T. Kurosawa, Y. Hao, T. Isaji, T. Tadano, H. Narimatsu, N. Taniguchi, J. Gu, Alpha1,6-fucosyltransferase-deficient mice exhibit multiple behavioral abnormalities associated with a schizophrenia-like phenotype: importance of the balance between the dopamine and serotonin systems, *J. Biol. Chem.* 286 (2011) 18434–18443.
- W. Gu, T. Fukuda, T. Isaji, H. Hashimoto, Y. Wang, J. Gu, alpha1,6-Fucosylation regulates neurite formation via the activin/phospho-Smad2 pathway in PC12 cells: the implicated dual effects of Fut8 for TGF-beta/activin-mediated signaling, *FASEB J* 27 (2013) 3947–3958.
- W. Gu, T. Fukuda, T. Isaji, Q. Hang, H.H. Lee, S. Sakai, J. Morise, J. Mitoma, H. Higashi, N. Taniguchi, H. Yawo, S. Oka, J. Gu, Loss of alpha1,6-Fucosyltransferase decreases Hippocampal long term potentiation: implications for core fucosylation in the regulation of ampa receptor heteromerization and cellular signaling, *J. Biol. Chem.* 290 (2015) 17566–17575.
- B.G. Ng, G. Xu, N. Chandy, J. Steyermark, D.N. Shinde, K. Radtke, K. Raymond, C.B. Lebrilla, A. Alasmari, S.F. Suchy, Z. Powis, E.A. Fageih, S.A. Berry, D.F. Kronn, H.H. Freeze, Biallelic mutations in FUT8 cause a congenital disorder of glycosylation with defective fucosylation, *Am. J. Hum. Genet.* 102 (2018) 188–195.
- X. Wang, S. Inoue, J. Gu, E. Miyoshi, K. Noda, W. Li, Y. Mizuno-Horikawa, M. Nakano, M. Asahi, M. Takahashi, N. Uozumi, S. Ihara, S.H. Lee, Y. Ikeda, Y. Yamaguchi, Y. Aze, Y. Tomiyama, J. Fujii, K. Suzuki, A. Kondo, S.D. Shapiro, C. Lopez-Otin, T. Kuwaki, M. Okabe, K. Honke, N. Taniguchi, Dysregulation of TGF-beta1 receptor activation leads to abnormal lung development and emphysema-like phenotype in core fucose-deficient mice, *Proc. Natl. Acad. Sci. U. S. A.* 102 (2005) 15791–15796.
- O.D. Howes, R. McCutcheon, Inflammation and the neural diathesis-stress hypothesis of schizophrenia: a reconceptualization, *Transl. Psychiatry* 7 (2017) e1024.
- O. Pasternak, M. Kubicki, M.E. Shenton, In vivo imaging of neuroinflammation in schizophrenia, *Schizophr. Res.* 173 (2016) 200–212.
- P.G. Haydon, GLIA: listening and talking to the synapse, *Nat. Rev. Neurosci.* 2 (2001) 185–193.
- V. Gundersen, J. Storm-Mathisen, L.H. Bergersen, Neuroglial Transmission, *Physiol. Rev.* 95 (2015) 695–726.
- C. Eroglu, B.A. Barres, Regulation of synaptic connectivity by glia, *Nature* 468 (2010) 223–231.
- K.A. Nave, Myelination and support of axonal integrity by glia, *Nature* 468 (2010) 244–252.
- C.K. Glass, K. Saijo, B. Winner, M.C. Marchetto, F.H. Gage, Mechanisms underlying inflammation in neurodegeneration, *Cell* 140 (2010) 918–934.
- L.J. Lawson, V.H. Perry, S. Gordon, Turnover of resident microglia in the normal adult mouse brain, *Neuroscience* 48 (1992) 405–415.
- D.P. Schafer, E.K. Lehrman, A.G. Kautzman, R. Koyama, A.R. Mardinly, R. Yamasaki, R.M. Ransohoff, M.E. Greenberg, B.A. Barres, B. Stevens, Microglia sculpt postnatal neural circuits in an activity and complement-dependent manner, *Neuron* 74 (2012) 691–705.
- R.C. Paolicelli, G. Bolasco, F. Pagani, L. Maggi, M. Scianni, P. Panzanelli, M. Giustetto, T.A. Ferreira, E. Guiducci, L. Dumas, D. Ragozzino, C.T. Gross, Synaptic pruning by microglia is necessary for normal brain development, *Science* 333 (2011) 1456–1458.
- S. Herculano-Houzel, The glia/neuron ratio: how it varies uniformly across brain structures and species and what that means for brain physiology and evolution, *Glia* 62 (2014) 1377–1391.
- L.E. Clarke, B.A. Barres, Emerging roles of astrocytes in neural circuit development, *Nat. Rev. Neurosci.* 14 (2013) 311–321.
- W.S. Chung, L.E. Clarke, G.X. Wang, B.K. Stafford, A. Sher, C. Chakraborty, J. Joung, L.C. Foo, A. Thompson, C. Chen, S.J. Smith, B.A. Barres, Astrocytes mediate synapse elimination through MEGF10 and MERTK pathways, *Nature* 504 (2013) 394–400.
- S.A. Liddelow, K.A. Guttenplan, L.E. Clarke, F.C. Bennett, C.J. Bohlen, L. Schirmer, M.L. Bennett, A.E. Munch, W.S. Chung, T.C. Peterson, D.K. Wilton, A. Frouin, B.A. Napier, N. Panicker, M. Kumar, M.S. Buckwalter, D.H. Rowitch, V.L. Dawson, T.M. Dawson, B. Stevens, B.A. Barres, Neurotoxic reactive astrocytes are induced by activated microglia, *Nature* 541 (2017) 481–487.
- T.A. Bayer, R. Buslei, L. Havas, P. Falkai, Evidence for activation of microglia in patients with psychiatric illnesses, *Neurosci. Lett.* 271 (1999) 126–128.
- A. Goudriaan, C. de Leeuw, S. Ripke, C.M. Hultman, P. Sklar, P.F. Sullivan, A.B. Smit, D. Posthuma, M.H. Verheijen, Specific glial functions contribute to schizophrenia susceptibility, *Schizophr. Bull.* 40 (2014) 925–935.
- J.M. Kippe, T.M. Mueller, V. Haroutunian, J.H. Meador-Woodruff, Abnormal N-acetylglucosaminyltransferase expression in prefrontal cortex in schizophrenia, *Schizophr. Res.* 166 (2015) 219–224.
- J. Tucholski, M.S. Simmons, A.L. Pinner, V. Haroutunian, R.E. McCullumsmith, J.H. Meador-Woodruff, Abnormal N-linked glycosylation of cortical AMPA receptor subunits in schizophrenia, *Schizophr. Res.* 146 (2013) 177–183.
- T.M. Mueller, V. Haroutunian, J.H. Meador-Woodruff, N-Glycosylation of GABAA receptor subunits is altered in schizophrenia, *Neuropsychopharmacology* 39 (2014) 528–537.
- T.M. Mueller, S.D. Yates, V. Haroutunian, J.H. Meador-Woodruff, Altered fucosyltransferase expression in the superior temporal gyrus of elderly patients with schizophrenia, *Schizophr. Res.* 182 (2017) 66–73.
- C.D. Rillahan, A. Antonopoulos, C.T. Lefort, R. Sonon, P. Azadi, K. Ley, A. Dell, S.M. Haslam, J.C. Paulson, Global metabolic inhibitors of sialyl- and fucosyltransferases remodel the glycome, *Nat. Chem. Biol.* 8 (2012) 661–668.
- N.M. Okesley, S.C. Alley, M.E. Anderson, T.E. Boursalian, P.J. Burke, K.M. Emmertson, S.C. Jeffrey, K. Klussman, C.L. Law, D. Sussman, B.E. Toki, L. Westendorf, W. Zeng, X. Zhang, D.R. Benjamin, P.D. Senter, Development of orally active inhibitors of protein and cellular fucosylation, *Proc. Natl. Acad. Sci. U. S. A.* 110 (2013) 5404–5409.
- M. Dumont, A. Lehner, M. Bardor, C. Burel, B. Vauzeilles, O. Lerouxel, C.T. Anderson, J.C. Mollet, P. Lerouge, Inhibition of fucosylation of cell wall components by 2-fluoro 2-deoxy-L-fucose induces defects in root cell elongation,

- Plant J. 84 (2015) 1137–1151.
- [38] T. Takada, T. Ebata, H. Noguchi, T.M. Keane, D.J. Adams, T. Narita, I.T. Shin, H. Fujisawa, A. Toyoda, K. Abe, Y. Obata, Y. Sakaki, K. Moriwaki, A. Fujiyama, Y. Kohara, T. Shiroishi, The ancestor of extant Japanese fancy mice contributed to the mosaic genomes of classical inbred strains, *Genome Res.* 23 (2013) 1329–1338.
- [39] C. Huang, Z.L. Hu, W.N. Wu, D.F. Yu, Q.J. Xiong, J.R. Song, Q. Shu, H. Fu, F. Wang, J.G. Chen, Existence and distinction of acid-evoked currents in rat astrocytes, *Glia* 58 (2010) 1415–1424.
- [40] F.A. Ran, P.D. Hsu, J. Wright, V. Agarwala, D.A. Scott, F. Zhang, Genome engineering using the CRISPR-Cas9 system, *Nat. Protoc.* 8 (2013) 2281–2308.
- [41] C.H. Latta, H.M. Brothers, D.M. Wilcock, Neuroinflammation in Alzheimer's disease; a source of heterogeneity and target for personalized therapy, *Neuroscience* 302 (2015) 103–111.
- [42] C. Cebrian, J.D. Loike, D. Sulzer, Neuroinflammation in Parkinson's disease animal models: a cell stress response or a step in neurodegeneration? *Curr. Top. Behav. Neurosci.* 22 (2015) 237–270.
- [43] K.S. Na, H.Y. Jung, Y.K. Kim, The role of pro-inflammatory cytokines in the neuroinflammation and neurogenesis of schizophrenia, *Prog. Neuro-Psychopharmacol. Biol. Psychiatry* 48 (2014) 277–286.
- [44] K. Matsumura, K. Higashida, H. Ishida, Y. Hata, K. Yamamoto, M. Shigetani, Y. Mizuno-Horikawa, X. Wang, E. Miyoshi, J. Gu, N. Taniguchi, Carbohydrate binding specificity of a fucose-specific lectin from *Aspergillus oryzae*: a novel probe for core fucose, *J. Biol. Chem.* 282 (2007) 15700–15708.
- [45] F.O. Martinez, S. Gordon, The M1 and M2 paradigm of macrophage activation: time for reassessment, *F1000Prime Rep* 6 (2014) 13.
- [46] B.J. Miller, P. Buckley, W. Seabolt, A. Mellor, B. Kirkpatrick, Meta-analysis of cytokine alterations in schizophrenia: clinical status and antipsychotic effects, *Biol. Psychiatry* 70 (2011) 663–671.
- [47] J.K.Y. Tse, Gut microbiota, Nitric Oxide, and Microglia as prerequisites for neurodegenerative disorders, *ACS Chem. Neurosci.* 8 (2017) 1438–1447.
- [48] Y. Ishida, T. Kondo, T. Takayasu, Y. Iwakura, N. Mukaida, The essential involvement of cross-talk between IFN-gamma and TGF-beta in the skin wound-healing process, *J. Immunol.* 172 (2004) 1848–1855.
- [49] W. Strober, B. Kelsall, I. Fuss, T. Marth, B. Ludviksson, R. Ehrhardt, M. Neurath, Reciprocal IFN-gamma and TGF-beta responses regulate the occurrence of mucosal inflammation, *Immunol. Today* 18 (1997) 61–64.
- [50] M.V. Sofroniew, H.V. Vinters, Astrocytes: biology and pathology, *Acta Neuropathol.* 119 (2010) 7–35.
- [51] J. Iijima, S. Kobayashi, S. Kitazume, Y. Kizuka, R. Fujinawa, H. Korekane, T. Shibata, S.I. Saitoh, S. Akashi-Takamura, K. Miyake, E. Miyoshi, N. Taniguchi, Core fucose is critical for CD14-dependent Toll-like receptor 4 signaling, *Glycobiology* 27 (2017) 1006–1015.
- [52] T.C. Frank-Cannon, L.T. Alto, F.E. McAlpine, M.G. Tansey, Does neuroinflammation fan the flame in neurodegenerative diseases? *Mol. Neurodegener.* 4 (2009) 47.
- [53] X. Wang, J. Gu, E. Miyoshi, K. Honke, N. Taniguchi, Phenotype changes of Fut8 knockout mouse: core fucosylation is crucial for the function of growth factor receptor(s), *Methods Enzymol.* 417 (2006) 11–22.
- [54] X. Wang, J. Gu, H. Ihara, E. Miyoshi, K. Honke, N. Taniguchi, Core fucosylation regulates epidermal growth factor receptor-mediated intracellular signaling, *J. Biol. Chem.* 281 (2006) 2572–2577.
- [55] K. Matsumoto, H. Yokote, T. Arao, M. Maegawa, K. Tanaka, Y. Fujita, C. Shimizu, T. Hanafusa, Y. Fujiwara, K. Nishio, N-Glycan fucosylation of epidermal growth factor receptor modulates receptor activity and sensitivity to epidermal growth factor receptor tyrosine kinase inhibitor, *Cancer Sci.* 99 (2008) 1611–1617.
- [56] Y. Zhao, S. Itoh, X. Wang, T. Isaji, E. Miyoshi, Y. Kariya, K. Miyazaki, N. Kawasaki, N. Taniguchi, J. Gu, Deletion of core fucosylation on alpha3beta1 integrin down-regulates its functions, *J. Biol. Chem.* 281 (2006) 38343–38350.
- [57] J.D. Cherry, J.A. Olschowka, M.K. O'Banion, Neuroinflammation and M2 microglia: the good, the bad, and the inflamed, *J. Neuroinflammation* 11 (2014) 98.
- [58] O. Matcovitch-Natan, D.R. Winter, A. Giladi, S. Vargas Aguilar, A. Spinrad, S. Sarrazin, H. Ben-Yehuda, E. David, F. Zelada Gonzalez, P. Perrin, H. Keren-Shaul, M. Gury, D. Lara-Astaiso, C.A. Thaïss, M. Cohen, K. Bahar Halpern, K. Baruch, A. Deczkowska, E. Lorenzo-Vivas, S. Itzkovitz, E. Elinav, M.H. Sieweke, M. Schwartz, I. Amit, Microglia development follows a stepwise program to regulate brain homeostasis, *Science* 353 (2016) aad8670.



Core Fucosylation of the T Cell Receptor Is Required for T Cell Activation

Wei Liang^{1†}, Shanshan Mao^{1†}, Shijie Sun^{1†}, Ming Li¹, Zhi Li², Rui Yu¹, Tonghui Ma¹, Jianguo Gu³, Jianing Zhang⁴, Naoyuki Taniguchi⁵ and Wenzhe Li^{1*}

¹ College of Basic Medical Sciences, Dalian Medical University, Dalian, China, ² Clinical Laboratory, Dalian Municipal Central Hospital, Dalian, China, ³ Division of Regulatory Glycobiology, Institute of Molecular Biomembrane and Glycobiology, Tohoku Medical and Pharmaceutical University, Sendai, Japan, ⁴ School of Life Science and Medicine, Dalian University of Technology, Panjin, China, ⁵ Systems Glycobiology Research Group, Advanced Science Institute, RIKEN, Saitama, Japan

OPEN ACCESS

Edited by:

Michael Loran Dustin,
Harvard University, United States

Reviewed by:

Balbino Alarcon,
Consejo Superior de Investigaciones
Científicas (CSIC), Spain
Christoph Wülfing,
University of Bristol, United Kingdom

*Correspondence:

Wenzhe Li
liwenzhe@dlmedu.edu.cn

[†]These authors have contributed
equally to this work.

Specialty section:

This article was submitted
to T Cell Biology,
a section of the journal
Frontiers in Immunology

Received: 30 September 2017

Accepted: 11 January 2018

Published: 29 January 2018

Citation:

Liang W, Mao S, Sun S, Li M, Li Z,
Yu R, Ma T, Gu J, Zhang J,
Taniguchi N and Li W (2018) Core
Fucosylation of the T Cell Receptor
Is Required for T Cell Activation.
Front. Immunol. 9:78.
doi: 10.3389/fimmu.2018.00078

CD4⁺ T cell activation promotes the pathogenic process of systemic lupus erythematosus (SLE). T cell receptor (TCR) complex are highly core fucosylated glycoproteins, which play important roles in T cell activation. In this study, we found that the core fucosylation of CD4⁺ T cells was significantly increased in SLE patients. Loss of core fucosyltransferase (Fut8), the sole enzyme for catalyzing the core fucosylation of N-glycan, significantly reduced CD4⁺ T cell activation and ameliorated the experimental autoimmune encephalomyelitis-induced syndrome in Fut8^{-/-} mice. T cell activation with OVA₃₂₃₋₃₃₉ loaded major histocompatibility complex II (pMHC-II) on B cell was dramatically attenuated in Fut8^{-/-}OT-II CD4⁺ T cells compared with Fut8^{+/+}OT-II CD4⁺ T cells. Moreover, the phosphorylation of ZAP-70 was significantly reduced in Fut8^{+/+}OT-II CD4⁺ T cells by the treatment of fucosidase. Our results suggest that core fucosylation is required for efficient TCR-pMHC-II contacts in CD4⁺ T cell activation, and hyper core fucosylation may serve as a potential novel biomarker in the sera from SLE patients.

Keywords: core fucosylation, T cell receptor, T cell activation, systemic lupus erythematosus, T-B cell interaction

INTRODUCTION

Systemic lupus erythematosus (SLE) is a severe autoimmune disease that characterized by the production of autoantibodies and the subsequent inflammatory disorders (1). Although the pathogenesis is not completely understood, the activation of CD4⁺ T cells seems plays an essential role in the onset and development of SLE (2). Appropriate CD4⁺ T cell activation is crucially important for adaptive immune responses and autoimmunity, but hyper-activation of these cells results in autoimmune diseases. T cell recognition of peptide-loaded major histocompatibility complex II (pMHC-II) on the antigen-presenting cells (APCs) by T cell receptors (TCRs) is the most important checkpoint for CD4⁺ T cell activation (3). During antigen recognition, the CD4 coreceptor binds to the non-polymorphic surfaces of the membrane-proximal domains of the same pMHCs, which results in a marked increase in the sensitivity of T cells to pMHCs on APC. When adequate agonistic TCR signaling creates a favorable microenvironment for binding, CD28-B7 molecules provide costimulatory lower the thresholds for TCRs triggering and activation. The signaling through TCR induces a conformational change in leukocyte function-associated antigen-1, which greatly

increases its affinity for intercellular adhesion molecule 1 and contributes to immune synapse formation T cells and APC (4, 5).

Glycosylation plays a regulatory and often pivotal role in T cell activation (6–10). Several studies have reported that glycosylation could contribute to higher activation thresholds of T cells. For instance, β 1,6N-acetylglucosaminyltransferase V (Mgat5) deficiency mediates lower T lymphocyte activation thresholds, and subsequently improves T cell activity *in vitro* and results in autoimmune disease *in vivo* (11, 12). Deletion of sialyltransferase ST3Gal-1 increase the sensitivity of TCRs to low-affinity ligands in CD8⁺ T cells (13). Fucosyltransferase 1 transgenic mice show increased TCR signaling and apoptosis that results in thymocyte maturation arrest (14). Notably, reduced N-glycosylation of TCR chains can improve functional avidity and recognition by T cells (15) suggesting that the glycosylation of TCR has a unique role in the regulation of T cell activation.

T cell receptors are heavily core-fucosylated glycoproteins. The core fucosylation of protein is catalyzed by core fucosyltransferase (Fut8), which transfers fucose residue from GDP-fucose to the innermost N-acetylglucosamine (GlcNAc) residue of N-linked glycans *via* an α 1,6 linkage in the Golgi apparatus of mammals (Figure S1 in Supplementary Material). Fut8-mediated core fucosylation is an important post-translational process (16), which regulates protein conformation, stability, and functional expression. Studies have shown that the N-glycans at Asn⁷⁰ [GlcNAc(α 1,6Fuc)- β 1,4GlcNAc: (A2G2F)], Asn¹⁸⁵ (A2G2F), and Asn²⁰³ in the α chain (C α) and Asn²³⁶ in the β chain (C β) extend from the surface of TCR on *Drosophila melanogaster* cells (6, 17). Interestingly, they found that the C α and C β of TCR were connected by the hydrogen bonds of the core fucose residue from Asn¹⁸⁵ (A2G2F) to side chains of Glu¹⁸¹ β and Ser¹⁸² β (6, 17), suggesting a crucial role of core fucosylation on the conformation of TCR. However, to the best of our knowledge, none of the previous studies had addressed the regulatory role of TCR core fucosylation on CD4⁺ T cell activation.

B cells play a role in evoking T cell responses by functioning as APCs, and the presentation of peptide by MHC-II on the B cells initiates T cell activation (18). Therefore, it is reasonable to anticipate that the core fucosylation has significant functional implications in T–B cell interaction, and thus affect the CD4⁺ T cell activation. In this study, we provide the first confirmation that SLE patients exhibited hyper core fucosylation on CD4⁺ T cells, which significantly enhanced the activation of their CD4⁺ T cells. Knockout of Fut8 gene resulted in attenuated T–B cell interaction *via* TCR–pMHC and the consequential reduced CD4⁺ T cell activation. Our data suggest that the core fucosylation may serve as a potential novel biomarker with promising clinical and therapeutic implications in SLE patients.

MATERIALS AND METHODS

Mice

Fut8^{-/-} mice were generated as previously described (19), and homozygous wild-type (Fut8^{+/+}) and Fut8^{-/-} mice on the C57BL/6 background were obtained by crossing heterozygous

Fut8^{+/-} mice (C57BL/6). OT-II (Jackson Laboratory) is a C57BL/6 TCR transgenic strain, expressing a receptor specific for peptide OVA_{323–339}. Fut8^{+/+}OT-II mice and Fut8^{-/-}OT-II mice were generated by crossing heterozygous Fut8^{+/-}OT-II mice. Mice were maintained in the specific pathogen-free laboratory animal facility of Dalian Medical University. All animal work was approved by the Ethics Committee at the Dalian Medical University.

Patients

Serum samples were collected from a total of 17 SLE patients (14 women, 3 men; mean age, 49 years; range, 18–67 years) with and healthy controls (12 women, 12 men; mean age, 18–48 years) (Table S1 in Supplementary Material). The diagnosis of underlying disease was made based on clinical manifestation, serology, imaging, and/or histopathology. These participants were Chinese, recruited at Dalian municipal central hospital. The anti-nuclear antibodies (ANA) titers of AD patients were detected with using Anti-nuclear Antibodies IgG Kit (EUROIMMUN, Germany). The Ethics Committee at the hospital approved the study protocol.

Antibodies

Anti-CD16/32 (2.4G2), anti-CD3(145-2c11), anti-CD28 (37.51), FITC-anti-MHC II (M5/114.15.2), FITC-anti-CD69 (H1.2F3), PE-labeled anti-CD4 (GK1.5), APC-labeled anti-CD8 (53-6.7), biotin-labeled anti-TCR β (H57-597), and PE-Cy5-labeled anti-TCR β (H57-597) were obtained from e-Bioscience; anti-GAPDH, horseradish peroxidase (HRP)-conjugated goat anti-mouse IgG and HRP-conjugated donkey anti-human IgG were obtained from proteintech; additional biotin-conjugated lens culinaris agglutinin (LCA) were purchased from Vector; anti-TCR $\alpha\beta$ (ab25336), anti-pZAP70 (ab194800), anti-ZAP70 (ab32410), Natural streptavidin protein (FITC) (ab136201), and streptavidin (HRP) (ab7403) were purchased from Abcam.

Histological Analysis

Formalin-fixed tissue samples were paraffin-embedded and sections were analyzed by hematoxylin–eosin (H&E) staining. The sections were stained with biotin-conjugated LCA. Briefly, sections were deparaffinized three times in xylene and hydrated through a 100, 90, 80, and 70% ethanol to phosphate-buffered saline (PBS). To quench the endogenous peroxidase activity, slides were incubated with 3% H₂O₂ for 30 min. Then, the slides were incubated with biotin-conjugated LCA, and washed three times with PBS. The slides probed with HRP–streptavidin for 30 min, and visualized with 3,3'-diaminobenzidine. The intensity of LCA-positive staining in the spleen was analyzed by integrated optical density using Image-Pro[®] Plus software (version 6.0; Media Cybernetics, USA).

Cell Lysate

Cells were solubilized in lysis buffer [Tris–HCl (50 mM), 1% Triton X-100, 10% glycerol, phenylmethylsulfonyl fluoride (100 μ M), leupeptin (5 μ g/mL), aprotinin (1 μ g/mL), NaF (100 mM), 150 mM NaCl, 2 mM EDTA, and sodium orthovanadate (1 mM)] for 15 min at 4°C. Cell lysate was centrifuged at

20,000 × *g* for 10 min at 4°C, and the supernatant was subjected to immunoprecipitation or Western blot, as indicated below.

Fut8 Enzyme Activity Assay

The Fut8 enzyme activity was measured by using the previous method (20). Five micrograms cell lysates as the enzyme source were added to the assay buffer (200 mM MES, 1% Triton X-100) supplemented with donor (500 μM GDP-L-fucose) and substrate [50 μM GnGn-Asn-4-(2-pyridylamine) butylamine (PABA)]. The mixture was incubated at 37°C for 8 h, and the reaction was stopped by heating at 100°C for 5 min. The reactive solution was then centrifuged at 12,000 × *g* for 10 min, and 10 μL of the reaction products were subjected to high-performance liquid chromatography (HPLC) with a Fluorescent detector (Waters Corporation, USA). The excitation and emission wavelengths are 320 and 400 nm, respectively.

PCR Array

Total RNAs were extracted from Fut8^{+/+} SPLs and Fut8^{-/-} SPLs with TRIzol reagent (Takara Bio). Mouse T Cell and B Cell Activation PCR Array (SA Biosciences) was carried out according to the protocol of the manufacturer. The difference of gene expression between Fut8^{+/+} SPLs and Fut8^{-/-} SPLs was calculated.

Animal Immunization

Mouse was immunized by subcutaneous injection with 200 μg OVA mixed with an equal volume of complete Freund's adjuvant (CFA) (Sigma). Two weeks later, mice were immunized with 200 μg OVA by subcutaneous injection. Mice sera were collected at 0, 7, and 14 days post-immunization.

Enzyme-Linked Immunosorbent Assay (ELISA)

The concentrations of IL-2 analyzed using mouse IL-2 ELISA kits (Boster Biological Engineering, Wuhan, China), according to the manufacturer's instructions. The concentrations of IL-2 were calculated according to a standard curve prepared using samples of known concentration. The absorbance was measured at a test wavelength of 450 nm with a microplate reader.

The immunoglobulin isotypes were measured by mouse mAb isotyping reagents (Sigma).

Cell Proliferation Assay

The growth rate of cells was measured using MTT assay. CD4⁺ T cells (1 × 10⁶) were cultured in 96-well culture plate with anti-CD3ε (2 μg/mL) and anti-CD28 mAbs (1 μg/mL). After 48 h of incubation, each well was added 10 μL of MTT solution, and then the absorbance was analyzed by a microplate reader (Thermo Multiskan Ascent, Finland) at 570 nm.

In addition, T cell proliferation with the OVA₃₂₃₋₃₃₉-loaded B cells was analyzed by carboxyfluorescein diacetatesuccinimidyl ester (CFSE, Sigma) dilution methods. CD4⁺ T cells (1 × 10⁶) were purified, and then labeled with 5 μM CFSE in PBS for 8 min at room temperature and coincubate with OVA₃₂₃₋₃₃₉ loaded Fut8^{+/+} OT-II B cells (1 × 10⁶) for 48 h, and then analyzed by flow cytometric analysis.

Western Blot and Lectin Blot Analysis

Protein samples were electrophoresed on 10% polyacrylamide gels. After electrophoresis at 240 mA for 30 min, proteins were transferred to PVDF membranes. Membranes were blocked in 5% BSA in TBS-T (10 mM Tris-HCl, 150 mM NaCl, and 0.1% Tween 20) at room temperature for 1 h, and then incubated with the biotin-labeled LCA, which preferentially recognizes the core fucose, or primary Abs in 1% BSA in TBS-T overnight at 4°C. After washing, the membranes were covered with the HRP-conjugated streptavidin or HRP-labeled secondary Abs at room temperature for 1 h, and visualized with an ECL system (Amersham).

Immunoprecipitation

Cell extracts (500 μg) were mixed with 20 μL of Protein G-Sepharose (50%) and corresponding Abs, and then incubated at 4°C overnight with continuous rotation. After washing three times in lysis buffer, the pull down samples were boiled for 5 min in Laemmli sample buffer with or without 2-mercaptoethanol.

T-B Cell Conjugate Formation

Conjugate formation between T cells and B cells were carried out as described previously with slight modification (21). T cells and 1 μg/mL OVA₃₂₃₋₃₃₉ (NH₂-ISQAVHAAHAEINEAGR-COOH)-pulsed B cells were mixed at a 1:1 ratio and a quick centrifugation to initiate cell-cell contact. To observe conjugate formation, B cells and T cells were labeled with MHC-II-FITC and TCRβ-PE-Cy5 before mixing. T-B cell conjugates were then analyzed by flow cytometry to determine the percentage of T-B cells that had both TCRβ-PE-Cy5 and MHC-II-FITC positive staining.

Remove of Core Fucose on Surface of T Cells

Purified CD4⁺ T cells (4 × 10⁶) were treated with 100 mU Glyko® α(1-2,3,4,6) Bovine Kidney Fucosidase (GKX-5006, Prozyme), incubate 3 h at 37°C in the reaction buffer. The enzyme reaction was terminated by centrifuging at 2,500 × *g* for 5 min and the cells were collected.

Confocal Microscopy

Conjugate formation between T cells and B cells were carried out as described previously with slight modification (21). T cells and 1 μg/mL OVA₃₂₃₋₃₃₉ pulsed B cells were mixed at a 1:1 ratio and a quick centrifugation to initiate cell-cell contact. Cell-cell conjugates were subsequently transferred to poly-D-lysine coated coverslips and incubated at 37°C for 30 min. Cells were fixed with 4% PFA for 20 min, and then blocked with 5% BSA and anti-CD16/CD32 (2.4G2) mAb for 30 min. After washing, cells were stained with anti-MHC-II Ab for 1 h. All images were taken using a spinning disk confocal microscope (Leica).

MACS Magnetic Cell Sorting

Single splenic cell suspensions were prepared by first grinding the tissues and then by passage through 30-μm nylon mesh. Red blood cells were lysed by incubation with 0.14 M NH₄Cl and 20 mM Tris (pH7.4) for 3 min at room temperature.

After the lysis of red blood cells, CD4⁺ T cells and B cells were positively isolated with anti-CD4 Ab and anti-CD45R Ab-conjugated magnetic beads (Miltenyi Biotec). The purified cell populations were detected by fluorescence activated cell sorting analysis.

Flow Cytometric Analysis (FACS)

Cells were isolated from tissue and incubated with an anti-CD16/CD32 (2.4G2) mAb to block Fcγ receptors. The cells were stained on ice for 15 min with several combinations of mAbs, as indicated in the figure legends. Flow cytometry was performed on a FACS-Calibur (Becton Dickinson, Mountain View, CA, USA) and analyzed using FlowJo software (Tree Star).

Induction of Experimental Autoimmune Encephalomyelitis (EAE)

For EAE induction, Fut8^{+/+} and Fut8^{-/-} mice were subcutaneously injected with 100 μg of myelin oligodendrocyte glycoprotein peptides (MOG₃₅₋₅₅) emulsified in CFA. Then, mice were injected intraperitoneally with 200 μg pertussis toxin (PTX) (List Biological Laboratories) on 0, 1, and 2 days. Clinical assessment of EAE was performed according to the following scale: 0, no disease; 1, limp tail; 2, hind-limb weakness; 3, partial hind-limb paralysis; 4, complete paralysis of hind-limbs; and 5, moribund state.

Statistical Analysis

Student's *t*-test was used for statistical analysis. Data are presented as mean values ± SEM, or as mean values ± SD. A probability value of *p* < 0.05 was considered significant. **p* < 0.05, ***p* < 0.01, ****p* < 0.001.

RESULTS

Core Fucosylation Is Significantly Upregulated in the Sera and CD4⁺ T Cells of SLE Patients

Higher circulating levels of ANA were detected in sera from SLE patients. In this study, we found that core fucosylation was dramatically increased in the sera from patients with SLE, as evidenced by LCA, which preferentially recognizes the core fucose structure (22) (*p* < 0.001) (Figures 1A,B). The expression of IgGs was also upregulated in sera of the SLE patients (*p* < 0.05) (Figure 1B). These observations pinpoint the contribution of hyper core fucosylation to SLE severity and pathogenesis.

The hyperactivity of B cells in SLE is T cell dependent, and CD4⁺ T cell activation plays a crucial role in SLE pathogenesis (23). We found that the percentage of CD4⁺ T cells in the peripheral blood of SLE patients is similar to those of healthy control (Figure 1C). However, the percentage of CD4⁺CD69⁺ T cells was significantly increased in the SLE (*n* = 17) (Figure 1D). Moreover, the enzyme activity of Fut8 was dramatically increased in the CD4⁺ T cells isolated from the SLE patients (Figures 1E,F), indicated that increased core fucosylation in SLE patients correlates with CD4⁺ T cell activation.

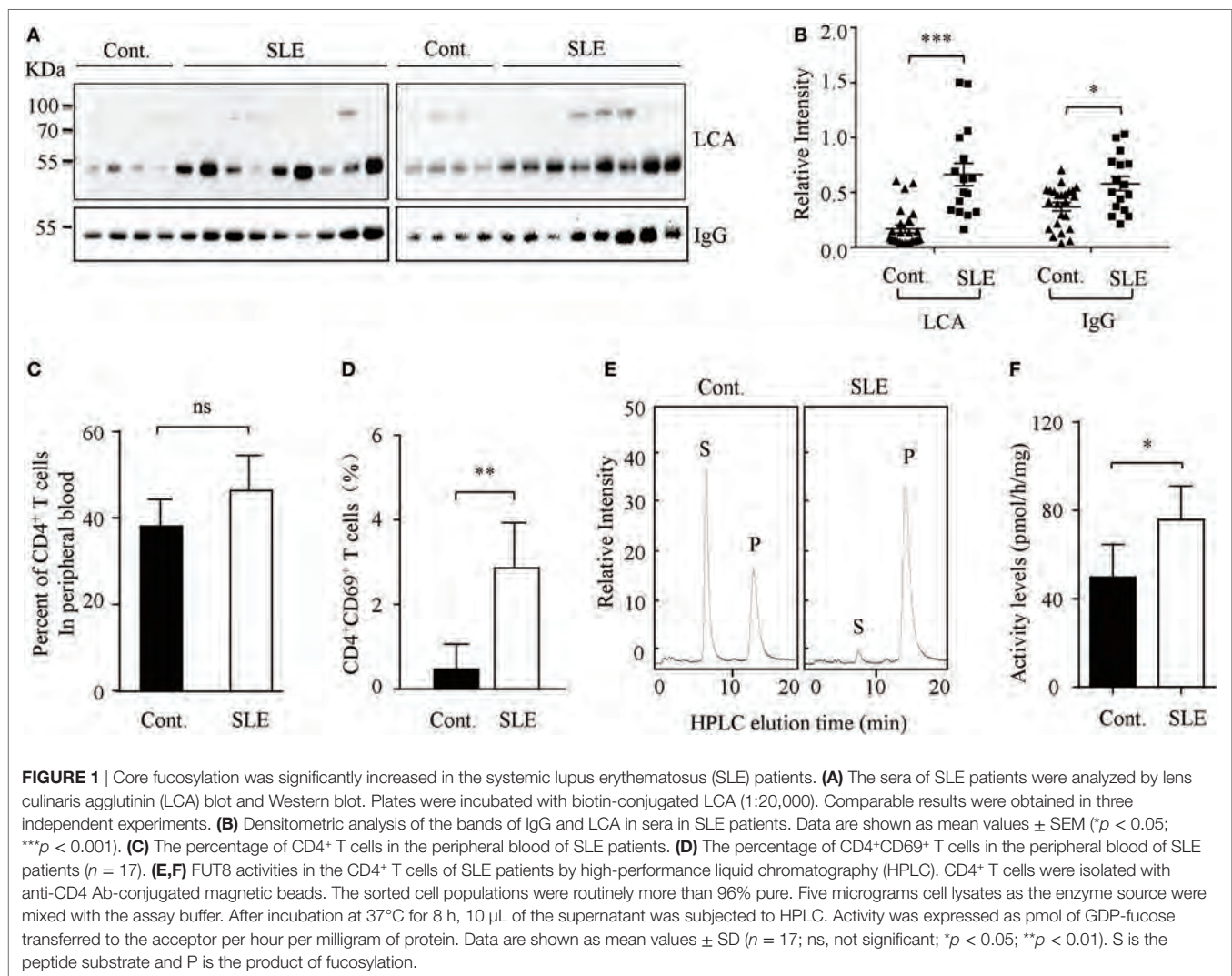
Lack of Core Fucosylation Ameliorated EAE Symptoms with Reduced CD4⁺ T Cell Activation

Wild-type (Fut8^{+/+}) and Fut8^{-/-} mice were generated previously (19). Histological analyses of the splenic architecture of Fut8^{+/+} and Fut8^{-/-} mice were unremarkable in H&E staining. The Fut8 products, core-fucosylated N-glycans, are ubiquitously expressed in the Fut8^{+/+} spleen, as confirmed by LCA (Figure 2A), while those were abolished in Fut8^{-/-} spleens. LCA blot analysis also confirmed the knockout of Fut8 expression in the whole cell lysates of Fut8^{-/-} SPLs (Figure 2B). The FUT8 enzymatic activity was not detected in the Fut8^{-/-} SPLs using HPLC analysis (Figure 2C).

Experimental autoimmune encephalomyelitis is an activated CD4⁺ T cell-mediated autoimmune disease model. Peptides (MOG₃₅₋₅₅) and PTX could induce the migration of activated T cells through the blood-brain barrier and caused several neurologic symptoms. To determine the association between core fucosylation and the activation of CD4⁺ T cells, EAE models were established using Fut8^{+/+} and Fut8^{-/-} mice. EAE is actively induced but appear more quickly upon adoptive transfer of activated MOG₃₅₋₅₅-specific T cells in Fut8^{+/+} mice (Figure 2D; Video S1 in Supplementary Material), while Fut8^{-/-} mice showed slight EAE symptoms (Figure 2D; Video S2 in Supplementary Material). The body weights of Fut8^{+/+} mice were significantly reduced, but no change was found in Fut8^{-/-} mice during EAE induction (Figure 2D). In addition, the proliferation of CD4⁺ T cells was significantly decreased in Fut8^{-/-} EAE mice. Moreover, the proliferation of CD4⁺ T cells with MOG₃₅₋₅₅-loaded B cells was remarkably reduced by de-core fucosylation (Figure 2E).

Lack of Core Fucosylation Suppressed the IgG Class-Switching by Impaired CD4⁺ T Cell Activation

Flow cytometry analysis revealed that, although Fut8^{-/-} mice contained normal proportions of CD4⁺ and CD8⁺ T cell populations in the spleen (Figures 3A,B), they were markedly reduced after OVA immunization contrast with the Fut8^{+/+} mice (Figures 3A,B). Immunoglobulin class-switching is a biological mechanism that changes a mature B cell's production of antibody *via* its B cell receptor from one class to another. For example, from an isotype called IgM to an isotype called IgGs. To illustrate the effects of Fut8 in the class-switching of immunoglobulin, we measured the class-switched (IgGs of different subclasses) and non-switched (IgM) in the sera of Fut8^{+/+} and Fut8^{-/-} mice using mouse mAb isotyping reagents. In 4-week-old Fut8^{-/-} mice, the amounts of IgG₁, IgG_{2a}, IgG_{2b}, and IgG₃ were significantly lower than those in Fut8^{+/+} mice after OVA immunization, while those of IgM were relatively normal (Figure 3C). The cytokines, such as IL-4, IL-5, IL-6, and IFNγ secreted by CD4⁺ T cells, contribute to the different IgG class-switching in the mice and human. It is reasonable to consider that the reduced IgG class-switching attributed to the low levels of cytokines secreted by CD4⁺ T cells in Fut8^{-/-} mice (Table 1). In addition, since the TGF receptor signaling was attenuated in the Fut8^{-/-} mice (19), the IgG₃



class-switching regulated by TGF signaling was also suppressed in the *Fut8*^{-/-} mice.

Loss of Core Fucosylation Impaired the Signal Transduction *via* TCR

T cell receptor signaling is very important for T cell activation. As illustrated in **Figure 4A**, no different expression of TCR was found in the *Fut8*^{+/+}CD4⁺ T and *Fut8*^{-/-}CD4⁺ T cells. Nonetheless, the core fucose of the N-glycans in the molecules was eliminated by a disruption of the *Fut8* (**Figure 4B**). Moreover, the MS spectra of N-glycans released from TCRs were analyzed. It is notable that the high levels of signals were corresponded to the core-fucosylated glycans bearing non-, mono-, or di-galactose in the *Fut8*^{+/+}CD4⁺ T cells, while those were completely disappeared in *Fut8*^{-/-}CD4⁺ T cells (Figure S2 in Supplementary Material). These results further confirmed in mice that TCRs are highly core-fucosylated proteins and contributes to its activities.

In order to examine the role of core fucosylation in the activation of CD4⁺ T cells, we isolated CD4⁺ T cells from *Fut8*^{+/+} and *Fut8*^{-/-} mice, and checked the level of core fucosylation.

FACS analysis showed that core fucosylation on the cellular surfaces was abolished in *Fut8*^{-/-} CD4⁺ T cells (**Figure 4C**). We compared the phosphorylation levels of *Fut8*^{+/+}CD4⁺ T cells with *Fut8*^{-/-}CD4⁺ T cells in response to costimulations with anti-CD3/CD28 Abs. In those comparisons, the levels of pZAP-70 in *Fut8*^{-/-}CD4⁺ T cells were significantly lower than those in *Fut8*^{+/+}CD4⁺ T cells (**Figure 4D**). Moreover, the populations of CD69⁺ cells (activated T cells) in *Fut8*^{-/-}CD4⁺ T cells were lower than those in *Fut8*^{+/+}CD4⁺ T cells following OVA immunization, while these were similar before immunization (**Figure 4E**). Furthermore, cell proliferation of *Fut8*^{-/-}CD4⁺ T cells was significantly reduced in response to the stimulation of anti-CD3/CD28 Abs (**Figure 4F**).

Core Fucosylation Is Essential for TCR-pMHC Conjugates in CD4⁺ T Cell Activation

B cells present antigenic peptide with MHC-II molecule as APCs, and CD4⁺ T cells physiologically recognize a complex of a peptide-loaded MHC-II in T-B cell interaction (18).

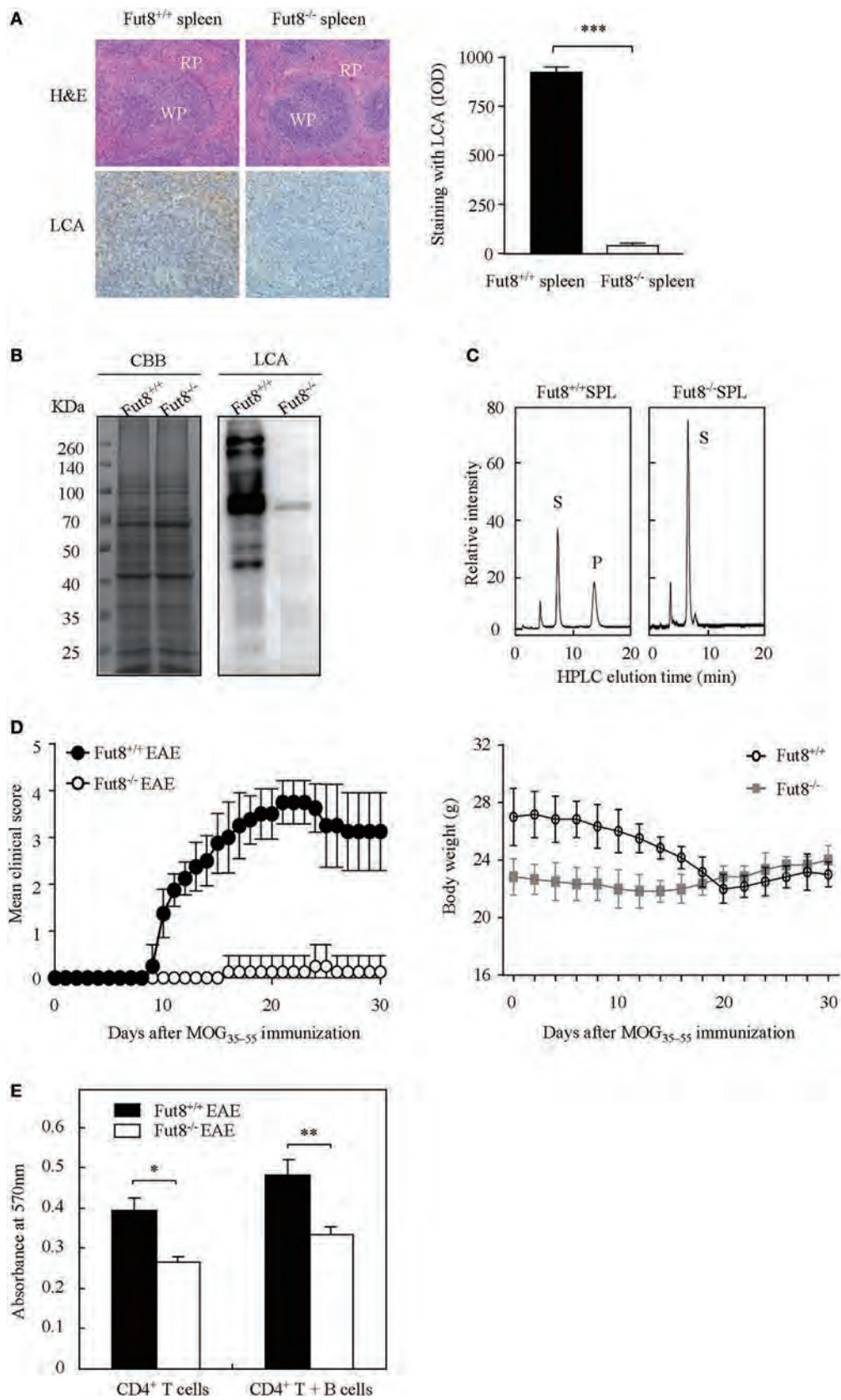
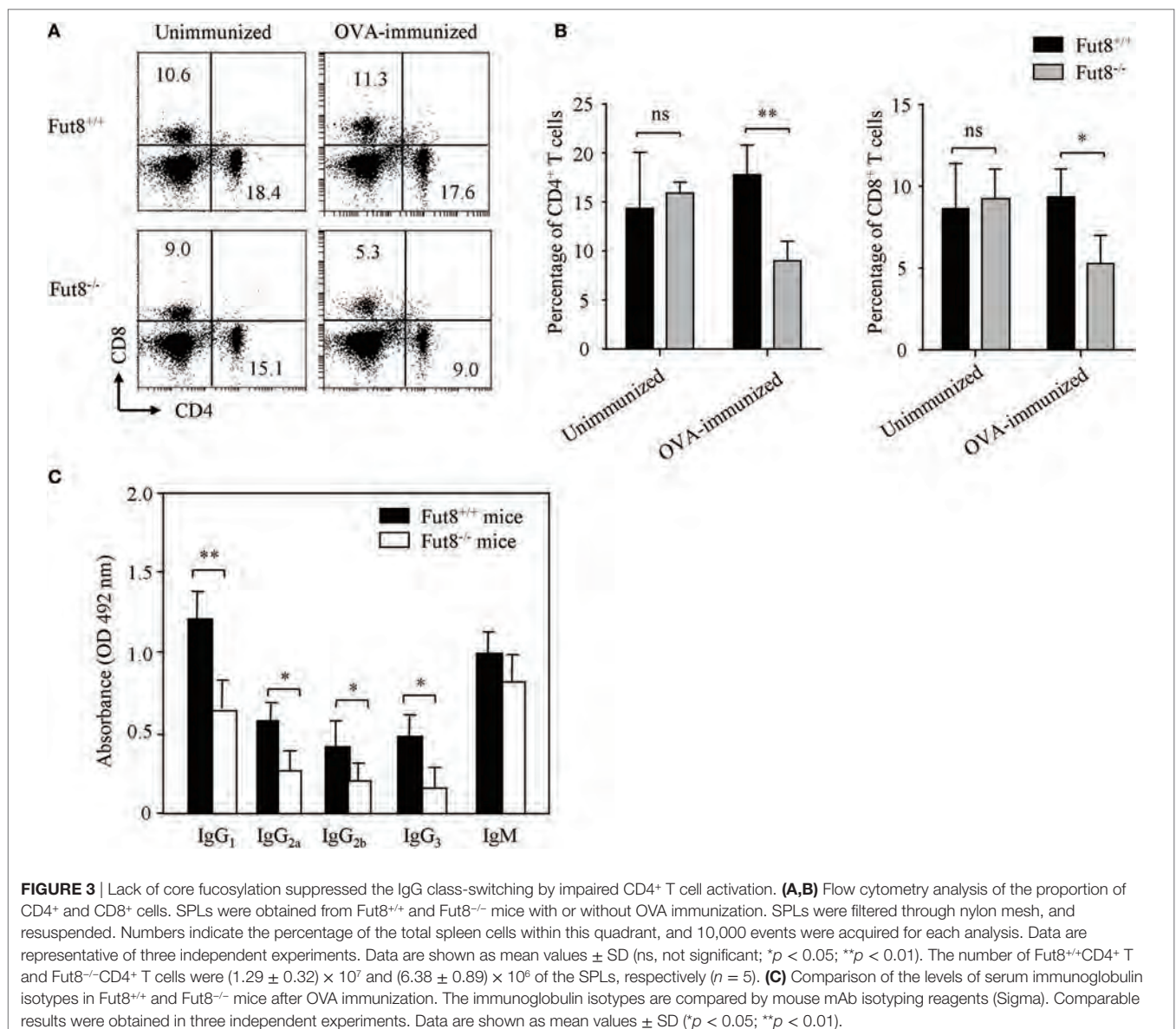


FIGURE 2 | Continued

FIGURE 2 | The experimental autoimmune encephalomyelitis (EAE) model was slightly induced in *Fut8*^{-/-} mice. **(A)** Immunohistochemical analysis of *Fut8*^{+/+} spleen and *Fut8*^{-/-} spleen. The paraffin sections of spleens were deparaffinized and hydrated through a graded series of ethanol to phosphate-buffered saline. One section was assessed by hematoxylin–eosin staining (magnification ×200). RP, red pulp; WP, white pulp. Another section was incubated with biotin-conjugated lens culinaris agglutinin (LCA) (1:200) for 1 h. Finally, the slides were visualized with 3,3'-diaminobenzidine. The staining with LCA was showed by integrated optical density analysis. Data are shown as mean values ± SD (***p* < 0.001). **(B)** Lectin blot of *Fut8*^{+/+} SPL and *Fut8*^{-/-} SPL. The SPL lysates were run on 10% SDS-PAGE gel and stained with Coomassie blue staining and LCA (1:5,000). **(C)** High-performance liquid chromatography (HPLC) analysis of *Fut8* activity. *Fut8* activities were examined using fluorescence-labeled sugar chain, GnGn-Asn-PABA, as an acceptor substrate, as described in Section "Materials and Methods." The substrate (S) and *Fut8* product (P) were eluted at 8 and 15 min, respectively. **(D)** Disease score of mice in *Fut8*^{+/+} and *Fut8*^{-/-} mice EAE model. EAE induction of *Fut8*^{+/+} and *Fut8*^{-/-} mice (*n* = 7). Mice were immunized with 100 μg MOG₃₅₋₅₅ peptide in complete Freund's adjuvant and injected with 200 μg pertussis toxin, and detected the signs of EAE daily for 30 days. Comparable results were obtained in four independent experiments. Body weights of mice were measured every 2 days after EAE induction of *Fut8*^{+/+} and *Fut8*^{-/-} mice (*n* = 7). **(E)** Cell proliferation from EAE mice. Purified splenic CD4⁺ T cells and/or MOG₃₅₋₅₅ peptide-loaded B cells from EAE models were incubated for 48 h at 37°C, and then the cell proliferation was detected by MTT assay. Comparable results were obtained in four independent experiments. Data are shown as mean values ± SD (**p* < 0.05; ***p* < 0.01).



Therefore, we were interested in determining whether core fucosylation is involved in the TCR sensitivity to pMHC-II. To explore the role of core fucosylation on the TCR interaction

with pMHC-II ligands, we crossed *Fut8*^{+/-} mice with OT-II TCR transgenic mice (expressing CD4⁺ TCR specific for OVA₃₂₃₋₃₃₉), and obtained *Fut8*^{+/+}OT-II and *Fut8*^{-/-}OT-II mice. LCA blots

TABLE 1 | Gene expression of Fut8^{-/-} SPLs after OVA immunization.

Gene name	Gene access number	Fold change (Fut8 ^{+/+} /Fut8 ^{-/-})
T-cell activation		
CD3e	NM-007648	2.15
CD4	NM-013488	3.16
CD8	NM-009858	2.51
CD40L	NM-011616	2.17
IL-2R α	NM-008367	3.04
IL-4	NM-021283	2.18
IL-6	NM-031168	2.14
IL-10	NM-010548	2.25
IL-12	NM-008352	3.89
IFN γ	NM-008337	3.08
CXCR4	NM-009911	2.04
CXCL12	NM-001012477	2.07
B-cell activation		
CD79a	NM-007655	3.35
CD81	NM-133655	2.82
Cell signaling		
MAPKKK	NM_009316	2.41
Vav1	NM-011691	3.28
PIK3	NM-001077495	2.36
PKC	NM-008859	2.00
Cyclin D3	NM-001081636	3.84

analysis showed that the core fucosylation level of T and B cells in Fut8^{-/-}OT-II mice (Figure S3 in Supplementary Material). Since MHC-II on the B cell surface can present peptides for recognition and activation of T cells, in this study, B cells were isolated from Fut8^{+/+}OT-II and Fut8^{-/-}OT-II spleen and incubated with monobiotin-labeled OVA₃₂₃₋₃₃₉. Although electron density was seen for the structures of I-A^d covalently linked to an OVA₃₂₃₋₃₃₉, with a single N-glycan (24), the core fucosylation did not affect the peptide presentation abilities of the MHCs between Fut8^{+/+}OT-II and Fut8^{-/-}OT-II B cells (Figure S4 in Supplementary Material). The CD4⁺ T cells were then stimulated with OVA₃₂₃₋₃₃₉ loaded B cells and subsequent T cell priming was investigated. The freshly purified *ex vivo* CD4⁺ T cells were stimulated with the OVA₃₂₃₋₃₃₉-loaded B cells. As shown in **Figure 5A**, compared with Fut8^{+/+}OT-II CD4⁺ T cells, the phosphorylation level of ZAP-70 was dramatically decreased in Fut8^{-/-}OT-II CD4⁺ T cells with stimulation of OVA₃₂₃₋₃₃₉-loaded B cells. Moreover, to remove the cell-surface fucosylation, the Fut8^{+/+}OT-II CD4⁺ T cells were treated with 100 mU Glyko[®] α (1-2,3,4,6) Fucosidase, which can cleaves α 1,6-linked fucose more efficiently than other α -fucose linkages (25). The signaling *via* TCR was significantly suppressed in OT-II CD4⁺ T cells treated with this fucosidase, when the T cells were stimulated with OVA₃₂₃₋₃₃₉-loaded B cells (**Figure 5B**), indicated that the Fut8 inactivation results in the less responsive for TCR stimulation with pMHC-II, despite similar TCR expression levels (**Figure 4A**). Moreover, the population of TCR⁺CD69⁺ cells was significantly reduced in Fut8^{-/-}OT-II CD4⁺ T/OVA₃₂₃₋₃₃₉-loaded B cells compared with Fut8^{+/+}OT-II CD4⁺ T/OVA₃₂₃₋₃₃₉-loaded B cells (**Figure 5C**).

To further determine how Fut8 deficiency affects the T–B cell interactions, the communication of CD4⁺ T cells and B cells was observed by confocal microscopy. OVA₃₂₃₋₃₃₉-loaded MHC-II was

markedly increased at the site of T–B cell contact in Fut8^{+/+}OT-II T cells for 30 min and was ubiquitous on the Fut8^{-/-}OT-II T cell surface (**Figures 5D,E**). Next, T–B cell conjugates were quantitatively analyzed *via* flow cytometry analysis. Few conjugates of T–B cells were observed in the absence of OVA₃₂₃₋₃₃₉ peptide, whereas peptide-pulsed B cells effectively interacted with CD4⁺ T cells. The percentages of T–B cell conjugates in Fut8^{+/+}OT-II and Fut8^{-/-}OT-II MHC-II⁺ TCR β ⁺ cells were 29.4 and 7.4%, respectively (**Figures 5F,G**), indicated that core fucosylation affected the T–B cell interaction. Moreover, the secretion of IL-2 was reduced in the culture media of Fut8^{-/-}OT-II T–B cells compared with Fut8^{+/+}OT-II T–B cells (**Figure 5H**). Furthermore, the T cell proliferation with OVA₃₂₃₋₃₃₉-loaded B cells was analyzed by CFSE dilution methods. Compared to the proliferation of Fut8^{+/+}OT-II CD4⁺ T cells, those of Fut8^{-/-}OT-II CD4⁺ T cells was significantly reduced with the cocultivation of OVA₃₂₃₋₃₃₉-loaded Fut8^{+/+}OT-II B cells (**Figure 5I**). These results indicated that Fut8 deficiency contributes to attenuated T–B cell communication, and follows attenuated T cell activation.

To further elucidate the underlying mechanism of the reduced T–B cell interaction caused by the disruption of Fut8, T and B cell Activation PCR Array was used to compare mRNA expression in Fut8^{+/+} SPLs with that in Fut8^{-/-} SPLs following OVA immunization. As illustrated in **Table 1**, the expression levels of four genes (CD3e, CD4, CD8, and CD40L) associated with TCR complex formation, eight genes (IL-2R α , IL-4, IL-6, IL-10, IL-12, IFN γ , CXCL12, and CXCR4) involved in T cell activation, and two genes (CD79a and CD81) associated with B cell activation, were downregulated in Fut8^{-/-} SPLs. Moreover, the gene expressions of signal molecules such as MAPKKK, Vav1, PIK3, PKC, and Cyclin D3 were downregulated in Fut8^{-/-} SPLs. Since core fucosylation of proteins is an important post-translational process, it is not surprising that many molecules involved in T and B cell activation were downregulated in Fut8^{-/-} SPLs.

DISCUSSION

The glycosylation and Golgi processing pathways have coevolved with the larger regulatory network that controls T cell activation. It is not surprising that changes of glycosylation are linked to AD pathogenesis, such as galactosylation (26, 27) and sialylation (28, 29). The lower levels of sialylated IgG were found in rheumatoid arthritis (RA) and Wegener's granulomatosis patients, and the sialylated IgG was increased in the sera of patients during remission (28, 29). Moreover, loss of galactose residues on IgG, is showed in the sera of RA patients (26, 27). The significant differences of O-glycan on T helper cells were detected in active SLE patients (30). Core-fucosylated glycans that contain bisecting GlcNAc was increased on the IgG of SLE (31). In this study, core fucosylations were associated with SLE severities, and significantly increased in the CD4⁺ T cells of SLE patients. Coincidentally, previous study by Fujii et al. found that the core fucosylation on T cells, required for activation of TCR signaling with anti-CD3/CD28 Abs and induction in colitis, is significantly increased in patients with inflammatory bowel disease (32). Hence, one possible consequence of hyper core

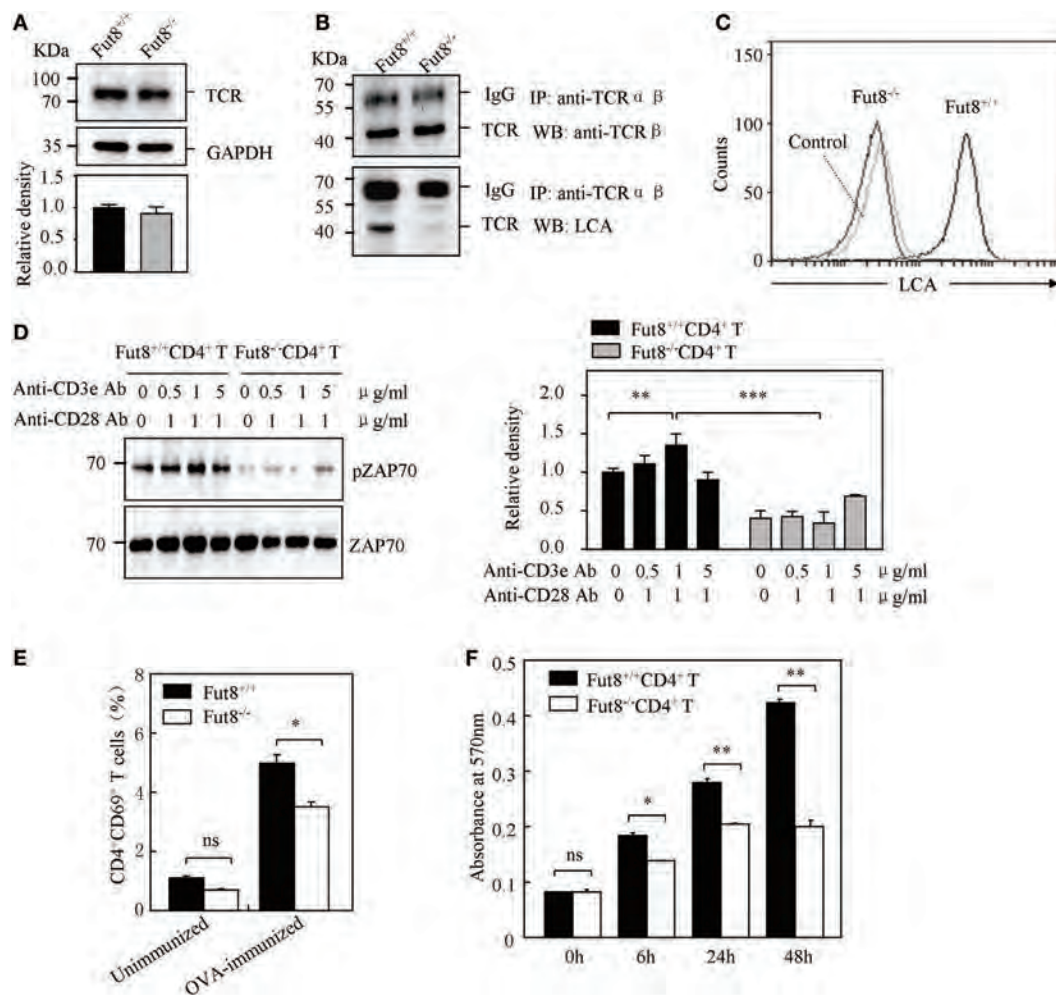


FIGURE 4 | Core fucosylation is required for the activation of CD4⁺ T cells. **(A)** Western blots analysis of T cell receptor (TCR). Whole cell lysates were resolved by SDS-PAGE on a 8% gel, transferred to a PVDF membrane, and probed with anti-TCRβ Ab. Densitometric analysis of the bands of TCRβ normalized against GAPDH. **(B)** Core fucose of N-glycan on TCRβ in *Fut8*^{-/-}CD4⁺ T cells was detected by LCA blot. Whole cell lysates were immunoprecipitated with an anti-TCRαβ antibody. The immunoprecipitates were resolved by SDS-PAGE on a 8% gel, and probed with the LCA and anti-TCRβ Ab. **(C)** Histograms of binding capacity with LCA. Core fucosylation level on the surface proteins of *Fut8*^{+/+}CD4⁺ T and *Fut8*^{-/-}CD4⁺ T cells investigated by FACS analysis. **(D)** Downregulation of phosphorylated Zap70 in *Fut8*^{-/-}CD4⁺ T cells. Purified CD4⁺ T cells were serum-starved and were stimulated with anti-CD3/CD28 Abs for 5 min at 37°C. Cells were lysated in lysis buffer for 15 min on ice. Whole cell lysates were subjected to 10% SDS-PAGE. The blots were probed by anti-pZAP70 Ab and anti-ZAP70 Ab. Densitometric analysis of the bands of pZAP70 normalized against ZAP70. Data are reported as the mean ± SD from three independent experiments (***p* < 0.01; ****p* < 0.001). **(E)** Loss of *Fut8* reduced the CD4⁺CD69⁺ cells populations in the SPL after OVA immunization. SPLs were isolated from OVA-immunized and unimmunized mice (*n* = 5). Cells were stained with anti-CD69 and anti-CD4 Abs, and then detected by FACS. Data are reported as the mean ± SD from three independent experiments (**p* < 0.05; ns, not significant). **(F)** Loss of *Fut8* decreased the proliferation of CD4⁺ T cells. Purified CD4⁺ T cells were stimulated with anti-CD3e Ab-coated microbeads and anti-CD28 Ab for 0, 6, 24, and 48 h at 37°C. The growth rates of CD4⁺ T cell were detected by MTT assay. Data are reported as the mean ± SD from three replicate cultures (**p* < 0.05; ***p* < 0.01). The absorbance related to the formazan dye level was measured with a microplate reader at 570 nm.

fucosylation-induced T cell activation could be the development of SLE. However, the underlying mechanisms of how core fucosylation regulate T cell activation with TCR-pMHC interaction remain unclear.

T cell recognition of pMHC-II ligands on B cells is thought to be carefully coordinated in CD4⁺ T cells. Conformational flexibility is likely responsible for the high degree of promiscuity or cross-reactivity that is evident in the TCR recognition of pMHCs (33–35). There are two models to explain how TCR-pMHC interactions result in T cell activation (36, 37). One

model involves an activation threshold based on the occupancy time of the TCR clustering with pMHCs. The alternative model is that pMHC could induce a specific conformational change of TCR complex and influence the quality of signal transductions *via* TCRs. Since the core fucose of N-glycan is located on the cellular surface of T and B cells, and the core fucosylation could affect the flexibility of N-glycan antenna (38) as well as the conformational stability of proteins (39), it is reasonable to assume that core fucosylation of TCR would affect the geometry and conformation of any TCR-pMHC clusters in the T-B cell

interactions. Based on a previous study in *D. melanogaster* cells, the closeness of the interaction of $C\alpha$ with $C\beta$ is shown by the hydrogen bonds of the core fucose residue (6, 17), suggested

core fucose possibly strengthens association of $C\alpha$ with $C\beta$. A water molecule also bridges the fucose exocyclic oxygen and the side chain of Arg^{150 β} (17). In this scenario, core fucosylation

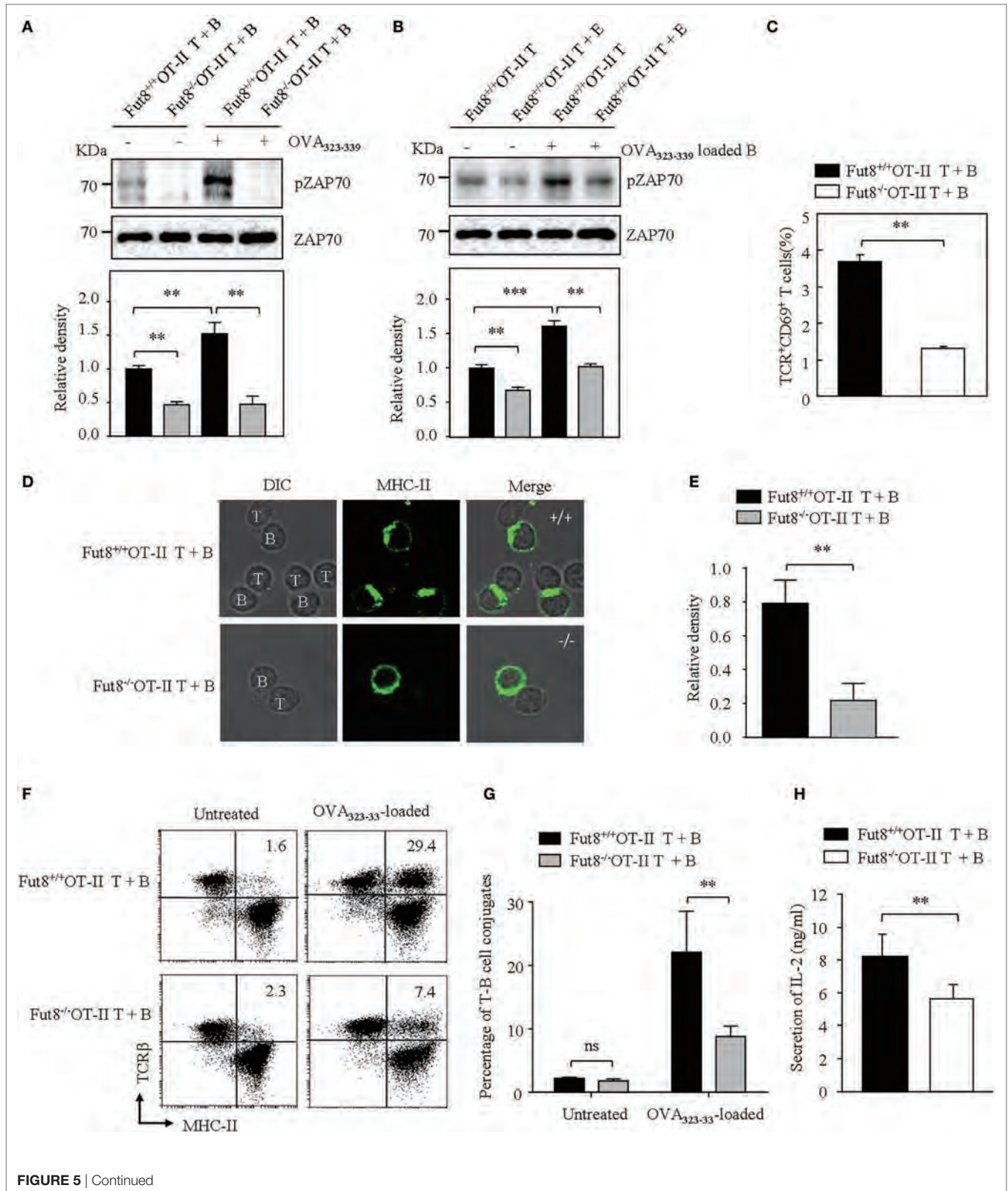
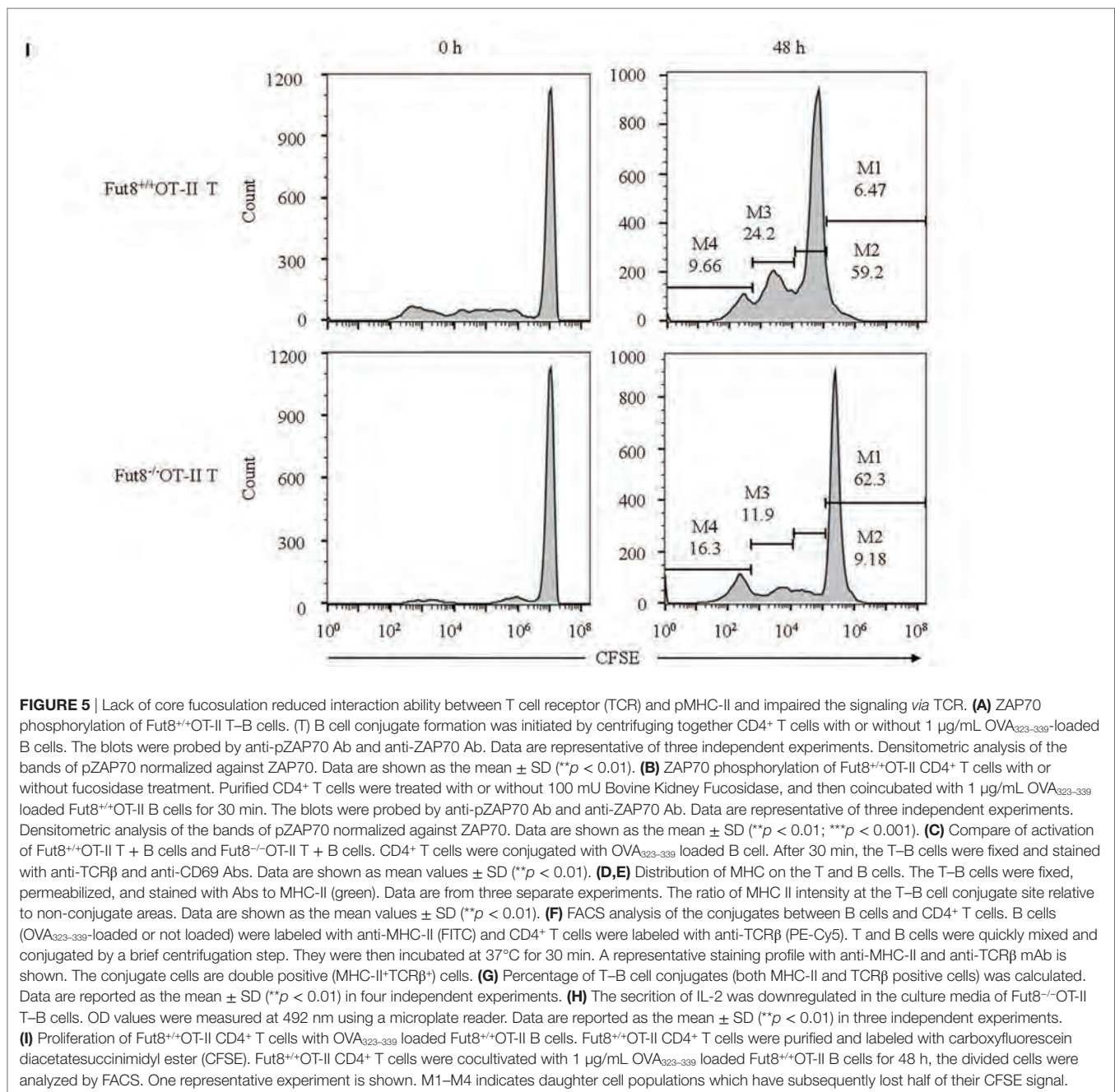


FIGURE 5 | Continued



is expected to provide exciting opportunities to control the TCR function. In the present study, the percentage of T-B cell conjugates (TCR⁺MHC-II⁺) was reduced by a factor of 3.97 (29.4/7.4%) in Fut8^{-/-}OT-II cells, indicated that the core fucosylation has significant functional implications in TCR-pMHC interaction.

Given the intimate relationship between pMHC recognition and TCR signaling, the signaling *via* TCR is also be regulated by glycosylation. It has long been appreciated that Mgat5 deficiency could enhance TCR recruitment to the synapse and results in greater TCR internalization/endocytosis (11). Physiologically,

TCR recognition of pMHC-II ligands on APCs such as dendritic cells and B cells are the most important checkpoint for CD4⁺ T cell activation (40). Engagement of the TCR complexes lead to a signaling cascade of protein tyrosine kinases, such as ZAP70. To explore the role of core fucosylation on the T cell activation, we generated Fut8^{+/+}OT-II and Fut8^{-/-}OT-II mice. Fut8 deficiency results in the attenuated phosphorylation of ZAP70 in Fut8^{-/-}OT-II CD4⁺ T cells with OVA₃₂₃₋₃₃₉-loaded B cells. Also, the phosphorylation of ZAP-70 was significantly reduced in Fut8^{+/+}OT-II CD4⁺ T cells by the treatment of fucosidase. Moreover, in Fut8^{-/-}OT-II cells, the number of CD4⁺ T cells activation (CD69⁺) was decreased

by a factor of 3.5. The proliferation of the Fut8^{-/-}OT-II CD4⁺ T cells cocultivated with OVA_{323–339}-loaded B cells was decreased compared with the Fut8^{+/+}OT-II CD4⁺ T cells. It is conceivable that low T–B cell conjugates was proportional to the decreased T cell activation and proliferation in Fut8^{-/-} CD4⁺ T cells. Core fucosylation is likely to be important in all three proposed stages involved in the T cell activation. First, core fucosylation is essential for the TCR structural formation. Second, core fucosylation of TCR could regulate the recognition of pMHC and affect T cell activation threshold. Third, fucose-specific lectins (41) might participate the events in the T–B cell interaction.

Systemic lupus erythematosus is characterized by the overproduction of auto antibodies, mainly IgG. However, B lymphocyte hyperactivity in SLE is T cell dependent. T cells from SLE patients are activated with a decreased activation threshold and regulated abnormally (32). Indeed, overactive CD4⁺ T cells had been implicated in the pathogenesis of SLE (42). Although we know that CD4⁺ T cell deregulation contributes to SLE pathogenesis, but the mechanism is still largely unknown. Studies in SLE patients and murine models of lupus have shown enhanced level of IL-4 (43), IFN γ (44), and IL-6 (45, 46). Compared to Fut8^{+/+} mice, the IgG class-switching was significantly reduced in the sera of Fut8^{-/-} mice after OVA immunization due to low levels of IL-4, IL-5, IL-6, IFN γ , and TGF secreted by Fut8^{-/-}CD4⁺ T cells. Development of SLE is associated with genetic, hormonal, environmental, and immunological factors, mainly those related to the helper T cell activation. To investigate the mechanisms of the CD4⁺ T cell activation that is important for SLE pathogenesis, we induced the EAE model using Fut8^{+/+} and Fut8^{-/-} mice. Loss of Fut8 reduced CD4⁺ T cell activation and ameliorated the EAE in Fut8^{-/-} mice. Fut8^{-/-} mice are resistant to the induction of EAE, whereas Mgat5^{-/-} mice are hypersensitive to it (47). In this regard, Fut8 and Mgat5 function as opposing regulators of T cell activation thresholds and susceptibility to AD. The hyper core fucosylations are associated with SLE severities, however, whether altered core fucosylation is a consequence or an underlying cause of the SLE cascade remains unclear.

FUT8 is able to modify multiple proteins, followed by the change of their functions. Because the most of immune response molecules are glycoproteins, FUT8 knockdown/knock out affected their function associated with immune response. Okada et al. (10) showed that loss of core fucosylation caused an inhibitory receptor PD-1 deprivation on the cellular surface and augmented T cell activation, when Fut8^{-/-}CD4⁺ T cells transferred

into Rag2^{-/-} mice. Although we did not measure the cell-surface PD-1 expression in the T cell activation and T–B cell interaction, the core fucosylation could regulate the PD-1 expression by modulating TCR signaling strength. Physiologically, there may be some equilibria of the core fucosylation on the TCR and PD-1 to regulate T cell activation. The complexity of *in vivo* condition made us cannot conclude the inability for TCR signaling pathway is the sole reason for the T cell activation, but our study first revealed that Fut8 is essential for TCR–pMHC contact and the following CD4⁺ T cell activation. The balance between specific and degenerate T cell recognition of pMHC-II holds important implications for protective immunity versus autoimmunity. With a better understanding of how core fucosylation regulates of the adaptive immune system, its use in therapy for SLE may prove to be a useful intervention.

ETHICS STATEMENT

All animal work was approved by the Ethics Committee at the Dalian Medical University. The Ethics Committee at the hospital approved the study protocol.

AUTHOR CONTRIBUTIONS

WL, SM, and SS designed research and performed experiment; ML, ZL, and RY analyzed the experimental data; TM, JG, JZ, and NT corrected paper; WL designed research and wrote paper. All authors reviewed the results and approved the final version of the manuscript.

FUNDING

This work was supported by the National Nature Science Foundation of China (31570797, 31270864, 30972675), and Natural Science Foundation of Liaoning Province (2015020253), China.

SUPPLEMENTARY MATERIAL

The Supplementary Material for this article can be found online at <http://www.frontiersin.org/articles/10.3389/fimmu.2018.00078/full#supplementary-material>.

VIDEO S1 | Experimental autoimmune encephalomyelitis symptoms in Fut8^{+/+} mice.

VIDEO S2 | Experimental autoimmune encephalomyelitis symptoms in Fut8^{-/-} mice.

REFERENCES

1. Yin Y, Choi SC, Xu Z, Perry DJ, Seay H, Croker BP, et al. Normalization of CD4⁺ T cell metabolism reverses lupus. *Sci Transl Med* (2015) 7(274):274ra18. doi:10.1126/scitranslmed.aaa0835
2. Rupanagudi KV, Kulkarni OP, Lichtneker J, Darisipudi MN, Mulay SR, Schott B, et al. Cathepsin S inhibition suppresses systemic lupus erythematosus and lupus nephritis because cathepsin S is essential for MHC class II-mediated CD4 T cell and B cell priming. *Ann Rheum Dis* (2015) 74(2):452–63. doi:10.1136/annrheumdis-2013-203717
3. Reinherz EL, Tan K, Tang L, Kern P, Liu J, Xiong Y, et al. The crystal structure of a T cell receptor in complex with peptide and MHC class II. *Science* (1999) 286(5446):1913–21. doi:10.1126/science.286.5446.1913
4. Lee KH, Holdorf AD, Dustin ML, Chan AC, Allen PM, Shaw AS. T cell receptor signaling precedes immunological synapse formation. *Science* (2002) 295(5559):1539–42. doi:10.1126/science.1067710
5. Johnson JL, Jones MB, Ryan SO, Cobb BA. The regulatory power of glycans and their binding partners in immunity. *Trends Immunol* (2013) 34(6):290–8. doi:10.1016/j.it.2013.01.006
6. Rudd PM, Wormald MR, Stanfield RL, Huang M, Mattsson N, Speir JA, et al. Roles for glycosylation of cell surface receptors involved in cellular immune recognition. *J Mol Biol* (1999) 293(2):351–66. doi:10.1006/jmbi.1999.3104
7. Daniels MA, Hogquist KA, Jameson SC. Sweet 'n' sour: the impact of differential glycosylation on T cell responses. *Nat Immunol* (2002) 3(10):903–10. doi:10.1038/ni1002-903

8. Lowe JB. Glycosylation, immunity, and autoimmunity. *Cell* (2001) 104(6): 809–12. doi:10.1016/S0092-8674(01)00277-X
9. Rudd PM, Elliott T, Cresswell P, Wilson IA, Dwek RA. Glycosylation and the immune system. *Science* (2001) 291(5512):2370–6. doi:10.1126/science.291.5512.2370
10. Okada M, Chikuma S, Kondo T, Hibino S, Machiyama H, Yokosuka T, et al. Blockage of core fucosylation reduces cell-surface expression of PD-1 and promotes anti-tumor immune responses of T cells. *Cell Rep* (2017) 20(5):1017–28. doi:10.1016/j.celrep.2017.07.027
11. Demetriou M, Granovsky M, Quaggin S, Dennis JW. Negative regulation of T-cell activation and autoimmunity by Mgat5 N-glycosylation. *Nature* (2001) 409(6821):733–9. doi:10.1038/35055582
12. Lau KS, Partridge EA, Grigorian A, Silvescu CI, Reinhold VN, Demetriou M, et al. Complex N-glycan number and degree of branching cooperate to regulate cell proliferation and differentiation. *Cell* (2007) 129(1):123–34. doi:10.1016/j.cell.2007.01.049
13. Starr TK, Daniels MA, Lucido MM, Jameson SC, Hogquist KA. Thymocyte sensitivity and supramolecular activation cluster formation are developmentally regulated: a partial role for sialylation. *J Immunol* (2003) 171(9):4512–20. doi:10.4049/jimmunol.171.9.4512
14. Moore GT, Brown SJ, Winterhalter AC, Lust M, Salvaris EJ, Selan C, et al. Glycosylation changes in hFUT1 transgenic mice increase TCR signaling and apoptosis resulting in thymocyte maturation arrest. *Mol Immunol* (2008) 45(8):2401–10. doi:10.1016/j.molimm.2007.11.006
15. Kuball J, Hauptrock B, Malina V, Antunes E, Voss RH, Wolf M, et al. Increasing functional avidity of TCR-redirected T cells by removing defined N-glycosylation sites in the TCR constant domain. *J Exp Med* (2009) 206(2):463–75. doi:10.1084/jem.20082487
16. Calderon AD, Liu Y, Li X, Wang X, Chen X, Li L, et al. Substrate specificity of FUT8 and chemoenzymatic synthesis of core-fucosylated asymmetric N-glycans. *Org Biomol Chem* (2016) 14(17):4027–31. doi:10.1039/c6ob00586a
17. Garcia KC, Degano M, Stanfield RL, Brunmark A, Jackson MR, Peterson PA, et al. An alpha T cell receptor structure at 2.5 Å and its orientation in the TCR-MHC complex. *Science* (1996) 274(5285):209–19. doi:10.1126/science.274.5285.209
18. Batista FD, Harwood NE. The who, how and where of antigen presentation to B cells. *Nat Rev Immunol* (2009) 9(1):15–27. doi:10.1038/nri2454
19. Wang X, Inoue S, Gu J, Miyoshi E, Noda K, Li W, et al. Dysregulation of TGF-beta1 receptor activation leads to abnormal lung development and emphysema-like phenotype in core fucose-deficient mice. *Proc Natl Acad Sci U S A* (2005) 102(44):15791–6. doi:10.1073/pnas.0507375102
20. Uozumi N, Teshima T, Yamamoto T, Nishikawa A, Gao YE, Miyoshi E, et al. A fluorescent assay method for GDP-L-Fuc:N-acetyl-beta-D-glucosaminide alpha 1-6fucosyltransferase activity, involving high performance liquid chromatography. *J Biochem* (1996) 120(2):385–92. doi:10.1093/oxfordjournals.jbchem.a021424
21. Watson AR, Lee WT. Differences in signaling molecule organization between naive and memory CD4+ T lymphocytes. *J Immunol* (2004) 173(1):33–41. doi:10.4049/jimmunol.173.1.33
22. Tateno H, Nakamura-Tsuruta S, Hirabayashi J. Comparative analysis of core-fucose-binding lectins from *Lens culinaris* and *Pisum sativum* using frontal affinity chromatography. *Glycobiology* (2009) 19(5):527–36. doi:10.1093/glycob/cwp016
23. Mao L, Hou H, Wu S, Zhou Y, Wang J, Yu J, et al. TIGIT signalling pathway negatively regulates CD4+ T-cell responses in systemic lupus erythematosus. *Immunology* (2017) 151(3):280–90. doi:10.1111/imm.12715
24. Scott CA, Peterson PA, Teyton L, Wilson IA. Crystal structures of two I-Ad-peptide complexes reveal that high affinity can be achieved without large anchor residues. *Immunity* (1998) 8(3):319–29. doi:10.1016/S1074-7613(00)80537-3
25. O'Flaherty R, Harbison AM, Hanley PJ, Taron CH, Fadda E, Rudd PM. Aminoquinoline fluorescent labels obstruct efficient removal of N-glycan core alpha(1-6) fucose by bovine kidney alpha(1)-fucosidase (BKF). *J Proteome Res* (2017) 16(11):4237–43. doi:10.1021/acs.jproteome.7b00580
26. Parekh RB, Roitt IM, Isenberg DA, Dwek RA, Ansell BM, Rademacher TW. Galactosylation of IgG associated oligosaccharides: reduction in patients with adult and juvenile onset rheumatoid arthritis and relation to disease activity. *Lancet* (1988) 1(8592):966–9. doi:10.1016/S0140-6736(88)91781-3
27. Ercan A, Cui J, Chatterton DE, Deane KD, Hazen MM, Brintnell W, et al. Aberrant IgG galactosylation precedes disease onset, correlates with disease activity, and is prevalent in autoantibodies in rheumatoid arthritis. *Arthritis Rheum* (2010) 62(8):2239–48. doi:10.1002/art.27533
28. Matsumoto A, Shikata K, Takeuchi F, Kojima N, Mizuochi T. Autoantibody activity of IgG rheumatoid factor increases with decreasing levels of galactosylation and sialylation. *J Biochem* (2000) 128(4):621–8. doi:10.1093/oxfordjournals.jbchem.a022794
29. Espy C, Morelle W, Kaviani N, Grange P, Goulvestre C, Viallon V, et al. Sialylation levels of anti-proteinase 3 antibodies are associated with the activity of granulomatosis with polyangiitis (Wegener's). *Arthritis Rheum* (2011) 63(7):2105–15. doi:10.1002/art.30362
30. Ramos-Martinez E, Lascunari R, Tenorio EP, Sanchez-Gonzalez A, Chavez-Rueda K, Chavez-Sanchez L, et al. Differential expression of O-glycans in CD4(+) T lymphocytes from patients with systemic lupus erythematosus. *Tohoku J Exp Med* (2016) 240(1):79–89. doi:10.1620/tjem.240.79
31. Vuckovic F, Kristic J, Gudelj I, Teruel M, Keser T, Pezer M, et al. Association of systemic lupus erythematosus with decreased immunosuppressive potential of the IgG glycome. *Arthritis Rheumatol* (2015) 67(11):2978–89. doi:10.1002/art.39273
32. Fujii H, Shinzaki S, Iijima H, Wakamatsu K, Iwamoto C, Sobajima T, et al. Core fucosylation on T cells, required for activation of T-cell receptor signaling and induction of colitis in mice, is increased in patients with inflammatory bowel disease. *Gastroenterology* (2016) 150(7):1620–32. doi:10.1053/j.gastro.2016.03.002
33. Alarcon B, Gil D, Delgado P, Schamel WW. Initiation of TCR signaling: regulation within CD3 dimers. *Immunol Rev* (2003) 191:38–46. doi:10.1034/j.1600-065X.2003.00017.x
34. Mason D. A very high level of crossreactivity is an essential feature of the T-cell receptor. *Immunol Today* (1998) 19(9):395–404. doi:10.1016/S0167-5699(98)01299-7
35. Kass I, Buckle AM, Borg NA. Understanding the structural dynamics of TCR-pMHC complex interactions. *Trends Immunol* (2014) 35(12):604–12. doi:10.1016/j.it.2014.10.005
36. Alam SM, Davies GM, Lin CM, Zal T, Nasholds W, Jameson SC, et al. Qualitative and quantitative differences in T cell receptor binding of agonist and antagonist ligands. *Immunity* (1999) 10(2):227–37. doi:10.1016/S1074-7613(00)80023-0
37. Schamel WW, Arechaga I, Risueno RM, van Santen HM, Cabezas P, Risco C, et al. Coexistence of multivalent and monovalent TCRs explains high sensitivity and wide range of response. *J Exp Med* (2005) 202(4):493–503. doi:10.1084/jem.20042155
38. Stubbs HJ, Lih JJ, Gustafson TL, Rice KG. Influence of core fucosylation on the flexibility of a biantennary N-linked oligosaccharide. *Biochemistry* (1996) 35(3):937–47. doi:10.1021/bi9513719
39. Wormald MR, Dwek RA. Glycoproteins: glycan presentation and protein-fold stability. *Structure* (1999) 7(7):R155–60. doi:10.1016/S0969-2126(99)80095-1
40. Wolfert NA, Boons GJ. Adaptive immune activation: glycosylation does matter. *Nat Chem Biol* (2013) 9(12):776–84. doi:10.1038/nchembio.1403
41. Lehrman MA, Hill RL. The binding of fucose-containing glycoproteins by hepatic lectins. Purification of a fucose-binding lectin from rat liver. *J Biol Chem* (1986) 261(16):7419–25.
42. Moulton VR, Tsokos GC. T cell signaling abnormalities contribute to aberrant immune cell function and autoimmunity. *J Clin Invest* (2015) 125(6):2220–7. doi:10.1172/jci78087
43. Mi XB, Zeng FQ. Hypomethylation of interleukin-4 and -6 promoters in T cells from systemic lupus erythematosus patients. *Acta Pharmacol Sin* (2008) 29(1):105–12. doi:10.1111/j.1745-7254.2008.00739.x
44. Gerez L, Shkolnik T, Hirschmann O, Lorber M, Arad G, Kaempfer R. Hyperinducible expression of the interferon-gamma (IFN-gamma) gene and its suppression in systemic lupus erythematosus (SLE). *Clin Exp Immunol* (1997) 109(2):296–303. doi:10.1046/j.1365-2249.1997.4471345.x
45. Linker-Israeli M, Deans RJ, Wallace DJ, Prehn J, Ozeri-Chen T, Klinenberg JR. Elevated levels of endogenous IL-6 in systemic lupus erythematosus. A putative role in pathogenesis. *J Immunol* (1991) 147(1):117–23.
46. Grondal G, Gunnarsson I, Ronnelid J, Rogberg S, Klareskog L, Lundberg I. Cytokine production, serum levels and disease activity in systemic lupus erythematosus. *Clin Exp Rheumatol* (2000) 18(5):565–70.

47. Grigorian A, Lee SU, Tian W, Chen IJ, Gao G, Mendelsohn R, et al. Control of T cell-mediated autoimmunity by metabolite flux to N-glycan biosynthesis. *J Biol Chem* (2007) 282(27):20027–35. doi:10.1074/jbc.M701890200

Conflict of Interest Statement: The authors declare that the research was conducted in the absence of any commercial or financial relationships that could be construed as a potential conflict of interest.

Copyright © 2018 Liang, Mao, Sun, Li, Li, Yu, Ma, Gu, Zhang, Taniguchi and Li. This is an open-access article distributed under the terms of the Creative Commons Attribution License (CC BY). The use, distribution or reproduction in other forums is permitted, provided the original author(s) and the copyright owner are credited and that the original publication in this journal is cited, in accordance with accepted academic practice. No use, distribution or reproduction is permitted which does not comply with these terms.

β 4-Integrin/PI3K Signaling Promotes Tumor Progression through the Galectin-3-*N*-Glycan Complex

Yukiko Kariya¹, Midori Oyama¹, Yasuhiro Hashimoto¹, Jianguo Gu², and Yoshinobu Kariya¹



Abstract

Malignant transformation is associated with aberrant *N*-glycosylation, but the role of protein *N*-glycosylation in cancer progression remains poorly defined. β 4-integrin is a major carrier of *N*-glycans and is associated with poor prognosis, tumorigenesis, and metastasis. Here, *N*-glycosylation of β 4-integrin contributes to the activation of signaling pathways that promote β 4-dependent tumor development and progression. Increased expression of β 1,6GlcNAc-branched *N*-glycans was found to be colocalized with β 4-integrin in human cutaneous squamous cell carcinoma tissues, and that the β 1,6GlcNAc residue was abundant on β 4-integrin in transformed keratinocytes. Interruption of β 1,6GlcNAc-branching formation on β 4-integrin with the introduction of bisecting GlcNAc by *N*-acetylglucosaminyltransferase III overexpression was correlated with suppression of cancer cell migration and tumorigenesis. *N*-Glycan deletion on β 4-integrin impaired β 4-dependent cancer cell migration, invasion, and growth *in vitro* and diminished tumorigenesis and proliferation *in vivo*. The reduced abilities of β 4-integrin were accompanied

with decreased phosphoinositol-3 kinase (PI3K)/Akt signals and were restored by the overexpression of the constitutively active p110 PI3K subunit. Binding of galectin-3 to β 4-integrin via β 1,6GlcNAc-branched *N*-glycans promoted β 4-integrin-mediated cancer cell adhesion and migration. In contrast, a neutralizing antibody against galectin-3 attenuated β 4-integrin *N*-glycan-mediated PI3K activation and inhibited the ability of β 4-integrin to promote cell motility. Furthermore, galectin-3 knockdown by shRNA suppressed β 4-integrin *N*-glycan-mediated tumorigenesis. These findings provide a novel role for *N*-glycosylation of β 4-integrin in tumor development and progression, and the regulatory mechanism for β 4-integrin/PI3K signaling via the galectin-3-*N*-glycan complex.

Implications: *N*-Glycosylation of β 4-integrin plays a functional role in promoting tumor development and progression through PI3K activation via the galectin-3-*N*-glycan complex. *Mol Cancer Res*; 16(6); 1024–34. ©2018 AACR.

Introduction

Integrins are a large family of heterodimeric transmembrane receptors comprising α and β subunits. The extracellular domains of integrin subunits bind to extracellular matrix proteins, such as collagen, fibronectin, and laminin, and the cytoplasmic domains interact with the actin cytoskeleton and signaling molecules. The interaction of integrin with its ligand can activate intracellular signaling and reorganize the actin cytoskeleton (1). Such integrin signaling regulates various cellular functions, such as cell adhesion, migration, and proliferation, not only in normal tissues but also in tumor tissues (1, 2).

The α 6 β 4-integrin (referred to herein as β 4-integrin because the β 4 subunit only pairs with the α 6 subunit) is a receptor for

laminin-332 and is an essential component of the hemidesmosome, an anchoring structure in the basal membrane of stratified epithelial cells (2, 3). In contrast to such a static role in normal epithelial cells, β 4-integrin was originally identified as a tumor-associated antigen (4, 5). β 4-integrin overexpression was found in several types of metastatic cancers, which correlates with poor prognosis and reduced survival (6, 7). Recent studies have shown that β 4-integrin is required for tumorigenesis in several *in vivo* mouse models (8–10). In addition, β 4-integrin promotes cell motility, invasion, and proliferation through activation of the phosphoinositol-3-kinase (PI3K) and ERK pathways (10–14).

Glycosylation is the most common posttranscriptional modification of proteins, and it modulates the folding, stability, and function of glycoproteins (15). Malignant transformation is associated with aberrant glycosylation of cell surface proteins, and the structural change of glycans is mainly due to the altered activity and expression of multiple glycosyltransferases in cancer cells. In addition, some glycans are used as tumor markers for cancer diagnosis (16). Overexpression of β 1,6GlcNAc-branched *N*-glycans, which is due to increased activity of *N*-acetylglucosaminyltransferase V (GnT-V; Fig. 1A), is often found in tumor tissues, and the increase in β 1,6GlcNAc-branched *N*-glycans is directly associated with malignancy and poor prognosis (17, 18). GnT-V knockout mice exhibit reduced mammary tumor growth and metastasis induced by the polyomavirus middle T oncogene (19). Furthermore, introduction of bisecting GlcNAc residues catalyzed

¹Department of Biochemistry, Fukushima Medical University School of Medicine, Fukushima, Japan. ²Division of Regulatory Glycobiology, Institute of Molecular Biomembrane and Glycobiology, Tohoku Medical and Pharmaceutical University, Miyagi, Japan.

Note: Supplementary data for this article are available at Molecular Cancer Research Online (<http://mcr.aacrjournals.org/>).

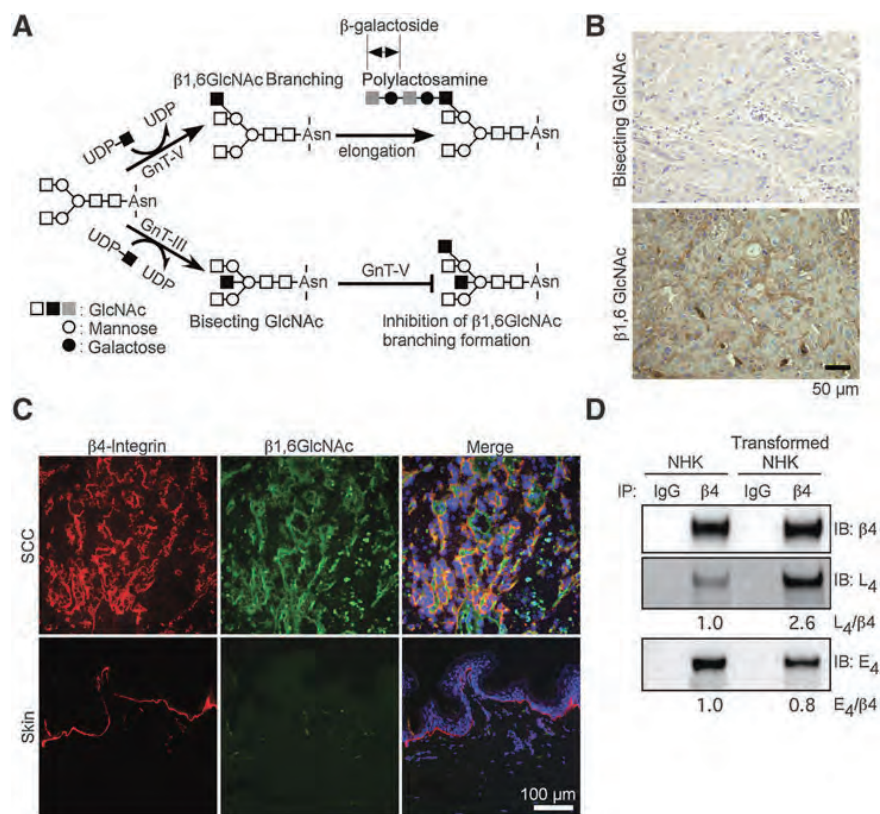
Corresponding Author: Yoshinobu Kariya, Fukushima Medical University School of Medicine, 1 Hikarigaoka, Fukushima City, Fukushima 960-1295, Japan. Phone: 81-24-547-1144; Fax: 81-24-548-8641; E-mail: kariya@fmu.ac.jp

doi: 10.1158/1541-7786.MCR-17-0365

©2018 American Association for Cancer Research.

Figure 1.

Increased expression of β 1,6GlcNAc residues on β 4-integrin in human carcinoma cells. **A**, Glycosylation reactions catalyzed by glycosyltransferases, GnT-III and GnT-V. β 1,6GlcNAc-branched *N*-glycans can be preferentially modified by poly-lactosamine *N*-glycan containing β -galactoside. Bisecting GlcNAc *N*-glycans inhibit β 1,6GlcNAc-branching formation catalyzed by GnT-V. **B**, Immunohistochemical analysis of bisecting GlcNAc and β 1,6GlcNAc expression in human cutaneous SCC using E_4 -PHA and L_4 -PHA lectins. **C**, Immunofluorescence microscopic analysis of β 4-integrin (red) and β 1,6GlcNAc (L_4 -PHA, green) in paraffin-embedded sections of human cutaneous SCC. Merged images are shown with nuclear Hoechst staining (blue). Normal human skin was stained as comparison. **D**, Western blot analysis of β 4-integrin immunoprecipitates from normal human keratinocytes (NHK) and Ras/I κ B-transformed NHK (transformed NHK) with L_4 -PHA and E_4 -PHA lectins, and anti- β 4-integrin polyclonal antibody. Results of the densitometric analysis are shown as the integrated density of lectin-recognized β 4 to total β 4 bands, which was 1.0 for NHK cells.



by *N*-acetylglucosaminyltransferase III (GnT-III) into *N*-glycans, which can disturb further processing and elongation of *N*-glycans, such as the formation of β 1,6GlcNAc-branched structures (Fig. 1A), suppresses cell migration and cancer metastasis (20).

β 1,6GlcNAc-branched *N*-glycans are often further modified by additional sugars to form poly-*N*-acetyl-lactosamine (poly-lactosamine) for the elongation of *N*-glycans consisting of β -galactoside sugars (Fig. 1A). This poly-lactosamine structure is a preferred ligand for one of the galectin isoforms, galectin-3 (21). Galectin-3 is widely expressed in epithelial and immune cells, and its expression is associated with cancer aggressiveness and metastasis (22–24). Cross-linking between glycoproteins by the binding of galectin-3 to poly-lactosamine on proteins regulates diverse cellular functions in cancer cells (25–27). We previously reported that *N*-glycosylation of β 4-integrin plays a crucial role in cell adhesion, migration, and galectin-3 binding in human keratinocyte cells (28). However, the contribution of *N*-glycosylation of β 4-integrin to tumor progression remains poorly defined. In the present study, we investigated the contribution of *N*-glycosylation to β 4-integrin-dependent tumor progression.

Materials and Methods

Antibodies and reagents

The following antibodies were used in this study: rat monoclonal antibodies specific for galectin-3 (M3/38; #sc-2393; Santa Cruz Biotechnology), α 6-integrin (GoH3; #sc-19622; Santa Cruz

Biotechnology), and β 4-integrin (439-9B; #555719; BD Transduction Laboratories); rabbit polyclonal antibodies against human β 4-integrin (H101; #sc-9090; Santa Cruz Biotechnology), phospho-Akt (pSer473; #9271; Cell Signaling Technology), and Akt (#9272; Cell Signaling Technology); and mouse monoclonal antibodies against Ki-67 (#610968; BD Transduction Laboratories), and β 4-integrin (3E1; #MAB1964; Merck Millipore). Alexa Fluor 488-conjugated leucoagglutinating phytohemagglutinin (L_4 -PHA; #L-11270), Alexa Fluor 546-conjugated goat anti-rabbit IgG secondary antibody (#A11035) and Alexa Fluor 546-conjugated goat anti-rat IgG secondary antibody (#A11081) were purchased from Thermo Fisher Scientific. Biotinylated L_4 -PHA (#B-1115) was obtained from Vector Laboratories. Hoechst 33342 (#382065) was obtained from Merck Millipore. Biotinylated erythroagglutinating phytohemagglutinin (E_4 -PHA; #300425) and biotinylated *Sambucus sieboldiana* agglutinin (SSA; #300442) were purchased from J-OIL MILLS. Purified human laminin-332 and galectin-3 were prepared as described previously (27, 29).

Cell culture

The human cancer MDA-MB435S cell line, which lacks β 4-integrin, was purchased from the American Type Culture Collection. Modified human 293 phoenix cells were received as a gift from Dr. M. Peter Marinkovich (Stanford University, Stanford, CA). The human epidermoid carcinoma cell line A431 (RCB0202) was provided by the RIKEN BRC through the National Bio-Resource Project of the MEXT, Japan. These cells

Kariya et al.

were cultured in DMEM supplemented with 10% FBS, penicillin and streptomycin sulfate at 37°C in a humidified 5% CO₂ incubator. Primary human keratinocytes isolated from normal skin (NHK) and Ras/IκB-transformed NHK (a gift from Dr. M. Peter Marinkovich; ref. 8) were cultured in a 50:50 mixture of defined keratinocyte serum-free medium (#10744-019; Life Technologies) and medium 154 (#M-154-500; Life Technologies) with human keratinocyte growth supplement (#S-001-5; Life Technologies) containing penicillin and streptomycin sulfate at 37°C in a humidified 5% CO₂ incubator. All cells were passaged fewer than 6 months after purchasing or receiving them for all the experiments and tested for *mycoplasma* contamination.

Immunohistochemistry/immunofluorescence

Human formalin-fixed paraffin-embedded sections were purchased from BioChain and US Biomax. Specimens were deparaffinized, rehydrated, and immersed in 0.3% hydrogen peroxidase-containing methanol for 20 minutes at room temperature to inactivate the intrinsic peroxidase. After blocking with 5% skim milk for 1 hour at room temperature, the sections were incubated with each biotinylated lectin overnight at 4°C, followed by peroxidase-labeled streptavidin (#426061; Nichirei Corp.) and 3,3'-diaminobenzidine detection using the Histofine DAB substrate kit (#425011; Nichirei Corp.). The slides were then counterstained with Mayer's hematoxylin solution (#131-09665; Wako). Images were obtained using a PROVIS AX-80 microscope (Olympus). For immunofluorescent staining, sections were deparaffinized, rehydrated, and treated with 0.05% protease XXIV in 50 mmol/L Tris-HCl (pH 7.5) for 20 minutes at room temperature. After blocking with 2% BSA in PBS for 1 hour at room temperature, the sections were visualized using a β4-integrin antibody (H101) and Alexa Fluor 488-conjugated L₄-PHA. Fluorescence images were obtained using an IX71 fluorescent microscope (Olympus). Lectin reactivity and β4-integrin expression were assessed as follows: positive, ≥10% positive tumor cells; negative, <10% positive tumor cells. For cross-linking inhibitory assay, glass-bottom dishes (#3971-035; IWAKI) were coated with laminin-332 proteins and blocked with 1% BSA in PBS. Cells (5 × 10⁴ cells) were incubated in serum-free medium in the presence of IgG or a functional blocking antibody against galectin-3 for 20 minutes. Then, the cells were plated to the glass-bottom dish and incubated for 1.5 hours at 37°C in a humidified 5% CO₂ incubator. The cells were fixed with 4% (w/v) paraformaldehyde in PBS for 10 minutes and blocked with 2% BSA in PBS for 1 hour at room temperature. The fixed cells were stained with a β4-integrin antibody (H101) and Alexa Fluor 488-conjugated anti-rabbit IgG antibody. Fluorescence images were obtained using an A1 confocal microscope (Nikon).

Preparation of cell lysates and immunoprecipitation

Cell lysates were prepared as follows. The cells were washed twice with cold PBS and then lysed with a lysis buffer [1% Triton X-100, 20 mmol/L Tris-HCl (pH 7.4), 150 mmol/L NaCl, 5 mmol/L EDTA] containing a protease inhibitor cocktail (#25955; Nacalai tesque) and a phosphatase inhibitor cocktail (#07575; Nacalai tesque). After incubation for 10 minutes on ice, the cell lysates were clarified by centrifugation at 15,000 rpm for 10 minutes at 4°C. The resulting supernatant was used in the following experi-

ments. The protein concentration was determined using a protein assay kit (#29449-44; Nacalai tesque). For immunoprecipitation, the primary antibody was added to the supernatant and rotated for 2 hours at 4°C. Then, protein G-Sepharose was added, followed by 3 hours of incubation at 4°C. Immunoprecipitates were washed five times with a washing buffer [50 mmol/L Tris-HCl (pH 7.5), 150 mmol/L NaCl, 2 mmol/L EDTA, 0.2% NP40 (v/v)], suspended in a reducing sample buffer, and heated at 95°C for 5 minutes.

Western blot analyses

Protein samples were resolved by SDS-PAGE under reducing conditions and then transferred to nitrocellulose membranes. The blots were probed with each specific antibody or biotinylated lectin. Immunoreactive bands were detected using an ImmunoStar Zeta (#297-72403; WAKO) or Trident femto-ECL (#GTX14698; GeneTex). Band intensity was calculated using NIH ImageJ software.

Expression vectors

Retroviral expression vectors encoding β4-integrin were prepared as previously described (28). Retroviral expression vector encoding active PI3K p110-CAAX was received as a gift from Dr. M. Peter Marinkovich. The cDNA encoding human GnT-III was amplified by PCR using a specific primer set and KOD Plus polymerase (#KOD-201; TOYOBO) for cloning into pENTR-D-TOPO (#K2400-20; Life Technologies) for the Gateway Conversion System according to the manufacturer's instructions. The final construct was recombined from pENTR-D-TOPO to the LZRS blast retroviral vector, including a Gateway cassette, using the LR clonase II Enzyme mix (#11791-020; Life Technologies) by a recombination reaction. The cDNA sequence was verified by sequencing.

Retrovirus infection

Retrovirus vectors were transfected into 293 phoenix cells using FuGENE6 transfection reagent (#11814443001; Roche). After transfection, cells were selected with 5 μg/mL puromycin (#P8833; Sigma-Aldrich). The retrovirus was then produced in 293 phoenix cells. One day before infection, 4 × 10⁵ cells were plated in 6-well plates. After incubation with 5 μg/mL polybrene (#10768-9; Sigma-Aldrich) for 15 minutes, media were exchanged to 3 mL retroviral supernatant and another 5 μg/mL polybrene was added. Plates were centrifuged at 1,200 rpm for 1 hour at 32°C using a Hitachi CR22N centrifuge machine. After centrifuge, the retroviral supernatant was replaced with growth medium and the cells were maintained. To establish a cell line, cells were selected with 5 μg/mL blasticidin S (#203350; Calbiochem).

Flow cytometry analysis

Cells were detached from a 10-cm dish using trypsin with 1 mmol/L EDTA. After quenching trypsinization with a medium that contained 10% FBS, the cells were washed twice with PBS that contained 1 mmol/L EDTA and incubated with a primary antibody or control IgG on ice for 30 minutes. The cells were then washed thrice with PBS that contained 1 mmol/L EDTA, followed by incubation for 15 minutes with the appropriate Alexa Fluor-conjugated secondary antibodies. After washing thrice with PBS containing 1 mmol/L EDTA, the cells were analyzed by flow

cytometry using a FACSCalibur and a CellQuest software program (BD Biosciences).

Cell migration assay

Cell migration was assayed using a 24-well chemotaxis chamber (BD Falcon cell culture companion plates; #353504 and 8.0- μ m insets; #353097; BD Biosciences). Two hundred microliters of 2.5×10^5 cells/mL (5×10^4 cells in serum-free DMEM) was inoculated into each upper well of a 24-well chemotaxis chamber, and 750 μ L of 10% FBS containing DMEM was placed in the bottom chamber to act as a chemoattractant. After incubating for 22 hours, the cells on the upper side of the membrane were removed with a cotton swab, and the cells on the lower side of the membrane were fixed with 4% paraformaldehyde and stained with 0.5% crystal violet in 20% methanol. Random fields were photographed using a phase contrast microscope and the number of migrated cells was counted.

In vivo tumorigenicity assay

All animal studies were performed in accordance with protocols approved by the Fukushima Medical University Animal Care and Use Committee. MDA-MB435S transfectants (1×10^6 cells/mouse) were injected subcutaneously along with Matrigel (#354234; BD Biosciences) into 6-week-old female nude mice. Tumor volume was measured weekly for a total of 6 weeks. Proliferating cells in 5- μ m frozen sections were detected with Ki-67 immunofluorescent staining. Proliferation was quantified as the ratio of Ki-67 staining to total nuclear staining.

Cell adhesion assay

Cell adhesion assays were performed as described previously (29). In brief, the wells of a 96-well ELISA plate (#3590; Corning) were coated with 50 μ L of indicated concentration of laminin-332 proteins and blocked with 1% BSA in PBS. Cell suspensions in serum-free medium were plated to each well (5×10^4 cells/well) and incubated at 37°C for 20 minutes in a 5% CO₂ incubator. After removing the non-adherent cells, the adherent cells were fixed with 25% (w/v) glutaraldehyde for 10 minutes and stained with 0.5% crystal violet in 20% (v/v) methanol for 10 minutes. Random fields were photographed using a phase contrast microscope, and the number of adherent cells was counted.

Cell proliferation assay

Cell suspensions in 1% serum-containing medium were plated to each well of a 96-well ELISA plate (5×10^3 cells/well) and incubated at 37°C for 45 hours in a 5% CO₂ incubator. After incubation, the number of growing cells was measured using a cell counting kit-8 (#347-07621; DOJINDO) according to the manufacturer's instructions.

Cell invasion assay

One hundred microliters of Matrigel, diluted to a final concentration of 1.6 mg/mL, was added to the upper chamber of 24-well Transwell plates and dried for 24 hours in a hood. The wells were reconstituted by incubation with 200 μ L of serum-free DMEM at 37°C for 1 hour. After removing the medium, 200 μ L of 5×10^5 cells/mL (1×10^4 cells in 0.1% BSA containing serum-free DMEM) were inoculated into each upper well of a 24-well chemotaxis chamber, and 750 μ L of 10% FBS containing DMEM was placed in the bottom chamber to act as a chemoattractant. After 6 hours of incubation, the cells on the upper side of the membrane were removed with a cotton swab, and the cells on the

lower side of the membrane were fixed with 4% paraformaldehyde and stained with 0.5% crystal violet in 20% methanol. Random fields were photographed using a phase contrast microscope and the number of invaded cells was counted.

Lentiviral short hairpin RNA (shRNA)

Lentiviral shRNA clones (Dharmacon RNAi consortium Lentiviral shRNA) targeting galectin-3 (#RHS3979-201759611, clone ID: TRCN0000029304) 5'-ATTGTACTGCAACAAGTGAGC-3' and control shRNA (#RHS4459) 5'-TACAACAGCCACAACGCTC-TAT-3' were purchased from GE Healthcare. These vectors were cotransfected with the packaging vectors into HEK293T cells using the Trans-Lentiviral shRNA Packaging kit (#TLP5912; GE Healthcare) according to the manufacturer's instructions. After incubation for 15 hours, media were exchanged to 5% FBS containing DMEM. After further incubation for 48 hours, viral supernatant was harvested and then centrifuged at 1,600 g for 10 minutes at 4°C. The supernatant was filtrated through a 0.45- μ m filter. Lentivirus was infected into MDA-MB435S cells using the same method as retrovirus infection. To establish a cell line, cells were selected with 5 μ g/mL puromycin.

Statistical analysis

Results are given as mean \pm SEM and are representative of two or three independent experiments. Statistical comparisons were calculated between two groups using unpaired Student *t* test and among the groups using one-way or two-way ANOVA followed by a Bonferroni posttest, with GraphPad Prism Version 5.0a software. A *P* value of <0.05 was considered statistically significant.

Results

β 1,6GlcNAc residue on β 4-integrin was associated with cell migration and tumorigenesis

Expression of β 1,6GlcNAc is associated with metastasis and poor prognosis, whereas bisecting GlcNAc suppresses the effect by inhibition of β 1,6GlcNAc-branching formation (20). Human cutaneous squamous cell carcinoma (SCC) showed positive expression of β 1,6GlcNAc (52 out of 75) and negative expression of bisecting GlcNAc (72 out of 75) by immunohistochemistry using L₄-PHA and E₄-PHA lectins (Fig. 1B, *n* = 75), which is consistent with previous observations that β 1,6GlcNAc was more likely to be associated with tumor malignancy (17). As over-expression of β 4-integrin in SCC has been reported (6, 30), we next examined the expression patterns of β 4-integrin and β 1,6GlcNAc in human cutaneous SCC. In skin cancer specimens (*n* = 37), β 4-integrin was abundantly present and colocalized with β 1,6GlcNAc-branched *N*-glycans. Thirty-three β 4-integrin positive tumor cells, 33 (100%) colocalized β 1,6GlcNAc-branched *N*-glycans (Fig. 1C). In contrast, β 4-integrin was clearly localized in the basement membrane, while the expression of β 1,6GlcNAc was almost undetectable in all tested normal human skin samples (*n* = 7). Taking these results into consideration, we hypothesized that the amount of β 1,6GlcNAc-branched *N*-glycans on β 4-integrin increases in cancer cells. To test this hypothesis, we examined whether β 1,6GlcNAc was attached to β 4-integrin upon transformation of NHK cells. Ras/I κ B-mediated transformation of NHK cells increased attachment of β 1,6GlcNAc to β 4-integrin while the extent of the bisecting GlcNAc modification of β 4-integrin was decreased after transformation (Fig. 1D). These

Kariya et al.

results suggest that the β 1,6GlcNAc modification of β 4-integrin is increased in cancer cells.

GnT-III inhibits the formation of β 1,6GlcNAc branching on *N*-glycans by the introduction of bisecting GlcNAc (Fig. 1A). To address the role of β 1,6GlcNAc modification of β 4-integrin in tumor malignancy, we used MDA-MB435S cells, which do not express β 4-integrin, for preparing stable transfectants retrovirally transduced with control lacZ, human β 4-integrin, lacZ with GnT-III, or β 4 with GnT-III. The FACS analysis exhibited that GnT-III expression did not affect the cell surface expression of β 4-integrin (Fig. 2A, lacZ versus lacZ+GnT-III and β 4 versus β 4+GnT-III). Overexpression of GnT-III in cells expressing β 4-integrin significantly reduced β 1,6GlcNAc-branched *N*-glycans on β 4-integrin accompanied with increased bisecting GlcNAc (Fig. 2B). Expression of β 4-integrin exhibited enhanced cell migration (Fig. 2C) and tumor formation (Fig. 2D) in the MDA-MB435S cells compared with the control cells, which were impaired by GnT-III expression. These results suggest that the β 1,6GlcNAc residue in β 4-integrin may be associated with primary tumor growth and metastatic cancer cell behavior.

N-Glycosylation of β 4-integrin drives proliferation, migration, and invasion through PI3K/Akt activation

GnT-III overexpression modifies not only β 4-integrin but also other glycoproteins (Supplementary Fig. S1). β 4-integrin contains five potential *N*-glycosylation sites in its extracellular domain (Fig. 3A). To directly address the biological role of *N*-glycosylation of β 4-integrin in cancer cell behavior, we prepared two β 4-integrin constructs; a full-length wild-type (WT) and a mutant lacking all five *N*-glycosylation sites (Δ N; ref. Fig. 3A). These constructs were retrovirally expressed in MDA-MB435S cells that endogenously expressed no β 4-integrin (Fig. 2A, lacZ). To confirm the loss of *N*-glycans on Δ N, we performed lectin blot analysis using L₄-PHA, E₄-PHA, and SSA lectins, which recognize β 1,6GlcNAc, bisecting GlcNAc, and

α 2,6 sialic acid in *N*-glycans, respectively. The WT reacted with all tested lectins, but the Δ N did not react (Fig. 3B), suggesting the loss of *N*-glycans in the Δ N. Similar to our previous reports using keratinocytes (28), the deletion of *N*-glycans had no effect on either cell surface expression (Supplementary Fig. S2A) or heterodimer formation of β 4-integrin with α 6-integrin (Supplementary Fig. S2B) in the MDA-MB435S cells. These results suggest that *N*-glycans on β 4-integrin were not required for either expression or heterodimer formation of α 6 β 4-integrin. We next assessed whether *N*-glycosylation on β 4-integrin can affect cell adhesion and spreading, which are generally associated with cancer progression, using the MDA-MB435S transfectants. Typically, β 4-integrin causes cellular signaling through cell adhesion to the extracellular matrix protein laminins in cancer progression (2, 31). Compared with the WT cells, the Δ N cells showed decreased cell adhesion and spreading on a laminin-332 substrate, which was comparable to those in the control lacZ cells (Fig. 3C), suggesting that *N*-glycans on β 4-integrin are related to β 4-integrin-dependent cell adhesion and spreading in MDA-MB435S cancer cells.

β 4-integrin regulates cell proliferation, migration, and invasion in cancer cell lines (2, 6). Therefore, we examined the cellular functions of MDA-MB435S cancer cells expressing WT and Δ N. The expression of β 4-integrin markedly enhanced cell proliferation, migration, and invasion of the MDA-MB435S cells (Fig. 3D–F, WT) compared with the control lacZ cells. The enhanced cellular functions were significantly impaired by the loss of *N*-glycans on β 4-integrin (Fig. 3D–F, Δ N). Previous studies have shown that β 4-integrin-dependent cell proliferation, migration, and invasion are closely associated with the PI3K pathway in several carcinoma cell lines (9, 13). To address whether the decreased cellular functions due to the deletion of *N*-glycosylation were correlated to the downregulation of PI3K signaling, we examined the activation of the PI3K signaling pathway by Western blot analysis with an anti-phosphorylated Akt antibody. The Δ N cells, as well

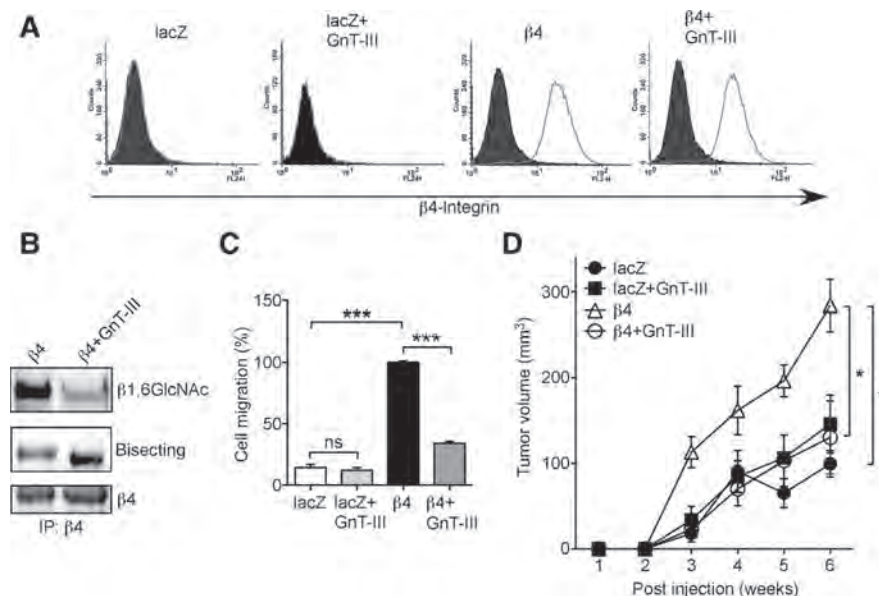
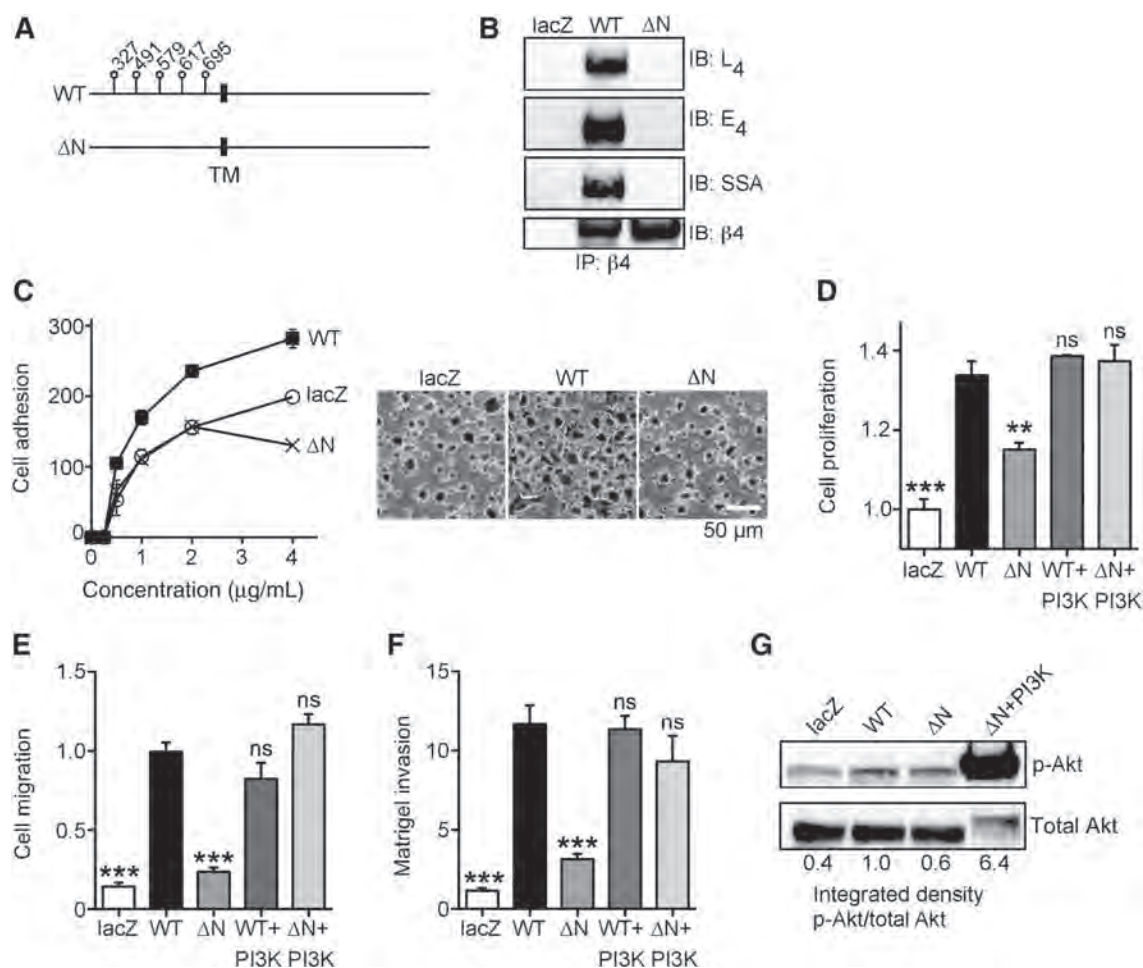


Figure 2. Decreased β 1,6GlcNAc residues in β 4-integrin by GnT-III correlates with suppression of cancer cell migration and tumorigenesis. **A**, Cell surface expression of β 4-integrin in MDA-MB435S cells expressing control lacZ, lacZ with GnT-III (lacZ+GnT-III), β 4, and β 4 with GnT-III (β 4+GnT-III). **B**, Lectin blot analysis of β 4-integrin immunoprecipitates from MDA-MB435S cells expressing β 4 and β 4 with GnT-III using L₄-PHA (β 1,6GlcNAc) and E₄-PHA (bisecting GlcNAc) lectins. Data are representative of three independent experiments. **C**, Effect of GnT-III overexpression on β 4-integrin-mediated cell migration. Results are the mean \pm SEM of three independent experiments conducted in triplicate. **D**, Tumor formation in nude mice injected subcutaneously with the indicated cells. Results are the mean \pm SEM of 5 mice per group. *, $P < 0.05$ (two-way ANOVA, Bonferroni posttest).

**Figure 3.**

N-Glycosylation of $\beta 4$ -integrin drives tumor cell proliferation, migration, and invasion through PI3K/Akt activation. **A**, Schematic diagram of the human $\beta 4$ -integrin cDNA constructs in this study. WT, wild-type $\beta 4$ -integrin; ΔN , *N*-glycosylation-defective $\beta 4$ -integrin mutant. The sites corresponding to the *N*-glycosylation sites on $\beta 4$ -integrin subunit (Asn327, Asn491, Asn579, Asn617, and Asn695) are shown by flags. Numbers indicate the number of amino acid residues. TM, transmembrane region. **B**, Lectin blot analysis of $\beta 4$ -integrin immunoprecipitates from MDA-MB435S cells expressing lacZ, WT, and ΔN with L_4 -PHA, E_4 -PHA, and SSA lectins. **C**, Cell adhesion and spreading of MDA-MB435S transfectants to laminin-332. Note that MDA-MB435S cells expressing no $\beta 4$ -integrin (lacZ) or ΔN showed decreased cell adhesion and spreading compared with the cells expressing WT. Cell spreading morphology was examined under a phase-contrast microscope after incubation for 20 minutes. **D–F**, Effect of the *N*-glycosylation defect in $\beta 4$ -integrin on cell proliferation (**D**), migration (**E**), and matrigel invasion (**F**). Note that cells expressing ΔN showed decreased cell proliferation, migration, and matrigel invasion, which were rescued by overexpression of constitutively active PI3K p110 α subunit (ΔN +PI3K). In contrast, overexpression of the active PI3K subunit had no significant effect on WT- $\beta 4$ -dependent cell proliferation, migration, or matrigel invasion (WT+PI3K). Results are the mean \pm SEM for three independent experiments conducted in triplicate. **, $P < 0.01$; ***, $P < 0.001$; ns, not significant (one-way ANOVA, Bonferroni posttest) versus WT. **G**, Western blot analysis of cell lysates from MDA-MB435S transfectants with phospho-Akt and total Akt antibody. Note that cells expressing lacZ or ΔN showed decreased PI3K/Akt pathway activation, which was rescued by overexpression of constitutively active p110 α PI3K subunit (ΔN +PI3K). Results of the densitometric analysis are shown as the integrated density of the ratio of phosphorylated protein to total protein bands. All blots are representative of at least three independent experiments.

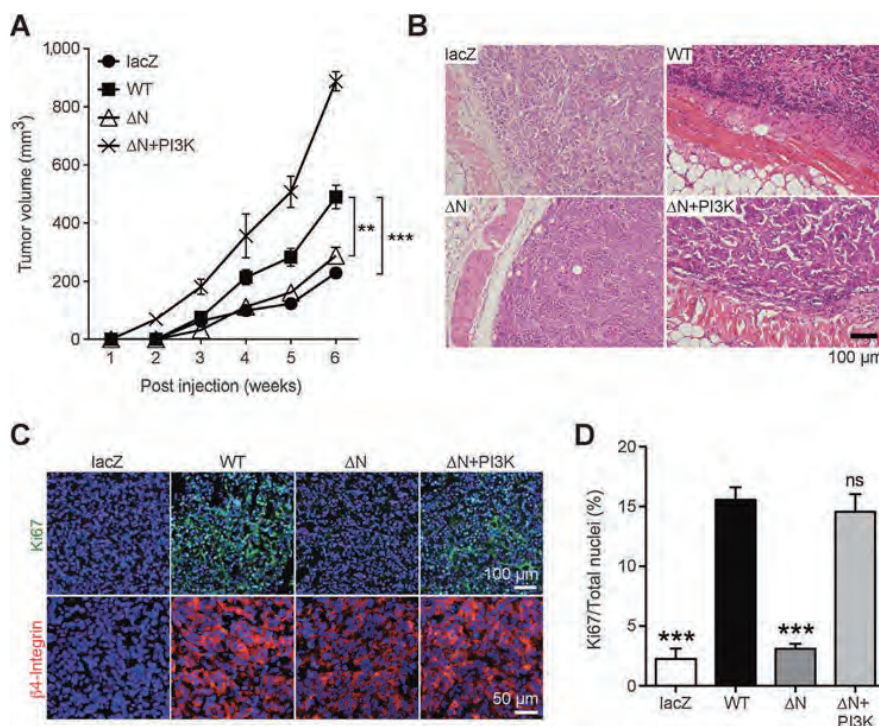
as the lacZ cells, showed decreased phosphorylation of Akt compared with the WT cells (Fig. 3G). We also found that the impairment of cellular functions in the ΔN cells was completely restored through overexpression of the constitutively active PI3K p110 α subunit (Fig. 3D–F, ΔN +PI3K). In contrast, overexpression of the active PI3K subunit in WT cells did not significantly affect the WT $\beta 4$ -dependent cell proliferation, migration, and invasion (Fig. 3D–F, WT+PI3K), suggesting that the WT $\beta 4$ -mediated PI3K/AKT activation is sufficient for such functions in the

cells and higher PI3K/AKT activation does not always promote activities of cancer cells. Together, these findings demonstrate that the *N*-glycosylation of $\beta 4$ -integrin plays a fundamental role in activating the PI3K pathway, thereby promoting cell proliferation, migration, and invasion.

N-Glycans of $\beta 4$ -integrin promote *in vivo* tumor growth.

To determine whether *N*-glycosylation of $\beta 4$ -integrin is related to tumorigenesis *in vivo*, we subcutaneously injected MDA-

Kariya et al.

**Figure 4.**

N-Glycosylation of β 4-integrin functionally contributes to tumorigenesis *in vivo*. **A**, Tumor growth after subcutaneous injection of MDA-MB435S cells expressing the indicated proteins into mice ($n = 5$ mice per group \pm SEM). **, $P < 0.01$; ***, $P < 0.001$ (one-way ANOVA, Bonferroni posttest). **B**, Hematoxylin/eosin staining of the indicated tumors. **C**, Immunofluorescent analysis of Ki-67 (green) and β 4-integrin (red) expression in the indicated tumors. Nuclei were stained with Hoechst 33342 (blue). **D**, Quantified percentage of Ki-67-positive cells to total cells in **C**. The bar graph represents the mean \pm SEM for three independent experiments. ***, $P < 0.001$; ns, not significant (one-way ANOVA, Bonferroni posttest) versus WT.

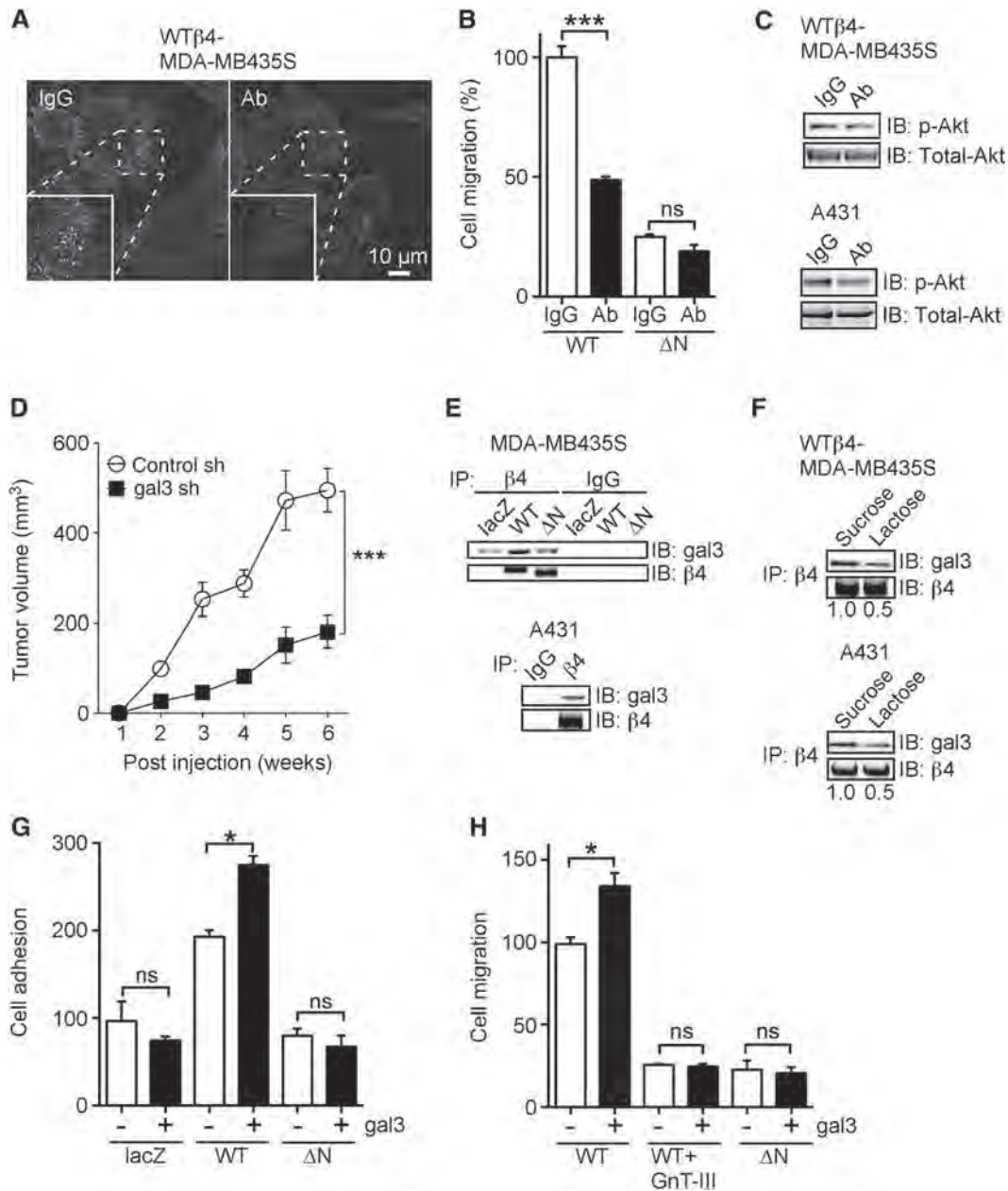
MB435S transfectants into nude mice and analyzed tumor growth. Compared with the WT cells, the Δ N cells showed significantly impaired tumorigenesis, which was comparable with the β 4 null (lacZ) cells (Fig. 4A and B). Impairment of the tumorigenesis in the Δ N cells was fully restored through overexpression of the constitutively active PI3K p110 α subunit (Fig. 4A, Δ N+PI3K). In comparison with the WT tumors, staining with anti-Ki-67 antibody demonstrated that the Δ N tumors included notably fewer proliferating cells, which was fully increased to WT tumor levels by overexpression of the constitutively active PI3K p110 α subunit (Fig. 4C and D). These results demonstrate that the ability of β 4-integrin to drive tumorigenesis, and tumor proliferation is associated with activation of PI3K pathway via *N*-glycans.

β 4-integrin-dependent tumor progression is associated with interaction between galectin-3 and β 1,6GlcNAc residue on β 4-integrin

Galectin-3 is known to be associated with cancer aggressiveness and metastasis (22–24). To examine the role of galectin-3 in β 4-integrin-mediated tumor progression, we performed inhibition assays using a functional blocking antibody against galectin-3 (M3/38). The functional blocking antibody against galectin-3 suppressed β 4-integrin clustering probably through inhibition of galectin-3 multimerization, suggesting that galectin-3 actually cross-links β 4-integrin (Fig. 5A). The antibody suppressed WT cell motility, whereas no effect was observed in the Δ N cells (Fig. 5B). Corresponding with the decreased cell motility of the WT cells, the galectin-3 antibody reduced Akt phosphorylation compared with control IgG in the WT cells (Fig. 5C). Furthermore, we tested the tumorigenicity of the WT cells expressing control shRNA or galectin-3 shRNA to confirm the importance of galectin-3

expression on tumor formation (Supplementary Fig. S3). The result showed that reduced expression of galectin-3 in WT cells suppressed tumor formation, suggesting that galectin-3 plays an important role in β 4-integrin-promoting tumor formation (Fig. 5D).

Galectin-3 has a high affinity for β 1,6GlcNAc-branched *N*-glycans modified by polylactosamine consisting of β -galactoside sugars. The oligomerization of integrins by galectin-3-mediated cross-linking between the β 1,6GlcNAc-branched *N*-glycans on integrins promotes integrin function (25, 27, 32). To understand why deletion of *N*-glycosylation suppressed the ability of β 4-integrin to promote cancer cell progression, we examined the relationship between galectin-3 binding to β 4-integrin and cellular functions of β 4-integrin. β 4-integrin immunoprecipitates from the WT cells contained high amounts of galectin-3 compared with those from the lacZ and Δ N cells, indicating that *N*-glycans on β 4-integrin promote complex formation by the two molecules (Fig. 5E). The association of β 4-integrin with galectin-3 was inhibited by a competitive inhibitor of galectin binding, β -lactose but not by control sucrose, suggesting that galectin-3 is bound to β 1,6GlcNAc-branched *N*-glycans modified by polylactosamine on β 4-integrin (Fig. 5F). Similar results were obtained from the squamous cell carcinoma cell line, A431 cells, which endogenously express β 4-integrin. The addition of galectin-3 significantly enhanced cell adhesion of the WT cells but not the lacZ or Δ N cells to a laminin-332 substrate (Fig. 5G). Furthermore, the addition of galectin-3 to the cell culture significantly promoted cell motility of the WT cells but not that of either the WT with GnT-III cells or Δ N cells (Fig. 5H). These findings suggest that galectin-3 binding to β 4-integrin through β 1,6GlcNAc-branched *N*-glycans promotes the ability of β 4-integrin to drive cell adhesion and motility.

**Figure 5.**

Galectin-3 is a key modulator of β 4-integrin function through *N*-glycan. **A**, Inhibitory effect of a functional blocking antibody against galectin-3 (Ab) or control IgG on β 4-integrin clustering. Note that MDA-MB435S cells expressing WT showed decreased β 4-integrin clustering by the treatment of a functional blocking antibody against galectin-3. **B**, Inhibitory effect of a functional blocking antibody against galectin-3 on *N*-glycosylation of β 4-integrin-mediated cell migration. Note that MDA-MB435S cells expressing WT but not Δ N showed decreased cell migration by the treatment of a functional blocking antibody against galectin-3. **C**, MDA-MB435S cells expressing WT and A431 cells were incubated in serum-free medium in the presence of IgG or a functional blocking antibody against galectin-3 (Ab) for 20 minutes. Cell lysates were analyzed by Western blot with phospho-Akt and total Akt antibody. **D**, Effect of galectin-3 (gal3) knockdown on tumor growth in MDA-MB435S cells expressing WT. Results are the mean \pm SEM of six mice per group. ***, $P < 0.001$ (unpaired Student *t* test). **E**, Western blot analysis of β 4-integrin immunoprecipitates from MDA-MB435S transfectants and A431 cells. **F**, MDA-MB435S cells expressing WT and A431 cells were serum-starved for 2 hours and were then incubated in serum-free medium in the presence of conditioned medium of MDA-MB435S cells and saccharides (0.2 mol/L) for 30 minutes. The β 4-integrin immunoprecipitates from the cells were analyzed by Western blot. Note that the binding of galectin-3 to β 4-integrin was inhibited by a competitive disaccharide, β -lactose, but not a noncompetitive disaccharide, sucrose. Results of the densitometric analysis are shown as the integrated density of the ratio of galectin-3 protein to β 4-integrin protein bands. **G**, Effect of galectin-3 on *N*-glycans of β 4-integrin-mediated cell adhesion. Note that galectin-3 enhanced cell adhesion of MDA-MB435S cells expressing WT but not either lacZ or Δ N to laminin-332. **H**, Effect of galectin-3 on *N*-glycosylation in β 4-integrin-mediated cell migration. Note that MDA-MB435S cells expressing WT, but not either WT with GnT-III or Δ N, showed increased cell migration in the presence of galectin-3. Results are the mean \pm SEM for two or three independent experiments conducted in triplicate. *, $P < 0.05$; ***, $P < 0.001$; ns, not significant (one-way ANOVA, Bonferroni posttest).

Kariya et al.

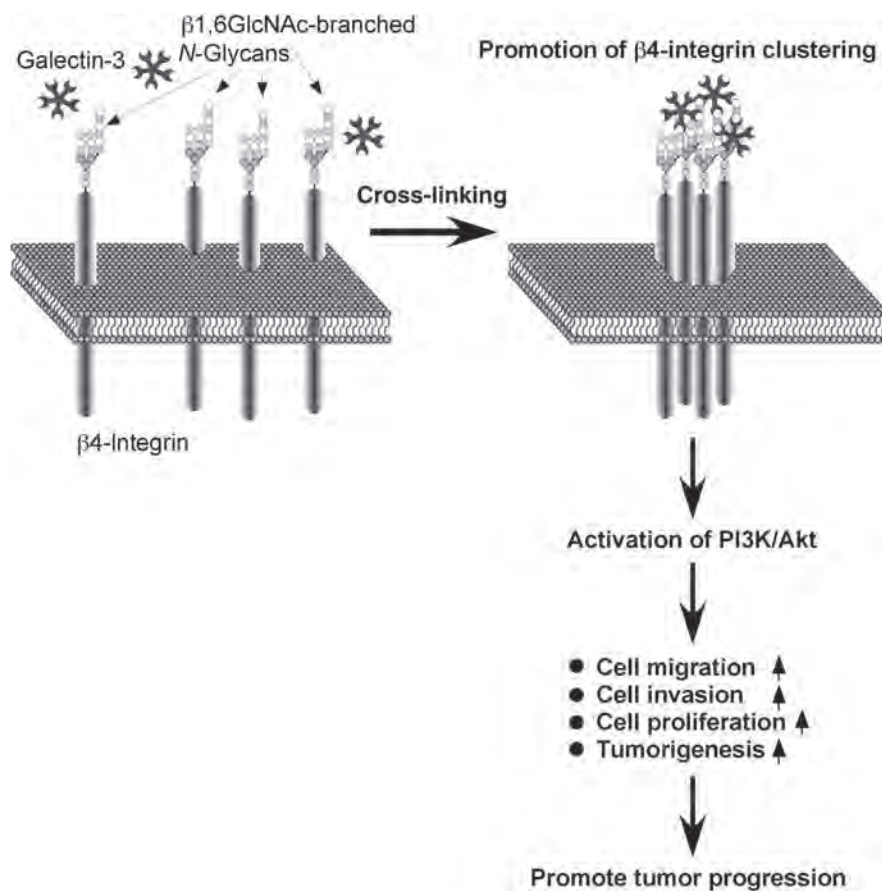


Figure 6. Hypothetical model of N-glycosylation-mediated $\beta 4$ -integrin-dependent tumor progression. Galectin-3 cross-links between $\beta 1,6$ GlcNAc-branched N-glycans, which in turn promotes $\beta 4$ -integrin clustering. The complex formation activates PI3K/Akt signaling, thereby promoting tumor progression by stimulating cell migration, invasion, proliferation, and tumorigenesis.

Discussion

In the current study, $\beta 4$ -integrin was colocalized with $\beta 1,6$ GlcNAc-branched N-glycans in tumor tissues. The suppression of the modification of $\beta 4$ -integrin by GnT-III was associated with reduced cancer cell migration and tumorigenesis in MDA-MB435S cells expressing $\beta 4$ -integrin. Deletion of N-glycosylation sites in $\beta 4$ -integrin, which was accompanied with downregulation of the PI3K signaling pathway, inhibited $\beta 4$ -integrin-dependent cancer cell migration, invasion, proliferation, and tumor formation. Furthermore, loss of association between galectin-3 and $\beta 4$ -integrin via $\beta 1,6$ GlcNAc-branched N-glycans abolished galectin-3-promoting cancer cell adhesion and migration. These results provide evidence that N-glycosylation of $\beta 4$ -integrin plays a functional role in promoting tumor development and progression through the PI3K activation.

$\beta 4$ -integrin promotes cell proliferation, migration, and invasion (31, 33), and plays pivotal roles in tumorigenesis (8). In the present study, deletion of N-glycosylation sites in $\beta 4$ -integrin suppressed those cellular functions *in vitro* as well as cell proliferation and tumorigenesis *in vivo*. GnT-V knockout mice have been reported to suppress polyomavirus middle T oncogene-induced mammary tumor growth and metastasis (19). Previous studies have shown that an increase of $\beta 1,6$ GlcNAc in the $\alpha 3$ -, $\alpha 5$ -, or $\beta 1$ -integrin subunit resulted in increased cancer cell migration (34, 35). Our findings indicate that modification of $\beta 4$ -integrin

with $\beta 1,6$ GlcNAc may be upregulated in tumor tissue. In addition, suppression of the $\beta 1,6$ GlcNAc modification in $\beta 4$ -integrin by overexpression of GnT-III reduced $\beta 4$ -integrin-dependent cancer cell migration and tumor formation. Therefore, this loss of $\beta 4$ -integrin function by the N-glycosylation defect may be mainly due to a lack of $\beta 1,6$ GlcNAc modification in $\beta 4$ -integrin.

Galectin-3 has a high affinity for $\beta 1,6$ GlcNAc-branched N-glycans through multivalent binding, and thereby cross-links glycoproteins on the cell surface and in the extracellular matrix to form molecular complexes (24). The formation of the macromolecular complexes on the cell surface by galectin-3 affects the distribution of glycoproteins and cellular signaling. Furthermore, integrin clustering mediated by galectin-3 promotes integrin activation (25, 27). In our study, we found that the deletion of N-glycans of $\beta 4$ -integrin, resulting in impaired galectin-3 binding to $\beta 4$, suppressed $\beta 4$ -integrin functions mainly through downregulation of the PI3K pathway. These results support the hypothesis that the cross-linking between $\beta 1,6$ GlcNAc-branched N-glycans of $\beta 4$ -integrins by galectin-3 directly or indirectly affects PI3K activation and cellular functions such as cell motility and tumorigenesis (Fig. 6); however, further investigation is required.

The association of $\beta 4$ -integrin with laminin-332 is known to induce PI3K activation, thereby promoting cell adhesion and migration (2). Our previous study showed that a decreased level of $\beta 1,6$ GlcNAc-branched N-glycans on laminin-332 by

introduction of bisecting GlcNAc suppressed its cell adhesion and migration activity as well as galectin-3-mediated β 4-integrin clustering (27). The present study showed that a defect of *N*-glycosylation in β 4-integrin suppressed the association with laminin-332 and PI3K activation, suggesting that *N*-glycosylation of β 4-integrin played a critical role in PI3K activation through the interaction with laminin-332. These results suggest that the association between laminin-332 and β 4-integrin through β 1,6GlcNAc-branched *N*-glycans may also be important for β 4-integrin-dependent tumor progression.

In the present study, we cannot exclude the potential effect of the lack of *N*-glycosylation on β 4-integrin protein folding. *N*-Glycosylation on integrins is important for such protein folding, which is required for heterodimer formation. In fact, the lack of *N*-glycans on α 5-integrin causes its misfolding and loss of heterodimer formation with β 1-integrin (36). In contrast, Δ N β 4-integrin could form a heterodimer with α 6-integrin (Supplementary Fig. S2B). Furthermore, FACS analysis showed that Δ N β 4 expressed on the cell surface, which is comparable with WT β 4 (Supplementary Fig. S2A). In essence, noncomplexed integrin is degraded immediately or remains in the endoplasmic reticulum (37). Therefore, the lack of *N*-glycans on β 4-integrin seems to affect its function and the association with other molecules, rather than β 4-integrin folding.

In conclusion, our study suggests that *N*-glycosylation of β 4-integrin is associated with tumor development and progression through β 4-integrin/PI3K signaling via the galectin-3-*N*-glycan complex. *N*-Glycosylation of β 4-integrin may therefore represent a potential therapeutic target for cancer.

Disclosure of Potential Conflicts of Interest

No potential conflicts of interest were disclosed.

Authors' Contributions

Conception and design: J. Gu, Y. Kariya

Development of methodology: Y. Kariya, Y. Kariya

Acquisition of data (provided animals, acquired and managed patients, provided facilities, etc.): Y. Hashimoto, Y. Kariya

Analysis and interpretation of data (e.g., statistical analysis, biostatistics, computational analysis): Y. Kariya, J. Gu, Y. Kariya

Writing, review, and/or revision of the manuscript: Y. Kariya, J. Gu, Y. Kariya

Administrative, technical, or material support (i.e., reporting or organizing data, constructing databases): Y. Kariya, M. Oyama, Y. Kariya

Study supervision: J. Gu, Y. Kariya

Acknowledgments

This work was supported by the Japan Society for Promotion of Science KAKENHI grant number 25860243, 17K08665 (Y. Kariya), 15H04354 (J. Gu), and the Fukushima Medical University Research Project from Fukushima Medical University No. KKI28001 (Y. Kariya).

The authors are grateful to Dr. M. Peter Marinkovich (Stanford University, Stanford, CA) for providing the cells. We thank the Fukushima Medical University English Editing Service for their English language review.

The costs of publication of this article were defrayed in part by the payment of page charges. This article must therefore be hereby marked *advertisement* in accordance with 18 U.S.C. Section 1734 solely to indicate this fact.

Received July 11, 2017; revised February 7, 2018; accepted March 12, 2018; published first March 16, 2018.

References

- Giancotti FG, Tarone G. Positional control of cell fate through joint integrin/receptor protein kinase signaling. *Annu Rev Cell Dev Biol* 2003; 19:173–206.
- Kariya Y, Kariya Y, Gu J. Laminin-332 and integrins: signaling platform for cell adhesion and migration and its regulation by *N*-glycosylation. *Laminins: structure, biological activity and role in disease*. Hauppauge, NY: Nova Science Publishers, Inc.; 2013. p. 29–51.
- Walko G, Castanon MJ, Wiche G. Molecular architecture and function of the hemidesmosome. *Cell Tissue Res* 2015;360:529–44.
- Falcioni R, Kennel SJ, Giacomini P, Zupi G, Sacchi A. Expression of tumor antigen correlated with metastatic potential of Lewis lung carcinoma and B16 melanoma clones in mice. *Cancer Res* 1986;46: 5772–8.
- Kimmel KA, Carey TE. Altered expression in squamous carcinoma cells of an orientation restricted epithelial antigen detected by monoclonal antibody A9. *Cancer Res* 1986;46:3614–23.
- Stewart RL, O'Connor KL. Clinical significance of the integrin α 6 β 4 in human malignancies. *Lab Invest* 2015;95:976–86.
- Masugi Y, Yamazaki K, Emoto K, Effendi K, Tsujikawa H, Kitago M, et al. Upregulation of integrin β 4 promotes epithelial-mesenchymal transition and is a novel prognostic marker in pancreatic ductal adenocarcinoma. *Lab Invest* 2015;95:308–19.
- Dajee M, Lazarov M, Zhang JY, Cai T, Green CL, Russell AJ, et al. NF- κ B blockade and oncogenic Ras trigger invasive human epidermal neoplasia. *Nature* 2003;421:639–43.
- Yoshioka T, Otero J, Chen Y, Kim YM, Koutcher JA, Satagopan J, et al. β 4 Integrin signaling induces expansion of prostate tumor progenitors. *J Clin Invest* 2013;123:682–99.
- Pylayeva Y, Gillen KM, Gerald W, Beggs HE, Reichardt LF, Giancotti FG. Ras- and PI3K-dependent breast tumorigenesis in mice and humans requires focal adhesion kinase signaling. *J Clin Invest* 2009; 119:252–66.
- Lim KH, Counter CM. Reduction in the requirement of oncogenic Ras signaling to activation of PI3K/AKT pathway during tumor maintenance. *Cancer Cell* 2005;8:381–92.
- Kariya Y, Miyazaki K. The basement membrane protein laminin-5 acts as a soluble cell motility factor. *Exp Cell Res* 2004;297: 508–20.
- Shaw LM, Rabinovitz I, Wang HH, Tokar A, Mercurio AM. Activation of phosphoinositide 3-OH kinase by the α 6 β 4 integrin promotes carcinoma invasion. *Cell* 1997;91:949–60.
- Kariya Y, Kariya Y, Gu J. Roles of integrin α 6 β 4 glycosylation in cancer. *Cancers* 2017 Jul 5;9: pii:E79.
- Dwek RA. Glycobiology: "towards understanding the function of sugars". *Biochem Soc Trans* 1995;23:1–25.
- Pinho SS, Reis CA. Glycosylation in cancer: mechanisms and clinical implications. *Nat Rev Cancer* 2015;15:540–55.
- Dennis JW, Laferte S. Oncodevelopmental expression of-GlcNAc β 1-6Man α 1-6Man β 1-4GalNAc6S-linked oligosaccharides in murine tissues and human breast carcinomas. *Cancer Res* 1989;49:945–50.
- Murata K, Miyoshi E, Kameyama M, Ishikawa O, Kabuto T, Sasaki Y, et al. Expression of N-acetylglucosaminyltransferase V in colorectal cancer correlates with metastasis and poor prognosis. *Clin Cancer Res* 2000;6: 1772–7.
- Granovsky M, Fata J, Pawling J, Muller WJ, Khokha R, Dennis JW. Suppression of tumor growth and metastasis in Mgat5-deficient mice. *Nat Med* 2000;6:306–12.
- Yoshimura M, Nishikawa A, Ihara Y, Taniguchi S, Taniguchi N. Suppression of lung metastasis of B16 mouse melanoma by N-acetylglucosaminyltransferase III gene transfection. *Proc Natl Acad Sci U S A* 1995;92:8754–8.
- Dumic J, Dabelic S, Fogel M. Galectin-3: an open-ended story. *Biochim Biophys Acta* 2006;1760:616–35.
- Takenaka Y, Fukumori T, Raz A. Galectin-3 and metastasis. *Glycoconj J* 2002;19:543–9.

Kariya et al.

23. Hittelet A, Legendre H, Nagy N, Bronckart Y, Pector JC, Salmon I, et al. Upregulation of galectins-1 and -3 in human colon cancer and their role in regulating cell migration. *Int J Cancer* 2003;103:370-9.
24. Liu FT, Rabinovich GA. Galectins as modulators of tumour progression. *Nat Rev Cancer* 2005;5:29-41.
25. Lagana A, Goetz JG, Cheung P, Raz A, Dennis JW, Nabi IR. Galectin binding to Mgat5-modified N-glycans regulates fibronectin matrix remodeling in tumor cells. *Mol Cell Biol* 2006;26:3181-93.
26. Partridge EA, Le Roy C, Di Guglielmo GM, Pawling J, Cheung P, Granovsky M, et al. Regulation of cytokine receptors by Golgi N-glycan processing and endocytosis. *Science* 2004;306:120-4.
27. Kariya Y, Kawamura C, Tabei T, Gu J. Bisecting GlcNAc residues on laminin-332 down-regulate galectin-3-dependent keratinocyte motility. *J Biol Chem* 2010;285:3330-40.
28. Kariya Y, Gu J. N-glycosylation of beta4 integrin controls the adhesion and motility of keratinocytes. *PLoS One* 2011;6:e27084.
29. Kariya Y, Kato R, Itoh S, Fukuda T, Shibukawa Y, Sanzen N, et al. N-Glycosylation of laminin-332 regulates its biological functions. A novel function of the bisecting GlcNAc. *J Biol Chem* 2008;283:33036-45.
30. Mercurio AM. Invasive skin carcinoma-Ras and alpha6beta4 integrin lead the way. *Cancer Cell* 2003;3:201-2.
31. Kariya Y, Kariya Y, Gu J. Roles of laminin-332 and alpha6beta4 integrin in tumor progression. *Mini Rev Med Chem* 2009;9:1284-91.
32. Yang EH, Rode J, Howlader MA, Eckermann M, Santos JT, Hernandez Armada D, et al. Galectin-3 alters the lateral mobility and clustering of beta1-integrin receptors. *PLoS One* 2017;12:e0184378.
33. Wilhelmsen K, Litjens SH, Sonnenberg A. Multiple functions of the integrin alpha6beta4 in epidermal homeostasis and tumorigenesis. *Mol Cell Biol* 2006;26:2877-86.
34. Guo HB, Lee I, Kamar M, Akiyama SK, Pierce M. Aberrant N-glycosylation of beta1 integrin causes reduced alpha5beta1 integrin clustering and stimulates cell migration. *Cancer Res* 2002;62:6837-45.
35. Zhao Y, Nakagawa T, Itoh S, Inamori K, Isaji T, Kariya Y, et al. N-acetylglucosaminyltransferase III antagonizes the effect of N-acetylglucosaminyltransferase V on alpha3beta1 integrin-mediated cell migration. *J Biol Chem* 2006;281:32122-30.
36. Isaji T, Sato Y, Zhao Y, Miyoshi E, Wada Y, Taniguchi N, et al. N-glycosylation of the beta-propeller domain of the integrin alpha5 subunit is essential for alpha5beta1 heterodimerization, expression on the cell surface, and its biological function. *J Biol Chem* 2006;281:33258-67.
37. Yoshida Y, Chiba T, Tokunaga F, Kawasaki H, Iwai K, Suzuki T, et al. E3 ubiquitin ligase that recognizes sugar chains. *Nature* 2002;418:438-42.

RESEARCH ARTICLE

Core fucosylation of copper transporter 1 plays a crucial role in cisplatin-resistance of epithelial ovarian cancer by regulating drug uptake

Xiaoxue Lv¹ | Jiazhe Song¹ | Kai Xue¹ | Zhi Li² | Ming Li¹ | Danishi Zahid¹ |
Hongyu Cao³ | Lu Wang¹ | Wanli Song¹ | Tonghui Ma¹ | Jianguo Gu⁴ |
Wenzhe Li¹ 

¹ College of Basic Medical Sciences, Dalian Medical University, Liaoning, China

² Clinical Laboratory, Dalian Municipal Central Hospital, Dalian, Liaoning, China

³ College of Life Science and Technology, Dalian University, Liaoning, China

⁴ Institute of Molecular Biomembrane and Glycobiology, Tohoku Medical and Pharmaceutical University, Miyagi, Japan

Correspondence

Wenzhe Li and Kai Xue, College of Basic Medical Sciences, Dalian Medical University, 9-Western Section, Lvshun South Road, Liaoning 116044, China.

Email: liwenzhe@dlmedu.edu.cn (W.L.); nkx123xuekai@dmu.edu.cn (K.X.)

Funding information

National Nature Science Foundation of China, Grant numbers: 31570797, 31870797; Nutrition and Care of Maternal & Child Research Fund Project of Guangzhou Biostime Institute of Nutrition & Care, Grant number: 2018BINCMCF39; Liaoning Provincial Program for Top Discipline of Basic Medical Sciences, China

Core fucosylation catalyzed by core fucosyltransferase (Fut8) contributes to the progressions of epithelial ovarian cancer (EOC). Copper transporter 1 (CTR1), which contains one N-glycan on Asn¹⁵, mediates cellular transport of cisplatin (cDDP), and plays an important role in the process of cDDP-resistance in EOC. In the present study, we found that the core fucosylation level elevated significantly in the sera of cDDP-treated EOC patients. The in vitro assays also indicate that core fucosylation of CTR1 was significantly upregulated in cDDP-resistant A2780CP cells compared to the cDDP-sensitive A2780S cells. Intriguingly, the hyper core fucosylation suppressed the CTR1-cDDP interactions and cDDP-uptake into A2780CP cells. Conversely, contrast to the *Fut8*^{+/+} mouse ovarian epithelial cells, the *Fut8*-deleted (*Fut8*^{-/-}) cells obviously showed higher cDDP-uptake. Furthermore, the recovered core fucosylation induced the suppression of cDDP-uptake in *Fut8*-restored ovarian epithelial cells. In addition, the core fucosylation could regulate the phosphorylation of cDDP-resistance-associated molecules, such as AKT, ERK, JNK, and mTOR. Our findings suggest that the core fucosylation of CTR1 plays an important role in the cellular cDDP-uptake and thus provide new strategies for improving the outcome of cDDP based chemotherapy of EOC.

KEYWORDS

cDDP-resistance, core fucosylation, CTR1, EOC, Fut8

1 | INTRODUCTION

Epithelial ovarian cancer (EOC) is the most lethal female genital tract cancer in the world.¹ The standard therapy scheme for the initial management of ovary cancer is based on cytoreductive surgery, followed by primary chemotherapy with a platinum-based regimen.² The first-line chemotherapy with platinum and

paclitaxel yields a response rate of more than 80%. Despite an initial high response rate, EOC has a poor prognosis due to the high proportion of chemo resistance (approximately 90%),² and the 5-year survival rate for advanced ovarian cancer is less than 30%. Reduced cellular accumulation of platinum-based drugs, enhanced detoxification capability, aberrant apoptosis pathways, and increased DNA repair ability from DNA damage are associated with the chemo resistance,^{3,4} however, the precise mechanisms of how EOC cells achieve resistance to platinum drugs have not been fully identified.

Xiaoxue Lv and Jiazhe Song contributed equally to this work.

The resistance to platinum drugs usually occurs during the ovarian tumor progressions, and the treatment for recurrent ovarian cancer is often difficult due to resistance to chemotherapeutic agents.^{4,5} Aberrant glycosylation is a universal feature of cancer malignancy and metastatic progress including EOC.^{1,5-12} Recent studies have reported that core fucosylation could participate in the EOC progression.^{1,5,12} Core fucosylation is catalyzed by core fucosyltransferase (Fut8) through transferring a fucose residue from GDP-fucose to the innermost N-acetylglucosamine (GlcNAc) residue of N-glycans via α 1,6-linkage (Figure 1A).¹³ It plays important roles in various cellular biological events.¹⁴ In our previous studies, we found that lack of core fucosylation in transforming growth factor β 1 (TGF β 1) receptor and epidermal growth factor receptor results in a marked dysregulation of their activation that is due to a decreased ligand affinity for the receptor.¹⁵ Moreover, core fucosylation of B cell receptor is required for antigen recognition.¹⁶ These findings indicate that core fucosylation is necessary for many molecular interactions on cell membrane. Since the drug uptake of cancer cell is based on the molecular interaction between cell surface proteins and drugs,¹⁷⁻²⁰ the relationship between core fucosylation and the membrane protein-dependent drug uptake should be a novel point for the studies on the drug-resistance of EOC.

The inhibition of cisplatin (cDDP) uptake is a main reason for the cDDP-resistance of EOC, which usually occurs during the malignant transformation in ovarian tumors.^{3,4,21,22} The transporters on the cell membrane play a key role in the cellular accumulation of platinum-based drugs, and several transporters of platinum compounds are glycoproteins, including the efflux ATPases (MRPs, ATP7A/B), and the solute carrier importers (SLCs, AQP2, and AQP9).³ Copper transporter 1 (CTR1) on the cell membrane contains three membrane-spanning segments. CTR1 is a transporter that play a key role in regulating copper homeostasis, and is also responsible for the uptake of cDDP in yeast and mammals.^{3,4,23-26} Over-expression of CTR1 in human ovarian tumor cells increases their sensitivity to platinum drugs.^{3,4,23-25} CTR1-mediated cDDP-uptake was dependant on its metal-binding ecto-domain, which is linked with the N-glycan (Asn¹⁵) and the O-glycan (Thr²⁷).¹⁹ Blocking CTR1 ecto-domain O-linked glycosylation by mutating Thr²⁷, increased the abundance of truncated CTR1.²⁷ In mammalian cells the N¹⁵Q mutant protein trafficked to the plasma membrane and copper transport was modestly reduced by the loss of glycosylation.²⁷ However, the role of core fucosylation of CTR1 in cDDP-uptake and in platinum-resistance in ovarian cancer has not been elucidated.

In order to investigate the role of core fucosylation in CTR1-mediated cDDP-uptake and cDDP-resistance of EOC, the core fucosylation level in the serum of cDDP-treated EOC patients was analyzed. Furthermore, we compared the ability of cDDP-uptake via CTR1 between different human EOC cell lines. By applying the *Fut8*-deleted (*Fut8*^{-/-}) mouse ovary epithelial cell model, we provide evidence that the core fucosylation of CTR1 is involved in the cDDP-uptake, followed by cell apoptosis or survival. Our data suggest that down-regulation of core fucosylation could improve the cDDP efficacy in EOC chemotherapy.

2 | MATERIALS AND METHODS

2.1 | Clinical samples

The ovarian cancer patients newly diagnosed and treated in Dalian Municipal Central Hospital from September 2016 to January 2017 were analyzed retrospectively. Pathology records were reviewed including morphology, immunophenotype, and cytogenetic and molecular findings. All cases met the criteria published by the World Health Organization (WHO). Serum samples were obtained from healthy people ($n = 20$) and ovarian cancer patients ($n = 21$). All our investigations were undertaken either for diagnostic purposes or with residual material obtained through diagnostic procedures. All procedures had been approved by the ethical committee of Dalian Municipal Central Hospital. Patient clinical characteristics were listed in Supplemental Table S1.

2.2 | Mice

Fut8^{-/-} mice were backcrossed eight times to the BALB/cA background. Homozygous wild (*Fut8*^{+/+}) and knockout (*Fut8*^{-/-}) mice were obtained by crossing heterozygous *Fut8*^{+/-} mice. Mice were maintained in a room illuminated for 12 h (08:00-20:00) and kept at 24 \pm 1°C with free access to food and water in the specific pathogen-free laboratory animal facility of Dalian Medical University. All animal procedures complied with the institutional animal protocol guidelines.

2.3 | Reagents

Antibodies for AKT, phospho-AKT (Ser473), mTOR, phospho-mTOR (Ser2448), CTR1, phospho-ERK (Thr202/Tyr204), JNK, phospho-JNK (Thr183/Tyr185) were purchased from Cell Signaling Technology (Beverly, MA), and rabbit polyclonal anti-GAPDH antibodies were purchased from Abcam (Cambridge, UK). Anti-cytokeratin 14 (K14) antibody and cDDP were purchased from Sigma (St. Louis, MO). *Lens Culinaris Agglutinin* (LCA) and *Aspergillus oryzae* lectin (AOL) were purchased from Vector Laboratories, Inc. (Burlingame, CA).

2.4 | Western blot and lectin blot analysis

Cells were washed with phosphate buffer solution (PBS) and then lysed with ice-cold buffer (50 mM Tris-HCl, 150 mM NaCl, 1% Triton-X 100, 5 mM EDTA, 10 mM NaF, 0.1 mM Na₃VO₄, supplemented with 0.1 mM phenylmethylsulfonyl fluoride, 1 mM DTT). Total protein concentrations were determined by bicinchoninic acid protein assay (BCA assay kit, Pierce, Rockford, IL). Ten microgram proteins from each sample were separated by 10% sodium dodecyl sulfate polyacrylamide gel electrophoresis (SDS-PAGE) and analyzed by immunoblotting for first antibody or the biotin-labeled LCA, which preferentially recognizes the core fucose,²⁸ followed by incubation with a HRP-conjugated secondary antibody or HRP-conjugated streptavidin for 1 h at room temperature. After washing, the membranes were visualized by chemiluminescence using an ECL kit (Pierce, Rockford, IL).

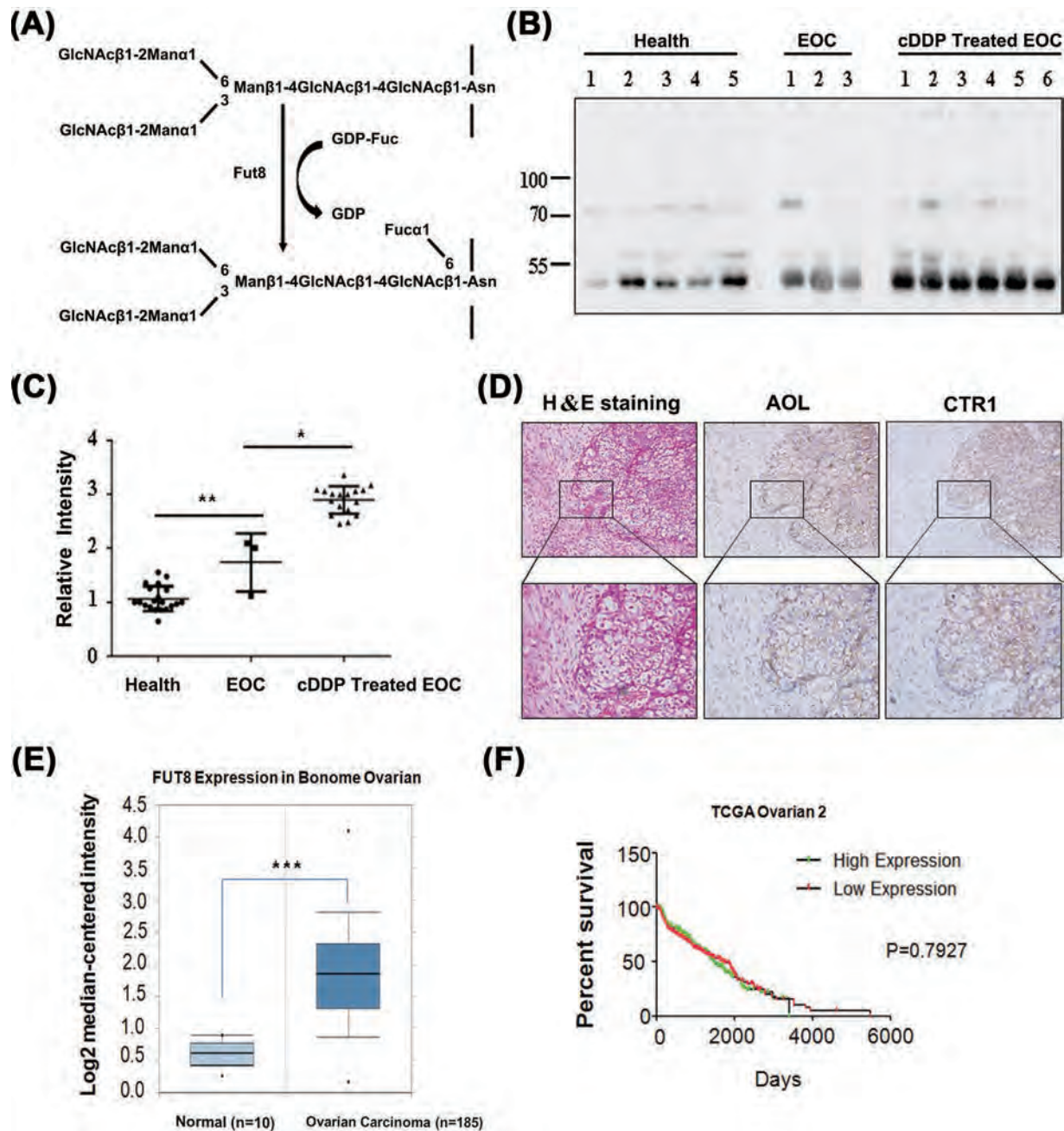


FIGURE 1 High level of core fucosylation frequently occurs in cDDP-treated EOC patients. A, The biological reaction of Fut8. Fut8 transfers fucose to the innermost GlcNAc residue of complex N-glycans via α 1, 6-linkage (core fucosylation) in the Golgi apparatus of mammal cells. Asn, asparagine; Fuc, fucose; GDP-Fuc, GDP-fucopyranoside; Man, mannose. B, Comparative analysis of the core fucosylation levels in sera of EOC patients and healthy controls. The core fucosylation levels in serum samples (5 μ g) were detected by LCA lectin blot. The represent image was shown. C, The statistical analysis of core fucosylation levels in the serum samples. Serum samples are from healthy control (n = 20), cDDP-treated (n = 15), and untreated (n = 3) EOC patients. The significantly difference was shown as * P < 0.05 or *** P < 0.01. D, Analysis of core fucosylated molecules and CTR1 expressions in EOC patient specimens using H&E (left), AOL (middle), and anti-CTR1 (right) staining. The paraffin sections were deparaffinized and hydrated through a graded series of ethanol to PBS and then incubated with biotin-conjugated AOL antibody or anti-CTR1 antibody. Finally, the slides were visualized with 3, 3'-diaminobenzidine. The original magnification of lower panel is x 400 (n = 3). E, The comparative analysis by Cancer Genome Atlas (TCGA) demonstrated that the expression of Fut8 was significantly increased in EOC patients (n = 185). The significantly difference was shown as *** P < 0.001. F, The overall survival between high Fut8 expressed and low Fut8 expressed patients were analyzed by TCGA dataset. [Color figure can be viewed at wileyonlinelibrary.com]

2.5 | Immunohistochemistry

Formalin-fixed ovarian tissue specimens were paraffin-embedded. For immunohistochemical analysis, the specimens were deparaffinized twice in xylene and hydrated through a graded series of ethanol to PBS. The endogenous peroxidase activity was blocked with 3% H₂O₂ for 5 min. Specimens were pretreated with avidin-biotin blocking and hydroxybenzoyl blocking for 10 min at 37°C, and then incubated with primary antibody (1:50 dilution) for 16 h at 4°C. Then the specimens were incubated with appropriate peroxidase-conjugated secondary antibody for 1 h at 37°C. The slides were visualized with 3, 3'-diaminobenzidine. Stained slides were mounted in anti-fade medium (PermaFluor Mountant Medium; Immunon, Pittsburgh, PA). Finally, the slides were examined under a fluorescence microscope (Leica, UK) at an x200 magnification using the appropriate filter. The specimens were analyzed by hematoxylin-eosin (H&E) staining.

2.6 | Cell culture

Two EOC cell lines, cisplatin-sensitive parental cell line (A2780S) and its cisplatin-resistant variant (A2780CP) were kindly provided in 2015 by Chun Peng (York University, Toronto, Canada) and Dr Shiyong Cui (Dalian Medical University), and were cultured in Dulbecco's modified Eagle's medium (DMEM) containing 10% fetal bovine serum and maintained at 37°C with 5% CO₂ as previously described.^{2,29} Cell line authentication and pathogen testing was performed upon receipt of cell lines. All experiments were performed on cells cultured for less than 2 months. The morphology of A2780S and A2780CP cells was shown in Supplemental Figure S1.

2.7 | Quantitative gene expression analysis by real-time PCR and RT-PCR

Total RNAs were extracted from ovarian cancer cell lines with the TRIzol™ reagent (Invitrogen, Carlsbad, CA). First-strand cDNA was synthesized using SuperScript II reverse transcriptase (Invitrogen) and the oligo (dT) 18 primer. Samples were analyzed in a triplicate 20 μL reaction (20 μmol/L of primers, 10 μL of Master Mix), which was adapted from the standard protocol provided by SYBR Green PCR Master Mix. The default PCR procedure was used on an Applied Biosystems Prism 7000 Sequence Detection System (Applied Biosystems, Tokyo, Japan). The primers used for PCR were listed in Supplemental Table S2. Using the 2- $\Delta\Delta$ Ct method, relative internal mRNA expression of target genes was normalized to GAPDH.

2.8 | Flow cytometry analysis

Cells were collected and blocked in 3% BSA for 10 min. Primary antibodies were incubated on ice for 30 min, and then stained with FITC-labeled secondary antibodies. Flow cytometry was performed on a FACS-Calibur (Becton Dickinson, Mountain View, CA), and the data was analyzed with Flowjo software (Treestar, San Carlos, CA).

2.9 | Immunoprecipitation

For immunoprecipitation (IP), 500 μg of cell extracts were mixed with 10 μL anti-CTR1 antibody and incubated at 4°C for 1 h with continuous rotation. Then 10 μL of a 50% suspension of Protein G-Sepharose (Amersham Pharmacia Biotech AB) was added and incubated at 4°C overnight with gentle agitation. The beads were washed four times with lysis buffer. The immunoprecipitated samples were eluted from the protein G-Sepharose by heating at 100°C for 5 min in 2 × loading buffer without 2-mercaptoethanol. After centrifugation, the supernatant were resolved by SDS-PAGE and Western blotted.

2.10 | Remove of fucosylation on the CTR1

The CTR1 from A2780CP and A2780S cells was purified by IP assay, and then purified CTR1 were treated with 100 mU Glyko® α (1-2, 3, 4, 6) Fucosidase (GKX-5006, Prozyme) for 16 h at 37°C to remove the core fucosylation.

2.11 | Molecular interactions

For molecular interaction analysis, the purified CTR1 proteins were mixed with different concentrations of cDDP, and detected by fluorescence measurement. The fluorescence measurements were performed on an FP-6500 fluorescence spectrophotometer (Jasco, Japan) equipped with a 150 W xenon lamp source. The fluorescence emission spectra were recorded with 1.0 cm quartz cell in the wavelength of 290–400 nm upon excitation at 280 nm at a scanning speed of 500 nm per min. The bandwidths for both excitation and emission were 3 and 5 nm, respectively. All synchronous fluorescence spectra were measured according to $\Delta\lambda = 20$ nm and $\Delta\lambda = 60$ nm, while the width of the excitation and emission slits were adjusted at 3 and 5 nm, respectively. The scanning speed of the synchronous fluorescence was 500 nm/min and the response time was 0.5 s with a medium sensitivity.

2.12 | Measurement of intracellular platinum content

Platinum contents were then measured by inductively coupled plasma-mass spectrometry (ICP-MS, Optima 2100dv) in Dalian Research Institute of Product Quality Testing as previously described.^{17,24} Cells were plated in dish at a density of 5×10^6 cells/dish followed by incubation with different concentration of cDDP for 4 h. Then cells were collected and digested in 1 mL of concentrated nitric acid and concentrated hydrochloric acid (1:3).

2.13 | Cell proliferation assay

For MTT [3-(4,5-dimethylthiazole-2-yl)-2,5-diphenyltetrazolium bromide] assay, cells were cultured in 96-well plates, and added cDDP at the indicated concentrations for 0, 24, 48, 72, 96 h. Ten microliter of 5 mg/mL of MTT was added in the each well. After incubation for 4 h,

DMSO (Sigma) was added to each well to dissolve the precipitate. The plate was read at 490 nm on a Benchmark microplate reader (BioRad, Hercules, CA). The percentage growth inhibition was calculated using following formula, cell survival inhibition (%) = $(Ac-At)/(Ac-Ab) \times 100\%$. At = Absorbance value of cDDP-treated; Ab = Absorbance value of blank; Ac = Absorbance value of control.

2.14 | CCK8 cell proliferation assay

Cell IC50 were measured by using CCK8 assay (APExBIO). Briefly, the A2780 and A2780-cp cells were plated in 96-well plates (5000 cells/well). After pre-culture for 12 h, the cells were treated with various concentrations of cisplatin (0, 10, 20, 30, 40, and 50 $\mu\text{g}/\text{mL}$) for 24 h, and 10 μL of CCK-8 solution (APExBIO) was subsequently added to each well of the plate. The bubbles were prohibited into the cells. Then the plate was incubated at 37°C for 3 h. The optical density (OD) value was measured at 450 nm using a microplate reader (BioTek Instruments, VT).

2.15 | Cell cycle and apoptosis analysis

For cell cycle analysis, cells were incubated with and without cDDP for 48 h. After extensive washing, the cells were fixed with 70% ethanol overnight at 4°C and incubated with propidium iodide (PI) (Sigma-Aldrich) and RNaseA (Sigma-Aldrich) for 1 h at room temperature, and analyzed using a FACS calibur instrument. The cell-cycle phase distribution was analyzed with the use of the CellQuest software.

For cDDP-induced cell apoptosis analysis, cells were harvested and fixed. Then, annexin V-APC/PI-FITC double staining were performed according to the manufacturer's instructions.

2.16 | Phosphorylation assay

Serum-starved cells were treated with indicated concentration of cDDP for 0, 5, 15, and 30 min. Stimulations were terminated by washing the cells once with ice-cold PBS supplemented with 0.4 mM sodium orthovanadate and then harvested by scraping. Cells were collected and solubilized for 30 min at 4°C in lysis buffer. After lysis, the lysate was centrifuged at 10 000g for 15 min at 4°C to precipitate insoluble materials, and the supernatant were subjected to immunoblotting.

2.17 | Establishment of FUT8^{+/+}, FUT8^{+/-}, FUT8^{-/-}, and Fut8-restored (Re) ovary epithelial cells

Ovary epithelial cells were obtained from homozygous wild type (FUT8^{+/+}), heterozygous (FUT8^{+/-}) and *Fut-8* gene-knockout (FUT8^{-/-}) mice.^{16,30} In detail, ovarian tissues were removed from the mice following by incubation in hyaluronidase (100 U) and collagenases (300 U) for 30 min. After centrifugation at 1000g, the cells was collected and cultured in DMEM supplemented with 10% FCS and incubated at 37°C. To obtain immortal cells, zeocine-resistant vector (pcDNA3.1) containing the SV40 gene was introduced to these

primary cells. Transfectants were screened in the presence of 400 $\mu\text{g}/\text{mL}$ zeocine, and Fut8^{+/+}, Fut8^{+/-} and Fut8^{-/-} mouse ovarian epithelial cells were established. The primers for Fut8^{+/+}, 5'-TTC CAG AGA GAT TAG CCT GTC T-3' and 5'-TCT CGA ACC AAA TGA CCA CCT A-3', and for FUT8^{-/-}, 5'-TTG CCG TCT TTT GGC AAT GTG A-3' and 5'-CCA GAT CAG ATC CCA TAC AAT G -3', were used for PCR to detect mouse genotyping.

To prepare Fut8-reintroduced cells, pLHCXsi-U6-Fut8 mutant expression vectors were prepared. The pLHCXsi-U6-Fut8 mutant vector was transduced into Fut8^{-/-} mouse ovary epithelial cells by Lipofectamine, and Fut8-restored (Re) mouse ovary epithelial cells were generated after selection with 200 $\mu\text{g}/\text{mL}$ hygromycin.

2.18 | Immunofluorescence assay

Cells were seeded onto 6-well chamber microscope slides and allowed to adhere overnight. Then cells were washed and fixed in methanol: acetone (1:1) for 30 min followed by block out in rabbit serum for 30 min. Primary antibody was incubated for 1 h at room temperature, then the secondary antibody was covered for 1 h and followed by DAPI staining for 5 min. Cell immunostaining was imaged on a fluorescence microscopy (Leica, Cambridge). The images were projected by using the Nikon Ez-C1 and Adobe Photoshop 8.0 software.

2.19 | Statistical analysis

Each experiment was performed at least three times and the mean was used to calculate significance. Data was expressed as mean values \pm standard error mean (SEM). Data analysis was performed with the statistical software package Graph Pad Prism 5. The statistical significance was assessed by one-way analysis of variance (ANOVA). The level of differences among groups was analyzed by Student's test. Differences were considered to be statistically significant at * $P < 0.05$, ** $P < 0.01$, and *** $P < 0.001$.

3 | RESULTS

3.1 | Core fucosylation of CTR1 is associated with the cDDP-resistance of EOC

During the therapy process of EOC, about 90% of patients exhibited chemo resistance.^{2,31} To investigate the role of core fucosylation in the cDDP-resistance of EOC, we evaluated the sera of 21 patients, who had received primary surgery. Among those, 18 EOC patients received cDDP-based primary therapy, and the other three were not received any chemotherapy (Supplementary Table S1). LCA staining demonstrated that the core fucosylation levels were dramatically up-regulated in cDDP-treated EOC patients, compared to the healthy controls and none cDDP-treated EOC patients (Figures 1B and 1C), indicating that high level of core fucosylation frequently occurs in cDDP-treated EOC patients. Moreover, the ovarian specimens of cDDP-treated EOC patients were analyzed by H&E staining and

immunohistochemical assay using AOL, which is another lectin specific for recognizing core fucosylation.³² As shown in Figure 1D, core fucosylation was markedly increased in ovarian carcinoma tissues contrast to the adjacent normal tissues. Here we also investigate CTR1 expressions of the specimens of ovary tissue from cDDP-treated EOC patients and found that CTR1 was mainly concentrated on the cell membrane of ovarian carcinoma (Figure 1D). Moreover, the Cancer Genome Atlas (TCGA) Bonome Ovarian Statistics demonstrates that the expression of Fut8 was significantly increased in EOC patients ($n = 185$, $***P < 0.001$) (Figure 1E), although there are no significant difference of the overall survival between high Fut8 expressed and low Fut8 expressed patients (Figure 1F, data from *Oncomine*). The colocalization of CTR1 with the core fucosylation in the cDDP-treated ovarian carcinoma tissues suggests that core fucosylation of CTR1 may be associated with the cDDP-resistance of EOC.

Next, we compared the core fucosylation levels of human EOC cell line A2780S and its cDDP-resistance variants A2780CP.^{2,29} The LCA blot indicated that core fucosylation levels of A2780CP cells are significantly higher than those of A2780S cells (Figure 2A). The *Fut8* mRNA and protein expressions are dramatically upregulated in A2780CP cells compared with A2780S cells (Figure 2B). No apparent changes were found in the expressions of other glycosyltransferase genes, such as N-acetylglucosaminyltransferase III (GnT III), GnT IV, GnT V, and α 2,6-sialyltransferase I (ST6Gal1). These findings were consistent with other previous report,¹⁵ suggesting that the up-regulation of core fucosylation is positively correlated to cDDP-resistant in EOC cells. Then we detected CTR1 expressions in the A2780S and A2780CP cells (Figures 2C and 2D). No significant difference of the CTR1 expression on the cell membrane was found between A2780S and A2780CP cells (Figure 2C). However, the core fucosylation level of CTR1 in A2780CP cells is dramatically higher than that in A2780S cells (Figure 2D). These findings also indicated that core fucosylation of CTR1 were associated with the cDDP-resistance of EOC cells.

To further explore the relationship between core fucosylation of CTR1 and the cDDP-resistance of EOC cells, the cDDP-treatment assays were performed. The cell survival inhibition assay showed that the A2780CP cells were more cDDP-resistant than that of A2780S cells during treatment with 10, 20, and 35 μ M cDDP (Figure 2E). To further determine whether cDDP influences cell survival via cell-cycle arrest, the cell-cycle was analyzed by flow cytometry. In the cell-cycle profiles the cDDP-treatment in A2780S cells induced higher proportion of G₂/M arrest than those in A2780CP cells, albeit the cDDP-treatment increased the G₂/M arrest in both cell lines (Figures 2F and S2). We next analyzed the effect of cDDP on cell apoptosis using annexin V and PI staining. As shown in Figure 2G, after cDDP-treatment, the percentages of early apoptotic cells (PI⁻ annexin V⁺ cells) in A2780S and A2780CP cells were 2.30% and 1.10%, respectively; the percentages of late apoptotic cells (PI⁺ annexin V⁺ cells) were 7.53% and 2.14%, respectively. Obviously, the rates of cell apoptosis in the A2780CP cells were significantly lower than those in A2780S cells. Moreover, in the CCK8 assay the IC₅₀ of the A2780CP cells

($28.3 \pm 0.06 \mu\text{g/mL}$) was significantly higher than that of the A2780S cells ($20.5 \pm 0.08 \mu\text{g/mL}$). These results indicated that the hyper core fucosylation of CTR1 in A2780CP cells is important for their survival against cDDP-treatment. Considering the colocalization of CTR1 with hyper core fucosylation in the ovarian carcinoma tissues of cDDP-treated EOC patients (Figure 1D) and the high proportion of cDDP-resistance in EOC patients,^{2,31} core fucosylation of CTR1 is associated with the cDDP-resistance of EOC.

3.2 | Core fucosylation of CTR1 plays a crucial role in the cDDP-uptake of EOC cells

CTR1 on cell membrane is the most important cDDP-transporting protein with the N-linked glycosylation on its metal-binding ecto-domain.^{3,4,19,23-25,33} The colocalization of CTR1 with core fucosylation of N-glycans on the cell membrane of ovarian carcinoma implied that the function of CTR1 may be correlated with core fucosylation in cDDP-treated EOC (Figure 1D). Given that the CTR1 plays a crucial role in regulating the influx of platinum drugs into the cells,^{3,4,23-26} we suspected that the core fucosylation is involved in the CTR1-mediated cDDP-uptake of cells. To determine the influence of core fucosylation on the interaction between CTR1 and cDDP, the CTR1 from A2780CP and A2780S cells was purified (Figure 3A) and treated with 100 mU Fucosidase, which can cleave α 1,6 fucose linkages more efficiently than other α -fucose linkages.³² As shown in Figure 3B, the core fucose was completely removed on the CTR1 by fucosidase treatment from A2780CP (A2780CP + E) and A2780S (A2780S + E). Surprisingly, loss of core fucosylation on the CTR1 exhibited no binding activity to cDDP (Figure 3C), suggesting that the fucosylation of CTR1 is essential to the interaction between CTR1 and cDDP. Indeed, the CTR1 of A2780S cells exhibited stronger binding activity to cDDP than those of A2780CP cells with a dose-dependent manner (Figure 3C). The signals of CTR1-cDDP complex reached a threshold at 100 nM of cDDP, evidenced by no change of the signals at 140 nM (Figure 3C). Since the core fucosylation of A2780CP cells are significantly higher than those of A2780S cells, it is reasonable to consider that the hyper core fucosylation of CTR1 suppressed the CTR1-cDDP interaction in A2780CP cells.

ICP-MS analysis is usually applied for detecting the cellular accumulation of platinum.^{23,33} To further clarify the association of core fucosylation with the CTR1-mediated cDDP-uptake, we measured the cellular accumulation of platinum in the cells by ICP-MS analysis. The cellular accumulation of platinum in A2780S cells was higher than those in A2780CP cells (Figure 3D). These results suggested that the hyper core fucosylation of CTR1 could suppress the CTR1-cDDP interactions and the following cDDP-uptake of EOC cells.

3.3 | Lack of core fucosylation weakens the cDDP-resistance of mouse ovarian epithelial cells by promoting cellular cDDP-uptake

Since Fut8 is the sole glycosyltransferase for core fucosylation, the *Fut8*^{-/-} mice, which were generated in our laboratory, were applied

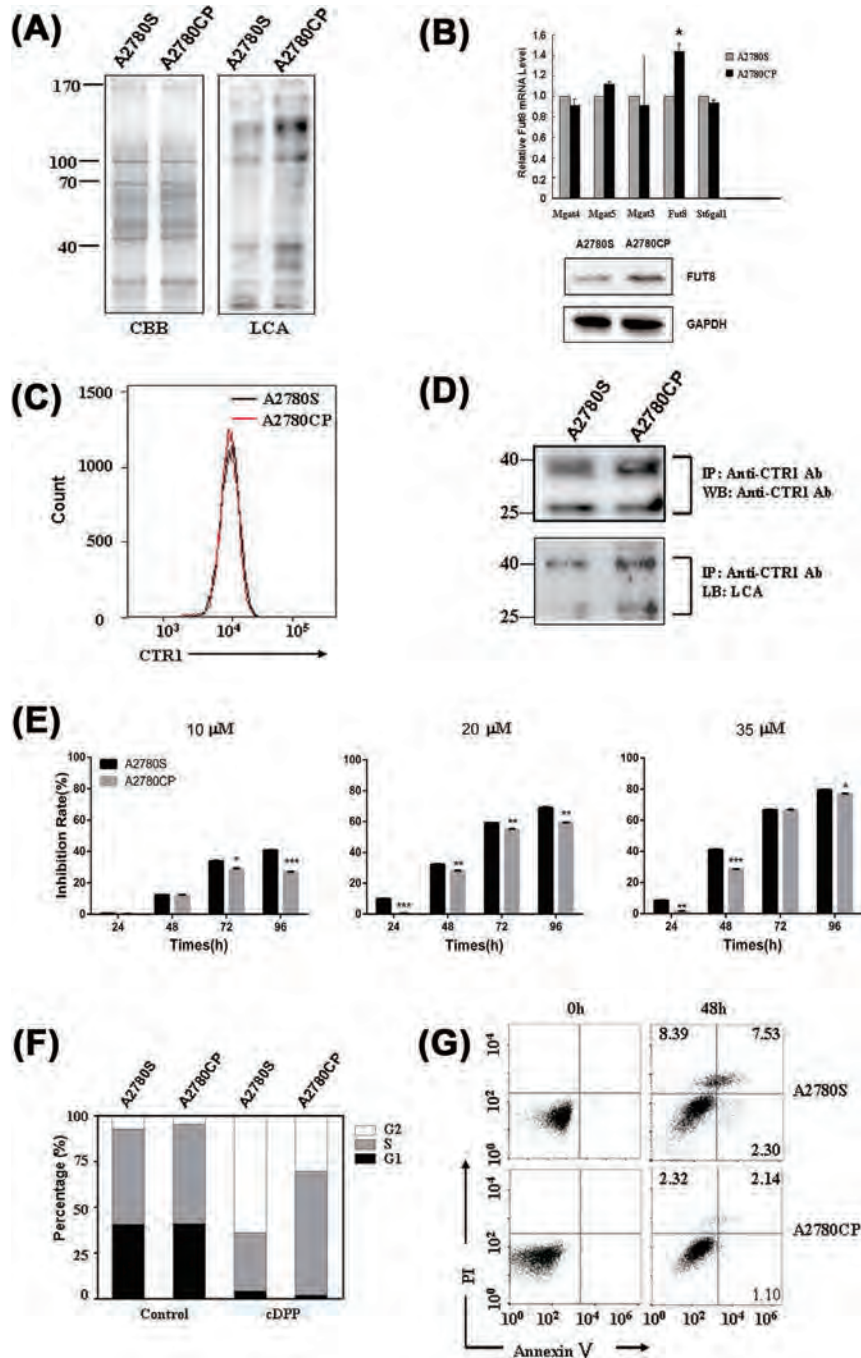


FIGURE 2 Core fucosylation are involved in the cDDP-resistance and survival of EOC cells. A, LCA staining of A2780S and A2780CP cells. The core fucosylation levels of A2780S and A2780CP cell lysates were detected using LCA staining. Coomassie brilliant blue (CBB) staining of gels showed the comparable amounts of protein. B, *Fut8* expressions of A2780S and A2780CP cell lines were analyzed by real time PCR and Western blot. The mRNA and protein levels of different genes were normalized with *GAPDH* expressions. The significantly difference was shown as * $P < 0.05$. C, Expressions of CTR1 on the surface of A2780S and A2780CP cells. Cells were stained with anti-CTR1 Ab for 30 min on ice, and the expression were analyzed by flow cytometry assay. D, Comparison of core fucosylation levels of CTR1 in A2780S and A2780CP cells. Whole lysates were immunoprecipitated by anti-CTR1 Ab, and followed by subjected to CTR1 Western blot and LCA blot analysis. E, The survival inhibition assay. A2780S and A2780CP cells were treated with 10, 20, and 35 μ M of cDDP for 24, 48, 72, and 96 h, and cell proliferation was analyzed by MTT assay. OD values were measured at 490 nm using microplate reader. Cell survival inhibition (%) = $(Ac-At)/(Ac-Ab) \times 100\%$. Ab, absorbance value of blank; Ac, absorbance value of control; At, absorbance value of cDDP-treated. The significantly difference was shown as * $P < 0.05$ or ** $P < 0.01$ or *** $P < 0.001$. F, Cell cycle analysis of A2780S and A2780CP cells. Cells were treated with 20 μ M cDDP for 48 h, the untreated cells were served as control. The PI staining was performed to measure the DNA content of cells; then the cell cycles were measured on a FACS Calibur cytometer. The percentages of cells were shown in different cell cycle phases (G₁, S, or G₂/M). G, The flow cytometry analysis was performed to measure the apoptosis of A2780S and A2780CP cells after PI and annexin V staining. Cells were exposed to 20 μ M cDDP for 48 h. [Color figure can be viewed at wileyonlinelibrary.com]

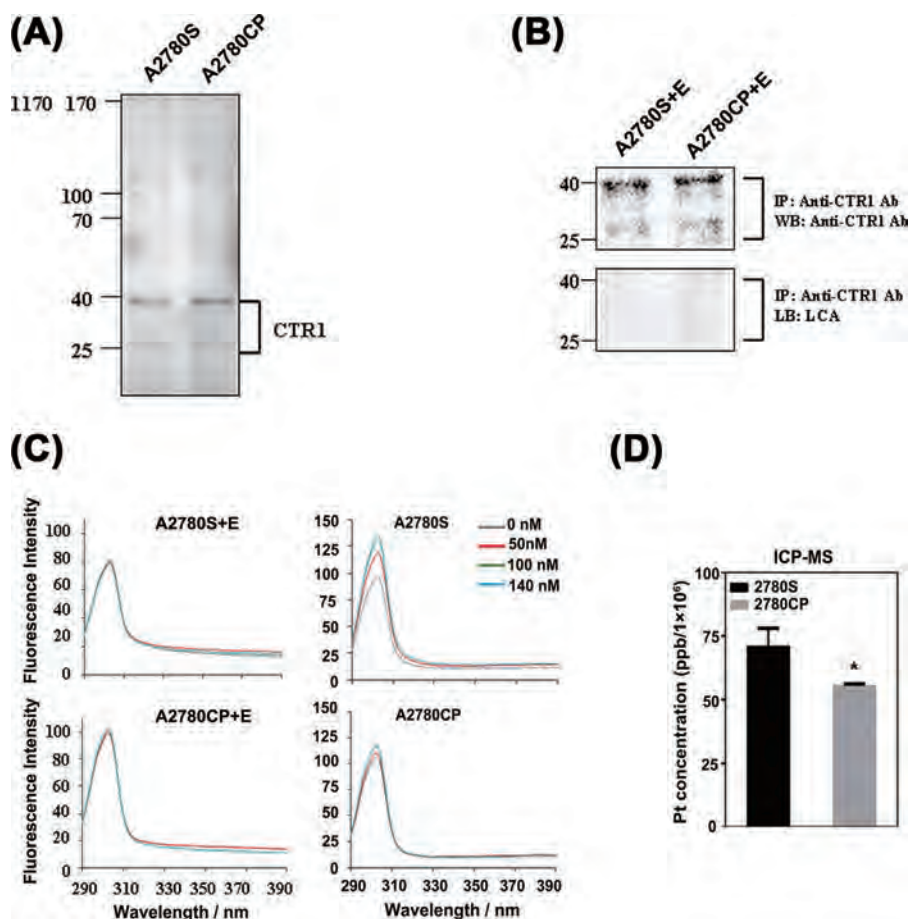


FIGURE 3 Core fucosylation regulates the CTR1-mediated cDDP uptake. A, Purification of CTR1. The proteins from A2780S and A2780CP cells were isolated, and CTR1 was further purified by the immunoprecipitation. B, Remove of fucose on the CTR1. The purified CTR1 was treated with 100mU Fucosidase. C, Molecular interactions between CTR1 proteins and cDDP. The cDDP solution (0, 50, 100, and 140 nM), was titrated into a fixed concentration of CTR1. Significant increase was observed in the fluorescence intensity, when the cDDP was interacted with CTR1. D, Cellular Pt accumulation after exposure to cDDP. A2780S and A2780CP were incubated with 50 μ M cDDP for 4 h. Cellular Pt accumulation was then measured by ICP-MS. The significantly difference was shown as * $P < 0.05$. [Color figure can be viewed at wileyonlinelibrary.com]

here to establish a *Fut8*-deleted mouse ovarian epithelial cell model.^{16,30} Immunohistochemistry assays with LCA show that core fucosylation was abolished in *Fut8*^{-/-} mouse ovary (Figure 4A). The purified ovarian epithelial cells were transfected with SV40 cDNA followed by screening with G418. Then the genotypes of immortalized *Fut8*^{-/-}, *Fut8*^{+/-}, and *Fut8*^{+/+} cells were proved by PCR assay (Figure 4B) and the epithelial type was identified by immunostaining of cytokeratin 14 (K14) in these three cell lines (Figure 4C). Furthermore, the CTR1 expressions in these three cell lines were examined by flow cytometry and western blot analysis. No significant difference of CTR1 expressions was found in *Fut8*^{-/-}, *Fut8*^{+/-}, and *Fut8*^{+/+} mouse ovarian epithelial cells (Figures 5A and 5B), however, the core fucosylation of *Fut8*^{-/-} mouse ovarian epithelial cells was abolished, and the core fucosylation level of *Fut8*^{+/-} cells was about half of *Fut8*^{+/+} cells (Figure 5B).

The cellular accumulation of platinum in *Fut8*^{-/-} cells were notably higher than that in *Fut8*^{+/-} and *Fut8*^{+/+} cells after incubation with 30 μ M of cDDP (Figure 5C). To determine the

role of core fucosylation in the cDDP-uptake of cells, we transduced *Fut8* cDNA to *Fut8*^{-/-} mouse ovarian epithelial cells and established *Fut8* restored cells (Re cells) (Figure 5D). As shown in Figure 5E, compared to *Fut8*^{+/+} cells, cDDP-uptake was significantly increased in *Fut8*^{-/-} cells, and that was restored in the Re cells. These results suggested that the lack of core fucosylation increased the CTR1-mediated cDDP-uptake of ovarian epithelial cells.

To further confirm the role of core fucosylation in cell survival after cDDP-treatment, we examined the proliferation of *Fut8*^{-/-}, *Fut8*^{+/-}, and *Fut8*^{+/+} mouse ovarian epithelial cells by MTT assay. Compared to *Fut8*^{+/+} cells, the survival rate of *Fut8*^{-/-} cells was dramatically reduced upon 10 and 20 μ M cDDP-treatment (Figure 5F). Moreover, the flow cytometry analysis shows that *Fut8*^{-/-} cells exhibited obviously increased apoptosis rate under 20 μ M cDDP-treatments (Figure 5G). Taken together, lack of core fucosylation weakens the cDDP-resistance of ovarian epithelial cells by promoting the cellular cDDP-uptake.

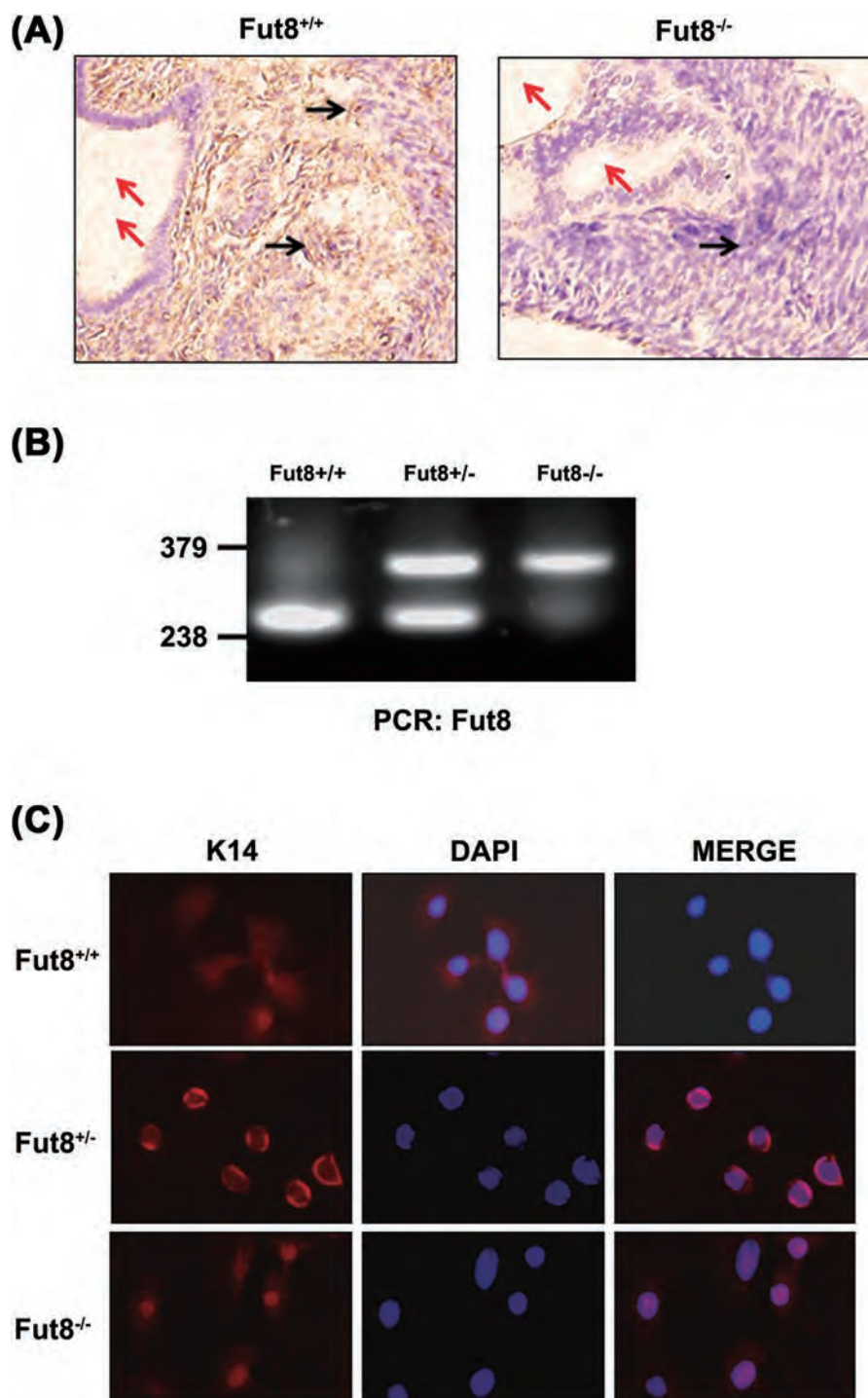


FIGURE 4 Establishment of the *Fut8*^{+/+}, *Fut8*^{+/-}, and *Fut8*^{-/-} ovary epithelial cells. A, Core fucosylation of *Fut8*^{+/+} and *Fut8*^{-/-} ovarian specimens by immunohistochemical analysis with LCA blot. Red arrows indicate antral follicles. Black arrows indicate primary follicles. B, PCR analysis of *Fut8* gene in the *Fut8*^{+/+}, *Fut8*^{+/-}, and *Fut8*^{-/-} cells. DNA were extracted from the *Fut8*^{+/+}, *Fut8*^{+/-}, and *Fut8*^{-/-} cells and were subjected to PCR assay. C, Identification of *Fut8*^{+/+}, *Fut8*^{+/-}, and *Fut8*^{-/-} ovarian epithelial cells. Cells were immunostained by antibody specific for epithelial marker (K14, red color, and DAPI, blue color). The magnification is 400-fold. [Color figure can be viewed at wileyonlinelibrary.com]

3.4 | Core fucosylation is involved in the cDDP-induced signal transduction in EOC cells

Several previous studies have proved that the uptake of cDDP initiates different signaling events, which modulating cell proliferation,

apoptosis, metabolism, and autophagy.^{3,34-37} To verify the impacts of core fucosylation on cell signaling, the A2780S and A2780CP cells were treated with 20 μ M of cDDP for 0, 5, 10, 15 min. Compared to low-core fucosylated A2780S cells, the phosphorylation levels of Akt, mTOR, ERK, and JNK was significantly enhanced in high-core

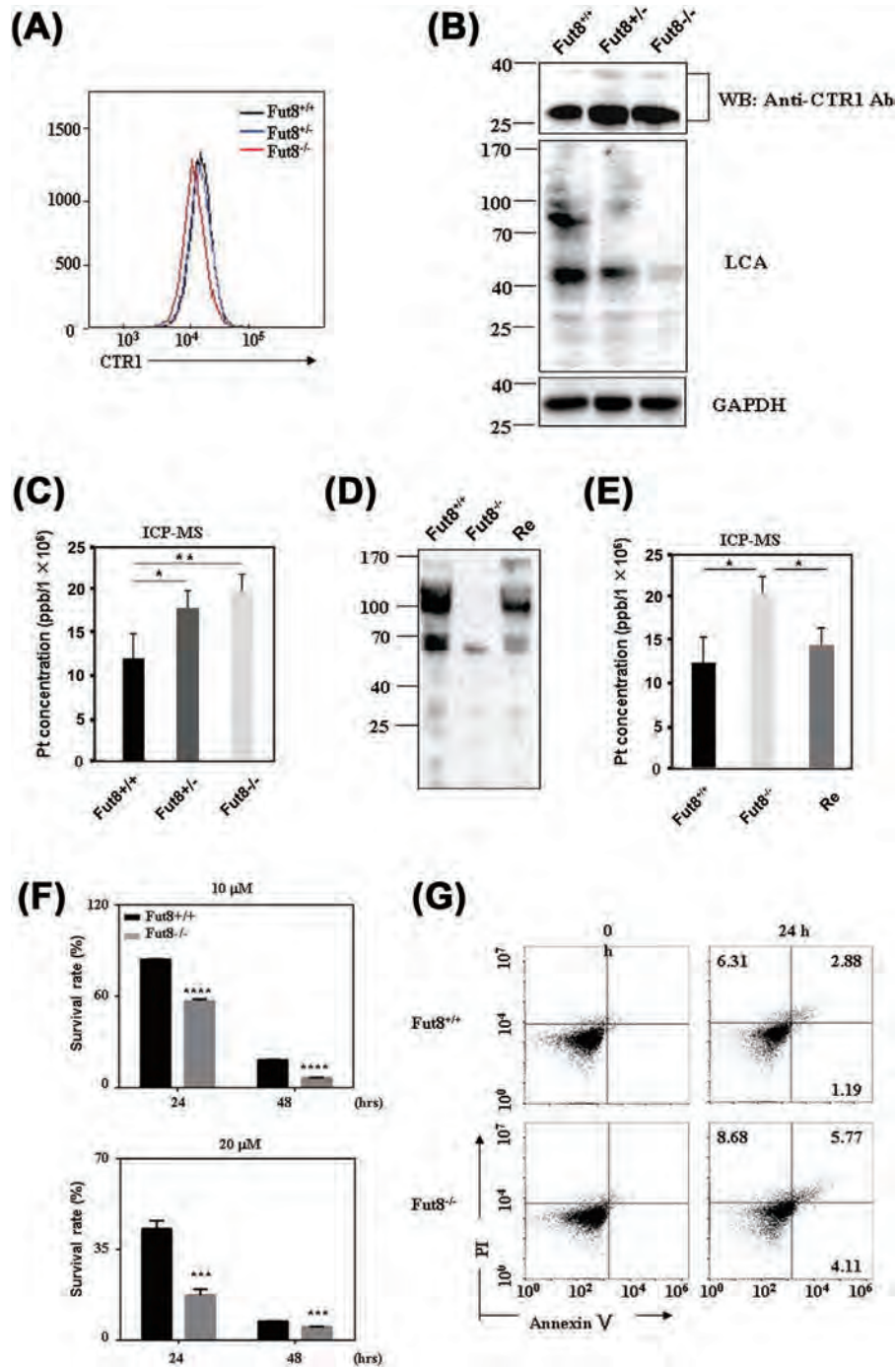


FIGURE 5 Loss of core fucosylation promotes CTR1-mediated cDDP uptake. A, Core fucosylation did not influence the CTR1 expressions on the surface of the *Fut8*^{+/+}, *Fut8*^{+/-}, and *Fut8*^{-/-} mouse ovarian epithelial cells. The CTR1 expressions on the cellular surface were analyzed by flow cytometry analysis. B, Immunoblot analysis. The CTR1 expressions were measured by Western blot. The core fucosylation of *Fut8*^{+/+}, *Fut8*^{+/-}, and *Fut8*^{-/-} cells were detected by LCA blot. GAPDH expressions were served as a control. C, Cellular Pt accumulation after exposure to cDDP. *Fut8*^{+/+}, *Fut8*^{+/-}, and *Fut8*^{-/-} mouse ovary epithelial cells were incubated with 30 μM cisplatin for 4 h. Platinum contents were then measured by ICP-MS. Data was expressed as mean ± SEM (n = 4). The significantly difference was shown as *P < 0.05. D, Establishment of Re cells. The Re cells were generated by introduction of *Fut8* cDNA to *Fut8*^{-/-} cells. The core fucosylation of *Fut8*^{+/+}, *Fut8*^{-/-}, and Re cells were detected by LCA blot. E, Cellular Pt accumulation of *Fut8*^{+/+}, *Fut8*^{-/-}, and Re cells by ICP-MS. Data was expressed as mean ± SEM (n = 4). The significantly difference was shown as *P < 0.05. F, MTT assay for cells viability. *Fut8*^{+/+} and *Fut8*^{-/-} cells were incubated with 10 and 20 μM of cDDP for 24 and 48 h. The significantly difference was shown as *P < 0.05 or **P < 0.01. G Flow cytometry analysis for cell apoptosis. After exposure to 20 μM cDDP for 48 h, *Fut8*^{+/+} and *Fut8*^{-/-} cell apoptosis was detected by double staining with PI and annexin V. [Color figure can be viewed at wileyonlinelibrary.com]

fucosylated A2780CP cells at 5, 15, and 30 min (Figures 6A and 6B). In addition, cDDP-induced cell signaling was also detected in *Fut8*^{-/-}, *Fut8*^{+/-}, and *Fut8*^{+/+} mouse ovary epithelial cells. Compared with *Fut8*^{-/-} ovary epithelial cells the enhanced activation of JNK and ERK signaling was found in *Fut8*^{+/+} cells under cDDP-treatment (Figures 6C and 6D). These results suggested that the core fucosylation is associated with the cDDP-induced signaling of EOC cells.

4 | DISCUSSION

Altered glycosylations contribute to the pathophysiological events during EOC progressions.^{1,5-12} In ovarian cancer, the mRNA expression and activity of the glycosyltransferase GnT-III, the enzyme responsible for the addition of bisecting N-linked glycans, were increased. The forced expression of ST6Gal-I, which catalyzes the addition of sialic acid to the termini of N-linked glycans, confers resistance to cisplatin, whereas ST6Gal-I knockdown conversely sensitizes cells to cisplatin.¹¹ The elevated fucosylation was also detected by AAL staining in ovarian cancer.⁶ Taniguchi and co-workers discovered that the mRNA levels and activity of FUT8 were increased in serous adenocarcinoma ovarian tissues compared with normal ovarian tissue.³⁸ These studies suggested the involvement of glycans in the ovarian cancer processes, but there are only a few reports available regarding the involvement of core fucosylation in resistance to platinum drugs in ovarian cancer. In the present study, we show that the level of core fucosylation was significantly increased in sera and cDDP-treated ovarian carcinoma tissues of cDDP-treated EOC patients. The elevated core fucosylation attributed to the cDDP-resistance of EOC by suppressing the binding of CTR1 with cDDP and the following cDDP-uptake, of which also affects cell signal transduction, survivals, and apoptosis (Figure 6E).

CTR1 transports cDDP via direct binding it by the Met-rich motifs within the ecto-domain.¹⁸ Thus the Met-rich motifs within the CTR1 ecto-domain are especially critical for cDDP acquisition of cells.^{18,19} Contrast to the CTR1^{-/-/WT} cells, the Pt content of CTR1^{-/-/M2} (⁴⁰MXXXM⁴⁵ was deleted) and CTR1^{-/-/Truncated} (the first N-terminal 45 amino acids were deleted) variants were increased by 2.5- and 2.3-fold, respectively.¹⁸ CTR1 contains one N-glycosylation site Asn¹⁵ on its metal-binding ecto-domain in mammalian cells. Fut8-catalyzed core fucosylation is one of the most prevalent glycosylations in mammalian N-glycans. Core fucosylation contributes to the folding, stability, and biological function of the molecules.^{15,30} Recently, Zhao et al⁵ detected a high level of core fucosylation in A2780CP cells by lectin array analysis. In agreement with this observation, we found that the core fucosylation levels in A2780CP cells are significantly higher than those of A2780S cells (Figure 2A) and the hyper core fucosylation suppressed the CTR1-cDDP interactions and cDDP-uptake in A2780CP cells (Figures 3C and 3D). Moreover, the capability of cDDP-uptake was obviously increased in the *Fut8*^{-/-} cells contrast to the *Fut8*^{+/+} cells, and suppressed in Re cells by re-introduction of *Fut8* gene. Since the cDDP-uptake of cancer cells is based on the molecular interaction between CTR1 and cDDP,⁴ and core fucosylation is

necessary for the molecular interactions such as receptor-ligand interaction on cell membrane,^{15,16} it is conceivable that core fucosylation is likely to be important in all three proposed stages involved in the cDDP-uptakes via CTR1. First, core fucosylation is essential for the conformation of metal-binding ecto-domain of CTR1. Second, core fucosylation of CTR1 could regulate the recognition of cDDP and affect the interaction between cDDP and CTR1. Third, core fucosylation is involved in the cDDP-uptake via CTR1 and the followed cell signaling.

CTR1 undergoes constitutive endocytosis and recycling to the plasma membrane. The removal of Asn¹⁵-linked glycan by mutation (N¹⁵Q) does not affect trafficking of the transporter to the cell surface.²⁷ Several studies on EOC cells reported that the expression levels of CTR1 are not correlated to the amount of cDDP accumulation.^{17,39,39} Conversely, it has been reported that the elevation of CTR1 expression in the tumor cells increased their sensitivity to platinum drugs and the survival of cancer patients.^{4,19,40} We found that there is no significant difference in CTR1 expressions of A2780S and A2780CP cells (Figure 2C), the CTR1 expression is not changed in A2780S and A2780CP cells after cDDP-treatment. It also reported that cDDP-treatment did not even change membrane CTR1 levels.^{17,39} However, cDDP induced down-regulation of human CTR1 expression in the CTR1^{-/-/WT}, CTR1^{-/-/M2}, and CTR1^{-/-/Truncated} cells.^{19,41} The discrepancy from our results may be caused by differences in the experimental procedure and the cell models. Although the changes of core fucosylation have no influence on the expression of CTR1 in *Fut8*^{+/+}, *Fut8*^{+/-}, and *Fut8*^{-/-} ovarian epithelial cells, loss of core fucosylation would give rise to the increased CTR1-cDDP interaction, thereby promotes cDDP-uptake, indicated that core fucosylation could sterically hinder cDDP-uptake within the ecto-domain. Therefore, it is reasonable to conceive that cDDP-uptake is mainly regulated by the core fucosylation of CTR1 rather than the cDDP expression.

The cDDP could initiate activation of different signaling pathways, such as ERK, MAPK, JNK, and AKT.^{3,34-37} which affect cell survival and apoptosis. Here we found that the different core fucosylations of CTR1 and distinct cDDP-uptakes existed between A2780S and A2780CP cells, implying that core fucosylation may be associated with cDDP-induced cell signal transductions by regulating CTR1-mediated cDDP-uptake. On the cell survival, cDDP caused the activation of ERK and JNK pathways that contribute to the increased proliferative rate of tumor cells.^{3,35,42} In our present study, the signaling in cDDP-resistant A2780CP cells was notably stronger than in cDDP-sensitive A2780S cells. In addition, compared with *Fut8*^{-/-} cells, the activation of JNK and ERK signaling were increased in *Fut8*^{+/+} cells under cDDP-treatment. On the apoptosis, AKT and its downstream molecular, mTOR, are correlated to the process of cDDP-resistance of ovarian cancer cells.^{3,34,36,37} In agreement with the previous study, the anti-apoptosis AKT-mTOR signaling was stronger in A2780CP cells than in A2780S cells, and the cell apoptosis in the A2780CP cells were significantly lower than those in A2780S cells, suggesting that the low apoptosis rate is correlated to the signal transductions via AKT-mTOR signaling. Beside the

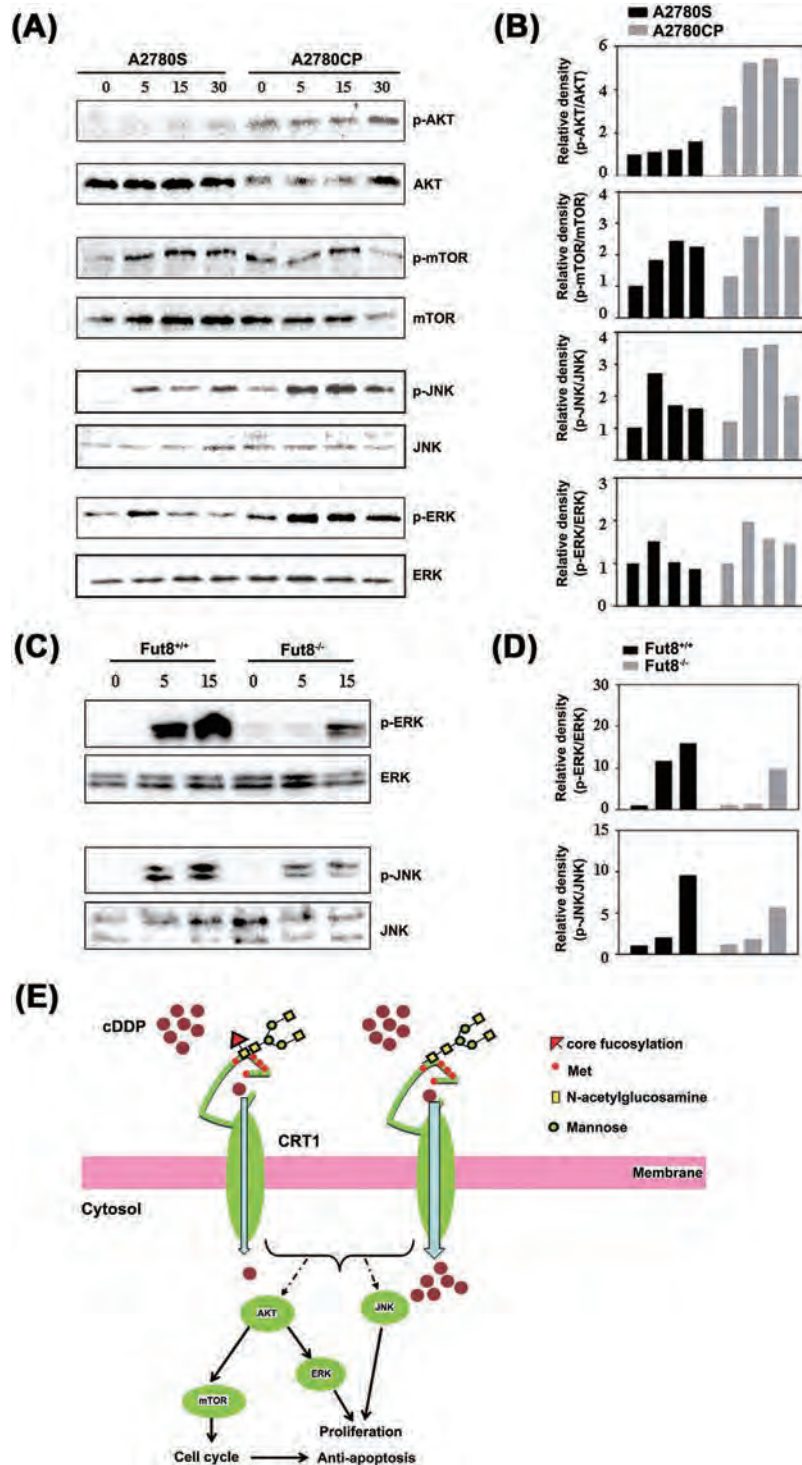


FIGURE 6 Core fucosylations regulate the cDDP-induced cell signal transduction. A, Phosphorylation assays. Phosphorylation assays for AKT, mTOR, JNK, and ERK. A2780S and A2780CP cells were serum starved for 24 h. The cells were harvested and treated with cDDP (20 μ M, for 0, 5, 15, and 30 min). Cell lysates were subjected to Western blot using anti-AKT, anti-pAKT, anti-mTOR, anti-pmTOR, anti-JNK, anti-pJNK, anti-ERK, and anti-pERK Abs. Data are representative of three independent experiment. B, The density of phosphorylated protein bands of A2780S and A2780CP cells was normalized to the corresponding density of total protein bands and the signal-activation are shown as Relative density. C, Phosphorylation assays. *Fut8*^{+/+} and *Fut8*^{-/-} mouse ovary epithelial cells were serum starved overnight. Then the harvested cells were incubated with cDDP (20 μ M, for 0, 5, and 15 min, and subjected to Western blot using anti-JNK, anti-pJNK, anti-ERK, and anti-pERK Abs. Data are representative of three independent experiment. D, The density of phosphor-protein bands of *Fut8*^{+/+} and *Fut8*^{-/-} mouse ovary epithelial cells was normalized to the corresponding density of total protein bands and the signal-activation are shown as relative density. E, Core fucosylation of CRT1 regulates the cDDP uptake and followed cell signaling and survival. [Color figure can be viewed at wileyonlinelibrary.com]

cDDP uptake of EOC cells, CTR1 also regulate the cellular pharmacology and sensitivity to platinum drugs.^{3,4,19,23–25,33} Similar to Cu⁺, platinum binds to Met-rich motifs within the CTR1 ectodomain,^{19,43} and CTR1 delivers platinum into cells via receptor mediated endocytosis rather than acting as a membrane channel as it does for Cu⁺.^{19,20} In this study, the cDDP-induced cellular signaling occurs by a short time (5 min), suggesting that the activation of signal pathway may depend on the receptor-mediated approaches. The precise biochemical mechanisms of how core fucosylation affects cDDP-induced cell signaling with or without CTR1 pathway remains to be elucidated in future study.

To our knowledge, this is the first attempt to show the alteration of core fucosylation in cDDP-resistance of EOC. The most important finding of the present study was the identification of the regulation role of core fucosylation in cDDP-uptake, which in turn, regulates several parameters of cDDP related events, such as cell survival, signal transduction, and cell apoptosis. Because the cDDP-uptake is a critical process during cDDP-resistance and the chemotherapy for the EOC,^{3,4,17,18} our results may have far-reaching implications that can enhance cDDP efficacy in resistant tumors or decrease the therapeutic dose needed for clinical efficacy by de-core fucosylation. An advanced understanding of the underlying mechanism of core fucosylation would provide new strategies for the treatment and diagnosis for malignant ovarian tumors from aspects of glycobiology.

ACKNOWLEDGMENTS

We gratefully acknowledge Chun Peng (York University, Toronto, Canada) and Dr. Shiyang Cui (Dalian Medical University) for the A2780S and A2780CP cell lines and Silethukuthula Natalie Ncube (Dalian Medical University) for critical reading of the manuscript. This work was supported by the National Nature Science Foundation of China (31570797, 31101717 and 31870797), and the Nutrition and Care of Maternal & Child Research Fund Project of Guangzhou Biostime Institute of Nutrition & Care (2018BINCMCF39), China. This work was also supported by Liaoning Provincial Program for Top Discipline of Basic Medical Sciences, China.

CONFLICTS OF INTEREST

The authors declare that they have no conflicts of interest with the contents of this article.

ORCID

Wenzhe Li  <http://orcid.org/0000-0001-7725-5325>

REFERENCES

- Zhang X, Wang Y, Qian Y, et al. Discovery of specific metastasis-related N-glycan alterations in epithelial ovarian cancer based on quantitative glycomics. *PLoS ONE*. 2014;9:e87978.
- Zhao H, Yu X, Ding Y, et al. MiR-770-5p inhibits cisplatin chemoresistance in human ovarian cancer by targeting ERCC2. *Oncotarget*. 2016;7:53254–53268.
- Dasari S, Tchounwou PB. Cisplatin in cancer therapy: molecular mechanisms of action. *Eur J Pharmacol*. 2014;740:364–378.
- Yoshida H, Teramae M, Yamauchi M, et al. Association of copper transporter expression with platinum resistance in epithelial ovarian cancer. *Anticancer Res*. 2013;33:1409–1414.
- Zhao R, Qin W, Qin R, et al. Lectin array and glycogene expression analyses of ovarian cancer cell line A2780 and its cisplatin-resistant derivative cell line A2780-cp. *Clin Proteomics*. 2017;14:20.
- Allam H, Johnson BP, Zhang M, Lu Z, Cannon MJ, Abbott KL. The glycosyltransferase GnT-III activates Notch signaling and drives stem cell expansion to promote the growth and invasion of ovarian cancer. *J Biol Chem*. 2017;292:16351–16359.
- Alley WR, Jr., Vasseur JA, Goetz JA, et al. N-linked glycan structures and their expressions change in the blood sera of ovarian cancer patients. *J Proteome Res*. 2012;11:2282–2300.
- Fuster MM, Esko JD. The sweet and sour of cancer: glycans as novel therapeutic targets. *Nat Rev Cancer*. 2005;5:526–542.
- Kuzmanov U, Jiang N, Smith CR, Soosaipillai A, Diamandis EP. Differential N-glycosylation of kallikrein 6 derived from ovarian cancer cells or the central nervous system. *Mol Cell Proteomics*. 2009;8:791–798.
- Saldova R, Wormald MR, Dwek RA, Rudd PM. Glycosylation changes on serum glycoproteins in ovarian cancer may contribute to disease pathogenesis. *Dis Markers*. 2008;25:219–232.
- Schultz MJ, Swindall AF, Wright JW, Sztul ES, Landen CN, Bellis SL. ST6Gal-I sialyltransferase confers cisplatin resistance in ovarian tumor cells. *J Ovarian Res*. 2013;6:25.
- Schwedler C, Kaup M, Weiz S, et al. Identification of 34 N-glycan isomers in human serum by capillary electrophoresis coupled with laser-induced fluorescence allows improving glycan biomarker discovery. *Anal Bioanal Chem*. 2014;406:7185–7193.
- Wilson JR, Williams D, Schachter H. The control of glycoprotein synthesis: N-acetylglucosamine linkage to a mannose residue as a signal for the attachment of L-fucose to the asparagine-linked N-acetylglucosamine residue of glycopeptide from alpha1-acid glycoprotein. *Biochem Biophys Res Commun*. 1976;72:909–916.
- Taniguchi N. A sugar-coated switch for cellular growth and arrest. *Nat Chem Biol*. 2007;3:307–309.
- Li W, Nakagawa T, Koyama N, et al. Down-regulation of trypsinogen expression is associated with growth retardation in alpha1,6-fucosyltransferase-deficient mice: attenuation of proteinase-activated receptor 2 activity. *Glycobiology*. 2006;16:1007–1019.
- Li W, Yu R, Ma B, et al. Core fucosylation of IgG B cell receptor is required for antigen recognition and antibody production. *J Immunol*. 2015;194:2596–2606.
- Kalayda GV, Wagner CH, Jaehde U. Relevance of copper transporter 1 for cisplatin resistance in human ovarian carcinoma cells. *J Inorg Biochem*. 2012;116:1–10.
- Larson CA, Adams PL, Jandial DD, Blair BG, Safaei R, Howell SB. The role of the N-terminus of mammalian copper transporter 1 in the cellular accumulation of cisplatin. *Biochem Pharmacol*. 2010;80:448–454.
- Ohrvik H, Logeman B, Turk B, Reinheckel T, Thiele DJ. Cathepsin protease controls copper and cisplatin accumulation via cleavage of the Ctr1 metal-binding ectodomain. *J Biol Chem*. 2016;291:13905–13916.
- Sinani D, Adle DJ, Kim H, Lee J. Distinct mechanisms for Ctr1-mediated copper and cisplatin transport. *J Biol Chem*. 2007;282:26775–26785.
- Kudoh K, Takano M, Koshikawa T, et al. Gains of 1q21-q22 and 13q12-q14 are potential indicators for resistance to cisplatin-based chemotherapy in ovarian cancer patients. *Clin Cancer Res*. 1999;5:2526–2531.

22. Muggia F. Platinum compounds 30 years after the introduction of cisplatin: implications for the treatment of ovarian cancer. *Gynecol Oncol.* 2009;112:275–281.
23. Ishida S, McCormick F, Smith-McCune K, Hanahan D. Enhancing tumor-specific uptake of the anticancer drug cisplatin with a copper chelator. *Cancer Cell.* 2010;17:574–583.
24. Kuo MT, Fu S, Savaraj N, Chen HH. Role of the human high-affinity copper transporter in copper homeostasis regulation and cisplatin sensitivity in cancer chemotherapy. *Cancer Res.* 2012;72:4616–4621.
25. Liang ZD, Long Y, Chen HH, Savaraj N, Kuo MT. Regulation of the high-affinity copper transporter (hCTR1) expression by cisplatin and heavy metals. *J Biol Inorg Chem.* 2014;19:17–27.
26. Ishida S, Lee J, Thiele DJ, Herskowitz I. Uptake of the anticancer drug cisplatin mediated by the copper transporter Ctr1 in yeast and mammals. *Proc Natl Acad Sci USA.* 2002;99:14298–14302.
27. Maryon EB, Molloy SA, Kaplan JH. O-linked glycosylation at threonine 27 protects the copper transporter hCTR1 from proteolytic cleavage in mammalian cells. *J Biol Chem.* 2007;282:20376–20387.
28. Tatenno H, Nakamura-Tsuruta S, Hirabayashi J. Comparative analysis of core-fucose-binding lectins from *Lens culinaris* and *Pisum sativum* using frontal affinity chromatography. *Glycobiology.* 2009;19:527–536.
29. Zhao JY, Liu CQ, Zhao HN, et al. Synchronous detection of miRNAs, their targets and downstream proteins in transferred FFPE sections: applications in clinical and basic research. *Methods.* 2012;58:156–163.
30. Li W, Liu Q, Pang Y, et al. Core fucosylation of mu heavy chains regulates assembly and intracellular signaling of precursor B cell receptors. *J Biol Chem.* 2011;287:2500–2508.
31. Williams TI, Touns KL, Saggese DA, Kalli KR, Cliby WA, Muddiman DC. Epithelial ovarian cancer: disease etiology, treatment, detection, and investigational gene, metabolite, and protein biomarkers. *J Proteome Res.* 2007;6:2936–2962.
32. O'Flaherty R, Harbison AM, Hanley PJ, Taron CH, Fadda E, Rudd PM. Aminoquinoline fluorescent labels obstruct efficient removal of N-glycan core alpha(1-6) fucose by bovine kidney alpha-L-fucosidase (BKF). *J Proteome Res.* 2017;16:4237–4243.
33. Holzer AK, Manorek GH, Howell SB. Contribution of the major copper influx transporter CTR1 to the cellular accumulation of cisplatin, carboplatin, and oxaliplatin. *Mol Pharmacol.* 2006;70:1390–1394.
34. Fraser M, Bai T, Tsang BK. Akt promotes cisplatin resistance in human ovarian cancer cells through inhibition of p53 phosphorylation and nuclear function. *Int J Cancer.* 2008;122:534–546.
35. Hayakawa J, Mittal S, Wang Y, et al. Identification of promoters bound by c-Jun/ATF2 during rapid large-scale gene activation following genotoxic stress. *Mol Cell.* 2004;16:521–535.
36. Mabuchi S, Kawase C, Altomare DA, et al. MTOR is a promising therapeutic target both in cisplatin-sensitive and cisplatin-resistant clear cell carcinoma of the ovary. *Clin Cancer Res.* 2009;15:5404–5413.
37. Yagyu T, Tsuji Y, Haruta S, et al. Activation of mammalian target of rapamycin in postmenopausal ovarian endometriosis. *Int J Gynecol Cancer.* 2006;16:1545–1551.
38. Takahashi T, Ikeda Y, Miyoshi E, Yaginuma Y, Ishikawa M, Taniguchi N. Alpha1,6fucosyltransferase is highly and specifically expressed in human ovarian serous adenocarcinomas. *Int J Cancer.* 2000;88:914–919.
39. Ivy KD, Kaplan JH. A re-evaluation of the role of hCTR1, the human high-affinity copper transporter, in platinum-drug entry into human cells. *Mol Pharmacol.* 2013;83:1237–1246.
40. Lee YY, Choi CH, Do IG, et al. Prognostic value of the copper transporters, CTR1 and CTR2, in patients with ovarian carcinoma receiving platinum-based chemotherapy. *Gynecol Oncol.* 2011;122:361–365.
41. Shang X, Lin X, Manorek G, Howell SB. Claudin-3 and claudin-4 regulate sensitivity to cisplatin by controlling expression of the copper and cisplatin influx transporter CTR1. *Mol Pharmacol.* 2013;83:85–94.
42. Johnson GL, Lapadat R. Mitogen-activated protein kinase pathways mediated by ERK, JNK, and p38 protein kinases. *Science.* 2002;298:1911–1912.
43. Crider SE, Holbrook RJ, Franz KJ. Coordination of platinum therapeutic agents to met-rich motifs of human copper transport protein1. *Metallomics.* 2010;2:74–83.

SUPPORTING INFORMATION

Additional supporting information may be found online in the Supporting Information section at the end of the article.

How to cite this article: Lv X, Song J, Xue K, et al. Core fucosylation of copper transporter 1 plays a crucial role in cisplatin-resistance of epithelial ovarian cancer by regulating drug uptake. *Molecular Carcinogenesis.* 2019;1–14.
<https://doi.org/10.1002/mc.22971>

Article

Sialic Acid-Binding Lectin from Bullfrog Eggs Exhibits an Anti-Tumor Effect Against Breast Cancer Cells Including Triple-Negative Phenotype Cells

Takeo Tatsuta¹, Shoko Sato², Toshiyuki Sato³, Shigeki Sugawara¹, Tsuneyoshi Suzuki², Akiyoshi Hara³ and Masahiro Hosono^{1,*} 

¹ Division of Cell Recognition Study, Institute of Molecular Biomembrane and Glycobiology, Tohoku Medical and Pharmaceutical University, Sendai, Miyagi 981-8558, Japan; t-takeo@tohoku-mpu.ac.jp (T.T.); ssuga@tohoku-mpu.ac.jp (S.S.)

² Department of Pharmaceutical Sciences, Tohoku Medical and Pharmaceutical University, Sendai, Miyagi 981-8558, Japan; shoko-s@tohoku-mpu.ac.jp (S.S.); tusuzuki@tohoku-mpu.ac.jp (T.S.)

³ Department of Clinical Pharmacotherapeutics, Tohoku Medical and Pharmaceutical University, Sendai, Miyagi 981-8558, Japan; hachikuma81@gmail.com (T.S.); hara-a@tohoku-mpu.ac.jp (A.H.)

* Correspondence: mhosono@tohoku-mpu.ac.jp; Tel.: +81-022-727-0114

Academic Editors: Tomohisa Ogawa and Hiroaki Tateno

Received: 18 September 2018; Accepted: 19 October 2018; Published: 21 October 2018



Abstract: Sialic acid-binding lectin from *Rana catesbeiana* eggs (cSBL) is a multifunctional protein that has lectin and ribonuclease activity. In this study, the anti-tumor activities of cSBL were assessed using a panel of breast cancer cell lines. cSBL suppressed the cell growth of all cancer cell lines tested here at a concentration that is less toxic, or not toxic at all, to normal cells. The growth suppressive effect was attributed to the cancer-selective induction of apoptosis. We assessed the expressions of several key molecules associated with the breast cancer phenotype after cSBL treatment by western blotting. cSBL decreased the expression level of estrogen receptor (ER) α , while it increased the phosphorylation level of p38 mitogen-activated protein kinase (MAPK). cSBL also suppressed the expression of the progesterone receptor (PgR) and human epidermal growth factor receptor type 2 (HER2). Furthermore, it was revealed that cSBL decreases the expression of the epidermal growth factor receptor (EGFR/HER1) in triple-negative breast cancer cells. These results indicate that cSBL induces apoptosis with decreasing ErbB family proteins and may have great potential for breast cancer chemotherapy, particularly in triple-negative phenotype cells.

Keywords: lectin; sialic acid-binding lectin; ribonuclease; breast cancer; ErbB family

1. Introduction

Lectins are proteins that bind to specific carbohydrate structures. They exist universally in plants, microorganisms, and animals, and have great potential for cancer therapy [1]. Even though only lectins play a role in recognizing sialic acids, i.e., sialic acid-binding lectins (SBLs), there are several lectins that reportedly have anti-tumor effects, such as *Maackia amurensis* seed lectin (MASL) [2], *Polygonatum odoratum* lectin (POL) [3], and *Haliotis discus discus* lectin (HddSBL) [4]. Sialic acids on the plasma membrane are generally observed to be linked to the terminal position of the carbohydrate groups of glycoproteins and glycolipids and have roles in the conformation, recognition, or binding of glycomolecules [5]. Given that altered sialylation is closely associated with malignant phenotypes, including metastasis and invasiveness [6,7], exploration of the effects of SBLs in cancer therapy is a field of great interest for basic studies, and also for clinical researchers.

The 12 kDa protein isolated from *Rana catesbeiana* oocytes was found to be a cell agglutinin [8] of many kinds of cancer cells, but not normal cells. These agglutinations were shown to be inhibited by

the sialic acid-containing complex, but not by their asialo-derivatives and, thus, the protein was named *R. catesbeiana* sialic acid-binding lectin (cSBL) [9]. Subsequent analyses revealed that it is homologous to the ribonuclease (RNase) A superfamily and it has substantial RNase activity [8,10,11]. An RNase purified from *R. catesbeiana* oocytes collected in Taiwan by Liao et al., and named RC-RNase, was found to be identical to cSBL [12,13]. Therefore, this interesting SBL is now consequently also called a leczyne (lectin + enzyme) [14,15].

Breast cancer is a molecularly heterogeneous disease [16]. Currently, the classification of breast cancer is based mainly on the expression of the estrogen receptor (ER), progesterone receptor (PgR), and the overexpression or amplification of human epidermal growth factor receptor 2 (HER2/c-ErbB2). In addition, tumors are characterized by grade and proliferative fraction (most commonly assessed by Ki-67). The intrinsic molecular subtypes of breast cancer are known as luminal A-like (strongly ER and PgR positive, HER2 negative, with lower proliferation markers), luminal B-like (variable degrees of ER/PgR expression, with higher proliferative fraction), HER2-enriched (ER and PgR negative, and HER2 positive) and basal-like (ER, PgR, and HER2 negative), and these are routinely used clinically to classify patients for prognostic predictions and to select treatments [17]. The basal-like subtype includes triple-negative breast cancer [18]. Patients diagnosed with triple-negative breast cancer have a poorer prognosis than HER2 and/or hormone receptor positive groups [19]. Recently, the three additional members of the HER/ErbB family of receptor tyrosine kinases (epidermal growth factor receptor (EGFR)/HER1/c-ErbB1, HER3/c-ErbB3 and HER4/c-ErbB4) have been of particular interest because of their ability to interact with HER2 [20]. Members of ErbB family are critically involved in the development and progression of breast cancer. The overexpression of HER1/EGFR is significantly associated with poor prognosis [21,22]. EGFR is well known as a treatment target for colorectal, head and neck, and non-small cell lung cancers, and is also a therapeutic target for breast cancer [23].

Since 2011, the efficacy of cSBL on breast cancer cells has been reported; however, the selectivity of cSBL to some cell lines is controversial. Tseng et al. showed that cSBL induces cell death selectively on ER-positive breast cancer cell lines (MCF7 and ZR-75-1), but not on ER-negative breast cancer cell lines (MDA-MB-231 and ZR-75-30) [24]. Their report indicates that ER is an important target of the RNase activity of cSBL. In contrast, our group has demonstrated that cSBL induces cell death in all cell lines tested in the report including MCF7 (ER-, PgR- and HER2-positive), SK-BR-3 (HER2-positive) and MDA-MB-231 (triple-negative) [25]. Here, we tested the effects of cSBL on a larger number of cell lines that represent distinct phenotypes, and also on a normal breast-derived cell line. It was revealed that cSBL exerts its pro-apoptotic effects on all cancer cells, but not on normal breast cells. Furthermore, we found that treatment with cSBL leads to the decrement of HER2 expression, and this reduced expression was also observed with regard to other ErbB family proteins expressed in each cell line. Our results suggest a potential application of cSBL in the treatment of breast cancers, including triple-negative breast cancer.

2. Results

2.1. Effects of cSBL on Breast Cancer Cell Growth

To evaluate the impact of cSBL on breast cancer cell growth, we first examined the effects of cSBL on cell proliferation in several breast cancer cell lines and a normal breast cell line by WST assay. The immortalized human mammary epithelial cell line, MCF 10A, was used as the normal breast cell line due to its non-tumorigenic origin [26]. The characteristic features of each cell lines used in this study are summarized in Table 1. As shown in Figure 1A, treatment with cSBL resulted in a significant reduction in the proliferation of breast cancer cells. In contrast, cSBL hardly showed any inhibitory effect on the proliferation of normal breast cells. Although statistical differences were detected at 10 and 20 μ M treatments with cSBL in MCF 10A cells, the viabilities were kept as 91% and 85%, respectively. The viabilities of each cell line with treatment of 20 μ M cSBL were as follows:

ZR-75-1, 69%; BT-474, 51%; MCF7, 45%; SK-BR-3, 46%; MDA-MB-231, 52%; MDA-MB468, 40%; and MCF 10A, 85%. MCF7 cells were shown to be the most sensitive to cSBL and the inhibitory effect was observed from relatively low concentrations, such as 1 μ M (viability: 50%).

Table 1. Classification of breast cancer cell lines [16,27].

Cell Line	ER ¹	PgR ¹	HER2 ²	Subtype
ZR-75-1	+	+	2+	Luminal A
BT-474	+	+	3+	Luminal B
MCF7	+	+	0-1+	Luminal A
SK-BR-3	-	-	3+	HER2
MDA-MB-231	-	-	0-1+	Basal
MDA-MB-468	-	-	-	Basal
MCF 10A	-	-	0-1+	Basal

¹ Data from mRNA, protein levels [16], and/or immunohistochemical (IHC) analysis [26]; ² Data from IHC analysis [26]. The Allred score was used for HER2.

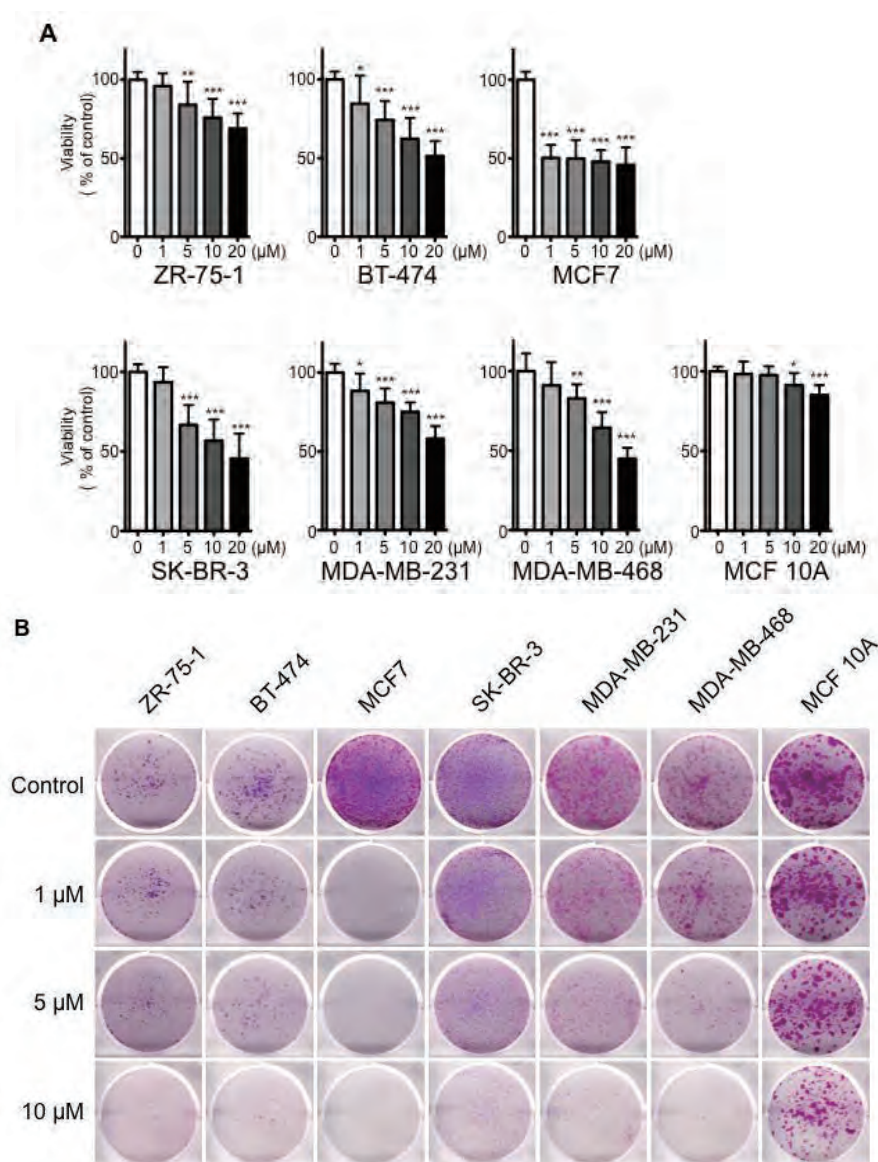


Figure 1. Cont.

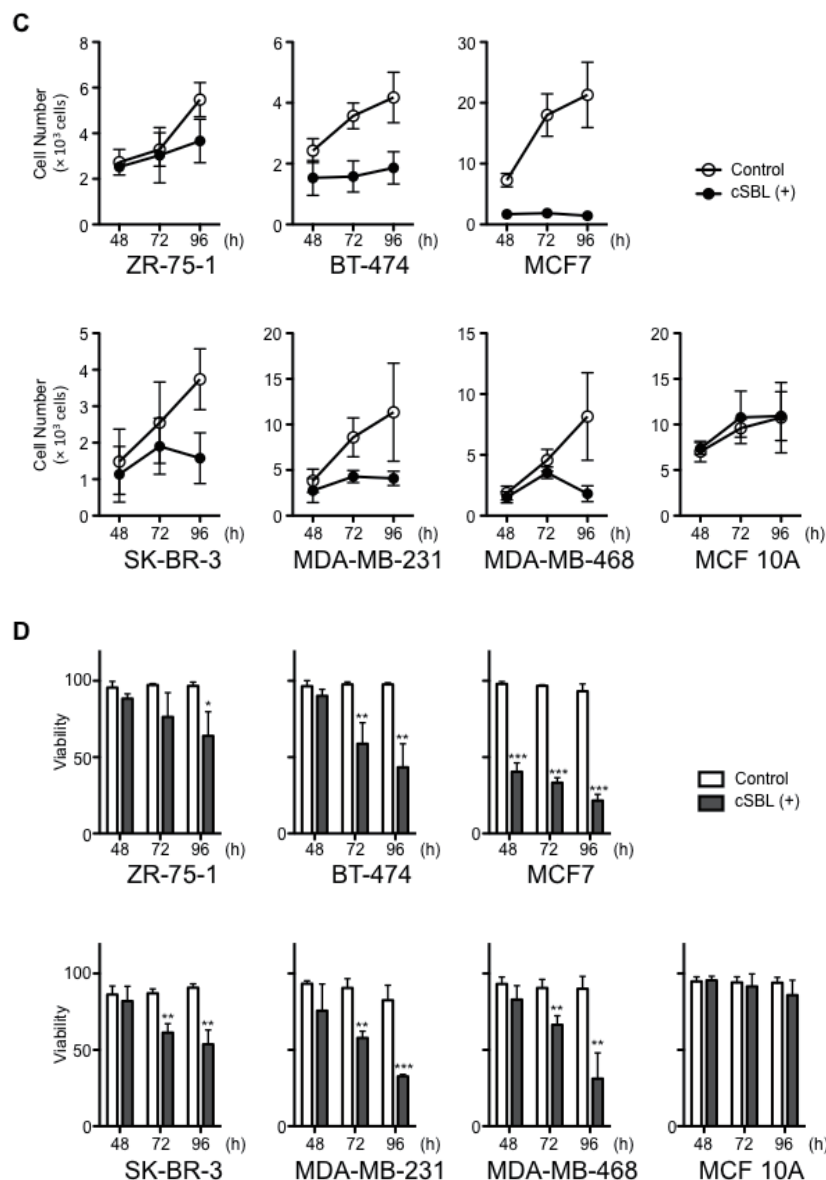


Figure 1. Anti-proliferative effects of *R. catesbeiana* sialic acid-binding lectin (cSBL) against breast cancer cell lines (ZR-75-1, BT-474, MCF7, SK-BR-3, MDA-MB-231, and MDA-MB-468) and a non-tumorigenic epithelial cell line (MCF 10A). (A) Viability of cells treated with cSBL. Cells were treated with cSBL (0.2–20 μ M) for 72 h. Each data point represents the mean \pm SD of three independent WST-8 assays conducted in triplicate. (B) The effects of cSBL on the clonogenic potential of the cells. Colony assays were performed on the cells in the absence or presence of cSBL (1, 5, and 10 μ M) for 72 h followed by incubation in cSBL-free medium for 7–28 days. Then, the cells were fixed with 2% paraformaldehyde and stained with crystal violet. Representative images from three independent experiments are shown. Cell growth (C) and viability were determined by trypan blue assay (D) of the cells treated with or without cSBL. Cells were treated with cSBL (10 μ M) for 48–96 h. Both live and dead cell numbers were counted by TC10. Each data point represents the mean \pm SD of three independent assays. For both graphs, * $p < 0.05$. ** $p < 0.01$. *** $p < 0.001$.

Next, we assessed the effects of cSBL on a clonogenic assay. At first, 5×10^3 cells were seeded, and then, the cells were treated with cSBL. cSBL markedly impaired the colony formation of breast cancer cells, whereas it had no profound effect on the growth of normal breast cells (Figure 1B). Untreated control cells of MCF7, MDA-MB-231, and MCF 10A exhibited higher colony forming rates, and ZR-75-1 and BT-474 exhibited low colony forming rates. Since the initial seeding concentration

of the cells affected the colony formation efficiency, we also performed the clonogenic assay with different cell seeding concentrations (Supplementary Figure S1). MCF7, SK-BR-3, MDA-MB-231, MDA-MB468, and MCF 10A cells were seeded with 2.5×10^3 cells per well (Figure S1A), ZR-75-1 and BT-474 cells were seeded with 1×10^4 cells per well (Figure S1B). As shown in Figure 1B and Figure S1A and B, similar tendencies were observed in all conditions. Namely, MCF7 showed the highest sensitivity; moderate effects were found in MDA-MB-231 and MDA-MB-468; SK-BR-3, ZR-75-1 and BT-474 exhibited relatively lower levels of sensitivity, but their effects on MCF 10A were limited. Furthermore, lower concentrations of cSBL were assessed with MCF7 and the significant inhibitory effects were confirmed for all cell seeding concentrations tested here, even with treatment of 0.1 μM (Figure S1C,D).

To obtain further evidence that cSBL only reduced the proliferation of breast cancer cells, we also measured the cell viability with the trypan blue dye exclusion assay (Figure 1C,D), since the assay counts the live and dead cells directly. All untreated control cells continued to proliferate over the experimental period; however, the proliferations of the cancer cells were impaired with cSBL treatment (Figure 1C). cSBL decreased the viability of all cancer cells significantly in a time- dependent manner. In MCF 10A, the effects of cSBL on cell growth and viability were not significant. In summary, cSBL showed concentration- and time-dependent cancer cell growth-suppressing effects. All assays showed a similar tendency, whereby MCF7 exhibited the highest, and MCF 10A exhibited the lowest sensitivity to cSBL. There were no correlations between cSBL effectiveness and the expression statuses of ER, PgR, or HER2. These results suggest that treatment with cSBL selectively leads to a cell growth inhibitory effect on breast cancer cells, regardless of the cancer cell phenotype.

2.2. cSBL-Induced Apoptosis

To investigate further insight into the growth inhibitory effects of cSBL, we assayed apoptotic cell death by detecting morphological and biochemical apoptotic changes. We analyzed nuclear morphological changes by Hoechst staining. As shown in Figure 2A, similar to the effects on cell proliferation, treatment with cSBL led to the induction of chromatin condensation and nuclear collapse in breast cancer cells, whereas it had almost no pro-apoptotic effects on normal cells. Since MCF7 is a type of caspase-3 deficient cell [28], and since the pro-apoptotic effects of cSBL are mainly initiated by caspase-9 activation [29], we analyzed the cleavage of procaspase-9 as an initiative event and that of poly-(ADP-ribose) polymerase (PARP) as an executive event. Treatment with cSBL cleaved the pro-caspase-9 and PARP in breast cancer cells, although the effects were relatively low in ZR-75-1 (Figure 2B). The cleaved form of PARP was detected slightly in MCF 10A treated with cSBL, but the level was comparable with the control. Taken together, these results suggest that cSBL induces apoptotic cell death via caspase cascade activation, particularly in cancer cells. Considering that cSBL decreased viabilities as well as cell numbers of breast cancer cells (Figure 1C,D), it is suggested that cSBL causes the death of cancer cells rather than the arrest of the cell cycle, and the induction of apoptosis is responsible for the cell death.

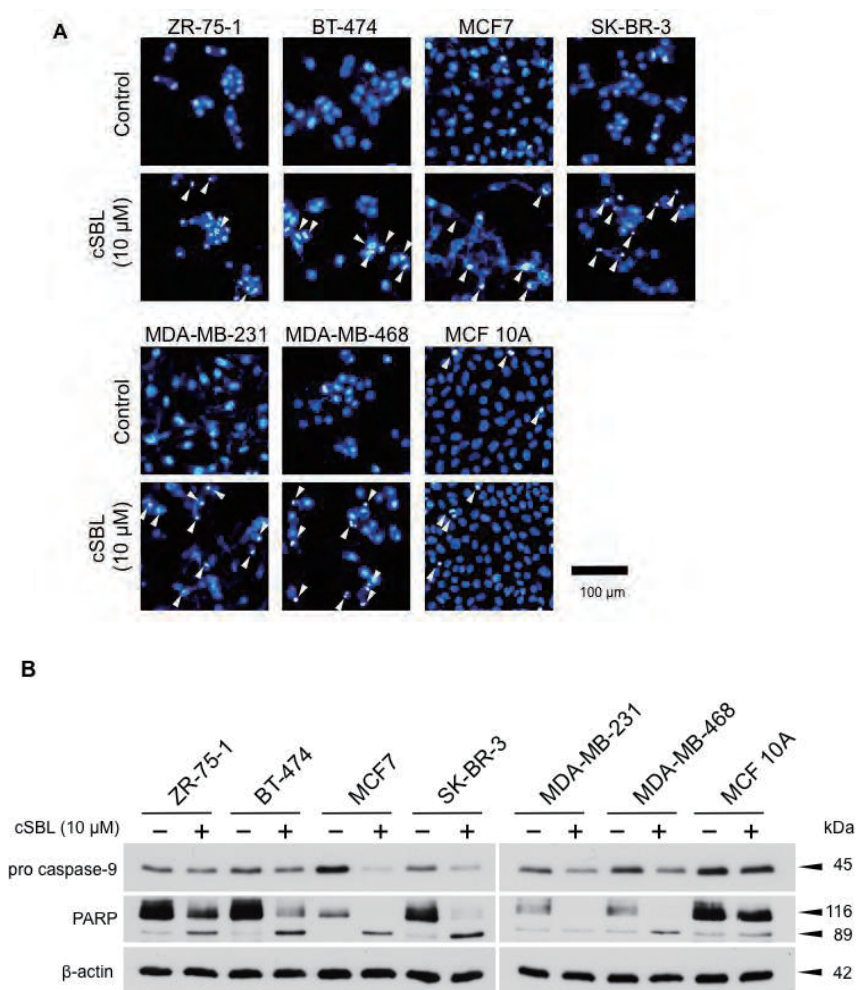


Figure 2. Apoptosis induction in breast cancer cell lines (ZR-75-1, BT-474, MCF7, SK-BR-3, MDA-MB-231, and MDA-MB-468) treated with cSBL. **(A)** Morphological changes of nuclei in cSBL-treated cells. Cells were treated with cSBL (10 μM) for 72 h and stained with Hoechst 33342. Nuclei were observed using a fluorescent microscope. Arrows indicate apoptotic nuclei. Magnification, 20×. **(B)** Cells were treated with cSBL (10 μM) for 72 h, and caspase-9 and PARP cleavage were detected by western blotting.

2.3. Effects of cSBL on Cell Survival-Related Molecules

We previously reported that cSBL induces p38 mitogen-activated protein kinase (MAPK) and consequently, activates caspase-3/7 in SBL-induced cell death [25]. Furthermore, Tseng et al., reported that cSBL induces cell death in ER-positive breast tumors through down-regulation of Bcl-2 and ER [24]. To confirm these phenomena and to further investigate cSBL-induced alterations on cell survival-related molecular expressions, we analyzed the phosphorylation of p38, JNK, and ERK MAPKs and protein expressions of the anti-apoptotic Bcl-2 family, as well as ERα, PgR, and HER2 in ER-positive ZR-75-1 and MCF7 cells. As shown in Figure 3A, consistent with previous reports, cSBL induced p38 phosphorylation. A slight phosphorylation of JNK was also observed in ZR-75-1 cells—whereas total JNK expression decreased in MCF7 cells, the phosphorylated JNK level was kept the same as control cells, and relative phosphorylation tended to increase. The phosphorylation status of ERK was not affected by cSBL treatment in both cell lines. Regarding the Bcl-2 family, although statistical significance was not observed, consistent with previous reports, cSBL tended to decrease the expression of Bcl-2 in MCF7, and decrements of Bcl-xL and Mcl-1 were detected in the cells (Figure 3B). In ZR-75-1 cells, Bcl-2 expression was very faint, and BCL-xL and Mcl-1 expression levels were slightly

increased. Thus, the effects of cSBL on the anti-apoptotic Bcl-2 family seem to vary depending on the cell line. ER α expression drastically decreased after exposure to cSBL in both cells, as expected (Figure 3C). Interestingly, cSBL also suppressed PgR in MCF7 and HER2 protein expression in both cell lines. These results indicate that cSBL works in an inhibitory manner concerning the protein expressions of key molecules that are implicated in breast cancer phenotypes.

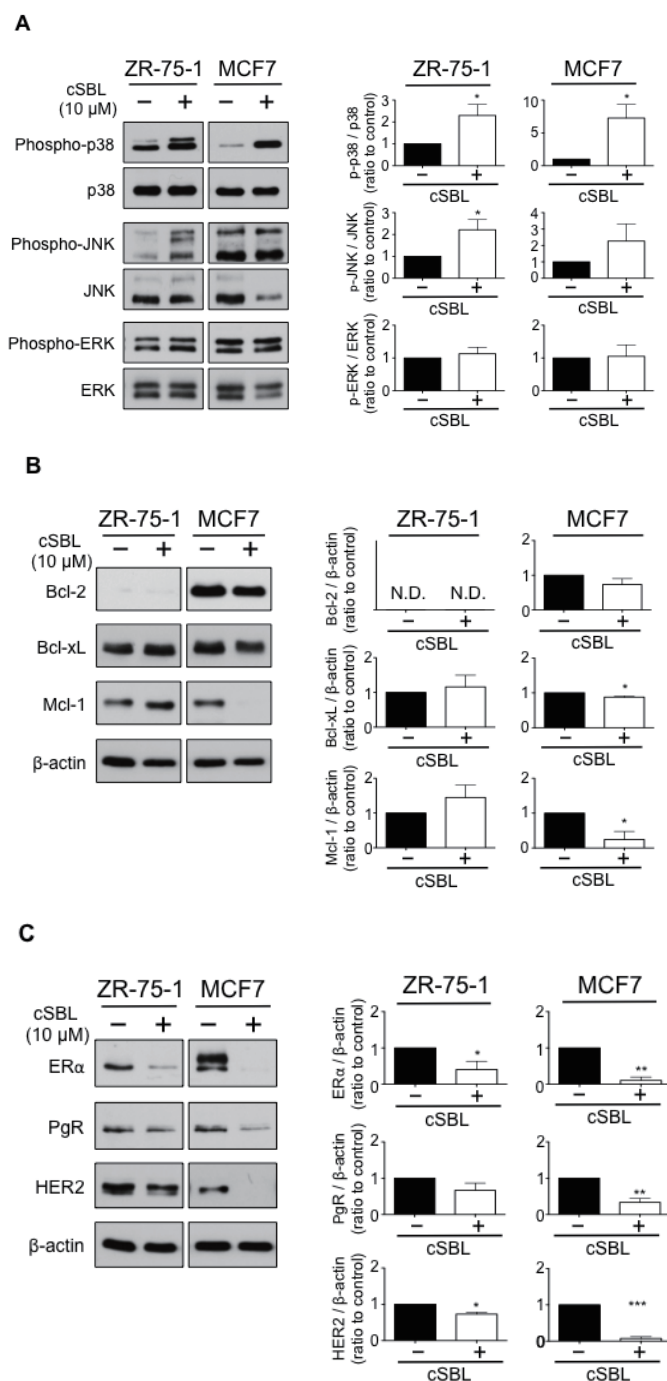


Figure 3. Effects of cSBL on the activations of mitogen-activated protein kinases (MAPKs) (A), and expressions of the anti-apoptotic Bcl-2 family (B), and breast cancer-related proteins (C) in ZR-75-1 and MCF7 cells. Cells were treated with cSBL (10 μ M) for 72 h, and the phosphorylation and expression levels of each molecule were detected by western blotting. The values relative to the controls are presented as the mean \pm SD of three independent experiments (right graphs). * $p < 0.05$, ** $p < 0.01$, *** $p < 0.001$.

2.4. Expressions of ErbB Family Protein in Breast Cancer Cells Treated with cSBL

Since the ErbB family proteins and their signals were generally attractive therapeutic targets, we evaluated the effects of cSBL on ErbB family expression in all breast cancer cell lines tested here (Figure 4). EGFR/HER1 was predominantly expressed in the triple-negative breast cancer cell lines, MDA-MB-231 and MDA-MB-468, and a faint band was also detected in SK-BR-3. HER2 expression was clearly observed in ZR-75-1, BT-474, SK-BR-3, and slightly in MCF7. HER3 expression was detected in MDA-MB-468 in addition to the four cell lines mentioned above. Slight expression of HER4 was found only in ZR-75-1 and MCF7. Then, the effects of cSBL on the levels of protein expression of these proteins were assessed in each cell line. Surprisingly, treatment with cSBL resulted in decreased protein levels of all ErbB proteins in each breast cancer cell line.

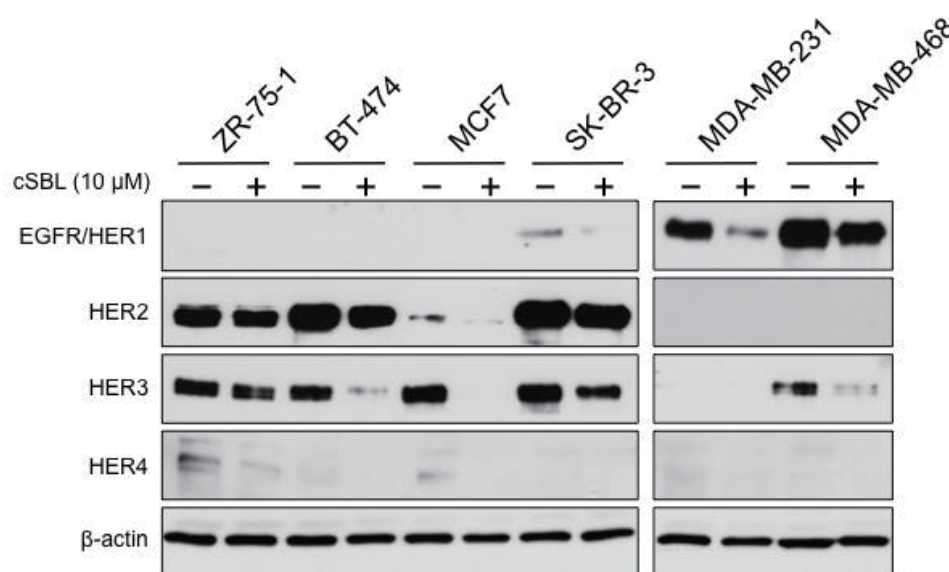


Figure 4. Effects of cSBL on the expression levels of ErbB family proteins in breast cancer cell lines (ZR-75-1, BT-474, MCF7, SK-BR-3, MDA-MB-231, and MDA-MB-468). Cells were treated with cSBL (10 μM) for 72 h and the expression levels of ErbB family in each cell line were detected by western blotting.

2.5. Expressions of EGFR and Its Signaling in Triple-Negative Breast Cancer Cells Treated with cSBL

Even though some drugs tailored to the breast cancer cell types, such as hormonal agents for ER-positive cells and HER2 targeted agents for HER2 positive cells, have achieved clinical effects to some extent, chemotherapeutic options for triple-negative phenotype breast cancers are very limited. Targeting EGFR/HER1, which is expressed in most patients of triple-negative breast cancer [23], or its signaling is a novel and attractive strategy. Since cSBL was shown to decrease EGFR/HER1 protein expression in triple-negative cell lines, we next sought to explore the downregulation mechanism of EGFR/HER1. Statistically significant reductions in EGFR/HER1 were observed after 24-h and 72-h of treatment with cSBL in MDA-MB-231 and MDA-MB-468, respectively (Figure 5A).

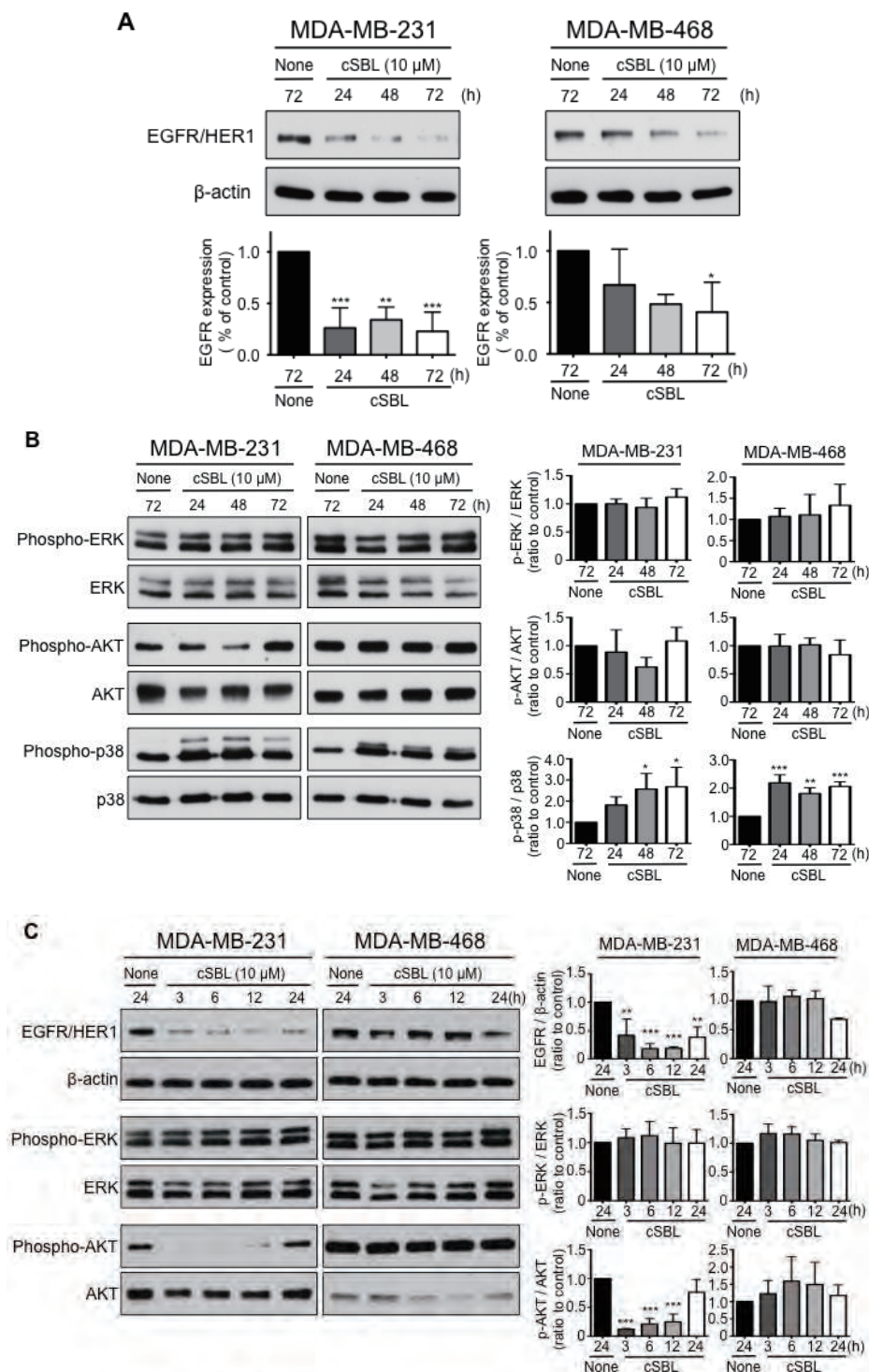


Figure 5. Effects of cSBL on EGFR/HER1 expression and downstream signaling in MDA-MB-231 and MDA-MB-468 cells. (A) Cells were treated with cSBL (10 μ M) for 24 to 72 h, and the expression levels of EGFR/HER1 in each cell line were detected by western blotting. Densitometric quantification of three independent experiments (mean \pm SD) was performed using Image J. (B) Cells were treated with cSBL (10 μ M) for 24 to 72 h, and the phosphorylation levels of AKT, ERK, and p38 were detected by western blotting. (C) Cells were treated with cSBL (10 μ M) for 3–24 h and the expression levels of EGFR/HER1 and the phosphorylation levels of AKT and ERK were detected by western blotting. The values relative to the controls are presented as the mean \pm SD from three independent experiments (right graphs). For both graphs, * $p < 0.05$; ** $p < 0.01$; *** $p < 0.001$.

In an effort to determine the contribution of EGFR/HER1 reduction to the cSBL-induced pro-apoptotic effect, we investigated the activation status of the EGFR signaling pathway. No change was observed in ERK activation in either MDA-MB-231 or MDA-MB-468 cells (Figure 5B). In MDA-MB-231, AKT phosphorylation seemed to slightly decrease after 48-h of treatment with cSBL, but increased after 72-h of treatment compared to the control. The phosphorylation level of AKT was unchanged in MDA-MB-468 cells. In contrast, phosphorylation of p38 increased in both cell lines.

Since the AKT activation status in MDA-MB-231 cells treated with cSBL was uncertain, we then further observed these events at an earlier time period (from 3 to 24 h of treatment). Even though low EGFR/HER1 levels were observed compared to 24-h untreated control throughout the time points, the level of phosphorylation of AKT gradually increased, and the level at 24-h treatment with cSBL was the same level as that of the 24-h untreated control in MDA-MB-231 (Figure 5C). Thus, it is suggested that AKT phosphorylation increased during the early period in our experimental culture period on cSBL-treated MDA-MB-231, although EGFR/HER1 expression was affected by the treatment. On the other hand, EGFR/HER1 expression was slightly decreased by 24-h of cSBL treatment. The AKT phosphorylation status tended to increase from 3 to 12-h of treatment even though statistical differences were not detected at all time points.

Taken together, the effects of cSBL treatment on ERK and AKT activation in MDA-MB-231 and MDA-MB-468 cells were not considered to be significant. Similarly, ERK activation was unchanged in ZR-75-1 and MCF7 cells (Figure 3A). Therefore, the EGFR signaling pathway might not be implicated in cSBL-induced apoptosis. P38 phosphorylation, which has been proven to, at least partially, contribute to caspase activation in cSBL-induced apoptosis [25], was observed, and this also supports this prediction. These results indicate that cSBL induces apoptosis to breast cancer cells, including triple-negative cells, accompanied by a decrease in the levels of ErbB family proteins, whereas EGFR signaling is not affected.

3. Discussion

In this study, the effects of cSBL on the breast cancer cell growth and on the expression of molecules that play key roles in breast cancer prognosis were evaluated. cSBL significantly suppressed the cell growth of six cancer cell lines representing a variety of phenotypes in ER α , PgR, and HER2 (Table 1 and Figure 1) through the induction of apoptosis (Figure 2). However, the effects of cSBL on normal breast cells were very limited; the viability of MCF 10A stayed over 85% in all concentration ranges tested, and pro-apoptotic changes were not detected under conditions that cause rigid apoptotic changes to cancer cells (Figures 1 and 2). We measured not only the activation of p38 and downregulation of ER α , consistent with previous reports, but also found varied effects on the expression of anti-apoptotic Bcl-2 family proteins depending on the cell types as well as the downregulation of PgR and HER2 in multiple cancer cell lines (Figure 3). Further investigation revealed that cSBL causes a reduction in all ErbB family proteins that are expressed in the breast cancer cell lines (Figure 4). The analysis of EGFR downstream signaling showed that the inhibition of EGFR signaling did not occur in the cSBL treatments (Figure 5). Accordingly, we propose that cSBL triggers apoptosis induction without affecting EGFR signaling, but the downregulation of ER α , PgR, and ErbB receptors are accompanied with cSBL-induced cell death under the experimental conditions used in the current study.

ER and PgR are nuclear hormone receptors whose activation is controlled by ligand binding, kinase activators, or phosphatase inhibitors [30–35]. The degradation of ER and PgR has been shown to be under the control of the ubiquitin proteasome system [35–39], and recent research revealed that the phosphorylation of ER α via p38 activation promotes ER α turnover in breast cancer cells [40]. The activation of p38 by cSBL treatment has been observed in leukemia cells [41], mesothelioma cells [42], and some breast cancer cells [25], as well as the cells tested here. Thus, the reduced expression levels of ER α and PgR in cSBL-treated cells may be associated with p38 activation. In the meantime, interaction and stabilization of these hormonal receptors with/by heat shock proteins (HSPs) has also been reported [36,43,44]. We previously found that reducing HSP70 expression attenuates the

apoptosis-inducing effects of cSBL [45]. Moreover, treatment with cSBL causes remarkable changes in the localization of HSP70 and HSC70; cSBL treatment has been shown to evoke increases of these proteins in the cytosol prior to the execution of apoptosis in mouse leukemia P388 cells [45]. This implies that HSP70 and HSC70 have important roles in the effects of cSBL, and, also, there is a possibility that cSBL decreases the expression of ER α and PgR through the regulation of HSPs. The implications of proteasome degradation and stabilization by HSPs are common in ErbB receptor turnover. EGFR/HER1 is known to be internalized after ligand binding and part of it is degraded by lysosomes or by the proteasome [46,47]. HSP70 and HSC70 act as key co-chaperones for HSP90 machinery, at least in part, by aiding in client protein recruitment [48]. The HSP70 and HSP90 chaperones work together to target certain client proteins, including EGFR/HER1 for degradation by the ubiquitin-proteasome system, and inhibitory agents targeting HSPs are one of the potential approaches for cancer therapeutics today [49,50]. Further works should be performed to determine the mechanisms by which p38 activation and/or HSPs are involved in the reduction of ER α , PgR, and ErbB receptors in cSBL-treated cells.

It has been reported that cSBL acts as an anti-cancer agent against various human cancer cells including carcinoma (cervical, oral, hepatocellular, and breast), leukemia, lymphoma, mesothelioma, and glioblastoma [24,41,42,51–57]. Interestingly, although cSBL induces apoptosis in those cancer cells, normal tissue-derived cells, such as fibroblasts, melanocytes, keratinocytes, and mesothelial cells, are relatively insensitive to this agent [53,56,58–60]. Moreover, our recent study using human malignant mesothelioma xenograft model mice showed that cSBL exerts significant anti-tumor effects without adverse effects *in vivo* [61]. It is also noteworthy that the members of the pancreatic-type RNase super-family, including cSBL, show high thermal stability and strong resistance to protein denaturants and to proteases [62,63]. Moreover, they are expected to have lower immunogenicity due to their compact structures and homology to human pancreatic RNases [64]. However, only limited information has been obtained regarding its cancer-selectivity so far. The known factors that affect cell susceptibility are summarized in our previous review [65]. To date, differences in the cSBL binding to the cell surface and its internalization into cytosol were considered to be the main reasons for the selectivity. In the present study, pro-apoptotic effects were observed irrespective of breast cancer cell type, and this is not consistent with previous reports; cSBL is effective towards breast cancer cells, including triple-negative breast cancers. It can be speculated that one of the reasons for this contradiction may be the variance of cell culture conditions. The elements that influence the cell dependency on particular hormones or growth factors, such as FBS, composed of complete medium may be an explanation. Our results also revealed obvious differences in sensitivity between MCF7 and MCF 10A to cSBL. Comparative studies on cSBL binding and/or internalization to these cells would give us evidence for the cancer selectivity of cSBL that could promote the development of novel anti-cancer agents. Furthermore, growth signals, such as the AKT and ERK activation of the cell lines investigated here, seem to be independent of EGFR/HER1 expression. Although involvement of alternative pathways such as PLC γ or STATs activated by EGFR/HER1 in the effects of cSBL needs to be elucidated, our results suggest that applications of cSBL against the cancer cells that depend on the ErbB receptors for growth may provide great benefit as a type of chemotherapy. Moreover, recent studies on triple-negative breast cancer therapeutics have been shown to affect the crucial parts of ErbB receptors [48,66,67]. Tao et al. reported that single treatment with an AKT inhibitor (GDC-0068) or a PI3K inhibitor (GDC-0941), inhibitors for EGFR downstream signaling, activates EGFR/HER1 and HER3 [68]. The blockade of EGFR and HER3 combined with drugs results in superior anti-tumor activity *in vitro* and *in vivo*, suggesting the importance of inhibition on both the upstream activation of key molecules and the downstream signaling pathway, due to the cellular response of activating an alternative pathway for cancer cell survival. Thus, the combination with cSBL that reduces the expressions of all ErbB family proteins with drugs such as AKT inhibitors could have a great potential for therapy in breast cancers, including triple-negative phenotype cells.

4. Materials and Methods

4.1. Reagents

cSBL was isolated using sequential chromatography with Sephadex G75, DEAE-cellulose, hydroxyapatite, and SP-Sepharose, as previously described [9]. The anti-caspase-9 antibody was purchased from Medical and Biological Laboratories Co., Ltd. (MBL; Nagoya, Japan). The anti-PARP (46D11), phospho-p38 (Thr180/182) (D3F9), p38 (D13E1), Phospho-ERK (Thr202/Tyr204) (F13.14.4E), ERK (137F5), Bcl-2 (D55G8), Bcl-xL (54H6), Mcl-1 (D35A5), EGFR/HER1 (D38B1), HER2 (29D8), HER3 (D22C5), HER4/ErbB4 (111B2), phospho-AKT (Ser473) (D9E), AKT (11E7), and phospho-AKT (Ser473), horseradish peroxidase (HRP)-conjugated anti-mouse IgG and anti-rabbit IgG antibodies were purchased from Cell Signaling Technology (Beverly, MA, USA). The anti- β -actin antibody was purchased from Sigma-Aldrich (Merck KGaA, Darmstadt, Germany). The anti-phospho-JNK (pT183/pY185), and JNK antibodies were purchased from BD Biosciences (Franklin Lakes, NJ, USA). The anti-ER α (E115) and PgR (ERP5489) antibodies were purchased from Abcam Biotechnology (Cambridge, UK).

4.2. Cell Culture

The breast cancer cell lines (ZR-75-1, BT-474, MCF7, SK-BR-3, MDA-MB-231, and MDA-MB-468), and a non-tumorigenic epithelial cell line, MCF 10A, were purchased from American Type Culture Collection (ATCC; Manassas, VA, USA). The cancer cells were cultured in Dulbecco's modified Eagle's medium (WAKO Pure Chemical Industries, Ltd., Osaka, Japan) supplemented with 10% fetal bovine serum (Biosera, Nuaille, France), 100 U/mL penicillin, and 100 μ g/mL streptomycin (Life Technologies, Carlsbad, CA, USA). MCF 10A cells were cultured in mammary epithelial cell growth medium (Lonza, Basel, Switzerland) supplemented with bovine pituitary extract, hydrocortisone, hEGF, insulin (Bullet Kit, Lonza) and 100 ng/mL cholera toxin (WAKO Pure Chemical Industries, Ltd.). All cell lines were cultured in a humidified atmosphere in 5% CO₂ at 37 °C.

4.3. WST Assays

WST-8 assay was performed to determine the cell viability. Cells (5×10^4 cells/mL) cultured in 96-well plates (100 μ L/well) were treated with cSBL (1, 5, 10, and 20 μ M) for 72 h. Then, the cells were incubated with Cell Count Reagent SF (Nacalai Tesque Inc., Kyoto, Japan) for 1–4 h. The absorbance of the resulting product at 450 nm was measured, and the background absorbance at 650 nm was subtracted. Experiments were conducted in triplicate.

4.4. Clonogenic Assay

The cells were seeded in six-well plates (5×10^3 cells/well) and allowed to adhere overnight. The cells were treated with 1–10 μ M cSBL for 72 h. The culture medium was subsequently replaced with cSBL-free culture medium and the cells were incubated for 7–28 more days (7 days: MCF7, MDA-MB-231, MCF 10A; 14 days: SK-BR-3, MDA-MB-468; 28 days: ZR-74-1, BT-474). The colonies were fixed with 2% paraformaldehyde and stained with crystal violet.

4.5. Trypan Blue Dye Exclusion Assay

A trypan blue dye exclusion assay was also performed to assess the effects of cSBL on cell viability. Cells (5×10^4 cells/mL) cultured in a 24-well plate (500 μ L/well) were treated with cSBL (10 μ M) for 48, 72, and 96 h. Then, the cells were harvested, and the numbers of live or dead cells were counted by TC10 (Bio-Rad Laboratories, Inc. Hercules, CA, USA) in accordance with to the manufacturer's instructions.

4.6. Observation of Nuclear Morphology

Cells (5×10^4 cells/mL) cultured in a Cell Carrier-96 Ultra Microplate (100 μ L/well) were treated with cSBL (10 μ M) for 72 h. Then, cells were stained with 2 μ g/mL Hoechst 33342 (Dojindo Laboratories, Kumamoto, Japan) for 1 h. The resulting images were acquired with the high-content analysis system Operetta CLSTM with NA 20 \times objectives.

4.7. Western Blotting

The cells (5×10^4 cells/mL) were cultured in six-well plates (4 mL/well) and were treated with cSBL (10 μ M) for the indicated time. Whole cell lysates were prepared using extraction buffer (150 mM NaCl, 10 mM Tris-HCl (pH 7.4), 5 mM EDTA, 1% Nonidet P-40, 0.1% sodium deoxycholate, and 0.1% sodium dodecyl sulfate) supplemented with cOmpleteTM Mini EDTA-free protease inhibitor cocktail tablets and PhosSTOP phosphatase inhibitor tablets (each 1 tablet/10 mL; Roche Applied Science, Indianapolis, IN, USA). Soluble proteins were collected, and the protein concentration was measured using a BCA protein assay kit (Thermo Fisher Scientific, Inc., Waltham, MA, USA) according to the manufacturer's instructions. The proteins were separated using 10% or 14% SDS-PAGE and transferred onto Immobilon-P transfer membranes (EMD Millipore, Billerica, MA, USA). The membranes were sequentially incubated with primary and secondary antibodies diluted in Can Get Signal solution (Toyobo Co., Ltd., Osaka, Japan). The protein bands were detected using ECL Prime Western Blotting Detection Reagent (GE Healthcare, Little Chalfont, Buckinghamshire, UK). The relative density of the protein bands was measured by ImageJ 1.51s software (National Institutes of Health, Bethesda, MD, USA). The experiments were repeated three times.

4.8. Statistical Analysis

Results are expressed as means \pm SE or SD and are the representative of at least three independent experiments. Statistical comparisons of two groups were made using Student's *t*-tests and among groups using one-way ANOVA, followed by Bonferroni's post hoc tests. All calculations were performed using GraphPad Prism version 5.0 (GraphPad Software Inc., San Diego, CA, USA). The significance threshold was $p < 0.05$.

5. Conclusions

In summary, our founding suggestion is that cSBL exhibits an apoptosis-inducing effect regardless of the breast cancer cell type and has high cancer selectivity. These effects are accompanied by a decrease in the ErbB family receptors. To explore the effects of cSBL on cancer cells showing ErbB family-dependent growths, a combinatorial study with EGFR signal-targeted drugs, such as AKT inhibitors, should be performed.

Supplementary Materials: The following are available online, Figure S1. Effects of cSBL on clonogenic potential of the cells seeded in distinct cell densities. Colony assays on the cells were performed in the absence or presence of cSBL for 72 h followed by incubation in cSBL-free medium for 7–28 days. The cells were fixed with 2% paraformaldehyde and stained with crystal violet. (A) 2.5×10^3 cells were seeded and allowed to adhere overnight, and then the cells were treated with 1–10 μ M cSBL. (B) 1×10^4 cells were seeded and allowed to adhere overnight, and then the cells were treated with 1–10 μ M cSBL. 5×10^3 (C) or 2.5×10^3 (D) cells were seeded and allowed to adhere overnight, and then the cells were treated with 0.1 and 0.5 μ M cSBL. Representative images are shown.

Author Contributions: T.T. conceived, designed, and performed the experiments, analyzed the data, and wrote the paper; S.S. (Shoko Sato) designed the experiments and wrote the paper; T.S. (Toshiyuki Sato) designed and performed the experiments; S.S. (Shigeki Sugawara) contributed reagents and analysis tools. T.S. (Tsuneyoshi Suzuki) and A.H. provided the laboratory support. M.H. provided the laboratory support, wrote the paper, and improved the manuscript.

Funding: This study was supported by the 'Strategic Research' Project (2012–2017) for Private Universities from the Ministry of Education, Culture, Sports, Science, and Technology of Japan, and funded by a Grant-in-Aid for Young Scientists (B), grant number 17K15029 to Takeo Tatsuta.

Conflicts of Interest: The authors declare that there is no conflict of interest.

References

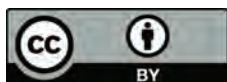
1. Yau, T.; Dan, X.; Ng, C.C.W.; Ng, T.B. Lectins with potential for anti-cancer therapy. *Molecules* **2015**, *20*, 3791–3810. [[CrossRef](#)] [[PubMed](#)]
2. Ochoa-Alvarez, J.A.; Krishnan, H.; Shen, Y.; Acharya, N.K.; Han, M.; McNulty, D.E.; Hasegawa, H.; Hyodo, T.; Senga, T.; Geng, J.-G.; et al. Plant Lectin Can Target Receptors Containing Sialic Acid, Exemplified by Podoplanin, to Inhibit Transformed Cell Growth and Migration. *PLoS ONE* **2012**, *7*, e41845. [[CrossRef](#)] [[PubMed](#)]
3. Liu, B.; Zhang, B.; Min, M.; Bian, H.; Chen, L.; Liu, Q.; Bao, J. Induction of apoptosis by Polygonatum odoratum lectin and its molecular mechanisms in murine fibrosarcoma L929 cells. *Biochim. Biophys. Acta Gen. Subj. USA/PAN* **2009**, *1790*, 840–844. [[CrossRef](#)] [[PubMed](#)]
4. Yang, X.; Wu, L.; Duan, X.; Cui, L.; Luo, J.; Li, G. Adenovirus carrying gene encoding discus sialic acid binding lectin induces cancer cell apoptosis. *Mar. Drugs* **2014**, *12*, 3994–4004. [[CrossRef](#)] [[PubMed](#)]
5. Miyagi, T.; Wada, T.; Yamaguchi, K.; Shiozaki, K.; Sato, I.; Kakugawa, Y.; Yamanami, H.; Fujiya, T. Human sialidase as a cancer marker. *Proteomics* **2008**, *8*, 3303–3311. [[CrossRef](#)] [[PubMed](#)]
6. Hakomori, S. Glycosylation defining cancer malignancy: New wine in an old bottle. *Proc. Natl. Acad. Sci. USA/PNAS* **2002**, *99*, 10231–10233. [[CrossRef](#)] [[PubMed](#)]
7. Dennis, J.W.; Granovsky, M.; Warren, C.E. Glycoprotein glycosylation and cancer progression. *Biochim. Biophys. Acta* **1999**, *1473*, 21–34. [[CrossRef](#)]
8. Kawauchi, H.; Sakakibara, F.; Watanabe, K. Agglutinins of frog eggs: A new class of proteins causing preferential agglutination of tumor cells. *Experientia* **1975**, *31*, 364–365. [[CrossRef](#)] [[PubMed](#)]
9. Nitta, K.; Takayanagi, G.; Kawauchi, H.; Hakomori, S. Isolation and characterization of *Rana catesbeiana* lectin and demonstration of the lectin-binding glycoprotein of rodent and human tumor cell membranes. *Cancer Res.* **1987**, *47*, 4877–4883. [[PubMed](#)]
10. Okabe, Y.; Katayama, N.; Iwama, M.; Watanabe, H.; Ohgi, K.; Irie, M.; Nitta, K.; Kawauchi, H.; Takayanagi, Y.; Oyama, F. Comparative base specificity, stability, and lectin activity of two lectins from eggs of *Rana catesbeiana* and *R. japonica* and liver ribonuclease from *R. catesbeiana*. *J. Biochem.* **1991**, *109*, 786–790. [[CrossRef](#)] [[PubMed](#)]
11. Nitta, K.; Ozaki, K.; Ishikawa, M.; Furusawa, S.; Hosono, M.; Kawauchi, H.; Sasaki, K.; Takayanagi, Y.; Tsuiki, S.; Hakomori, S. Inhibition of cell proliferation by *Rana catesbeiana* and *Rana japonica* lectins belonging to the ribonuclease superfamily. *Cancer Res.* **1994**, *54*, 920–927. [[PubMed](#)]
12. Titani, K.; Takio, K.; Kuwada, M.; Nitta, K.; Sakakibara, F.; Kawauchi, H.; Takayanagi, G.; Hakomori, S. Amino acid sequence of sialic acid binding lectin from frog (*Rana catesbeiana*) eggs. *Biochemistry* **1987**, *26*, 2189–2194. [[CrossRef](#)] [[PubMed](#)]
13. Liao, Y.-D. A pyrimidine-guanine sequence-specific ribonuclease from *Rana catesbeiana* (bullfrog) oocytes. *Nucleic Acids Res.* **1992**, *20*, 1371–1377. [[CrossRef](#)] [[PubMed](#)]
14. Nitta, K.; Ozaki, K.; Tsukamoto, Y.; Hosono, M.; Ogawakono, Y.; Kawauchi, H.; Takayanagi, Y.; Tsuiki, S.; Hakomori, S. Catalytic lectin (leczyme) from bullfrog (*Rana catesbeiana*) eggs. *Int. J. Oncol.* **1996**, *9*, 19–23. [[CrossRef](#)] [[PubMed](#)]
15. Sharon, N.; Lis, H. *Lectins*; Springer: Dordrecht, The Netherlands, 2007; ISBN 978-1-4020-6605-4.
16. Neve, R.M.; Chin, K.; Fridlyand, J.; Yeh, J.; Baehner, F.L.; Fevr, T.; Clark, L.; Bayani, N.; Coppe, J.P.; Tong, F.; et al. A collection of breast cancer cell lines for the study of functionally distinct cancer subtypes. *Cancer Cell* **2006**, *10*, 515–527. [[CrossRef](#)] [[PubMed](#)]
17. Curigliano, G.; Burstein, H.J.; Winer, E.P.; Gnant, M.; Dubsy, P.; Loibl, S.; Colleoni, M.; Regan, M.M.; Piccart-Gebhart, M.; Senn, H.-J.; et al. De-escalating and escalating treatments for early-stage breast cancer: The St. Gallen International Expert Consensus Conference on the Primary Therapy of Early Breast Cancer 2017. *Ann. Oncol.* **2017**, *28*, 1700–1712. [[CrossRef](#)] [[PubMed](#)]
18. Prat, A.; Perou, C.M. Deconstructing the molecular portraits of breast cancer. *Mol. Oncol.* **2011**, *5*, 5–23. [[CrossRef](#)] [[PubMed](#)]
19. Jitariu, A.-A.; Cîmpean, A.M.; Ribatti, D.; Raica, M. Triple negative breast cancer: The kiss of death. *Oncotarget* **2017**, *8*, 46652–46662. [[CrossRef](#)] [[PubMed](#)]
20. Schlessinger, J. Cell signaling by receptor tyrosine kinases. *Cell* **2000**, *103*, 211–225. [[CrossRef](#)]

21. Park, H.S.; Jang, M.H.; Kim, E.J.; Kim, H.J.; Lee, H.J.; Kim, Y.J.; Kim, J.H.; Kang, E.; Kim, S.-W.; Kim, I.A.; et al. High EGFR gene copy number predicts poor outcome in triple-negative breast cancer. *Mod. Pathol.* **2014**, *27*, 1212–1222. [[CrossRef](#)] [[PubMed](#)]
22. Sassen, A.; Rochon, J.; Wild, P.; Hartmann, A.; Hofstaedter, F.; Schwarz, S.; Brockhoff, G. Cytogenetic analysis of HER1/EGFR, HER2, HER3 and HER4 in 278 breast cancer patients. *Breast Cancer Res.* **2008**, *10*, R2. [[CrossRef](#)] [[PubMed](#)]
23. Costa, R.; Shah, A.N.; Santa-Maria, C.A.; Cruz, M.R.; Mahalingam, D.; Carneiro, B.A.; Chae, Y.K.; Cristofanilli, M.; Gradishar, W.J.; Giles, F.J. Targeting Epidermal Growth Factor Receptor in triple negative breast cancer: New discoveries and practical insights for drug development. *Cancer Treat. Rev.* **2017**, *53*, 111–119. [[CrossRef](#)] [[PubMed](#)]
24. Tseng, H.-H.; Yu, Y.-L.; Chen, Y.-L.S.; Chen, J.-H.; Chou, C.-L.; Kuo, T.-Y.; Wang, J.-J.; Lee, M.-C.; Huang, T.-H.; Chen, M.H.-C.; et al. RC-RNase-induced cell death in estrogen receptor positive breast tumors through down-regulation of Bcl-2 and estrogen receptor. *Oncol. Rep.* **2011**, *25*, 849–853. [[CrossRef](#)] [[PubMed](#)]
25. Kariya, Y.; Tatsuta, T.; Sugawara, S.; Kariya, Y.; Nitta, K.; Hosono, M. RNase activity of sialic acid-binding lectin from bullfrog eggs drives antitumor effect via the activation of p38 MAPK to caspase-3/7 signaling pathway in human breast cancer cells. *Int. J. Oncol.* **2016**, *49*, 1334–1342. [[CrossRef](#)] [[PubMed](#)]
26. Liu, S.; Lin, Y.C. Transformation of MCF-10A human breast epithelial cells by zeranone and estradiol-17 β . *Breast J.* **2004**, *10*, 514–521. [[CrossRef](#)] [[PubMed](#)]
27. Subik, K.; Lee, J.F.; Baxter, L.; Strzepak, T.; Costello, D.; Crowley, P.; Xing, L.; Hung, M.C.; Bonfiglio, T.; Hicks, D.G.; et al. The expression patterns of ER, PR, HER2, CK5/6, EGFR, KI-67 and AR by immunohistochemical analysis in breast cancer cell lines. *Breast Cancer Basic Clin. Res.* **2010**, *4*, 35–41. [[CrossRef](#)]
28. Jänicke, R.U. MCF-7 breast carcinoma cells do not express caspase-3. *Breast Cancer Res. Treat.* **2009**, *117*, 219–221. [[CrossRef](#)] [[PubMed](#)]
29. Tatsuta, T.; Sugawara, S.; Takahashi, K.; Ogawa, Y.; Hosono, M.; Nitta, K. Leczyme: A new candidate drug for cancer therapy. *Biomed. Res. Int.* **2014**, *2014*, 421415. [[CrossRef](#)] [[PubMed](#)]
30. Lee, H.; Bai, W. Regulation of Estrogen Receptor Nuclear Export by Ligand-Induced and p38-Mediated Receptor Phosphorylation. *Mol. Cell. Biol.* **2002**, *22*, 5835–5845. [[CrossRef](#)] [[PubMed](#)]
31. Khan, J.A.; Amazit, L.; Bellance, C.; Guiochon-Mantel, A.; Lombès, M.; Loosfelt, H. p38 and p42/44 MAPKs Differentially Regulate Progesterone Receptor A and B Isoform Stabilization. *Mol. Endocrinol.* **2011**, *25*, 1710–1724. [[CrossRef](#)] [[PubMed](#)]
32. Driggers, P.H.; Segars, J.H. Estrogen action and cytoplasmic signaling pathways. Part II: The role of growth factors and phosphorylation in estrogen signaling. *Trends Endocrinol. Metab.* **2002**, *13*, 422–427. [[CrossRef](#)]
33. Bunone, G.; Briand, P.A.; Miksicek, R.J.; Picard, D. Activation of the unliganded estrogen receptor by EGF involves the MAP kinase pathway and direct phosphorylation. *EMBO J.* **1996**, *15*, 2174–2183. [[CrossRef](#)] [[PubMed](#)]
34. Kato, S.; Endoh, H.; Masuhiro, Y.; Kitamoto, T.; Uchiyama, S.; Sasaki, H.; Masushige, S.; Gotoh, Y.; Nishida, E.; Kawashima, H.; et al. Activation of the estrogen receptor through phosphorylation by mitogen-activated protein kinase. *Science* **1995**, *270*, 1491–1494. [[CrossRef](#)] [[PubMed](#)]
35. Shen, T.; Horwitz, K.B.; Lange, C.A. Transcriptional hyperactivity of human progesterone receptors is coupled to their ligand-dependent down-regulation by mitogen-activated protein kinase-dependent phosphorylation of serine 294. *Mol. Cell. Biol.* **2001**, *21*, 6122–6131. [[CrossRef](#)] [[PubMed](#)]
36. Lange, C.A.; Shen, T.; Horwitz, K.B. Phosphorylation of human progesterone receptors at serine-294 by mitogen-activated protein kinase signals their degradation by the 26S proteasome. *Proc. Natl. Acad. Sci. USA* **2000**, *97*, 1032–1037. [[CrossRef](#)] [[PubMed](#)]
37. Reid, G.; Hübner, M.R.; Métivier, R.; Brand, H.; Denger, S.; Manu, D.; Beaudouin, J.; Ellenberg, J.; Gannon, F. Cyclic, proteasome-mediated turnover of unliganded and liganded ER α on responsive promoters is an integral feature of estrogen signaling. *Mol. Cell.* **2003**, *11*, 695–707. [[CrossRef](#)]
38. Laïos, I.; Journé, F.; Nonclercq, D.; Vidal, D.S.; Toillon, R.-A.; Laurent, G.; Leclercq, G. Role of the proteasome in the regulation of estrogen receptor α turnover and function in MCF-7 breast carcinoma cells. *J. Steroid Biochem. Mol. Biol.* **2005**, *94*, 347–359. [[CrossRef](#)] [[PubMed](#)]

39. Calvo, V.; Beato, M. BRCA1 counteracts progesterone action by ubiquitination leading to progesterone receptor degradation and epigenetic silencing of target promoters. *Cancer Res.* **2011**, *71*, 3422–3431. [[CrossRef](#)] [[PubMed](#)]
40. Bhatt, S.; Xiao, Z.; Meng, Z.; Katzenellenbogen, B.S. Phosphorylation by p38 mitogen-activated protein kinase promotes estrogen receptor α turnover and functional activity via the SCF(Skp2) proteasomal complex. *Mol. Cell. Biol.* **2012**, *32*, 1928–1943. [[CrossRef](#)] [[PubMed](#)]
41. Tatsuta, T.; Hosono, M.; Sugawara, S.; Kariya, Y.; Ogawa, Y.; Hakomori, S.; Nitta, K. Sialic acid-binding lectin (lecyzime) induces caspase-dependent apoptosis-mediated mitochondrial perturbation in Jurkat cells. *Int. J. Oncol.* **2013**, *43*, 1402–1412. [[CrossRef](#)] [[PubMed](#)]
42. Tatsuta, T.; Hosono, M.; Takahashi, K.; Omoto, T.; Kariya, Y.; Sugawara, S.; Hakomori, S.; Nitta, K. Sialic acid-binding lectin (lecyzime) induces apoptosis to malignant mesothelioma and exerts synergistic antitumor effects with TRAIL. *Int. J. Oncol.* **2014**, *44*, 377–384. [[CrossRef](#)] [[PubMed](#)]
43. Dhamad, A.E.; Zhou, Z.; Zhou, J.; Du, Y. Systematic proteomic identification of the heat shock proteins (Hsp) that interact with estrogen receptor alpha (ER α) and biochemical characterization of the ER α -Hsp70 Interaction. *PLoS ONE* **2016**, *11*, e0160312. [[CrossRef](#)] [[PubMed](#)]
44. Paul, A.; Garcia, Y.A.; Zierer, B.; Patwardhan, C.; Gutierrez, O.; Hildenbrand, Z.; Harris, D.C.; Balsiger, H.A.; Sivils, J.C.; Johnson, J.L.; et al. The cochaperone SGTA (small glutamine-rich tetratricopeptide repeat-containing protein alpha) demonstrates regulatory specificity for the androgen, glucocorticoid, and progesterone receptors *. *J. Biol. Chem.* **2014**, *289*, 15297–15306. [[CrossRef](#)] [[PubMed](#)]
45. Tatsuta, T.; Hosono, M.; Ogawa, Y.; Inage, K.; Sugawara, S.; Nitta, K. Downregulation of Hsp70 inhibits apoptosis induced by sialic acid-binding lectin (lecyzime). *Oncol. Rep.* **2013**, *1*, 13–18. [[CrossRef](#)] [[PubMed](#)]
46. Sigismund, S.; Argenzio, E.; Tosoni, D.; Cavallaro, E.; Polo, S.; Di Fiore, P.P. Clathrin-Mediated Internalization Is Essential for Sustained EGFR Signaling but Dispensable for Degradation. *Dev. Cell.* **2008**, *15*, 209–219. [[CrossRef](#)] [[PubMed](#)]
47. Hatton, N.; Lintz, E.; Mahankali, M.; Henkels, K.; Gomez-Cambronero, J. Phosphatidic acid (PA) increases EGF receptor (EGFR) expression by stabilizing mRNA, inhibiting RNase-A, and by inhibiting lysosomal and proteasomal degradation of the internalized EGFR. *Mol. Cell. Biol.* **2015**, *35*, MCB.00286-15. [[CrossRef](#)] [[PubMed](#)]
48. Esser, C.; Alberti, S.; Höhfeld, J. Cooperation of molecular chaperones with the ubiquitin/proteasome system. *Biochim. Biophys. Acta Mol. Cell. Res.* **2004**, *1695*, 171–188. [[CrossRef](#)] [[PubMed](#)]
49. Leu, J.I.-J.; Pimkina, J.; Pandey, P.; Murphy, M.E.; George, D.L. HSP70 inhibition by the small-molecule 2-phenylethynylsulfonamide impairs protein clearance pathways in tumor cells. *Mol. Cancer Res.* **2011**, *9*, 936–947. [[CrossRef](#)] [[PubMed](#)]
50. Sawai, A.; Chandarlapaty, S.; Greulich, H.; Gonen, M.; Ye, Q.; Arteaga, C.L.; Sellers, W.; Rosen, N.; Solit, D.B. Inhibition of Hsp90 down-regulates mutant epidermal growth factor receptor (EGFR) expression and sensitizes EGFR mutant tumors to paclitaxel. *Cancer Res.* **2008**, *68*, 589–596. [[CrossRef](#)] [[PubMed](#)]
51. Liao, Y.D.; Huang, H.C.; Chan, H.J.; Kuo, S.J. Large-scale preparation of a ribonuclease from *Rana catesbeiana* (bullfrog) oocytes and characterization of its specific cytotoxic activity against tumor cells. *Protein Expr. Purif.* **1996**, *7*, 194–202. [[CrossRef](#)] [[PubMed](#)]
52. Hu, C.C.; Tang, C.H.; Wang, J.J. Caspase activation in response to cytotoxic *Rana catesbeiana* ribonuclease in MCF-7 cells. *FEBS Lett.* **2001**, *503*, 65–68. [[CrossRef](#)]
53. Hu, C.C.; Lee, Y.H.; Tang, C.H.; Cheng, J.T.; Wang, J.J. Synergistic cytotoxicity of *Rana catesbeiana* ribonuclease and IFN- γ on hepatoma cells. *Biochem. Biophys. Res. Commun.* **2001**, *280*, 1229–1236. [[CrossRef](#)] [[PubMed](#)]
54. Wei, C.W.; Hu, C.C.A.; Tang, C.H.A.; Lee, M.C.; Wang, J.J. Induction of differentiation rescues HL-60 cells from *Rana catesbeiana* ribonuclease-induced cell death. *FEBS Lett.* **2002**, *531*, 421–426. [[CrossRef](#)]
55. Tang, P.-C.; Huang, H.-C.; Wang, S.-C.; Jeng, J.-C.; Liao, Y.-D. Regulation of ribonuclease expression by estradiol in *Rana catesbeiana* (Bullfrog). *Nucleic Acids Res.* **2002**, *30*, 3286–3293. [[CrossRef](#)] [[PubMed](#)]
56. Tang, C.-H.A.; Hu, C.-C.A.; Wei, C.-W.; Wang, J.-J. Synergism of *Rana catesbeiana* ribonuclease and IFN- γ triggers distinct death machineries in different human cancer cells. *FEBS Lett.* **2005**, *579*, 265–270. [[CrossRef](#)] [[PubMed](#)]

57. Chen, J.; Yiang, G.; Lin, Y.; Chou, P.; Wu, T.; Chang, W.; Chen, C.; Yu, Y. Rana catesbeiana ribonuclease induces cell apoptosis via the caspase-9/-3 signaling pathway in human glioblastoma DBTRG, GBM8901 and GBM8401 cell lines. *Oncol. Lett.* **2015**, 2471–2476. [[CrossRef](#)] [[PubMed](#)]
58. Satoh, T.; Tatsuta, T.; Sugawara, S.; Hara, A.; Hosono, M. Synergistic anti-tumor effect of bullfrog sialic acid-binding lectin and pemetrexed in malignant mesothelioma. *Oncotarget* **2017**, 8, 42466–42477. [[CrossRef](#)] [[PubMed](#)]
59. Lee, Y.-H.; Wei, C.-W.; Wang, J.-J.; Chiou, C.-T. Rana catesbeiana ribonuclease inhibits Japanese encephalitis virus (JEV) replication and enhances apoptosis of JEV-infected BHK-21 cells. *Antiviral Res.* **2011**, 89, 193–198. [[CrossRef](#)] [[PubMed](#)]
60. Ogawa, Y.; Sugawara, S.; Tatsuta, T.; Hosono, M.; Nitta, K.; Fujii, Y.; Kobayashi, H.; Fujimura, T.; Taka, H.; Koide, Y.; et al. Sialyl-glycoconjugates in cholesterol-rich microdomains of P388 cells are the triggers for apoptosis induced by Rana catesbeiana oocyte ribonuclease. *Glycoconj. J.* **2014**, 31, 171–184. [[CrossRef](#)] [[PubMed](#)]
61. Tatsuta, T.; Satoh, T.; Sugawara, S.; Hara, A.; Hosono, M. Sialic acid-binding lectin from bullfrog eggs inhibits human malignant mesothelioma cell growth in vitro and in vivo. *PLoS ONE* **2018**, 13, e0190653. [[CrossRef](#)] [[PubMed](#)]
62. Rosenberg, H.F.; Zhang, J.; Liao, Y.-D.; Dyer, K.D. Rapid diversification of RNase A superfamily ribonucleases from the bullfrog, Rana catesbeiana. *J. Mol. Evol.* **2001**, 53, 31–38. [[CrossRef](#)] [[PubMed](#)]
63. Notomista, E.; Catanzano, F.; Graziano, G.; Piaz, F.D.; Barone, G.; D’Alessio, G.; Di Donato, A. Onconase: An unusually stable protein. *Biochemistry* **2000**, 39, 8711–8718. [[CrossRef](#)] [[PubMed](#)]
64. Costanzi, J.; Sidransky, D.; Navon, A.; Goldsweig, H. Ribonucleases as a novel pro-apoptotic anticancer strategy: Review of the preclinical and clinical data for ranpirnase. *Cancer Invest.* **2005**, 23, 643–650. [[CrossRef](#)] [[PubMed](#)]
65. Tatsuta, T.; Sugawara, S.; Takahashi, K.; Ogawa, Y.; Hosono, M.; Nitta, K. Cancer-selective induction of apoptosis by leczyne. *Front. Oncol.* **2014**, 4, 139. [[CrossRef](#)] [[PubMed](#)]
66. Serra, V.; Scaltriti, M.; Prudkin, L.; Eichhorn, P.J.A.; Ibrahim, Y.H.; Chandarlapaty, S.; Markman, B.; Rodriguez, O.; Guzman, M.; Rodriguez, S.; et al. PI3K inhibition results in enhanced HER signaling and acquired ERK dependency in HER2-overexpressing breast cancer. *Oncogene* **2011**, 30, 2547–2557. [[CrossRef](#)] [[PubMed](#)]
67. Rodrik-Outmezguine, V.S.; Chandarlapaty, S.; Pagano, N.C.; Poulikakos, P.I.; Scaltriti, M.; Moskatel, E.; Baselga, J.; Guichard, S.; Rosen, N. mTOR kinase inhibition causes feedback-dependent biphasic regulation of AKT signaling. *Cancer Discov.* **2011**, 1, 248–259. [[CrossRef](#)] [[PubMed](#)]
68. Tao, J.J.; Castel, P.; Radosevic-robin, N.; Elkabets, M.; Aceto, N.; Weitsman, G.; Barber, P.; Vojnovic, B.; Morse, N.; Viola-villegas, N.T.; et al. Antagonism of EGFR and HER3 Enhances the Response to Inhibitors of the PI3K-Akt Pathway in Triple-Negative Breast Cancer. *Sci. Signal.* **2015**, 7, ra29. [[CrossRef](#)] [[PubMed](#)]

Sample Availability: Samples of cSBL are not available from the authors.



© 2018 by the authors. Licensee MDPI, Basel, Switzerland. This article is an open access article distributed under the terms and conditions of the Creative Commons Attribution (CC BY) license (<http://creativecommons.org/licenses/by/4.0/>).

RESEARCH ARTICLE

Sialic acid-binding lectin from bullfrog eggs inhibits human malignant mesothelioma cell growth *in vitro* and *in vivo*

Takeo Tatsuta¹, Toshiyuki Satoh^{1,2}, Shigeki Sugawara¹, Akiyoshi Hara², Masahiro Hosono^{1*}

1 Division of Cell Recognition Study, Institute of Molecular Biomembrane and Glycobiology, Tohoku Medical and Pharmaceutical University, Aobaku, Sendai, Japan, **2** Department of Clinical Pharmacotherapeutics, Tohoku Medical and Pharmaceutical University, Aobaku, Sendai, Japan

☞ These authors contributed equally to this work.

* mhosono@tohoku-mpu.ac.jp



OPEN ACCESS

Citation: Tatsuta T, Satoh T, Sugawara S, Hara A, Hosono M (2018) Sialic acid-binding lectin from bullfrog eggs inhibits human malignant mesothelioma cell growth *in vitro* and *in vivo*. PLoS ONE 13(1): e0190653. <https://doi.org/10.1371/journal.pone.0190653>

Editor: Irina V. Lebedeva, Columbia University, UNITED STATES

Received: September 19, 2017

Accepted: December 18, 2017

Published: January 3, 2018

Copyright: © 2018 Tatsuta et al. This is an open access article distributed under the terms of the [Creative Commons Attribution License](https://creativecommons.org/licenses/by/4.0/), which permits unrestricted use, distribution, and reproduction in any medium, provided the original author and source are credited.

Data Availability Statement: All relevant data are within the paper.

Funding: This study was supported by the 'Strategic Research' Project (2012-2017) for Private Universities from the Ministry of Education, Culture, Sports, Science and Technology of Japan, and a Grant-in-Aid for Young Scientists (B) [grant no. 17K15029 (to Takeo Tatsuta)]. The funders had no role in study design, data collection and analysis, decision to publish, or preparation of the

Abstract

Malignant mesothelioma is an aggressive cancer that results from exposure to asbestos. The therapeutic options for this type of cancer are limited; therefore, the development of novel therapeutic agents is urgently required. Sialic acid-binding lectin isolated from *Rana catesbeiana* oocytes (cSBL) is a novel therapeutic candidate for cancer, which exhibits antitumor activity mediated through RNA degradation. In the present study, we evaluated the effect of cSBL *in vitro* and *in vivo*. Xenograft-competent H2452 and MSTO human mesothelioma cell lines were treated with cSBL, and the pathway by which cSBL induces apoptosis was analyzed. *In vivo* studies were performed using nude mice inoculated with one of the two cell lines, and the effects of cSBL and pemetrexed were monitored simultaneously. Furthermore, the pharmacological interactions between the three agents (pemetrexed, cisplatin and cSBL) were statistically assessed. It was demonstrated that cSBL treatments caused morphological and biochemical apoptotic changes in both cell lines. Caspase cascade analysis revealed that an intrinsic pathway mediated cSBL-induced apoptosis. The administration of cSBL significantly inhibited tumor growth in two xenograft models, without any adverse effects. Furthermore, the combination index and dose reduction index values indicated that the cSBL + pemetrexed combination showed the highest synergism, and thus potential for reducing dosage of each drug, compared with the other combinations, including the existing pemetrexed + cisplatin regimen. cSBL exerted prominent antitumor effects on malignant mesothelioma cells *in vitro* and *in vivo*, and showed favorable effects when combined with pemetrexed. These results suggest that cSBL has potential as a novel drug for the treatment of malignant mesothelioma.

Introduction

Malignant mesothelioma is an aggressive cancer of the mesothelial cells of serous membranes, involving the pleural and peritoneal spaces, which results from exposure to asbestos [1–3]. The mechanisms underlying the induction of DNA damage by asbestos fibers in mesothelial cells remain unclear. The production and use of asbestos is now forbidden in the majority of

manuscript. There was no additional external funding received for this study.

Competing interests: The authors have declared that no competing interests exist.

industrialized countries; however, it is still actively used in many developing countries [4]. As the time between asbestos exposure and disease diagnosis is >40 years on average, the incidence of mesothelioma is increasing and is projected to peak in the late 2020s, even in developed countries [5].

Malignant mesothelioma may have an epithelioid, sarcomatoid or biphasic morphology [6]. The epithelioid type is associated with a longer survival time compared with the biphasic and sarcomatoid types [7,8]. Although chemotherapeutic approaches are limited for malignant mesothelioma, it is generally accepted that patients with the epithelioid subtype respond better to treatment [9,10]. Additionally, other factors, including sex, performance status, disease stage, serum lactate dehydrogenase level, anemia and leukocytosis, reportedly influence survival in malignant mesothelioma [11]. However, it is difficult to identify the biological factors that clearly differentiate between patients with a poor prognosis and those with a more favorable prognosis, as long-term survival is rare in malignant mesothelioma [6].

There are few therapeutic options (surgery, radiation therapy, and chemotherapy) for mesothelioma [1]. The folate antimetabolite pemetrexed is a chemotherapeutic agent, which is typically used in combination with platinum-containing drugs, such as cisplatin [12,13]. This combination therapy improves the response rate, progression-free survival, overall survival, and quality of life of patients with mesothelioma [12]; however, any treatment-induced regression observed is typically transient, and local tumors rapidly relapse due to the high chemoresistance of this cancer type [4]. So far, some progresses were obtained by multimodality therapy [14]. A median survival time of up to 29 months has been reported for those who complete a trimodal therapy including chemotherapy, surgery, and hemithoracic radiation therapy [15–18]. Moreover, pleurectomy/decortication with intraoperative photodynamic therapy and adjuvant pemetrexed-based chemotherapy demonstrated 36 months median survival [19]. However, even with these aggressive approaches, the prognosis of malignant mesothelioma remains poor. Considering the predicted incidence peak and poor prognosis, as well as the fact that intrinsic and acquired resistance to existing drugs is common, further research into developing therapeutic agents for mesothelioma is essential.

There is growing interest in the use of naturally derived molecules as potential cancer therapeutics. Lectins, carbohydrate-binding proteins that occur in all organisms, are representative of such natural compounds that have great potential for cancer therapy. Among them, several sialic acid-binding lectins (SBLs), including mistletoe lectin (ML1) [20], *Maackia amurensis* seed lectin (MASL) [21], *Polygonatum cyrtonema* lectin (POL) [22] and *Haliotis discus discus* lectin (HddSBL) [23], have been reported to have antitumor effects. SBL isolated from *Rana catesbeiana* oocytes (cSBL) is a unique compound that has multifunctional activity with lectin [24,25] and ribonuclease (RNase) [26], as well as antitumor activity [25]. cSBL exerts potent cytotoxicity in various cancer cell types, but low cytotoxicity in normal cells [27]. *Rana catesbeiana* RNase (RC-RNase), an RNase purified from *R. catesbeiana* oocytes collected in Taiwan by Liao *et al.* is identical to cSBL [28,29]. cSBL consists of 111 amino acid residues with four disulfide bonds [29], and belongs to the vertebrate-secreted RNase family (RNase A superfamily) [30]. It has high thermal stability and strong resistance to protein denaturants [31]. These features are considered one reason for the potent antitumor activity, and provide benefits for commercialization. Furthermore, that cSBL does not associate with endogenous mammalian RNase inhibitors, and that it exerts cytotoxicity in human cancer cells via its RNase activity [25], has facilitated further research into its antitumor effects. The mechanism of cSBL-induced cytotoxicity is proposed to be as follows: cSBL binds to the cancer cell surface and is internalized. It subsequently degrades RNA in the cytosol, leading to the induction of apoptotic signaling [27]. In human leukemia Jurkat cells, cSBL was found to activate p38 and JNK mitogen-activated protein kinase (MAPK) signals and induce apoptosis via the intrinsic

(mitochondrial) pathway [32]. The RNase activity was also determined to be critical for apoptosis induction in MDA-MB231 human breast cancer cells, as an amino acid-replaced mutant of cSBL that lacked RNase activity did not exhibit the apoptosis-inducing effect, even when internalized into the cells like native cSBL [33]. The efficacy of cSBL on malignant mesothelioma cells has previously been reported [34,35]; Even though cSBL hardly show cytotoxicity to normal mesothelial cell Met5A, it efficiently reduced the viability of H28 malignant mesothelioma cells, and exhibited synergistic effects with TRAIL and pemetrexed on these cells.

In our previous study, *in vivo* experiments with cSBL were performed using mice transplanted with related ascites carcinoma, Ehrlich, Mep II and Sarcoma 180 cells. cSBL prolonged their survival at non-toxic dose levels [25]. However, to date, the effect of cSBL on human malignant mesothelioma cells *in vivo* has not been elucidated. In the present study, to assess the therapeutic potential of cSBL on malignant mesothelioma, we conducted an *in vivo* study of cSBL using human malignant mesothelioma cell xenografts, and analyzed its antitumor effects on these xenograft-competent cells.

Materials and methods

Cell culture

The human malignant mesothelioma cell lines NCI-H2452 (H2452, #CRL-5946) and MSTO-211H (MSTO, #CRL-2081) were purchased from the American Type Cell Culture Collection (ATCC; Manassas, VA, USA). The cells were cultured in RPMI-1640 medium (Nissui Pharmaceutical Co., Tokyo, Japan) supplemented with 10% fetal bovine serum (FBS, Biosera, Nuaille, France), 100 U/mL penicillin and 100 µg/mL streptomycin (Life Technologies, Carlsbad, CA, USA) at 37°C in an atmosphere of 95% air and 5% CO₂.

Animals

Eggs-bearing bullfrogs (domestically caught) and 5-week-old male nude mice (BALB/c nu/nu Slc) were purchased from Japan SLC, Inc (Shizuoka, Japan). All animal experiments were carried out in accordance with the Guidelines for Animal Experiments of the Tohoku Medical and Pharmaceutical University (permission number: A16012-cn). Housing condition of the mice was kept under standard conditions approved by the institutional guidelines with free food- and water-consumptions.

Reagents

cSBL was isolated using sequential chromatography with Sephadex G75, DEAE-cellulose, hydroxyapatite and SP-Sepharose, as previously described [24]. Pemetrexed disodium heptahydrate was purchased from LC Laboratories (Woburn, MA, USA). The caspase-3 and caspase-8 antibodies were purchased from Cell Signaling Technology, Inc. (Danvers, MA, USA). The caspase-9 antibody was purchased from Medical & Biological Laboratories Co., Ltd. (MBL; Nagoya, Japan). The β-actin antibody was obtained from Sigma-Aldrich (Merck KGaA, Darmstadt, Germany) and a horseradish peroxidase (HRP)-conjugated anti-mouse IgG antibody was purchased from Zymed Laboratories (Thermo Fisher Scientific, Inc., Waltham, MA, USA). An HRP-conjugated anti-rabbit IgG antibody was purchased from Cedarlane Laboratories (Burlington, Ontario, Canada).

Annexin V staining assay

To investigate the induction of apoptosis, we evaluated Annexin V binding using an MEB-CYTO apoptosis kit (MBL, Nagoya, Japan) according to the manufacturer's instructions. Cells

(5×10^4 cells/mL) were cultured in 6-well plates (2 mL/well) and treated with cSBL (H2452: 1 μ M; MSTO: 0.4 μ M) for 24–72 h at 37°C in an atmosphere of 95% air and 5% CO₂. Fluorescence intensity was subsequently detected using a FACSCalibur™ flow cytometer, and the data was analyzed using CELLQuest™ software version 6.0 (BD Biosciences, Franklin Lakes, NJ, USA).

Detection of nuclear fragmentation

Cells (5×10^4 cells/mL) cultured in a Cell Carrier-96 Ultra Microplate (100 μ L/well) were treated with cSBL (H2452: 5 μ M; MSTO: 2 μ M) for 6, 24, 48 and 72 h, in triplicate. Then, cells were stained with 2 μ g/mL Hoechst 33342 (Dojindo Laboratories, Kumamoto, Japan) for 1 h. The resulting images were acquired with the High-Content Analysis System Operetta CLS™ with NA 20X or 40X objectives, and the fragmentation index was calculated using Harmony™ Imaging and Analysis Software 4.6 (PerkinElmer Japan Co., Ltd., Kanagawa, Japan).

Detection of caspase activity

The protein expression levels of activated caspase-3, -8, and -9 were analyzed using western blot assays. Cells (1×10^5 cells/mL) cultured in 6-well plates (2 mL/well) were treated with cSBL (H2452: 5 μ M; MSTO: 2 μ M) for 1, 3, 6, 24, 48, and 72 h. Whole cell lysates were prepared using extraction buffer [150 mM NaCl, 10 mM Tris-HCl (pH 7.4), 5 mM EDTA, 1% Nonidet P-40, 0.1% sodium deoxycholate, and 0.1% sodium dodecyl sulfate] supplemented with cOmplete™ Mini EDTA-free Protease Inhibitor Cocktail tablets and PhosSTOP phosphatase inhibitor tablets (each 1 tablet/10 mL; Roche Applied Science, Indianapolis, IN, USA). Soluble proteins were collected, and the protein concentration was measured using a BCA protein assay kit (Thermo Fisher Scientific, Inc.) according to the manufacturer's instructions. The proteins were separated using 10 or 14% SDS-PAGE and transferred onto Immobilon-P transfer membranes (EMD Millipore, Billerica, MA, USA). The membranes were sequentially incubated with primary and secondary antibodies diluted in Can Get Signal® solution (Toyobo Co, Ltd., Osaka, Japan). The protein bands were detected using ECL Prime Western Blotting Detection Reagent (GE Healthcare, Little Chalfont, USA) or Chemi-Lumi One Super (Nacalai Tesque Inc., Kyoto, Japan).

Caspase enzymatic activity was measured using a Cell Meter™ Multiplexing Caspase-3/7, -8 and -9 Activity Assay Kit (AAT Bioquest, Inc., Sunnyvale, CA). Cells (5×10^4 cells/mL) cultured in black 96-well plates (100 μ L/well) were treated with cSBL (H2452: 5 μ M; MSTO: 2 μ M) for 1, 3, 6, 24, 48, and 72 h in triplicate. Substrate solution (100 μ L) was added to each well, and the contents of the wells were mixed using a plate shaker for 30 sec. The cells were incubated at 37°C in a 5% CO₂ atmosphere for 1 h. The luminescence in each well was measured using Infinite™ 200 PRO and i-control™ software (Tecan Japan Co., Ltd., Kanagawa, Japan).

In vivo experiment

H2452 (5×10^6 cells) and MSTO (2×10^6 cells) cells were mixed with an equal volume of ice-cooled Corning™ Matrigel™ Basement Membrane Matrix (Corning, NY, USA), and an aliquot (100 μ L) of suspended cells was subcutaneously injected into the lower backs of the mice. 2–4 weeks after inoculation (day 1), mice bearing tumors of 100–150 mm³ in volume were randomly divided into three groups, with 10 mice in each group. Group 1 was injected with 1 mL/kg vehicle (PBS) as the control. Group 2 was daily injected intraperitoneally with 100 mg/kg pemetrexed dissolved in sterile PBS on days 1–5 and 15–19. The method of administration the dosage of pemetrexed selected were based on the previously reported maximum tolerated dosage [36,37]. Group 3 was injected intratumorally with 2.5 mg/kg cSBL, twice weekly for four

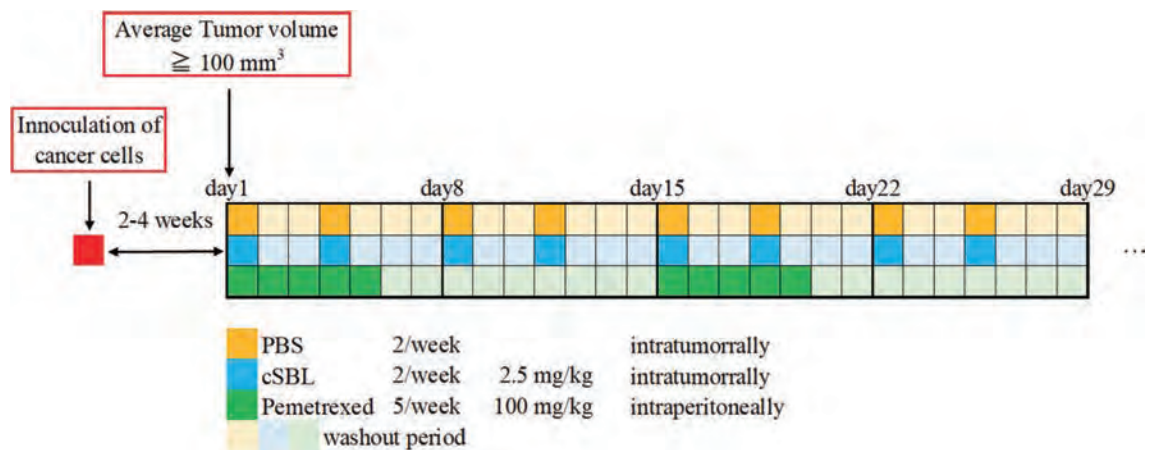


Fig 1. A schematic overview of the cancer cell injection and drug administration schedule. The cell suspension (100 μ L/mouse, H2452; 5×10^6 cells, MSTO; 2×10^6 cells) was injected subcutaneously into the lower backs of mice. After 2–4 weeks, mice bearing tumors of 100–150 mm^3 were randomly divided into 3 groups with 10 mice per group. Group 1 was administered PBS as control. Group 2 was injected intraperitoneally with pemetrexed (100 mg/kg) dissolved in sterile PBS on days 1–5 and 15–19. Group 3 was injected intratumorally with cSBL (2.5 mg/kg) twice per week for 4 weeks. Body weights and tumor sizes were measured twice per week. The endpoint of experiment was when the tumor diameter exceeded 200 mm^3 .

<https://doi.org/10.1371/journal.pone.0190653.g001>

weeks. Body weights and tumor sizes were measured twice weekly. Solid tumor volumes were calculated as follows: $0.4 \times A \times B^2$, with A and B representing the long and short tumor diameters (measured in mm), respectively. Tumor growth and body weight changes were evaluated as the ratio of each value against the baseline (day 1). Fig 1 shows the administration schedule used in the experiments. Mice were sacrificed by neck dislocation under ether anesthesia when tumor volumes reached 200 mm^3 .

Drug combination studies

The effect of combination treatment on cell viability was determined using a WST-8 assay. Cells (5×10^4 cells/mL) were cultured in 96-well plates (100 μ L/well). The concentration of pemetrexed, cisplatin, or cSBL was based on the IC_{50} values obtained in the single-treatment experiments conducted in our prior study [35]. After 72 h, the cells were incubated with Cell Count Reagent SF (Nacalai Tesque Inc., Kyoto, Japan) at 37°C in a 5% CO_2 atmosphere for 1–4 h. The absorbance of the resulting product at 450 nm was measured, and the background absorbance at 650 nm was subtracted. Combination Index (CI) and Dose Reduction Index (DRI) values were calculated using CompuSyn software (ComboSyn, Inc., Paramus, NJ), as described by Chou *et al* [38]. The experiments were conducted in triplicate. CI = 1 indicated an additive effect; CI < 1 indicated a synergistic effect; CI > 1 indicated an antagonistic effect. DRI = 1 indicated no dose reduction, whereas DRI > 1 and < 1 indicated favorable and unfavorable dose reductions, respectively.

Statistical analysis

The results from ≥ 3 independent experiments, each performed in triplicate, are expressed as the mean \pm standard deviation. Statistical analyses were conducted using GraphPad Prism 5.0, and comparisons were made using one-way analysis of variance (ANOVA) or two-way ANOVA followed by Bonferroni’s post hoc test. A P-value of < 0.05 was considered statistically significant.

Results

cSBL induces apoptosis to H2452 and MSTO cells

In order to investigate the antitumor activity of cSBL on xenograft-competent malignant mesothelioma cells, H2452 and MSTO cells were treated with cSBL and the antitumor mechanisms were analyzed. The percentage of Annexin V-positive cells was significantly increased in both H2452 (16.13%, 72 h) and MSTO (40.05%, 72 h) cells (Fig 2A and 2B). In addition, chromatin condensation and nuclear collapse were observed in the two cell types treated with cSBL

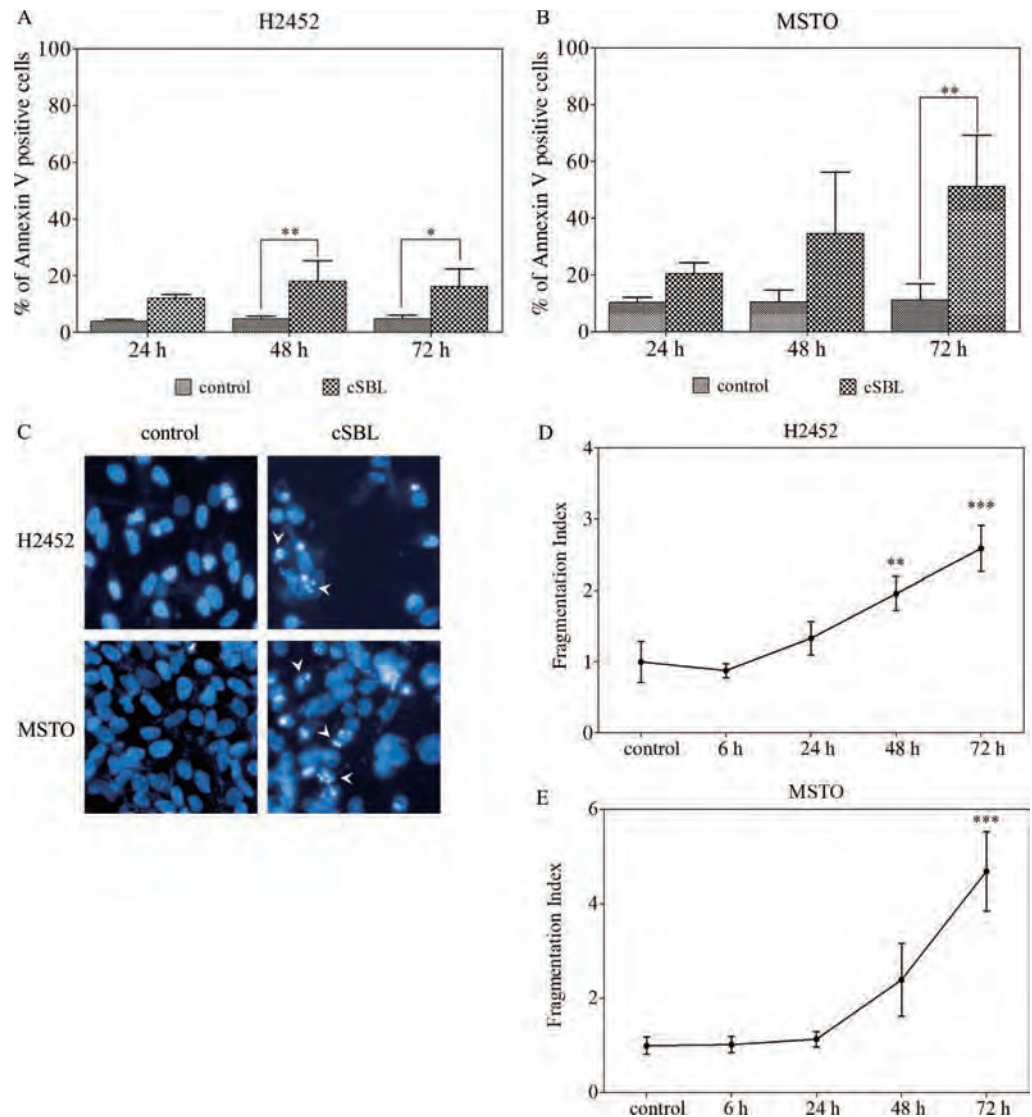


Fig 2. cSBL induced apoptotic changes in H2452 and MSTO cells. Cells were treated with cSBL for the indicated times. (A, B) Rate of apoptosis as indicated by the percentage of annexin V-positive cells. (C) Nuclear fragmentation images were captured using 40X objective; a false-colored image of the nuclei (blue) is shown. White arrowheads indicate the cells with condensed or fragmented nuclei. (D, E) Fragmentation index indicating the degree of nuclear fragmentation; a higher index indicates greater occurrence of fragmentation, calculated using the High-Content Analysis System. All data are expressed as the mean \pm SD of three independent experiments. The statistical significance of these experiments compared with the control is shown as follows: * $P < 0.05$, ** $P < 0.01$, *** $P < 0.001$.

<https://doi.org/10.1371/journal.pone.0190653.g002>

(Fig 2C). Alterations to nuclear morphology were detected by High-Content Analysis Systems and numerically output as fragmentation indexes. As shown in Fig 2D and 2E, cSBL provoked significant nuclear morphology changes in time-dependent manner.

cSBL-induced apoptosis is mediated by the intrinsic pathway

To obtain further insight into the mechanisms of cSBL-induced apoptosis in H2452 and MSTO cells, the activation of three key caspases was analyzed chronologically. The expression levels of activated caspase-9, -8 and -3 were detected by western blotting, and the substantial enzymatic activities of these caspases were evaluated by fluorometric analysis. As shown in Fig 3A and 3B, increased levels of activated caspase-9 were observed from 6 h and 1 h in H2452 and MSTO cells, respectively. After that, activated caspase-8 began to be observed from 24 h in H2452 and 6 h in MSTO cells. The appearance of activated caspase-3 was recorded from 48 h in H2452 and 24 h in MSTO cells. Consistently, the enzymatic activity of caspase-9 was significantly enhanced from 1 h in H2452 and MSTO cells, and the levels of caspase-8 and -3/7 increased almost simultaneously (H2452: 48 h; MSTO: 24 h; Fig 3C and 3D). Thus, caspase-9 was activated prior to caspase-8 and -3, indicating that the intrinsic apoptotic pathway was involved.

cSBL inhibits cancer cell proliferation without inducing weight loss in xenograft models

To examine the effects of cSBL on tumor growth *in vivo*, nude mice were inoculated with H2452 and MSTO cells. cSBL was administered intratumorally and the effects of pemetrexed were also assessed according to previously reported experimental conditions [36,37] (Fig 1).

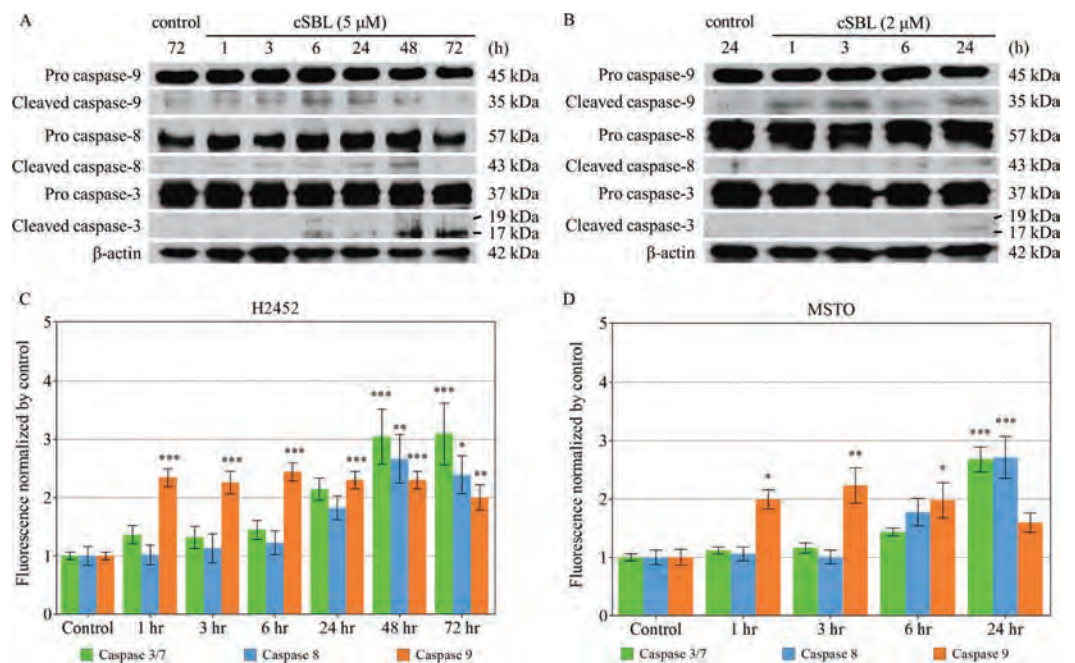


Fig 3. cSBL induced apoptosis in H2452 and MSTO cells via activation of the caspase pathway. Caspase-3, -8, and -9 activation was detected by western blotting (A, B) or fluorometry (C, D). Fluorometry was performed independently three times and data are expressed as the mean ± SD. The statistical significance of these experiments compared with the control is shown in as follows: *P<0.05, **P<0.01, ***P<0.001.

<https://doi.org/10.1371/journal.pone.0190653.g003>

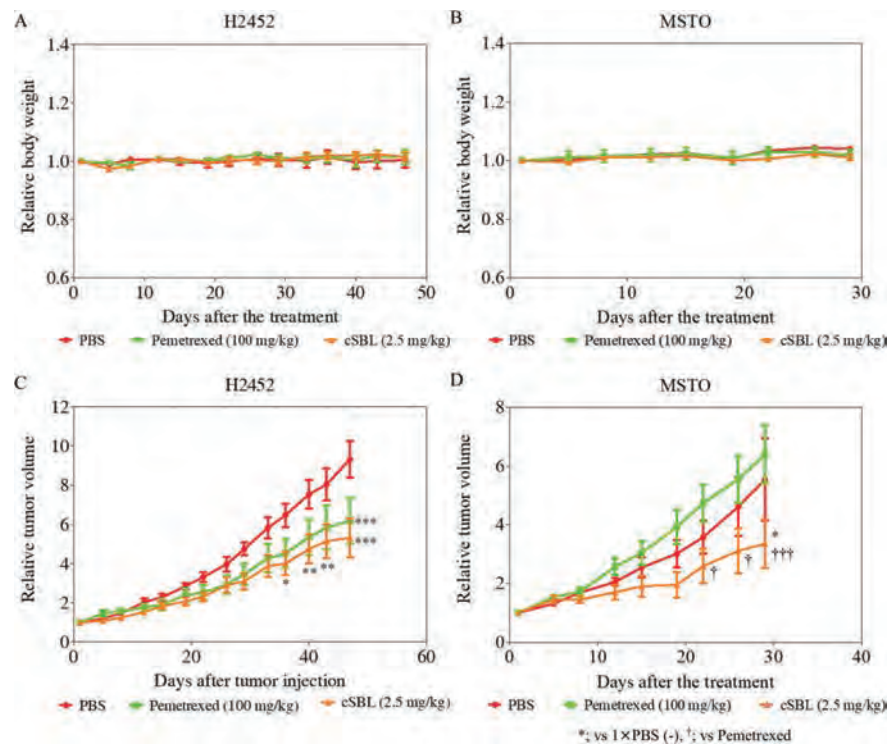


Fig 4. cSBL showed *in vivo* cytotoxicity without inducing loss of body weight. Mice were randomly divided into 3 groups with 10 mice in each group. Groups 1, 2, and 3 were injected PBS, pemetrexed (100 mg/kg, intraperitoneally), and cSBL (2.5 mg/kg, intratumorally), respectively. Body weights and tumor sizes were measured twice per week. Tumor volumes were calculated as follows: $0.4 \times A \times B^2$, where A and B represent the long and short diameters (in mm) of the tumor, respectively. Relative body weight (A, B) and relative tumor volume (C, D) are plotted as the mean of each group \pm SD at each timepoint. The statistical significance of these experiments compared with PBS (*) or pemetrexed (†) is shown as follows: * $P < 0.05$, ** $P < 0.01$, *** $P < 0.001$, † $P < 0.01$, ††† $P < 0.001$.

<https://doi.org/10.1371/journal.pone.0190653.g004>

The rate of changes to animal weights and tumor volumes were monitored following the administration of each agent. As shown in Fig 4A and 4B, body weight changes were not observed in any of the groups. In the H2452 xenograft model, cSBL and pemetrexed each significantly inhibited tumor growth compared with the PBS group ($P < 0.05$), and the cSBL group showed a growth inhibition effect earlier (after 36 days of treatment) than that of the pemetrexed group (after 47 days of treatment) (Fig 4C). Conversely, for the MSTO xenograft group, significant inhibition of cancer growth was observed only in the cSBL-treated group after 29 days of treatment ($P < 0.05$; Fig 4D).

cSBL and pemetrexed exhibit a strong synergistic effect in H2452 and MSTO cells

Finally, we performed the *in vitro* combination study of cSBL with other reagents. In addition to pemetrexed, cisplatin, an existing drug for malignant mesothelioma usually used in combination with pemetrexed, was chosen for the test reagent. Pharmacological interactions between these three agents were investigated by evaluating the viability of H2452 and MSTO cells treated with pemetrexed + cisplatin, cSBL + pemetrexed, and cSBL + cisplatin. The drug concentration in each combination regimen was based on the IC_{50} value for each agent previously determined via single treatments [35]. The viability curves for each drug in single or

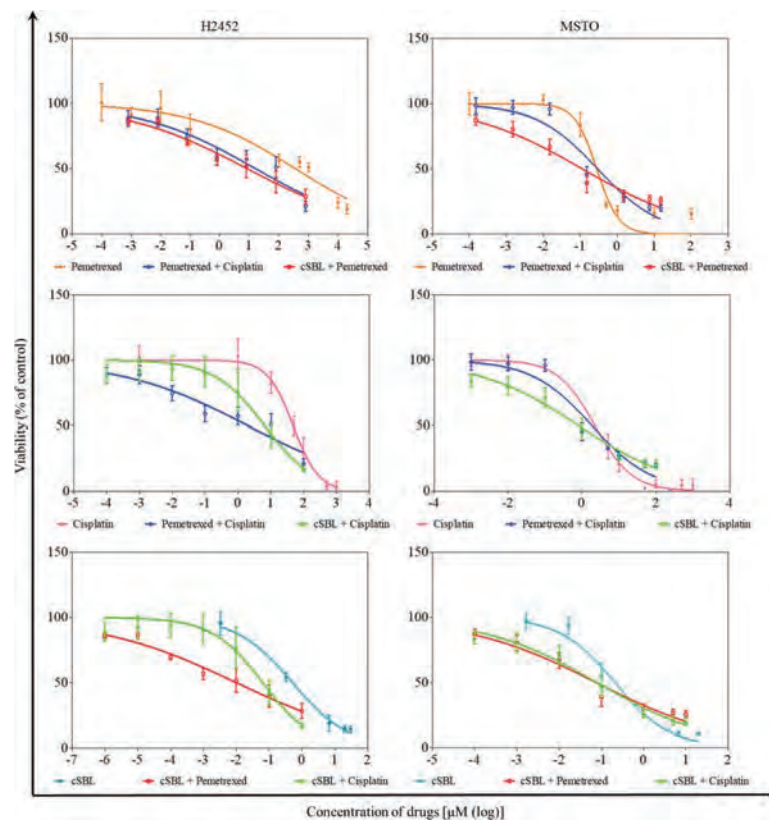


Fig 5. Viability curves of H2452 and MSTO cells treated with pemetrexed, cisplatin, and cSBL, either alone or in combination. Each group of cells was treated with fixed concentration ratios of pemetrexed: cisplatin:cSBL as follows: 800:100:1 (for H2452 cells) or 3:20:2 (for MSTO cells). Each data point represents the mean \pm SD of at least three independent WST-8 assays. Each sample was plated in triplicate. The y-axis indicates the viability of cells. The x-axis indicates the concentration of pemetrexed (upper), cisplatin (middle), or cSBL (lower).

<https://doi.org/10.1371/journal.pone.0190653.g005>

combination treatments are presented in Fig 5. In H2452 cells, all combinations decreased cell viability to a greater extent than each single treatment over the whole concentration range. Similar tendencies were observed in MSTO cells over a wide concentration range, although the combination effects appeared to saturate at a higher concentration. To evaluate the synergistic effect of each drug combination, CI values were calculated. At each experimental concentration (Fig 6A) in H2452 cells, the CI values for all combinations were <1 , indicating that all combinations were synergistic. cSBL + pemetrexed showed the highest synergistic effect at all concentration points. In MSTO cells, CI values at the highest two concentration points of all combinations exhibited antagonism rather than synergism; however, cSBL-containing combinations (cSBL + pemetrexed; cSBL + cisplatin) exhibited high synergism in the mid-low concentration range. The pemetrexed + cisplatin combination in MSTO cells showed dispersion and high CI values at various concentrations. Furthermore, we calculated DRI values, representing the index of the fold-number that each drug combination dose could be reduced by compared with that of each drug alone (Fig 6B). In H2452 cells, all combinations had high DRI values. In MSTO cells, high DRI values were observed in the cSBL-containing combinations, particularly in the low concentration range. However, the pemetrexed + cisplatin combination had low DRI values at all concentrations.

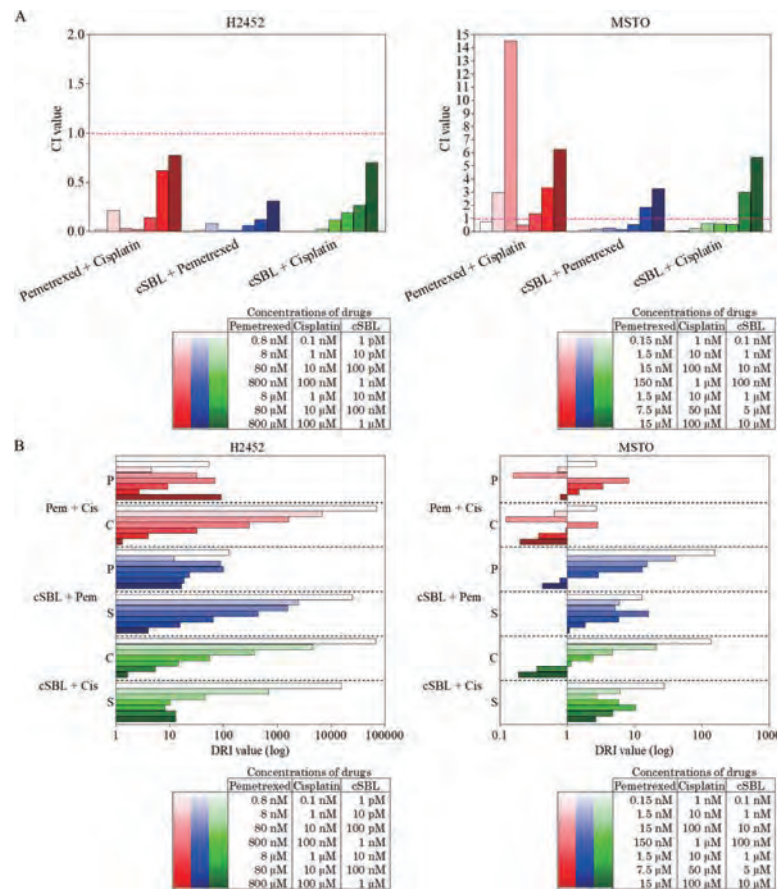


Fig 6. Pharmacological interactions between pemetrexed, cisplatin and cSBL in H2452 and MSTO cells. (A) CI values of each combination (CI = 1 indicates an additive effect; CI < 1 indicates a synergistic effect; and CI > 1 indicates an antagonistic effect). (B) DRI values of each reagent (DRI = 1 indicates no dose reduction; whereas DRI > 1 and < 1 indicate favorable and unfavorable dose-reductions, respectively). Pem or P, pemetrexed; Cis or C, cisplatin; S, cSBL.

<https://doi.org/10.1371/journal.pone.0190653.g006>

Discussion

We previously demonstrated that cSBL induces apoptosis in H28 (sarcomatoid histological type), MESO-1 and MESO-4 (epithelioid type) cells, but not in normal Met5A mesothelial cells, by detecting elevated proportions of Annexin V positive cells following cSBL treatment [34]. Furthermore, from the investigations in which H2452 (epithelioid type) and MSTO (biphasic type) were utilized, in addition to aforementioned cell lines, higher cancer-selectivity of cSBL was observed compared with either pemetrexed or cisplatin in their antiproliferative effects [35]. The antitumor mechanism of cSBL in malignant mesothelioma has been well-documented in H28 cells; it was revealed that cSBL treatment activates the caspase cascade, the proapoptotic Bcl-2 family proteins Bik and Bim, as well as JNK and p38 MAPKs, consequently inducing apoptosis in these cells. However, although the effectiveness of cSBL against mesothelioma *in vitro* has been reported, the *in vivo* efficacy of cSBL has not been investigated to date.

Although H28, MESO-1, and MESO-4 cells did not show tumorigenicity in the nude mice used, we succeeded in establishing malignant mesothelioma xenografts with H2452 and MSTO cells. First, the antitumor effects of cSBL on these two cell lines were investigated *in vitro*. cSBL induced typical apoptotic changes, such as phosphatidylserine externalization,

nuclear condensation and fragmentation, in both cells in a time-dependent manner (Fig 2). Moreover, caspase-9 was activated by cSBL treatment earlier and more strongly than caspase-8, indicating that apoptosis was induced through the intrinsic pathway (Fig 3). In the *in vivo* studies, no obvious toxicities or body weight changes were observed during the experimental period in any group (Fig 4A and 4B). In both types of xenograft, significant tumor growth suppression was observed in cSBL-treated groups compared with control groups. In H2452 xenografted groups, cSBL showed a tumor-suppressive effect earlier than that of the pemetrexed-treated group, and the antitumor effect of pemetrexed was not observed in the MSTO xenografts (Fig 4C and 4D). The reason for the lack of effect by pemetrexed is uncertain; we speculate that the high growth rate of MSTO cells in the xenograft model may contribute to this phenomenon. We were unable to compare the effects of cSBL and pemetrexed directly due to the differences in the dosing conditions; however, our observations indicate that cSBL could potentially inhibit the tumor growth of mesothelioma without any toxicity, even if previously established pemetrexed administration had little or no effect. From these results, it was suggested that cSBL had the capability to inhibit tumor growth in xenografted mice. Thus, cSBL may be safely used, and further studies are required to determine the maximal tolerated dose of cSBL in order to optimize its efficacy.

Combination therapy, a treatment modality that combines two or more therapeutic agents to reduce the risk of drug resistance or adverse effects while simultaneously providing therapeutic anti-cancer benefits, is a mainstay of current cancer therapy [39]. In fact, combination treatments comprising pemetrexed and cisplatin are used for the treatment of mesothelioma as a standard regimen. We previously demonstrated that the cSBL + pemetrexed combination exerted stronger cytotoxicity and synergism compared with the pemetrexed + cisplatin combination in H28 cell lines. The cytostatic effect of pemetrexed and the cytotoxic effect of cSBL cooperated without any repulsion, although the effects of pemetrexed and cisplatin on cyclin A expression were counteractive when used in combination [35]. In the present study, we evaluated the generality of the prominent synergistic effect of the cSBL + pemetrexed combination, utilizing H2452 and MSTO cells, by calculating CI and DRI values. The cSBL + pemetrexed combination exhibited the highest synergism of the three combinations tested in both cell lines (Fig 5B). Surprisingly, in MSTO cells, the pemetrexed + cisplatin combination appeared to be antagonistic rather than synergistic or additive at the most of concentration points tested. High DRI values (Fig 5C) were calculated for all combinations, except for pemetrexed + cisplatin in MSTO cells. These results suggest that cSBL + pemetrexed may be a rational treatment combination for several types of malignant mesothelioma. On the other hand, the current gold-standard regimen for malignant mesothelioma, pemetrexed + cisplatin, may be ineffective, depending on the cell type, with respect to synergism (i.e., undesired adverse effects may easily occur in some circumstances, depending on the patient).

Although the combination of pemetrexed and cisplatin has been demonstrated to prolong the survival of patients with malignant mesothelioma, the median survival is only 12 months, and the response rate is ~40% [12]. Thus, almost half of all mesothelioma patients are initially resistant, and all eventually develop resistance [40]. Therefore, researches to improve the malignant mesothelioma therapy have been actively attempt. The combinations of carboplatin and pemetrexed, or gemcitabine and cisplatin showed comparable outcomes with pemetrexed and cisplatin combination in phase- II trials [41–43]. The French Mesothelioma Avastin Cisplatin Pemetrexed Study (MAPS) demonstrated a statistically significant improvement in the median overall survival time using a combination of cisplatin, pemetrexed and bevacizumab, a monoclonal antibody that binds VEGF and blocks its interaction with the VEGF receptor [44]. In addition, several other molecular targeting and immunotherapeutic agents, such as anti-EGFR signaling agent and anti-programmed cell death 1 (PD-1) antibodies, are currently

being investigated in clinical trials [43]. In this study, cSBL was demonstrated to induce apoptosis and inhibit tumor cell growth in xenografted mice. CI analysis also evidenced a prominent combinatory effect of cSBL with pemetrexed. As cSBL is a novel candidate anti-cancer agent that exerts antitumor activity through targeting RNA (which represents a novel class of potential therapeutic targets), it may provide a new option for the chemotherapeutic treatment of malignant mesothelioma. This is particularly true among patients with pemetrexed resistance, as cSBL was effective in pemetrexed-resistant cells, as shown in the current study and in previous report [35].

Conclusions

cSBL induced apoptosis in H2452 and MSTO cells via the intrinsic apoptotic pathway. *In vivo*, cSBL treatment inhibited tumor growth in multiple xenograft models without any undesirable adverse effects. A higher efficacy was achieved by the use of cSBL + pemetrexed in mesothelioma cells compared with pemetrexed + cisplatin. To the best of our knowledge, this is the first report to demonstrate the antitumor efficacy of cSBL in human malignant mesothelioma xenograft models. cSBL has potential as a novel treatment for malignant mesothelioma.

Author Contributions

Conceptualization: Takeo Tatsuta, Masahiro Hosono.

Data curation: Takeo Tatsuta, Toshiyuki Satoh, Masahiro Hosono.

Formal analysis: Takeo Tatsuta, Toshiyuki Satoh.

Funding acquisition: Takeo Tatsuta, Akiyoshi Hara, Masahiro Hosono.

Investigation: Takeo Tatsuta, Toshiyuki Satoh, Shigeki Sugawara.

Methodology: Takeo Tatsuta, Toshiyuki Satoh, Shigeki Sugawara.

Project administration: Akiyoshi Hara, Masahiro Hosono.

Resources: Takeo Tatsuta, Toshiyuki Satoh, Shigeki Sugawara.

Supervision: Akiyoshi Hara, Masahiro Hosono.

Validation: Takeo Tatsuta, Masahiro Hosono.

Visualization: Takeo Tatsuta, Toshiyuki Satoh, Shigeki Sugawara.

Writing – original draft: Takeo Tatsuta, Toshiyuki Satoh.

Writing – review & editing: Takeo Tatsuta, Toshiyuki Satoh, Masahiro Hosono.

References

1. Tsao AS, Wistuba I, Roth JA, Kindler HL. Malignant pleural mesothelioma. *J Clin Oncol*. 2009; 27: 2081–90. <https://doi.org/10.1200/JCO.2008.19.8523> PMID: 19255316
2. Robinson BWS, Lake RA. Advances in malignant mesothelioma. *N Engl J Med*. 2005; 353: 1591–603. <https://doi.org/10.1056/NEJMra050152> PMID: 16221782
3. Antman KH. Natural history and epidemiology of malignant mesothelioma. *Chest*. The American College of Chest Physicians; 1993; 103: 373S–376S. <https://doi.org/10.1378/chest.103.4> PMID: 8462328
4. Bonelli MA, Fumarola C, La Monica S, Alfieri R. New therapeutic strategies for malignant pleural mesothelioma. *Biochem Pharmacol*. Elsevier Inc.; 2017; 123: 8–18. <https://doi.org/10.1016/j.bcp.2016.07.012> PMID: 27431778
5. Robinson BM. Malignant pleural mesothelioma: an epidemiological perspective. *Ann Cardiothorac Surg*. 2012; 1: 491–6. <https://doi.org/10.3978/j.issn.2225-319X.2012.11.04> PMID: 23977542

6. Davidson B. Prognostic factors in malignant pleural mesothelioma. *Hum Pathol*. Elsevier Inc.; 2015; 46: 789–804. <https://doi.org/10.1016/j.humpath.2015.02.006> PMID: [25824607](https://pubmed.ncbi.nlm.nih.gov/25824607/)
7. Musk AW, Olsen N, Alfonso H, Reid A, Mina R, Franklin P, et al. Predicting survival in malignant mesothelioma. *Eur Respir J*. 2011; 38: 1420–4. <https://doi.org/10.1183/09031936.00000811> PMID: [21737558](https://pubmed.ncbi.nlm.nih.gov/21737558/)
8. Brims FJH, Meniawy TM, Duffus I, de Fonseka D, Segal A, Creaney J, et al. A Novel Clinical Prediction Model for Prognosis in Malignant Pleural Mesothelioma Using Decision Tree Analysis. *J Thorac Oncol*. Elsevier Inc; 2016; 11: 573–82. <https://doi.org/10.1016/j.jtho.2015.12.108> PMID: [26776867](https://pubmed.ncbi.nlm.nih.gov/26776867/)
9. Billé A, Krug LM, Woo KM, Rusch VW, Zauderer MG. Contemporary Analysis of Prognostic Factors in Patients with Unresectable Malignant Pleural Mesothelioma. *J Thorac Oncol*. Elsevier Inc; 2016; 11: 249–55. <https://doi.org/10.1016/j.jtho.2015.10.003> PMID: [26845118](https://pubmed.ncbi.nlm.nih.gov/26845118/)
10. Muruganandan S, Alfonso H, Franklin P, Shiikn K, Segal A, Olsen N, et al. Comparison of outcomes following a cytological or histological diagnosis of malignant mesothelioma. *Br J Cancer*. Nature Publishing Group; 2017; 116: 703–708. <https://doi.org/10.1038/bjc.2017.20> PMID: [28196068](https://pubmed.ncbi.nlm.nih.gov/28196068/)
11. Campbell N, Kindler H. Update on Malignant Pleural Mesothelioma. *Semin Respir Crit Care Med*. 2011; 32: 102–110. <https://doi.org/10.1055/s-0031-1272874> PMID: [21500129](https://pubmed.ncbi.nlm.nih.gov/21500129/)
12. Vogelzang NJ, Rusthoven JJ, Symanowski J, Denham C, Kaukel E, Ruffie P, et al. Phase III study of pemetrexed in combination with cisplatin versus cisplatin alone in patients with malignant pleural mesothelioma. *J Clin Oncol*. 2003; 21: 2636–44. <https://doi.org/10.1200/JCO.2003.11.136> PMID: [12860938](https://pubmed.ncbi.nlm.nih.gov/12860938/)
13. Krug LM. An overview of chemotherapy for mesothelioma. *Hematol Oncol Clin North Am*. 2005; 19: 1117–36. <https://doi.org/10.1016/j.hoc.2005.09.010> PMID: [16325127](https://pubmed.ncbi.nlm.nih.gov/16325127/)
14. Nelson DB, Rice DC, Niu J, Atay S, Vaporciyan AA, Antonoff M, et al. Long-term survival outcomes of cancer-directed surgery for malignant pleural mesothelioma: Propensity score matching analysis. *J Clin Oncol*. 2017; 35: 3354–3362. <https://doi.org/10.1200/JCO.2017.73.8401> PMID: [28817374](https://pubmed.ncbi.nlm.nih.gov/28817374/)
15. de Perrot M, Feld R, Cho BCJ, Beziak A, Anraku M, Burkes R, et al. Trimodality therapy with induction chemotherapy followed by extrapleural pneumonectomy and adjuvant high-dose hemithoracic radiation for malignant pleural mesothelioma. *J Clin Oncol*. 2009; 27: 1413–8. <https://doi.org/10.1200/JCO.2008.17.5604> PMID: [19224855](https://pubmed.ncbi.nlm.nih.gov/19224855/)
16. Krug LM, Pass HI, Rusch VW, Kindler HL, Sugarbaker DJ, Rosenzweig KE, et al. Multicenter phase II trial of neoadjuvant pemetrexed plus cisplatin followed by extrapleural pneumonectomy and radiation for malignant pleural mesothelioma. *J Clin Oncol*. 2009; 27: 3007–13. <https://doi.org/10.1200/JCO.2008.20.3943> PMID: [19364962](https://pubmed.ncbi.nlm.nih.gov/19364962/)
17. Bölükbas S, Manegold C, Eberlein M, Bergmann T, Fisseler-Eckhoff A, Schirren J. Survival after trimodality therapy for malignant pleural mesothelioma: Radical Pleurectomy, chemotherapy with Cisplatin/Pemetrexed and radiotherapy. *Lung Cancer*. 2011; 71: 75–81. <https://doi.org/10.1016/j.lungcan.2009.08.019> PMID: [19765853](https://pubmed.ncbi.nlm.nih.gov/19765853/)
18. Weder W, Stahel RA, Bernhard J, Bodis S, Vogt P, Ballabeni P, et al. Multicenter trial of neo-adjuvant chemotherapy followed by extrapleural pneumonectomy in malignant pleural mesothelioma. *Ann Oncol Off J Eur Soc Med Oncol*. 2007; 18: 1196–202. <https://doi.org/10.1093/annonc/mdm093> PMID: [17429100](https://pubmed.ncbi.nlm.nih.gov/17429100/)
19. Friedberg JS, Simone CB, Culligan MJ, Barsky AR, Doucette A, McNulty S, et al. Extended Pleurectomy-Decortication-Based Treatment for Advanced Stage Epithelial Mesothelioma Yielding a Median Survival of Nearly Three Years. *Ann Thorac Surg*. 2017; 103: 912–919. <https://doi.org/10.1016/j.athoracsur.2016.08.071> PMID: [27825687](https://pubmed.ncbi.nlm.nih.gov/27825687/)
20. Pryme IF, Bardocz S, Pusztai A, Ewen SWB. Suppression of growth of tumour cell lines in vitro and tumours in vivo by mistletoe lectins. *Histol Histopathol*. 2006; 21: 285–99. <https://doi.org/10.14670/HH-21.285> PMID: [16372250](https://pubmed.ncbi.nlm.nih.gov/16372250/)
21. Ochoa-Alvarez JA, Krishnan H, Shen Y, Acharya NK, Han M, McNulty DE, et al. Plant lectin can target receptors containing sialic acid, exemplified by podoplanin, to inhibit transformed cell growth and migration. *PLoS One*. 2012;7. <https://doi.org/10.1371/journal.pone.0041845> PMID: [22844530](https://pubmed.ncbi.nlm.nih.gov/22844530/)
22. Liu B, Zhang B, Min M wei, Bian H jiao, Chen L fei, Liu Q, et al. Induction of apoptosis by Polygonatum odoratum lectin and its molecular mechanisms in murine fibrosarcoma L929 cells. *Biochim Biophys Acta—Gen Subj*. Elsevier B.V.; 2009; 1790: 840–844. <https://doi.org/10.1016/j.bbagen.2009.04.020> PMID: [19414060](https://pubmed.ncbi.nlm.nih.gov/19414060/)
23. Yang X, Wu L, Duan X, Cui L, Luo J, Li G. Adenovirus carrying gene encoding *Haliotis discus discus* sialic acid binding lectin induces cancer cell apoptosis. *Mar Drugs*. 2014; 12: 3994–4004. <https://doi.org/10.3390/md12073994> PMID: [24983642](https://pubmed.ncbi.nlm.nih.gov/24983642/)
24. Nitta K, Takayanagi G, Kawauchi H, Hakomori S. Isolation and characterization of *Rana catesbeiana* lectin and demonstration of the lectin-binding glycoprotein of rodent and human tumor cell membranes.

- Cancer Res. 1987; 47: 4877–83. Available: <http://www.ncbi.nlm.nih.gov/pubmed/3497712> PMID: [3497712](https://doi.org/10.1371/journal.pone.0190653)
25. Nitta K, Ozaki K, Ishikawa M, Furusawa S, Hosono M, Kawauchi H, et al. Inhibition of cell proliferation by *Rana catesbeiana* and *Rana japonica* lectins belonging to the ribonuclease superfamily. *Cancer Res.* 1994; 54: 920–7. Available: <http://www.ncbi.nlm.nih.gov/pubmed/8313382> PMID: [8313382](https://doi.org/10.1371/journal.pone.0190653)
 26. Nitta K, Oyama F, Oyama R, Sekiguchi K, Kawauchi H, Takayanagi Y, et al. Ribonuclease activity of sialic acid-binding lectin from *Rana catesbeiana* eggs. *Glycobiology.* 1993; 3: 37–45. Available: <http://www.ncbi.nlm.nih.gov/pubmed/8448385> PMID: [8448385](https://doi.org/10.1371/journal.pone.0190653)
 27. Tatsuta T, Sugawara S, Takahashi K, Ogawa Y, Hosono M, Nitta K. Cancer-selective induction of apoptosis by leczyne. *Front Oncol.* 2014; 4: 139. <https://doi.org/10.3389/fonc.2014.00139> PMID: [24926439](https://doi.org/10.1371/journal.pone.0190653)
 28. Liao Y di. A pyrimidine-guanine sequence-specific ribonuclease from *Rana catesbeiana* (bullfrog) oocytes. *Nucleic Acids Res.* 1992; 20: 1371–1377. <https://doi.org/10.1093/nar/20.6.1371> PMID: [1373237](https://doi.org/10.1371/journal.pone.0190653)
 29. Titani K, Takio K, Kuwada M, Nitta K, Sakakibara F, Kawauchi H, et al. Amino acid sequence of sialic acid binding lectin from frog (*Rana catesbeiana*) eggs. *Biochemistry.* 1987; 26: 2189–2194. <https://doi.org/10.1021/bi00382a018> PMID: [3304421](https://doi.org/10.1371/journal.pone.0190653)
 30. Tatsuta T, Sugawara S, Takahashi K, Ogawa Y, Hosono M, Nitta K. Leczyme: a new candidate drug for cancer therapy. *Biomed Res Int.* Hindawi Publishing Corporation; 2014; 2014: 421415. <https://doi.org/10.1155/2014/421415> PMID: [24864241](https://doi.org/10.1371/journal.pone.0190653)
 31. Irie M, Nitta K, Nonaka T. Biochemistry of frog ribonucleases. *Cell Mol Life Sci.* 1998; 54: 775–784. <https://doi.org/10.1007/s000180050206> PMID: [9760986](https://doi.org/10.1371/journal.pone.0190653)
 32. Tatsuta T, Hosono M, Sugawara S, Kariya Y, Ogawa Y, Hakomori S, et al. Sialic acid-binding lectin (leczyme) induces caspase-dependent apoptosis-mediated mitochondrial perturbation in Jurkat cells. *Int J Oncol.* 2013; 43: 1402–12. <https://doi.org/10.3892/ijo.2013.2092> PMID: [24008724](https://doi.org/10.1371/journal.pone.0190653)
 33. Kariya Y, Tatsuta T, Sugawara S, Kariya Y, Nitta K, Hosono M. RNase activity of sialic acid-binding lectin from bullfrog eggs drives antitumor effect via the activation of p38 MAPK to caspase-3/7 signaling pathway in human breast cancer cells. *Int J Oncol.* 2016; 49: 1334–42. <https://doi.org/10.3892/ijo.2016.3656> PMID: [27513956](https://doi.org/10.1371/journal.pone.0190653)
 34. Tatsuta T, Hosono M, Takahashi K, Omoto T, Kariya Y, Sugawara S, et al. Sialic acid-binding lectin (leczyme) induces apoptosis to malignant mesothelioma and exerts synergistic antitumor effects with TRAIL. *Int J Oncol.* 2014; 44: 377–84. <https://doi.org/10.3892/ijo.2013.2192> PMID: [24297392](https://doi.org/10.1371/journal.pone.0190653)
 35. Satoh T, Tatsuta T, Sugawara S, Hara A, Hosono M. Synergistic anti-tumor effect of bullfrog sialic acid-binding lectin and pemetrexed in malignant mesothelioma. *Oncotarget.* 2017; 8: 42466–42477. <https://doi.org/10.18632/oncotarget.17198> PMID: [28476017](https://doi.org/10.1371/journal.pone.0190653)
 36. Kawabata S, Chiang C-T, Tsurutani J, Shiga H, Arwood ML, Komiya T, et al. Rapamycin downregulates thymidylate synthase and potentiates the activity of pemetrexed in non-small cell lung cancer. *Oncotarget.* 2014; 5: 1062–70. <https://doi.org/10.18632/oncotarget.1760> PMID: [24658085](https://doi.org/10.1371/journal.pone.0190653)
 37. Tonkinson JL, Worzalla JF, Teng CH, Mendelsohn LG. Cell cycle modulation by a multitargeted antifolate, LY231514, increases the cytotoxicity and antitumor activity of gemcitabine in HT29 colon carcinoma. *Cancer Res.* 1999; 59: 3671–6. Available: <http://www.ncbi.nlm.nih.gov/pubmed/10446980> PMID: [10446980](https://doi.org/10.1371/journal.pone.0190653)
 38. Chou T-C. Drug combination studies and their synergy quantification using the Chou-Talalay method. *Cancer Res.* 2010; 70: 440–6. <https://doi.org/10.1158/0008-5472.CAN-09-1947> PMID: [20068163](https://doi.org/10.1371/journal.pone.0190653)
 39. Mokhtari RB, Homayouni TS, Baluch N, Morgatskaya E, Kumar S, Das B, et al. Combination therapy in combating cancer. *Oncotarget.* 2015; 8: 38022–38043. <https://doi.org/10.18632/oncotarget.16723> PMID: [28410237](https://doi.org/10.1371/journal.pone.0190653)
 40. Røe OD, Szulkin A, Anderssen E, Flatberg A, Sandeck H, Amundsen T, et al. Molecular resistance fingerprint of pemetrexed and platinum in a long-term survivor of mesothelioma. *PLoS One.* 2012; 7: e40521. <https://doi.org/10.1371/journal.pone.0040521> PMID: [22905093](https://doi.org/10.1371/journal.pone.0190653)
 41. Castagneto B, Botta M, Aitini E, Spigno F, Degiovanni D, Alabiso O, et al. Phase II study of pemetrexed in combination with carboplatin in patients with malignant pleural mesothelioma (MPM). *Ann Oncol Off J Eur Soc Med Oncol.* 2008; 19: 370–3. <https://doi.org/10.1093/annonc/mdm501> PMID: [18156144](https://doi.org/10.1371/journal.pone.0190653)
 42. Jänne PA, Simon GR, Langer CJ, Taub RN, Dowlati A, Fidias P, et al. Phase II trial of pemetrexed and gemcitabine in chemotherapy-naïve malignant pleural mesothelioma. *J Clin Oncol.* 2008; 26: 1465–71. <https://doi.org/10.1200/JCO.2007.14.7611> PMID: [18349397](https://doi.org/10.1371/journal.pone.0190653)
 43. Levin PA, Dowell JE. Spotlight on bevacizumab and its potential in the treatment of malignant pleural mesothelioma: the evidence to date. *Onco Targets Ther.* 2017; 10: 2057–2066. <https://doi.org/10.2147/OTT.S113598> PMID: [28435296](https://doi.org/10.1371/journal.pone.0190653)

44. Zalcman G, Mazieres J, Margery J, Greillier L, Audigier-Valette C, Moro-Sibilot D, et al. Bevacizumab for newly diagnosed pleural mesothelioma in the Mesothelioma Avastin Cisplatin Pemetrexed Study (MAPS): a randomised, controlled, open-label, phase 3 trial. *Lancet*. 2016; 387: 1405–1414. [https://doi.org/10.1016/S0140-6736\(15\)01238-6](https://doi.org/10.1016/S0140-6736(15)01238-6) PMID: [26719230](https://pubmed.ncbi.nlm.nih.gov/26719230/)

ナマズ卵レクチンのがん治療への応用を目指した基礎研究

菅原 栄 紀

Application of Lectin from Catfish Eggs to Cancer Therapy: A Fundamental Study

Shigeki Sugawara

Division of Cell Recognition Study, Institute of Molecular Biomembrane and Glycobiology, Tohoku Medical and Pharmaceutical University; 4-4-1 Komatsushima, Aoba-ku, Sendai 981-8558, Japan.

(Received June 3, 2018)

Silurus asotus egg lectin (SAL) is an α -galactoside-binding protein, isolated from the egg of catfish. It belongs to the rhamnose-binding lectin family that binds to Gb3 glycan (Gal α 1-4Gal β 1-4Glc). SAL has resulted in the induction of early apoptosis in the Raji cell line, which is a Burkitt's lymphoma cell line expressing Gb3. The apoptosis was characterized by i) increased externalization of phosphatidylserin *via* multidrug resistance 1 P-glycoprotein (MDR1 P-gp), and ii) reduced cell size through the activation of voltage-gated potassium channel Kv1.3. Although the incorporation of propidium iodide (PI) was observed, SAL did not cause apoptosis in Raji cells. This event may be due to an increased expression of membrane-anchored tumor necrosis factor α (TNF α) and TNF receptor 1 (TNFR1) after the binding of SAL to Gb3. Moreover, SAL arrested the cell cycle at the G_{0/1} phase, thus inhibiting cell proliferation. The suppression of cell proliferation by SAL was likely due to the enhanced expression of p21 caused by the phosphorylation of ERK_{1/2} through the Ras-MEK-ERK_{1/2} pathway. Combination of SAL with anti-cancer drugs was also examined in this study. Interestingly, SAL increased the incorporation of doxorubicin (Dox) into Raji cells, consequently enhancing its cytotoxic effect. Similarly, the cytotoxic effects of vinblastine and irinotecan were also significantly increased in Raji cells treated with SAL. These studies demonstrate that SAL may be applied to cancer therapy.

Key words—*Silurus asotus* egg lectin; globotriaosylceramide; cell cycle arrest; anti-cancer drug

1. はじめに

ヒトにおける糖鎖形成では、数種類の糖が単純に連結した直鎖構造ではなく、多種の結合様式により枝分かれした構造を有することから、糖鎖は情報分子として、多様性という点で核酸やアミノ酸よりも優れていることが示唆されてきた。¹⁾しかし、一方でその多様性が、タンパク質などの機能解明と比較して糖鎖の持つ情報機能の解析を困難にしている一因になっている。糖鎖の機能を理解する試みに、動物から植物まで生物界全体に普遍的に存在し、特定の糖に対して特異的に結合する性質を持つレクチンが利用されてきた。現在まで、受精、発生、免疫、ウイルス感染などのメカニズムの一部は、いずれも糖鎖とそれを認識するタンパク質であるレクチンと

の特異的な相互作用に起因することが明らかにされている。^{2,3)}近年の生命科学の進歩において、レクチンは、生体における情報分子として位置づけられる糖鎖の受け手として注目されている。細胞内で作られるタンパク質のおよそ半分が糖鎖修飾を受けているとされ、糖タンパク質の機能解析を行うにあっても、糖鎖及び糖鎖を認識するレクチンの重要性が再認識されている。

古くから動物レクチンの原材料として卵が重用されており、筆者の研究室ではウシガエル卵より単離・精製したシアル酸結合性レクチン (cSBL) に、正常中皮細胞に対しては効果を示さず、悪性中皮腫細胞選択的に細胞死を誘導する効果があることを見出した。⁴⁻⁶⁾

一方、魚卵には動物レクチンの二大ファミリーであるガレクチンや C-タイプレクチンとは異なるユニークな糖特異性を有するレクチンが多数見つまっている。^{7,8)}このレクチンの特徴は、L-ラムノースや α -ガラクトシドに対して非常に高い親和性を示し、

東北医科薬科大学分子生体膜研究所分子認識学部門
(〒981-8558 仙台市青葉区小松島 4-4-1)

e-mail: ssuga@tohoku-mpu.ac.jp

本総説は、平成 29 年度日本薬学会東北支部奨励賞の受賞を記念して記述したものである。

かつ後述する特徴的な糖認識配列を共有することである。⁹⁾このような性質を持つレクチンを総称して、ラムノース結合性レクチン (rhamnose-binding lectin; RBL) という呼称が現在使用されている。⁹⁻¹⁴⁾ RBL の中には、がん細胞膜に発現しているスフィンゴ糖脂質の一種でセラミドに結合している三糖の非還元末端にガラクトシル α 結合を持つグロボトリアオシルセラミド (Gb3) に結合することにより細胞死を引き起こすものが報告されている。¹⁵⁻¹⁷⁾

本稿では、RBL の一種であるナマズ卵より得られたレクチン (*Silurus asotus* egg lectin; SAL) に着目し、Gb3 を高発現しているパーキットリンパ腫細胞株 Raji に対する作用を検討した結果を中心に詳述するとともに、がん治療への応用の可能性を概説する。

2. 魚卵由来ラムノース結合性レクチンについて

サケ目、ナマズ目、キュウリウオ目、スズキ目及びコイ目に属する多くの魚の未受精卵より RBL が発見されている。^{10-14,18-22)} これらのタンパク質のアミノ酸配列を比較すると類似した約 95 アミノ酸残基よりなるドメインが 2 あるいは 3 つ並んだタンデムリピート構造を持つという特徴を持つことが明らかとなっている。このドメインには、RBL モチーフと呼ばれている、よく保存された配列が存在し、N-末端部に ANYGR 配列、C 末端部に DPC-KYL 配列がみられ、このドメインが RBL における糖結合ドメイン (RBL-carbohydrate recognition domain; RBL-CRD) であると報告されている。¹¹⁾ Nitta らは、一次構造の類似性、ヒト赤血球凝集活性及びラクトースによる阻害の有無から、RBL ファミリーを 5 つのタイプに分類し、²³⁾ その後、Ogawa らにより、タンパク質配列データベースを利用した包括的な解析がなされ、RBL ファミリーが有する RBL-CRD を進化的相同性の観点から 6 つに分類し (RBL-CRD1-6)、この RBL-CRD の組み合わせから 13 のサブタイプに分類された。²⁴⁾ SAL は、RBL-CRD が 3 つ並んだタイプ Ia (CRD: 5-3-3) に分類される。これまで、魚卵からは、1 つの RBL-CRD よりなる RBL の報告はなされていないが、ウニ卵からは、タンデムリピートではなく二量体としての RBL が見つかっている。また、魚卵より単離・精製されたという報告ではないが、2014 年に Thongda らにより、RNA-sequencing (RNA-seq) データ

を利用し構築されたアメリカナマズ (*Ictalurus punctatus*) データベースから、このナマズには 6 つの異なる推定アミノ酸配列を有する RBL (IpRBL1a, 1b, 1c, 3a, 3b, 5a) が存在することを示し、このうち IpRBL5a は、1 つの RBL-CRD からなるものであることが報告された。²⁵⁾

3. SAL によるホスファチジルセリン (phosphatidylserine; PS) の細胞膜外層側への移行及び細胞縮小に関する分子機構

細胞毒性を有するガラクトース結合性レクチンである ricin, abrin 及び misletoe (ヤドリギ) レクチンは、細胞に PS の外層側への移行などアポトーシス様の変化をもたらし、最終的に細胞死を引き起こすことが知られている。²⁶⁻²⁸⁾ 一方、2 量体化したガラクトシン-1 (dGal-1) は、PS の外層側への移行を誘導するものの、アポトーシスを誘導しない。²⁹⁾ これらのレクチンによる PS の細胞膜外層側への移動に係わる分子機構はまだ明らかにされておらず、それぞれ異なる機構により引き起こされるものと考えられている。また、RNA *N*-glycosidase 活性を持つ A サブユニット及びレクチンとして機能を有する B サブユニットから構成される AB-毒素の代表例である志賀毒素 (Shiga toxin; Stx) は、細胞膜上に発現している Gb3 に結合することにより、アポトーシスを誘導することが知られている。³⁰⁾ SAL も Gb3 に結合することから [Fig. 1 (A)], Gb3 発現細胞に対して細胞死を誘導できるのではないかと考えたが、実験の結果、Raji 細胞において SAL 処理による細胞死は認められなかった。しかし、一般的にアポトーシス初期に起こることが知られている PS の細胞膜外層側への移行 (アネキシン V の結合で評価) 及び細胞縮小が認められたため [Figs. 1 (B) and (C)], これらの現象がどのような過程を経て引き起こされるのか、またなぜ細胞死が誘導されないのかという点について検討した。

PS の細胞膜外層側への移行に関する分子を同



菅原栄紀

2000 年東北薬科大学薬学部卒業。2002 年東北大学大学院薬学研究所修士課程修了。2005 年東北薬科大学大学院薬学研究所博士課程修了。同年同大学助手。2007 年同助教。2017 年東北医科薬科大学薬学部講師、現在に至る。研究テーマと抱負：魚卵レクチンのがん治療への応用を目指した研究。

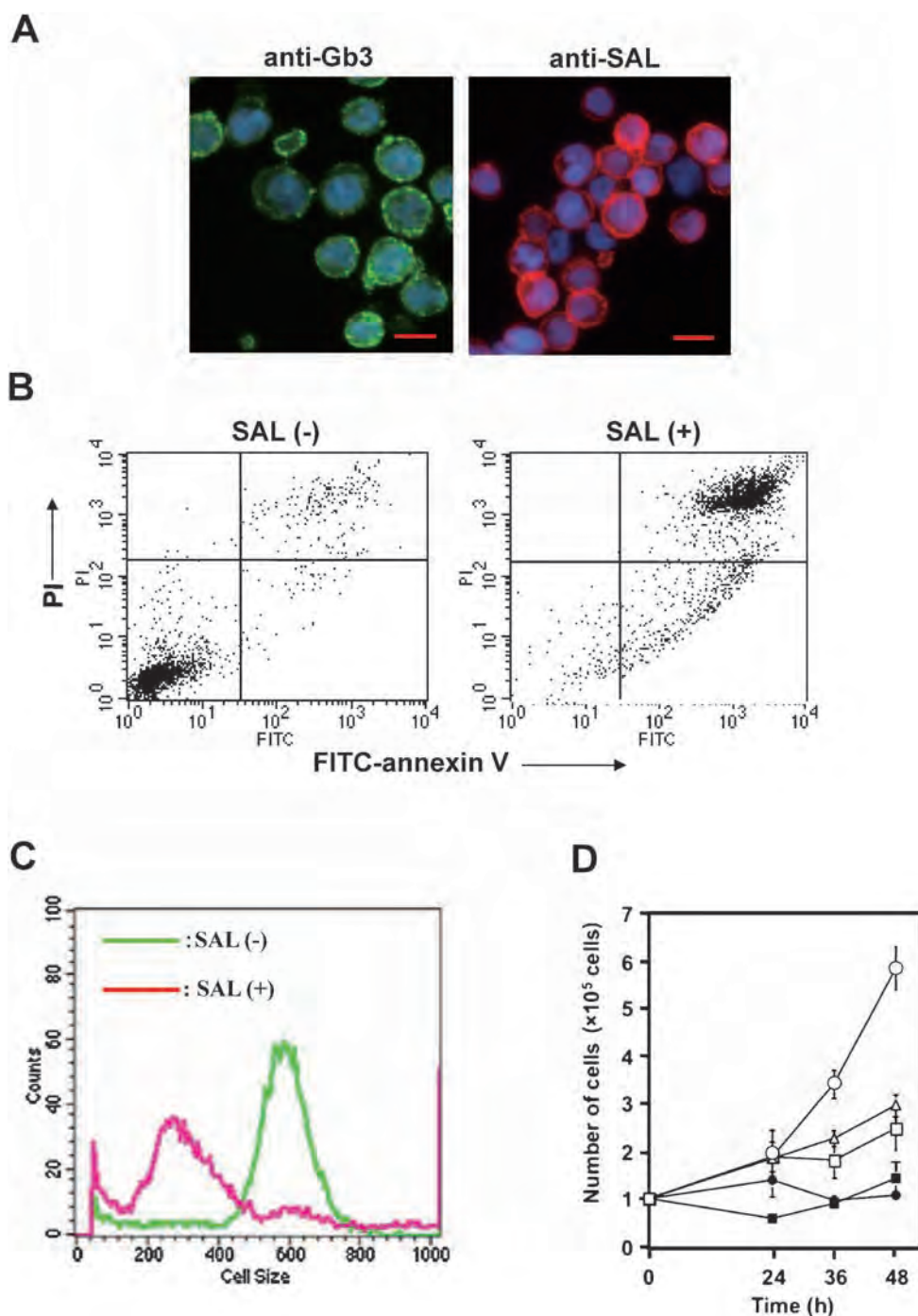


Fig. 1. Effect of SAL on Raji Cells

(A) Expression of Gb3 in Raji cells (green) and binding of SAL (red). (B) Externalization of phosphatidylserine (PS) and incorporation of propidium iodide (PI) in Raji cells. (C) Flow cytometry based data to show shrinkage of Raji cells induced by SAL. (D) Reduction of proliferation of Raji cells by SAL as measured by trypan blue dye exclusion assay. Control (○); 1 μg/mL (△); 5 μg/mL (□); 50 μg/mL (■); 100 μg/mL (●).

定するため、細胞膜脂質二重層を維持あるいは制御する分子として知られている phospholipid scramblase (PLS), aminophospholipid translocase (APTL), ATP-binding cassette (ABC) transporter に属する MDR1 P-gp 及び multidrug resistance protein (MRP) 1 に着目して検討を行った。³¹⁻³⁴⁾ Raji

における PLS の発現レベルは非常に低く phospholipid 1-palmitoyl-1-[6-(7-nitro-2-1,3-benzoxadiazol-4-yl) amino] dodecanoyl]-PC (NBD-PC) の取り込みがほとんど認められなかったため、Raji における PS の細胞膜外層側への移行に、PLS が関与している可能性は低いと考えた。³⁵⁾ 一方、Raji 細胞では、

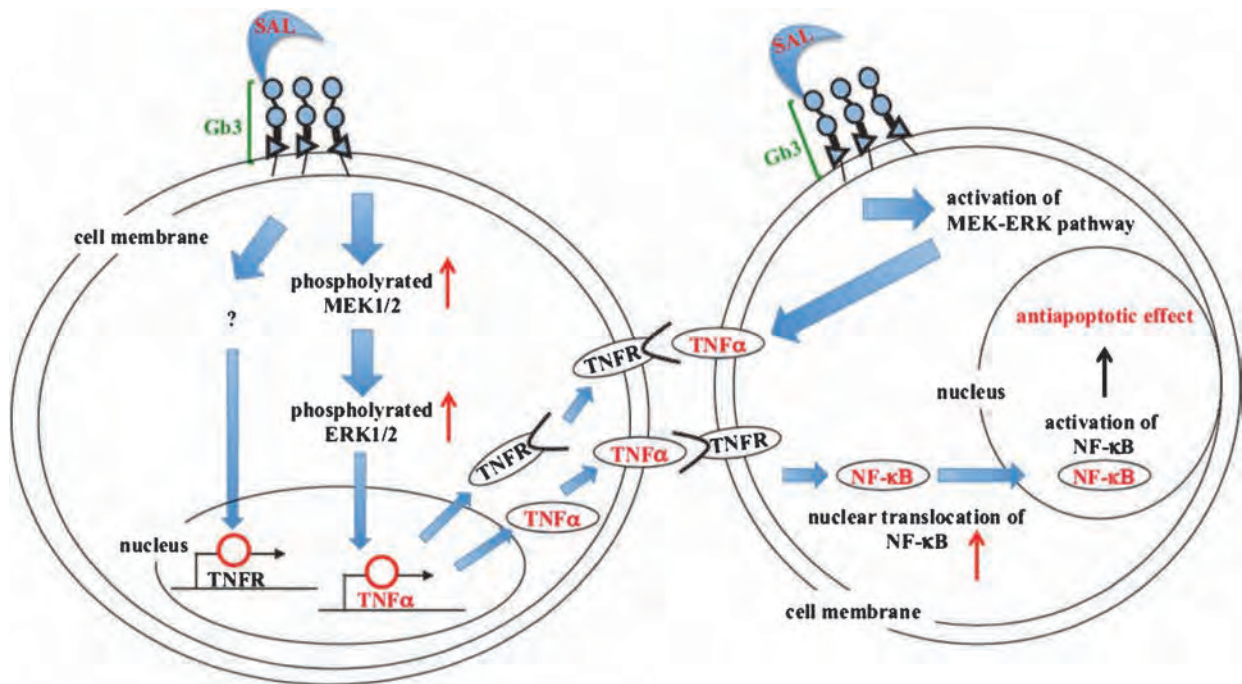


Fig. 2. An Insight into the Molecular Mechanism of Antiapoptotic Effect Caused by SAL

Treatment of Gb3 expressing Raji cells with SAL causes binding of TNF α to TNFR1, resulting in translocation of NF- κ B, thus inducing an anti-apoptotic effect.

PS やホスファチジルエタノールアミン (PE) の細胞膜外層から内層側への移行に参与している APTL の発現が非常に高いことが報告されていたが、こちらも SAL 処理 Raji 細胞における APTL 活性の減少は観察されなかった。以上のことから、PLS と APTL は SAL が誘導する PS の移行には関与していないと考えられた。次に、MRP1 及び MDR1 P-gp の関与について検討した。Raji 細胞においては、MRP1 の発現が高く、反対に MDR1 P-gp 発現は非常に低いものであった。次に、MDR1 P-gp 阻害剤であるシクロスポリン A (cyclosporin A; CsA) 及び MRP1 阻害剤である MRK16 を用いた実験を行った結果、SAL 処理により PS の細胞膜外層側への移行が CsA でのみ阻害された。これらの結果から、SAL は Raji 細胞膜上に発現している Gb3 に結合し、選択的に MDR1 P-gp を活性化していることが示唆された。³⁵⁾

細胞膜には、膜内外の電位差の変化によって開閉する電位依存型カリウムチャンネル (voltage-gated potassium channel; Kv), カルシウムイオン又は他のシグナル分子により開閉するカルシウム依存型カリウムチャンネル及び G タンパク質共役型の内向き整流カリウムチャンネルが発現している。このような

カリウムチャンネルは、カリウムを選択的に細胞内に流入あるいは排出することにより細胞の大きさを常に一定に保つように働いている。³⁶⁾ また、アポトーシスによる細胞縮小は、カリウムチャンネルからのカリウムイオンの流出によって起こることも知られている。³⁷⁾ SAL 処理した Raji 細胞でみられる細胞縮小も同様な機構により起こるのかを検討した結果、SAL の処理時間及び濃度依存的に細胞内カリウムイオンの減少が認められた。一方、Gb3 を発現していない K562 細胞ではこのような現象はみられないことから、これらの現象は SAL の Gb3 への結合が引き金となって引き起こされていることを示している。したがって、Gb3 に SAL が結合することによりこのチャンネルが活性化し、細胞外へのカリウムイオンの放出と同時に水分子が流出するため、腫瘍細胞の縮小が引き起こされるというストーリーが推測される。³⁸⁾

4. SAL は tumor necrosis factor (TNF) α 及び TNF receptor (TNFR) の発現を増加させる

SAL は、Raji 細胞をアポトーシス初期状態に変化させるが、結果的に細胞死を引き起こさない。なぜ細胞死を誘導しないのか、その原因については不明であった。Watanabe らは魚由来の培養細胞であ

る RTM5 (繊維芽細胞) 及び RTG-2 (腹腔内マクロファージ細胞) に対して CSL は、サイトカインの一種である $TNF\alpha$ と interleukin (IL) -8 の発現を誘導することを報告し,³⁹⁾ 筆者のデータからも SAL 処理 Raji 細胞において $TNF\alpha$ が上昇するという結果が得られている。 $TNF\alpha$ には membrane form (膜結合型) と soluble form (可溶型) が存在することが知られているが、SAL は膜結合型 $TNF\alpha$ の発現を上昇させる効果を示す。¹⁶⁾ 後述にするように、SAL は、ERK シグナル伝達機構を活性化するため、膜結合型 $TNF\alpha$ の発現上昇もこの機構により引き起こされている可能性を考えている。また $TNF\alpha$ は、細胞膜上に発現している TNFR に結合することにより細胞内にシグナル伝えるが、SAL は、 $TNF\alpha$ の発現上昇だけではなく、その受容体である TNFR1 及び TNFR2 の発現も上昇させる。 $TNF\alpha$ が TNFR に結合すると nuclear factor- κ B (NF- κ B) が活性型に変化し、この NF- κ B が核内に移行することにより様々な遺伝子の発現が誘導されることから、SAL 処理により活性型 NF- κ B が核内に核移行することが明らかとなった。¹⁶⁾ Qin らにより、 $TNF\alpha$ が TNFR1 に結合することにより抗アポトーシス作用を誘導することが報告されている。⁴⁰⁾ このことから、SAL 処理により細胞死が誘導されないのは、膜結合型 $TNF\alpha$ 及び TNFR1 の発現上昇によりこれらの分子を介して細胞同士が結合することによる NF- κ B の抗アポトーシス効果が原因ではないかと推察している (Fig. 2)。現在、NF- κ B の核移行が抗アポトーシスに関与しているのか否かを直接的に証明する実験に取り組んでいる。

5. SAL はバーキットリンパ腫細胞の増殖を抑制する

上記のように、Raji 細胞を SAL 処理しても細胞死は起きない。そこで、SAL の細胞増殖におよぼす影響を検討したところ、100 μ g/mL の SAL 処理で細胞増殖が止まることが分かった [Fig. 1 (D)]。さらに、この現象は、ハプテン糖により Gb3 に結合した SAL を解離させると解除されることから、SAL の糖結合能が直接関与していると考えられる。そこで、この細胞増殖抑制が細胞周期の停止によるのか否かを検討したところ、SAL は細胞周期を G1 期で停止させることにより細胞増殖を抑制している可能性が示された。細胞周期の G1 期から S

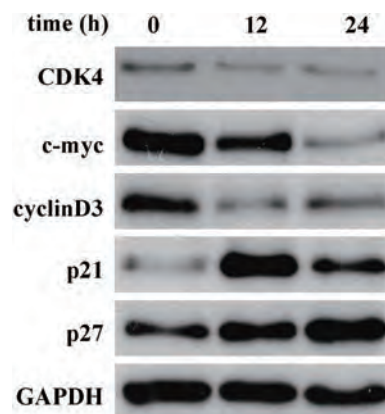


Fig. 3. SAL Alters the Expression of Proteins CDK4, c-MYC, cyclin D3, p21, and p27

Cells (1×10^6) were treated with SAL (100 μ g/mL) at 37°C for 0, 12, or 24 h. Whole cell extract was subjected to western blotting using antibodies against CDK4, c-MYC, cyclin D3, p21, and p27.

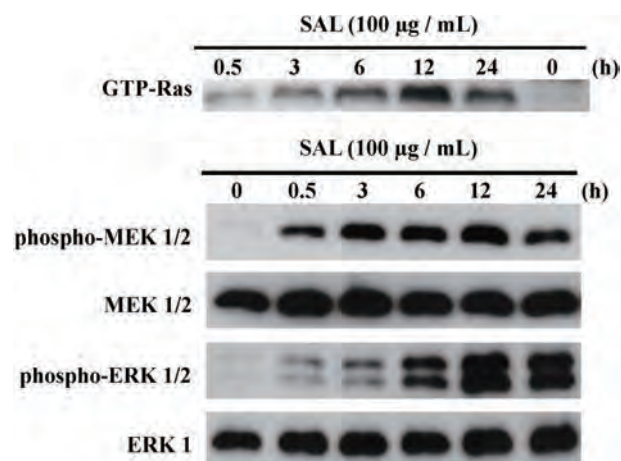


Fig. 4. SAL Causes Activation of Ras-MEK-ERK Pathway

Cells (1×10^6) were treated with SAL (100 μ g/mL) at 37°C for various durations from 0 to 24 h. Whole cell extracts were subjected to western blotting using antibodies directed against Ras, pMEK_{1/2}, MEK_{1/2}, pERK_{1/2}, and ERK₁.

期への移行には、cyclin-dependent kinase (CDK) 4, c-myc, cyclin D3, p21 及び p27 が関与していることが知られている。SAL 処理によるこれらのタンパク質発現量の変化を検討した結果、CDK4, c-myc, 及び cyclin D3 の発現が減少し、反対に p21 と p27 は SAL 処理により発現が上昇することが明らかとなった (Fig. 3).⁴¹⁾ 次に、ERK 経路に着目してこれらの分子の制御機構について検討したところ、SAL 処理により Ras-MEK-ERK 経路が活性化するという結果が得られた (Fig. 4)。この結果を単純に解釈すると細胞を増殖させる方向に働くことになり、SAL が細胞増殖を抑制する、という事実と相反することからメカニズム解明を悩ませた。し

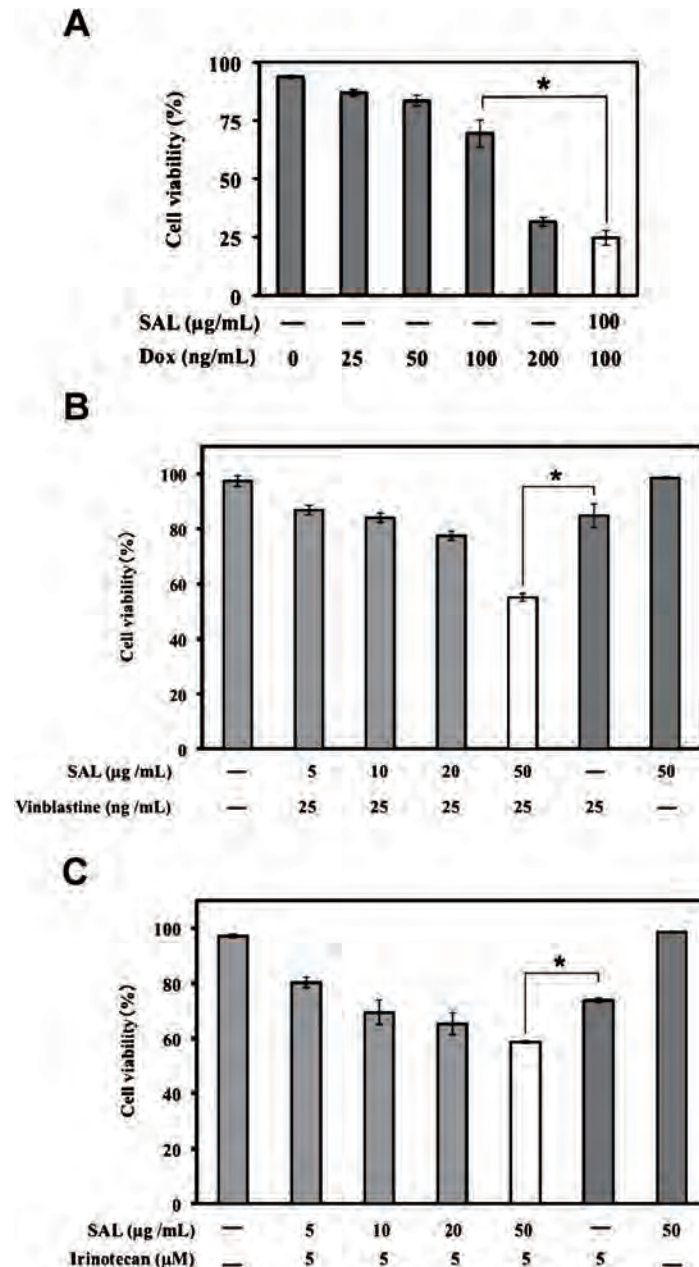


Fig. 5. Cytotoxic Effect of Anti-cancer Drugs in Raji Cells Pre-treated with SAL

(A) Cells (5×10^4) were treated with Dox (25, 50, 100, 200 ng/mL) at 37°C for 60 h. Raji cells pre-treated with 100 $\mu\text{g/mL}$ SAL at 37°C for 24 h, were subjected to treatment with Dox (100 ng/mL) at 37°C for 60 h. (B) Raji cells pre-treated with SAL (5, 10, 20 and 50 $\mu\text{g/mL}$) at 37°C for 24 h were treated with vinblastine (25 ng/mL) at 37°C for 48 h. (C) Raji cells pre-treated with SAL (5, 10, 20 and 50 $\mu\text{g/mL}$) at 37°C for 24 h were treated with irinotecan (5 μM) at 37°C for 48 h. Cell viability was measured by trypan blue dye exclusion assay. Each value represents the mean \pm S.E. for three independent experiments. * $p < 0.05$ versus doxorubicin, vinblastine, or irinotecan-treated cells.

かし、2011年にMoonらにより、JNK阻害剤SP600125で処理された細胞では、ERKのリン酸化レベル上昇に伴い、転写因子であるSp1が活性化することにより、p21の発現が上昇し細胞増殖を抑制するという報告がなされた。⁴²⁾ SALもこれと同様の作用機序を持つとすれば、一連の結果を矛盾なく説明できるかもしれない。現在、この仮説を証明するエビデンスを得るための実験が進行中である。

6. SALと抗がん剤との併用効果

ヨウ化プロピジウム(propidium iodide; PI)は、細胞膜が健全な生細胞には取り込まれず、細胞死により細胞膜が崩壊した細胞に取り込まれることが知られている。先にも述べたように、SALは細胞死を誘導しない。しかし、理由は分からないが、細胞膜不透過物質であるPIがSAL処理細胞には促進的に取り込まれるという興味深い現象を見出した

[Fig. 1 (B)]. この現象をがん治療に応用できなかいと考え、PIを抗がん剤に置き換えてSALと抗がん剤との併用効果について検討した。

まずはじめに、ドキソルビシン (doxorubicin; Dox) との併用効果を検討した。Doxの持つ自家蛍光を利用して細胞内の取り込み量を測定した結果、SAL処理により増加していることが示された。⁴³⁾ Doxは、処理濃度依存的にRaji細胞の生存率を低下させるが、SALを前処理することにより生存率がさらに低下し、100 ng/mLのDoxとSALの併用により、200 ng/mLのDox処理と同程度まで生存率を低下させることが示された [Fig. 5 (A)]. さらに、他の抗がん剤との併用も検討したところ、25 ng/mLビンブラスチン (vinblastine; Vin) 単独処理時のRaji細胞の生存率は85%であったが、SALを併用することにより生存率が55%まで低下した [Fig. 5 (B)]. イリノテカン (irinotecan; Iri) も同様にSAL併用時における生存率の変化を調べたところ、5 μ M Iri単独処理では生存率が74%であったが、SALとの併用により生存率が59%に低下した [Fig. 5 (C)].⁴⁴⁾ これらの結果から、抗がん剤をSALと併用することにより薬剤の濃度を下げても高濃度と同じ効果を得られることが分かった。抗がん剤治療で最も問題となるのは副作用の発現であるが、SALは、がん細胞の薬剤感受性を高める効果を発揮することでこの問題を解決できる可能性を有している。また、パーキットリンパ腫のみならずGb3を発現しているがん細胞であれば、SALは併用する抗がん剤の用量低減に貢献できる可能性を有するものと考えている。

7. おわりに

RBLのがん細胞に対する作用は、前述したCSL3とSALでは異なり、前者はcytotoxicに、また後者はcytostaticに働く。この要因が、レクチン分子のCRD組成による(それぞれ2個及び3個)か否かを証明するエビデンスはまだ得られていないが、CSL3と同様に2個のCRDからなるOLLは、SALと異なりcytotoxicな作用を示すことを確認している。表面プラズモン共鳴スペクトル (surface plasmon resonance; SPR) 解析により、SALとOLLの糖結合性を速度論的に比較したところ、Gal α 結合及びGal β 結合に対する親和性は、SALがGal α \gg Gal β である一方、OLLはGal α \geq Gal β

で、若干の相違が認められた。この傾向は、レクチンのRaji細胞への結合性が、SALの場合抗Gb3抗体の前処理ではほぼ完全に阻害されるのに対し、OLLでは同じ処理でも結合が一部残存するという結果にもあらわれている。すなわち、Gb3のみを介するSALのcytostaticな作用は、同時にGal β 結合を介する他の糖鎖との相互作用の追加によりcytotoxicな方向に舵を切るようになるのではないか。また、Gb3発現のみられないK562細胞にGb3を強制発現させると、SALの結合は観察されるものの、Raji細胞でみられるような細胞縮小や増殖抑制は起こらない。そもそもGb3は膜貫通分子ではないので、SALのシグナルを細胞内に伝達するためのアダプター分子の存在が推測されたことから、現在Gb3の近傍に存在し、かつRBLの結合によりシグナルを仲介する分子を、enzyme-mediated activation of radical sources (EMARS) 法などを駆使して探索中である。⁴⁵⁾ さらに最近、がん細胞の種類によりGb3の分子組成(主にセラミド部分を構成しているアシル鎖の違い)が異なり、それに伴ってSALの効果も変化するという興味ある知見も得ている。

抗腫瘍戦略にレクチンを参入させる新しい試みが最近報告された。2017年に筑波大学と産業技術総合研究所のグループが*Burkholderia cenocepacia*由来のBC2LC-Nレクチンに緑膿菌外毒素であるPE38を融合させたlectin drug conjugate (LDC)を開発し、膵がんを標的とした抗腫瘍薬創製の可能性を示した。このLDCの膵がん細胞株に対する効果は、既存の抗体-薬剤融合体 (antibody-drug conjugate; ADC) よりも1000倍高く、かつマウスを用いた*in vivo*の実験でもその効果が確認された。⁴⁶⁾ これはレクチンが標的細胞を捕捉する能力において抗体を凌駕している点で、従来の認識を覆す重要な知見である。またこの報告は、レクチンのがん治療への応用に道を拓くものであり、今後LDCの応用研究が加速されていくことになろう。一方で、筆者のナマズ卵レクチンによる、「がん細胞の薬剤感受性を高め、副作用を軽減する」戦略も、LDCとはコンセプトが異なるが、これまでにないユニークなものであると考えている。細胞膜ラフト画分におけるGb3の機能解明あるいは未同定の仲介タンパク質の解析など課題は山積しているが、「レクチンに

よるがん治療」実現に向けて研究を進めていきたい。

謝辞 本研究は東北医科薬科大学薬学部分子認識学教室 細野雅祐教授並びに仁田一雄名誉教授の指導により行われた研究成果であります。この場を借りて御礼申し上げます。本総説中で述べた当研究室関連の研究の一部は、文部科学省私立大学戦略的研究基盤形成支援事業の助成により行われたものです。

利益相反 開示すべき利益相反はない。

REFERENCES

- 1) Varki A., "Essential of Glycobiology," ed. by Varki A., Cummings R., Esko J., Freeze H., Hart G., Marth J., Cold Spring Harbor Laboratory Press, Cold Spring Harbor, 1999.
- 2) Dodson K. W., Pinkner J. S., Rose T., Magnusson G., Hultgren S. J., Waksman G., *Cell*, **105**, 733–743 (2001).
- 3) Karlson K. A., *Annu. Rev. Biochem.*, **58**, 309–350 (1989).
- 4) Krajhanzl A., *Adv. Lectin Res.*, **3**, 83–131 (1990).
- 5) Satoh T., Tatsuta T., Sugawara S., Hara A., Hosono M., *Oncotarget*, **8**, 42466–42477 (2017).
- 6) Tatsuta T., Satoh T., Sugawara S., Hara A., Hosono M., *PLoS One*, **13**, e0190653 (2018).
- 7) Barondes S. H., Castronovo V., Cooper D. N. W., Cummings R. D., Drickamer K., Feizi T., Gitt M. A., Hirabayashi J., Hughes C., Kasai K., Leffler H., Liu F. T., Lotan R., Mercurio A. M., Monsigny M., Pillai S., Poirer F., Raz A., Rigby P. W. J., Rini J. M., Wong J. L., *Cell*, **76**, 597–598 (1994).
- 8) Barondes S. H., Cooper D. N. W., Gitt M. A., Leffler H., *J. Biol. Chem.*, **269**, 20807–20810 (1994).
- 9) Hosono M., Kawauchi H., Nitta K., Takayanagi Y., Shiokawa H., Mineki R., Murayama K., *Biol. Pharm. Bull.*, **16**, 239–243 (1993).
- 10) Hosono M., Ishikawa K., Mineki R., Murayama K., Numata C., Ogawa Y., Takayanagi Y., Nitta K., *Biochem. Biophys. Acta*, **1472**, 668–675 (1999).
- 11) Hosono M., Kawauchi H., Nitta K., Takayanagi Y., Shiokawa H., Mineki R., Murayama K., *Biol. Pharm. Bull.*, **16**, 1–5 (1993).
- 12) Hosono M., Matsuda K., Kawauchi H., Takayanagi Y., Shiokawa H., Mineki R., Murayama K., Nitta K., *Biomed. Res.*, **13**, 443–449 (1992).
- 13) Tateno H., Saneyoshi A., Ogawa T., Muramoto K., Kamiya H., Saneyoshi M., *J. Biol. Chem.*, **273**, 19190–19197 (1998).
- 14) Shiina N., Tateno H., Ogawa T., Muramoto K., Saneyoshi M., Kamiya H., *Fish. Sci.*, **68**, 1352–1366 (2002).
- 15) Hosono M., Sugawara S., Matsuda A., Tatsuta T., Koide Y., Hasan I., Ozeki Y., Nitta K., *Fish. Physiol. Biochem.*, **40**, 1559–1572 (2014).
- 16) Shirai T., Watanabe Y., Lee M., Ogawa T., Muramoto K., *J. Mol. Biol.*, **391**, 390–403 (2009).
- 17) Hatakeyama T., Ichise A., Unno H., Goda S., Oda T., Tateno H., Hirabayashi J., Sakai H., Nakagawa H., *Protein Sci.*, **26**, 1574–1583 (2017).
- 18) Tateno H., Ogawa T., Muramoto K., Kamiya H., Saneyoshi M., *Biosci. Biotechnol. Biochem.*, **66**, 1356–1365 (2002).
- 19) Terada T., Watanabe Y., Tateno H., Naganuma T., Ogawa T., Muramoto K., Kamiya H., *Biochem. Biophys. Acta*, **1770**, 617–629 (2007).
- 20) Watanabe Y., Shiina N., Shiozaki F., Yokoyama H., Kominami J., Nakamura-Tsuruta S., Hirabayashi J., Sugahara K., Kamiya H., Matsubara H., Ogawa T., Muramoto K., *Dev. Comp. Immunol.*, **32**, 487–499 (2008).
- 21) Jimbo M., Usui R., Sakai R., Muramoto K., Kamiya H., *Comp. Biochem. Physiol.*, **B147**, 164–171 (2007).
- 22) Yu H., Murata K., Hedrick J. L., Almaraz R. T., Xiang F., Franz A. H., *Arch. Biochem. Biophys.*, **463**, 1–11 (2007).
- 23) Nitta K., Kawano T., Sugawara S., Hosono M., *Yakugaku Zasshi*, **127**, 553–561 (2007).
- 24) Ogawa T., Watanabe M., Naganuma T., Muramoto K., *J. Amino Acid*, 838914 (2011).
- 25) Thongda W., Li C., Luo Y., Beck B. H., Peatman E., *Dev. Comp. Immunol.*, **44**, 320–331

- (2014).
- 26) Kageyama A., Kusano I., Tamura T., Oda T., Muramatsu T., *Biosci. Biotechnol. Biochem.*, **66**, 835–839 (2000).
- 27) Ohba H., Moriwaki S., Bakalova R., Yasuda S., Yamasaki N., *Toxicol. Appl. Pharmacol.*, **195**, 182–193 (2004).
- 28) Hajtó T., Berki T., Boldizsár F., Németh P., *Immunol. Lett.*, **86**, 23–27 (2003).
- 29) Dias-Baruffi M., Zhu H., Cho M., Karmakar S., McEver R. P., Cummings R. D., *J. Biol. Chem.*, **278**, 41282–41293 (2003).
- 30) Katagiri Y. U., Mori T., Nakajima H., Katagiri C., Taguchi T., Takeda T., Kiyokawa N., Fujimoto J., *J. Biol. Chem.*, **274**, 35278–35282 (1999).
- 31) Fadeel B., Gleiss B., Högstrand K., Chandra J., Wiedmer T., Sims P. J., Henter J. I., Orrenius S., Samali A., *Biochem. Biophys. Res. Commun.*, **266**, 504–511 (1999).
- 32) Bratton D. L., Fadok V. A., Richter D. A., Kailey J. M., Guthrie L. A., Henson P. M., *J. Biol. Chem.*, **272**, 26159–26165 (1997).
- 33) van Helvoort A., Smith A. J., Sprong H., Fritzsche I., Schinkel A. H., Borst P., van Meer G., *Cell*, **87**, 507–517 (1996).
- 34) Borst P., Zelcer N., van Helvoort A., *Biochim. Biophys. Acta*, **1486**, 128–144 (2000).
- 35) Sugawara S., Hosono M., Ogawa Y., Takayanagi M., Nitta K., *Biol. Pharm. Bull.*, **28**, 434–441 (2005).
- 36) Okada Y., Maeno E., Shimizu T., Dezaki K., Wang J., Morishima S., *J. Physiol.*, **532**, 3–16 (2001).
- 37) Bortner C. D., Cidlowski J. A., *Biochem. Pharmacol.*, **56**, 1549–1559 (1998).
- 38) Kawano T., Sugawara S., Hosono M., Tatsuta T., Ogawa Y., Fujimura T., Taka H., Murayama K., Nitta K., *Biol. Pharm. Bull.*, **32**, 345–353 (2009).
- 39) Watanabe Y., Tateno H., Nakamura-Tsuruta S., Kominami J., Hirabayashi J., Nakamura O., Watanabe T., Kamiya H., Naganuma T., Ogawa T., Naudé R. J., Muramoto K., *Dev. Comp. Immunol.*, **33**, 187–197 (2009).
- 40) Qin J., Shang L., Ping A. S., Li J., Li X. J., Yu H., Magdalou J., Chen L. B., Wang H., *Arthritis. Res. Ther.*, **14**, R242 (2012).
- 41) Sugawara S., Im C., Kawano T., Tatsuta T., Koide Y., Yamamoto D., Ozeki Y., Nitta K., Hosono M., *Glycoconj. J.*, **34**, 127–138 (2017).
- 42) Moon D. O., Choi Y. H., Kim G. Y., *Cell. Mol. Life. Sci.*, **68**, 3249–3260 (2011).
- 43) Sugawara S., Sasaki S., Ogawa Y., Hosono M., Nitta K., *Yakugaku Zasshi*, **125**, 327–334 (2005).
- 44) Sugawara S., Araya K., Hosono M., Tatsuta T., Nitta K., *J. Tohoku Pharm. Univ.*, **58**, 41–46 (2011).
- 45) Kotani N., Gu J., Isaji T., Udaka K., Taniguchi N., Honke K., *Proc. Natl. Acad. Sci. USA*, **105**, 7405–7409 (2008).
- 46) Shimomura O., Oda T., Tateno H., Ozawa Y., Kimura S., Sakashita S., Noguchi M., Hirabayashi J., Asashima M., Ohkohchi N., *Mol. Cancer Ther.*, **17**, 183–195 (2018).

原 著

Gb3 検出に利用する抗 Gb3 抗体 (1A4) の有用性の検討

菅原 栄紀,^{a*} 鷹薮 祥子,^a 本田 捷太,^a 立田 岳生,^a 伊藤 淳,^b
佐藤 信,^b 大山 力,^c 細野 雅祐^a

Examination of the Usability of Anti-Gb3 Antibody (1A4) for Detection of Gb3

Shigeki SUGAWARA,^{a*} Shoko TAKANOHASHI,^a Shota HONDA,^a Takeo TATSUTA,^a Jun ITO,^b
Makoto SATO,^b Chikara OHYAMA,^c and Masahiro HOSONO^a

^aDivision of Cell Recognition Study, Institute of Molecular Biomembrane and Glycobiology, Faculty of Pharmaceutical Sciences, Tohoku medical and Pharmaceutical University; ^bDepartment of Urology, Faculty of Medicine, Tohoku medical and Pharmaceutical University; ^cDepartment of Urology, Hirosaki University Graduate School of Medicine.

(Received November 20, 2018)

Globotriaosylceramide (Gb3) is the most important cell surface ligand of the rhamnose-binding lectins such as *Sirulus asotus* lectin (SAL). SAL recognizes and binds to Gb3 expressing tumor cells such as Burkitts' lymphoma Raji cells and induces them to the G0/G1 phase growth arrest. Thus, a fine detecting probe, or monoclonal antibody (mAb) of Gb3, is important for operating immunocytochemical analyses of SAL. In this experiments, we established simple and convenience preparation method to obtain the mAb, 1A4 (isotype: IgM), from the culture medium of the provided hybridoma cell line (originally from Ishigami F., and Hakomori S., method unpublished), and compared its reactivity and stability with BGR23 (isotype: IgG) which is commonly used and commercially available mAb against Gb3. mAb 1A4 was simply purified by using Rapid SPiN L column within an hour and showed higher reactivity than BGR23 on the flow cytometric analyses against Gb3 expressing tumor cells. The optimum concentration of 1A4 was 0.6 $\mu\text{g}/\text{mL}$ for the adequate detection while four and ten times higher concentrations were needed to obtain equal reactivity on Raji and TOS-1 cells, respectively, by using BGR23. Although purified 1A4 was stable in the 0.1 M Tris-Glycine after one-month storage at 4°C or -80°C, its reactivity was slightly decreased when the buffer was changed to 10 mM PBS. These results suggest that mAb 1A4 possesses relatively higher binding capacity to cell surface Gb3 than BGR23 and highly concentrated buffer could also suitable for its storage condition.

Key words — globotriaosylceramide; monoclonal antibody; flowcytometry

緒 論

分子生物学研究に用いられている免疫組織染色法, 免疫沈降法, ウエスタンブロッティング法, フローサイトメトリー法などにおいて, 必須の材料は「抗体」である. これらの研究に利用される抗体には, 様々なエピトープを認識する抗体が含まれているポリクローナル抗体と, 1つのエピトープのみを認識するモノクローナル抗体 (mAb) が存在し, 研究の目的に応じて使い分けられている. mAb の作製方法は, 1975年にケーラーおよびミルステインにより確立され (1984年「免疫制御

機構に関する確立とモノクローナル抗体の作製法の開発」によりノーベル医学・生理学賞を受賞),¹⁾ この方法により, mAbの大量作製が可能になった. がん細胞膜表面の分子組成は, 正常細胞と比べ異なる点が多く, 特定の分子の消長に注目すれば, それはがん特異抗原として理解される. mAbという優れたプローブの出現は, 腫瘍病理の分野における腫瘍マーカー研究を急速に発展させることに大きく貢献した.²⁾ 診断への応用のみならず, 1990年代後半からは, 非ホジキンリンパ腫治療薬であるリツキサン (リツキシマブ, 抗CD20抗体) に代表されるように, がんの治療に利用可能なmAbが開発され,³⁾ 現在もその特異性の観点からがんに対して治療効果の高い抗体医薬品の開発が進行している. 本年 (2018年) のノーベル医学・生理学賞は, 活性化したT細胞の表面に発現する

^a東北医科薬科大学薬学部分子生体膜研究所分子認識学教室, ^b東北医科薬科大学医学部泌尿器科学教室, ^c弘前大学大学院医学研究科泌尿器科学講座

*e-mail: ssuga@tohoku-mpu.ac.jp

受容体である Programmed cell death 1 (PD-1) を標的とした抗体医薬であるニボルマブ (商品名オプジーボ) を開発した, 京都大学の本庶佑博士らに授与されたことは記憶に新しい。⁴⁾

細胞の表面は, 稠密な複合糖質に覆われている (糖衣) ため, 細胞表面抗原は糖鎖に由来するものが多く, 特に腫瘍関連抗原としての膜糖脂質に対する mAb は豊富に準備されている。しかし, 糖脂質はそれ自身低分子であることに加え, 分子構造として疎水性尾部は膜に埋め込まれ, また, 細胞外に表出する糖鎖部分はそれほど長く (大きく) ないため, いわゆる “潜在性” が抗体作製の際に問題となる。⁵⁾ 例えば, ガンクリオシド GM3 に対する mAb である M2950 は, 細胞表面の GM3 の密度によって反応性が変わることが知られている。^{6,7)} また, 極性頭部 (糖鎖部分) の配向や他の糖脂質との相互作用によっても抗体の反応性は変化する。⁸⁾ 当研究室では, 中性糖脂質であるグロボトリアオシルセラミド (Gb3, Gal α 1-4Gal β 1-4Glc-Cer) に結合するナマズ卵レクチン (*Silurus asotus* lectin, SAL) に関する研究を行っており, これまでに, Gb3 を高発現しているパーキットリンバ腫細胞株 Raji に対し, SAL が細胞縮小, ヨウ化プロピジウム (PI) の取り込み増加, ホスファチジルセリン (PS) の細胞膜外層側への移行および細胞増殖抑制を引き起こすことを報告している。^{9,11)} Gb3 の検出には, 一般に特異抗体として市販されているマウス mAb (Isotype: IgG, Clone: BGR23) およびラット mAb (Isotype: IgM, Clone: 38-13) が利用されている。^{12,14)} Raji 細胞膜において Gb3 は, 脂質ラフトと呼ばれるマイクロドメイン (glycolipid enriched microdomain, GEM と呼ばれる) に存在するが, フローサイトメトリーで調べるとその反応性 (感度) は若干異なる。一方, 抗 Gb3 mAb は, これら以外にも研究室レベルで樹立されたハイブリドーマから得られるものがいくつか存在するが, 今回我々は, 米国ワシントン大学名誉教授である箱守仙一郎博士らのグループによりテラトカルシノーマを抗原として作製されたマウス mAb (Isotype: IgM, Clone: 1A4) を産生するハイブリドーマを入手した。本論文では, SAL の細胞膜リガンドとして機能する Gb3 の高感度で安定した検出法の確立を目的とし, 1A4 の簡便な精製方法および精製した抗体の反応性と貯法について検討した結果について述べる。

実験材料および実験方法

1. 実験材料

パーキットリンバ腫細胞株 Raji およびヒト慢性骨髄性白血病細胞株 K562 は, 東北大学加齢医学研究所医用細胞資源センターより, また, ヒト腎がん細胞株 TOS1 は, 東北医科薬科大学医学部泌尿器科学教室から供与されたものを用いた。この細胞を, 10% 非働化ウシ胎児血清を含む RPMI 1640 培地 (日水製薬社製, 東京) またはダルベッコ改変イーグル培地 (和光純薬工業社製, 大阪) 中で, 37°C, 5% CO₂ 存在下で培養した。抗 Gb3 抗体 (BGR23) は, 東京化成工業 (東京) より購入した。

2. 抗 Gb3 抗体 (1A4) 産生ハイブリドーマの培養

1A4 産生ハイブリドーマは, 弘前大学大学院医学研究科泌尿器科学講座から供与されたものを用いた。ハイブリドーマは, 25 cm² のフラスコ (Nunc 社製, Roskilde, Denmark) を用いて, 5 mL の培養液中に 7×10^5 細胞を播種して 37°C で 2 日間培養した。培養後, 細胞を除去した培養上清 (5 mL \times 2 で Total 10 mL) を回収した。

3. Rapid SPiN L カラムを用いた 1A4 の精製

イムノグロブリン軽鎖を構成する κ 鎖を含む抗体を精製することができるプロテイン L 固定化アフィニティーゲルが充填されている Rapid SPiN L カラム (プロテノバ社製, 東かがわ) に培養上清 (500 μ L) を加え, 1 回転あたり 30 sec の速度で 4 分間攪拌した後, 2,000 \times g で 5 秒間遠心分離を行い, 素通り画分を回収する操作を培養上清がなくなるまで繰り返した。中和バッファーとして 1 M Tris (5 μ L) を添加した回収用マイクロチューブにカラムを付け替え, 溶出液として 0.1 M グリシン塩酸塩 (pH 2.5, 200 μ L) を加えて 1 分間放置した。その後, 2,000 \times g, 5 分間遠心分離して 1A4 (Gly) を溶出した。

4. 保存溶液の置換

上記で溶出した 1A4 (Gly) の一部をウルトラフリー遠心フィルターユニット (分画分子量 10,000, Millipore 社製, Bedford, MA) に加え, 12,000 \times g, 15 分間遠心分離を行った。溶出液を廃棄した後, フィルター内の残液にダルベッコリン酸緩衝液 (D-PBS, pH 7.2) を 500 μ L 加え, 12,000 \times g, 15 分間遠心分離を行った。フィルター内の溶液を回収し, 全量 200 μ L になるように D-PBS を加え, さら

に、保存剤として終濃度 0.2% になるようにアジ化ナトリウム (Sigma 社製, St. Louis, MO, USA) を添加し、保存溶液を PBS に置換した 1A4 (PBS) を作製した。

5. タンパク質の定量

精製した抗体の定量は、Bicinchoninic Acid (BCA) protein assay kit (Pierce 社製, Rockford, IL, USA) を用いて行った。検量線作成用にはウシ血清アルブミン (BSA) を用い、得られた検量線からそれぞれの抗体の濃度を算出した。

6. SDS-ポリアクリルアミドゲル電気泳動 (SDS-PAGE)

SDS-PAGE は Laemmli の方法により行った。¹⁵⁾ 抗体の分子量の確認は、BGR23 と 1A4 (PBS) を 2-メルカプトエタノール存在下または非存在下で処理して試料を作製した。SDS-PAGE では 7.0% ゲルを用い、1 レーンあたり 1 μ g になるように添加して分離後、Silver Stain MS kit (和光純薬工業社製) で染色した。

7. フローサイトメトリー法による細胞膜 Gb3 の検出

Raji, K562 および TOS1 (2×10^5 cells) を回収し、PBS で洗浄後、一次抗体として PBS で希釈した BGR23 または 1A4 を加え、水中で 30 分間処理した。次いで、PBS で洗浄後、PBS で希釈した FITC 標識抗マウス IgG/IgM 抗体 (Jackson ImmunoResearch Laboratories 社製, West Grove, PA, USA) または Alexa488 標識マウス IgG 抗体 (Thermo Scientific 社製, Rockford, IL, USA) を加え混和し、水中で 30 分間処理した。処理後、FACScalibur (Becton Dickinson 社製, San Jose, CA, USA) を用いて細胞膜上の Gb3 発現量を測定した。

8. 免疫染色法による細胞膜 Gb3 の検出

Raji (1×10^6 cells) を回収し、4% パラホルムアルデヒド (和光純薬工業社製) を加え、室温で 15 分間処理した。PBS で洗浄後、一次抗体として PBS で希釈した BGR23 または 1A4 を加え、水中で 30 分間処理した。次いで、PBS で洗浄後、PBS で希釈した FITC 標識抗マウス IgG/IgM 抗体 (Jackson ImmunoResearch Laboratories 社製) または Alexa488 標識マウス IgG 抗体 (Thermo Scientific 社製) を加え混和し、水中で 30 分間処理した。さらに、DRAQ5 (Biostatus 社製, Leicestershire, UK) を終濃度 0.5 μ M になるように加え、核染色し

た後、fluoromount (DiagnosticBioSystems 社製, Pleasanton, CA) を用いてスライドガラスにマウントし、FV1000 共焦点レーザー顕微鏡 (Olympus 社製, 東京) により細胞膜上の Gb3 発現量を測定した。

結 果

1. SDS-PAGE による精製した 1A4 アイソタイプの確認

供与されたハイブリドーマの抗体産生能および Rapid SPiN L を利用して 1A4 のアイソタイプである IgM が簡単に精製可能か否か調べる目的で、1A4 およびアイソタイプが IgG である BGR23 を試料とし、還元および非還元条件下での SDS-PAGE を行った。還元条件で行った結果より、BGR23 ではマウス IgG の H 鎖を示す約 55 kDa のバンドが認められ、1A4 ではマウス IgM の H 鎖を示す約 80 kDa のバンドが検出された。また、非還元条件において、BGR23 は約 252 kDa 付近にバンドが見られるのに対して、1A4 は同じ条件で分離用ゲルに入らない、すなわち多量体であることを確認した (Fig. 1)。このことから、このハイブリドーマは IgM を産生しており、Rapid SPiN L を利

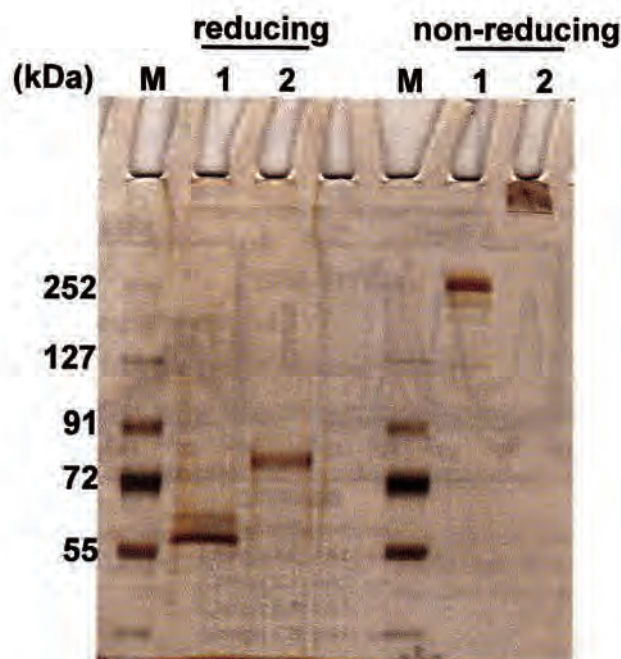


Fig. 1. SDS-PAGE pattern of purified 1A4 from hybridoma supernatants.

SDS-PAGE was performed using homogeneous 7.0% gel under reducing and non-reducing condition. Lane 1: BGR23, Lane 2: 1A4, M: protein ladder maker.

用することにより簡便な抗体精製が可能であることが示された。

2. ハイブリドーマが産生した抗体の Gb3 に対する反応性および検出する際の適切な条件の決定

ハイブリドーマの産生した IgM が Gb3 を特異的に認識する 1A4 であるか否かを, Gb3 を高発現していることが知られている Raji および Gb3 の陰性コントロールとして用いられている K562 を利用して検討した。Raji では, IgM の濃度が高くなるにつれてピークの蛍光強度が強い方にシフトし, IgM を処理した K562 では, 一次抗体未処理のコントロールと大きな差が認められないことから, この IgM は Gb3 を認識する 1A4 であることが示された。一方, 1A4 を処理した K562 では, 濃度によって大きな変化は見られないが, わずかに蛍光強度のポジティブ側へのシフトが認められた (Fig. 2A)。Gb3 が発現していない K562 で若干の反応性が見られるという結果から, この実験に用いた 1A4 の処理条件は適切ではないと考えられたため, より適切な条件を検討した。Gb3 の高感度な検出という目的から, 1A4 の濃度が低すぎると検出感度自体が低下することを考慮して, Fig. 2A の結果から使用濃度を $0.6 \mu\text{g}/\text{mL}$ に設定した。また, 蛍光標識二次抗体の濃度については, 500 および 2000 倍希釈の 2 種類の濃度に関して検討を行った。その結果, K562 では, どちらの濃度でも 1A4 で処

理後に見られる蛍光強度は, 1A4 未処理のネガティブコントロールと同程度であった (Fig. 2B)。一方, Raji においては, 二次抗体の希釈倍率が高くなるにつれて, 蛍光強度のピークがネガティブコントロールに近づいた。これらの結果から, Gb3 に対する検出感度が保たれ, Gb3 陰性細胞には反応しない条件として 1A4 の濃度を $0.6 \mu\text{g}/\text{mL}$ および二次抗体を 500 倍希釈で行うと設定して以降の実験を行うことにした。

3. Gb3 発現細胞に対する BGR23 および 1A4 (Gly) の反応性

Raji に発現している Gb3 に対する 1A4 および BGR23 の反応性の違いを, それぞれの濃度を変えて比較検討した。1A4 のサブタイプは IgM であり, BGR23 のそれは IgG であるため, それぞれの検出に用いる標識二次抗体が異なる。したがって, 二種類の抗体の比較検討の際には, それぞれの標識二次抗体のみで処理された細胞で見られる蛍光強度 (negative control) の値をできるだけ揃えて実施した。Raji に対し, 1A4 を $0.6 \mu\text{g}/\text{mL}$, BGR23 を $2.4 \mu\text{g}/\text{mL}$ で反応させた場合, フローサイトメトリー法で検出されるピークの蛍光強度はほぼ同程度であったが (Fig. 3A), BGR23 を $0.6 \mu\text{g}/\text{mL}$ とした場合には 1A4 の蛍光強度よりも明らかに低下し (Fig. 3A), この条件で共焦点レーザー顕微鏡を用いて解析を行っても, フローサイトメトリー

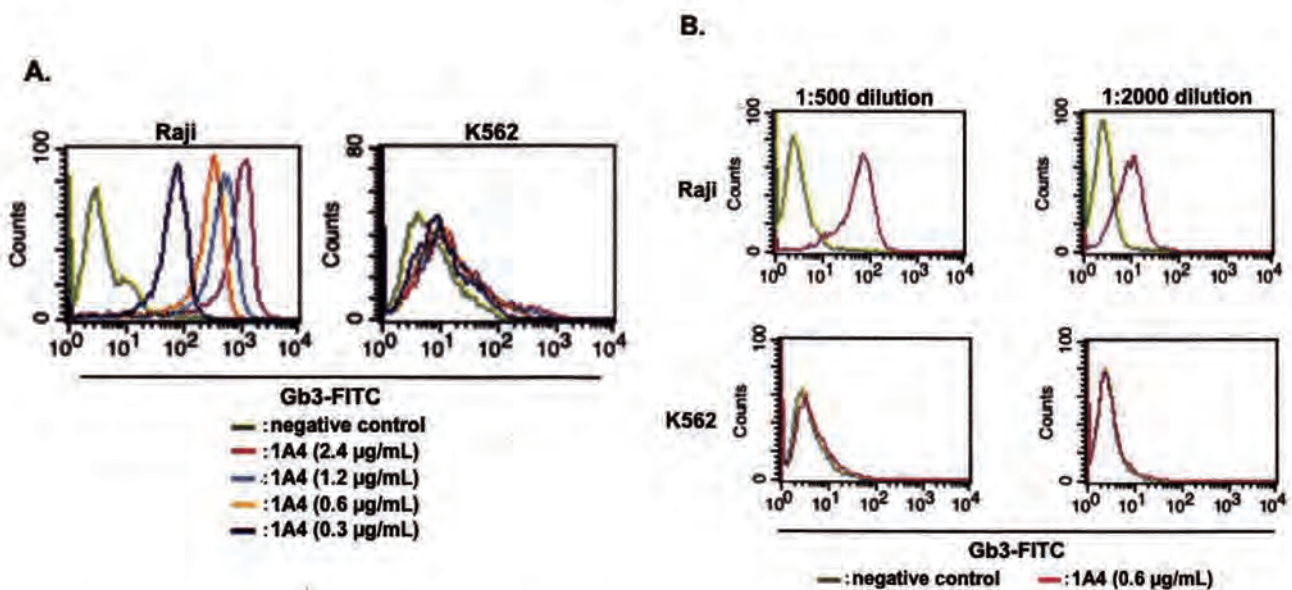


Fig. 2. Reactivity of 1A4 (Gly) against Raji and K562 cells.

(A) Raji and K562 cells were treated with 1A4 (0.3, 0.6, 1.2, and $2.4 \mu\text{g}/\text{mL}$), and then with FITC-conjugated goat anti-mouse IgM Ab (diluted 1 : 200). (B) Cells were stained with 1A4 ($0.6 \mu\text{g}/\text{mL}$) and FITC-conjugated goat anti-mouse IgM Ab (diluted 1 : 500 or 1 : 2000) (red line). Flow cytometric analysis was performed by use of FACScalibur. Green line: fluorescence intensity of control cells.

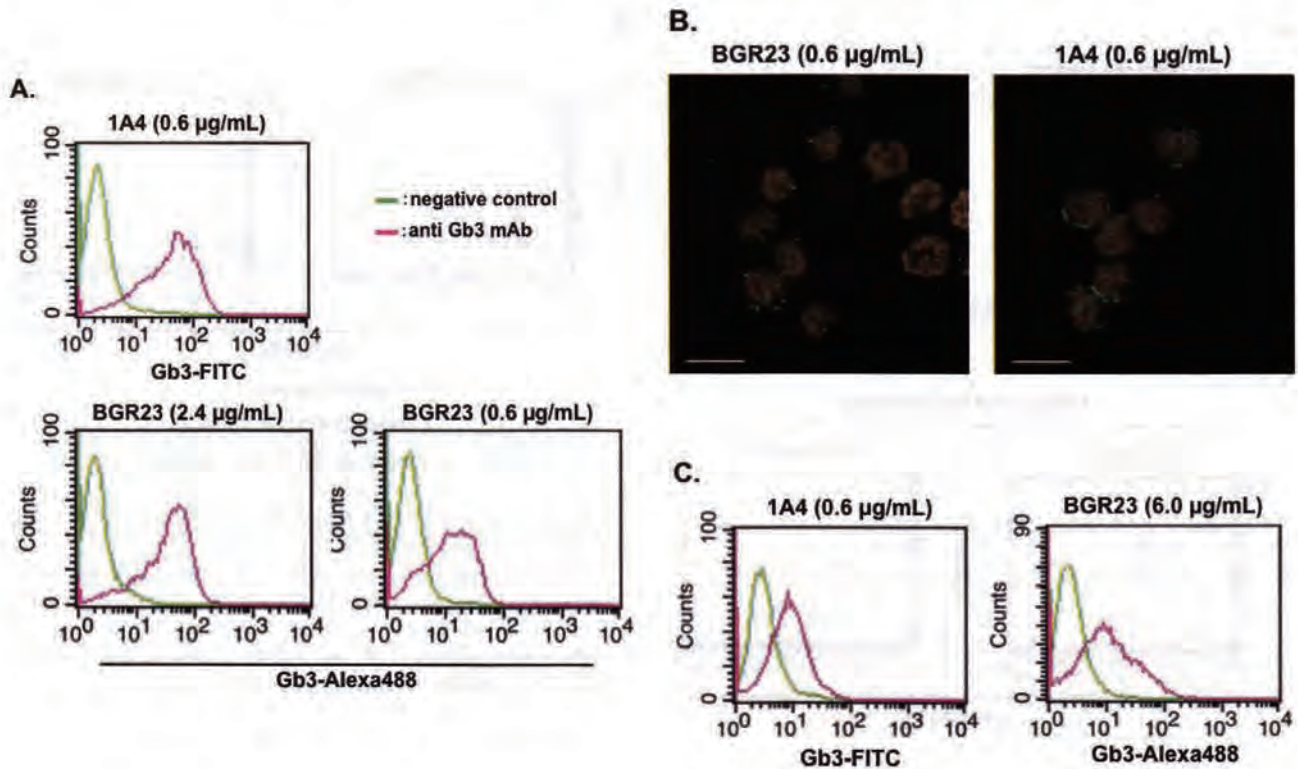


Fig. 3. Comparison of reactivities between BGR23 and 1A4 (Gly) antibodies with Gb3-expressing Raji and TOS1 cells.

(A) Raji cells were treated with 1A4 (0.6 $\mu\text{g}/\text{mL}$) or BGR23 (0.6 and 2.4 $\mu\text{g}/\text{mL}$), and then with FITC-conjugated goat anti-mouse IgM Ab or Alexa488-conjugated goat anti-mouse IgG Ab (red line). (B) Raji cells were stained as described above (green). Nuclei were counterstained with DRAQ5 (orange). Photographs were made by use of a 60X objective lens (scale: 10 μm). (C) TOS1 cells were treated with 1A4 (0.6 $\mu\text{g}/\text{mL}$) or BGR23 (0.6 $\mu\text{g}/\text{mL}$). Flow cytometric analysis was performed by use of FACScalibur.

法と同様に 1A4 において Gb3 を示す強い蛍光が観察された (Fig. 3B). TOS1 は、Gb3 の発現量が Raji よりも低いことが知られている。この細胞に対しては、BGR23 を 6.0 $\mu\text{g}/\text{mL}$ にすることで 1A4 (0.6 $\mu\text{g}/\text{mL}$) と同程度のピークの蛍光強度が得られた (Fig. 3C)。

4. 1A4 (Gly) の保存状態による反応性の変化

1A4 (Gly) の保存期間における Gb3 に対する反応性の変化を検討したところ、1 カ月間凍結保存を行っても Gb3 に対する反応性に変化は見られなかった (Fig. 4)。1A4 (Gly) は、中和されているものの一般的な抗体の保存に利用されるリン酸緩衝生理食塩水 (PBS, pH 7.4) とは異なるため、バッファー交換により PBS 置換した 1A4 (PBS) を作製して、保存バッファーが Gb3 に対する反応性に影響を与えるか否かを検討した。抗体を精製した直後、4°C で 1 週間および 1 カ月間保存したときの反応性の変化を調べた結果、精製した直後の 1A4 は保存溶液による反応性に違いは見られないが、1 週間および 1 カ月間保存すると 1A4 (PBS) において反応性が低下するという結果が得られた

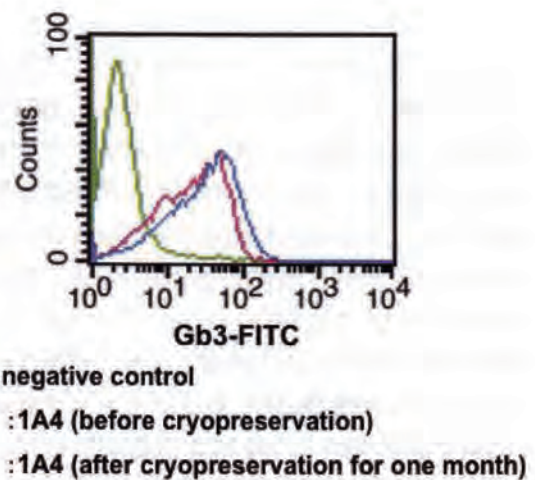


Fig. 4. Storage effect after cryopreservation on a 1A4 reactivity.

Raji cells were treated with 1A4 (0.6 $\mu\text{g}/\text{mL}$), and then with FITC-conjugated goat anti-mouse IgM Ab (diluted 1:500). Flow cytometric analysis was performed as described above.

(Fig. 5A). さらに、保存温度により Gb3 に対する反応性が変化するか否かについても検討したところ、精製してから 4°C で保存した抗体と -80°C 凍結保存した抗体では、どちらの保存温度でも 1A4

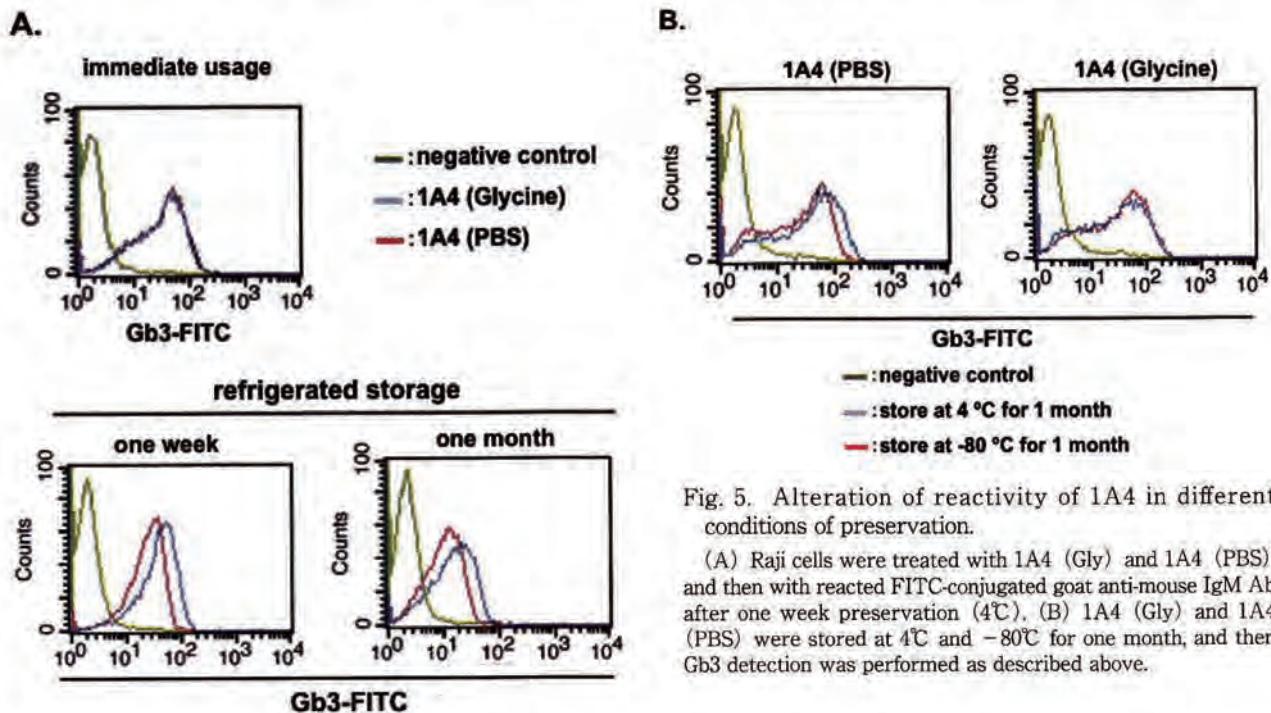


Fig. 5. Alteration of reactivity of 1A4 in different conditions of preservation.

(A) Raji cells were treated with 1A4 (Gly) and 1A4 (PBS), and then with reacted FITC-conjugated goat anti-mouse IgM Ab after one week preservation (4°C). (B) 1A4 (Gly) and 1A4 (PBS) were stored at 4°C and -80°C for one month, and then Gb3 detection was performed as described above.

(Gly) および 1A4 (PBS) において反応性に大きな変化は見られなかった (Fig. 5B).

考 察

タンパク質にはエピトープとなる部位が複数存在し、そのため1つのタンパク質に対して複数の抗体が作製される。同時に、単一のエピトープに着目した場合でも、それに対して作られる抗体は1種類とは限らない。これを抗体の不均一性という。糖脂質を抗原とする場合、脂質部分は膜の脂質二重層に埋め込まれていることからエピトープとなることは稀であり、ほぼ糖鎖部分が抗体によって認識されることになる。この場合でも、同じエピトープを認識する抗体でありながら、例えば TLC 上での発色 (結合) 様態と免疫沈降させたときに見られる結果が異なるケースが報告されている。¹⁶⁾ 抗体は、抗原と単に結合するだけではなく、結合することによって細胞に様々な変化を及ぼすが、もちろんこの変化も抗体の種類によって変わる。さらに、糖脂質の細胞膜上における局在密度 (一定面積に存在する分子の数) や糖鎖の配向 (膜面に対して直立しているか平行しているか) などによっても抗体の反応性が異なることが報告されている。¹⁷⁾

Gb3 は B 細胞の分化抗原 CD77 として、また、

ヒト赤血球の血液型 Pk 抗原として知られるグロボ系スフィンゴ糖脂質であり、同時に病原性大腸菌が産生するシガ毒素 (Stx) の受容体として機能していることが知られている。一方で Gb3 は、主に海洋生物に多く存在するラムノース結合性レクチン (RBL) の細胞膜レセプターであることが明らかになっているが、我々が研究している SAL も RBL の一つである。SAL はバーキッドリンパ腫 (Raji, Ramos など) に対して細胞増殖抑制効果を示すが、これはアポトーシス誘導のような細胞に対する不可逆的毒性ではなく、G₀G₁ arrest による細胞周期の停滞によるものであることが分かっている。¹¹⁾ がん細胞に対する SAL の効果を検討する上で、細胞膜 Gb3 の有無や存在形態は決定的なファクターとなる。事実、Gb3 の発現が認められていない K562 は、SAL に対する反応がまったく見られないことから、良いネガティブコントロール細胞として利用可能である。Table 1 で示されるように Gb3 に対する mAb は、BGR23 および 38-13 の 2 種類のクローンが市販されており、前者は、*Salmonella minnesota* を抗原として作製され、後者は Gb3 発現細胞を抗原として作製された抗体であり、^{12,13)} この 2 種はそれぞれ反応性が異なることが実験的に分かっている。Kim らは、ヒト急性単球性白血病細胞株 THP-1 について、BGR23, 38-13 お

Table 1. Characteristics of antibody against Gb3.

Clone name	Isotype	Host species	Immno-gen	Optimized storage buffer	Optimized storage temperature (°C)
BGR23	IgG2b	mouse	Purified Gb3 adsorbed to <i>Salmonella Minnesota</i>	PBS	-80
38-13	IgM	rat	Burkitt's lymphoma cell line Daudi	PBS	-80
1A4	IgM	mouse	Teratocarcinoma	unknown	unknown

よび市販されていない 5B5 を用いて Gb3 の検出に最適な濃度を検討し、BGR23 は $20 \mu\text{g}/\text{mL}$ 、38-13 は $5 \mu\text{g}/\text{mL}$ であり、5B5 は最も低い $1.25 \mu\text{g}/\text{mL}$ であると報告している。¹⁸⁾ この報告と今回我々が精製した 1A4 (Gly) を比較すると、細胞は異なるもの $0.6 \mu\text{g}/\text{mL}$ で Gb3 を検出できることから (Fig. 2B)、利用することができる抗体の中では 1A4 が最も有用な抗体ではないかと考えた。1A4 は IgM クラスの抗体であることから、BGR23 (IgG) と比較し 5 倍の結合価数をもっているが、Gb3 の三糖構造に対する結合を考えた場合、その空間配置や立体障害の関係で全てが結合に関わるとは考えにくい。さらに、分子量からのモル比を考慮すると、1A4 の反応性が有意に高いことは明らかである。

マウス IgM は、ヒト IgM と比較すると protein A に対する結合能が低く、その抗体精製には protein L が利用され、一般的に protein L と IgM 結合させるためには、 4°C で 2~4 時間あるいは一夜処理する必要があるとされている。しかし、今回利用した Rapid SPiN L カラムは、高結合改変 protein L 固定化アフィニティーゲルが充填されたカラムであり、結合に要する時間は 4 分間とかなり短く、抗体溶出までの所要時間は約 10 分である。このカラムの IgM 精製に対する適性は、Fig. 1 で示した通りであり、迅速かつ簡便に純度の高い抗体を得る方法を確立できたものと考えている。

今回、我々は Gb3 に対する反応性がより高い抗体の取得を目的とし、市販されていない 1A4 と BGR23 と直接比較した。その結果 1A4 は、Gb3 に対する反応性が BGR23 より高い抗体である可能性が示された (Fig. 3A, B)。しかしながら、今回の実験では結合解離定数などの速度論解析は行っておらず、抗体の反応性を定量化するには至っていない。今後、分子間相互作用解析装置等を用いて比較検討することにより、1A4 の Gb3 に対する反

応性の有意性がさらに明確になると思われる。また、抗体貯法に関して、保存温度および一般に mAb の保存溶媒として使用されている PBS と、Rapid SPiN L カラム溶出後の Tris-Glycine 塩酸塩のどちらが適しているかについて検討した結果、どちらの保存溶液でも 4°C あるいは -80°C 保存で反応性に変化は見られなかったことから、温度そのものは 1A4 の反応性に影響を及ぼさないことが示された (Fig. 5B)。一方、 4°C で 1 週間から 1 カ月保存した場合、PBS に溶解したもののほうが Tris-Gly 塩酸塩よりも反応性が低下した (Fig. 5A)。抗体に限らず、酵素や増殖因子などの生物活性をもつタンパク質を溶液中で保存する場合は、比較的高濃度の緩衝液に溶解する方がタンパク質の活性な立体構造を保つ上で都合が良いとされている。今回得られたデータからも、凍結保存しない場合、1 カ月程度であれば、スピナカラム精製・中和後、バッファー交換せずにそのまま保存した方が反応性が低下しないことが分かった。本研究により、Gb3 の検出に用いる mAb として 1A4 は、ハイブリドーマから迅速簡便に精製可能であり、また、既存の市販抗体と比較して抗原検出感度の点で優れていること、さらに貯法として、高塩濃度緩衝液を利用することで、溶液状態での保存が可能であることが明らかとなり、SAL に関する今後の実験プロトコールに資する結果が得られた。

近年、抗体依存性細胞障害活性 (ADCC) を利用して mAb を直接がんの治療に応用しようという試みが数多く検討されている。¹⁹⁾ Gb3 を標的とした研究でも、パーキットリンパ腫細胞に対してアポトーシスを誘導する活性 (1A4) が報告され、²⁰⁾ また Desselle らは、新たな抗 Gb3 mAb である 3E2 が、*in vitro* および *in vivo* において腫瘍血管新生とがんの成長に抑制的に作用することを報告している。²¹⁾ これらの情報を踏まえ、SAL の抗腫瘍効

果を検討することと並行して, 膜糖脂質としての Gb3 にも着目し, その機能についても視野を広げていく必要があると考えている。

利益相反

開示すべき利益相反はない。

REFERENCES

- 1) Köhler G., Milstein C., *Nature*, **256**, 495–497 (1975).
- 2) Zhang X., Soori G., Dobleman T. J., Xiao G. G., *Expert Rev. Mol. Diagn.*, **14**, 97–106 (2014).
- 3) Salles G., Barrett M., For R., Maurer J., O'Brien S., Wenger M., Maloney D. G., *Adv. Ther.*, **34**, 2232–2273 (2017).
- 4) Ishida Y., Agata Y., Shibahara K., Honjo T., *EMBO J.*, **11**, 3887–3895 (1992).
- 5) Kasahara K., *Trends Glycosci. Glycotechnol.*, **26**, 79–87 (2014).
- 6) Nores G. A., Dohi T., Taniguchi M., Hakomori S., *J. Immunol.*, **139**, 3171–3176 (1987).
- 7) Tatewaki K., Yamaki T., Maeda Y., Tobioka H., Piao H., Ibayashi Y., Sawada N., Hashi K., *Exp. Cell Res.*, **233**, 145–154 (1997).
- 8) Greenshields K. N., Halstead S. K., Zitman F. M., Rinaldi S., Brennan K. M., O'Leary C., Chamberlain L. H., Easton A., Roxburgh J., Pediani J., Furukawa K., Goodyear C. S., Plomp J. J., Willison H. J., *J. Clin. Invest.*, **119**, 595–610 (2009).
- 9) Sugawara S., Hosono M., Ogawa Y., Takayanagi M., Nitta K., *Biol. Pharm. Bull.*, **28**, 424–441 (2005).
- 10) Kawano T., Sugawara S., Hosono M., Tatsuta T., Ogawa Y., Fujimura T., Taka H., Murayama K., Nitta K., *Biol. Pharm. Bull.*, **32**, 345–353 (2009).
- 11) Sugawara S., Im C., Kawano T., Tatsuta T., Koide Y., Yamamoto D., Ozeki Y., Nitta K., Hosono M., *Glycoconj. J.*, **34**, 127–138 (2017).
- 12) Kotani M., Kawashima I., Ozawa H., Ogura K., Ariga T., Tai T., *Arch. Biochem. Biophys.*, **310**, 89–96 (1994).
- 13) Wiels J., Fellous M., Turz T., *Proc. Natl. Acad. Sci. USA*, **78**, 6485–6488 (1981).
- 14) Nudelman E., Kannagi R., Hakomori S., Parsons M., Lipinski M., Wiels J., Fellous M., Tursz T., *Science*, **220**, 509–511 (1983).
- 15) Laemmli U.K., *Nature*, **227**, 680–685 (1970).
- 16) Iwabuchi K., Nakayama H., *Seikagaku*, **89**, 62–72 (2017).
- 17) Hanashima T., Miyake M., Yahiro K., Iwamura Y., Ando A., Morinaga N., Noda M., *Microb. Pathog.*, **45**, 124–133 (2008).
- 18) Kim M., Binnington B., Sakac D., Fernandes K. R., Shi S.P., Lingwood C. A., Branch D. R., *J. Immunol. Methods*, **371**, 48–60 (2011).
- 19) Ochoa M. C., Minute L., Rodriguez I., Garasa S., Perez-Ruiz E., Inogés S., Melero I., Berraondo P., *Immunol. Cell Biol.*, **95**, 347–355 (2017).
- 20) Tétaud C., Falguières T., Carlier K., Lécluse Y., Garibal J., Coulaud D., Busson P., Steffensen R., Clausen H., Johannes L., Wiels J., *J. Biol. Chem.*, **278**, 45200–45208 (2003).
- 21) Desselle A., Chaumette T., Gaugler M. H., Cochonneau D., Fleurence J., Dubois N., Hulin P., Aubry J., Birklé S., Paris F., *PLoS One*, **7**, e45423 (2012).

東北医科薬科大学分子生体膜研究所年報

2019年3月31日発行

発行者・発行所 東北医科薬科大学分子生体膜研究所

宮城県仙台市青葉区小松島 4-4-1



東北医科薬科大学

TOHOKU MEDICAL AND PHARMACEUTICAL UNIVERSITY